molecules

Special Issue Dedicated to Late Professor Takuo Okuda, Tannins and Related Polyphenols Revisited

Chemistry, Biochemistry and Biological Activities

Edited by
Hideyuki Ito, Tsutomu Hatano and Takashi Yoshida

MDPI

Special Issue Dedicated to Late Professor Takuo Okuda

Special Issue Dedicated to Late Professor Takuo Okuda

Tannins and Related Polyphenols Revisited: Chemistry, Biochemistry and Biological Activities

Special Issue Editors

Hideyuki Ito
Tsutomu Hatano
Takashi Yoshida

Special Issue Editors
Hideyuki Ito
Okayama Prefectural University
Japan

Tsutomu Hatano
Okayama University
Japan

Takashi Yoshida
Okayama University
Japan

For citation purposes, cite each article independently as indicated on the article page online and as indicated below:

LastName, A.A.; LastName, B.B.; LastName, C.C. Article Title. *Journal Name* **Year**, *Article Number*, Page Range.

Contents

About the Special Issue Editors

Hideyuki Ito, He worked as a Research Associate at Okayama University (Professor Takashi Yoshida), Japan in 1992 and obtained his PhD from the same university in 1999. He worked as an Associate Professor at the same university in 2005. He moved as a Professor to Okayama Prefectural University in 2013. His research interests include the isolation and structural elucidation of ellagitannins and related polyphenols and bioavailability of polyphenols. A part of his research has been published as review articles in this area (*Planta Medica*, 11, 1110–1115 (2011)., *Molecules*, 16, 2191–2217 (2011)).

Tsutomu Hatano, He received his PhD degree from Kyoto University in 1991. His research as Assistant Professor at Faculty of Pharmaceutical Sciences, Okayama University started in 1979. He has continued his research as Associate Professor, Faculty of Pharmaceutical Sciences, Okayama University since 1993, and as Professor, Okayama University Graduate School of Medicine, Dentistry and Pharmaceutical Sciences since 2005.

Takashi Yoshida, He obtained his PhD from Kyoto University (Japan) in 1969 and worked as a Research Associate at the same university. He then moved as an Associate Professor to Okayama University (Japan, Professor Takuo Okuda) in 1970 and succeeded Professor Okuda after his retirement in 1993. He also worked at the College of Pharmacy, Matsuyama University (Japan, Professor) (2006–2012) after his departure from Okayama University in 2005. His research interests include the isolation and structural determination of ellagitannins and related polyphenols and studies on their physiological activities. His group has published many papers extensively in this area, including a book edition "Plant Polyphenols 2" (Kluwer/Academic, Plenum Publishers, 1999, edited together with Drs. R. Hemingway and G.G. Gross).

Preface to "Special Issue Dedicated to Late Professor Takuo Okuda"

This book is a specially designed reprint of the Special Issue in Molecules, "Tannins and Related Polyphenols Revisited: Chemistry, Biochemistry and Biological Activities", which was dedicated to Dr. Takuo Okuda, on the occasion of his passing away in December 2016.

Takuo Okuda Ph.D. (1927–2016)

He obtained his PhD from Kyoto University (Pharmacognosy, Japan) in 1955, followed by postdoctoral study at Pennsylvania State University (USA, 1955–1957). After serving as a Lecturer (1958–1961) and an Associate Professor at Kyoto University (1962–1969), he moved to Okayama University (Faculty of Pharmaceutical Sciences, Professor) in 1970 and retired in 1993 (Emeritus Professor of Okayama University).

Dr. Okuda received the Tannin Award in the 4th Tannin Conference in 2004 (Philadelphia, USA), Groupe Polyphenol Medal in 2014 (Nagoya), and an honor of The Order of the Sacred Treasure, Gold Rays with Neck Ribbon in 2016 (the Imperial Household Agency of Japan) for his outstanding achievements in the field of polyphenolic natural products.

Antioxidant polyphenols, especially those classified as tannins and flavonoids, have currently been attracting increased interest as important constituents in vegetables, fruits, and

beverages as well as natural medicines because of their multiple biological activities that are beneficial to human health. Dr. Takuo Okuda largely contributed as one of the pioneers in development and promotion of polyphenol research ever since the early stage of the chemical study on tannins and related polyphenols in medicinal plants traditionally used in Japan, China and/or South-East Asian countries. He first characterized a tannin constituent (geraniin) in a popular official crude drug (anti-diarrheic: Geranium thunbergii) in Japan, in 1982, and since then and for two decades developed the studies on the isolation and characterization of tannins and related polyphenols in various plant species to find more than 150 new compounds at Okayama University, Japan. He also reported a broad range of pharmacological functions of tannins and related polyphenols, suggesting chemoprevention of life-related diseases such as cancers, diabetes, arteriosclerosis, and heart diseases, which largely led to a basis of the current concept for "polyphenols". His prolific scientific activity is documented by 392 papers which contain a review of his life-work (In "Progress in the Chemistry of Organic Natural Products 66" (Founded by L. Zechmeister, Springer-Verlag, 1995)).

This book contains 4 reviews and 14 original articles by experts of the tannin and polyphenol research, which are arranged with classification of polyphenols (ellagitannins, condensed tannins, flavonoids, and others). This will be useful for all scientists to understand a current trend of research on various polyphenols and to recognize their significance in herbal medicines and food science, and for young scientists to encourage to explore these important class of natural compounds.

Hideyuki Ito, Tsutomu Hatano, Takashi Yoshida
Guest Editors

Review

Chemical and Biological Significance of Oenothein B and Related Ellagitannin Oligomers with Macrocyclic Structure

Takashi Yoshida [1,2], Morio Yoshimura [1] and Yoshiaki Amakura [1,*]

[1] College of Pharmaceutical Sciences, Matsuyama University, 4-2 Bunkyo-cho, Matsuyama, Ehime 790-8578, Japan; xp769b@bma.biglobe.ne.jp (T.Y.); myoshimu@g.matsuyama-u.ac.jp (M.Y.)

[2] Okayama University, Okayama 701-1152, Japan

[*] Correspondence: amakura@g.matsuyama-u.ac.jp; Tel.: +81-89-925-7111

Abstract: In 1990, Okuda et al. reported the first isolation and characterization of oenothein B, a unique ellagitannin dimer with a macrocyclic structure, from the *Oenothera erythrosepala* leaves. Since then, a variety of macrocyclic analogs, including trimeric–heptameric oligomers have been isolated from various medicinal plants belonging to Onagraceae, Lythraceae, and Myrtaceae. Among notable in vitro and in vivo biological activities reported for oenothein B are antioxidant, anti-inflammatory, enzyme inhibitory, antitumor, antimicrobial, and immunomodulatory activities. Oenothein B and related oligomers, and/or plant extracts containing them have thus attracted increasing interest as promising targets for the development of chemopreventive agents of life-related diseases associated with oxygen stress in human health. In order to better understand the significance of this type of ellagitannin in medicinal plants, this review summarizes (1) the structural characteristics of oenothein B and related dimers; (2) the oxidative metabolites of oenothein B up to heptameric oligomers; (3) the distribution of oenotheins and other macrocyclic analogs in the plant kingdom; and (4) the pharmacological activities hitherto documented for oenothein B, including those recently found by our laboratory.

Keywords: oenothein B; ellagitannin; macrocyclic oligomer; Onagraceae; Myrtaceae; Lythraceae; antioxidants; antitumor effect; immunomodulatory effect; anti-inflammation

1. Introduction

Antioxidant polyphenols in medicinal plants, foods, and fruits are currently acknowledged as important beneficial constituents that reduce the risk of life-related diseases closely associated with active oxygen damage, such as cancers, arteriosclerosis, diabetes, and coronary heart diseases, and have been explored as plausible chemopreventive agents for the human healthcare market. Polyphenols have thus received increasing attention for the discovery and development of their new physiological functions. Among various types of antioxidant plant polyphenols are low molecular weight compounds, represented by flavonoids and lignans, and higher molecular weight polyphenols classified as tannins. Vegetable tannins are classified into two large groups: (1) condensed tannins (proanthocyanidin polymers and oligomers); and (2) hydrolysable tannins, which are subgrouped into gallotannins (polygalloyl esters of glucose) and ellagitannins, which are characterized as hexahydroxydiphenoyl (HHDP) esters of sugar, mostly glucose, as represented by geraniin (**1**), tellimagrandin I (**2**), and II (**3**). In contrast to condensed tannins and gallotannins (Turkish or Chinese gall), which were long recognized in the leather industry [1], ellagitannins in medicinal plants had been little studied before the discovery of geraniin (**1**) from a Japanese folk medicine, *Geranium thunbergii* (Geraniaceae), by Okuda's group in 1976 [2,3]. Since 1976,

remarkable progress in the field of ellagitannin chemistry, promoted by the development of high resolution NMR and MS spectrometers and new separation methods, has led to the isolation and characterization of more than 500 ellagitannins with diverse arrays of structures from the traditional medicines long used in Japan, China, and South East Asia. The structural diversity of the ellagitannins are brought by various oxidative modifications of the HHDP group producing dehydroellagitannins, such as **1** or by intermolecular C–O oxidative coupling(s) among multiple molecules, leading to oligomeric ellagitannins [4–7]. The first dimeric ellagitannin encountered in nature was agrimoniin from *Agrimonia pilosa* (Rosaceae), which was characterized as a dimer of potentillin (1-*O*-galloyl-2,3/4,6-di-*O*-(*S*)-HHDP-α-D-glucose), produced through the formation of a dehydrodigalloyl linking unit by intermolecular C–O oxidative coupling between two galloyl groups at C-1 [8]. Among the more than 300 oligomers, up to heptamer, reported after the discovery of agrimoniin, oenothein B (**4**) is a unique macrocyclic ellagitannin dimer, which is biogenetically produced by double C–O couplings of two molecules of tellimagrandin I (**2**), as illustrated in Figure 1.
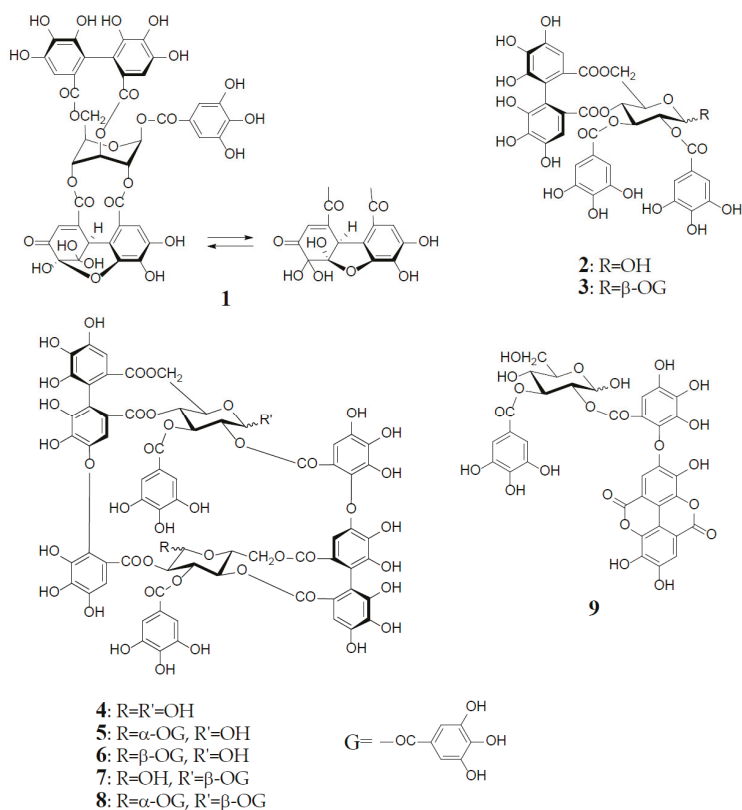
Figure 1. Structures of geraniin (**1**), tellimagrandin I (**2**), and II (**3**), oenothein B (**4**), woodfordin C (**5**), eugeniflorin D$_1$ (**6**), cuphiin D$_2$ (**7**), cuphiin D$_1$ (**8**), and oenothein C (**9**).

Oenothein B (**4**) was first isolated as a major component from the leaves of *Oenothera erythrosepala* (Onagraceae) in 1990 [9], and later found widely distributed in other plant species belonging to Myrtaceae and Lythraceae, as well as Onagraceae [5,6,10,11]. It was an important leading compound that made easier the structure elucidation of analogous oligomers co-occurring in various plant species.

Furthermore, oenothein B and related oligomers have been reported to exhibit a variety of in vitro or in vivo physiological activities beneficial to human health.

This review summarizes the structural characteristics of oenothein B (**4**) and related oxidized metabolites, up to heptameric oligomer, found in medicinal plants and their diverse biological functions hitherto reported, including those discovered recently in our laboratory. This review provides a better understanding of the significance of those antioxidant tannin constituents in medicinal plants, which may lead to future developments of preventive or therapeutic agents for various chronic diseases associated with oxygen stress by active oxygen species and free radicals.

2. Structural Characteristics of Oenothein B

Oenothein B (**4**), FABMS m/z 1569 [M + H]$^+$, was obtained as an amorphous powder forming an inseparable mixture of theoretically four anomers at two C-1 unacylated glucosyl cores, which caused extreme difficulty in its structure elucidation by spectroscopic analysis. In fact, the ^{1}H-NMR spectrum in acetone-d_6-D$_2$O recorded at ambient temperature is poorly informative due to severe broadening and multiplication of each proton signal. This spectral feature is characteristic of this type of macrocyclic oligomers owing to the anomerization at each glucose core, and also to a poor flexibility of the macro ring arising from a restricted rotation around the ether linkages of two valoneoyl groups. The structure determination of **4** was performed by spectral and chemical methods, briefly described below.

The ^{1}H-NMR measurement at an elevated temperature (40–50 °C) provided a more informative spectrum, indicating the presence of a predominant anomer with anomeric proton signals at δ 6.20 (d, J = 3.5 Hz) and δ 4.48 (d, J = 7.5 Hz), due to the α- and β-anomers of glucose-I and II, respectively; however, some of the aromatic and sugar proton signals still broadened, probably due to the poor flexibility of the macro ring. A conclusive clue for the structure elucidation of **4** was brought by the NaBH$_4$ reduction at the anomeric centers, which gave a sole tetrahydro derivative with two glucitol cores showing a well-resolved simple NMR spectrum. The spectrum clearly indicated the presence of two each of valoneoyl, galloyl, and glucitol groups as components, as revealed by the characteristic six 1H-singlets and two 2H-singlets in the aromatic region. These units were chemically substantiated by acid hydrolysis of **4**, which produced glucose, and by permethylation followed by methanolysis, which afforded methyl tri-*O*-methylgallate and trimethyl (*S*)-octa-*O*-methylvaloneate in a 1:1 molar ratio. The binding modes of the valoneoyl and galloyl groups on the glucose cores in **4** were determined from the long-range ^{1}H-^{13}C shift correlation spectrum of the tetrahydro derivative and identification of partial hydrolysates, including oenothein C (**9**), obtained upon treatment of **4** with hot water. The ^{13}C-NMR and CD (large positive Cotton effect at 218–236 nm) spectra of oenothein B were all consistent with the gross structure (**4**) [9] (Figure 1).

It is noteworthy that the purity of oenothein B (**4**) is hard to assess by reversed-phase HPLC, because of the appearance of multiple peaks on the chromatograph, depending on the different ratio of the anomers. The LC-MS/MS data for oenothein B reported by Toth et al. might be valuable for its identification [11]. Although expensive, oenothein B is now commercially available as analytical standard, and thus can be used as reference compound for the identification of oenothein B isolated from natural sources, by comparisons of the normal and reversed-phases HPLC with those of the commercial reagent.

Among interesting analogs of oenothein B (**4**) are oenotheins D (**10**) and F (**11**), which were isolated together with **4** (major principle) from the leaves of *Oenothera laciniata*, and characterized as regioisomers of **4**, differing at the binding site of the valoneoyl group linking each monomeric unit, as illustrated in Figure 2 [12]. Contrary to oenothein B (**4**), oenothein D (**10**) displayed a well-resolved ^{1}H-NMR spectrum at ambient temperature, and indicated the presence of predominant anomers at each glucose core, as revealed by the unacylated anomeric proton signals at δ 5.89 (d, J = 4 Hz; glucose-I) and 4.85 (d, J = 8 Hz; glucose-II). The positions of the two valoneoyl moieties in **10** were

determined in a similar way to **4**, i.e., long-range ^{1}H-^{13}C correlation spectrum and partial degradation in hot water.

The ^{1}H-NMR spectrum of oenothein F (**11**) in acetone-d_6-D$_2$O (2 drops) indicated that it exists as a mixture of four anomers at the glucose cores, as shown by the valoneoyl 1H- and galloyl 2H-singlets, each forming four lines in a ratio of ca. 1:2:2:6. It is noteworthy that the relative peak intensity of the four lines for each proton signal changed to ca. 1:4:4:23 after leaving the NMR sample in solution for two days. The ^{1}H-NMR spectrum of the most dominant anomer looked like that of a monomeric tannin, namely the appearance of three singlets (δ 6.21, 6.40, and 7.30, each 2H) and one singlet (δ 7.04, 4H) assignable to two valoneoyl and two galloyl units. The sugar proton signals were also apparently those of a monomeric tannin closely similar to those of an α-anomer of tellimagrandin I (**2**). Such a monomer-like ^{1}H-NMR spectrum suggested that **11** has a symmetrical structure with a considerably flexible macro ring (Figure 2).
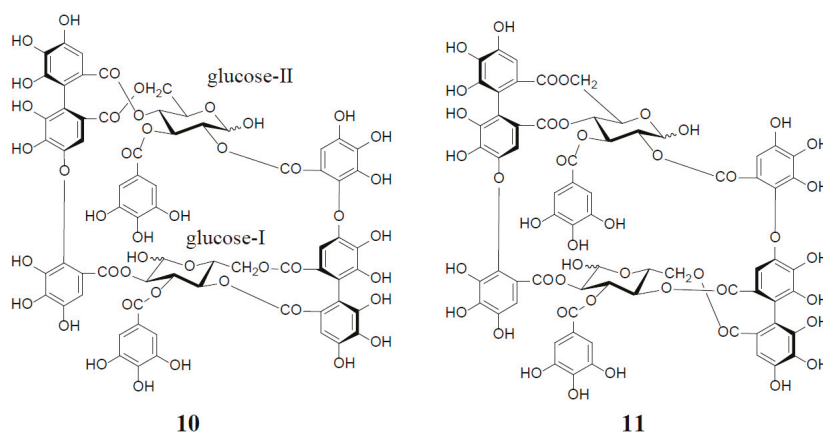
Figure 2. Structures of oenotheins D (**10**) and F (**11**).

Oenothein B (**4**) and related dimers were also found in plant species of Lythraceae and Myrtaceae, as well as Oenotheraceae. Notably, the lythraceous and myrtaceous plants, unlike Oenotheraceae, produce the galloylated oenothein B together with 4. Woodfordin C (**5**) and eugeniflorin D$_1$ (**6**), which are monogalloyl isomers at glucose-I of 4, were obtained from *Woodfordia fruticosa* (Lythraceae), a popular traditional Jamu medicine in Indonesia and Malaysia [13,14], and *Eugenia uniflora* (Myrtaceae), an evergreen fruit tree called Brazilian cherry [15], respectively. The ^{1}H-NMR spectrum of 5 (α-gallate at glucose-I), recorded at ambient temperature, displayed broad signals for some of the aromatic and glucose protons, while the spectrum recorded at an elevated temperature (38 °C), which largely contributed to its structure elucidation, was much simpler, and displayed a preferred β-anomer at glucose-II [anomeric proton, δ 4.38 (br. d, J = 8 Hz)] [13]. Cuphiin D$_2$ (**7**), a β-gallate at glucose-II of 4, was isolated along with a digallate, cuphiin D$_1$ (**8**), as well as 4 and 5 from the aerial parts of *Cuphea hyssopifolia* (Lythraceae), which has been used as a folk medicine for treating stomach disorders and oral contraceptive in South and Central Americas [16]. The existence of a dominant α-anomer at glucose-I in 7 (δ 6.18, d, J = 3 Hz) was evidenced by the absence of duplicates of any proton signal in the NMR spectra recorded at 40 °C, and also the observation of a single peak in the reversed-phase HPLC. The structural relationship of cuphiins D$_1$ (**8**) and D$_2$ (**7**) was verified by enzymatic degalloylation of 8, with tannase affording 4, 5, and 7, besides gallic acid (Figure 1).

3. Oxidized Metabolites (Dimers and Oligomers) of Oenothein B

An old hypothetical biogenesis of ellagitannins [1,4,17] has now been proven by the intensive enzymatic studies of Gross et al. Using crude enzyme preparations from the *Tellima grandiflora* leaves, they demonstrated the in vitro biosynthesis of ellagitannins, which includes an intramolecular C–C oxidative coupling of pentagalloylglucose to tellimagrandin II (**3**) [18], followed by an oxidative intermolecular C–O coupling between two moles of **3** to yield a dimeric ellagitannin, cornusiin E (**12**) [19] (Figure 3). These in vitro C–C and C–O couplings in the biosynthesis of hydrolysable tannins are thought to occur in vivo through free radical coupling processes involving laccase-type phenolase, with a lower redox potential than those concerned in lignification processes.
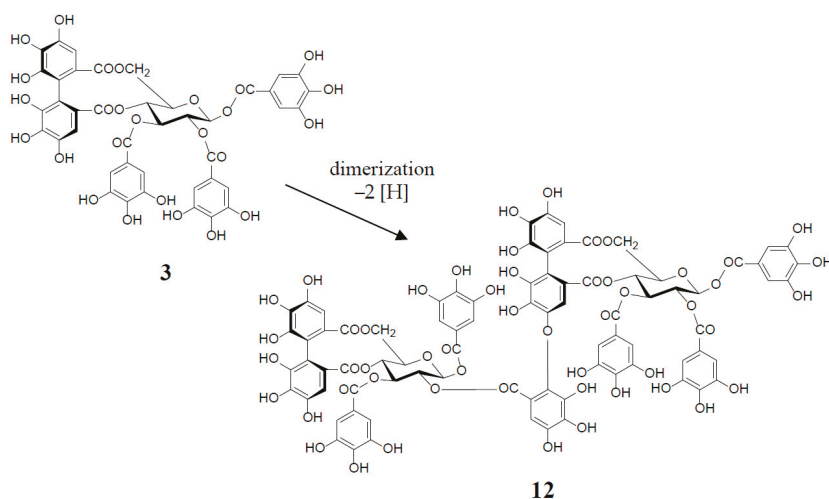
Figure 3. in vitro biosynthesis of cornusiin E (**12**) from tellimagrandin II (**3**) (2 moles).

Similar intermolecular oxidative coupling(s) of oenothein B and related dimers with additional monomeric ellagitannin(s) are believed to lead to trimeric and higher oligomeric analogs. Such examples in nature are oenothein A (**13**) from *Oenothera* and *Epilobium* species, and its gallate, woodfordins D (**14**) (trimer) [20], E (**15**) (trimer) and F (**16**) (tetramer), together with woodfordin I (**17**) (dimer) from the *W. fruticosa* flowers [21]. The presence of oenothein B-related oligomers larger than **16** in *Epilobium angustifolium* (willowherb) was recently reported by Salminen et al. [22]. They isolated the oenothein B-based oligomers using preparative HPLC, and characterized them as oenothein B (**4**), oenothtein A (**13**), woodfordin F (**16**), and related pentameric (**18**) to heptameric (**20**) oligomers, chiefly based on the analysis of the fragmentation pattern in the ESI-microTOF-Q mass spectra (negative mode) (Figure 4). The structures of these oligomers were postulated as those produced by the formation of the valoneoyl group through sequential intermolecular oxidative coupling(s) of a galloyl unit at C2 of monomeric tellimagrandin I (**2**) with an HHDP unit of the terminal glucose-IV of woodfordin F (**16**). In the mass spectra, basic fragmentation occurred reversely through the sequential removal of a molecule of tellimagrandin I (**2**) by the oxidative cleavage of an ether bond of the valoneoyl unit from the terminal glucose core, leading to a fragment ion due to the remaining HHDP (*o*-quinone) ester part(s). Quantitative analyses of individual oligomers in the extracts of flowers, leaves, and stems of *E. angustifolium* were successfully performed by ultra-high performance liquid chromatography coupled with tandem mass spectra (UHLC-MS/MS) [22,23]. This analytical method was reported to offer the advantages of good repeatability and sensitivity for an accurate quantification of this class of oligomers, with limits of detection ranging from 0.1 to 1.3 μg/mL.

13: R=OH
14: R=α-OG

16
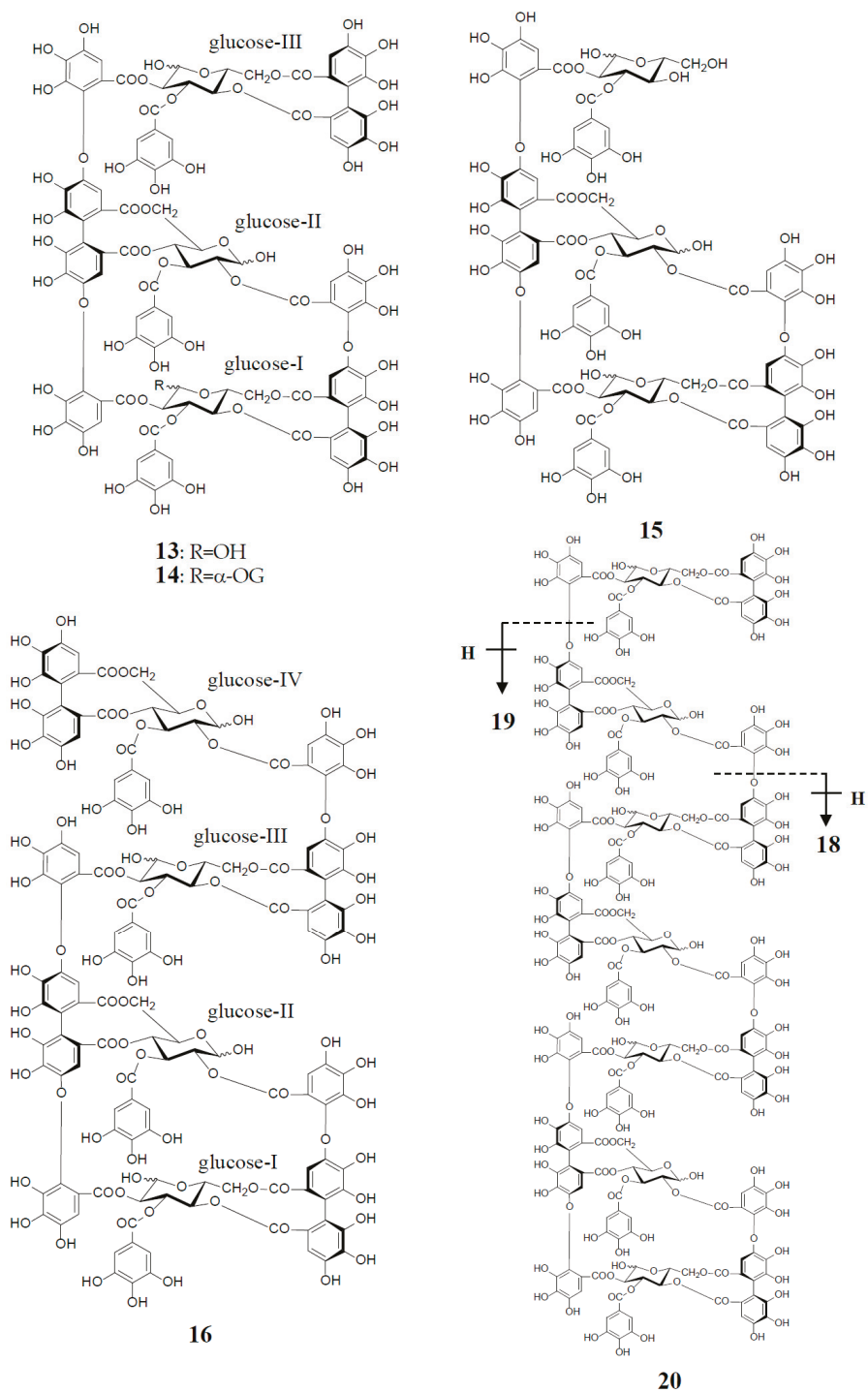
Figure 4. *Cont.*
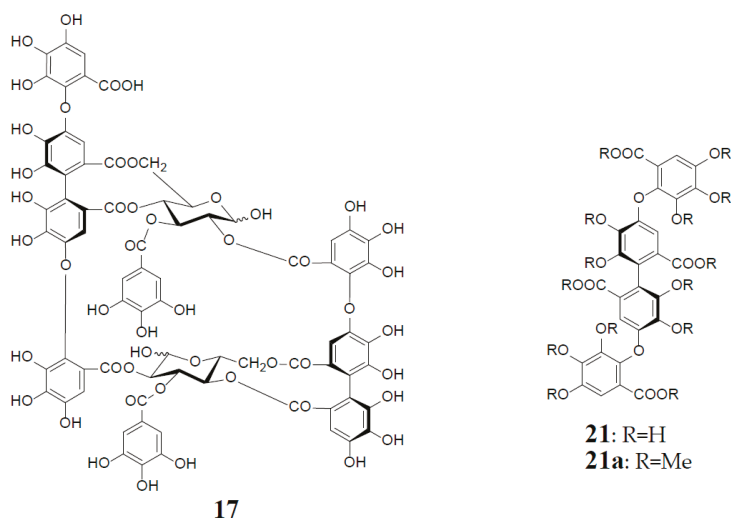
Figure 4. Structures of oenothein A (**13**), woodfordins D (**14**), E (**15**), and F (**16**), pentamer (**18**), hexamer (**19**), and heptamer (**20**), Structures of woodfordin I (**17**) and woodfordinic acid (**21**).

Woodfordinic acid (**21**), which is the parent acid participating in the linkage of three glucose cores (I–III) in oenothein A (**13**) and woodfordin D (**14**), was characterized as a gallic acid tetramer by spectral analyses (NMR, MS, and CD) of its methylated derivative (21a; $C_{42}H_{46}O_{20}$) obtained upon permethylation of 14 followed by methanolysis [21]. Its symmetrical structure was evidenced by 2 aromatic proton singlets and 7 methoxy proton signals, and 21 carbon signals comprising of 12 sp^2, 2 ester carbonyl and 7 sp^3 carbon signals in the ^{1}H- and ^{13}C-NMR spectra, respectively (Figure 4). Woodfordin I (**17**), a dimer possessing the woodfordinoyl group, is likely a catabolic metabolite of 13 and 14. Interestingly, woodfordin I was also isolated from a traditional Chinese medicine, *Chamaenerion* (= *Epilobium*) *angustifolium* [24].

Analogs eugeniflorin D_2 (**22**), and oenotherin T_1 (**23**) and T_2 (**24**), all containing an oxidized valoneoyl group, were found in *Eugenia uniflora* [15] and *O. tetraptera* [25,26], respectively. The structural confirmation of oenotherin T_1 (**23**) was conducted by the $Na_2S_2O_4$ reduction of the isodehydrovaloneoyl group affording oenothein A (**13**), similar to the conversion of a dehydrohexahydroxyl group to an HHDP group [3]. Notably, in contrast to many *Oenothera* species producing mainly oenothein A (**13**) and B (**4**), the most abundant constituent of *O. tetraptera* was oenotherin T_1. On the other hand, eugeniflorin D_2 (**22**), with a dehydrovaloneoyl group isomeric to that in oenotherin T_1 (**23**), was also found in the leaves of *Eucalyptus cypellocarpa* [27] and *Myrtus communis* of Myrtaceae [28]. Eurobustin C (**25**), isolated from *Eucalyptus robusta* [6], as well as oenotherin T_2 (**24**), had a new unique linking unit in place of the valoneoyl group, as shown in Figure 5.

In a study on the production of ellagitannins by callus cultures, Taniguchi et al. reported the establishment of callus tissues induced from the *Oenothera laciniata* leaves, which yielded large amounts of oenotheins A (**13**) and B (**4**), as well as oenotherin T_1 (**23**) [25,29]. It is noteworthy that oenothein B content (65 mg/g dry wt) in the calli cultured on modified Linsmaier–Skoog's medium was 1.8 times higher than that of intact leaves [29].
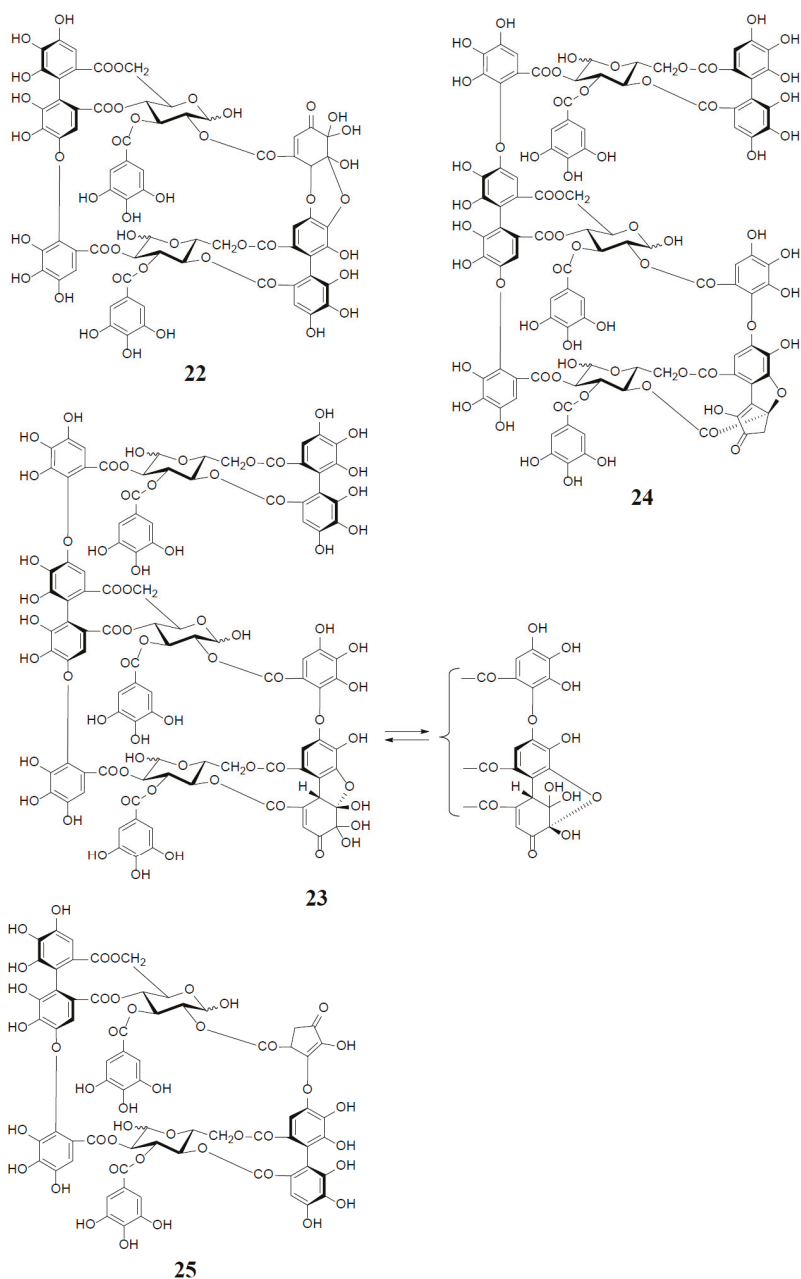
Figure 5. Structures of eugeniflorin D$_2$ (**22**), oenotherins T$_1$ (**23**), T$_2$ (**24**), and eurobustin C (**25**).

4. Distribution of Oenothein B and Its Analogs

As described earlier, oenotheins A (**13**) and B (**4**) have been isolated as main ingredients accompanying various analogs from the plant species of Onagraceae, Lythraceae, and Myrtaceae [5,10,11,20,30,31].

The distribution of oenothein B (**4**) in further species of these plant families was examined by HPLC to reveal its considerable wide occurrence, particularly in *Eucalyptus* species of Myrtaceae [30,32]. The oenothein B-containing plants reported so far are summarized in Table 1. Recently, the dried pericarps of *Punica granatum* belonging to Lythraceae (Punicaceae) were reported to produce oenothein B, along with new tellimagrandin I-based linear oligomers, pomegraniin A (tetramer) (**28**) and B (pentamer) (**29**), as well as eucalbanin B (dimer) (**26**) and eucarpanin T$_1$ (trimer) (**27**), which were first isolated from the leaves of *Eucalyptus alba* [33] and *E. cypellocarpa* [27] (Myrtaceae), respectively [34] (Figure 6). Although in the classical plant taxonomy Punicaceae belonged to its own family, it is currently included in the Lythraceae family in the phylogenetic system APG III [35]. It is chemotaxonomically interesting that the oligomeric ellagitannins of *P. granatum* showed close resemblance with those of the genera *Cuphea*, *Lythrus*, and *Woodfordia*, which are closely related genera in this family [36], although *P. granatum* is distinguished from the species of the other genera in the elongation mode of the monomers; that is, the presence of an oenothein B-based trimer (**13**) in the latter three, or absence in the former.

Table 1. Distribution of oenothein B and related macrocyclic oligomers in plants.

Family Species	Tannins	Ref.
Oenotheraceae		
Oenothera erythrosepala Bordas	oenothein B	[9]
O. biennis L.	oenotheins A, B	[20,37,38]
O. laciniata Hill.	oenotheins A, B, D, F, G	[12]
O. tetraptera Cav.	oenotheins A, B, oenotherins T$_1$, T$_2$	[25,26]
O. paradoxa Hudziok	oenothein B	[38]
Epilobium capense Buch.	oenotheins A, B	[10,11]
E. angustifolium L.	oenotheins A, B, woodfordin I, tetramer–heptamer	[10,11,22,24,39]
E. pyrricholophum Franch. et Sav.	oenotheins B	[39]
E. hirsutum L.	oenotheins B	[10,39]
E. palustre L.	oenotheins A, B	[39]
E. dodonoei Vill.	oenothein B (HPLC) *	[10]
E. stereophyllum Fres.	oenothein B (HPLC)	[10]
E. salignum Hausskn.	oenothein B (HPLC)	[10]
E. parviflorum Schreb.	oenothein B (HPLC)	[10]
E. roseum Schreb.	oenothein B (HPLC), (LC/MS) *	[10,11]
E. tetragonum L.	oenothein B (LC/MS)	[11]
E. montanum L.	oenothein B (HPLC), (LC/MS)	[10,11]
Lythraceae		
Lythrum anceps Makino	oenothein B	[31]
Woodfordia fruticosa Kurz.	oenotheins A, B, woodfordins C, D, E, F, I	[13,14,20,21]
Cuphea hyssopifolia Humb.	oenotheins A, B, woodfordin C, cuphiins D$_1$, D$_2$	[16]
Punica granatum L.	oenothein B	[34]
Myrtaceae		
Eugenia uniflora L.	oenothein B, eugeniflorins D$_1$, D$_2$	[15,40]
Melaleuca leucadendron L.	oenothein B	[5]
Myrtus communis L.	oenothein B, eugeniflorin D$_2$	[28]
Eucalyptus alba Reinw. Ex Blume	oenothein B	[33]
E. robusta Sm.	oenothein B, eugeniflorin D$_2$, eurobustin C	[27]
E. cypellocarpa LAS Johnson	oenothein B, eugeniflorin D$_2$	[27]
E. globulus Labill.	oenothein B	[30]
E. consideniana Maiden	oenothein B	[32]
E. viminalis Labill.	oenothein B	[32]
E. pulverulenta Sims.	oenothein B (HPLC) *	[30]
E. nicholii Box Hill. Merbourne	oenothein B (HPLC)	[30]
E. camaldulensis Dehnh.	oenothein B (HPLC)	[30]
Myrtus communis var. *microphylla* Willk.	oenothein B (HPLC)	[30]
Austromyrtus dulcis L.S. Sm.	oenothein B (HPLC)	[30]

* Method for identification, characterization, or detection.
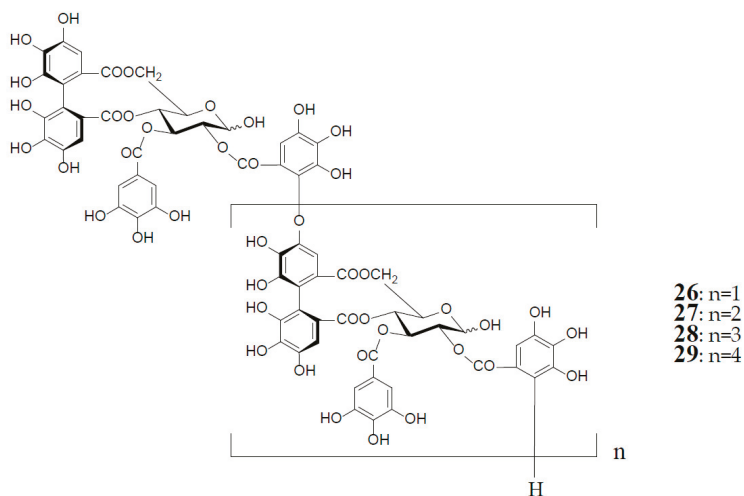
Figure 6. Structures of eucalbanin B (**26**), eucarpanin T_1 (**27**), pomegraniin A (tetramer) (**28**), and B (pentamer) (**29**).

5. Biological Activities of Oenothein B and Related Oligomers

Numerous medicinal plants rich in tannins have long been used worldwide as folk medicines or traditional medicines for various purposes, represented by antidiarrheic, hemostatic, and the treatment of gastrointestinal disorders, wound healing, and skin stress [4,7]. The active components of these plant extracts responsible for such therapeutic effects were ascribed to the tannins (large molecular polyphenols), which were long recognized to have non-specific binding ability with proteins (astringency), inducing a peristaltic action. However, the remarkable progress in the structural characterization of ellagitannin constituents in those medicinal plants since the 1980s has enabled studies on various pharmacological activities of individual tannin constituents with defined structures. As a result, diverse biological effects, such as antioxidant, antimicrobial, antitumor, antiulcer, and anti-inflammatory effects, have been found by various in vitro and in vivo studies [4,6,7] and citations therein [41]. The efficacies of such biological activities have been reported to be largely dependent on the difference of types or structures of tannins and related polyphenols, and on their concentrations. Advance in the structural study of ellagitannins also has enabled investigation of the interaction between structure-defined ellagitannins and certain proteins, amino acids, or metals. These studies revealed that tannin–protein complex formations are not due to nonspecific binding with proteins, as previously thought, but largely dependent on the structure and concentration of tannins and targeted proteins. Recently, the importance of molecular size and structural flexibility of ellagitannins in the interaction with bovine serum albumin was emphasized, based on the thermodynamic study of the interaction using isothermal titration calorimetry and fluorescence spectroscopy [42].

As oenothein B (**4**) constitutes a unique class of ellagitannins in its macrocyclic structure with limited flexibility of rotational bond, and also in its high content in many medicinal *Oenothera*, *Epilobium*, and *Eucalyptus* species, its biological activities have been widely studied [5–7,39,43]. Among such pharmacological effects, hitherto documented for oenothein B and its analogs, this review summarizes selected papers, reporting (1) antioxidant and anti-inflammation activity; (2) antitumor activity; (3) immunomodulatory effects; and (4) antimicrobial effects, including our recent findings.

5.1. Antioxidant and Anti-Inflammation Activity

The active oxygen damage or formation of reactive oxygen species (ROS), caused by an imbalance in the body's antioxidant system, has been related with the pathogenesis of various human diseases, such as cancer and cardiovascular diseases, and inflammation [44]. Antioxidant activity is the most basic biological property of polyphenols, ranging from flavonoids and lignans of small molecules to tannins of higher molecular weight [4,7,45]. Okuda's early in vitro studies on the antioxidant effects of polyphenols estimated by (1) 1,1-diphenyl-2-picrylhydrazyl (DPPH) radical scavenging test, (2) Cu(II)-catalyzed autoxidation of ascorbic acid, and (3) lipid peroxidation in rat liver mitochondria and microsomes, demonstrated that the antioxidative potencies of ellagitannins, including oligomers, were generally higher than those of small molecular polyphenols, as well as α-tocopherol and ascorbic acid [46].

These properties are ascribable to the potent radical scavenging ability of ellagitannins, which can terminate free radical chain reaction of other compounds, e.g., lipid peroxidation, by their self-oxidation, thus preventing the oxidation of lipids, proteins, or DNA. A stable radical of an ellagitannin, geraniin (**1**), generated upon air oxidation in an alkaline DMSO solution, was substantiated by the observation of its free radical signals with modulation width 0.05 G in the ESR spectrum [47]. The reactivity of a phenolic radical generated upon donating a phenolic hydrogen radical to another free radical (ROS) was indicated by the treatment of an alkyl gallate with DPPH radical, which produced a dialkyl ester of hexahydroxydiphenic acid by mutual coupling of transient *C*-centered galloyl radicals [48] (Figure 7). This radical coupling reaction is reminiscent of the ellagitannin biosynthesis by laccase-like enzymes, as described earlier.

R=CH₃, CH₃CH₂, CH₃CH₂CH₂, or
CH₃CH₂CH₂CH₂
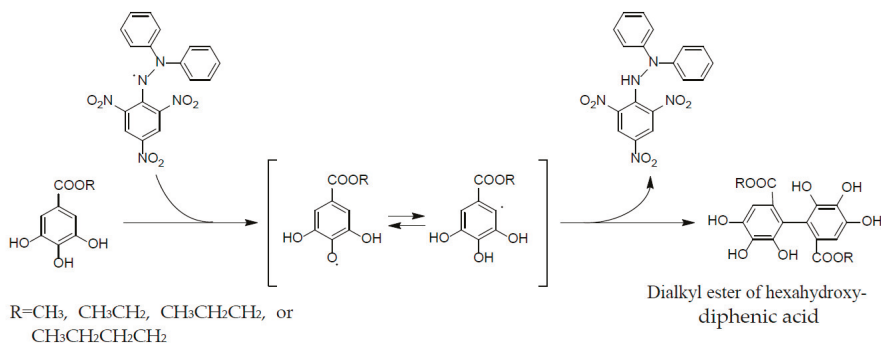
Figure 7. Formation of dialkylester of hexahydroxydiphenic acid in radical reaction of alkyl gallate with DPPH.

The biological antioxidant efficacies of representative condensed tannins, hydrolysable tannins, and related simple phenolics, such as catechin, methyl gallate, and pyrogallol, were also evaluated by cyclic voltammetry. In these studies, the redox potentials of all polyphenols at pH 6-8 were reported to be substantially below 1000 mV, thus implicating that they act as reducing agents (radical scavengers) for the peroxyl (E^-1000 mV) and hydroxyl (E^-2300 mV) radicals [49].

Although these redox potentials of the tannins were similar to those of simple polyphenols, tannins were 15–30 times more effective at quenching peroxyl radicals than simple phenolics or Trolox (6-hydroxy-2,5,7,8-tetramethyl-chroman-2-carboxylic acid) in a metmyoglobin assay [50]. This result suggests a significance of high molecular weight and the proximity of many aromatic rings and hydroxyl groups for the free radical scavenging ability.

Antioxidant and anti-inflammatory effects of oenothein B-rich *Epilobium* and *Oenothera* species against oxygen stress have been studied, in order to justify their traditional usages as herbal supplements or tea [11,37,38,51]. *Epilobium* species (willowherbs) have long been used to improve

urogenital functions (prostate, bladder, and hormone troubles) in European folk medicine. The extracts of the three most popular *Epilobium* species (*E. angustifolium*, *E. hirsutum*, and *E. parviflorum*), which contained oenothein B (**4**) in high quantities (20–35%), exhibited inhibitory effects on lipoxygenase and hyaluronidase, with IC_{50} around 25 μg/mL and 5 μg/mL, respectively. Additionally, the radical scavenging properties of these extracts were demonstrated by the significant reduction of ROS generated from *N*-formyl-methionyl-leucyl-phenylalanine (f-MLP) and phorbol myristate acetate (PMA)-induced neutrophils, with IC_{50} 5 μg/mL and 25 μg/mL, respectively. A plausible active constituent responsible for these activities was considered as the predominant oenothein B. In fact, oenothein B (**4**) inhibited myeloperoxidase (MPO) release from stimulated neutrophils with IC_{50} 7.7 μM, similarly to the anti-inflammatory drug indomethacin (IC_{50} 15.4 μM), and hyaluronidase with IC_{50} 1.1 μM [39,51]. Similarly, Kiss et al. reported that extracts of *Oenothera paradoxa* and *O. biennis* exhibited anti-inflammatory activity by inhibiting hyaluronidase and lipoxygenase in a concentration-dependent manner, and an inhibitory effect against ROS production from human neutrophils [37,38]. The antioxidant property of extracts from the most common *Epilobium* species, all of which were shown to be rich in oenothein B (**4**) as estimated by LC/MS, were measured by a simple spectrophotometric method using 2,2′-azinobis-(3-ethylbenzthiazoline-6-sulfonic acid) (ABTS), and the extract of *E. parviflorum* was shown to have the highest radical-scavenger activity among these extracts, and comparable to that of well-known antioxidants, Trolox and ascorbic acid [11].

5.2. Antitumor Effect

5.2.1. Cytotoxicity against Tumor Cell Lines

Tumor cell growth is regulated in the balance between proliferation and apoptosis. There is considerable amount of evidence indicating that ellagitannins reduce the growth of cancer cells by inhibiting cell proliferation and inducing apoptotic cell death.

In in vitro studies of macrocyclic ellagitannins performed with cancer cell lines, oenothein B (**4**), woodfordin C (**5**), and cuphiins D_1 (**8**) and D_2 (**7**) significantly inhibited the growth of the human oral epidermoid (KB), cervical (HeLa), prostate carcinoma (DU-145), and hepatocellular (Hep-3B) carcinoma cell lines, and the promyelocytic leukemia (HL-60) cell lines, and showed less cytotoxicity than adriamycin against a normal cell line (WISH) [52]. The mechanism for the cyctotoxicity of cuphiins D_1 (**8**) was examined using HeLa cell lines, and was suggested to be due to induction of apoptosis by inhibition of Bcl-2 expression [53]. Moreover, oenothein B, woodfordin C (**5**) and D (**14**) showed higher cytotoxic activity against human oral squamous cell carcinoma and salivary gland tumor cell lines than against normal human gingival fibroblasts. These cytotoxicities were also indicative of induction of apoptotic cell death as characterized by DNA fragmentation and cleavage of cytokeratin 18 by activated caspase(s) [27,54]. Woodfordin I (**17**) suppressed the proliferation and induced apoptosis in human chronic myelogenous leukemia K 562 cells, which was mediated through the intrinsic mitochondria-dependent pathway [24].

5.2.2. Antitumor Effect Caused by Tumor-Related Enzyme Inhibition

Activity-guided fractionation of the bioactive components of *Epilobium capense* led to the isolation and identification of oenotheins A (**13**) and B (**4**) as potent inhibitors of 5α-reductase and aromatase, enzymes involved in the etiology of benign prostatic hyperplasia. Potencies of the inhibitory effects against 5α-reductase were IC_{50} 1.24 μM for oenothein A (**13**) and IC_{50} 0.44 μM for oenothein B (**4**), respectively, although they were substantially weaker than the positive control finasteride, with IC_{50} 5 nM. On the other hand, against aromatase, oenotheins A (**13**) and B (**4**) displayed 70% and 33% inhibition at 50 μM, respectively, higher and comparable with the synthetic reference compound aminoglutethimide (37% inhibition at 50 μM) [10]. Similarly, oenothein B (**4**) from *E. angustifolium* was found to be specifically able to induce neutral endopeptidase in prostate cancer PC-3 cells, which inactivates growth stimulatory neuropeptides [55]. This enzyme is also known to be involved

in prostate cancer progression. Thus, these results might offer a pharmacological explanation for the use (improvement of prostate diseases) of *Epilobium* extract as a folk medicine. As the bioavailability of oenothein B (**4**) still remains unsolved, Kiss et al. further investigated the consistency between the in vitro and in vivo effects of *E. angustifolium* (EA) aqueous extract, using LNCaP human prostate carcinoma cells (in vitro) and rats intraperitonially implanted with LNCaP cells (in vivo) [56]. EA extract (20, 50, 70 μg/mL) and oenothein B (**4**) (2, 5, 10 μM) showed a significant reduction of proliferation of LNCaP cells in dose-dependent manner without affecting the normal human skin fibroblast cells, which was correlated with the induction of apoptosis. These effects were indicated to be comparable to reference compound camptothecin. Similar reduction of the prostatic adenoma up to 13% was observed upon oral administration of EA extract (50–200 mg/kg) to rats implanted with LNCaP cells, suggesting significant and consistent effects in the in vitro and in vivo assays. In order to characterize active metabolites of EA extract (oenothein B) produced by intestinal bacteria, the urinary metabolites obtained from rat and human volunteers supplemented with EA extract were investigated by an application of UHPLC-DAD-MS/MS analysis of ellagitannin metabolites, such as urolithins [57]. Although any bioactive metabolites of oenothein B remained uncharacterized, oenothein B metabolism was suggested to be obviously different from those of other ellagaitannins [56].

In a screen conducted to find inhibitors of DNA topoisomerase-II (topo-II), woodfordin C (**5**) isolated from the leaves of *Woodfordia fruticosa* [14] was shown to inhibit topo-II dose dependently [58]. This in vitro potency was much stronger than those of the clinically used drugs, adriamycin (ADR) and etoposide (ETP). This compound inhibited DNA synthesis, rather than RNA and protein synthesis, in a similar way to ETP. Upon evaluation against cultured human tumor cell lines, woodfordin C (**5**) showed remarkable antitumor activity (IC_{50} 0.07 μg/mL) against PC-1 (lung carcinoma) cells, and moderate activity against MKN 45 (stomach cancer) (IC_{50} 1.73 μg/mL) and KB cells (IC_{50} 5.58 μg/mL), in comparison with ADR and ETP (IC_{50} 0.12–0.67 μg/mL). Also, in vivo antitumor activity of woodfordin C (**5**) against colon 38 (mouse colon adenocarcinoma), subcutaneously inoculated to the flank of a BDF_1 mouse was shown by 55% inhibition of tumor growth, 16 days after i.v. administration of **5** with 1.5 mg/kg/day (once daily for 5 consecutive days). This result suggested that antitumor mechanism may be through the inhibition of topo-II [58]. It is noted in the literature that **5** may not be taken directly into tumor cells, because of its large molecular mass and a high anionic charge, thus, further studies on bioavailability of **5**, as well as **4**, are still needed.

Epstein–Barr virus (EBV) is a human B lymphotropic herpes virus known to be closely associated with nasopharyngeal carcinoma (NPC). Inhibitory activity against EBV-DNA polymerase, which is a key enzyme during EBV replication, was estimated for the macrocyclic dimers, eugeniflorin D_2 (**22**) and oenothein B (**4**), isolated from *Eugenia uniflora*, and the former (**22**) exhibited a remarkable inhibition with IC_{50} 3.5 μM, while the latter (**4**) showed weaker activity with IC_{50} 62.3 μM in comparison with a positive control, phosphonoacetic acid (EBV replication inhibitor) (IC_{50} 16.4 μM) [40].

On the other hand, degradation of poly(ADP-ribose) on specific chromosomal proteins in eukaryotic cells, mainly by poly(ADP-ribose) glycohydrolase, is considered to be an important factor in the regulation of gene activation, DNA replication and transcription, and cell death [59]. In a search for potent and specific inhibitors of poly(ADP-ribose) glycohydrolase purified from human placenta, oligomeric ellagitannins were found to be more potent inhibitors (IC_{50} 0.3–7.1 μM) than condensed tannins and monomeric hydrolysable tannins (IC_{50} 15.5–31.8 μM), and also than the previously known inhibitors, daunomycin and ethadridine (IC_{50} 50–100 μM), and cAMP (IC_{50} 5–10 mM) [60]. The most potent inhibitory activity was exhibited by nobotanin K (a tetramer from *Tibouchina semidecandra*; Melastomataceae [61]) and oenothein B (**4**), with IC_{50} 0.3 and 1.8 μM, respectively, on a molar concentration basis. It is notable that the condensed tannins (epicatechin gallate dimer to tetramer) and flavan-3-ols tested were not active even at 100 mM. As depoly(ADP-ribosyl)ation of chromosomal proteins was suggested to be involved in the initiation of glucocorticoid-sensitive mouse mammary tumor virus (MMTV) transcription, the inhibitory effect of oenothein B (**4**) on MMTV gene expression in intact 34I cells, derived from C3H mouse mammary carcinoma, was examined.

As a result, pretreatment with oenothein B (**4**) potently suppressed, dose-dependently in a range of 1–50 μM, the induction of MMTV mRNA by dexamethasone (100 nM). It is noteworthy that oenothein B showed no inhibitory effect against other poly(ADP-ribose) metabolizing enzymes tested, such as poly(ADP-ribose) polymerase and NAD$^+$ glycohydrolase, even at 0.5 mM, thus indicating that oenothein B is specific for poly(ADP-ribose) glycohydrolase [62]. Although poly(ADP-ribosyl)ation has been suggested to be involved in regulation of DNA repair, transcription, centrosome duplication, and chromosome stability, the regulation of the degradation of poly(ADP-ribose) and its significance remain less understood [59,63,64]. Therefore, oenothein B (**4**) may not only be a promising therapeutic candidate, but also one of the useful chemicals in pharmacological experiments for elucidation of the physiological role of poly(ADP-ribose).

5.2.3. Host Mediated Antitumor Activity

Detailed investigations on the host-mediated antitumor effect of ellagitannins and other related polyphenols were reported by Miyamoto and Okuda's group [65–67]. Oenothein B (**4**) exhibited remarkable host-mediated antitumor activity upon intraperitoneal (ip) injection several days before or after inoculation of sarcoma-180 (S-180) tumor cells into the abdomen of mice [65]. The evaluation of the activity was evaluated by the number of survivors (in six mice/group), and the percent increase in life span (%ILS) 60 days after administration. Treatment with a 10 mg/kg dose of oenothein B (**4**) four days before inoculation of S-180 resulted in four survivors out of six mice, and 196 %ILS, demonstrating that oenothein B was the most potent among the approximately 100 polyphenols tested, including condensed tannins and ellagitannins (monomers-tetramers), as well as related small molecular polyphenols, such as caffeic acid derivatives and gallotannins. Oenothein A (**13**) and woodfordin D (**14**) showed 102.7 and 123.0 %ILS, respectively, and each with one survivor. Oenothein B also exhibited anticancer activity against murine mammary carcinoma MM2 in C3H/He mice by i.p. administration at 10 mg/kg dosage, at one, four, and seven days after the cancer inoculation. The effect evaluated after 60 days showed high %ILS (126.8%), and four survivors out of six mice [63]. This effect was stronger than that of OK-432, a streptococcal preparation with a potent immunostimulatory activity [68]. in vivo treatment with these antitumor-active dimers induced cytotoxic adherent peritoneal exudate cells, including stimulated macrophages producing and secreting interleukin (IL)-1β [65,67,69]. Cuphiin D$_1$ (**8**) was also shown to stimulate human peripheral blood mononuclear cells (PBMCs) and release, dose-dependently, IL-1β, IL-2, and TNF-α, and then activate T cells. Therefore, cuphiins D$_1$-activated T cells via IL-1β, in vitro, might account for the host-mediated mechanism of 8. Thus, the antitumor effect of these tannins was attributed to the enhancing of the immune response of the host, and not due to their direct cytotoxic action on tumor cells [70].

5.3. Immunomodulatory Effect

In order to understand the mechanisms underlying diverse biological activities of macrocyclic ellagitannins, such as anti-inflammatory, antitumor, and antimicrobial effects, the immunomodulatory effects of oenothein B (**4**) have been investigated in various in vitro or in vivo immune systems.

Oenothein B (**4**) was reported [71] to activate a number of phagocyte functions in an in vitro evaluation using neutrophils and monocytes purified from healthy human blood, resulting in the induction of intracellular Ca^{2+} flux, production of ROS, NF-kB activation, and proinflammatory cytokine production. On the other hand, intraperitoneal administration of **4** to female BALB/c mice induced significant levels of keratinocyte, which directly correlated with the neutrophil influx into the peritoneum. However, the oenothein B-related small molecular weight polyphenols, gallic acid, pyrogallol, pyrocatechol, and 3,4-dihydroxybenzoic acid, were all inactive, suggesting the necessity of the whole structure of **4** for the modulation of the phagocyte functions, both in vitro and in vivo [71]. Oenothein B (**4**) was also shown to reduce, dose-dependently, nitric oxide (NO) production, inducible nitric oxide synthase (iNOS) mRNA, and iNOS protein levels, without inhibiting the iNOS enzymatic activity in lipopolysaccharide (LPS)-stimulated murine RAW 264.7 macrophage

cells [72,73]. The IC_{50} value of **4** for inhibition of inducible NO production was 17.7 μM, while gallic acid, a component unit of **4**, showed much weaker activity, with IC_{50} 631.6 μM, implying the requirement of the entire structure of **4** for this effect, in agreement with the above results [71]. The inhibition of inducible NO synthesis by **4** in a dose-dependent manner was also observed in Toll-like receptor (TLR)-stimulated RAW 264.7 cells, which were stimulated using TLR4 and TLR2 agonists. Such an inhibitory effect by **4** was shown to be NF kB-dependent, but independent from the interferon (IFN)-γ/JAK-STAT pathway [72]. As inappropriate or excessive NO production by iNOS is closely associated with numerous inflammatory diseases and neuropathic pain states, oenothein B (**4**) might be a promising lead for the development of therapeutic agents as the effective inhibitors of NO production. Ramstead et al. reported that oenothein B (**4**) stimulated innate lymphocytes, including bovine and human γδ T cells and NK cells, resulting in either increased CD25 and/or CD69 expression. Oenothein B thus enhanced the production of IFNγ by bovine and human NK cells, and also by human T cells. These responses were not observed with other commonly studied polyphenols. Since IFNγ is known to contribute to antitumor, antibacterial, and antiviral cell responses, these data suggested an additional mechanism for the immune-enhancing properties of oenothein B [74]. Innate immune cell responsiveness is known to be affected by aging. Then, the responsiveness of oenothein B (**4**) in T cells from individuals over a broad range of ages (cord blood, young, and adult donors) was estimated by measuring IFNγ production, and clear differences depending on the ages were observed, that is, oenothein B (**4**) induced IFNγ production in T cells from adult humans and cattle, but not in T cells from human cord blood and bovine calves [75].

Recently Yoshimura et al. [76] reported the significant immunomodulatory effects of oenothein B (**4**) on human dendritic cells (DCs), which are widely present in various tissues in contact with the external environment, such as the skin, nose, lungs, stomach, and intestines, and have critical functions in the initial immune response as antigen presenting cells. Oenothein B (**4**) had significant immunoregulatory effects on DCs through suppression of cell surface molecules, downregulation of cytokine production, and induction of their apoptosis. When oenothein B (**4**) (25 μM or 100 μM) was added to the cultured immature DCs (iDCs) supplemented with TNF-α (75 ng/mL) and LPS (100 ng/mL), the expression of cell surface molecules, CD1a and CD83, was shown to be suppressed significantly at 100 μM of **4**, resulting in the dysfunction of DC-mediated immune responses by the inhibition of cell maturation and subsequent antigen presentation. The suppressive effect on DCs was shown to be due to the induction of apoptosis by a flow cytometric assay. However, in the apoptosis induced by **4**, none of caspase-3/7, 8, and 9, which play crucial roles in cell apoptosis, was activated, suggesting a caspase-independent mechanism for this apoptosis. Morphological change of tannin-treated DCs was confirmed by fluorescence microscopy, showing significant nuclear condensation without DNA fragmentation, similar to that of AIF (apoptosis-inducing factor)/PARP [poly (ADP-ribose) polymerase]-dependent cell death [77]. Oenothein B also markedly suppressed the production of inflammatory cytokines, such as IL-1β and IL-6, in a dose-dependent manner at 25 mM and 100 mM. Plant tannins, including condensed tannins, are generally considered to be stable in acidic conditions [78], and thus could travel unmodified, or form complexes with some inner biomacromolecules, such as proteins and dietary fiber, through the pharyngeal tube and stomach, until metabolized in the small intestine. These effects on DCs may thus be significant in the traditional usages of oenothein B- or related ellagitannin-containing medicinal plants for the treatment of a variety of inflammatory diseases.

Apart from inflammatory effects in peripheral tissues, in vivo effects of oenothein B (**4**) on the damage to the central nervous system due to systemic inflammation was reported by Okuyama et al. [79]. Peripherally injected LPS is reported to induce a depressive-like abnormal behavior through induction of microglial immune responses in the brain of mice [80]. In an open-field test using mice treated with LPS (i.p.) (1 mg/kg mouse), orally administered (p.o.) oenothein B (300 mg/kg) showed significant increase of the locomotive activity at 24 h after LPS treatment, compared with that of the control group with depressive-like behavior. Immunohistochemical and

biochemical investigation of oenothein B-administered mice indicated suppression of LPS-induced microglial activation and LPS-induced cyclooxygenase-2 production in the hippocampus and striatum of these mice. These results suggested that oenothein B has the ability to reduce neuroinflammation in the brain during systemic inflammation. Since oenothein B itself might hardly pass through the blood–brain barrier (BBB), some metabolites of 4 produced by intestinal microflora [57,81,82] were considered to likely affect the peripheral inflammation, which was followed by the suppression of the inflammatory responses in the brain, although the possibility that these metabolites can pass through BBB and act directly in the brain as anti-inflammation agents was not excluded.

5.4. Antimicrobial Effects

Antimicrobial effects of ellagitannins, including antibacterial, antivirus, and antiprotozoal activities, have been documented in many papers and reviews, including those by Okuda, Haslam, and Kolodziej [4,6,46,83,84]. Among them, a notable activity was the synergistic effects of certain polyphenols with currently used antibiotics against drug-resistant bacteria. Many pathogenic bacteria, such as methicillin-resistant *Staphylococcus aureus* (MRSA), have acquired resistance to various clinical antibiotics. This worldwide problem is likely driving the development of new antibiotic drugs in an endless stream. Synergistic effects of ellagitannins, including oenothein B (**4**) and tellimagrandin I (**2**), with β-lactam antibiotics (e.g., oxacillin), were found to restore the effectiveness of these antibiotics against MRSA. When used together with these tannins, the MICs of oxacillin against MRSA strains were markedly lowered to 1/250 or 1/500 [85]. These results may provide one strategy for overcoming emergent bacterial resistance.

6. Conclusions

Since the discovery in 1990 of oenothein B (**4**) and woodfordin C (**5**), a unique class of dimeric ellagitannins with macrocyclic structures, many analogous ellagitannins (oenotheins, woodfordins, cuphiins, eugeniflorins, and oenotherins), including oxidized oligomers up to heptamer with molecular weight 5488, have been isolated from various medicinal plants belonging to Onagraceae, Lythraceae, and Myrtaceae. Their novel structures were elucidated by spectroscopic analyses (ESIMS, 1D and 2D NMR, CD) and chemical degradation. Oenothein B is commonly the most abundant constituent in plants containing this class of macrocyclic ellagitannins.

Oenothein B (**4**) and its analogs were documented to possess diverse in vitro and in vivo pharmacological properties, including antioxidants, antitumor, immunomodulatory, and antimicrobial effects, and their potencies were, in general, much higher than those of the related polyphenols with small molecular weight, suggesting the necessity of the entire structure of tannins for exhibiting activities. Hence, this type of oligomer may provide promising leads for the development of novel therapeutics and chemopreventive agents. An often-claimed problem is that high molecular weight tannins (polyphenols) have a limited bioavailability in biological systems due to their low solubility, stability, and membrane permeability. Therefore, biological activities of tannins and related polyphenols found in in vitro and in vivo assays have to be interpreted with caution, as noted in many papers or reviews, for the necessity of further studies. Increased interest for the fate of ellagitannins in the gastrointestinal tract has thus prompted investigations on the bioavailability or actual metabolites of ellagitannins in detail [55–57,81,82,86], and these aspects were reviewed by Tomas-Barberan et al. [87] and Torronen [88]. On the other hand, an oral delivery device, which encapsulates oenothein B or other ellagitannins, was reported for their enhanced protection through the gastrointestinal tract [89]. Further studies on these matters, including different manners of intestinal metabolism from those of non-macrocyclic ellagitannins, are strongly encouraged, for a better understanding and effective usage of these bioactive macrocyclic ellagitannins.

Author Contributions: T.Y., M.Y. and Y.A. contributed equally to this work and T.Y. finalized the manuscript.

References

1. Haslam, E. The metabolism of gallic and hexahydroxydiphenic acid in higher plant. *Fortschr. Chem. Org. Naturstoffe* **1982**, *41*, 1–46.
2. Okuda, T.; Yoshida, T.; Hatano, T. Geraniin, a new ellagitannin from *Geranium thunbergii*. *Tetrahedron Lett.* **1976**, *17*, 3721–3724. [CrossRef]
3. Okuda, T.; Yoshida, T.; Hatano, T. Constituents of *Geranium thunbergii* Sieb. et Zucc. Part 12. Hydrated stereostructure and equilibration of geraniin. *J. Chem. Soc. Perkin Trans. 1* **1982**, 9–14. [CrossRef]
4. Okuda, T.; Yoshida, T.; Hatano, T. Hydrolyzable tannins and related polyphenols. *Prog. Chem. Organ. Nat. Prod.* **1995**, *66*, 1–117.
5. Yoshida, T.; Amakura, Y.; Yoshimura, M. Structural Features and Biological Properties of Ellagitannins in the Myrtales. *Int. J. Mol. Sci.* **2010**, *11*, 79–106. [CrossRef] [PubMed]
6. Yoshida, T.; Hatano, T.; Ito, H.; Okuda, T. Highly Oxidized Ellagitannins and Their Biological Activity. In *Plant Polyphenols 2*; Gross, G.G., Hemingway, R.W., Yoshida., T., Eds.; Kluwer/Plenum: New York, NY, USA, 1999; pp. 127–144.
7. Okuda, T.; Yoshida, T.; Hatano, T.; Ito, H. Ellagitannins Renewed the Concept of Tannins. In *Chemistry and Biology of Ellagitannins*; Quideau, S., Ed.; World Scientific: Hackensack, NJ, USA, 2009; pp. 1–54.
8. Okuda, T.; Yoshida, T.; Kuwahara, M.; Memon, M.; Shingu, T. Agrimoniin and potentillin, ellagitannin dimer and monomer having α-glucose cores. *J. Chem. Commun.* **1982**, 163–164. [CrossRef]
9. Hatano, T.; Yasuhara, T.; Matsuda, M.; Yazaki, K.; Yoshida, T.; Okuda, T. Oenothein B, a Dimeric, hydrolysable tannin with macrocyclic structure, and accompanying tannins from *Oenothera erythrosepala*. *J. Chem. Soc. Perkin Trans. 1* **1990**, 2735–2743. [CrossRef]
10. Ducrey, B.; Marston, A.; Göhring, S.; Hartmann, R.W.; Hostettmann, K. Inhibition of 5α-reductase and aromatase by the ellagitannins oenothein A and oenothein B from *Epilobium species*. *Planta Med.* **1997**, *63*, 111–114. [CrossRef] [PubMed]
11. Tóth, B.H.; Blazics, B.; Kéry, A. Polyphenol composition and antioxidant capacity of *Epilobium* species. *J. Pharm. Biomed. Anal.* **2009**, *49*, 26–31. [CrossRef] [PubMed]
12. Yoshida, T.; Chou, T.; Shingu, T.; Okuda, T. Oenotheins D, F and G, Hydrolysable Tannin Dimers from *Oenothera laciniata*. *Phytochemistry* **1995**, *40*, 555–561. [CrossRef]
13. Yoshida, T.; Chou, T.; Nitta, A.; Miyamoto, K.; Koshiura, R.; Okuda, T. Woodfordin C, a macro-ring hydrolyzable tannin dimer with antitumor activity, and accompanying dimers from *Woodfordia fruticosa* flowers. *Chem. Pharm. Bull.* **1990**, *38*, 1211–1217. [CrossRef] [PubMed]
14. Kadota, S.; Takamori, Y.; Nyein, K.N.; Kikuchi, T.; Tanaka, K.; Ekimoto, H. Constituents of the leaves of *Woodfordia fruticosa* Kurz. I. Isolation, structure, and proton and carbon-13 nuclear magnetic resonance signal assignments of woodfruticosin (woodfordin C), an inhibitor of deoxyribonucleic acid topoisomerase II. *Chem. Pharm. Bull.* **1990**, *38*, 2687–2697. [CrossRef] [PubMed]
15. Lee, M.; Nishimoto, S.; Yang, L.L.; Yen, K.Y.; Hatano, T.; Yoshida, T.; Okuda, T. Two macrocyclic hydrolysable tannin dimers from *Eugenia uniflora*. *Phytochemistry* **1997**, *44*, 1343–1349.
16. Chen, L.G.; Yen, K.Y.; Yang, L.L.; Hatano, T.; Okuda, T.; Yoshida, T. Macrocyclic ellagitannin dimers, cuphiins D$_1$ and D$_2$, and accompanying tannins from *Cuphea hyssopifolia*. *Phytochemistry* **1999**, *50*, 307–312. [CrossRef]
17. Haddock, E.A.; Gupta, R.K.; Al-Shafi, S.M.K.; Layden, K.; Haslam, E.; Magnolato, D. The Metabolism of gallic acid and hexahydroxydiphenic acid in plants; biogenetic and molecular taxonomic considerations. *Phytochemistry* **1982**, *21*, 1049–1062. [CrossRef]
18. Niemetz, R.; Schilling, G.; Gross, G.G. Ellagitannin Biosynthesis: Oxidation of pentagalloylglucose to tellimagrandin II by an emzyme from *Tellima grandiflora* leaves. *Chem. Commun.* **2001**, *1*, 35–36. [CrossRef]
19. Niemetz, R.; Schilling, G.; Gross, G.G. Biosynthesis of dimeric ellagitannin, cornusiin E, in *Tellima grandiflora*. *Phytochemistry* **2003**, *64*, 109–114. [CrossRef]
20. Yoshida, T.; Chou, T.; Matsuda, M.; Yasuhara, T.; Yazaki, K.; Hatano, T.; Nitta, A.; Okuda, T. Woodfordin D and oenothein A, trimeric hydrolyzable tannins of macro-ring structure with antitumor activity. *Chem. Pharm. Bull.* **1991**, *39*, 1157–1162. [CrossRef] [PubMed]
21. Yoshida, T.; Chou, T.; Nitta, A.; Okuda, T. Tannins and related polyphenols of lythraceous plants. III. Hydrolyzable tannin oligomers with macrocyclic structure and accompanying tannins from *Woodfordia fruticosa* KURTZ. *Chem. Pharm. Bull.* **1992**, *40*, 2023–2030. [CrossRef]

22. Baert, N.; Karonen, M.; Salminen, J.P. Isolation, characterization and quantification of the main oligomeric macrocyclic ellagitannins in *Epilobium angustifolium* by ultra-high performance chromatography with diode array detection and electrospray tandem mass spectrometry. *J. Chromatogr. A* **2015**, *1419*, 26–36. [CrossRef] [PubMed]

23. Baert, N.; Kim, J.; Karonen, M.; Salminen, J.P. Inter-population and inter-organ distribution of the main polyphenolic compounds of *Epilobium angustifolium*. *Phytochemistry* **2017**, *134*, 54–63. [CrossRef] [PubMed]

24. Liu, M.J.; Wang, Z.; Li, H.X.; Wu, R.C.; Liu, Y.Z.; Wu, Q.Y. Mitochondrial dysfunction as an early event in the process of apoptosis induced by woodfordin I in human leukemia K562 cells. *Toxicol. Appl. Pharmacol.* **2004**, *194*, 141–155. [CrossRef] [PubMed]

25. Taniguchi, S.; Imayoshi, Y.; Yabu-uchi, R.; Ito, H.; Hatano, T.; Yoshida, T. A macrocyclic ellagitannin trimer, oenotherin T$_1$, from *Oenothera* species. *Phytochemistry* **2002**, *59*, 191–195. [CrossRef]

26. Taniguchi, S.; Imayoshi, Y.; Yoshida, T.; Hatano, T. A new trimeric hydrolysable tannin, oenotherin T$_2$, isolated from aerial parts of *Oenothera tetraptera* Cav. *Heterocyles* **2009**, *79*, 617–626.

27. Yoshida, T.; Hatano, T.; Ito, H. Chemistry and function of vegetable polyphenols with high molecular weights. *BioFactors* **2000**, *13*, 121–125. [CrossRef] [PubMed]

28. Yoshimura, M.; Amakura, Y.; Tokuhara, M.; Yoshida, T. Polyphenolic compounds isolated from the leaves of *Myrtus communis*. *J. Nat. Med.* **2008**, *62*, 366–368. [CrossRef] [PubMed]

29. Taniguchi, S.; Nakamura, N.; Nose, M.; Takeda, S.; Yabu-uchi, R.; Ito, H.; Yoshida, T.; Yazaki, K. Production of macrocyclic ellagitannin oligomers by *Oenothera laciniata* callus cultures. *Phytochemistry* **1998**, *48*, 981–985. [CrossRef]

30. Amakura, Y.; Yoshimura, M.; Sugimoto, N.; Yamazaki, T.; Yoshida, T. Marker constituents of the natural antioxidant *Eucalyptus* leaf extract for the evaluation of food additives. *Biosci. Biotechnol. Biochem.* **2009**, *73*, 1060–1065. [CrossRef] [PubMed]

31. Okuda, T.; Yoshida, T.; Hatano, T.; Yazaki, K.; Kira, R.; Ikeda, Y. Chromatography of tannins II: Preparative fractionation of hydrolyzable tannins by centrifugal partition chromatography. *J. Chromatogr. A* **1986**, *362*, 375–381. [CrossRef]

32. Santos, S.C.; Waterman, P.G. Polyphenols from *Eucalyptus consideniana* and *Eucalyptus viminalis*. *Fitoterapia* **2001**, *72*, 95–97. [CrossRef]

33. Yoshida, T.; Maruyama, T.; Nitta, A.; Okuda, T. Eucalbanins A, B and C, monomeric and dimeric hydrolyzable tannins from *Eucalyptus alba* REINW. *Chem. Pharm. Bull.* **1992**, *40*, 1750–1754. [CrossRef]

34. Ito, H.; Li, P.; Koreishi, M.; Nagatomo, A.; Nishida, N.; Yoshida, T. Ellagitannin oligomers and a neolignan from pomegranate arils and their inhibitory effects on the formation of advanced glycation end products. *Food Chem.* **2014**, *152*, 323–330. [CrossRef] [PubMed]

35. The Angiosperm Phylogeny Group. An update of the Angiosperm Phylogeny Group classification for the orders and families of flowering plants. APG III. *Bot. J. Linn. Soc.* **2009**, *161*, 105–121.

36. Graham, S.A.; Hall, J.; Sytsma, K.; Shi, S. Phylogenetic analysis of the Lythraceae based on four gene regions and morphology. *Int. J. Plant Sci.* **2005**, *166*, 995–1017. [CrossRef]

37. Granica, S.; Czerwińska, M.E.; Piwowarski, J.P.; Ziaja, M.; Kiss, A.K. Chemical composition, antioxidative and anti-inflammatory activity of extracts prepared from aerial parts of *Oenothera biennis* L. and *Oenothera paradoxa* Hudziok obtained after seeds cultivation. *J. Agric. Food Chem.* **2013**, *30*, 801–810. [CrossRef] [PubMed]

38. Kiss, A.K.; Kapłon-Cieślicka, A.; Filipiak, K.J.; Opolski, G.; Naruszewicz, M. Ex vivo effects of an *Oenothera paradoxa* extract on the reactive oxygen species generation and neutral endopeptidase activity in neutrophils from patients after acute myocardial infarction. *Phytother. Res.* **2012**, *26*, 482–487. [CrossRef] [PubMed]

39. Granica, S.; Piwowarski, J.P.; Czerwińska, E.M.; Kiss, A.K. Phytochemistry, pharmacology and traditional uses of different *Epilobium* species (Onagraceae): A review. *J. Ethnopharmacol.* **2014**, *156*, 316–346. [CrossRef] [PubMed]

40. Lee, M.H.; Chiou, J.F.; Yen, K.Y.; Yang, L.L. EBV DNA polymerase inhibition of 4 tannins from *Eugenia uniflora*. *Cancer Lett.* **2000**, *54*, 131–136. [CrossRef]

41. Yoshida, T.; Hatano, T.; Ito, H.; Okuda, T. Structural diversity and antimicrobial activities of ellagitannins. In *Chemistry and Biology of Ellagitannins*; Quideau, S., Ed.; World Scientific: Hackensack, NJ, USA, 2009; pp. 55–93.

42. Dobreva, M.A.; Green, R.J.; Muller-Harvey, I.; Salminen, J.P.; Howlin, B.J.; Frazier, R.A. Size and molecular flexibility affect the binding of ellagitannins to bovine serum albumin. *J. Agric. Food Chem.* **2014**, *62*, 9186–9194. [CrossRef] [PubMed]

43. Schepetkin, I.A.; Ramstead, A.G.; Kirpotina, L.N.; Voyich, J.M.; Jutila, M.A.; Quinn, M.T. Therapeutic potential of polyphenols from *Epilobium angustifolium* (Fireweed). *Phytother. Res.* **2016**, *30*, 1287–1297. [CrossRef] [PubMed]

44. Jassen, Y.M.V.; Van Houten, B.; Borm, P.J.A.; Mossman, B.T. Cell and tissue responses to oxidative damage. *Lab. Investig.* **1993**, *69*, 261–274.

45. Haslam, E. Natural polyphenols (vegetable tannins) as drugs: possible models of action. *J. Nat. Prod.* **1996**, *59*, 205–215. [CrossRef] [PubMed]

46. Okuda, T.; Yoshida, T.; Hatano, T. Pharmacologically active tannins isolated from medicinal plants. In *Plant Polyphenols*; Hemingway, R.W., Lacks, P.E., Eds.; Plenum Press: New York, NY, USA, 1992; pp. 530–569.

47. Fujita, Y.; Komagoe, K.; Sasaki, Y.; Uehara, I.; Okuda, T.; Yoshida, T. Inhibition mechanism of tannins on Cu(II)-catalyzed autoxidation of ascorbic acid. *Yakugaku Zasshi* **1987**, *107*, 17–22. [CrossRef]

48. Yoshida, T.; Mori, K.; Hatano, T.; Okumura, T.; Uehara, I.; Komagoe, K.; Fujita, Y.; Okuda, T. Radical-scavenging effects of tannins and related polyphenols on 1,1-diphenyl-2-picrylhydrazyl radical. *Chem. Pharm. Bull.* **1989**, *37*, 1919–1921. [CrossRef]

49. Hagerman, A.E.; Riedl, K.M.; Rice, R.E. Tannins as biological antioxidants. In *Plant Polyphenols 2*; Gross, G.G., Hemingway, R.W., Yoshida, T., Eds.; Kluwer Academic/Plenum Publishers: New York, NY, USA, 1999; pp. 495–505.

50. Hagerman, A.E.; Riedl, K.M.; Jones, G.A.; .Sovik, K.N.; Ritchard, N.T.; Hartzfeld, P.W.; Riechel, T.L. High molecular weight plant polyphenolics (Tannins) as biological antioxidants. *J. Agric. Food Chem.* **1998**, *46*, 1887–1892. [CrossRef] [PubMed]

51. Kiss, A.K.; Bazylko, A.; Filipek, A.; Granica, S.; Jaszewska, E.; Kiarszys, U.; Kośmider, A.; Piwowarski, J.P. Oenothein B's contribution to the anti-inflammatory and antioxidant activity of *Epilobium* sp. *Phytomedicine* **2011**, *18*, 557–560. [CrossRef] [PubMed]

52. Wang, C.C.; Chen, L.G.; Yang, L.L. Antitumor activity of four macrocyclic ellagitannins from *Cuphea hyssopifolia*. *Cancer Lett.* **1999**, *140*, 195–200. [CrossRef]

53. Wang, C.C.; Chen, L.G.; Yang, L.L. Cytotoxic effects of cuphiin D$_1$ on the growth of human cervical carcinoma and normal cells. *Anticancer Res.* **2002**, *22*, 2677–2684. [PubMed]

54. Sakagami, H.; Jiang, Y.; Kusama, K.; Atsumi, T.; Ueha, T.; Toguchi, M.; Iwakura, I.; Satoh, K.; Ito, H.; Hatano, T.; et al. Cytotoxic activity of hydrolyzable tannins against human oral tumor cell lines—A possible mechanism. *Phytomedicine* **2000**, *7*, 39–47. [CrossRef]

55. Kiss, A.; Kowalski, J.; Melzig, M.F. Induction of neutral endopeptidase activity in PC-3 cell by aqueous extract of *Epilobium angustifolium* and Oenothein B. *Phytomedicine* **2006**, *13*, 284–289. [CrossRef] [PubMed]

56. Piwowarski, J.P.; Bobrowska-Korczak, B.; Stanislawska, I.; Bielecki, W.; Wrzesien, R.; Granica, S.; Krupa, K.; Kiss, A.N. Evaluation of the effect of *Eepilobium angustifolium* aqueous extract on LNCap cell proliferation in in vitro and in vivo medels. *Planta Med.* **2017**, *83*, 1159–1168. [PubMed]

57. Piwowarski, J.P.; Granica, S.; Stefarska, J.; Kiss, A.K. Differences in metabolism of ellagitannins by human gut microbiota ex vivo cultures. *J. Nat. Prod.* **2016**, *79*, 3022–3030. [CrossRef] [PubMed]

58. Kuramochi-Motegi, A.; Kuramochi, H.; Kobayashi, F.; Ekimoto, H.; Takahashi, K.; Kadota, S.; Takamori, Y.; Kikuchi, T. Woodfruticosin (woodfordin C), a new inhibitor of DNA topoisomerase II. Experimental antitumor activity. *Biochem. Pharmacol.* **1992**, *44*, 1961–1965. [PubMed]

59. Tanuma, S.; Johnson, L.D.; Johnson, G.S. ADP-ribosylation of chromosomal proteins and mouse mammary tumor virus gene expression. *J. Biol. Chem.* **1983**, *258*, 15371–15375. [PubMed]

60. Aoki, K.; Nishimura, K.; Abe, H.; Maruta, H.; Sakagame, H.; Hatano, T.; Okuda, T.; Yoshida, T.; Tsai, Y.J.; Uchiumi, F.; et al. A novel inhibitors of poly(ADP-ribose) glycohydrolase. *Biochim. Biophys. Acta* **1993**, *1158*, 251–256. [CrossRef]

61. Yoshida, T.; Haba, K.; Arata, R.; Nakata, F.; Shingu, T.; Okuda, T. Tannins and related polyphenols of Melastomataceous plants. VII. Nobotanins J and K, trimeric and tetrameric hydrolyzable tanins from *Heterocentron roseum*. *Chem. Pharm. Bull.* **1995**, *43*, 1101–1106. [CrossRef]

62. Aoki, K.; Maruta, H.; Uchiumi, F.; Hatano, T.; Yoshida, T.; Tanuma, S. A macrocircular ellagitannin, oenothein B, suppresses mouse mammary tumor gene expressionvia inhibition of poly(ADP-ribose) glycohydrolase. *Biochim. Biophys. Res. Commun.* **1995**, *210*, 329–337. [CrossRef] [PubMed]

63. Hanai, S.; Kanai, M.; Ohashi, S.; Okamoto, K.; Yamada, M.; Takahashi, H.; Miwa, M. Loss of poly(ADP-ribose) glycohydrolase causes progressive neurodegeneration in Drosophila melanogaster. *Proc. Natl. Acad. Sci. USA* **2004**, *101*, 82–86. [CrossRef] [PubMed]

64. Feng, X.; Koh, D.W. Roles of poly(ADP-ribose) glycohydrolase in DNA damage and apoptosis. *Int. Rev. Cell Mol. Biol.* **2013**, *304*, 227–281. [PubMed]

65. Miyamoto, K.; Kishi, N.; Koshiura, R.; Yoshida, T.; Hatano, T.; Okuda, T. Relationship between the structures and the antitumor activities of tannins. *Chem. Pharm. Bull.* **1987**, *35*, 814–822. [CrossRef] [PubMed]

66. Miyamoto, K.; Nomura, M.; Sasakura, M.; Matsui, E.; Koshiura, R.; Murayama, T.; Furukawa, T.; Hatano, T.; Yoshida, T.; Okuda, T. Antitumor activity of oenothein B, a unique macrocyclic ellagitannin. *Jpn. J. Cancer Res.* **1993**, *84*, 99–103. [CrossRef] [PubMed]

67. Murayama, T.; Kishi, N.; Koshiura, R.; Takagi, K.; Furukawa, T.; Miyamoto, K. Agrimoniin, an antitumor tannin of *Agrimonia pilosa* Ledeb., induces interleukin-1. *Anticancer Res.* **1992**, *12*, 1471–1474. [PubMed]

68. Murayama, T.; Natsuume-Sakai, S.; Ryoyama, K.; Koshiura, S. Studies on the properties of a streptococcal preparation, OK-432 (NSC-B116209), as an immunopotentiator. II. Mechanism of macrophage activation by OK-432. *Cancer Immunol. Immunother.* **1982**, *12*, 141–146. [CrossRef]

69. Miyamoto, K.; Murayama, T.; Nomura, M.; Hatano, T.; Yoshida, T.; Furukawa, T.; Koshiura, R.; Okuda, T. Antitumor activity and interleukin-1 induction by tannins. *Anticancer Res.* **1993**, *13*, 37–42. [PubMed]

70. Wang, C.C.; Chen, L.G.; Yang, L.L. in vitro immunomodulatory effects of cuphiin D_1 on human mononuclear cells. *Anticancer Res.* **2002**, *22*, 4233–42336. [PubMed]

71. Schepetkin, I.A.; Kirpotina, L.N.; Jarissa, L.; Khlebnikov, A.I.; Blaskovich, C.L.; Jutila, M.A.; Quinn, M.T. Immunomodulatory activity of oenothein B isolated from *Epilobium angustifolium*. *J. Immun.* **2009**, *183*, 6754–6766. [CrossRef] [PubMed]

72. Schmid, D.; Gruber, M.; Piskaty, C.; Woehs, F.; Renner, A.; Nagy, Z.; Kaltenboeck, A.; Wasserscheid, T.; Bazylko, A.; Kiss, A.K. Inhibition of NF-κB-dependent cytokine and inducible nitric oxide synthesis by the macrocyclic ellagtannin oenothein B in TLR-stimulated RAW 264.7 macrophages. *J. Nat. Prod.* **2012**, *75*, 870–875. [CrossRef] [PubMed]

73. Chen, Y.; Yang, L.L.; Lee, T.J. Oroxylin A inhibition of lipopolysaccharide-induced iNOS and COX-2 gene expression via suppression of nuclear factor-kappaB activation. *Biochem. Pharmacol.* **2000**, *59*, 1445–1457. [CrossRef]

74. Ramstead, A.G.; Schepetkin, I.A.; Quinn, M.T.; Jutila, M.A. Oenothein B, a cyclic dimeric ellagitannin isolated from *Epilobium angustifolium*, enhances IFNγ production by lymphocytes. *PLoS ONE* **2012**, *7*, e50546. [CrossRef] [PubMed]

75. Ramstead, A.G.; Schepetkin, I.A.; Todd, K.; Loeffelholz, J.; Berardinelli, J.G.; Quinn, M.T.; Jutila, M.A. Aging influences the response of T cells to stimulation by the ellagitannin, oenothein B. *Int. Immunopharmacol.* **2015**, *26*, 367–377. [CrossRef] [PubMed]

76. Yoshimura, M.; Akiyama, H.; Kondo, K.; Sakata, K.; Matsuoka, H.; Amakura, Y.; Teshima, R.; Yoshida, T. Immunological effects of oenothein B, an ellagitannin dimer, on dendritic cells. *Int. J. Mol. Sci.* **2013**, *14*, 46–56. [CrossRef] [PubMed]

77. Yu, S.W.; Wang, H.; Poitras, M.F.; Coombs, C.; Bowers, W.J.; Federoff, H.J.; Poirier, G.G.; Dawson, T.M.; Dawson, V.L. Mediation of poly(ADP-ribose) polymerase-1-dependent cell death by apoptosis-inducing factor. *Science* **2002**, *297*, 259–263. [CrossRef] [PubMed]

78. Rios, L.Y.; Bennett, R.N.; Lazarus, S.A.; Rémésy, C.; Scalbert, A.; Williamson, G. Cocoa procyanidins are stable during gastric transit in humans. *Am. J. Clin. Nutr.* **2002**, *76*, 1106–1110. [CrossRef] [PubMed]

79. Okuyama, S.; Makihata, N.; Yoshimura, M.; Amakura, Y.; Yoshida, T.; Nakajima, M.; Furukawa, Y. Oenothein B suppresses lipopolysaccharide (LPS)-induced inflammation in the mouse brain. *Int. J. Mol. Sci.* **2013**, *14*, 9767–9778. [CrossRef] [PubMed]

80. O'Connor, J.C.; Lawson, M.A.; André, C.; Moreau, M.; Lestage, J.; Castanon, N.; Kelley, K.W.; Dantzer, R. Lipopolysaccharide-induced depressive-like behavior is mediated by indoleamine 2,3-dioxygenase activation in mice. *Mol. Psychiatry* **2009**, *14*, 511–522. [CrossRef] [PubMed]

81. Ito, H.; Iguchi, A.; Hatano, T. Identification of urinary and intestinal bacterial metabolites of ellagitannin geraniin in rats. *J. Agric. Food Chem.* **2008**, *56*, 393–400. [CrossRef] [PubMed]

82. Giménez-Bastida, J.A.; Larrosa, M.; González-Sarrías, A.; Tomás-Barberán, F.; Espín, J.C.; García-Conesa, M.T. Intestinal ellagitannin metabolites ameliorate cytokine-induced inflammation and associated molecular markers in human colon fibroblasts. *J. Agric. Food Chem.* **2012**, *60*, 8866–8876. [CrossRef] [PubMed]

83. Kolodziej, H.; Kayser, O.; Latte, K.P.; Kiderlen, A.F. Enhancement of antimicrobial activity of tannins and related compounds by immune modulatory effects. In *Plant Polyphenols 2*; Gross, G.G., Hemingway, R.W., Yoshida, T., Eds.; Kluwer Academic/Plenum Publishers: New York, NY, USA, 1999; pp. 575–594.

84. Kolodziej, H.; Kayser, O.; Latte, K.P.; Kiderlen, A.F.; Ito, H.; Hatano, T.; Yoshida, T.; Foo, L.Y. Antileishmnial activity of hydrolysable tannins and their modulatory effects on nitric oxide and tumor necrosis factor-a release in macrophages in vitro. *Planta Med.* **2001**, *67*, 825–832. [CrossRef] [PubMed]

85. Hatano, T.; Tsugawa, M.; Ohyabu, T.; Kusuda, M.; Shiota, S.; Tsuchiya, T.; Yoshida, T. Effects of polyphenols in tea and foods on methicillin-resistant *Staphylococcus aureus* and the sustainability of the antibacterial effects in the presence of food additives. *Assoc. J. Jpn. Soc. Med. Use Funct. Foods* **2006**, *4*, 43–48.

86. Ishimoto, H.; Shibata, M.; Myojin, Y.; Ito, H.; Sugimoto, Y.; Tai, A.; Hatano, T. in vivo anti-inflammatory and antioxidant properties of ellagitannin metabolite urolithin A. *Bioorg. Med. Chem. Lett.* **2011**, *21*, 5901–5904. [CrossRef] [PubMed]

87. Tomas-Barberan, F.A.; Espin, J.C.; Garcia-Conesa, M.T. Bioavailability and metabolism of ellagic acid and ellagitannins. In *Chemisty and Biology of Ellagitannins*; Quideau, S., Ed.; World Scientific: Hackensack, NJ, USA, 2009; pp. 273–297.

88. Torronen, R. Sources and health effects of dietry ellagitannins. In *Chemisty and Biology of Ellagitannins*; Quideau, S., Ed.; World Scientific: Hackensack, NJ, USA, 2009; pp. 298–319.

89. Lan, Y.; Wang, L.; Cao, S.; Zhong, Y.; Li, Y.; Cao, Y.; Zhao, L. Rational design of food-grade polyelectrolyte complex coacervate for encapsulation and enhanced oral delivery of oenothein B. *Food Funct.* **2017**, *8*, 4070–4080. [CrossRef] [PubMed]

MDPI

Review

Structural Revisions in Natural Ellagitannins

Hidetoshi Yamada [1],*, Shinnosuke Wakamori [1], Tsukasa Hirokane [2], Kazutada Ikeuchi [3] and Shintaro Matsumoto [1]

[1]   School of Science and Technology, Kwansei Gakuin University, Sanda 669-1337, Japan;
      shinnosuke1010@kwansei.ac.jp (S.W.); ean89778@kwansei.ac.jp (S.M.)
[2]   Faculty of Pharmaceutical Sciences, Tokushima Bunri University, Tokushima 770-8514, Japan;
      hiro-tks@ph.bunri-u.ac.jp
[3]   Department of Chemistry, Faculty of Science, Hokkaido University, Sapporo 060-0810, Japan;
      ikeuchi@sci.hokudai.ac.jp
*   Correspondence: hidetosh@kwansei.ac.jp; Tel.: +81-795-65-8342

check for
updates

Abstract: Ellagitannins are literally a class of tannins. Triggered by the oxidation of the phenolic parts on β-pentagalloyl-D-glucose, ellagitannins are generated through various structural conversions, such as the coupling of the phenolic parts, oxidation to highly complex structures, and the formation of dimer and lager analogs, which expand the structural diversity. To date, more than 1000 natural ellagitannins have been identified. Since these phenolic compounds exhibit a variety of biological activities, ellagitannins have potential applications in medicine and health enhancement. Within the context of identifying suitable applications, considerations need to be based on correct structural features. This review describes the structural revisions of 32 natural ellagitannins, namely alnusiin; alnusnin A and B; castalagin; castalin; casuarinin; cercidinin A and B; chebulagic acid; chebulinic acid; corilagin; geraniin; isoterchebin; nobotanin B, C, E, G, H, I, J, and K; punicalagin; punicalin; punigluconin; roxbin B; sanguiin H-2, H-3, and H-6; stachyurin; terchebin; vescalagin; and vescalin. The major focus is on the outline of the initial structural determination, on the processes to find the errors in the structure, and on the methods for the revision of the structure.

Keywords: ellagitannin; structure; revision

1. Introduction

Tannins are astringent polyphenolic compounds with high diversity in biological activities [1–3]. Many of the compounds have antioxidative effects and affect various organisms, such as fungi, tumor cells, and viruses. Originally, the term tannin meant a compound that could be used for the tanning of animal hides. Today, tannins are divided into multiple classes according to the source and the chemical structures; however, they are roughly classified into two categories: condensed and hydrolyzable tannins [4,5]. Of the two, ellagitannins belong to the hydrolyzable tannins.

Ellagitannins arise through biosynthetic pathways that allow for the production of diversity. In the early stage of the biosynthesis, the galloyl groups of the β-pentagalloyl glucose (**1**) couple oxidatively to produce the hexahydroxydiphenoyl (HHDP) group (Figure 1) [6–10]. Two of the five galloyl groups of **1** can couple and, in addition, the occurrence of *R* or *S* axial chirality on the HHDP group may be possible. Therefore, the number of combinations is 20 ($_5C_2 \times 2$). After the occurrence of the first HHDP group, the production of the second HHDP group as cuspinin ((a*R*,a*S*)-**2**) and the cleavage of the ester bonds of the HHDP and the rest of the galloyl groups as corilagin ((a*R*)-**3**) may expand the variation. The oxidative coupling continues further to construct the trimer and tetramer of the galloyl group, which are called the nonahydroxytriphenoyl (NHTP) (alias: flavogallonyl) and gallagyl groups, respectively [11,12]. In addition, the galloyl and HHDP groups can connect

oxidatively through a C–O bond, which produces sanguisorboyl, tergalloyl, valoneoyl, and other groups [13]. Production of the C–O connected components often involves the generation of dimeric and larger ellagitannins to drastically increase the diversity. The HHDP group can be further oxidized to form the dehydrohexahydroxydiphenoyl (DHHDP), chebuloyl, and other groups, which brings the structures beyond the patterned restriction. Further, ellagitannins can join to the components outside of ellagitannins, such as acutissimin A and hirsunin, to illustrate illimitable possibilities in structure [14,15].
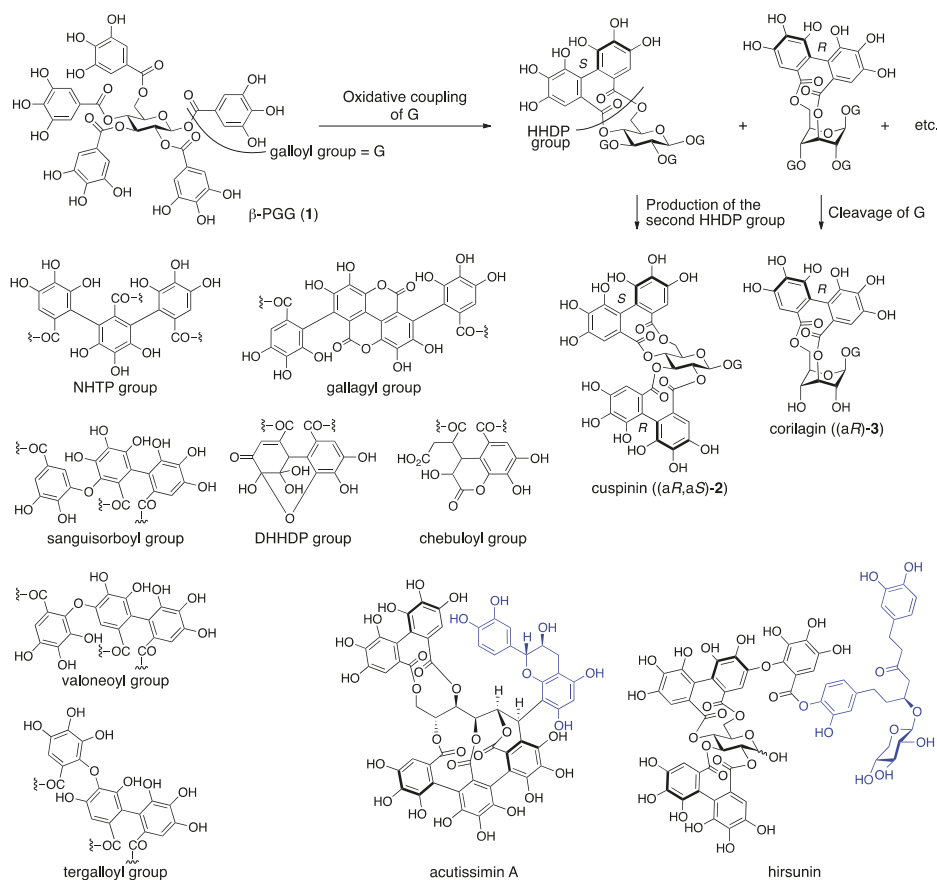
Figure 1. The oxidative intramolecular coupling of the galloyl groups and the structures of components of ellagitannin, acutissimin A, and hirsunin.

The structural diversity expands in the direction that makes the structures become more complex. Today, structures of complicated ellagitannins can be elucidated. However, during their development, studies for structural determinations had tackled the most difficult subjects at the time. Therefore, situations in which it was difficult to narrow down the options or which led to incorrect structures could not be avoided. The reported structures have been exposed to verification by history, including the development of analytical methods and confirmation by chemical synthesis, and some of them were revised. In the meantime, the reported structures were diffused by a secondary medium, such as books, reviews, and websites. Although the structures were revised afterward, most of the exhibited information remains as it was, which causes confusion and misunderstanding.

Hence, reviewing structural revisions is worthwhile as Amagata and McPhail have done already in an independent publication [16,17]. However, there has been no review article featuring structural revisions of ellagitannins, which is the topic of this article.

2. Notice

In this review article, the following contrivance is used in order to improve intelligibility. For the revised compounds, all of the previously reported structures are exhibited inside a square frame with angular corners (for example, Figure 2). In the frame, the words "*1st*", "*2nd*", "*3rd*", and "*latest*" indicate the transition of the structure. As a guide, the reported year and the representative of the report are appended in a parenthesis. Arrows with "revision" also show the transition. The flame appears first in each description for revised ellagitannins, which might help in understanding the overall transition. Regarding the initial structural determination, the processes to find the errors in the structure, and the methods for the revision of the structure, glancing at figures might not be enough to understand; so, reading the text while referring to the figures is recommended. Degraded compounds that arose in the processes of the structural determination are also illustrated similarly in square frames with angular corners (for example, Figure 10). Frames with round corners are used to indicate the simplified expression of frequent components (for example, Figure 8) and to separate adjacent figures clarifying different contents (for example, Figure 10). We refer to more than 100 original papers in this review article. Except for References [18,19], every outcome was published by several authors. However, when we refer to authors in the review, we restricted ourselves to a delegate to avoid the repeating phrase "and co-workers", of course, with respect for all of the co-workers.

3. Structural Revision in Ellagitannins

3.1. Correction of the Bonding Positions of the Galloyl and HHDP Groups and Correction of the Axial Chirality of the HHDP Group

3.1.1. Corilagin

Corilagin was first isolated from dividivi (*Caesalpinia coriaria*) by Schmidt in 1951 [20]. Three years later, the first structure (**3**) was determined (Figure 2), where the axial chirality of the HHDP group remained unknown [21]. In the second structure, the axial chirality was revealed as *S* by Djerassi on the basis of an empirical rule named the amide rule [22]. After that, Okuda revised the axial chirality to be *R* with undeniable facts [23].
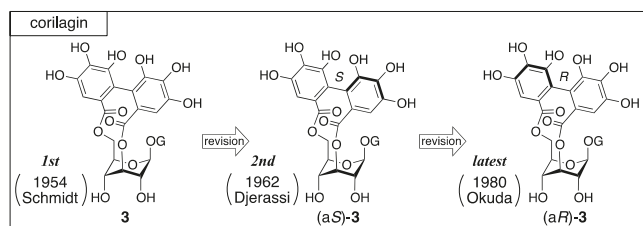
Figure 2. The transition of the structure of corilagin.

The first structure **3** was determined by methylation/degradation and comparison of the fragments with known analogs [21]. The treatment of corilagin with diazomethane provided nonamethylcorilagin, the hydrolysis of which released D-glucose, tri-*O*-methylgallic acid (**4**), and hexamethoxydiphenic acid (**5a**) (Figure 3a) [24]. Therefore, corilagin is an esterified glucose with galloyl and HHDP groups. On the other hand, the methylation of nonamethylcorilagin with MeI/Ag$_2$O yielded undecamethylcorilagin, the methanolysis of which produced a mixture of an

anomeric isomer that arose by the release of the galloyl moiety. The subsequent transformation of the hemiacetal to the corresponding methyl acetal followed by the hydrolysis of the remaining HHDP group furnished 1,2,4-tri-*O*-methylglucose (**6**) [25,26]. These results were evidence for the structure **3** that possessed the HHDP group bridging between the O-3 and O-6 of glucose and the galloyl group at O-1. The β-stereochemistry came from the behavior of a specific optical rotation. Thus, according to the knowledge that the anomeric isomerization of levorotatory β-**7** provides dextrorotatory α-**7** (Figure 3b) [27], levorotatory undecaacetylcorilagin provided an anomeric mixture of undecaacetylcorilagin after a similar isomerization whose specific optical rotation in gross was dextrorotatory. Later on, Schmidt confirmed the structure **3** using a ^{1}H-NMR spectrum [28].
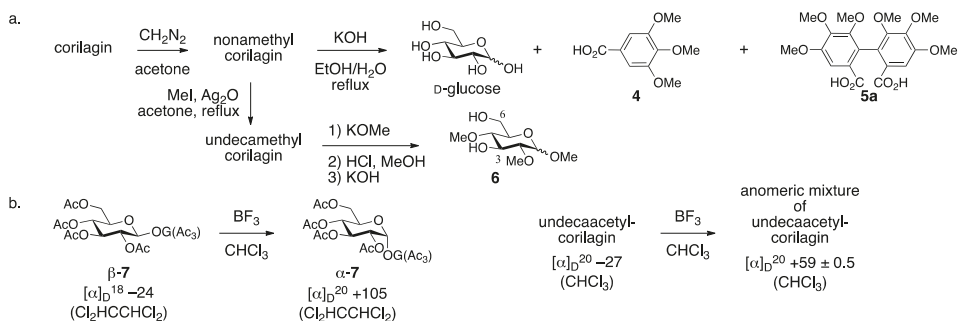
Figure 3. (**a**) The successive methylation and degradation of corilagin and (**b**) the basis for β-stereochemistry at the anomeric position.

The axial chirality in (a*S*)-**3** was attributed to an empirical rule for the prediction of axial chirality employing optical rotatory dispersion (ORD) spectra [22]. The grounds for the rule are the behavior of the ORD values of the amides **8c** and **9c**, which are smaller than those of the respective carboxylic acids **8a** and **9a** and methyl esters **8b** and **9b** (Figure 4). Djerassi compared the ORD values of the dicarboxylic acid derivative of the HHDP group **5a**, the methyl ester **5b**, and the amide **5c** to find that the value of **5c** was obviously smaller than those of **5a** and **5b**; here, **5b** and **5c** were derived from the carboxylic acid (+)-**5a** [29]. According to the observation, the axial chirality of the HHDP group was determined to be *S* [22].

Okuda corrected the axial chirality of corilagin to give the latest structure (a*R*)-**3** in a reliable manner. They confirmed that both of the specific optical rotations were dextrorotatory between the two dimethyl esters **5b** derived from nonamethylcorilagin and from the schizandrin (**10**) bearing the definite *R*-axial chirality; hence, the axial chirality in corilagin was *R* (Figure 5) [23]. After that, Okuda and Seikel independently clarified that the conformation of the glucopyranose core was in [1]C$_4$ by ^{1}H-NMR analyses [30,31]. In addition, corilagin was obtained as a hydrolysate of geraniin (Section 3.2.1) [32], the structure of which was elucidated by an X-ray diffraction study of the singe crystal [33]. Afterward, Yamada synthesized (a*R*)-**3** [34].

R	O$_2$N NO$_2$ *S* R R **8** [M]$_D$ (°)	Me Me *S* R R **9** [M]$_D$ (°)	MeO MeO OMe OMe MeO OMe * R R **5** [M]$_D$ (°)
CO$_2$H (**a**)	−422	+70	+116
CO$_2$Me (**b**)	−346	+128	+167
CONH$_2$ (**c**)	−958	0	−432

Figure 4. The data used for the determination of the *S*-axial chirality in the second structure of corilagin.
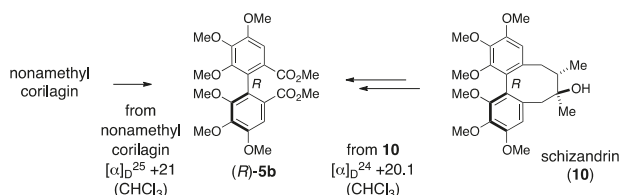
Figure 5. The determination of the *R*-axial chirality in the latest structure of corilagin.

3.1.2. Punigluconin

Punigluconin was isolated from *Punica granatum* L. by Nishioka [35]. For the first structure, **11** that possessed the galloyl groups on O-2 and O-3 of gluconic acid was reported (Figure 6). After that, the structure was revised to the 2,5-di-*O*-galloylated **12**, which is the latest structure [36].
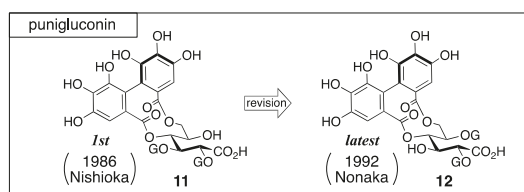
Figure 6. The transition of the structure of punigluconin.

The structure **11** was determined on the basis of an NMR study and chemical transformations [35]. ^{1}H-NMR indicated that punigluconin possessed two galloyl groups and one HHDP group. ^{13}C-NMR exhibited the existence of an aldonic acid. The treatment of punigluconin with diluted sulfuric acid produced gluconic acid (Figure 7); hence, the aldonic acid was gluconic acid. On the other hand, the full methylation of punigluconin followed by methanolysis provided methyl tri-*O*-methylgallate (**13**) and the dimethyl ester (*S*)-**5b** [37] derived from the (*S*)-HHDP group. The ^{1}H-NMR spectrum of the tannase-hydrolysate of punigluconin showed a high-field shift of H-2 and H-3. No remarkable change in the chemical shifts was observed on H-4 and H-6. Thus, the hydrolysate was **14**.
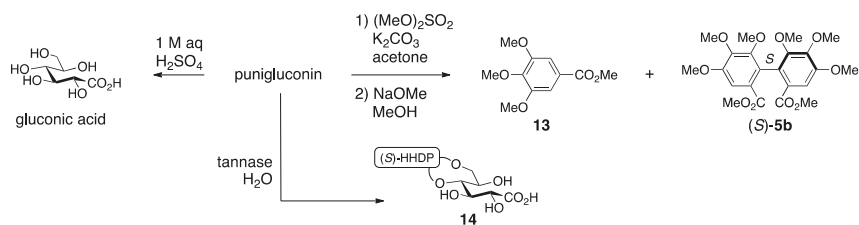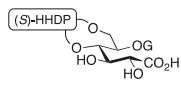
Figure 7. The transformations used in the determination for the first structure of punigluconin (**11**).

After that, Nonaka isolated lagerstannin C from *Lagerstroemia speciose* (L.) PERS. and determined its structure to be **15** (Figure 8) [36]. Comparison of the ^{1}H-NMR spectrum of punigluconin to that of **15** showed a notable difference at H-2 and similar values at the other hydrogens. Accordingly, the position of the galloyl group was changed to revise the structure to be **12**. Note that the ^{1}H-NMR assignments of H-3 and H-5 in the reports of the structural determinations for **11** [35] and for **12** [36] were swapped, which seemed to cause the error in the initial structure.

position	**15**	punigluconin [ref. 36]
H-2	4.25	5.36
H-3	4.15	4.45
H-4	5.47	5.82
H-5	5.74	5.51
H-6	4.95	4.82
H–6	4.16	4.06

^{1}H–NMR chemical shifts (in acetone-d_6)

lagerstannin C (**15**)

Figure 8. The comparison of the ^{1}H-NMR chemical shifts between lagerstannin C (**15**) and punigluconin.

3.1.3. Cercidinin A and B

Cercidinin A and B were isolated from *Cercidiphyllum japonicum* SIEB. *Et* ZUCC by Nishioka and first given the structures (a*R*)-**16** and (a*R*)-**17** (Figure 9), respectively [38]. Khanbabaee synthesized (a*R*)-**16** and (a*R*)-**17** in 1998, but the synthesized compounds were different from natural cercidinin A and B [39]. Following the result, Kouno revised the structure to **18** [40]. Yamada synthesized **18** to confirm the structure in 2013 [41].
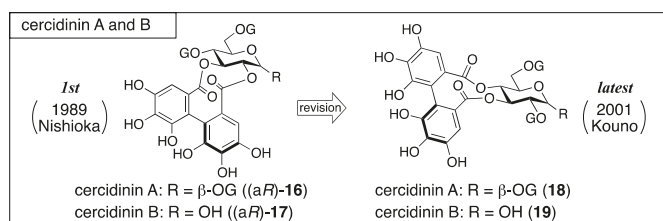
Figure 9. The transition of the structure of cercidinin A and B.

The process for the determination of (a*R*)-**16** and (a*R*)-**17** consists of NMR studies and the degradation of the natural products. The ^{1}H-NMR spectrum of cercidinin A indicated that the compound consisted of three galloyl groups and one HHDP group and that all the hydroxy groups of the glucose moiety were acylated. The hydrolysis of cercidinin A produced D-glucose, gallic acid, and ellagic acid (Figure 10a). On the other hand, the methanolysis of pentadecamethylcercidinin A yielded methyl tri-*O*-methylgallate (**13**) and dimethyl hexamethoxydiphenoate ((*R*)-**5b**). The *R*-axial chirality was based on the comparison of the specific optical rotation of **5b** to the data in the literature [42]. In the ^{1}H-NMR data of pentadecamethylcercidinin A, the coupling constants of the hydrogens on glucose displayed that the conformation of the glucose part was in the typical $^4C_1$ form. The tannase-hydrolysate of cercidinin A was a mixture of anomers (Figure 10b). In addition, the chemical shift of H-6 of the tannase-hydrolysate shifted to a higher magnetic field than that of cercidinin A. Therefore, the HHDP group was situated at the 2,3- or 3,4-positions of the glucose moiety. The reason for the decision on the 2,3-HHDP isomer (a*R*)-**20** was the similarity of the ^{1}H-NMR spectra (100 MHz) to that of the known (a*S*)-**20** [43]. The β-anomeric stereochemistry in cercidinin A was supported by the coupling constant of H-1 (*J* = 8 Hz) in the ^{1}H-NMR spectrum. The ^{1}H-NMR of cercidinin B exhibited that the compound possessed two galloyl groups and one HHDP group and that a hydroxy group was situated at the anomeric position. The hydrolysis of cercidinin B using tannase provided the same compound with the tannase-hydrolysate of cercidinin A.

a.

b.
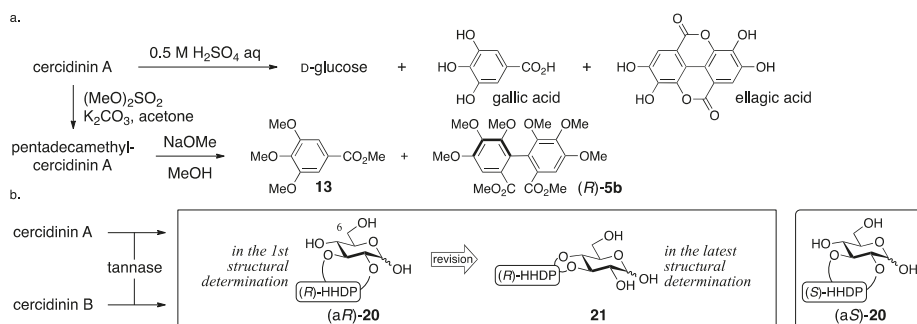
Figure 10. The transformations used in the determination for the first structure of cercidinin A ((aR)-**16**) and B ((aR)-**17**).

In Khanbabaee's synthesis that indicated the error in (aR)-**16** and (aR)-**17**, both the setting of the position of the HHDP group and the process that determined the axial chirality are reliable (Figure 11) [39]. They synthesized the bridged compound **24** through the double esterification of the 2,3-diol **22** with the racemic diphenic acid *rac*-**23**. The obtained bislactone was a mixture of diastereomers which was separable by column chromatography. The *R*-axial chirality was ascribed to the dextrorotation of **23**, that is, the hydrolysate of **24**, because its hexamethyl analog (*R*)-**5a** had been known to be dextrorotatory (Figure 4) [42]. The conversion of **24** through several steps produced (aR)-**16** and (aR)-**17**, which were eventually found to be different from natural cercidinin A and B. Namely, both (aR)-**16** and (aR)-**17** actually represent new compounds, which were subsequently named mahtabin A and Pariin M, respectively.
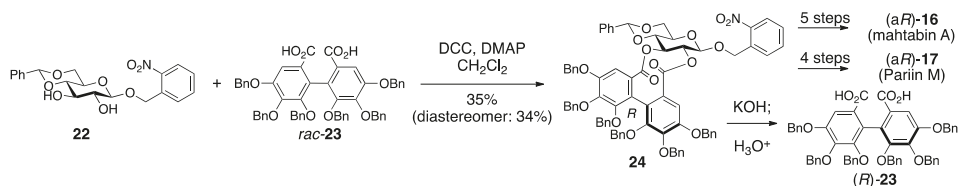
Figure 11. The synthesis of (aR)-**16** and (aR)-**17**.

Nishioka's structural revisions are grounded on the following observations. Reviewing the logic for the first structure (aR)-**16**, the determinations of the axial chirality and of the conformation of the glucose moiety were factually correct. The assignment of all the hydrogens and carbons of the carbohydrate part in cercidinin A was possible by employing a 500 MHz NMR instrument. On the basis of the assignments, the specification of the 3,4-HHDP structure was possible using hetero-nuclear multiple-bond coherence (HMBC) correlations between the carbonyl carbons of the HHDP group and the H-3/H-4 as displayed on the structure of **18** (Figure 12). Furthermore, the HMBC experiment determined the structure of **21** that was the hydrolysate of cercidinins with tannase. These results advocated for the structure **18**. In Nishioka's report, the structural revision of cercidinin A was only described. However, the structure of cercidinin B should be corrected to **19** as the difference between cercidinin A and B has been known to be the existence or non-existence of the anomeric galloyl group [38].
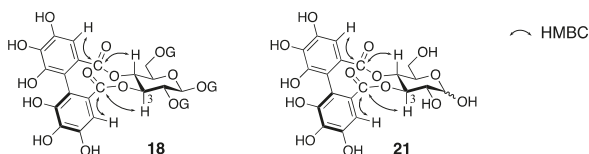
Figure 12. The significant HMBC relationships used for the determination of the structure **18** and **21**.

In Yamada's synthesis of **18**, a protected (*R*)-HHDP diacid **23** is introduced between the O-3 and O-4 of glucose (Figure 13) [41]. The double esterification of the diol **25** with the dicarboxylic acid (*R*)-**23**, the enantiomeric purity of which was 100%, yielded the bislactone **26**. The subsequent three steps provided **18**, which was identical to natural cercidinin A.
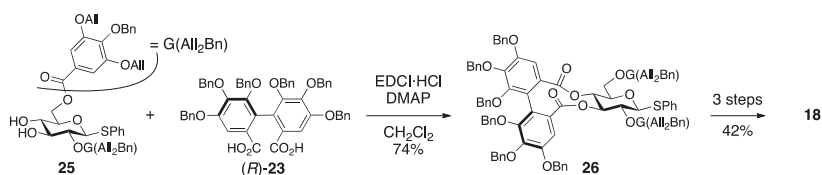
Figure 13. The key steps in the synthesis of **18**.

3.1.4. Roxbin B

Roxbin B was isolated from *Rosa roxburghii* TRATT and first given the structure (a*S*,a*S*)-**27** by Okuda (Figure 14) [44]. After that, Yamada synthesized (a*S*,a*S*)-**27**, but the synthesized compound was not identical to the natural product [45]. Yamada reviewed the process of the structural determination for (a*S*,a*S*)-**27**, presumed on the basis of the review that roxbin B was the same compound with cuspinin ((a*R*,a*S*)-**2**), and confirmed the presumption by total syntheses [46].
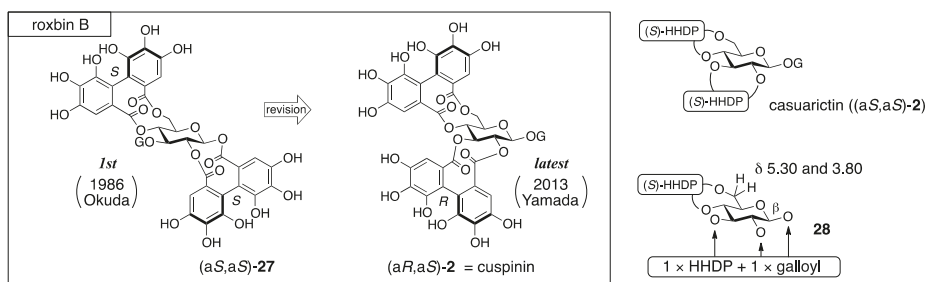
Figure 14. The transition of the structure of roxbin B, the structure of casuarictin ((a*S*,a*S*)-**2**), and the reliable partial structure **28** of roxbin B.

The structure (a*S*,a*S*)-**27** was determined by degradation, ^{1}H-NMR and circular dichroism (CD) spectra, and an HPLC chromatogram [44]. The ^{1}H-NMR spectrum of roxbin B revealed the numbers of the galloyl and HHDP groups. The hydrolysis of roxbin B produced gallic acid, ellagic acid, and D-glucose. The determination of the *S*,*S*-axial chiralities of the two HHDP groups was based on the Cotton effects that were positive at 225 nm and negative at 255 nm in the CD spectrum. Because the behavior was similar to that of casuarictin ((a*S*,a*S*)-**2**) [37], Okuda assessed that roxbin B was an isomer of (a*S*,a*S*)-**2**. In the ^{1}H-NMR spectrum, one of the two H-6s shifted to a lower field (δ5.30 and 3.80, see **28**), which indicated that one of the HHDP groups bridged between O-4 and O-6 [47].

The spectrum also demonstrated the β-anomeric stereochemistry ($^3J_{\text{H-1–H-2}}$ = 8.5 Hz) and the $^4C_1$ conformation of the pyranose ring. When the second HHDP group bridged between O-1 and O-3, the conformation of the pyranose should be in a boat form; thus, this could be excluded. The HPLC chromatogram of tannase-treated roxbin B indicated peaks due to gallic acid and another component. If roxbin B was an O-1 gallate, the component would be a mixture of anomers. The authors considered that such a mixture of anomers could be separated into two peaks in the chromatogram; hence, O-1 was judged not to be galloylated. Therefore, they concluded the 1,2-*O*-HHDP structure (a*S*,a*S*)-**27**.

In the synthesis of (a*S*,a*S*)-**27**, the introduced position and axial chirality of the HHDP groups were secure [45]. The stepwise esterification of the 1,2-diol **29** and the (*S*)-HHDP acid anhydride **30** (Figure 15), of which the optical purity was >99%, provided the 1,2-*O*-(*S*)-HHDP bridged compound **31**. The removal of the *p*-methoxybenzylidene acetal from **31** released the corresponding 4,6-diol, to which dicarboxylic acid (*S*)-**23** was introduced in a double esterification manner. Finally, the removal of all benzyl groups provided (a*S*,a*S*)-**27**. However, the ^{1}H/^{13}C-NMR spectra of the synthesized (a*S*,a*S*)-**27** were totally different from those of the natural roxbin B.
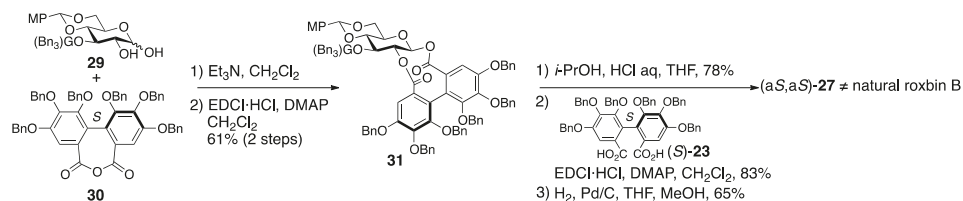
Figure 15. The synthesis of (a*S*,a*S*)-**27**.

The revised structure of roxbin B ((a*R*,a*S*)-**2**) was obtained by reviewing Okuda's process for the structure (a*S*,a*S*)-**27** [46]. Tracing Okuda's structural determination, it was trustworthy that roxbin B contained the partial structure **28** (Figure 14). In the review, a sample of roxbin B preserved for more than 20 years was found to degrade and provide strictinin (**32**) (Figure 16). This observation was associated with the 4,6-*O*-(*S*)-HHDP structure. On the other hand, the weak Cotton effect at 236 nm in the CD spectrum raised a doubt about whether the axial chiralities of the HHDP groups were both *S*. Thus, a hypothesis that one of the two HHDP groups had an *R*-axial chirality supposed two possible structures, (a*R*,a*S*)-**2** (Figure 14) and (a*R*,a*S*)-**27** (Figure 16). Of the two, (a*R*,a*S*)-**2** was cuspinin that had already been isolated by Nishioka [38]. The data in the literature on cuspinin were in good agreement with those of roxbin B. In Nishioka's report [38], the three main subjects of discussion were the structures of cercidinin A and B (Section 3.1.3) and cuspinin. Among the three, the structures of cercidinin A and B were revised and that of cuspinin supported the structural revision of roxbin B.

Figure 16. The structure of strictinin (**32**) and of a candidate (a*R*,a*S*)-**27** for revised roxbin B.

The synthesis aiming at confirmation of the structure of cuspinin ((a*R*,a*S*)-**2**), which is the revised structure of roxbin B, is conducted using HHDP compounds with secure axial chirality [46]. The sequential bridge formation between O-2 and O-3 of **33** adopting the HHDP derivative (*R*)-**23**, the removal of the benzylidene acetal, and the introduction of the (*S*)-HHDP group between O-4 and O-6 of **34** provided **35** (Figure 17). The debenzylation of **35** provided (a*R*,a*S*)-**2**, the ^{1}H/^{13}C-NMR of which were identical to those of cuspinin (and also roxbin B). Moreover, (a*R*,a*S*)-**27** was synthesized similarly and used to illustrate that its ^{1}H/^{13}C-NMR were obviously different from those of (a*R*,a*S*)-**2**.
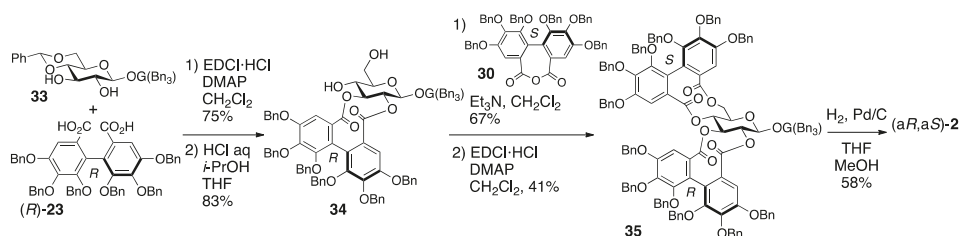
Figure 17. The synthesis of cuspinin ((aR,aS)-**2**), the structure of which was the revised structure of roxbin B.

The supposed cause to reach the first structure (aS,aS)-**27** was also reported [46]. Thus, from the comparison of the CD spectra of (aS,aS)-**27** (a synthesized compound), (aR,aS)-**2**, (aR,aS)-**27** (a synthesized compound), and (aR)-**36** emerged a tendency that the Cotton effect of a compound bearing the (R)-HHDP group indicated a 20 nm smaller wavelength than that of an (S)-HHDP compound (Figure 18). In addition, in the case where both the (R)- and (S)-HHDP groups were in a molecule, the intensity of the Cotton effect was weakened due to compensation for each other (compare (aS,aS)-**27** and (aR,aS)-**27**, Figure 18). Yamada explained that the determination of the structure (aS,aS)-**27** was attributed to the unnoticed negative Cotton effect around 220 nm.
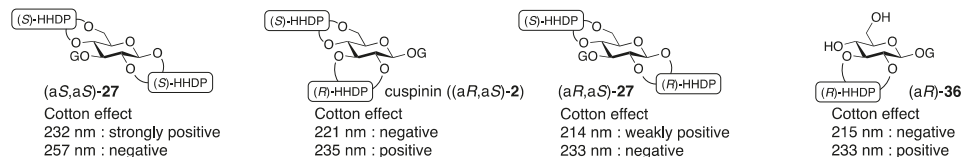
Figure 18. The comparison of the Cotton effects observed on (aS,aS)-**27**, cuspinin ((aR,aS)-**2**), (aR,aS)-**27**, and (aR)-**36**.

3.2. Correction Based on the Structure of the DHHDP Group

3.2.1. Geraniin

For geraniin, its first isolation, the structural determination, and all structural revisions were conducted by Okuda. Geraniin has been isolated from various plants, but initially it was isolated from *Geranium thunbergii* Sieb. *et* Zucc. and **37** was given as the first structure (Figure 19) [32,48]. After that, the structure of the DHHDP group was revised twice. For the second structure, the equilibrium mixture **38** was proposed [49]. Later on, the structure was revised to another equilibrium mixture **39** and the axial chirality of the HHDP group was revealed to be *R* [23]. The hemiacetal structure with the six-membered ring **39**-I was confirmed by an X-ray diffraction study [33].
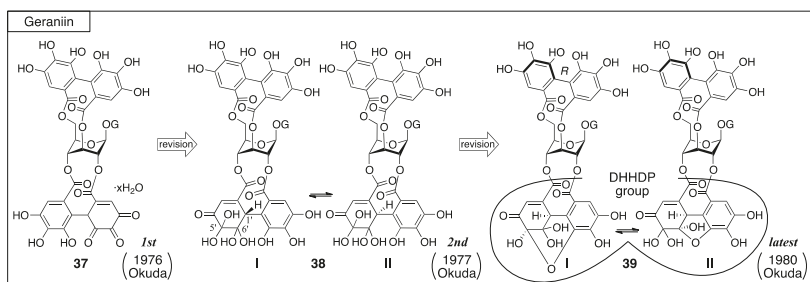
Figure 19. The transition of the structure of geraniin.

In the determination of the first structure (**37**), the use of the phenazine derivative is a feature [32]. Boiling water hydrolyzed geraniin to release corilagin (Section 3.1.1) (Figure 20); therefore, geraniin contained corilagin as a partial structure. Because the ^{1}H-NMR chemical shift of H-2 and H-4 of geraniin was over 1 ppm larger than those of corilagin, there were esters on O-2 and O-4 in geraniin. The treatment of geraniin with benzene-1,2-diamine and acetic acid produced phenazine-*do*. The phenazine-*do* gradually changed to phenazine-*re*, the hydrolysis of which provided phenazine-*mi* (**46**). The evidence for the structure **46** was the identity of two dimethyl esters **47**, which were derived from **46** and from the known **48** [50] through **49** that was obtained by the hydrogenolytic removal of only one benzyl group from **48** [48]. These results demonstrated that the component on the O-2 and O-4 was a partly oxidized HHDP group, the DHHDP group. In addition, the high-field shift of the H-1 (from 6.55 to 6.14 ppm) in ^{1}H-NMR observed in the transformation from phenazine-*do* to -*re* suggested that the phenazine skeleton was on the O-2 side because of the proximity. Hence, the structure of geraniin was **37**. Similarly, the structures of phenazine-*do* and -*re* were decided to be **40** and **43**, respectively. Note that the structure **40** seems to be one that would aromatize immediately, but it was copied as reported.
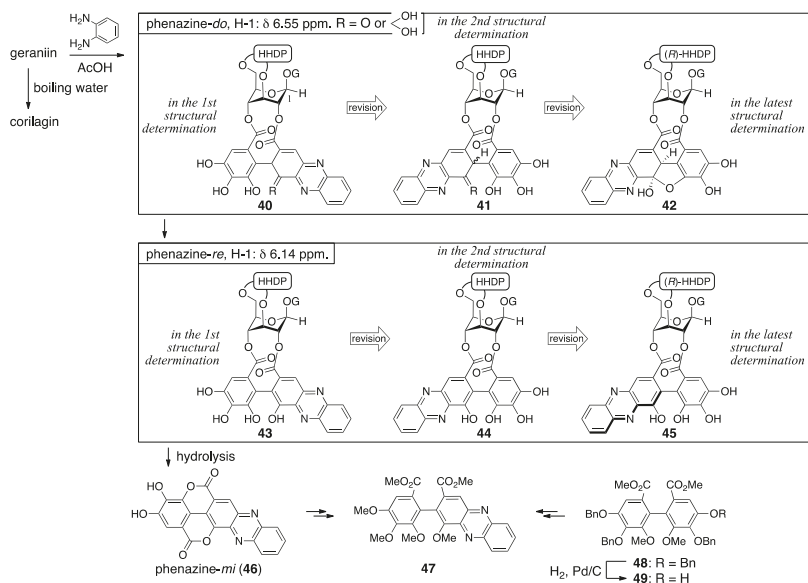
Figure 20. The hydrolysis and derivatization of geraniin.

The revision to the second structure of geraniin (**38**) was the positional swap of the quinone ring in the 2,4-*O*-DHHDP group [49]. The diazomethane treatment of phenazine-*re* produced **50** (Figure 21a), in which the ester bond "on O-2" was cleaved. The reason for the "on O-2" was the lower field shift of H-2 in the acetylated **51**. In the ^{1}H-NMR spectrum of the monocarboxylic acid **52**, which was derived by the hydrolysis of **51**, the chemical shift of H$_A$ situated on the phenazine skeleton shifted to the lower field by the addition of pyridine-d_5. Generally, the chemical shift of a neighboring (*o*-position in this case) hydrogen of a carboxylic acid slides to the lower field when the carboxylic acid forms a salt. By contrast, in the ^{1}H-NMR spectra of the corresponding dimethyl ester **47** and the dicarboxylic acid **53**, which were derived from **52**, the chemical shifts of H$_A$ and H$_B$ of **47** showed no significant shifts and both of H$_A$ and H$_B$ in **53** shifted lower. Thus, the phenazine moiety was on the O-4 side; hence, the structure of geraniin was **38**. This alteration revised the structures of phenazine- *do* and -*re* to be **41** and **44**, respectively (Figure 20). When a crystal of geraniin was dissolved in acetone-d_6 containing 10% D$_2$O, the compound was changed to be a 1:1 mixture within 6 h (Figure 21b). On the other hand, more than 12 h was required to reach a 1:1 mixture in anhydrous acetone-d_6. Accordingly, water participated in the equilibrium. The ^{1}H-NMR of the equilibrium mixture displayed each set of two signals due to methine hydrogens and vinyl hydrogens. Additionally, in the ^{13}C-NMR, each set of the two carbons was observed due to two kinds of hydrated ketones and a carbonyl carbon of conjugated ketone. These results provided the structures **38**-I and -II, which were the epimers at C-1′ and included two hydrated ketones at C-5′ and C-6′.
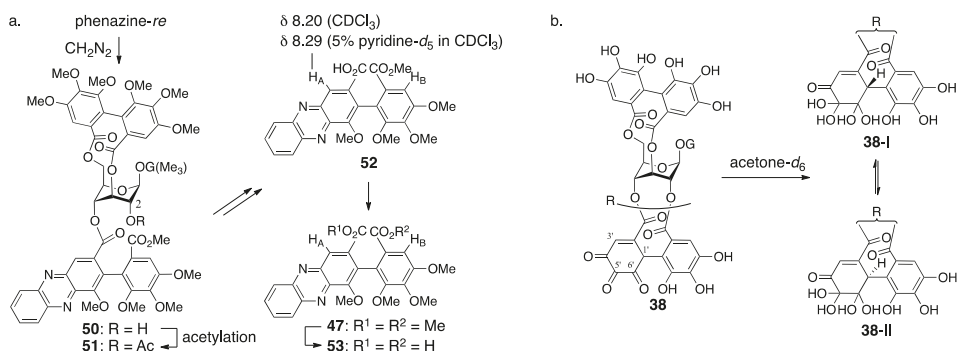
Figure 21. (**a**) The transformations that lead to the second structure of geraniin (**38**) and (**b**) the equilibrium between the two hydrated structures.

The doubt in **38** commenced with the fact that the observation of ^{1}H-NMR in the presence of D$_2$O did not induce the deuteration of the methine hydrogen [23]. There are two isomers in geraniin, crystalline type-I and non-crystalline type-II that occurs in a solution. Okuda focused on the notable difference of the ^{13}C-NMR chemical shifts of C-6′ (Figure 22a) to presume the type-II hemiacetal structure containing the five-membered ring. The structure was associated with the coupling constant between H-1′ and H-3′. The determination of stereochemistries at C-1′ and C-6′ of **39**-II commenced with consideration of the ^{1}H-NMR chemical shifts of H-1, which shifted to a higher field when phenazine-*do* was transformed to -*re* (Figure 22b). Okuda inferred that the shielding effect due to the phenazine rings induced the shift and supposed the structure **45**, where the phenazine moiety and H-1 could be close. For the formation of **45** that bears the *R*-axial chirality, the *R*-stereochemistry is necessary for C-1′ in its precursor **42**. The relative configuration between C-1′ and C-6′ was *cis* since **42** had a hemiacetalic structure with a fused five/six-membered ring. Moreover, the precursor **39**-II for **42** included a similar hemiacetalic structure; thus, the stereochemistry of **39**-II was determined to be 1′*R*, 6′*R*. On the other hand, for the type-I structure, the six-membered ring hemiacetal **39**-I, hydrated **38**-I, and **38**-II were the candidates. Among them, **39**-I was chosen because the ^{13}C-NMR spectrum

using the deuterium-induced differential isotope shift (DIS) method [51] revealed that the O-6″ was not a hydroxy group. The *R*-axial chirality of the HHDP group in **39** was introduced according to the *R*-chirality in corilagin, which had just been revealed (Section 3.1.1) [23]. In addition, the conformation of the glucopyranose of **39** was determined to be $^1C_4$ in acetone-d_6, which was similar to that in corilagin [30]. Finally, structure **39-I** was confirmed by an X-ray diffraction study [33].
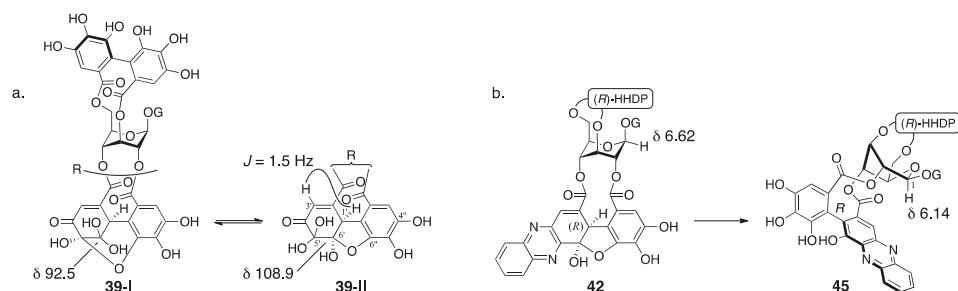
Figure 22. (**a**) The revised hemiacetalic structures and (**b**) the determination of the (*R*)-stereochemistry for C-1′.

3.2.2. Terchebin

Terchebin was isolated by Schmidt from myrobalans (fruit of *Terminalia chebula*) [52]. From this plant, chebulinic acid and chebulagic acid were also isolated (Section 3.3) [52]. Schmidt firstly gave **54** for the structure of terchebin, which possessed a cyclohexane-trione ring on the O-2 side [52]. In the ensuing year, they revised the structure to the mixture of isomers **55** [28]. Later, Okuda further revised the structure to **56** (I and II) that possessed the DHHDP group bridging between O-2 and O-4 (Figure 23) [53].
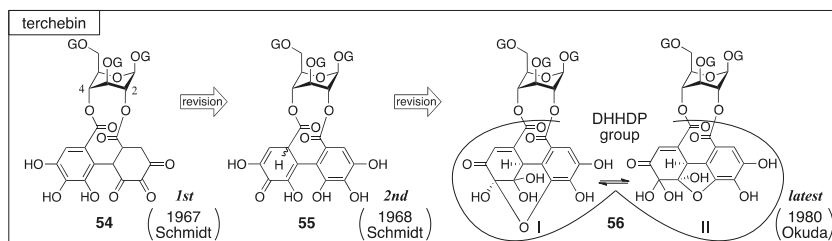
Figure 23. The transition of the structure of terchebin.

The structural determination of terchebin began with degradation experiments. The treatment of terchebin with benzene-1,2-diamine and AcOH provided the known compounds 1,3,6-tri-*O*-galloyl-β-glucose (**57**) [54] and phenazine-*mi* **46** (Figure 24a) [55]. According to the observation that **46** was obtained in the structural determination of brevilagin 1 (**58**), they considered that terchebin contained the same DHHDP group bridging between O-2 and O-4 through ester bonds [55]. On the other hand, the treatment of **58** with concentrated hydrochloric acid provided chloroellagic acid (**59**). However, a similar treatment of terchebin did not produce **59**. Furthermore, **58** did not provide a hydrogenated compound but terchebin did (Figure 24c), and the obtained product reduced the Tillmans reagent [56] to suggest that the product contained a reducing structure similar to ascorbic acid. According to these facts, Schmidt reached the conclusion that the structure of the hydrogenated compound was **60** and exhibited the structure of **54**. In the structure, there was no experimental evidence for the direction of the isohexahydroxydiphenoyl (*iso*-HHDP) group.

The authors supposed the direction on the basis of the similarity of the first structures of chebulinic acid and chebulagic acid (Section 3.3) [57,58].
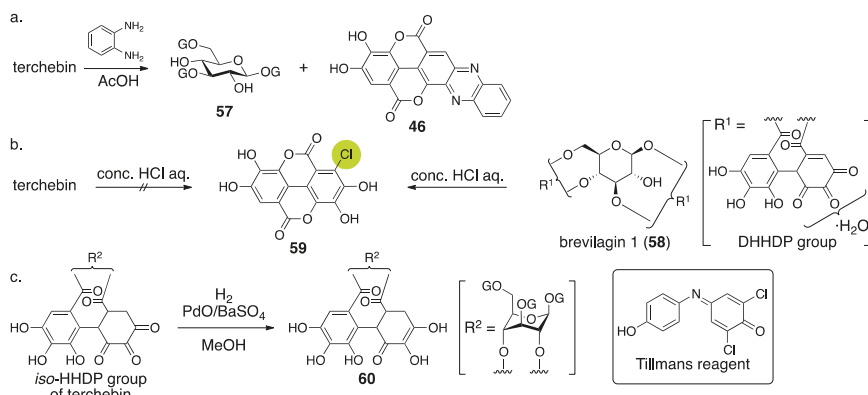
Figure 24. The transformations used for the determination of the first structure of terchebin (**54**).

Consideration of the ^{1}H-NMR spectrum of terchebin caused Schmidt to become aware of the error in the structure **54**. The ^{1}H-NMR spectrum of terchebin in DMSO-d_6 did not show any signal due to the –CH$_2$– group that was in the cyclohexane-trione ring in **54**. Moreover, signals from groups, such as the hydroxy groups other than those of phenol, H-2′, H-3′, and H-3″, were observed as $\frac{1}{2}$ H integrated intensity (Figure 25). According to the observations, Schmidt presumed the diastereomeric mixture **61** for the *iso*-HHDP moiety. With the knowledge of the revisions of the structurally related chebulinic acid and chebulagic acid to their second structures (Section 3.3), structure **55**, in which the benzene ring at the O-4 side was oxidized, was given [28].
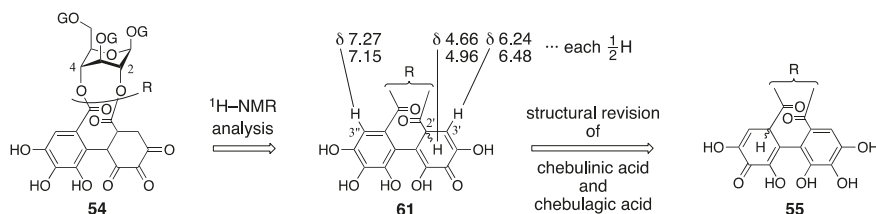
Figure 25. The pathway of the structural revision to **55**.

According to the structural revision of geraniin (Section 3.2.1) [23], Okuda reinvestigated the structure of terchebin [53]. The hydrolysis of terchebin with concentrated hydrochloric acid followed by methylation provided a mixture, the mass spectrum of which displayed a molecular ion peak that corresponded to tetra-*O*-methylated chloroellagic acid (**62**) (Figure 26). The result was contrary to Schmidt's report. In addition, Okuda confirmed that the hydrogenated geraniin reduced Tillmans reagent. According to the facts, the existence of the same DHHDP group in geraniin was supposed for the component situated between O-2 and O-4 of terchebin. With the following two observations, Okuda concluded that the structure of terchebin was **56** (I and II). The first observation was that the ^{1}H/^{13}C-NMR spectra of terchebin indicated signals that were similar to those of the DHHDP group of geraniin. The second observation was that the H-1 of the phenazine **64**, derived from terchebin via **63**, shifted to a higher field. The shift was similar to that observed in geraniin.
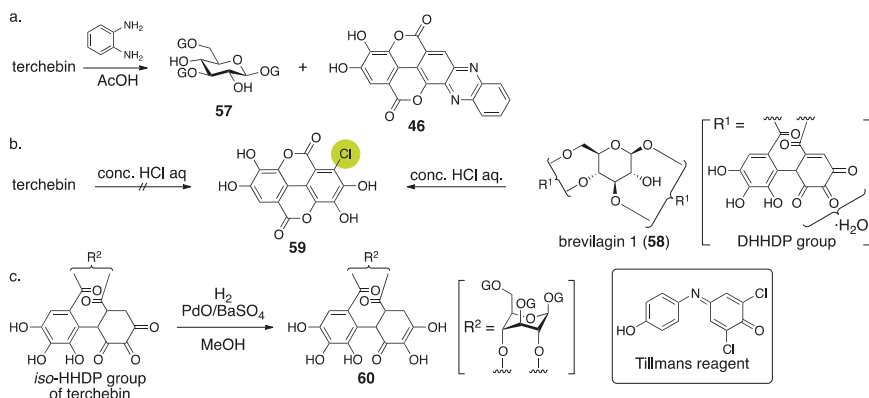
Figure 26. The transformations used for the structural revision to **56**.

3.2.3. Isoterchebin

Isoterchebin was isolated from *Cytinus hypocisris* by Schildknecht and firstly given the structure **65** [59] (Figure 27). After that, Okuda isolated cornus-tannin I from *Cornus officinalis*, revealed its structure, and found that the structure of cornus-tannin I (**66**) was identical to isoterchebin. Consequently, at this time, the structure of isoterchebin was revised to be **66** [60]. Later, Nishioka isolated a tannin, trapain, from *Trapa japonica* FLEROV, which also had the structure **66** [61].
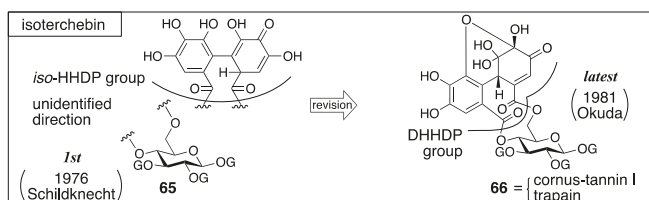
Figure 27. The transition of the structure of isoterchebin.

The structure **65** was determined by the combination of classic methods and NMR studies [59]. Hydrolysis with 5% sulfuric acid provided ellagic acid, D-glucose, and gallic acid (Figure 28). Meanwhile, one of the products derived by the methylation of the AcOEt extracts of the hydrolysates was **67** [62]. In those days, no ellagitannin containing structure **68** had been found. On the other hand, it was known that the hydrolysis of terchebin and brevilagins (**58** and **69**) [28], which had been considered to have the *iso*-HHDP and DHHDP groups, respectively, produced ellagic acid and **68** [63]. In addition, a method for the discrimination of the DHHDP and *iso*-HHDP groups had been known [52], which was that the treatment of dehydrohexahydroxydiphenic acid (**70**) with concentrated hydrochloric acid precipitated **59** out, but the treatment of **71** did not result in the same outcome. Because the hydrolysis of isoterchebin using concentrated hydrochloric acid did not provide **59**, Schildknecht considered that isoterchebin likely had the *iso*-HHDP group. From the ^{1}H-NMR spectrum of isoterchebin, they identified the existence of three unsubstituted galloyl groups, a gallic acid moiety modified at the 2-position, a vinyl proton, phenolic hydroxy groups, and enolic hydroxy groups. Among them, the chemical shifts of the vinyl proton and enolic hydroxy groups were in good agreement with those of terchebin. Therefore, they assessed that isoterchebin had the *iso*-HHDP group on the basis of the structure **55** (Figure 23). The signals due to the glucose moiety also displayed

that the pyranose was in the $^4C_1$ form and the existence of a bridging group between O-4 and O-6. The observations collectively lead to the structure **65** [59].
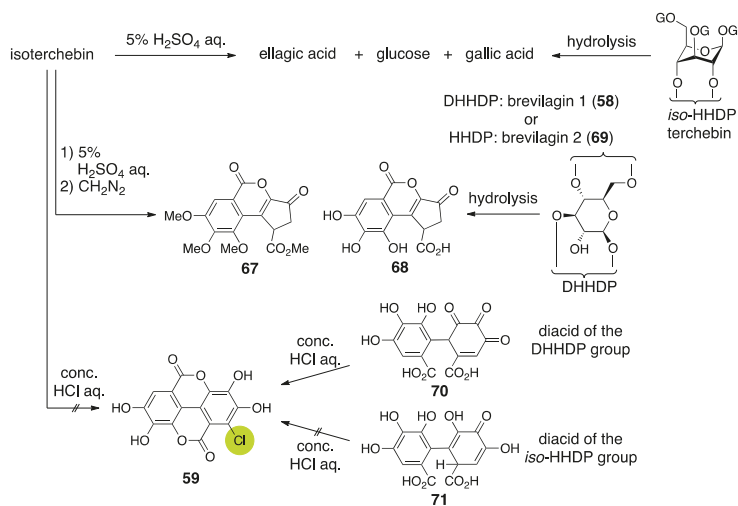
Figure 28. The transformations used for the determination of the structure **65**.

When Okuda isolated and determined the structure of cornus-tannin I, the structure that had been understood as the *iso*-HHDP group was revised to be the DHHDP group [53]. Accordingly, they doubted **65** that possessed the *iso*-HHDP group and concluded that cornus-tannin I and isoterchebin were the same compound because of their identical ^{1}H-NMR spectra and physical properties. The NMR experiments revealed, in addition to Schildknecht's observations, that three galloyl groups and one DHHDP group composed the molecule, that the DHHDP group was in the hemiacetal structure, and that no equilibrium mixture due to the existence of water occurred, which had been observed in geraniin. The condensation of isoterchebin with benzene-1,2-diamine provided the phenazine **72** (Figure 29a), which was transformed to known (*S*)-**47** [53] to exhibit the *S*-axial chirality. Hence, the chirality of the methine carbon of the DHHDP group was *S*. The decision that the phenazine formed on the O-6 side in structure **72** was attributed to the high-field shift of the C-6 of **72** compared to those of isoterchebin (−1.3 ppm) and **73** (−2.5 ppm) in the ^{13}C-NMR. In addition, the conformational change due to the formation of the phenazine was exposed by the high- and low-field shifts of H-4 and H-6, respectively, in the transformation of isoterchebin to **72**.
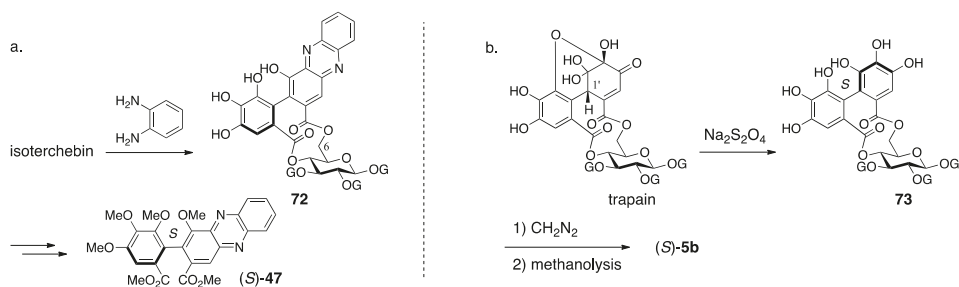
Figure 29. (**a**) The determination of the stereochemistry of the DHHDP group of isoterchebin (**66**) and (**b**) the reduction of trapain, which is the same compound with isoterchebin.

Nishioka's structural determination of trapain [61], which is the same compound with isoterchebin, was similar to that examined by Okuda [60]. The differences were in the method for disclosing the absolute structure of the DHHDP group and in the confirmation that the DHHDP group was in the six-membered hemiacetalic ring. Thus, the reduction of the DHHDP group of trapain using aqueous $Na_2S_2O_4$ produced **73** (Figure 29b) [64]. Full methylation of **73** followed by methanolysis provided (*S*)-**5b**, the axial chirality of which was confirmed by optical rotation [42]. Therefore, the chirality of C-1′ in the DHHDP group was also *S*. For the confirmation of the six-membered hemiacetalic ring of the DHHDP group, long range proton decoupling was applied. Their discovery that the DHHDP group of trapain did not generate a mixture of isomers by the addition of water corresponded to previous discussions.

3.3. Correction Based on the Structure of the Chebuloyl Group: Chebulinic Acid and Chebulagic Acid

Chebulinic acid and chebulagic acid are the major ellagitannins of myrobalans (fruit of *Terminalia chebula*) [65]. Fridolin isolated chebulinic acid for the first time in 1884 [18]. From this plant, terchebin was also isolated (Section 3.2.2). The first structures of chebulinic acid (**74**) and chebulagic acid (**76**) were determined by Schmidt (Figure 30) [57,58]. Subsequently, Haslam revised **74** to be **75a** [66]. Accordingly, Schmidt revised **76** to be **77a** [28]. These structures were revised once more by Okuda to be **75b** and **77b** [67].
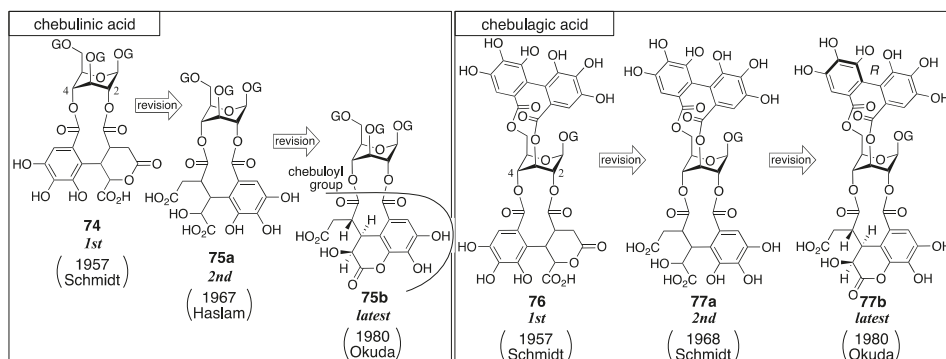
Figure 30. The transition of the structures of chebulinic acid and chebulagic acid.

Schmidt's structural determination of **74** and **76** is based on decomposition experiments. The hydrolysis of chebulinic acid provided the known 1,3,6-tri-*O*-galloyl-β-glucose (**57**) [54] and chebulic acid (**78**) [68] (Figure 31a) along with a new compound named neochebulinic acid (**79**, $C_{41}H_{34}O_{28}$ by elemental analysis). The successive full methylation of **79** and hydrolysis produced 2-*O*-methylglucose (**80**). Therefore, **79** is a seco acid with an unmodified 2-OH of glucose. With the authors' consideration that the chebuloyl group was an oxidized HHDP group [65] and with the structure of **78** in mind, the authors gave the structure **81** for the chebuloyl group. The determination suggests structures **79a** and **79b** for neochebulinic acid. They adopted **79a** considering that the aliphatic ester, which is more reactive, was hydrolyzed swiftly [58]. As the structure of chebulinic acid is lactonized **79a** at O-2, it was **74**. On the other hand, the hydrolysis of chebulagic acid released corilagin [69], **78**, and a halfway hydrolysate named neochebulagic acid (**82**) that possessed unmodified 2-OH (Figure 31b). These products indicated structure **76** [57].
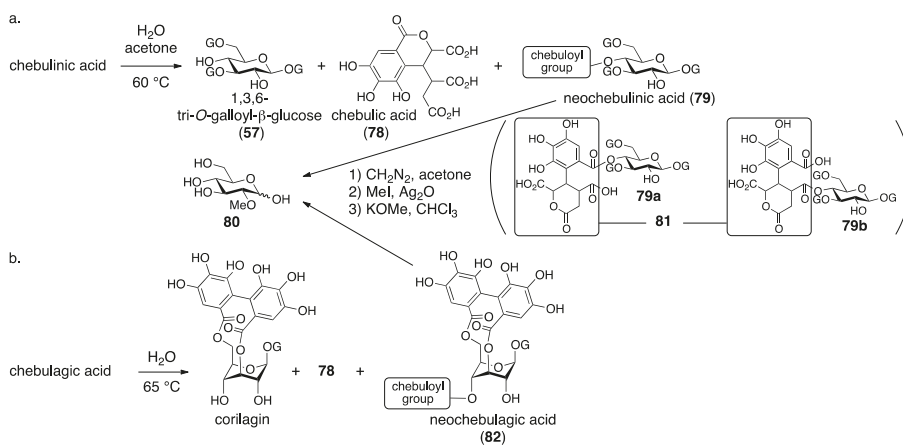
Figure 31. (**a**) The hydrolysis of chebulinic acid and the determination of the position of the chebuloyl group and (**b**) the hydrolysis of chebulagic acid.

Haslam observed two signals indicating methoxycarbonyl groups on a ^{1}H-NMR spectrum of diazomethane-treated chebulinic acid (Figure 32a). The result could not be explained with structure **74** that bore only one carboxy group. Hence, the structure of the chebuloyl group was not **81**, but was supposed to be non-lactonized **83**. In addition, they considered that the intramolecular lactonization due to the nucleophilic attack of a hydroxy group in the chebuloyl group produced neochebulinic acid (Figure 32b). With the fact that the ester bond on the O-2 of glucose was easier to cleave, they proposed structure **75a** [66]. After that, Schmidt revised the structure of **76** to **77a** according to Haslam's revision [28]. In the same report, Schmidt mentioned the *cis*-relationship between H-2″ and H-3″ of **79c** on the basis of the ^{1}H-NMR coupling constant.
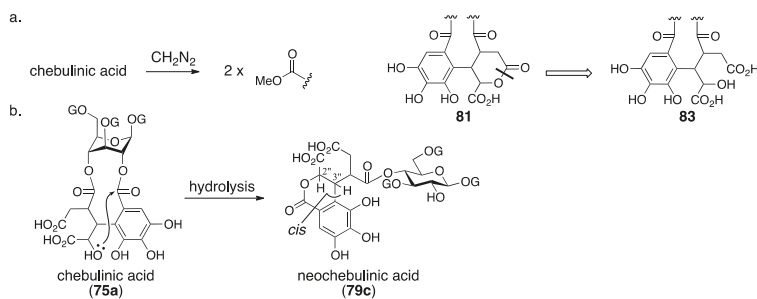
Figure 32. The consideration of the structural revision to the second structures of chebulinic acid and chebulagic acid.

Okuda re-examined the structure of chebulinic acid using the DIS method [51] that had been effective in the structural determination of geraniin (Section 3.2.1) [23]. Consequently, they revealed that only C-4′ and C-5′ had the structure of "C–OH" among the aromatic carbons bearing an oxygen atom in the chebuloyl group (Figure 33a). Since the revelation could not be explained with structure **83**, they conceived structure **84** that was a lactone mediated by O-6′. Structure **84** was ensured by three facts: (1) the DIS spectrum disclosed that only one of the four –CO$_2$– structures in the chebuloyl group was –CO$_2$H; (2) only one signal shifted to the lower magnetic field in the ^{13}C-NMR spectrum of the Et$_3$N salt of chebulinic acid; and (3) the reported IR absorptions (1775 and 1730–1700 cm^{-1}) by

Haslam were relevant to the dihydrocoumarin ring [66]. Thus, the structure of chebulinic acid was elucidated to be **75b**, and, similarly, the structure of chebulagic acid was revised to be **77b**. However, these structures might not generate "the two methoxy carbonyl groups", which Haslam previously observed on the methylated chebulinic acid. Okuda considered the inconsistency and concluded that the lactone of **84** was easy to cleave by treatment with diazomethane, which allowed for the formation of the two methyl esters. The stereochemistry indicated in structures **75b** and **77b** is based on the following consideration. Because chebulinic acid and chebulagic acid were isolated from the same plant from which terchebin (Section 3.2.2) was isolated, the stereochemistry of the C-3″ position was estimated to be *S*, that is, the same stereochemistry of C-3″ in terchebin (Figure 33b). The relative configuration of chebulic acid (**78**) was determined by an X-ray diffraction study of triethyl chebulate (**85**) (Figure 33c) [70]. The absolute configuration of **78** was confirmed to be *2″S, 3″S, 4″S* on the basis of the comparison of the CD spectrum of fully methylated chebulic acid (**86**) [71] to that of **87**, derived from bergenin (**88**), of which the absolute structure had been known (Figure 33d) [72,73]. The result indicated that the absolute stereochemistries of chebulinic acid and chebulagic acid were *2″S, 3″S, 4″S*. The axial chirality of the HHDP group of chebulagic acid was identified to be *R* because chebulagic acid contained corilagin, of which the axial chirality of the HHDP group was known to be *R* [23].
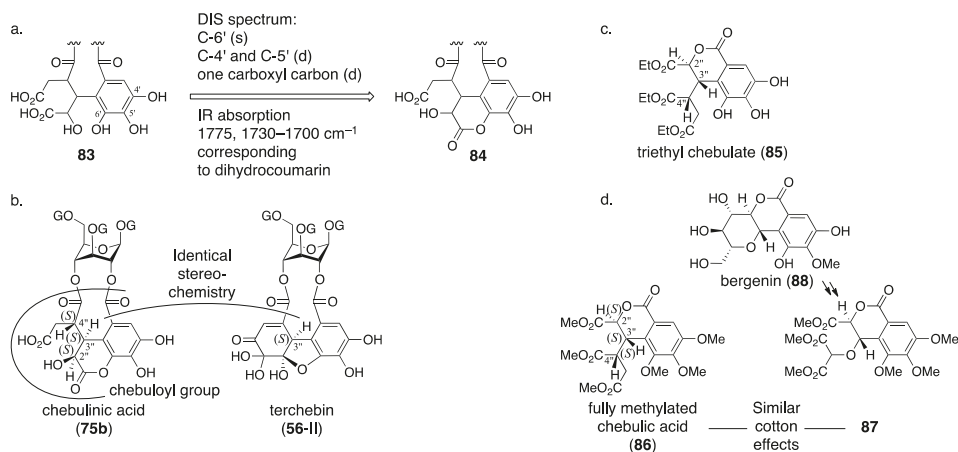
Figure 33. The structural revision of the chebuloyl group for the latest structures of chebulinic acid (**75b**) and chebulagic acid (**77b**). DIS, differential isotope shift.

3.4. Compounds Containing a C–C-Connected Trimer and Tetramer of the Galloyl Group

3.4.1. Castalin, Vescalin, Castalagin, Vescalagin, Casuarinin, and Stachyurin

All of the six ellagitannins listed above have a *C*-glycosidic bond in common (Figure 34). Mayer isolated castalin and vescalin from *Castanea sativa* and *Quercus sessiliflora* in 1967 [74] and gave their first structures as (1*S*)-**89** and (1*R*)-**89**, respectively, which comprised the NHTP group [75,76]. They also isolated castalagin and vescalagin from the same plants [74] and gave their first structures as (1*S*)-**90** and (1*R*)-**90**, respectively [77,78]. Subsequently, Okuda isolated casuarinin and stachyurin from *Casuarina stricta* and *Stachyurus praecox* and reported the respective structures (1*S*)-**91** and (1*R*)-**91** [37,79]. In 1987, Nishioka determined the axial chirality of the NHTP group to be *S,S* and reported the second structures for castalagin and vescalagin [80]. Thus, the axial chirality was also added to the structures of castalin and vescalin, resulting in their second structures. After that, Nishioka corrected the stereochemistries of the 1-OH of casuarinin and stachyurin, which lead their latest structures, (1*R*)-**91** and (1*S*)-**91**, respectively [81]. In accordance with the correction, the C-1 stereochemistries of castalin, vescalin,

castalagin, and vescalagin were revised, resulting in their third structures. Twenty-five years later, in 2015, Tanaka corrected the axial chirality of the NHTP group and revised the structures of castalin and vescalin to be (1*R*,a*S*,a*R*)-**89** and (1*S*,a*S*,a*R*)-**89**, respectively [82]. Consequently, the structures of castalagin and vescalagin were revised, resulting in the latest structures. In 2017, Quideau synthesized the latest structure of vescalin [83].
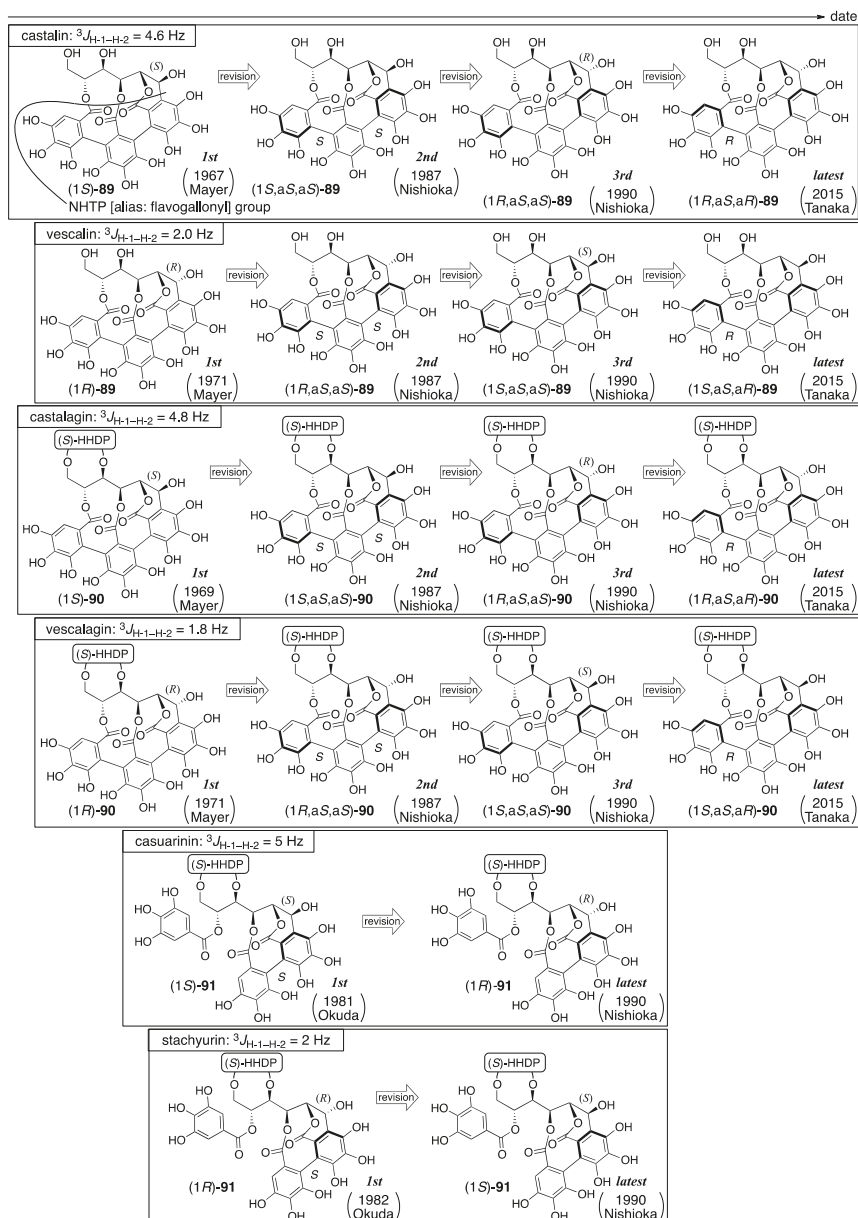
Figure 34. The transition of the structure of castalin, vescalin, castalagin, vescalagin, casuarinin, and stachyurin.

The first structure of castalin was revealed on the basis of the decomposition of the natural product and NMR studies [75]. The decomposition of castalin with hydrochloric acid and MeOH followed by the treatment of the decomposed products with diazomethane gave structurally unknown derivatives. A fragment ion peak in the mass spectrum of the derived compound indicated the existence of the NHTP group. Chemical shifts of the ^{1}H-NMR spectrum of castalin showed that (1) the NHTP group combined with a glucose moiety at O-2, O-3, and O-5 through ester bonds and (2) there was a *C*-glycosidic bond at C-1. The *S*-stereochemistry of C-1 was ascribed to the coupling constant of 4.6 Hz for $^3J_{\text{H-1–H-2}}$.

The first structure of castalagin was determined on the basis of the first structure of castalin, (1*S*)-**89** [77]. The hydrolysis of castalagin yielded castalin [74,75] and ellagic acid (Figure 35). Hence, castalagin has the structure (1*S*)-**90** that is composed of the HHDP group and castalin.
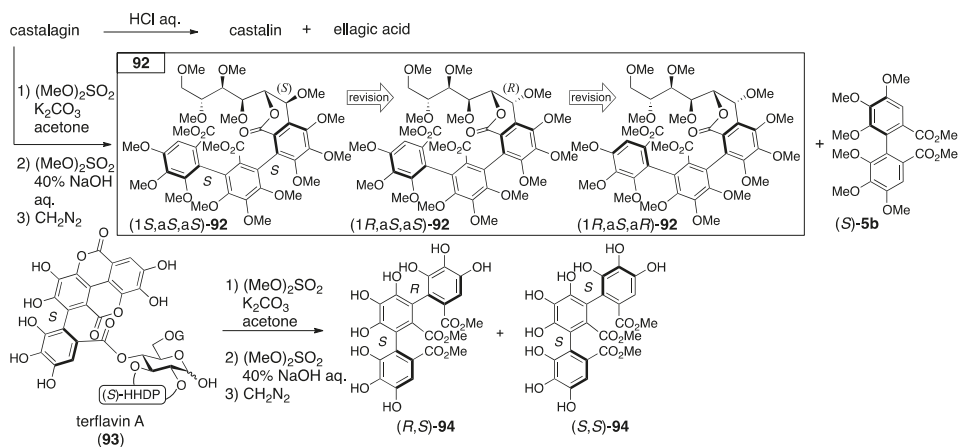
Figure 35. The hydrolysis of castalagin, and the determination of the axial chiralities in the second structure of castalagin.

The first structures of vescalin and vescalagin were disclosed in a manner similar to that above [76,78]. Because the hydrolysis of vescalagin provided vescalin and ellagic acid, structure (1*R*)-**90** was illustrated. The C-1 *R*-stereochemistry was given according to the coupling constant of 1.8 Hz for $^3J_{\text{H-1-H-2}}$.

In the determination of the axial chirality of the NHTP group that lead to the second structure of castalagin, CD spectra were used [80]. Thus, starting from castalagin, the three-step transformation introduced **92** along with (*S*)-**5b** (Figure 35). On the other hand, terflavin A (**93**), of which the absolute stereochemistry had been known [84], was converted to (*R,S*)-**94** and (*S,S*)-**94** in three steps. Of these, the optically inactive (*R,S*)-**94** was the *meso*-isomer. The axial chirality of the optically active isomer was (*S,S*)-**94** since the relevant part in **93** was *S*. The CD spectra of **92** showed a similar waveform to that of (*S,S*)-**94** in which the Cotton effect was negative at around 230 nm and positive at around 252 nm. According to the observation, the axial chirality of the NHTP group in **92** was determined as being *S,S*; hence, the structure was (1*S*,a*S*,a*S*)-**92**. The heating of an aqueous solution of vescalagin gave rise to the isomerization at C-1 to produce castalagin [74]; therefore, the stereochemistry of the NHTP group of vescalagin was the same as *S,S* and, thus, the structure was (1*R*,a*S*,a*S*)-**90** [80]. Similarly, as castalin and vescalin were structural parts of castalagin and vescalagin [80], these second structures might be revised to (1*S*,a*S*,a*S*)-**89** and (1*R*,a*S*,a*S*)-**89** at this time despite its absence in the literature.

The first structures of casuarinin and stachyurin were introduced by decomposition and NMR studies [37]. The tannase hydrolysis of casuarinin provided **95** (Figure 36). By the transformation,

the ^{1}H-NMR chemical shift of H-5 shifted to a higher magnetic field. In addition, because the coupling constant was 5 Hz for the $^3J_{\text{H-1–H-2}}$ of casuarinin (Figure 34), the stereochemistry of C-1 was demonstrated to be *S* according to the structure of castalin ((1*S*)-**89**). On the other hand, the sequential treatment of casuarinin with diazomethane followed by the methanolysis of the product gave (*S*)-**5b**, **13**, and **96**. The CD spectrum of **96** partially indicated a similar Cotton effect to that of (*S*)-**5b**. Therefore, the *S*-axial chirality in **96** was provided. In the determination of the first structure of stachyurin ((1*R*)-**91**), the following two facts were the conclusive factors: (1) the $^3J_{\text{H-1–H-2}}$ value was 2 Hz; and (2) the heating of the aqueous solution of casuarinin caused the occurrence of isomerization to yield stachyurin [79].
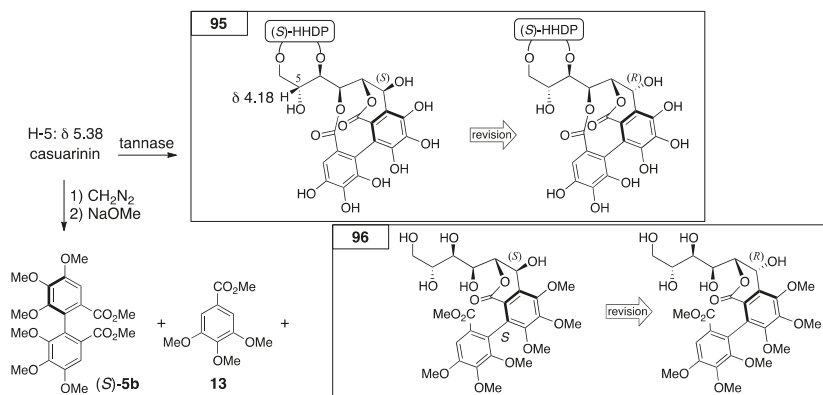
Figure 36. The transformations used for the determination of the first structure of casuarinin ((1*S*)-**91**).

In the structural revision to the latest structures of casuarinin and stachyurin, nuclear Overhauser effect (NOE) difference spectroscopy played a key role. The natural products casuarinin and stachyurin were introduced to **98** and the acetate **99** through **97** and *epi*-**97**, respectively (Figure 37) [81]. The NOE difference spectrum of **99** indicated a *cis*-configuration at H-1 and C-3. Therefore, the stereochemistry of C-1 was *S*. By contrast, there was no decisive NOE relationship in **98** for the determination of the stereochemistry of C-1, but it was the epimer at C-1; hence, the stereochemistry of **98** was *R*.
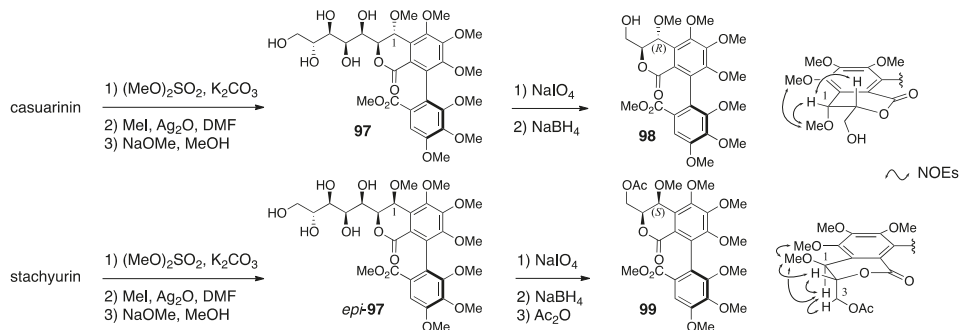
Figure 37. The grounds for swapping the stereochemistry of C-1 to lead to the latest structures of casuarinin and stachyurin. NOE, nuclear Overhauser effect.

The correction of the C-1 stereochemistry of casuarinin and stachyurin affected the structures of castalagin and vescalagin. Thus, on the basis of the similarity of the coupling constants ($^3J_{\text{H-1–H-2}}$)

(Figure 34), the C-1 stereochemistries of castalagin and vescalagin were changed to be *R* and *S*, respectively; hence, the structures were revised to be (1*R*,a*S*,a*S*)-**90** and (1*S*,a*S*,a*S*)-**90** (the third structures). Likewise, despite their absence in the literature, the structures of castalin and vescalin could be revised to be their third structures (1*R*,a*S*,a*S*)-**89** and (1*S*,a*S*,a*S*)-**89**, respectively, where the stereochemistry at C-1 was swapped.

In the correction of the axial chirality of the NHTP group in 2015, chemical calculations were utilized [82]. Using the density functional theory (DFT) method, Tanaka calculated each electronic circular dichroism (ECD) spectrum of four isomers of the castalin/vescalin **89** (Figure 38), in which the C-1 stereochemistry and the axial chirality of the NHTP group differed. As a result, the calculated spectrum for (1*R*,a*S*,a*R*)-**89** and the actual spectrum of castalin [75] were in good agreement. Similarly, the calculated data for (1*S*,a*S*,a*R*)-**89** were similar to the measured spectra of vescalin [76]. As castalin and vescalin were the hydrolysates of castalagin and vescalagin, respectively [74], these structures were also revised to be (1*R*,a*S*,a*R*)-**90** and (1*S*,a*S*,a*R*)-**90** [82]. In the report, Tanaka points out that the correction of the axial chirality would affect the structures of the other natural ellagitannins containing the NHTP group, such as roburins A−D [85], castaneanins A−D [86], acutissimins A (Figure 1) and B [14], anogeissusins A and B [87], anogeissinin [87], and several related metabolites, such as mongolicains A and B [88].
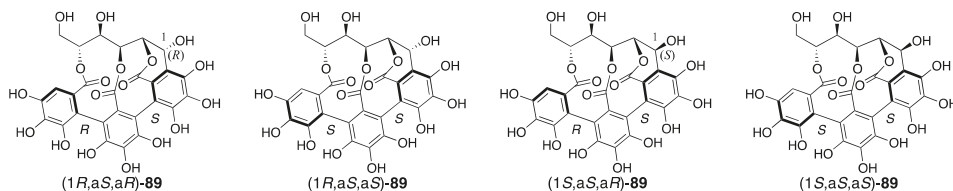
Figure 38. The computer-calculated compounds that led to the structural revisions of castalin and vescalin to the latest structures.

Quideau's synthesis of vescalin was achieved by the development of a novel method for synthesizing the NHTP group (Figure 39) [83]. The six-step transformation of **100** provided **101** that possessed the (*S*)-HHDP group between O-2 and O-3. An additional six-step transformation, including hydrolysis, oxidation at the anomeric position, and the introduction of the galloyl group to O-5, gave **102**. The removal of the TBS groups from **102** triggered the *C*-glycosylation. Oxidation by CuCl₂ and *N*,*N*′-dimethylbispidine constructed the NHTP group to provide **103**. Further hydrogenolysis of the benzyl groups and hydrolysis of the benzylidene acetal afforded vescalin. The synthetic method for the NHTP group developed in the total synthesis showed, for the first time, that the group could be chemically synthesized using the oxidative coupling of phenols.
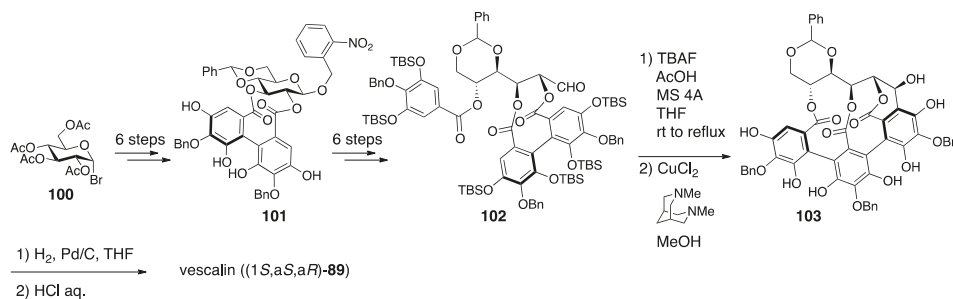
Figure 39. The first total synthesis of vescalin.

3.4.2. Punicalin and Punicalagin

Punicalin and punicalagin were isolated from pomegranate (*Punica granatum*) their first structures, **104** and **106**, were reported by Mayer in 1977, in which the gallagyl group bridged between the O-2 and O-6 of glucose (Figure 40) [89]. Nishioka revised the structures to **105** and **107** in 1986 [90]. In the revision, the bridging position of the gallagyl group was altered and the axial chirality was determined.
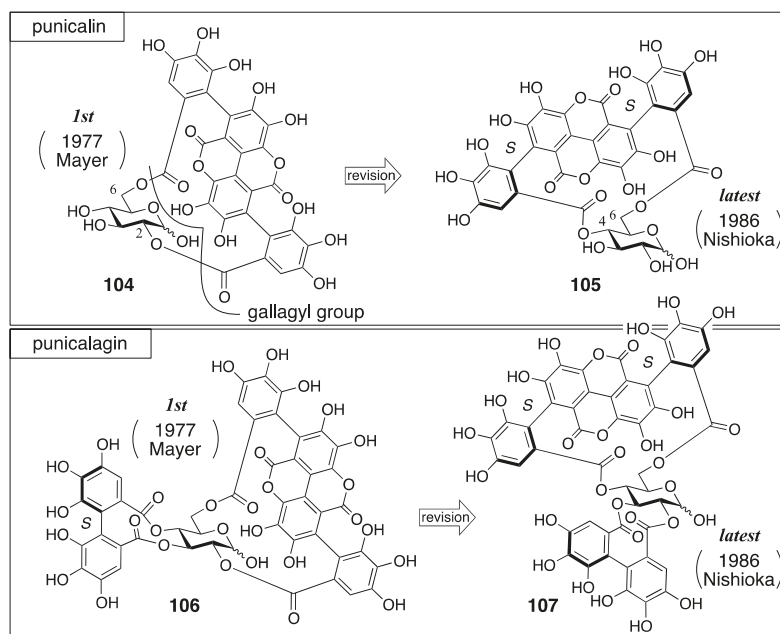
Figure 40. The transition of the structures of punicalin and punicalagin.

The first structures were determined using degradation (Figure 41), NMR studies, and the consideration of molecular models. The hydrolysis of punicalagin provided ellagic acid and punicalin. Therefore, punicalin was a component of punicalagin. The treatment of punicalagin with diazomethane and the subsequent methanolysis produced **108**, (*S*)-**5b** [77], and **109**. The hydrolysis of **109** yielded dicarboxylic acid **110**. On the basis of the ^{1}H-NMR and mass spectra, structures **109** and **110** were determined. Taken together, Mayer supposed that punicalagin had a hydroxy group on the C-1 of glucose and that there were HHDP and gallagyl groups on the other oxygens. The fact that punicalin and punicalagin were negative to the qualitative analysis using aniline hydrogen phthalate [19] and the knowledge that 2-*O*-galloyl glucose is basically negative to detection [91] lead to the prediction that the O-2 of both punicalin and punicalagin was esterified. The other connecting site, O-6, was revealed according to the consideration that the gallagyl group could connect only with O-6 in assembling a molecular model. Thus, the HHDP group bridged between the residual O-3 and O-4 in the structure of punicalagin. Later, Schilling reported that the glucose moieties in punicalin and punicalagin were both in the $^4C_1$ form on the basis of the ^{1}H-NMR coupling constants [92].
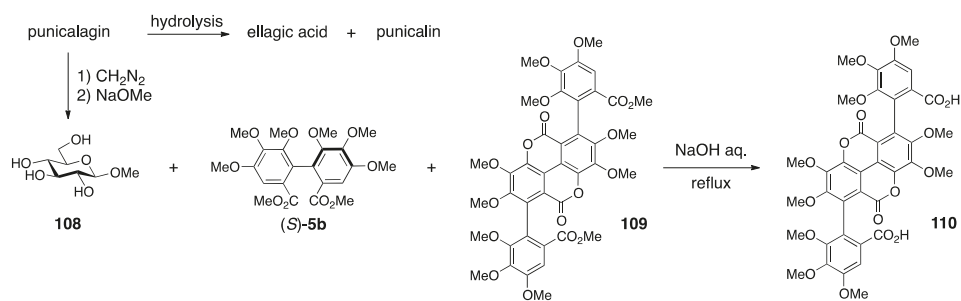
Figure 41. The degradation used for the structural determination of the first structures of punicalin and punicalagin.

The revision to the latest structures was triggered by the discovery of the related natural tannin **111** (no specific name) (Figure 42) [90]. First, the connecting positions of the gallagyl group in punicalin and punicalagin were revised. The ^{1}H-NMR spectrum of **111** indicated the existence of one galloyl group. The tannase-mediated hydrolysis of **111** produced punicalin where the ^{1}H-NMR chemical shifts of the H-2 shifted to a higher field ($\Delta\delta$ −1.5 ppm). After the acetylation of **111**, the ^{1}H-NMR chemical shifts of the H-1 and H-3 of the obtained **112** were in a lower field than those of **111**, which demonstrated that O-1 and O-3 were acetylated. The above led to the conclusion that **111** possessed hydroxy groups on C-1 and C-3, a galloyl group on O-2, and a gallagyl group bridging between O-4 and O-6. The fact that punicalin was a hydrolysate of **111** meant that the gallagyl group bridged between O-4 and O-6. Since the position of the gallagyl group in punicalin was the same in punicalagin, the position of the HHDP group in punicalagin was revised to be between O-2 and O-3. Then, the *S,S*-axial chiralities in the gallagyl group were given. Thus, the methylation of **111** and the subsequent methanolysis released (*S,S*)-**109**, which was converted to (*S,R,S*)-**113** and (*S,S,S*)-**113** by additional two steps, although the axial chiralities were unknown at this point. On the other hand, the Ullmann coupling of the known (*S*)-**114** [43] yielded (*S,R,S*)-**113** and (*S,S,S*)-**113**, which were identical to those derived from **109**. Hence, these axial chiralities were *S,R,S* and *S,S,S* from which the disappearance of the middle axial chirality due to bislactonization revealed the *S,S*-structure.
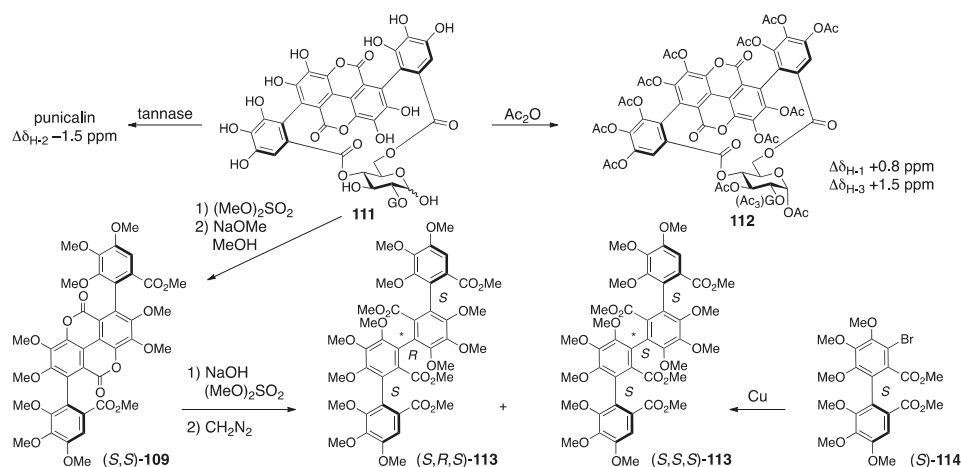
Figure 42. The transformations that led to the latest structures of punicalin and punicalagin.

3.5. Correction Based on the Bonding Position of C–O-Connected Components

3.5.1. Sanguiin H-2, H-3, and H-6

Sanguiin H-2, H-3, and H-6 were isolated from great burnet (*Sanguisorba officinalis*) and given their respective first structures by Nishioka (Figure 43) [93,94]. Three years later, Nishioka revised them to the latest structures, in which the bridging positions were altered [43], the axial chirality of the sanguisorboyl group was changed, and the α-stereochemistry was determined for the anomeric gallate.
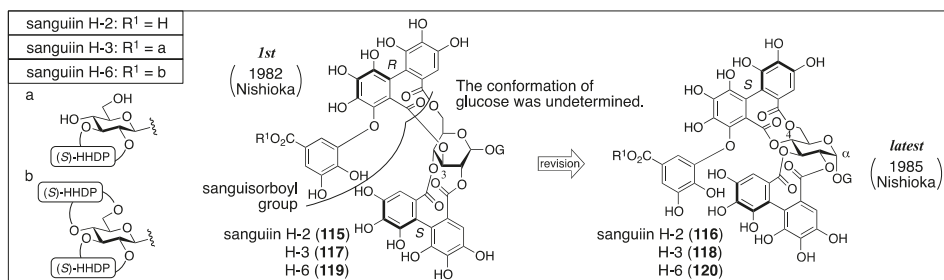
Figure 43. The transition of the structure of sanguiin H-2, H-3, and H-6. The conformation of the glucose moiety in the first structures was undetermined.

The process for the determination of the first structure of sanguiin H-2 (**115**) consisted of transformations of the natural product and NMR studies (Figure 44) [93]. The methylation of sanguiin H-2 provided the per-*O*-methylated **121**, the mass spectrum of which indicated the existence of sanguisorboyl, HHDP, and galloyl groups. The ^{1}H-NMR of **121** exhibited signals for seven hydrogens on aromatic rings; thus, each one of the sanguisorboyl, HHDP, and galloyl groups was contained in sanguiin H-2. The methanolysis of **121** and the subsequent treatment with diazomethane produced (*S*)-**5b** and **122**. The *S*-axial chirality was provided by a comparison of the specific optical rotation to that of the known (*R*)-**5b** [42]. The reason for the *R*-axial chirality of **122** was the opposite Cotton effect observed at 244 and 265 nm in the CD spectra of (*S*)-**5b** and **122**. The hydrolysis of sanguiin H-2 with tannase provided two products. One was an anomeric mixture bearing the sanguisorboyl and HHDP groups; hence, the galloyl groups were situated on O-1 in sanguiin H-2. The other was determined to be **125**, which possess a 3,6-*O*-bridged structure. The bridge position was revealed by a comparison of its ^{1}H-NMR spectra to those of the known (a*R*)-**3** [31] and **127** [64]. Embodying the information presented structure **115**.

The structural determinations for sanguiin H-3 (**117**) and H-6 (**119**) were proceeded similarly [93,94]. The ^{1}H/^{13}C-NMR spectrum of sanguiin H-3 indicated that a glucose derivative possessing one HHDP group had combined with sanguiin H-2. The methylation of sanguiin H-3 provided triicosa-*O*-methylsanguiin H-3 (Figure 45); further methylation and subsequent hydrolysis released 4,6-di-*O*-methyl-D-glucose (**130**). In addition, the partial hydrolysis of sanguiin H-3 provided sanguiin H-2 and (a*S*)-**20**. The *S*-axial chirality of the HHDP group in (a*S*)-**20** was confirmed by the transformation of it to (*S*)-**5b**. By integrating these pieces of information, structure **117** was determined. The ^{1}H-NMR spectrum of sanguiin H-6 demonstrated a structure that had one more HHDP group merged with sanguiin H-3. The partial hydrolysis of sanguiin H-6 gave sanguiin H-2, sanguiin H-3, and (a*S*)-**20**. The determination of the *S*-axial chirality of the 4,6-*O*-HHDP in **119** relied on the similarity of the ^{13}C-NMR spectrum of sanguiin H-6 and casuarictin ((a*S*,a*S*)-**2**).
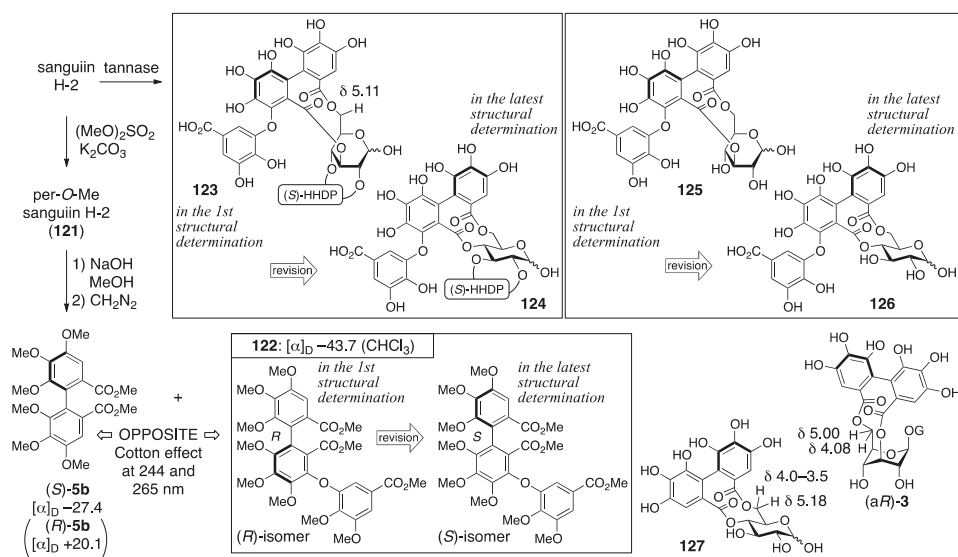
Figure 44. The observations used for the structural determination of sanguiin H-2 (**115**). The conformation of the glucose moiety of **123** and **125** was undetermined.
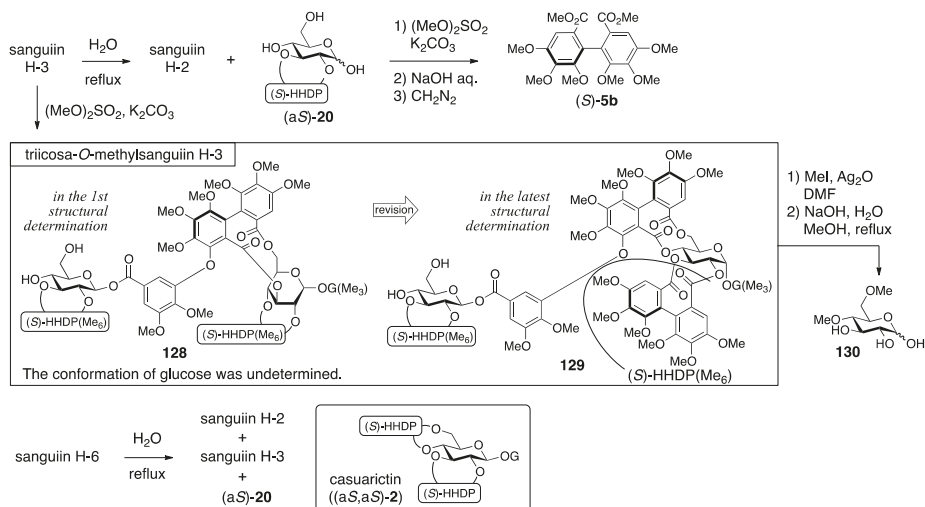
Figure 45. The transformations that led to the first structures of sanguiin H-3 (**117**) and H-6 (**119**). The conformation of the glucose moiety of **128** was undetermined.

The structural revision to the latest structures is founded on identification and synthesis [43]. First, the hydrolysate of sanguiin H-7 (**131**) (Figure 46), which possessed the sanguisorboyl group between O-4 and O-6, was identical to the tannase hydrolysate derived from sanguiin H-2 (see also Figure 44). Therefore, the bridging position of the sanguisorboyl group in the hydrolysate was corrected to be between O-4 and O-6 as in **126**. Due to this correction, the position of the HHDP group in sanguiin H-2 was altered to be between O-2 and O-3 from between O-2 and O-4. Then, the axial

chirality of the sanguisorboyl group was revised from *R* to *S*. Thus, the Cu_2O-mediated coupling [95] of **114**, which was a brominated (*S*)-HHDP compound derived from (*S*)-**5b**, and the gallic acid derivative **132** provided (*S*)-**122**. The ^{1}H-NMR spectrum and the sign of the specific optical rotation of (*S*)-**122** were identical to those of **122** derived from **121** (Figure 44). The stereochemistry of the anomeric position was determined to be α on the basis of the ^{1}H-NMR coupling constant ($^3J_{H-1–H-2}$ = 4 Hz). Hence, the structure of sanguiin H-2 was **116**. The structures of sanguiin H-3 and H-6 were similarly revised to be **118** and **120**, respectively.
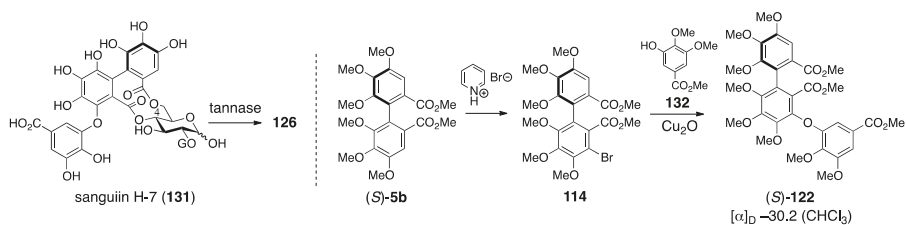
Figure 46. The information referred to in the structural revision to **116**.

3.5.2. Alnusiin

Alnusiin was isolated from the fruits of *Alnus sieboldiana* by Okuda in 1981. Initially, the structure **133** was advocated (Figure 47) [96]. In the structure, the direction of the bridging component between O-4 and O-6 of the glucose moiety was unspecified. The structure **133** was revised to **134** in 1989 by Okuda [97]. The structure of the partly lactonized macaranoyl group in **133** had included an error. The component was a partly lactonized tergalloyl group.
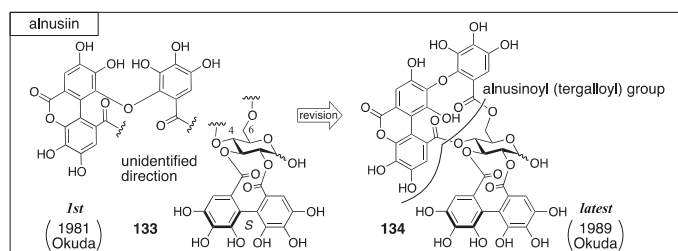
Figure 47. The transition of the structure of alnusiin.

In the process leading to **133**, several types of methylation were effectively used [96]. The observation of two anomeric carbons in ^{13}C-NMR revealed that alnusiin was a mixture of anomers. The methylation of the phenolic hydroxy groups of alnusiin produced trideca-*O*-methylalnusiin (**135**) (Figure 48a). The methanolysis of **135** provided D-glucose, (*S*)-**5b**, and a decamethylated compound. The further methylation of this provided an undecamethylated compound whose mass spectrum was similar to that of known **140**, but these ^{1}H-NMR spectra were different [98]; hence, the "tricarboxylic acid" was a new compound and named alnusinic acid. Structure **141**, composed of the macaranoyl-group skeleton, was determined according to the additivity of the substituent effect in the ^{13}C-NMR spectrum. The facts that the product obtained by methanolysis of **135** was not an "undecamethylated compound" but a "decamethylated compound" and that one of the carbonyl carbons appeared with an upfield shift (δ 164.1) in the ^{13}C-NMR indicated the existence of the lactone. Therefore, the fragment that consisted of three condensed galloyl groups was called the alnusinic acid monolactone group. The conformation of the glucose moiety in the thoroughly methylated alnusiin (Figure 48b), which was prepared by the treatment of alnusiin with dimethyl sulfate, was $^4C_1$

according to the ^{1}H-NMR coupling constants. The conformation limited the positions of the bridges to be between O-2 and O-3 and between O-4 and O-6. The mild methanolysis of the α-isomer of the thoroughly methylated alnusiin with CD_3OD cleaved the ester bond on O-2 of the glucose, which was confirmed by the disappearance of the esterification shift, to give **143**. The subsequent methylation produced the O-2-metylated compound **144**. The molecular weight of a fragment observed in the mass spectrum of **144** was 439, which corresponded to that of the HHDP derivative **145**. Accordingly, the HHDP group bridged between O-2 and O-3. The other component, which was the alnusinic acid monolactone group, bridged between O-4 and O-6.
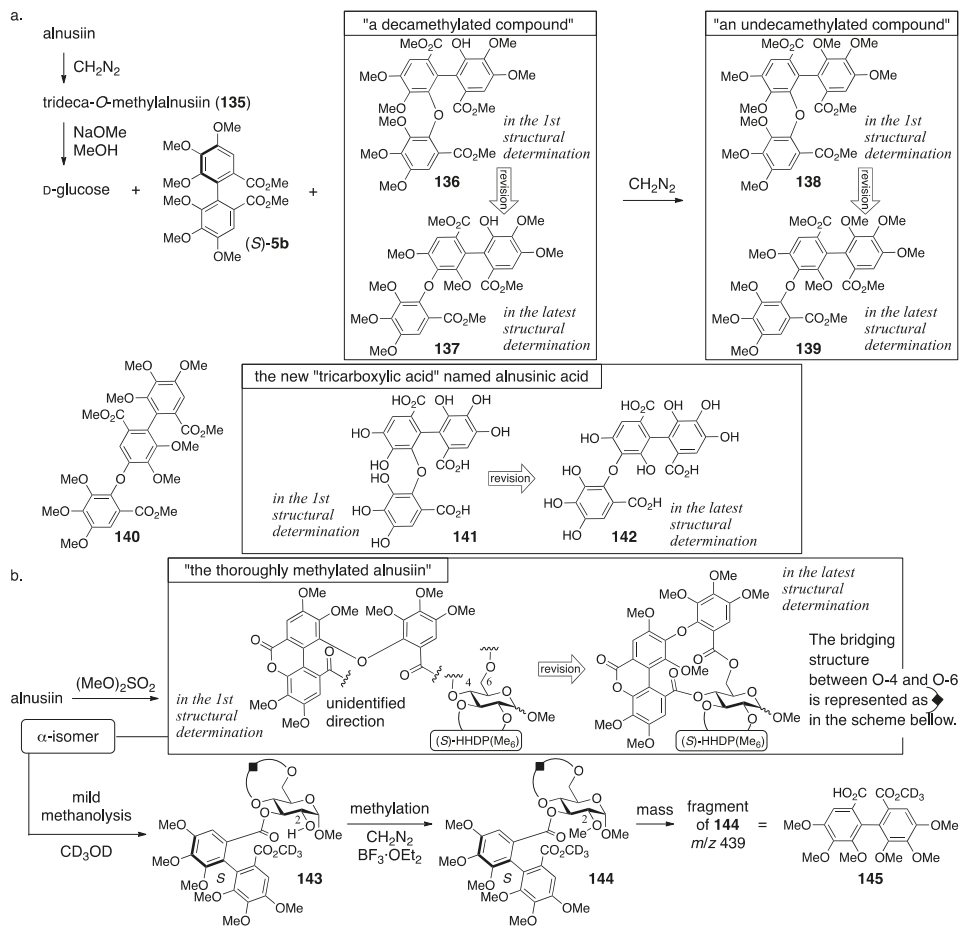
Figure 48. The information that led to **133**.

In the revision to the latest structure, the component bridging between O-4 and O-6 was changed from a derivative of the macaranoyl group to that of the tergalloyl group [97,99]. The hydrolysate of alnusiin was found to be **146a** (Figure 49). Methanolysis of the trideca-*O*-methylalnusiin (**135**) yielded **137**. These results limit the structure of the fragment to only **146b** and **146c**. An NMR analysis observing the [1]H–[13]C long-range shift correlations showed a cross-peak between H-3″ on the B-ring and a carbonyl carbon of lactone (see the thoroughly methylated alnusiin); hence, it was determined to be **146b**. The long-range correlation experiment also displayed cross-peaks between H-6‴ and C-2‴

and between H-6′′′ and a carbonyl carbon. In addition, the carbonyl carbon exhibited a correlation with the H-6 of glucose. These correlations are the conclusive evidence for the determination of the direction of the alnusinoyl (that is alnusinic acid monolactone) group in the structure of **134**. Note that the alnusinoyl group has the same framework as the tergalloyl group. The alnusinoyl group's name likely refers to the lactonized structure, but the name is used only in this report to the best of our knowledge. There is a report that calls the lactone fragment "the monolactonized tergalloyl group" [99].
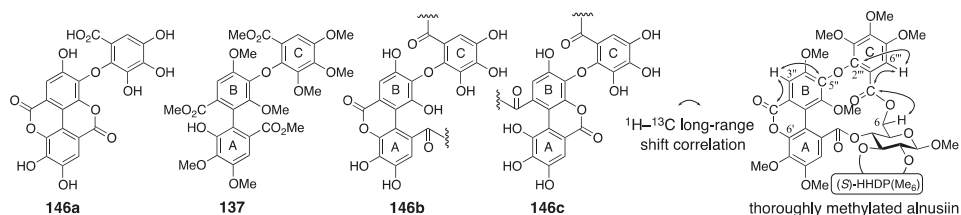
Figure 49. The compounds used for considering the latest structure of alnusiin **134**.

3.5.3. Alnusnin A and B

Alnusnin A and B were first isolated from *Alnus sieboldiana* and given their first structures **147** and **149**, respectively, by Nishioka in 1989 (Figure 50) [100]. In 1993, Nishioka isolated platycaryanin A and B. The determined structures of platycaryanins were **147** and **149**, respectively. Because platycaryanin A and B were not identical to alnusnin A and B, they reconsidered the structures. Each of the revised structures **148** and **150** contains a lactonized tergalloyl group [101].
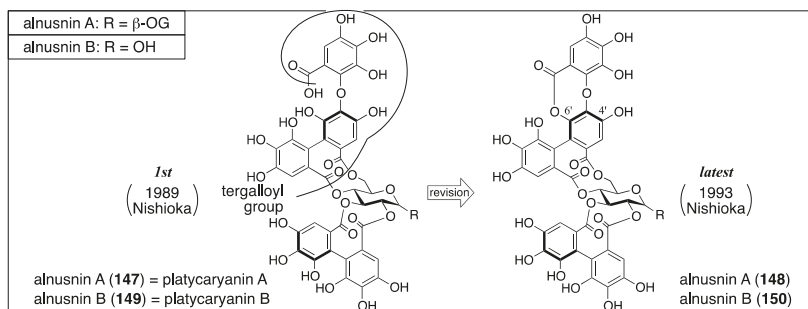
Figure 50. The transition of the structure of alnusnin A and B.

In the determination of the first structures of alnusnin A and B (**147** and **149**) [100], the presence of the galloyl, HHDP, and "triphenoyl" groups in alnusnin A were suggested by the ^{1}H/^{13}C-NMR spectra. Here, the "triphenoyl" means a component that has three hydroxylated benzoyl groups. The spectra of alnusnin A indicated that the chemical shifts and coupling patterns of sugar signals were in good agreement with those found in casuarictin ((aS,aS)-**2**) (Figure 51a) [47]. The hydrolysis of alnusnin A by tannase provided alnusnin B and gallic acid (Figure 51b). The FAB-MS spectra of alnusnin A and B supported their structures in terms of their molecular weights. The presence of the HHDP and triphenoyl groups in alnusnin B was indicated by the ^{1}H/^{13}C-NMR spectra with the information that the glucose moiety was in a hemiacetal form. The spectra also exhibited evidence that the signals, due to the sugar moiety, were similar to those found in the known **151**, of which the conformation of the glucose moiety was $^4C_1$. The information demonstrated that the HHDP and the triphenoyl groups were attached to the 2,3- and 4,6-positions of the glucose moiety. The structures of the HHDP and the triphenoyl groups were determined by comparison of (*S*)-**5b** and **139** (Figure 51c),

which is derived from alnusnin B, through the full-methylation of the hydroxy groups and subsequent methanolysis. The axial chirality of the (*S*)-HHDP group was provided by comparison of the optical rotation of **5b** derived from alnusnin B to the known **5b** [42]. The triphenoyl group was determined to be the tergalloyl group on the basis of the identical ^{1}H-NMR signals of **139** derived from alnusnin B to those of **139**-d_3 derived from a known compound, tergallagin (**152**), except for OCH$_3$ on C-6′ (Figure 51d) [84]. The *S*-axial chirality of the tergalloyl group was estimated by the similarity of its CD spectrum to that of the known (*S*)-**5b**. The 2,3-location of the (*S*)-HHDP group in alnusnin B was established by the fact that the partial hydrolysis of alnusnin B yielded the known (a*S*)-**20** [31] together with **146a** (Figure 51e) [84].
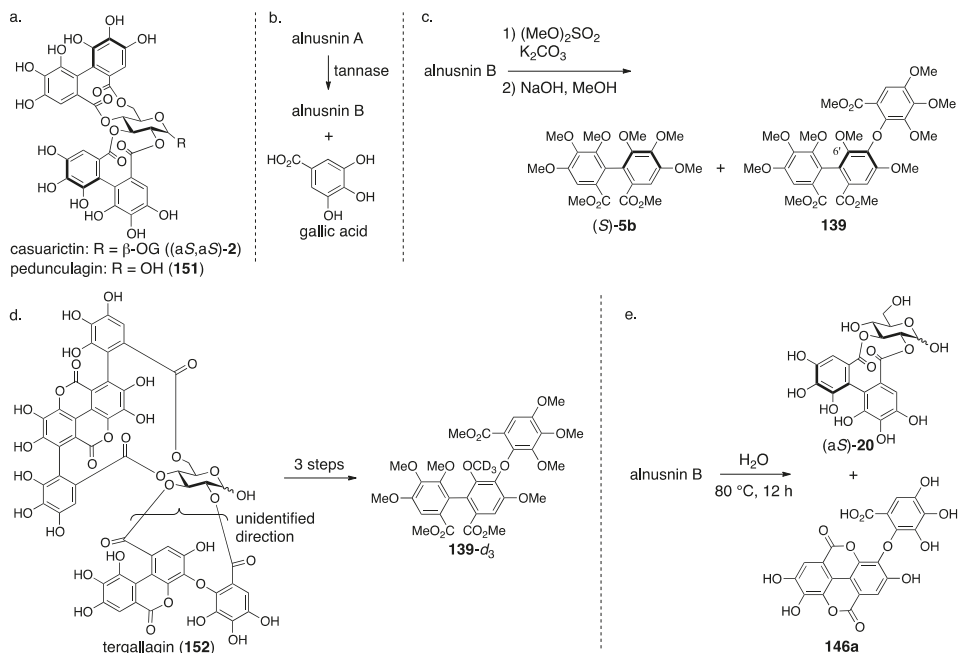
Figure 51. The transformations used in the determination of the first structures of alnusnin A (**147**) and B (**149**).

The discovery of platycaryanins A and B in 1993 triggered the structural revision of alnusnins A and B [101]. The structures **147** and **149** were given for the structures of platycaryanins A and B, respectively, on the basis of NMR studies and transformation to known compounds. Despite the identical structures of platycaryanins and alnusnins, their NMR spectra were different. Thus, the authors reinvestigated the structures of alnusnin A and B. In the reinvestigations, the FAB-MS of alnusnin A and B showed their molecular weights, both of which were 18 smaller than the molecular weights of structures **147** and **149**. Therefore, the authors supposed the lactone forms **148** and **150**. Lactonization was possible at O-4′ and O-6′, from which the position was determined to be O-6′ according to the ^{13}C-NMR chemical shifts and the ^{1}H–^{13}C long-range correlation spectroscopy (COSY) spectrum. The supposition was confirmed by the fact that the lactonization of platycaryanin B (**149**) using EDCI·HCl provided alnusnin B (**150**).

Hatano also isolated alnusnin A (**148**) and platycaryanin A (**147**) in 2012 [102]. In the NMR studies, they realized that: (1) the chemical shifts of H-3′ in the "depside bond"-forming lactonized (namely, depsidone) tergalloyl groups indicated more downfield shifts than those in the normal tergalloyl groups (Figure 52a); and (2) that the chemical shifts of H-6″ in the tergalloyl groups shift to be more upfield than those in the valoneoyl groups (Figure 52b). The "depside" refers to two aromatic moieties connected through an ester bond. These subtle but remarkable characteristics would be useful for structural determinations of other ellagitannins.
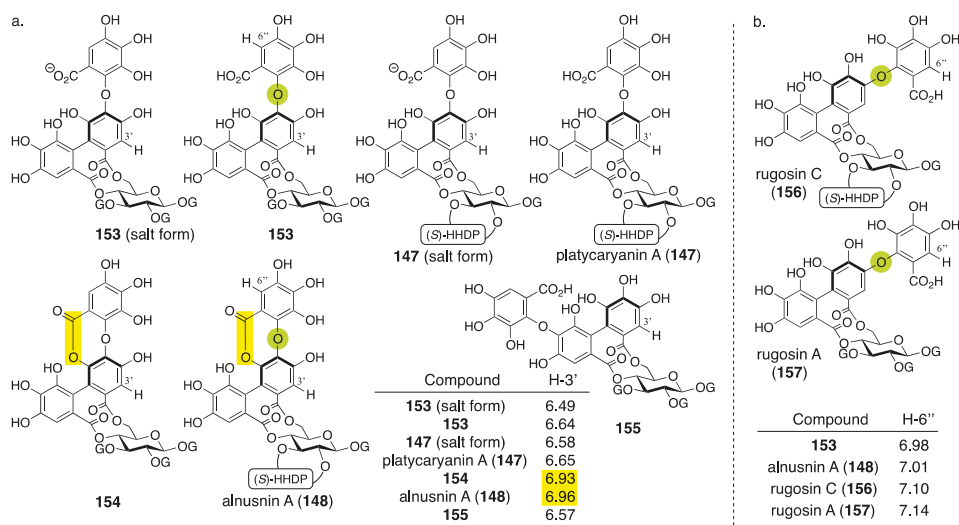
Figure 52. The notable difference of the ¹H-NMR chemical shift observed (**a**) between the lactonized and non-lactonized forms of the tergalloyl moieties and (**b**) between the tergalloyl and valoneoyl moieties. Yellow indicates lactone. Green indicates the oxygen of diaryl ethers listed in the Table in (**b**).

3.5.4. Nobotanin B, C, E, G, H, I, J, and K

Nobotanins are ellagitannins derived from *Tibouchina semidecandra* and other plants and involve 22 analogs: nobotanin A–V. Among them, the initial structures of B, C, E, and G–K have been revised (Figure 53). For the nobotanins, the isolations, structural determinations, and revisions were all conducted by Okuda. The first structure of nobotanin B (**158**) was provided in 1986 [103]. In the following year, the first structures of nobotanins C (**160**), E (**162**), G (**164**), H (**166**), I (**168**), and J (**170**) were determined [104]. In 1988, the tetrameric structure **172** was reported for nobotanin K [105]. The main point of the changes in the structural revisions was the direction of the valoneoyl group. Firstly, the structures of nobotanin B, C, and E were corrected to **159**, **161**, and **163**, respectively, in 1991 [106]. In the ensuing year, the latest structures were reported for nobotanin G (**165**), H (**167**), I (**169**), and J (**171**) [107]. The revision of nobotanin I involves the change of the direction of the valoneoyl group and of its lactone structure from the macrocyclic ring to the seven-membered one. In 1995, nobotanin K was corrected to be **173** [108].
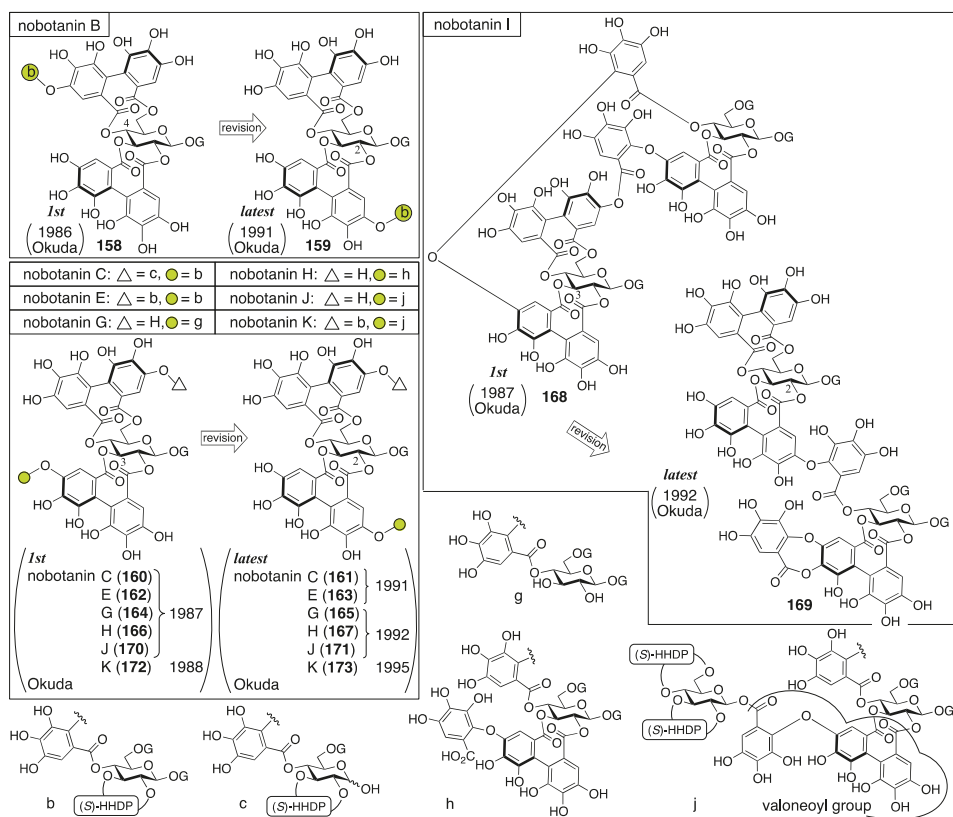
Figure 53. The transition of the structure of nobotanins B, C, E, G, H, I, J, and K. The green is merely a mark. The usage is the same in the following figures.

Among the nobotanins, initially, the first structure of nobotanin B (**158**) was determined along with nobotanin A, D, and F [103]. The CD and ^{1}H/^{13}C-NMR spectra indicated that nobotanin B was an isomer of nobotanin F (**174**) (Figure 54). In the hydrolysis of nobotanin B, the 1:1 production of isostrictinin ((aS)-**36**) [109] and **175** was observed at an early stage. The prolonged reaction time increased the yield of **176**. The structures for **175** and **176** were provided through a subsequent process. Thus, the ^{1}H-NMR and UV spectra of **175** and **176** indicated the existence of: (1) the galloyl group; and (2) the valoneoyl group, in which the HHDP part was lactonized to be the structure of ellagic acid. The reason for the determination, which was that one of the two galloyl groups was on O-1, was the observation that the tannase treatment of **175** provided a hydrolysate that reacted at O-1. The position of the HHDP group in **175**, which was between O-2 and O-3, came from comparison of the ^{1}H-NMR spectra of **175** and **176**. Regarding the remaining O-4 and O-6, on which the other galloyl group and the lactonized valoneoyl group were situated, their positions were determined on the basis of an unusual upfield shift (δ 6.89) of a hydrogen on one galloyl group. Okuda considered that the shift was the result of the magnetic anisotropy effect derived by the ellagic acid moiety. Because the shift was observed on only one of the galloyl groups, the authors distributed the second galloyl group onto O-6 and the lactonized valoneoyl onto O-4. Structure **158** was the combination of (aS)-**36** and **175**, with the exception of **174**.
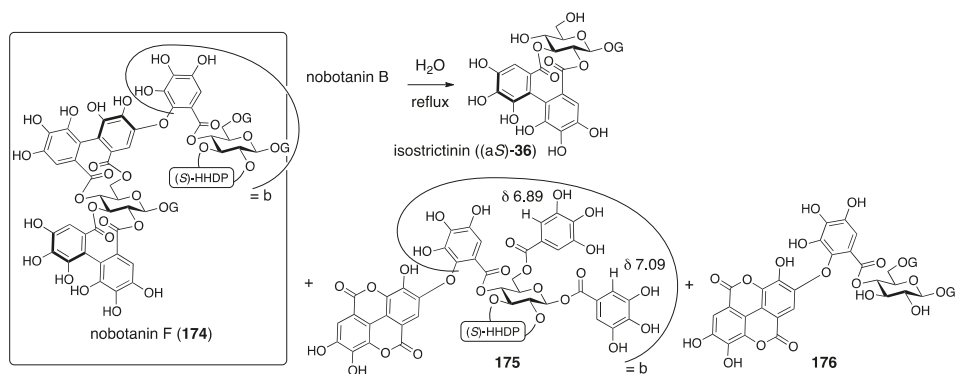
Figure 54. The information that led to the first structure of nobotanin B (**158**).

The first structures of nobotanins C (**160**) and E (**162**) were introduced on the basis of their hydrolysis [104]. The grounds for nobotanin C being a trimeric ellagitannin was its ^{1}H/^{13}C-NMR spectra and a GPC analysis. The ^{1}H-NMR indicated the existence of two valoneoyl, two HHDP, and four galloyl groups, each as a 5:3 pair of signals. Therefore, nobotanin C was assessed as a mixture of anomers. Hydrothermal degradation provided **175**, **176**, **177**, **178**, **179**, and **180** (Figure 55a). Among them, **175**, **176**, **177**, and **178** were the known degradation products of nobotanins B and F (**174**) [103]; **178** was identical to the degradation product of nobotanin A (**181**) [103]; and **179** was that which was derived from nobotanin B. Note that structure **179** should be corrected according to the structural revision of nobotanin B to the latest structure. The structure of **180** was presumed based on its ^{1}H-NMR spectrum. The *S*-axial chiralities for all the HHDP groups of nobotanin C were determined on the basis of the CD spectrum. Although arranging the above information could not narrow the direction of the valoneoyl group to one, structure **160** was illustrated according to the structure of nobotanin I, the structural determination of which is explained in the following paragraph. The reason that structure **162** was given for nobotanin E, which was the galloylated nobotanin C, was that the tannase hydrolysate of nobotanin E was nobotanin C (Figure 55b).
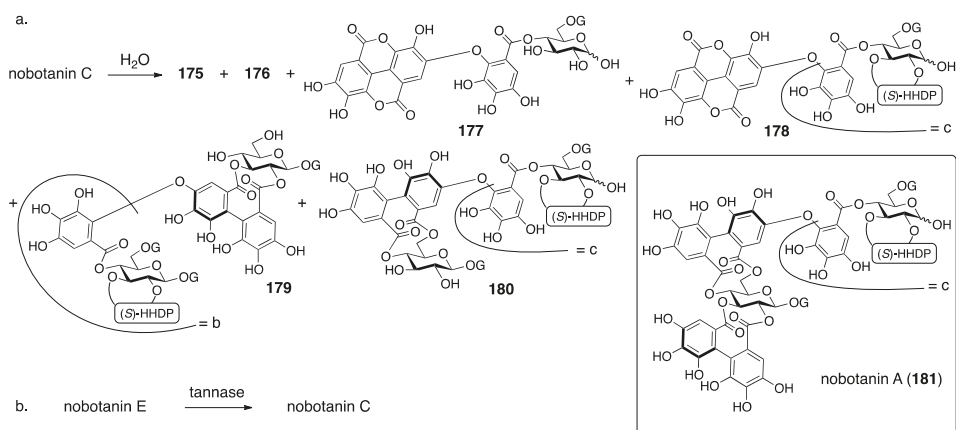
Figure 55. The information referred to in the structural determination of the first structures of nobotanins C (**160**) and E (**162**).

The first structures of nobotanins G (**164**), H (**166**), and I (**168**) were revealed by association of their hydrolysates to related known compounds [104]. The ¹H-NMR and COSY spectra led to the dimeric structure for nobotanin G, in which the O-2 and O-3 of one of the two glucoses were hydroxy groups and the other hydroxy groups were all acylated. With the observation that strictinin (**32**) and **176** were given as the hydrolysates (Figure 56) [103], structure **164** was provided. The reason for the determined direction of the valoneoyl group is described later. Nobotanin H was presumed to have the structure that a valoneoyl group was attached to nobotanin G on the basis of the ¹H-NMR and COSY spectra. The additional information that the hydrolysis of nobotanin H produced **32** and nobotanin G led to structure **166**. Leaving a 0.1% aqueous solution of nobotanin I at 37 °C for 36 h provided nobotanin H quantitatively. In addition, leaving a solution of nobotanin I in MeOH at room temperature for a week provided a methanolysate of nobotanin I (**182**) quantitatively. Such hydrolysis and methanolysis that proceeded under mild conditions had been observed on compounds containing depside bonds (Section 3.5.3 for the meaning of depside). Therefore, the results strongly supposed the existence of a depside bond in nobotanin I. The comparison of the ¹³C-NMR spectra of nobotanin H to nobotanin I demonstrated that the signals at δ 166.8 and 137.7 of nobotanin H were shifted to a higher magnetic field to be δ 163.2 and 132.2, respectively. By contrast, the signal δ 145.2 of nobotanin H shifted lower to be δ 151.7 in nobotanin I. This phenomenon had been observed in the comparison of rugosin C (**156**) and praecoxin C (**184**) [110]. Accordingly, the structure of nobotanin I was considered to have a lactonized structure of nobotanin H, where the direction of the valoneoyl group was attributed by considering a molecular model in which the diaryl ether part was situated on the O-3 side of the glucose. Hence, the structure was **168** (Figure 53). The determined direction of the valoneoyl group affected the structure of nobotanins C (**160**), E (**162**), G (**164**), and H (**166**).
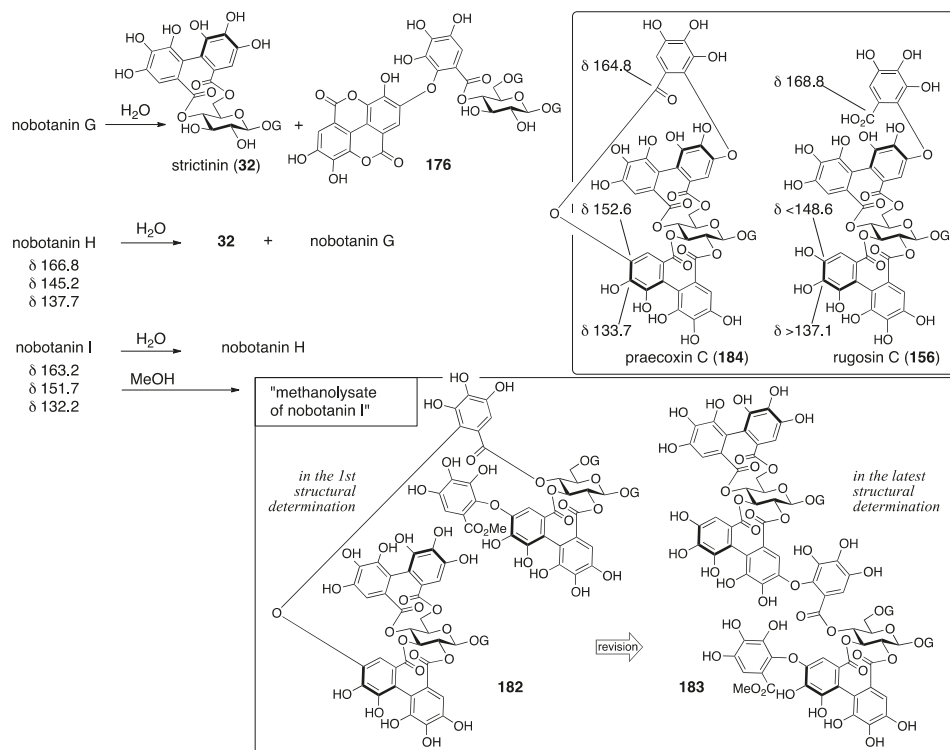
Figure 56. The observations that led to the first structures of nobotanins G, H, and I (**164**, **166**, and **168**).

The first structure of nobotanin J (**170**) was determined according to its fragments [104]. The ^{1}H/^{13}C-NMR spectra indicated: (1) that the compound was trimeric; (2) the existence of two valoneoyl, three HHDP, and three galloyl groups; and (3) that all the hydroxy groups of glucose were acylated. A dilute aqueous solution of nobotanin J hydrolyzed it to provide pedunculagin (**151**) and nobotanin H (Figure 57). Leaving its methanol solution at room temperature gave a compound that was the same as the "methanolysate of nobotanin I" and **151**.
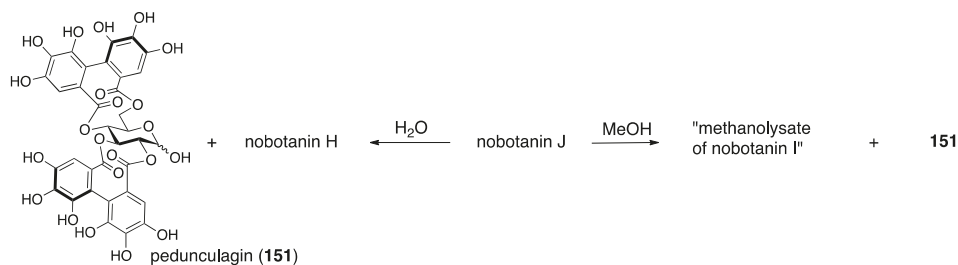
Figure 57. The transformation used in the structural determination for the first structure of nobotanin J (**170**).

For the structural determination of nobotanin K (**172**), nothing has been reported to international journals. A summary of a conference presentation suggests that the structure was identified on the basis of a comparison of the decomposed product of nobotanin K to nobotanins E and J [105].

Okuda revised nobotanins B, C, and E to their latest structures, **159**, **161**, and **163**, respectively, in 1991 [106]. In the structural revision of nobotanin B, the position of the valoneoyl group was changed. It had been known that the NMR chemical shifts of hydrogens on the HHDP moiety of a valoneoyl group indicated an obvious difference at the sides with and without the aryl-O-aryl bond [111–113]. According to this knowledge, the hydrogens H$_A$ and H$_B$ of the valoneoyl groups were assigned as illustrated in Figure 58a. Among them, the H$_A$ (δ 6.45) was associated with the H-3′ of glucose in a ^{1}H–^{13}C long-range COSY experiment, which determined the direction of the valoneoyl group. In addition, the long-range data ensured that the galloyl moiety of the valoneoyl group was attached to the O-4 of glucose, the bonding position of which had remained uncertain since the structural determination in 1986. Note that the clear differences in the chemical shifts—δ H-4′ < δ H-4 and δ H-5′ > δ H-5—were observed in the ^{1}H-NMR spectrum of nobotanin B. This phenomenon is a common feature when the HHDP part of a valoneoyl group is attached to the O-2′ and O-3′ of one glucose and the galloyl part is connected to the O-4 of the other glucose as seen in **159** [113]. In the revision to the latest structure of nobotanin C (**161**), the following three facts served as the evidence. First, the differences in the chemical shifts between H-4′ and H-4 and between H-5′ and H-5 were similar to those in nobotanin B (Figure 58b). Second, in the ^{1}H/^{13}C-NMR spectrum, the signals due to glucose moieties resembled those of nobotanin B and praecoxin B ((a*S*)-**17**) [110] closely. Third, compound **185** was found among the hydrolysates of nobotanin C. The structure of **185** was revealed using ^{1}H-NMR and mass spectra. Nobotanin E had been known as galloylated nobotanin C (Figure 55b); therefore, the structure was revised to be **163**.
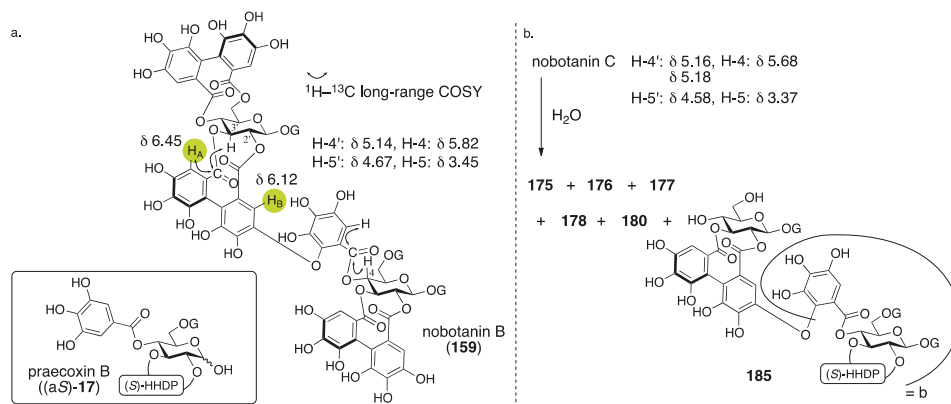
Figure 58. The data used for the revision to the latest structures of nobotanins B, C, and E (**159**, **161**, and **163**, respectively).

The common point in the revision to the latest structures of nobotanins G–J is the overturning of the valoneoyl group [107,114]. The structural revision of nobotanin G was ascribed to the observations that: (1) the differences in the chemical shifts between H-4′ and H-4 and between H-5′ and H-5 were similar to those in nobotanin B; and (2) that **186** was found among the hydrolysates of nobotanin G (Figure 59a). The grounds for the structural revision of nobotanin H were: (1) the similar differences in the chemical shifts between H-4′ and H-4 and between H-5′ and H-5; and (2) the ^{1}H–^{13}C long-range shift correlation coherence spectroscopy (COLOC) (see **167** in Figure 59b). The bases for the structural revision of nobotanin I were: (1) the revision of nobotanin H; and (2) the comparison of the ^{13}C-NMR chemical shifts of nobotanin H to rugosin A (**157**) [112] and prostratin C (**187**) [115,116]. Regarding the assertion (1), as nobotanin H was a hydrolysate of nobotanin I (Figure 56), the structural revision of nobotanin H affected the structure of nobotanin I. In terms of the assertion (2), the feature of the ^{13}C-NMR chemical shifts of the carbons that might construct the seven-membered lactone observed in the non-lactonized **157** and the lactonized **187** were exactly like those observed in nobotanins H and I [115]. The structural revision of nobotanin J came from the revision of nobotanin H.

The structure of nobotanin K was revised in 1995 [108]. On the occasion of the revision, the tetrameric structure and existence of three valoneoyl, three HHDP, and five galloyl groups were reconfirmed. Another reaffirmation was that nobotanin K had a structure that was composed of nobotanin J and pterocaryanin C ((aS)-**16**), which was carried out by a comparison of the NMR data of it to nobotanin J and (aS)-**16** [114]. Therefore, the structure of nobotanin K was influenced by the revision of nobotanin J. The hydrothermal degradation of nobotanin K provided **175** (Figure 60), which had also been obtained by the hydrolysis of nobotanins B, E, and F (**174**). On the other hand, the methanolysis of nobotanin K gave **188** and **189** in addition to **151**. The structures of **188** and **189** were determined on the basis of their ^{1}H-NMR spectra. Taking the above information together, the structure was revised to **173**.
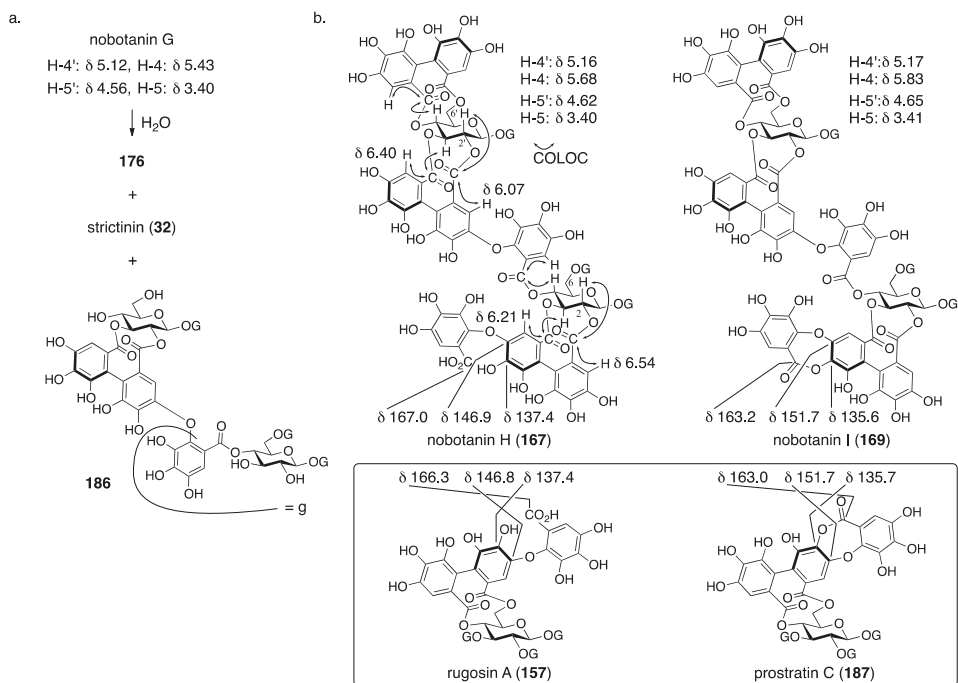
Figure 59. The information that led to the latest structures of nobotanins G, H and I (**165**, **167** and **169**, respectively).
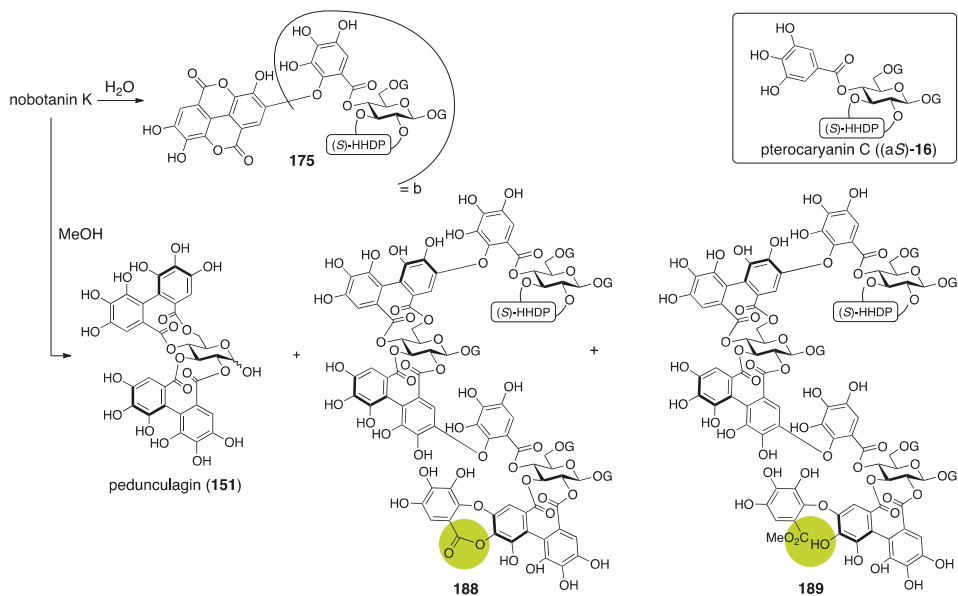
Figure 60. The information used for the revision to the latest structure of nobotanin K (**173**).

4. Summary

Table 1 summarizes the causes for wrong structures, how the error was realized, and the methods used for latest structural revision for each ellagitannin introduced in this review. The content given to each item is expressed roughly since the principal description has already been given in Section 3. The most common cause for a wrong structure is in a prediction based on "similarity" (red text), where CD/ORD is the most-used data for the similarity.

Table 1. Causes for wrong structures, how the error was realized, and methods used for the latest structural confirmation.

Section	Compound Name	Cause(s) for Wrong Structure	How the Error Was Realized	Methods Used for Latest Structural Confirmation
4.1.1.	corilagin	Prediction based on similarity of CD/ORD spectra	unclear	Identification with a known fragment Total synthesis and identification
4.1.2.	punigluconin	Misassignment of NMR data	Structural determination of analogous compounds	NMR studies
4.1.3.	cercidinins A and B	Prediction based on similarity of NMR data with analogous compounds	Total synthesis	NMR studies with long-range methods Total synthesis and identification
4.1.4.	roxbin B	Prediction based on similarity of CD/ORD spectra	Total synthesis	Identification of NMR data to a known compound Total synthesis and identification
4.2.1	geraniin	Misinterpretation of NMR data	Contradiction between NMR data and reported structure	NMR studies Single-crystal X-ray diffraction
4.2.2.	terchebin	Prediction based on analogous compounds Incorrect experimental results	Contradiction between NMR data and reported structure	Structural determination from the beginning
4.2.3.	isoterchebin	Incorrect experimental results	Identification of the reported structure to the other compound	Structural determination from the beginning involving identification
4.3.	chebulinic acid and chebulagic acid	Unreasonable structure determination under lack of evidence	Contradiction between NMR data and reported structure	Structural determination from the beginning Single-crystal X-ray diffraction of a fragment
4.4.1.	castalin, vescalin, castalagin, vescalagin, casuarinin, and stachyurin	Misinterpretation of NMR data Prediction based on similarity of CD/ORD spectra	unclear	NMR studies Chemical calculation Total synthesis and identification
4.4.2.	punicalin and punicalagin	Use of molecular model for the final basis	Structural determination of analogous compounds	Structural determination from the beginning involving identification
4.5.1	sanguiin H-2, H-3, and H-6	Prediction based on similarity of CD/ORD spectra	Structural determination of analogous compounds	Structural determination from the beginning Synthesis of a fragment and identification
4.5.2.	alnusiin	Use of the additivity of the substituent effect in the ^{13}C-NMR spectrum	unclear	NMR studies with long-range methods
4.5.3	alnusnins A and B	Incorrect experimental results	Structural determination of analogous compounds	Correct mass spectra
4.5.4.	nobotanins B, C, E, G, H, I, J, and K	Prediction based on wrong structures Use of molecular model for the final basis	Structural determination of analogous compounds	NMR studies with long-range methods

Red: prediction based on "similarity". Green: structural determination on similar compounds. Lite blue: contradiction between NMR data and the reported structure. Blue: methods based on identification. Purple: use of long-range correlation methods in NMR spectroscopy. CD, circular dichroism; ORD, optical rotatory dispersion.

The most common reason for noticing structural errors is a structure determination on similar compounds (green text). A contradiction between NMR data and the reported structure is also a common reason (light blue text). Indication of errors in ellagitannin structures by total synthesis is a minor reason.

In the latest structural determination, methods based on identification are chiefly used (blue text). The reason why there are only two examples using X-ray analysis is probably due to the unique circumstances of ellagitannins, for which it is difficult to obtain good single crystals. The long-range correlation methods in NMR spectroscopy, such as the HMBC method, which had been generalized in the 1990s, is quite useful for a structural determination on ellagitannins (purple text). Structure determination incorporating support for chemical calculation is a new trend, and this method revised the structures of castalin, vescalin, castalagin, and vescalagin 25 years after the previous structure determination (Section 3.4.1). These are revisions of those structures that had previously been "believed". By the way, among the ellagitannins appearing in this review, the initial structure of roxbin B ((a*S*,a*S*)-**27**) had been believed for 27 years, which is the longest period. However, roxbin B disappeared as the compound was found to have the same structure as an already known ellagitannin, cuspinin ((a*R*,a*S*)-**2**) (Section 3.1.4).

Recently, support for computational chemistry in structure determination [117] and techniques for an X-ray diffraction analysis without crystallization are advancing [118]. As examples that have already been used in the structural revision of ellagitannins, these new methods might change the isolation/structural determination protocols, together with the advancement of separation methods, to enable the use of smaller amounts of samples with a shorter time period. In the course of promoting the new methods, verification using "identification" based on reliable information will be important.

Conflicts of Interest: The authors declare no conflict of interest.

Abbreviations

Ac	acetyl
All	allyl
aq	aqueous
Bn	benzyl
CD	circular dichroism
COLOC	correlation spectroscopy via long-range coupling spectrum
conc	concentrated
COSY	correlation spectroscopy
D	deuterium, dextrorotatory
DCC	*N,N'*-dicyclohexylcarbodiimide
DFT	density functional theory
DHHDP	dehydrohexahydroxydiphenoyl
DIS	differential isotope shift
DMAP	4-(dimethylamino)pyridine
DMF	*N,N*-dimethylformamide
DMSO	dimethyl sulfoxide
ECD	electronic circular dichroism
EDCI·HCl	1-(3-dimethylaminopropyl)-3-ethylcarbodiimide hydrochloride
Et	ethyl
epi	epimer
FAB-MS	fast atom bombardment-mass spectrometry
G	galloyl
G(Ac₃)	tri-*O*-acetylgalloyl

G(Bn₃)	tri-*O*-benzylgalloyl
G(All₂Bn)	3,5-di-*O*-allyl-4-*O*-benzylgalloyl
G(Me₃)	tri-*O*-methylgalloyl
GPC	gel permeation chromatography
h	hour(s)
HHDP	hexahydroxydiphenoyl
HHDP(Me₆)	hexa-*O*-methyl-hexahydroxydiphenoyl
HMBC	hetero-nuclear multiple-bond coherence
i	iso
IR	infrared
Me	methyl
MP	4-methoxyphenyl
MS	mass spectrum (or spectra)
MS 4A	molecular sieves 4A
n	normal
NHTP	nonahydroxytriphenoyl
NMR	nuclear magnetic resonance
NOE	nuclear Overhauser effect
ORD	optical rotatory dispersion
Ph	phenyl
Pr	propyl
rac	racemic
rt	room temperature
t	tertiary
TBAF	tetra-*n*-butylammonium fluoride
TBS	*t*-butyldimethylsilyl
THF	tetrahydrofuran
UV	ultraviolet

References

1. Okuda, T. Novel aspects of tannins–Renewed concepts and structure-activity relationships. *Curr. Org. Chem.* **1999**, *3*, 609–622.
2. Ascacio-Valdés, J.A.; Fuenrostro-Figueroa, J.J.; Aguilera-Carbo, A.; Prado-Barragán, A.; Rodríguez-Harrera, R.; Aguilar, C.N. Ellagitannins: Biosynthesis, biodegradation and biological properties. *J. Med. Plants Res.* **2011**, *5*, 4696–4703.
3. Quideau, S. *Chemistry and Biology of Ellagitannins—An Underestimated Class of Bioactive Plant Polyphenols*; World Scientific: Singapore, 2009.
4. Okuda, T.; Ito, H. Tannins of constant structure in medicinal and food plants—Hydrolyzable tannins and polyphenols related to tannins. *Molecules* **2011**, *16*, 2191–2217. [CrossRef]
5. Quideau, S.; Deffieux, D.; Douat-Casassus, C.; Pouységu, L. Plant polyphenols: Chemical properties, biological activities, and synthesis. *Angew. Chem. Int. Ed.* **2011**, *50*, 586–621.
6. Schmidt, O.T.; Mayer, W. Natürliche Gerbstoffe. *Angew. Chem.* **1956**, *68*, 103–115.
7. Haslam, E. Gallic acid and its metabolites. In *Plant Polyphenols*; Hemingway, R.W., Laks, P.E., Eds.; Springer: New York, NY, USA, 1992; pp. 169–194.
8. Haslam, E. *Che Faro Senza Polifenoli: Plant Polyphenols 2*; Gross, G.G., Hemingway, R.W., Yoshida, T., Eds.; Springer: New York, NY, USA, 1999; pp. 15–40.
9. Niemetz, R.; Schilling, G.; Gross, G.G. Ellagitannin biosynthesis: Oxidation of pentagalloylglucose to tellimagrandin II by an enzyme from *Tellima grandiflora* leaves. *Chem. Commun.* **2001**, *1*, 35–36. [CrossRef]
10. Niemetz, R.; Gross, G.G. Oxidation of pentagalloylglucose to the ellagitannin, tellimagrandin II, by a phenol oxidase from *Tellima grandiflora* leaves. *Phytochemistry* **2003**, *62*, 301–306. [CrossRef]
11. Buckingham, J. Tannins. In *Dictionary of Natural Products*; Chapman & Hall: London, UK, 1994.
12. Pouységu, L.; Deffieux, D.; Malik, G.; Natangelo, A.; Quideau, S. Synthesis of ellagitannin natural products. *Nat. Prod. Rep.* **2011**, *28*, 853–874. [PubMed]

13. Li, H.; Tanaka, T.; Zhang, Y.J.; Yang, C.R.; Kouno, I.; Rubusuaviins, A.F. Monomeric and Oligomeric Ellagitannins from Chinese Sweet Tea and Their α-Amylase Inhibitory Activity. *Chem. Pharm. Bull.* **2007**, *55*, 1325–1331. [CrossRef] [PubMed]

14. Ishimaru, K.; Nonaka, G.I.; Nishioka, I. Tannins and related compounds. LV. Isolation and characterization of acutissimins A and B, novel tannins from *Quercus* and *Castanea* species. *Chem. Pharm. Bull.* **1987**, *35*, 602–610. [CrossRef]

15. Lee, M.W.; Tanaka, T.; Nonaka, G.I.; Nishioka, I. Hirsunin, an ellagitannin with a diarylheptanoid moiety, from Alnus hirsuta var. Microphylla. *Phytochemistry* **1992**, *31*, 967–970.

16. Amagata, T. Misaligned Structures: Case Examples from the Past Decade. In *Comprehensive Natural Products II, Chemistry and Biology*; Liu, H.W., Ed.; Elsevier: Amsterdam, The Netherlands, 2010; Volume 2, pp. 581–621.

17. Suyama, T.L.; Gerwick, W.H.; McPhail, K.L. Survey of marine natural product structure revisions: A synergy of spectroscopy and chemical synthesis. *Bioorg. Med. Chem.* **2011**, *19*, 6675–6701. [CrossRef] [PubMed]

18. Fridolin. Chebulinic acid. *Chem. Zentralbl.* **1884**, 641.

19. Partridge, S.M. Aniline Hydrogen Phthalate as a Spraying Reagent for Chromatography of Sugars. *Nature* **1949**, *164*, 443. [CrossRef] [PubMed]

20. Schmidt, O.T.; Lademann, R. Corilagin, ein weiterer kristallisierter gerbstoff aus dividivi. *Liebigs Ann. Chem.* **1951**, *571*, 232–237. [CrossRef]

21. Schmidt, O.T.; Schmidt, D.M.; Herok, J. Die konstitution und konfiguration des corilagins XIX. Mitteilung uber natürliche gerbstoffe. *Liebigs Ann. Chem.* **1954**, *587*, 67–74. (In German) [CrossRef]

22. Mislow, K.; Glass, M.A.W.; O'brien, R.E.; Rutkin, P.; Steinberg, D.H.; Weiss, J.; Djerassi, C. Configuration, conformation and rotatory dispersion of optically active biaryls. *J. Am. Chem. Soc.* **1962**, *84*, 1455–1478. [CrossRef]

23. Okuda, T.; Yoshida, T.; Hatano, T. Equilibrated stereostructures of hydrated geraniin and mallotusinic acid. *Tetrahedron Lett.* **1980**, *21*, 2561–2564. [CrossRef]

24. Schmidt, O.T.; Blinn, F.; Lademann, R. Über die bindung der ellagsäure in corilagin und chebulagsäure. XII. Mitteilung über natürliche gerbstoffe. *Liebigs Ann. Chem.* **1952**, *576*, 75–84. (In German) [CrossRef]

25. Reeves, R.E.; Goebel, W.F. Chemoimmunological studies on the soluble specific substance of pneumococcus V. The structure of the type III polysaccharide. *J. Biol. Chem.* **1941**, *139*, 511–519.

26. For β-isomer: Adams, M.H.; Reeves, R.E.; Goebel, W.F. The synthesis of 2,4-dimethyl-β-methylglucoside. *J. Biol. Chem.* **1941**, *140*, 653–661.

27. Schmidt, O.T.; Herok, J. α-Glucogallin XVIII. Mitteilung über natürliche gerbstoffe. *Liebigs Ann. Chem.* **1954**, *587*, 63–66. (In German) [CrossRef]

28. Jochims, J.C.; Taigel, G.; Schmidt, O.T. Uber natürliche gerbstoffe, XLI. Protonenresonanz-spektren und konformationsbestimmung einiger natürlicher gerbstoffe. *Liebigs Ann. Chem.* **1968**, *717*, 169–185. (In German)

29. Schmidt, O.T.; Demmler, K. Racemische und optisch aktive 2,3,4,2′,3′,4′-hexaoxydiphenyl-6,6′-dicarbonsaure. XVII. Mitteilung uber natürliche gerbstoffe. *Liebigs Ann. Chem.* **1954**, *586*, 179–193. (In German) [CrossRef]

30. Hatano, T.; Yoshida, T.; Shingu, T.; Okuda, T. ^{13}C Nuclear magnetic resonance spectra of hydrolyzable tannins. III. Tannins having ^{1}C$_4$ glucose and C-glucosidic linkage. *Chem. Pharm. Bull.* **1988**, *36*, 3849–3856.

31. Seikel, M.K.; Hills, W.E. Hydrolysable tannins of *Eucalyptus delegatensis* wood. *Phytochemistry* **1970**, *9*, 1115–1128.

32. Okuda, T.; Yoshida, T.; Nayeshiro, H. Geraniin, a new ellagitannin from *Geranium thunbergii. Tetrahedron Lett.* **1976**, 3721–3722. [CrossRef]

33. Luger, P.; Weber, M.; Kashino, S.; Amakura, Y.; Yoshida, T.; Okuda, T.; Beurskens, G.; Dauter, Z. Structure of the tannin geraniin based on conventional X-ray data at 295 K and on synchrotron data at 293 and 120 K. *Acta Cryst.* **1998**, *B54*, 687–694. [CrossRef]

34. Yamada, H.; Nagao, K.; Dokei, K.; Kasai, Y.; Michihata, N. Total synthesis of (–)-corilagin. *J. Am. Chem. Soc.* **2008**, *130*, 7566–7567. [CrossRef] [PubMed]

35. Tanaka, T.; Nonaka, G.-I.; Nishioka, I. Tannins and related compounds. XLI. Isolation and characterization of novel ellagitannins, punicacorteins A, B, C and D, and punigluconin from the bark of *Punica granatum* L. *Chem. Pharm. Bull.* **1986**, *34*, 656–663. [CrossRef]

36. Tanaka, T.; Tong, H.-H.; Xu, Y.-M.; Ishimaru, K.; Nonaka, G.-I.; Nishioka, I. Tannins and related compounds. CXVII. Isolation and characterization of three new ellagitannins, lagerstannins A, B, and C, having a gluconic acid core, from *Lagerstroemia speciosa* (L.) P$_{ERS}$. *Chem. Pharm. Bull.* **1992**, *40*, 2975–2980. [CrossRef]

37. Okuda, T.; Yoshida, T.; Ashida, M. Casuarictin and casuarinin, two new ellagitannins from *Casuarina stricta*. *Heterocycles* **1981**, *16*, 1681–1685.

38. Nonaka, G.-I.; Ishimatsu, M.; Ageta, A.; Nishioka, I. Tannins and related Compounds. LXXVI. Isolation and characterization of cercidinins A and B and cuspinin, unusual 2,3-(*R*)-hexahydroxydiphenoyl glucoses from *Cercidiphyllum japonicum and Castanopsis cuspidate* var. *sieboldii*. *Chem. Pharm. Bull.* **1989**, *37*, 50–53.

39. Khanbabaee, K.; Lötzerich, K. Synthesis of enantiomerically pure unusual ellagitannins 1,4,6-tri-*O*-galloyl 2,3-(*R*)-hexahydroxydiphenoyl-β-ᴅ-glucoside. The proposed chemical structures for cercidinin A and B must be revised. *J. Org. Chem.* **1998**, *63*, 8723–8728. [CrossRef]

40. Tanaka, T.; Nonaka, G.-I.; Ishimatsu, M.; Nishioka, I.; Kouno, I. Revised structure of cercidinin A, a novel ellagitannin having (*R*)-hexahydroxydiphenoyl esters at the 3,4-postions of glucopyranose. *Chem. Pharm. Bull.* **2001**, *49*, 486–487. [CrossRef] [PubMed]

41. Yamada, H.; Ohara, K.; Ogura, T. Total synthesis of cercidinin A. *Eur. J. Org. Chem.* **2013**, 7872–7875. [CrossRef]

42. Ikeya, K.; Taguchi, H.; Yoshioka, I.; Kobayashi, H. The constituents of *Schisandra chinensis* BAILL. I. Isolation and structure determination of five new lignans, gomisin A, B, C, F, and G, and the absolute structure of schizandrin. *Chem. Pharm. Bull.* **1979**, *27*, 1383–1394. [CrossRef] [PubMed]

43. Tanaka, T.; Nonaka, G.-I.; Nishioka, I. Tannins and related compounds. Part 28. Revision of the structures of sanguiins H-6, H-2, and H-3, and isolation and characterization of sanguiin H-11, a novel tetrameric hydrolysable tannin, and seven related tannins, from *Sanguisorba officinalis*. *J. Chem. Res. (S)* **1985**, 176–177.

44. Yoshida, T.; Chen, X.; Hatano, T.; Fukushima, M.; Okuda, T. Tannins and related polyphenols of rosaceous medicinal plants. IV. Roxbin A and B from *Rosa roxburghii* Fruits. *Chem. Pharm. Bull.* **1987**, *35*, 1817–1822. [PubMed]

45. Yamaguchi, S.; Ashikaga, Y.; Nishii, K.; Yamada, H. Total synthesis of the proposed structure of roxbin B; the nonidentical outcome. *Org. Lett.* **2012**, *14*, 5928–5931. [CrossRef] [PubMed]

46. Yamaguchi, S.; Hirokane, T.; Yoshida, T.; Tanaka, T.; Hatano, T.; Ito, H.; Nonaka, G.-I.; Yamada, H. Roxbin B is cuspinin: Structural revision and total synthesis. *J. Org. Chem.* **2013**, *78*, 5410–5417. [CrossRef] [PubMed]

47. Gupta, R.K.; Al-Shari, S.M.K.; Layden, K.; Haslam, E. The metabolism of gallic acid and hexahydroxydiphenic acid in plant. Esters of (*S*)- hexahydroxydiphenic acid with ᴅ-glucopyranose($^4C_1$). *J. Chem. Perkin. Trans.* **1982**, *1*, 2525–2534. [CrossRef]

48. Okuda, T.; Yoshida, T.; Nayeshiro, H. Constituents of *Geranium thunbergii* S$_{IEB}$. *et* Zucc. IV. Ellagitannins. (2). Structure of geraniin. *Chem. Pharm. Bull.* **1977**, *25*, 1862–1869.

49. Okuda, T.; Nayeshiro, H.; Seno, K. Structure of geraniin in the equilibrium state. *Tetrahedron Lett.* **1977**, *18*, 4421–4424. [CrossRef]

50. Schmidt, O.T.; Voigt, H.; Puff, W.; Köster, R. Benzyläther der ellagsäure und hexaoxy-diphensäure XVI. Mitteilung über natürliche gerbstoffe. *Liebigs Ann. Chem.* **1954**, *586*, 165–178. (In German)

51. Pfeffer, P.E.; Valentine, K.M.; Parrish, F.W. Deuterium-induced differential isotope shift ^{13}C NMR. 1. Resonance reassignments of mono- and disaccharides. *J. Am. Chem. Soc.* **1979**, *101*, 1265–1274. [CrossRef]

52. Schmidt, O.T.; Schulz, J.; Wurmb, R. Uber natürliche gerbstoffe, XXXVI. Terchebin. *Liebigs Ann. Chem.* **1967**, *706*, 169–179. (In German) [CrossRef]

53. Okuda, T.; Hatano, T.; Nitta, H.; Fujii, R. Hydrolysable tannins having enantiomeric dehydrohexahydroxydiphenoyl group: Revised structure of terchebin and structure of granatin B. *Tetrahedron Lett.* **1980**, *21*, 4361–4364. [CrossRef]

54. Schmidt, O.T.; Klinger, G. Über natürliche gerbstoffe XXVIII. Synthese der 1.3.6-trigalloyl-glucose. *Liebigs Ann. Chem.* **1957**, *609*, 199–208. [CrossRef]

55. Schmidt, O.T.; Schanz, R.; Eckert, R.; Wurmb, R. Über natürliche gerbstoffe, XXXIV. Brevilagin 1. *Liebigs Ann. Chem.* **1967**, *706*, 131–153. (In German) [CrossRef]

56. Tillmans, J.; Hirsch, P.; Hirsch, W. Uber die anwendung von 2,6-dichlorphenol-indophenol als reduktionsindicator bei der untersuchung yon lebensmitteln. *Z. Unters. Lebensm.* **1928**, *56*, 272–292. (In German) [CrossRef]

57. Schmidt, O.T.; Hensler, R.H.; Stephan, P. Über natürliche gerbstoffe XXVI. *Neochebulagsäure Liebigs Ann. Chem.* **1957**, *609*, 186–191. (In German)

58. Schmidt, O.T.; Demmler, K.; Bittermann, H. Über natürliche gerbstoffe XXVII. Neochebulinsäure und 1.3.6-trigalloyl-glucose. *Liebigs Ann. Chem.* **1957**, *609*, 192–199. (In German) [CrossRef]

59. Fürstenwerth, H.; Schildknecht, H. Isoterchebin, der gerbe Farbestoff des Zistrosenwürgers *Cytinus hypocistis* (Rafflessiaceae, Schmarotzerblumengewächse). *Liebigs Ann. Chem* **1976**, 112–123. (In German) [CrossRef]

60. Okuda, T.; Hatano, T.; Yasui, T. Revised structure of isoterchebin, isolated from *Cornus Officinalis*. *Heterocycles* **1981**, *16*, 1321–1324. [CrossRef]

61. Nonaka, G.I.; Matsumoto, Y.; Nishioka, I.; Nishizawa, M.; Yamagishi, T. Trapain, a new hydrolysable tannin from *Trapa japonica* Flerov. *Chem. Pharm. Bull.* **1981**, *29*, 1184–1187. [CrossRef]

62. Schmidt, O.T.; Bernauer, K. Brevifolin and Brevifolin-carbosäure XXI. Mitteilung über natürliche Gerbstoffe. *Libigs Ann. Chem.* **1954**, *588*, 211–230. (In German) [CrossRef]

63. Schmidt, O.T.; Wurmb, R.; Schulz, J. Hexahydroxy-diphensäure (ellagsäure), brevifolin-carbosäure und chebulsäure als Umwandlungsprodukte der brevilagin und des terchebins. *Libigs Ann. Chem.* **1967**, *706*, 180–186. (In German) [CrossRef]

64. Nonaka, G.I.; Harada, M.; Nishioka, I. Eugeniin, a new ellagitannin from cloves. *Chem. Pharm. Bull.* **1980**, *28*, 685–687. [CrossRef]

65. Schmidt, O.T.; Schulz, J.; Fiesser, H. Über natürliche gerbstoffe XXVIII. Die gerbstoffe der myrobalanen. *Liebigs Ann. Chem.* **1967**, *706*, 187–197. (In German) [CrossRef]

66. Haslam, E.; Uddin, M. Gallotannins. Part XV. Some observations on the structures of chebulinic acid and its derivatives. *J. Chem. Soc. (C)* **1967**, 2381–2384.

67. Yoshida, T.; Fujii, R.; Okuda, T. Revised structures of chebulinic acid and chebulagic acid. *Chem. Pharm. Bull.* **1980**, *28*, 3713–3715. [CrossRef]

68. Schmidt, O.T.; Mayer, W. Die Konstitution der spaltsaure $C_{14}H_{12}O_{11}$ aus chebulin- und chebulagsäure. *Liebigs Ann. Chem.* **1951**, *571*, 1–15.

69. Schmidt, O.T.; Schmidt, D.M. Die umwandlung von chebulagsäure in corilagin XIV. Mitteilung über natürliche gerbstoffe. *Liebigs Ann. Chem.* **1952**, *578*, 25–30. [CrossRef]

70. Schilling, G.; Schweiger, R.; Weis, G.; Mayer, W.; Weiβ, J.; Siegel, R. Die relative konfiguration der chebulsäure. *Liebigs Ann. Chem.* **1981**, *1981*, 603–609. [CrossRef]

71. Yoshida, T.; Okuda, T.; Koga, T.; Toh, N. Absolute configurations of chebulic, chebulinic and chebulagic acid. *Chem. Pharm. Bull.* **1982**, *30*, 2655–2658. [CrossRef]

72. Hay, J.E.; Haynes, L.J. Bergenin, a C-glycopyranosyl derivative of 4-*O*-methylgallic acid. *J. Chem. Soc.* **1958**, 2231–2238. [CrossRef]

73. Ito, T.; Harada, N.; Nakanishi, K. Application of the aromatic chirality method to the bergenin system. *Agric. Biol. Chem.* **1971**, *35*, 797–798. [CrossRef]

74. Mayer, W.; Gabler, W.; Riester, A.; Korger, H. Die Isolierung von Castalagin, Vescalagin, Castalin und Vescalin. *Liebigs Ann. Chem.* **1967**, *707*, 177–181. [CrossRef]

75. Mayer, W.; Einwiller, A.; Jochims, J.C. Die Struktur des Castalins. *Liebigs Ann. Chem.* **1967**, *707*, 182–189. (In German) [CrossRef]

76. Mayer, W.; Kuhlmann, F.; Schilling, G. Die Struktur des Vescalins. *Liebigs Ann. Chem.* **1971**, *747*, 51–59. (In German)

77. Mayer, W.; Seitz, H.; Jochims, J.C. Die Struktur des Castalagins. *Liebigs Ann. Chem.* **1969**, *721*, 186–193. (In German) [CrossRef]

78. Mayer, W.; Seitz, H.; Jochims, J.C.; Schauerte, K.; Schilling, G. Struktur des Vescalagins. *Liebigs Ann. Chem.* **1971**, *751*, 60–68. (In German) [CrossRef]

79. Okuda, T.; Yoshida, T.; Ashida, M.; Yazaki, K. Casuarinin, stachyurin and strictinin, new ellagitannins from *Casuarina stricta* and *Stachyurus praecox*. *Chem. Pharm. Bull.* **1982**, *30*, 766–769. [CrossRef]

80. Nonaka, G.I.; Ishimaru, K.; Watanabe, M.; Nishioka, I.; Yamauchi, T.; Wan, A.S.C. Tannins and Related Compounds. LI. Elucidation of the Stereochemistry of the Triphenoyl Moiety in Castalagin and Vescalagin, from *Eugenia grandis*. *Chem. Pharm. Bull.* **1987**, *35*, 217–220. [CrossRef]

81. Nonaka, G.I.; Sakai, T.; Tanaka, T.; Mihashi, K.; Nishioka, I. Tannins and Related Compounds. XCVII. Structure Revision of *C*-Glycosidic Ellagitannins, Castalagin, Vescalagin, Casuarinin and Stachyurin, and Related Hydrolyzable Tannins. *Chem. Pharm. Bull.* **1990**, *38*, 2151–2156. [CrossRef]

82. Matsuo, Y.; Wakamatsu, H.; Omar, M.; Tanaka, T. Reinvestigation of the Stereochemistry of the *C*-Glycosidic Ellagitannins, Vescalagin and Castalagin. *Org. Lett.* **2015**, *17*, 46–49. [PubMed]

83. Richieu, A.; Peixoto, P.; Pouységu, L.; Denis, D.; Quideau, S. Bio-inspired Total Synthesis of (–)-Vescalin, A Nonahydroxytriphenoylated *C*-Glucosidic Ellagitannin. *Angew. Chem. Int. Ed.* **2017**, *56*, 13833–13837.

84. Tanaka, T.; Nonaka, G.I.; Nishioka, I. Tannins and Related Compounds. XLII. Isolation and Characterization of Four New Hydrolyzable Tannins, Terflavins A and B, Tergallagin and Tercatain from the Leaves of *Terminalia catappa* L. *Chem. Pharm. Bull.* **1986**, *34*, 1039–1049. [CrossRef]

85. Hervé du Penhoat, C.L.M.; Michon, V.M.F.; Peng, S.; Viriot, C.; Scalbert, A.; Gage, D. Structural elucidation of new dimeric ellagitannins from *Quercus robur* L. roburins A–E. *J. Chem. Soc. Perkin Trans. 1* **1991**, 1653–1660. [CrossRef]

86. Tanaka, T.; Ueda, N.; Shinohara, H.; Nonaka, G.I.; Fujioka, T.; Mihashi, K.; Kouno, I. *C*-glycosidic ellagitannin metabolites in the heartwood of Japanese chestnut tree (*Castanea crenate* SIEB. *et* ZUCC.). *Chem. Pharm. Bull.* **1996**, *44*, 2236–2242. [CrossRef]

87. Lin, T.C.; Tanaka, T.; Nonaka, G.I.; Nishioka, I.; Young, T.J. Tannins and related compounds. CVIII. Isolation and characterization of novel complex tannins (flavono-ellagitannins), anogeissinin and anogeissusins A and B, from *Anogeissus acuminata* (ROXB *ex* DC.) GUILL. *et* PERR. var. *lanceolata* WALL. *ex* CLARKE. *Chem. Pharm. Bull.* **1991**, *39*, 1144–1147. [CrossRef]

88. Nonaka, G.I.; Ishimaru, K.; Mihashi, K.; Iwase, Y.; Ageta, M.; Nishioka, I. Tannins and related compounds. LXIII. Isolation and characterization of mongolicains A and B, novel tannins from *Quercus* and *Castanopsis* species. *Chem. Pharm. Bull.* **1988**, *36*, 857–869. [CrossRef]

89. Mayer, W.; Görner, A.; Andrä, K. Punicalagin und Punicalin, zwei Gerbstoffe aus den Schalen der Granatäpfel. *Liebigs Ann. Chem.* **1978**, *1977*, 1976–1986. [CrossRef]

90. Tanaka, T.; Nonaka, G.-I.; Nishioka, I. Tannins and Related Compounds. XL. Revision of the Structures of Punicalin and Punicalagin, and Isolation and Characterization of 2-*O*-Galloylpunicalin from the Bark of *Punica granatum* L. *Chem. Pharm. Bull.* **1986**, *34*, 650–655. [CrossRef]

91. Schmidt, O.T.; Würtele, L.; Harréus, A. Pedunculagin, eine 2.3;4.6-Di-[(–)-hexahydroxy-diphenoyl]glucose aus Knoppern. *Liebigs Ann. Chem.* **1965**, *690*, 150–162. [CrossRef]

92. Schilling, G.; Schick, H. Zur Struktur des Punicalagins und Punicalins. *Liebigs Ann. Chem.* **1985**, *1985*, 2240–2245. [CrossRef]

93. Nonaka, G.I.; Tanaka, T.; Nishioka, I. Tannins and Related Compounds. Part 3. A New Phenolic Acid, Sanguisorbic Acid Dilactone, and Three New Ellagitannins, Sanguiins H-1, H-2, and H-3, from *Sanguisorba officinalis*. *J. Chem. Soc., Perkin Trans.* **1982**, *1*, 1067–1073. [CrossRef]

94. Nonaka, G.I.; Tanaka, T.; Nishioka, I. A dimeric hydrolyzable tannin, sanguiin H-6 from *Sanguisorba officinalis* L. *Chem. Pharm. Bull.* **1982**, *27*, 2255–2257.

95. Bacon, R.G.R.; Stewart, O.J. Metal Ions and Complexes in Organic Reactions. Part IV. Copper-promoted Preparations of Diaryl Ethers and Competing Hydrogen-transfer Processes. *J. Chem. Soc.* **1965**, 4953–4961.

96. Yoshida, T.; Memon, M.U.; Okuda, T. Alnusiin, a novel ellagitannin from *Alnus sieboldiana* fruits. *Heterocycles* **1981**, *16*, 1085–1088.

97. Yoshida, T.; Yazaki, K.; Memon, M.U.; Maruyama, I.; Kurokawa, K.; Okuda, T. Bicornin, a new hydrolysable tannin from *Trapa bicornis*, and revised structure of alnusiin. *Heterocycles* **1989**, *29*, 861–864.

98. Mayer, W.; Bilzer, W.; Schilling, G. Castavaloninsäure, isolierung und strukturermittlung. *Liebigs Ann. Chem.* **1976**, *1976*, 876–881.

99. Yoshida, T.; Yazaki, K.; Memon, M.U.; Maruyama, I.; Kurokawa, K.; Shingu, T.; Okuda, T. Structures of alnusiin and bicornin, new hydrolysable tannins having a monolactonized tergalloyl group. *Chem. Pharm. Bull.* **1989**, *37*, 2655–2660. [CrossRef]

100. Ishimatsu, M.; Tanaka, T.; Nonaka, G.I.; Nishioka, I. Alnusnins A and B, from the leaves of *Alnus sieboldiana*. *Phytochemistry* **1989**, *28*, 3179–3184. [CrossRef]

101. Tanaka, T.; Kirihara, S.; Nonaka, G.I.; Nishioka, I. Tannins and related compounds CXXIV. Five new ellagitannins, platycaryanins A, B, C, and D, and platycariin, and new complex tannin, strobilanin, from the fruits and bark of *Platycarya strobilacea* SIEV *et al* ZUCC., and biomimetic synthesis of *C*-glycoside ellagitannins from glucopyranose-based ellagitannins. *Chem. Pharm. Bull.* **1993**, *41*, 1708–1716.

102. Eerdunbayaer, L.B.; Nozaki, A.; Takahashi, E.; Okamoto, K.; Ito, H.; Hatano, T. Hydrolyzable tannins isolated from *Syzygium aromaticum*: structure of a new *C*-glucosidic ellagitannin and spectral features of tannins with a tergalloyl group. *Heterocycles* **2012**, *85*, 365–381.

103. Yoshida, T.; Ikeda, Y.; Ohbayashi, H.; Ishihara, K.; Ohwashi, W.; Shingu, T.; Okuda, T. Dimeric ellagitannins in plants of melastomataceae. *Chem. Pharm. Bull.* **1986**, *34*, 2676–2679. [CrossRef]

104. Yoshida, T.; Haba, K.; Arata, R.; Okuda, T. Structures of new hydrolysable tannin oligomers from Melastomataceae plants. *Tennen Yuki Kagobutsu Toronkai Koen Yoshishu* **1987**, *29*, 676–683.

105. Yoshida, T.; Haba, K.; Arata, R.; Okuda, T. Presented at 108th Annual Meeting of the Pharmaceutical Society of Japan, Hiroshima, Japan, 4 April 1988; p. 339.

106. Yoshida, T.; Ohwashi, W.; Haba, K.; Ohbayashi, H.; Ishihara, K.; Okano, Y.; Shingu, T.; Okuda, T. Tannins and Related Polyphenols of Melastomaceous Plants. II. Nobotanins B, C, and E, Hydrolyzable Tannin Dimer and Trimers from *Tibouchina semidecandra* COGN. *Chem. Pharm. Bull.* **1991**, *39*, 2264–2270. [CrossRef]

107. Yoshida, T.; Haba, K.; Nakata, F.; Okano, Y.; Shingu, T.; Okuda, T. Tannins and Related Polyphenols of Melastomaceous Plants. III. Nobotanins G, H, and I, Dimeric Hydrolyzable Tannins from *Heterocentron roseum*. *Chem. Pharm. Bull.* **1992**, *40*, 66–71. [CrossRef]

108. Yoshida, T.; Haba, K.; Arata, R.; Nakata, F.; Shingu, T.; Okuda, T. Tannins and Related Polyphenols of Melastomaceous Plants. VII. Nobotanins J and K, Trimeric Hydrolyzable Tannins from *Heterocentron roseum*. *Chem. Pharm. Bull.* **1995**, *43*, 1101–1106. [CrossRef]

109. Okuda, T.; Yoshida, T.; Hatano, T.; Yazaki, K.; Ashida, M. Ellagitannins of the Casuarinaceae, Stachyuraceae and Myrtaceae. *Phytochemistry* **1982**, *21*, 2871–2874. [CrossRef]

110. Okuda, T.; Hatano, T.; Yazaki, K. Praecoxin B, C, D and E, novel ellagitannins from *Stachyurus praecox*. *Chem. Pharm. Bull.* **1983**, *31*, 333–336. [CrossRef]

111. Hatano, T.; Kira, R.; Yasuhara, T.; Okuda, T. Tannins of Hamamelidaceous Plants. III. Isorugosins A, B and D, New Ellagitannins from *Liquidambar formosana*. *Chem. Pharm. Bull.* **1988**, *36*, 3920–3927. [CrossRef]

112. Hatano, T.; Ogawa, N.; Yasuhara, T.; Okuda, T. Tannins of Rosaceous Plants. VIII. Hydrolyzable Tannin Monomers Having a Valoneoyl Group from Flower Petals of *Rosa rugosa* THUNB. *Chem. Pharm. Bull.* **1990**, *38*, 3308–3313. [CrossRef]

113. Yoshida, T.; Hatano, T.; Namba, O.; Atallah, A.F.; Chu, T.; Okonogi, A.; Kuwajima, T.; Okuda, T. Determination of orientation of acyl group in hydrolyzable tannin oligomers. *Tennen Yuki Kagobutsu Toronkai Koen Yoshishu* **1991**, *33*, 401–408.

114. Yoshida, T.; Nakata, F.; Hosotani, K.; Nitta, A.; Okuda, T. Dimeric hydrolysable tannins from *Melastoma malabathricum*. *Phytochemistry* **1992**, *31*, 2829–2833.

115. Hatano, T.; Namba, O.; Chen, L.; Yasuhara, T.; Yazaki, K.; Yoshida, T.; Okuda, T. Hydrolyzable tannins having a depsidone-forming valoneoyl group. *Heterocycles* **1990**, *31*, 1221–1224.

116. Yoshida, T.; Namba, O.; Chen, L.; Liu, Y.; Okuda, T. Ellagitannin Monomers and Oligomers from *Euphorbia prostrata* AIT. and Oligomers from *Loropetalum chinense* OLIV. *Chem. Pharm. Bull.* **1990**, *38*, 3296–3302. [CrossRef]

117. Elyashberg, M.; Williams, A.J.; Blinov, K. Structural revisions of natural products by Computer-Assisted Structure Elucidation (CASE) systems. *Nat. Prod. Rep.* **2010**, *27*, 1296–1328. [PubMed]

118. Inokuma, Y.; Yoshioka, S.; Ariyoshi, J.; Arai, T.; Hitora, Y.; Takada, K.; Matsunaga, S.; Rissanen, K.; Fujita, M. X-ray analysis on the nanogram to microgram scale using porous complexes. *Nature* **2013**, *495*, 461–466. [CrossRef] [PubMed]

molecules

MDPI

Vegetable Tannins Used in the Manufacture of Historic Leathers

Lina Falcão [1,2] and Maria Eduarda M. Araújo [2,*]

[1] Artistic Studies Research Centre, Faculty of Fine Arts, University of Lisbon, Largo da Academia Nacional de Belas-Artes, 1249-058 Lisboa, Portugal; linafalcao@gmail.com
[2] Centre of Chemistry and Biochemistry, Department of Chemistry and Biochemistry, Faculty of Sciences, University of Lisbon, Campo Grande, Edifício C-8, 1749-016 Lisboa, Portugal
*   Correspondence: mearaujo@fc.ul.pt; Tel.: +351-217-500-968

check for updates

Abstract: In this review, a brief description of how animal skins were transformed in leathers in Europe using different vegetable tannins will be presented. Special attention will be dedicated to the description of the type of tannins and the characteristics of the most important type of historic leathers thus obtained. The text will also focus on the description of the techniques used in the identification of these tannins in historic objects: colorimetric tests and spectroscopic analysis.

Keywords: tannins; vegetable tanning; European historic leathers; colorimetric tests; spectroscopy; UV-Vis; FTIR

1. Introduction

Natural tannins, stricto sensu, are polyphenolic compounds of vegetal origin with the property to precipitate proteins. It is assumed that the oldest application of this tannins chemical property in technology is the stabilization of animal skins protein against putrefaction [1].

According to some authors [2–5], it may have been by the end of Neolithic period and in the eastern Mediterranean region that man began to use, incipiently, plant materials, such as leaves, twigs, fruits, barks or roots, to prevent animal skins degradation, transforming them into a more durable and useful material. Empirical development of this process during Classical Antiquity resulted in one of the most important animal skin transformation technique: vegetable tanning. This millenary technology, which is still in use, is one of the oldest processes used to produce leather. It was introduced in the north western regions of Europe after the Roman conquest [6], reaching thereafter a great importance in leather production which lasted until the end of the 19th century, when mineral tanning based on chromium (III) salts was developed and implemented in tanneries. Mineral tanning is nowadays the most used tanning process. In the early of the 20th century synthetic tannins, based on different organic molecules, were introduced in leather industry with the purpose of aiding vegetable tanning [1,7].

Succinctly, the vegetable tanning method can be described as the treatment of animal skin—previously washed, limed, dehaired, fleshed, delimed-, with crushed vegetable materials, or liquors/macerations (oozes), infusions, or decoctions, or extracts prepared with those materials. The result is the transformation of animal skin into what is termed by leather: a stable and non-putrescible material, resistant to deterioration promoted both by microorganisms and heat, when wetted. This is due to the chemical bonds established between collagen, the main constitutive protein of skin, and the tannins present in the vegetable materials. Collagen stabilization occurs when 15% to 40% of tannins, per dry weight of skins, are absorbed and incorporated into the collagen fibres matrix, depending of the type of leather produced [1,8–10].

The origin of the term 'tannin' it is also close related to the vegetable tanning process and came into use in France at the end of the 18th century by the French chemist Armand Séguin (1767–1835), who had previously worked with Antoine Lavoisier. Séguin firstly used the word *tannin* to define the organic substance present in the aqueous extracts of plants responsible for the transformation of skin into leather. The word derives from the French word *tan*, which corresponds to the ground oak bark, an important widespread and extensively used European vegetable source for leather making.

The term tanning (and *tannage* in French) itself has also a root in the word *tan*, and it was originally reserved for leather production with tannins but, since the 19th century with the development of other processes, the word has been applied for all different processes of leather making [11,12].

Vegetable tanning could be performed in different ways mostly depending on the size of animal skins, but since the medieval period three main techniques could be found in Europe: pit, vat and bag tanning [13–16].

Tanning in pits—large tanks set on the ground—was a slow and static process mostly reserved to the treatment of large animal skins (hides) and to produce heavy and strong leathers for shoe soles, belting or harness. Succinctly, hides were set in horizontal layers inside the pits (or *layaways*) with the ground vegetable material, one layer of hide another layer of crushed barks or leaves. Water or oozes was then added to the pits until all the skins were immersed and left for about 6 to 12 months.

The tanning of small to medium skins was mostly performed in wooden or clay vats where they were put together with the vegetable material, or an aqueous liquor of these materials, and stirred together for a few weeks until the required amount tanning material had been absorbed.

The last process, bag tanning, mostly used in south of Europe, was a faster process since it took only two to three weeks to complete. This method was used to produce light and fancy leathers that were then applied in lavish items such as jewellery and cases coverings, etc. To obtain these exquisite leathers, the skins were folded, sewed like a small bag and filled up with water and with the ground vegetable material inside. Then "bags" were immersed in an identical infusion or liquors used to fill it and shake to speed up the process of tanning. Basils (*badanas*, in Iberian languages), cordovans and morocco are some examples of vegetable tanned leathers traditionally produced by bag tanning technique [17–20].

With the Industrial Revolution, and the need of faster tanning processes, all vegetable tanned leathers started to be produced in drums which consist of a wooden cylinder rotating around its own axis filled with skins, tanning agents and water.

Leather produced with tannins, or vegetable tanned leather, was one of the most important pre-industrial materials in Western world, very much appreciated and demanded due to its versatility. Its characteristics, ranging from rigid to flexible, depend on the raw materials used, both skins and vegetable tannins, and the tanning techniques. It was a fundamental material for the production a wide range of artefacts such as footwear, garments, book bindings, saddlery, wall-hangings, furniture upholstery, cases coverings, carriages or liquids containers [7,21]. Beyond its utilitarian function, it was also used as support material for artistic and decorative paintings, wall hangings or screen coverings. Different ornamental techniques such as dyeing, painting, gilding, moulding, tooling, embroidering, cutting-out, scorching or sewing, have been often incorporated transforming vegetable tanned leather into a valuable and luxurious material. Gilt leather (Spanish leather, *guadameci*) is one of the finest examples created in Europe: it is a silvered and then "golden" varnished, painted and tooled or moulded vegetable tanned leather, mostly produced between the 16th and 18th centuries [13,22,23].

Therefore, vegetable tanned leather is the most common type of heritage leather found in museums and collections [24,25].

2. Vegetable Tanning Materials: The Sources of Tannins

Vegetable tannins are polyphenolic secondary metabolites produced by higher plants. They can precipitate not only proteins, as it was stated before, but also polysaccharides and alkaloids. They are large molecules with a molecular weight comprised from 500 to 30,000 Da. However, not all tannins

are useful for tanning, only those with a molecular weight lower than 3000 Da are efficient in leather making since large molecules are unable to penetrate into the skin's fibre structure and tend to be water insoluble [1,26].

Tannins can be divided in four classes: hydrolysable, condensed, complex and phlorotannins [27–29]. Complex tannins have a molecular structure that can be considered a mixture of hydrolysable and condensed, including gallic, ellagic and catechin sub-units. Phlorotannins are a small group of tannins isolated mainly from brown seaweeds. None of the two groups is important for leather tanning.

Hydrolysable tannins consist in a monosaccharide core, usually glucose, esterified with gallic acid, forming the gallotannins, or with hexahydrodiphenoic acid, the precursor of ellagic acid, and gallic acid, forming the ellagitannins. Upon heating in acidic aqueous medium, they hydrolyse to yield gallic and ellagic acid. Thermal decomposition originates pyrogallol which gave the traditional and former name to this class of compounds.

Condensed tannins have a flavonoid origin. They are oligo- or polymeric proanthocyanidins were the phenolic hydroxyls are totally or partially esterified with gallic acid.

Many plants rich in tannins had been used over time. Table 1 lists the most important sources of tannins used in European tanneries until development of mineral tanning since before the 18th century the autochthonous plants were the main raw vegetable tanning materials. However, with the growing need for leather and the increase in trading between Europe and other continents such as Africa, Australia and South America, other exotic sources arrived at Europeans tanneries in large amounts and low cost [15,30,31].

The selection of the appropriate vegetable tanning material was crucial to obtain leathers with specific characteristics [32]. Leathers produced with hydrolysable tannins are light brown, yellow or greenish, and are lightfast. Leathers produced with condensed tannins have a brown to reddish colour, becoming darker if exposed to light. This latter type of leather tends to absorb more easily atmospheric pollutants like sulphur dioxide, promoting the acidic hydrolysis of collagen, leading to its degradation. The so-called red rot is an advanced stage of degradation where cohesion is lost due to the disintegration of collagen fibres. Leather produced with condensed tannins is more prone to this occurrence than the one produced with hydrolysable tannins [9,25].

2.1. Barks

Barks from different tree species were, and some still are, very important raw materials in the production of vegetable tanned leathers.

In Europe, oak (*Quercus* spp.) barks were the most used. In the British Isles and other western European countries, the prevailing species were English (pedunculated) oak (*Quercus robur* syn. *Q. pedunculata*) and sessile oak (*Quercus petraea* syn. *Q. sessiliflora*), while in the south predominated Pyrenean oak (*Quercus pyrenaica*) and Portuguese oak (*Quercus faginea*). In the Mediterranean and Atlantic regions of south Europe, the bark of smaller and endemic species belonging to the *Quercus* genus such as cork oak (*Quercus suber*), holm oak (*Quercus rotundifolia* syn. *Q. ilex* subsp. *rotundifolia*) and kermes oak (*Quercus coccifera*) were also used since these species grow spontaneously [12,18,33].

Barks were removed from trees with 12 to 15 years old, between spring and early summer, since it is the time when barks are richer in tannins and, at the same time, easier to separate from the trunk. Barks were dried and then ground into a powder containing 6–17% weight of a mixture of condensed tannins and ellagitannins [1,7].

Early analysis of *Quercus robur* and *Q. petraea* barks found that they contained proanthocyanidins of the procyanidin and prodelphinidin type. Nevertheless only 23% of the water-soluble oak bark tannins consisted of oligomeric proanthocyanidins [34,35].

Quercus spp., namely *Q. robur*, such the other species known by the common name of oak, are also a rich source of ellagitannins. The main ellagitannins that account for 40–60% of components of the bark are vescalagin and castalagin. These are complex molecules comprising a linear glucose unit with

OH at the 4 and 6 positions esterified with a hexahydrodiphenoic acid (HHDP acid). At the same time, it also exists a C-C coupling between C-1 of glucose and C-2 of a nonahydroxytriphenoyl moyaty. This unit esterifies the remaining OH of glucose at the 3, 4 and 5 positions (Figure 1). Vescalagin and castalagin are epimers at the C-1 position of glucose unit [26,36].

Vescalagin, R₁=OH, R₂=H
Castalagin, R₁=H, R₂=OH
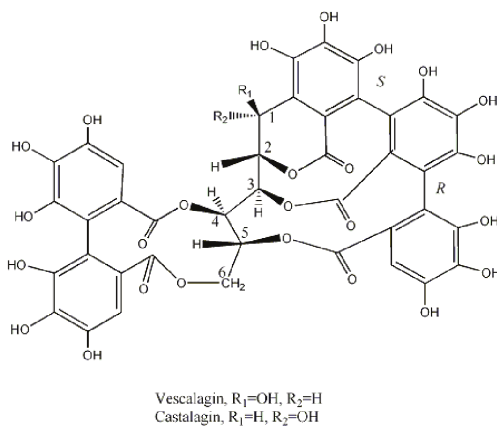
Figure 1. Structure of vescalagin and castalagin.

Steriochemistry of the C-C bond between the two galloyl unit, linked to C-3 and C-5 OH of glucose has recently been reinvestigated [37].

Quercus suber, cork oak, was also used in tanning. The inner part of the bark was removed and used in Portugal, Spain and Corsega. It was also exported to Ireland [20,33,38]. Investigation of cork from Spanish specimen indicates that the main tannins were common to the other *Quercus* species, the ellagitannins grandinin (Figure 2), vescalagin, and castalagin, being grandinin and castalagin the main components [39].

Quercus coccifera, kermes oak, was very used in the French Provence where it was known as *garouille*. *Rusque*, the name of the husk of the root, was used to produce shoe sole of high quality [19,20].
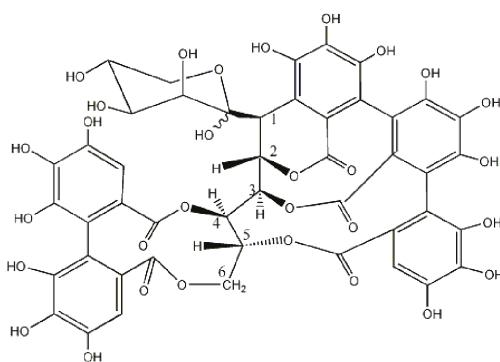
Figure 2. Structure of grandinin.

Table 1. Post-medieval and traditional vegetable tanning materials used in Europe [18–20,33].

Botanical Name	Common Name	Origin and Distribution	Part of the Plant Used	Main Tannins	Geographical Uses	Observations
Acacia mearnsii	mimosa, wattle	Australia, cultivated in South Africa since 1864 and South America	barks	condensed	imported since second decade of 19th century, commercial extracts	
Betula spp.	birch	northern Europe, Russia	barks	condensed	northern Europe, Russia	used to produce Russia leather
Caesalpinia coriaria	divi-divi	Central and South America	pods	hydrolysable: gallotannins	imported since late 18th century	
Castanea sativa	chestnut, sweet chestnut	Mediterranean region	wood	hydrolysable: ellagitannins	since 19th century, commercial extracts	used mixed with other vegetable materials to produce firm leather
Coriaria myrtifolia	Mediterrenean coriaria (*emborrachacabras*, redoul, roldor, rodor)	southern France and Mediterranean coastal Spain	leaves (redoul)	hydrolysable	southern France and Mediterranean coastal Spain	
Cotinus coggygria (syn *Rhus cotinus*)	smoke tree	southern Europe, Mediterranean region	leaves (Venetian or Turkish sumac)	hydrolysable: gallotannins	southern Europe	
Larix	larch	northern Europe	bark	condensed	northern Europe	
Mirtus communis	myrtle	southern Europe	leaves	hydrolysable: ellagitannins	Italic Peninsula	
Picea abies	Norway spruce	Alps, Pyrenees, Germany, Scandinavia	barks	condensed	northern and central Europe	
Pinus halepensis	Aleppo pine	coastal areas of the western Mediterranean region	barks	condensed	northern Europe	yields a reddish leather
Quercus aegilops	valonea oak, Turkish oak	eastern Mediterranean region	acorn cups	hydrolysable: ellagitannins	Middle Ages in Turkey, Greece, Italy	
Quercus coccifera	garouille	Mediterranean region	husk of root (*rusque*)	hydrolysable	south of France	
Quercus infectoria	Aleppo oak	eastern Mediterranean region	galls (Allepo galls)	hydrolysable: gallotannins	Europe	

Table 1. *Cont.*

Botanical Name	Common Name	Origin and Distribution	Part of the Plant Used	Main Tannins	Geographical Uses	Observations
Quercus ilex	holm oak	central-western part of the Mediterranean	barks	condensed and hydrolysable	Iberian Peninsula	
Quercus spp. (*Q. ilex*, *Q. robur*, *Q. petraea*, *Q. pyrenaica*)	oak	Europe	barks	condensed and hydrolysable: ellagitannins	Europe	
			wood	hydrolysable: ellagitannins		
Quercus suber	cork oak		inner bark	condensed and hydrolysable: ellagitannins	Iberian Peninsula	
Rhus coriaria	sumac	Mediterranean region	leaves (*Sicilian sumac*)	hydrolysable: gallotannins	southern Europe	yields light coloured, soft and supple leathers. Used to produce basil and cordovan leather.
Salix spp.	willow	northern Europe, Russia	barks	condensed	northern Europe, Russia	yields a light coloured, yellowish-brown leather that is soft and flexible
Schinopsis balansae, *S. lorentzii*	quebracho	south America	wood	condensed	imported and used in Europe since last decades of 19th century	
Terminalia chebula	myrabolans	India	fruits	hydrolysable	British Islands	used in mixed tannages for sole leather

In northern Europe and Russia, the main vegetable tanning materials were the barks of local trees like *Betula* spp., birch, *Salix* spp., willow, *Larix* spp., larch, or *Picea* spp., spruce. The use of these barks was restricted to these regions [20,33].

One of the finest examples of vegetable tanned leathers produced in Eastern Europe was Russia leather, which was obtained by tanning the hides or skins with birch or willow barks. It was a highly valued leather, being exported from Moscow to Western Europe from the 17th to the 19th centuries where it was very appreciated for furniture upholstery and lavish coverings [7,18].

The above species biosynthesise condensed tannins although these compounds were found in small percentages [40].

In Scandinavia, barks from *Salix arenaria* and *Salix resseliana* containing 7–11% of condensed tannins were traditionally used to produce leather for gloves [20].

Tannins from the bark of *Picea abies* (Norway spruce) were identified as combinations of (epi)catechin and (epi)gallocatechin units with a polymerization degree of up to 13 units [41].

During the late 18th and 19th century there existed a great demand on tanning vegetable material. To overcome the problem, barks from what was called exotic trees were imported from South America, South Africa, Australia and New Zealand. One of the most imported material was the bark of *Acacia mearnsii*, black wattle, endemic in Australia and New Zealand and cultivated in South Africa. This material is still very used today in Europe by leather industry. Barks were collected from August to October. The outer part was discarded, and the inner part was milled. It could be used as a powder or boiled to produce liquor that was evaporated to dryness and traded for all Europe [20,42]. *Acacia* bark contains 22–48% of condensed tannins. This source of tannins is a very effective tanning agent and is used to produce different types of leathers, with a light red colour when new becoming darker with time.

Wattle tannins consist of about 9% monomers, 42% dimers, 40% trimers, 9% tetramers and 1% pentamers and higher oligomers by mass. The starter unit is either catechin or gallocatechin and the extender units, fisetinidol or robinetinidol (Figure 3a). The second extender unit is always linked to the starter unit to give angular trimers (Figure 3b). The predominance of trimers in the vegetable material is essential for leather tanning since high molecular weight oligomers would not be able to penetrate skin collagen fibres. *A. mearnsii* proanthocyanidin has recently been investigated. The percentage of the different monomers in the tannin of mimosa are around 15% of catechin, 65–70% of robinetidinol and 15–20% of fisetinidol. It can be considered as a mixture of procyanidin or profisetidin and prorobinetidin or prodelphinidin substructures (Table 2) most probably as a mixture of procyanidin and prorobinetidin or prodelphinidin since the proportion of OH/H substitution at position 5 is 6.8:1 and the proportion of OH/H substitution at position 5′ is 3:2 [43,44].

Catechin and epicatechin: R=OH, R'=H
Gallocatechin and epigallocatechin: R=OH, R'=OH
Fisetinidol: R=H, R'=H
Robinetidinol: R=H, R'=OH

(a)   (b)
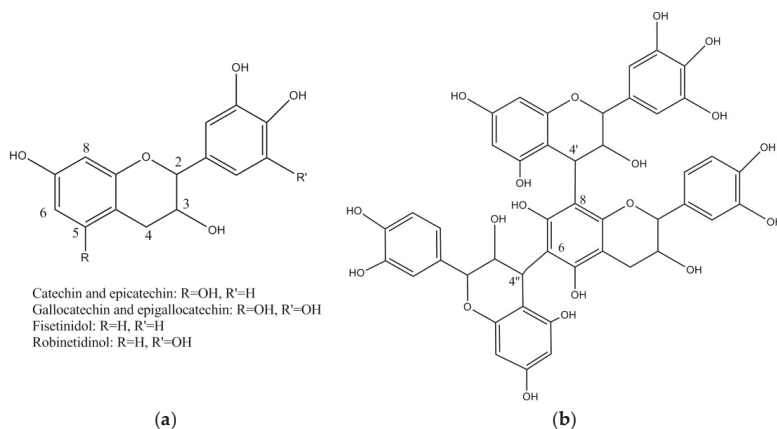
Figure 3. Structure of flavan-3-ol monomers (**a**) and mimosa condensed tannin (**b**).

2.2. Wood

Wood was mainly used in furniture and buildings, so its use in tanning was scarce until the beginning of the 19th century when an urge need for new tanning materials appeared. Both chestnut and oak wood began to be used as ground or aqueous extracts [45]. The wood of these species, like the barks, are also rich in ellagitannins. Nowadays, chestnut extracts are still used in industry being mainly produced in Italy, Central Europe and Baltic region. Research of chestnut heartwood indicated that has a polyphenolic constitution similar to oak wood. Monomeric vescalagin and castalagin predominate in oak wood representing 40–60% of the ellagitannins. Dimers (roburin A and roburin D, (Figure 4a) and other compounds were other sugar unit like lyxose/xylose derivatives grandinin, roburin B, roburin C, and roburin E (Figure 4a,b), were also identified in oak woods [46]. Some of the previous roburins like roburin A and roburin E were also identified in small amounts in oak bark [39].
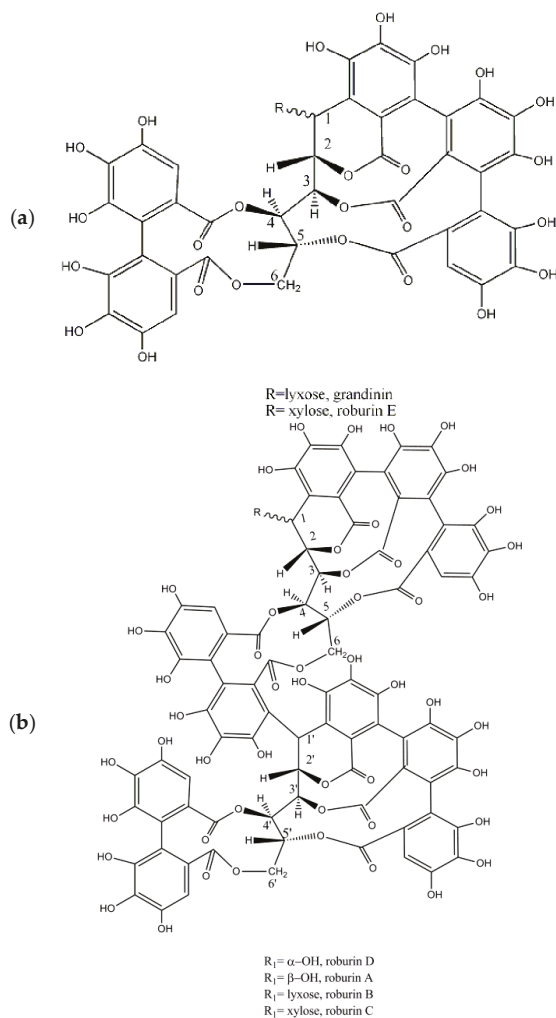
Figure 4. Structure of ellagitanins present in oak wood: (**a**) grandinin and roburin D; (**b**) roburins A, B, C and D.

During the last decades of the 19th century Europe began to import an exotic wood, quebracho, *Schinopsis lorentzii* and *S. balasae*, from south America [18,47]. This tree has hard and reddish wood rich in condensed tannins, about 14–26% weight of the heartwood. Quebracho tannins extracts contains oligomers based on catechin as starter unit linked to one, two, three, etc. *ent*-fisetinidol extender units (Table 2, Figure 5). The trimer is angular with one fisetinidol linked to the C-8 position and the other to the C-6-position of catechin. Analysis of the tannin indicates that is composed by about 33% dimers, 37% trimers, 21% tetramers, 8% pentamers, and 1% heptamers. Compounds with higher degree of polymerisation, if present, exist in low concentration [1,48,49].
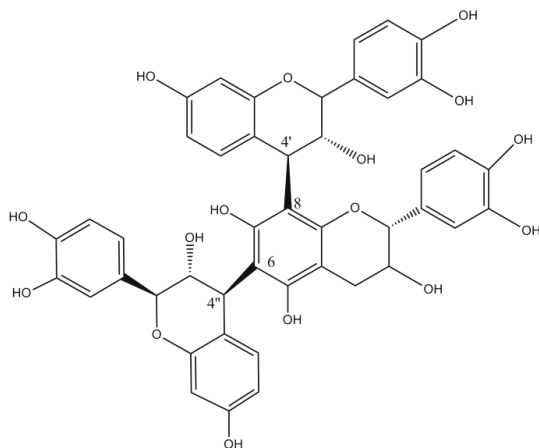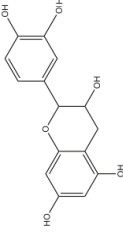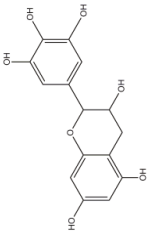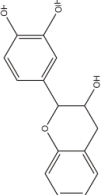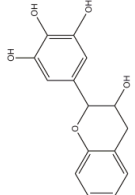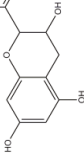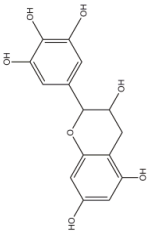
Figure 5. Structure of quebracho tannin.

2.3. Leaves

In Europe, until the 20th century, sumac (*Rhus coriaria*) leaves, together with oak bark, were one of the most important materials used to produce leathers. Sumac has been used since Antiquity and it is even mentioned in Pedanius Dioscorides book "De Materia Medica" written between 50–70 AD. During the Middle Age it was a valuable material used to produce delicate, light colored and great durability leathers. It was also used in the dying of leathers and textiles. In Iberian Peninsula it was used to prepare the famous cordovan, leather prepared with goat skins, and basils. The word sumac refers to several species belonging to the genera *Rhus* of the Anacardean family. It also refers to the powder obtained milling the leaves and small branches of the shrub collected from July to September. Good quality sumac contains 25–35% of gallotannins. *Rhus coriaria* grew spontaneously or cultivated in several regions of the South Europe, namely Portugal, Spain and Sicilia, produced a light yellow to green tanning powder.

During the 17th and 18th centuries there was a great demand for Portuguese sumac produced in the north of the country and it is described in the firsts encyclopedias as having a superior quality. It was exported to France and British Islands to be used by the textile and leather manufactures of Northern Europe. However, during the 20th century Spanish and *Sicilian sumac* surpassed the demand for Portuguese sumac [18,33,50].

Table 2. Proanthocyanidins monomers.

	Tannins Name			
	Procyanidin	**Profisetidin**	**Prorobinetidin**	**Prodelphinidin**
Chemical structure of the building block				
Coupling position	4-8	4-6	4-6	4-8

In Turkey and in the Oriental Mediterranean another specie of sumac was used, named Turkish or Venezian sumac, *Rhus cotinus* (syn. *Cotinus coggygria*) used in the Mediterranean region but containing less amount of tannins. Both sumacs tanning materials produces pale and soft leathers, contrasting with other tanning agents that originate brown coloured leathers. Pale leathers were much appreciated since they could be dyed in light and bright colours without dark background interference. There are however some drawbacks: sumac infusions ferment and hydrolyse easily and the resulting material has no tanning properties. They were used in vat or bag tanning.

Besides sumac leaves other plants leaves were also used for leather production, such as myrtle, mastic and *rédoul*. The last one is of French provenance, very used in the French regions of Languedoc and Provence and also in Catalonia where was called *redon*. It was also known as French or fake sumac and it was poorer tanning material, with only about 15% of tannins [7,20,51].

As stated above, sumac is a source of gallotannins. The simplest gallotannin is pentagalloyl glucose, β-1,2,3,4,6-pentagalloyl-*O*-D-glucopyranose (PGG). This compound has the five free hydroxyls of glucose esterified with a galloyl residues. The α anomer is not usual in nature. More galloyl residues can be attached to PGG through a meta- or para depside bond (Figure 6) [26].

Tannic acid is considered the tanning agent in sumac. Commercial tannic acid has a molecular weight of 1701.206 g/mol and a molecular formula of $C_{76}H_{52}O_{46}$, corresponding to a decagalloyl glucose, sumac leaves contain a mixture of gallotannins, from penta to decagalloyl-glucoside [52–54].

In Spain, true sumac was many times forged with mastic (*Pistacia lentiscus*) leaves. However this plant contains condensed tannins and leathers thus obtained were darker and got a reddish colour with light.

Leaves of *Myrtus communis* were widely used for leather production in Italic Peninsula. This plant contains the following ellagitannins: oenothein B, eugeniflorin D2, and tellimagrandins I and II [55].
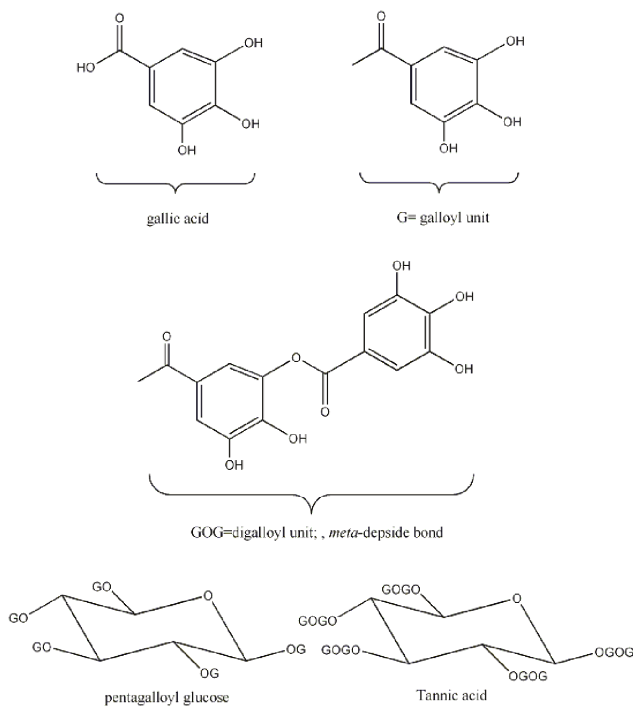
Figure 6. Structure of gallic acid and pentagalloyl glucose and tannic acid

2.4. Fruits

A few fruits were also used as tanning materials, the most important being valonia and divi-divi. Valonia is the acorns of *Quercus aegilops*, a tree also known as Turkish oak, which grows abundantly in Turkey, Greece and adjacent countries. Acorns are usually picked up in August and then dried out from the domes. It has been widely used in the production of leather in Austria, Germany and France and allows producing faster, harder, firmer, heavier and quite impermeable to water leather. Valonia is a source of ellagitannins, whose main constituents are castalagin, vescalagin and pentagalloylglucose (Figures 1 and 6) [56]. This material was often mixed with ground oak bark to produce soles that were considered of excellent quality and durability [18,20].

The divi-divi is a pod of a shrub, *Caesalpinia coriaria*, native to South America. It became to be imported and used in English tanneries in the 19th century. This material, mainly a source of gallotannins containing a small amount of condensed tannins, produces very porous leathers of brown or reddish-brown colour [20,57].

2.5. Galls

Galls are pathological excrescences formed in the branches, leaves or domes of plants as a response to the bites of certain insects or other parasites. They are anomalous grow of plant tissues and have different size, shape and composition depending on the plant and the agent that causes them. Galls used in tanning have a spherical (globose) shape, are smooth or have a crown and are characterized by a high content of tannins, 40% to 70% of gallotannins. The most important are the so-called Turkish galls, Aleppo or Levant galls, and are produced by the insect *Cynips gallae tinctoriae* in the branches of the *Quercus infectoria* (syn *Q. lusitanica*) growing mainly in Asia Minor. These galls have a greenish or brownish colour, are rigid, compact, very astringent, bitter to taste and are one of the raw materials used to obtain tannic acid [33].

The so-called white galls, brownish-yellow, lighter, less astringent and with bitter taste, having less tannin content than greenish galls, are another type of galls produced by *Q. infectoria* [19,20]. Since Ancient Greece that both have commercial importance and, in addition to tanneries, were widely used in traditional medicine, dyeing and to make writing ink (iron gallic ink).

Another important gall is known as *knoppern*, or acorn gall, which is caused by the insect *C. quercus-calycis* and found in many Central European *Quercus (Q. robur, Q. pyrenaica)* (Austria, Hungary, Serbia, Slovenia) and Greece [20].

3. Detection and Characterization of Tannins in Historic Vegetable Tanned Leathers

Vegetable tanned leathers, i.e., leathers produced with plant materials rich in tannins, are the commonest European cultural heritage leathers.

In heritage conservation, identification of leather making process is important to comprehend leather technology, degradation susceptibility and condition.

The analysis of tannins is a relatively common procedure in historic leather conservation and heritage science studies. Tannins characterisation allows to elucidate aspects on historic leathers composition, technology, and condition, but also to evaluate the suitability of new vegetable tanned leathers for conservation purposes [9,58].

Tannins characterisation in leathers can be based on spot tests, formerly the ferric test and vanillin test and more recently the rhodanine, nitrous acid and the acid butanol tests. These chemical tests are employed for a fast-preliminary material characterisation, especially by leather conservators [58–63].

Some studies using chromatographic techniques, namely high-performance liquid chromatography (HPLC) have been also used, but more costly and time consuming and only allows to distinguish the broad classes of condensed versus hydrolysable tannins [64].

3.1. Colorimetric Tests

Different colorimetric tests developed in the field of phytochemistry [26] have been adapted for tannins detection in historic and archaeological leathers. These tests, particularly ferrous and vanillin test, have been performed as spot test directly in fibres collected from leathers [61,62,65]. Recently, more specific chemical tests have been adapted to analyse both leather fibres and extracts prepared from those fibres. The analysis of fibres with these tests is done visually. However, the identification of tannins can be difficult to interpret in coloured or aged leathers samples due to the presence of colorants or degradation products of the leather itself. To overcome these limitations, chemical analysis of historic leathers can be performed in leather fibres extracts and analysed spectrophotometrically [66].

Colorimetric tests can be used as a global and fast tool to detect and classify vegetable tannins. When specific tests for the detection of condensed tannins (HCl/butanol test), ellagitannins (nitrous acid test) and gallic acid/gallotannins (rhodanine test) are performed, a combined evaluation of results is possible allowing a more specific detection of the chemical nature of tannins used in the manufacture of the leather (Figure 7) [66].
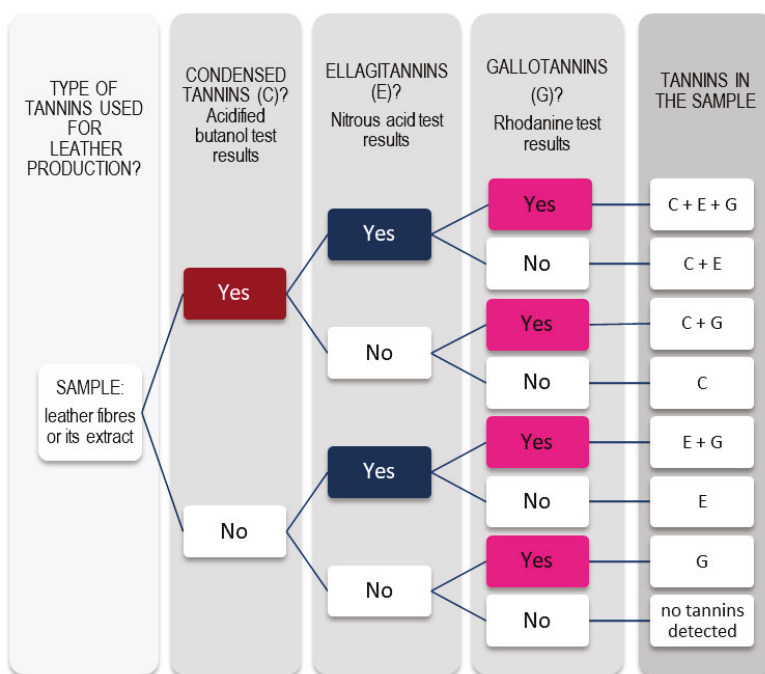
Figure 7. Key-guide for the identification of tannins by colorimetric tests.

3.1.1. Ferric Test

This type of test is specific for phenolic compounds and not only tannins. It is based on the principle that phenolics react with iron salts forming a bluish or greenish black (or grey) product [58,64]. Iron salts such as iron sulfate (III) ($Fe_2(SO_4)_3$) or iron chloride ($FeCl_3$) are the commonest reagents used in ferric test.

Some literature refers that this test can be used to distinguish hydrolysable from condensed tannins. Hydrolysable tannins, namely tannic acid, form blue black products while condensed tannins form green black products. This subtle distinction is very difficult to observe in leather fibres,

particularly in aged dark leathers or when mixtures of different types of tannins are present and if diverse coloured fibres are to be compared [61,62].

3.1.2. Acidified Vanillin Test

Vanillin test has been widely used to detect condensed tannins. In acid conditions, vanillin reacts specifically with meta-substitued flavanols, not only condensed tannins, to form a red product. Widely distributed flavanols such as catechin and epicatechin, condensed tannins monomers, also react with the disadvantage they give higher colour yield than the condensed tannins. Furthermore, this test is very sensitive to the presence of water that quenchs colour yield. In addition, quebracho proanthocyanidins do not produce an intense colour with this reagent [26].

Reactivity with vanillin cannot be considered sufficient evidence for the presence of condensed tannins [23,67]. Furthermore, vanillin reacts reluctantly with aged leathers, becoming very difficult to undoubtedly identify the presence of condensed tannins [59,61,62,68].

3.1.3. Acidified Butanol Test

Acid butanol test is a depolymerization method specific for condensed tannins detection. With this method it is promoted an oxidative cleavage of interflavanoid bond of proanthocyanidins in hot acidified alcohol solutions to yield correspondent red anthocyanidins with absorbance maxima around 550 nm. The red colour can vary significantly depending on the anthocyanidin formed and on the position of interflavan links (C4 → C6 were found to be more resistant to cleavage than C4 → C8) [23,67].

This test, specific to condensed tannins, is more sensitive than vanillin test and results are unequivocally [62].

3.1.4. Nitrous Acid Test

Ellagitannins react with nitrous acid, obtained by dissolving sodium nitrite in a diluted acid, forming a red or pink colour, which slowly changes to purple or blue [23,67,69].

Nitrous acid test can also be used to detect ellagic acid, an ellagitannins degradation product. With this reagent ellagic acid forms a red chromophore product while other phenolics can form yellow or orange products.

Ellagic acid can be present in aged leather due to acid hydrolysis promoted by moisture and acidic pollutants. The red colour formed in tested historic samples indicates ellagic acid may be present [62].

3.1.5. Rhodanine Test

Rhodanine test is specific for gallic acid detection and was developed by Inoue and Hagerman for gallotannins determination in plant materials. In basic solution, this reagent (2-thio-4-ketothiazolidine) reacts with the vicinal hydroxyl groups of free gallic acid producing a red complex, with a maximum absorbance around 520 nm. This red colour is not formed with galloyl esters of gallotannins, ellagic acid, ellagitannins or condensed tannins. However, this method can be used indirectly to detect gallotannins presence performing the test before and after hydrolysis of tannins [70].

Rhodanine test was adapted to detect free gallic acid in fibres and, indirectly, to estimate gallotannins, without hydrolysing samples, by comparing results with acid butanol and nitrous acid tests. The presence of free gallic acid in historic leathers may be due not only to gallotannins degradation (hydrolysis), but also to ellagitannins, complex tannins and even condensed tannins degradation. Therefore, an unequivocal assumption of a leather tanning with a vegetable source of gallotannins is only possible if ellagitannins and condensed tannins are not detected (Figure 7) [62,66].

3.2. Spectroscopic Techniques

3.2.1. UV-Vis

Ultraviolet-visible (UV-Vis) spectroscopy has been used to analyse tannins extracted from European historic leathers, such as bookbinding and upholstery leathers, principally as a complementary technique to other spectroscopic research studies.

It is well established that the different classes of tannins from different vegetable sources present characteristic UV absorption bands. Briefly, and considering hydrolysable tannins, the wavelength of the maximum absorbance (λ_{max}) and the respective inflection point (λ_{min}) are as follows: while gallotannins show two characteristic absorption maximums, λ_{max1} around 212 nm and λ_{max2} around 275 nm, with distinctive inflection point around 242 nm; ellagitannins present strong absorption near 200 nm and a shoulder around 277 nm. Regarding condensed tannins, they present a strong absorption around 200 nm, an inflection point (λ_{min}) between 258–259 nm and λ_{max} between 279–281 nm [71,72].

This distinctive spectral data has been found when analysing leather fibers extracts gathered from leathers of different periods and geographical origins. Studies demonstrate that UV spectra can clearly indicate if gallotannins or condensed tannins are present in extracts obtained from leathers tanned exclusively with one of these types of tannins. UV spectra obtained from samples containing ellagitannins, mixtures of different types of tannins or combined tannages are more difficult to interpret [66].

Other authors [73] present similar values for bookbinding and upholstery leathers.

3.2.2. FTIR

Fourier transform infra-red (FTIR) spectroscopy is a very useful and common analytical technique in heritage science studies and in the last decade different studies have been published describing this technique to analyse tannins in historic leathers [36,66,73–77].

Tannins from different vegetable sources present characteristic absorption bands in mid- infrared region of spectrum. The 1750–700 cm^{-1} region was considered the most informative. All tannins FTIR spectra exhibit four strong bands, two of them at 1615–1606 cm^{-1} and 1452–1446 cm^{-1} assigned to aromatic ring stretch vibrations and the other two at 1211–1196 cm^{-1} and 1043–1030 cm^{-1} assigned to stretch vibrations of C–O bond. Tannins also present another weak band at 1518–1507 cm^{-1} due to skeletal vibration of the aromatic rings.

And it is also demonstrated that the fingerprint region (1800–650 cm^{-1}) of hydrolysable tannins presents an absorption pattern distinct from condensed tannins. Hydrolysable tannins presented bands at 1731–1704 and 1325–1317 cm^{-1}. The gallotannins sub class present three distinctive bands at 1088–1082, 872–870 and 763–758 cm^{-1}.

Vegetable tanning materials classified as condensed tannins, showed three strong bands at 1288–1283 cm^{-1}, 1160–1155 cm^{-1} and 1116–1110 cm^{-1} and two other weak bands at 976 and 844–842 cm^{-1}. These bands are not found in the spectra of gallo- and ellagitannins. The 1288–1283 cm^{-1} indicates a characteristic feature for the flavonoid-based tannins. This band can be assigned to the ethereal C–O asymmetric stretching vibration arising from the pyran-derived ring structure of this class of tannins [78,79].

The tanning materials in historical leathers can be analysed by FTIR technique after extraction with aqueous acetone, followed by lyophilization. The presence of the four strong bands at 1615–1030 cm^{-1}, as referred above, is a strong indication that the material had been tanned with vegetable tannins. Further characterization is possible looking for the marker bands of each class (Table 3). Ellagitannins can only be identified if marker bands for hydrolysable tannins are present and marker bands for condensed and gallotannins are missing. Table 3 presents data obtained with ATR device. If other technique is used like KBr pellet or diffuse reflectance identical or very close values are obtained.

Usually historic leather tanned with sumac like morocco leather are easily identified since the characteristic bands of gallotannins are well defined. However, if leathers were tanned with oak, which

contains a mixture of ellagi- and condensed tannins, or if the leather was tanned with more than one type of tannin, FTIR spectra present the characteristic bands of hydrolysable and condensed tannins, do not allowing the differentiation between these two situations.

When spectra display intense bands around 1650 and 1550 cm^{-1} corresponding to the amide I and II bands of collagen, respectively, is an indication that leather had suffered a considerable degradation of the proteinaceous material.

Table 3. Main ATR-FTIR bands of vegetable tanning materials and their assignment [36].

Bands (cm^{-1})	Assignment	Tannin Identification
1731–1704 (m-s)	ν C=O phenolic esters lactones / ν C=O phenolic esters	hydrolysable tannins
1615–1606 (m-vs)	ν C=C aromatic ring	present in all classes of tannins
1518–1507 (w-m)	ν C=C skeletal ring	present in all classes of tannins
1452–1446 (m-s)	ν C=C aromatic ring	present in all classes of tannins
1325–1317 (m-s)	ν C-O lactones and O-H deformation	hydrolysable tannins
1288–1282 (ms-vs)	ν C-O pyran ring, flavonoids	condensed tannins
1211–1196 (m-vs)	ν aromatic C-OH	present in all classes of tannins
1162–1155 (s)	ν, asymmetric, C-O-C cyclic ether	condensed tannins
1116–1110 (s-vs)	ν, asymmetric, C-O-C cyclic ether	condensed tannins
1088–1082 (m)	ν, symmetric, C-O-C aryl phenolic ester	gallotannins
1043–1030 (m-vs)	β = C-H deformation	present in all classes of tannins
976 (w)		condensed tannins
844–842 (w)	γ tetrasubsituted aromatic C-H	condensed tannins
872–870 (w)	γ OH and γ tetrasubsituted aromatic C-H	gallotannins
763–758 (w-m)	ν, symmetric skeletal (sugar ring, breathing vibration)	gallotannins

ν stretching, β in plane, γ out-of plane; vs: very strong, s: strong, m: medium, w: weak.

3.2.3. Other Spectroscopic Techniques: Fluorescence Spectroscopy and Solid State ^{13}C-NMR

There are few reports than the above mentioned of other spectroscopic techniques used to characterize vegetable tannins in historical leathers.

Emission fluorescence spectra of five tannins, oak, valonea, chestnut, quebracho and mimosa, were recorded between 200 and 800 nm after excitation at 220 nm and 250. Results were used by the authors to confirm the conclusions obtained by FTIR and UV spectroscopy [73].

Solid state ^{13}C-NMR was used to distinguish between leather tanned with vegetable material from leather tanned with mineral tanning agents. Special attention was paid to the spectra between about 165–171 ppm. In this region peaks of vegetable tannins are very important while those from collagen are small and scarce. The technique was applied only to new tanned leathers and requires the use of small amount of material, 1–2 mm, which were freeze in liquid nitrogen and then milled to a powder. Besides the distinction between hydrolysable and condensed tannins the authors also to distinguish leather tanned with mimosa from the leather tanned with quebracho [80].

Conflicts of Interest: The authors declare no conflict of interest.

References

1. Covington, A.D. *Tanning Chemistry: The Science of Leather*; Royal Society of Chemistry: Cambridge, UK, 2009; ISBN 978-1-84973-434-9.
2. Forbes, R.J. *Studies in Ancient Technology*, 2nd ed.; Brill Publishers: Leiden, The Netherlands, 1966; Volume V.
3. Reed, R. *Ancient Skins, Parchments and Leathers*; Seminar Press: London, UK; New York, NY, USA, 1972; ISBN 978-0-129-03550-3.
4. Haslam, E. Vegetable tannage: Where do the tannins go? *J. Soc. Leather Technol. Chem.* **1997**, *81*, 45–51.
5. Goffer, Z. *Archaeological Chemistry*, 2nd ed.; John Wiley & Sons: Hoboken, NJ, USA, 2007; ISBN 978-0-471-25288-7.
6. Van Driel-Murray, C. Tanning and leather. In *The Oxford Handbook of Engineering and Technology in the Classical World*; Oleson, J.P., Ed.; Oxford University Press: New York, NY, USA, 2009; pp. 483–495.
7. Chahine, C. *Cuir et Parchemin ou la Métamorphose de la Peau*; CNRS Éditions: Paris, France, 2013; ISBN 978-2-271-07686-1.
8. Sharphouse, J.H. *Leather Technician's Handbook*, 75th ed.; Leather Producers' Association: Northampton, UK, 1995; ISBN 978-0950228518.
9. Florian, M.-L. *Protein Facts: Fibrous Proteins in Cultural Artifacts*; Archetype Publications: London, UK, 2008; ISBN 978-1873132340.
10. Thomson, R. Skin, leather and tanning: Some definitions. In *Leather Tanneries: The Archaeological Evidence*; Thomson, R., Mould, Q., Eds.; Archetype Publications—Archaeological Leather Group: London, UK, 2011; pp. 3–7. ISBN 978-1904982616.
11. Seymour-Jones, F.L. The beginnings of leather chemistry. *J. Chem. Educ.* **1927**, *4*, 831–835. [CrossRef]
12. Azéma, J.-P. *Moulins du Cuir et de la Peau: Moulins a Tan et à Chamoiser en France*; Éditions Creer: Nonette, France, 2004; ISBN 978-2848190143.
13. Waterer, J.H. *Leather Craftsmanship*; G. Bell and Sons: London, UK, 1968.
14. Thomson, R. Leather manufacture in the postmedieval period with special reference to Northamptonshire. *Post Med. Archaeol.* **1981**, *15*, 161–175. [CrossRef]
15. Clarkson, L.A. Developments in tanning methods during the Post-Medieval Period (1500–1850). In *Leather Manufacture through the Ages, Proceedings of the 27th East Midlands Industrial Archaeology Conference*; Thomson, R., Beswick, J.A., Eds.; Arkle Print Ltd.: Northampton, UK, 1983; pp. 11–21.
16. Sol, B. L'évolution des procédés de tannage végétal. In *Environnement et Conservation de l'Écrit, de l'Image et du Son*; Association pour la Recherche Scientifique sur les Arts Graphiques-ARSAG: Paris, France, 1994; pp. 89–95.
17. Miguelez, C. *Arte de Curtir ó Instruccion General de Curtidos*; Imprenta Real: Madrid, Spain, 1805.
18. Procter, H.R. *A Text-Book of Tanning: A Treatise on the Conversion of Skins into Leather*; E. & F. N. Spon: London, UK, 1885.
19. Villon, A.-M. *Traité Pratique de la Fabrication des Cuirs et du Travail des Peaux*; Librairie Polytechnique: Paris, France, 1889.
20. Bennett, H.G. *The Manufacture of Leather*; Constable & Company Ltd.: London, UK, 1920.
21. Mould, Q.; Carlisle, I.; Cameron, E. *Leather and leatherworking in Anglo-Scandinavian and Medieval York*; Council for the British Archaeology: York, UK, 2003; Volume 17, ISBN 978-1902771366.
22. Departament de Cultura. *L'Art en la Pell. Cordovans i Guadamassils de la Collecció Colomer Munmany*; Departament de Cultura: Vich, Spain, 1992.
23. Nenno, R.; Rathke, C. *Lederlust: Meisterwerke der Angewandten Kunst aus dem Deutschen Ledermuseum Offenbach*; Kerber Christof Verlag: Darmstadt, Germany, 2006; ISBN 978-3-938025-67-3.
24. Thomson, R. Leather. In *Conservation Science: Heritage Materials*; The Royal Society of Chemistry: Cambridge, UK, 2006; pp. 92–120.
25. Larsen, R. The chemical degradation of leather. *Chimia* **2008**, *62*, 899–902. [CrossRef]
26. Hagerman, A.E. The Tannin Handbook. 2018. Available online: http://chemistry.muohio.edu/hagerman (accessed on 28 March 2018).
27. Khanbabaee, K.; van Ree, T. Tannins: Classification and definition. *Nat. Prod. Rep.* **2001**, *18*, 641–649. [PubMed]

28. Arbenz, A.; Avérous, L. Chemical modification of tannins to elaborate aromatic biobased macromolecular architectures. *Green Chem.* **2015**, *17*, 2626–2646. [CrossRef]

29. Quideau, S.; Deffieux, D.; Douat-Casassus, C.; Pouységu, L. Plant Polyphenols: Chemical Properties, Biological Activities, and Synthesis. *Angew. Chem.* **2011**, *50*, 586–621. [CrossRef] [PubMed]

30. Thomson, R. The manufacture of leather. In *Conservation of Leather and Related Materials*; Kite, M., Thomson, R., Eds.; Butterworth Heinemann-Elsevier: Oxford, UK, 2006; pp. 121–129.

31. Trommer, B. *Archäologisches Leder: Herkunft, Gerbstoffe, Technologien, Alterungs–und Abbauverhalten*; VDM: Saarbrücken, Germany, 2008; ISBN 978-3836496292.

32. Hilbert, F.L. Tanning materials (vegetable). In *Encyclopedia of Chemical Technology*; Kirk, R.E., Othmer, D., Eds.; The Interscience Encyclopedia: New York, NY, USA, 1954; Volume 13, pp. 578–586.

33. Howes, F.N. *Vegetable Tanning Materials*; Butterworths Scientific Publications: London, UK, 1953.

34. Kuliev, Z.A.; Vdovin, A.D.; Abdullaev, N.D.; Makhmatkulov, A.B.; Malikov, V.M. Study of the catechins and proanthocyanidins of Quercus robur. *Chem. Nat. Compd.* **1997**, *33*, 642–652. [CrossRef]

35. Pallenbach, E.; Scholz, E.; König, M.; Rimpler, H. Proanthocyanidins from Quercus petraea Bark. *Planta Med.* **1993**, *59*, 264–268. [CrossRef] [PubMed]

36. Falcão, L.; Araújo, M.E.M. Application of ATR–FTIR spectroscopy to the analysis of tannins in historic leathers: The case study of the upholstery from the 19th century Portuguese Royal Train. *Vib. Spectrosc.* **2014**, *74*, 98–103. [CrossRef]

37. Matsuo, Y.; Wakamatsu, H.; Omar, M.; Tanaka, T. Reinvestigation of the stereochemistry of the C-glycosidic ellagitannins, vescalagin and castalagin. *Org. Lett.* **2015**, *17*, 46–49. [CrossRef] [PubMed]

38. Matos, A.M.C. A indústria no distrito de Évora, 1836-90. *Anal. Soc.* **1991**, *26*, 561–581.

39. Conde, E.; Cadahía, E.; García-Vallejo, M.C.; Fernández de Simón, B. Polyphenolic Composition of *Quercus suber* Cork from Different Spanish Provenances. *J. Agric. Food Chem.* **1998**, *46*, 3166–3171. [CrossRef]

40. Palo, R.T. Distribution of birch (*Betula* spp.), willow (*Salix* spp.), and poplar (*Populus* spp.) secondary metabolites and their potential role as chemical defense against herbivores. *J. Chem. Ecol.* **1984**, *10*, 499–520. [CrossRef] [PubMed]

41. Kemppainen, K.; Siikaahoa, M.; Pattathil, S.; Giovando, S.; Kruus, K. Spruce bark as an industrial source of condensed tannins and non-cellulosic sugars. *Ind. Crops Prod.* **2014**, *52*, 158–168. [CrossRef]

42. No II. Extract of Mimosa-Bark, for the Use of Tanners. 1823. Available online: http://www.jstor.org/stable/41325900 (accessed on 28 March 2018).

43. Reid, D.G.; Bonnet, S.L.; Kemp, G.; van der Westhuizen, J.H. Analysis of commercial proanthocyanidins. Part 4: Solid state ^{13}C NMR as a tool for in situ analysis of proanthocyanidin tannins, in heartwood and bark of quebracho and acacia, and related species. *Phytochemistry* **2013**, *94*, 243–248. [CrossRef] [PubMed]

44. Crestini, C.; Lange, H.; Bianchetti, G. Detailed Chemical Composition of Condensed Tannins via Quantitative ^{31}P NMR and HSQC Analyses: *Acacia catechu*, *Schinopsis balansae*, and *Acacia mearnsii*. *J. Nat. Prod.* **2016**, *79*, 2287–2295. [CrossRef] [PubMed]

45. Smout, T.C. Oak as a commercial crop in the eighteenth and nineteenth centuries. *Bot. J. Scotl.* **2005**, *57*, 107–114. [CrossRef]

46. Zhang, B.; Cai, J.; Duan, C.-Q.; Reeves, M.J.; He, F. A Review of Polyphenolics in Oak Woods. *Int. J. Mol. Sci.* **2015**, *16*, 6978–7014. [CrossRef] [PubMed]

47. Jumelle, H. Le Quebracho. *Rev. Bot. Appl. Agric. Colon.* **1924**, *30*, 88–98. [CrossRef]

48. Venter, P.B.; Sisa, M.; van der Merwe, M.J.; Bonnet, S.L.; van der Westhuizen, J.H. Analysis of commercial proanthocyanidins. Part 1: The chemical composition of quebracho (*Schinopsis lorentzii* and *Schinopsis balansae*) heartwood extract. *Phytochemistry* **2012**, *73*, 95–105. [CrossRef] [PubMed]

49. Kardel, M.; Taube, F.; Schulz, H.; Schutze, W.; Gierus, M. Different approaches to evaluate tannin content and structure of selected plant extracts—Review and new aspects. *J. Appl. Bot. Food Qual.* **2013**, *86*, 154–166. [CrossRef]

50. Córdoba de la Llave, R. Cuatro textos sobre literatura técnica medieval sobre el trabajo del cuero. *Merid. Rev. Hist. Med.* **2002**, *5–6*, 171–204.

51. Cardon, D.; Pinto, A. Le redoul, herbe des tanneurs et des teinturiers. Collecte, commercialisation et utilisations d'une plante sauvage dans l'espace meridional (XIIIe-XVe siècles). *Médiévales* **2007**, *53*, 51–64. [CrossRef]

52. Zalacain, A.; Prodanov, M.; Carmona, M.; Alonso, G.L. Optimisation of extraction and identification of gallotannins from sumac leaves. *Biosyst. Eng.* **2003**, *84*, 211–216. [CrossRef]

53. Regazzonia, L.; Arlandinia, E.; Garzona, D.; Santagatib, N.A.; Berettaa, G.; Facinoa, R.M. A rapid profiling of gallotannins and flavonoids of the aqueous extract of *Rhus coriaria* L. by flow injection analysis with high-resolution mass spectrometry assisted with database searching. *J. Pharm. Biomed. Anal.* **2013**, *72*, 202–207. [CrossRef] [PubMed]

54. Romeo, F.V.; Ballistreri, G.; Fabroni, S.; Pangallo, S.; Nicosia, M.G.L.D.; Schena, L.; Rapisarda, P. Chemical Characterization of Different Sumac and Pomegranate Extracts Effective against *Botrytis cinereal* Rots. *Molecules* **2015**, *20*, 11941–11958. [CrossRef] [PubMed]

55. Yoshimura, M.; Amakura, Y.; Tokuhara, M.; Yoshida, T. Polyphenolic compounds isolated from the leaves of *Myrtus communis*. *J. Nat. Med.* **2008**, *62*, 366–368. [CrossRef] [PubMed]

56. Abdalla, S.; Pizzi, A.; Bahabri, F.; Ganash, A. Analysis of Valonia Oak (*Quercus aegylops*) Acorn Tannin and Wood Adhesives Application. *BioResources* **2015**, *10*, 7165–7177. [CrossRef]

57. Pérez, M.A.; Rengifo, R.; Pereira, C.; Hernández, V. Dividivi tannins: An ecological product for water-based drilling fluids. *Environ. Dev. Sustain.* **2017**, *19*, 1815–1829. [CrossRef]

58. Florian, M.-L. Vegetable tannins. *Leather Conserv. News* **1984**, *1*, 37–38.

59. Larsen, R.; Wouters, J.; Chahine, C.; Brimblecombe, P.; Calnan, C. Recommendations on the production, artificial ageing, assessment, storage and conservation of vegetable tanned leather. In *Environment Leather Project: Deterioration and Conservation of Vegetable Tanned Leather—Research Report No. 6*; Larsen, R., Ed.; The Royal Danish Academy of Fine Arts: Copenhagen, Denmark, 1996; pp. 189–202.

60. Van Driel-Murray, C. Practical evaluation of a field test for the identification of ancient vegetable tanned leathers. *J. Archaeol. Sci.* **2002**, *29*, 17–21. [CrossRef]

61. Poulsen, D.V. Presentation and evaluation of spot tests for identification of the tannin type in vegetable tanned leather. In Proceedings of the 13th Triennal Meeting ICOM Committee for Conservation, Rio de Janeiro, Brazil, 22–27 September 2002; Vontobel, R., Ed.; James and James: London, UK, 2002; pp. 792–797.

62. Falcão, L.; Araújo, M.E.M. Tannins characterisation in new and historic vegetable tanned leathers fibres by spot tests. *J. Cult. Herit.* **2011**, *12*, 149–156. [CrossRef]

63. Johnson, A. Evaluation of the use of SC6000 in conjunction with Klucel G as a conservation treatment for bookbinding leather: Notes on a preliminary study. *J. Inst. Conserv.* **2013**, *36*, 125–144. [CrossRef]

64. Wouters, J. High-performance liquid chromatography of vegetable tannins extracted from new and old leathers. In Proceedings of the 10th Triennal Meeting ICOM Committee for Conservation, Washington, DC, USA, 22–27 August 1993; James & James for ICOM-CC: London, UK, 1993; pp. 669–673.

65. Odegaard, N.; Carroll, S.; Zimmt, W.S. *Material Characterization Tests for Objects of Art and Archaeology*, 2nd ed.; Archetype Publications: London, UK, 2005; ISBN 1904982093.

66. Falcão, L.; Araújo, M.E.M. Tannins characterization in historic leathers by complementary analytical techniques ATR-FTIR, UV-Vis and chemical tests. *J. Cult. Herit.* **2013**, *14*, 499–508. [CrossRef]

67. Scalbert, A. *Quantitative methods for the estimation of tannins in plant tissues, In Plant. Polyphenols: Synthesis, Properties, Significance*; Hemingway, R.W., Laks, P.E., Eds.; Plenum Press: New York, NY, USA, 1992; pp. 259–278.

68. Nikolova, D.; Goshev, I. Modification of the method of Broadhurst and Jones for proving of tannins in cultural-historical objects. *C. R. Acad. Bulg. Sci.* **2009**, *62*, 825–830.

69. Wilson, T.C.; Hagerman, A.E. Quantitative determination of ellagic acid. *J. Agric. Food Chem.* **1990**, *38*, 1678–1683. [CrossRef]

70. Inoue, K.H.; Hagerman, A.E. Determination of gallotannins with rhodanine. *Anal. Biochem.* **1988**, *169*, 363–369. [CrossRef]

71. Nakagawa, K.; Sugita, M. Spectroscopic characterization and molecular weight of vegetable tannins. *J. Soc. Leather Technol. Chem.* **1999**, *83*, 261–264.

72. Laghi, L.; Parpinello, G.P.; Del Rio, D.; Calani, L.; Mattioli, A.U.; Versari, A. Fingerprint of enological tannins by multiple techniques approach. *Food Chem.* **2010**, *121*, 783–788. [CrossRef]

73. Giurginca, M.; Badea, N.; Miu, L.; Meghea, A. Spectral technics for identifying tanning agents in the heritage leather items. *Rev. Chim.* **2007**, *58*, 923–927.

74. Derrick, M.R.; Stulik, D.C.; Landry, J.M. *Infrared Spectroscopy in Conservation Science*; The Getty Conservation Institute: Los Angeles, CA, USA, 1999.

75. Stuart, B.H. *Analytical Techniques in Materials Conservation*; John Wiley & Sons: Chichester, UK, 2007; ISBN 978-0470012802.

76. Bonnot-Diconne, C.; Robinet, L.; Pacheco, C.; Ioele, M.; Paris, M. Multi-technique analysis of gilt-leather wall coverings (16th–18th centuries). In Proceedings of the ICOM-CC 17th Triennial Conference Preprints, Melbourne, Australia, 15–19 September 2014; International Council of Museums: Paris, France, 2014.

77. Falcão, L.; Pereira, F.A.B.; Araújo, M.E.M. Caracterização de cabedais adamascados e guadamecis dos séculos XVII e XVIII por ATR. *Conserv. Patrim.* **2018**, *27*, 49–61. [CrossRef]

78. Ricci, A.; Olejar, K.J.; Parpinello, G.P.; Kilmartin, P.A.; Versari, A. Application of Fourier transform infrared (FTIR) spectroscopy in the characterization of tannins. *Appl. Spectrosc. Rev.* **2015**, *50*, 407–442. [CrossRef]

79. Tondi, G.; Petutschnigg, A. Middle infrared (ATR FT-MIR) characterization of industrial tannin extracts. *Ind. Crops Prod.* **2015**, *65*, 422–428. [CrossRef]

80. Romer, F.H.; Underwood, A.P.; Senekal, N.D.; Bonnet, S.L.; Duer, M.J.; Reid, D.G.; van der Westhuizen, J.H. Tannin fingerprinting in vegetable tanned leather by solid state NMR spectroscopy and comparison with leathers tanned by other processes. *Molecules* **2011**, *16*, 1240–1252. [CrossRef] [PubMed]

molecules

MDPI

Review

Tannins from *Acacia mearnsii* De Wild. Bark: Tannin Determination and Biological Activities

Sosuke Ogawa [1,*,†] and Yoshikazu Yazaki [2,†]

[1]   Mimozax Co., Ltd., 4291-1, Miyauchi, Hatsukaichi-shi, Hiroshima 738-0034, Japan
[2]   Department of Chemical Engineering, Monash University, Clayton, Victoria 3800, Australia;
      yoshi.yazaki@monash.edu
*   Correspondence: ogawa@mimozax.co.jp; Tel.: +81-829-306-100
†   These authors contributed equally to this work.

check for
updates

Abstract: The bark of *Acacia mearnsii* De Wild. (black wattle) contains significant amounts of water-soluble components acalled "wattle tannin". Following the discovery of its strong antioxidant activity, a wattle tannin dietary supplement has been developed and as part of developing new dietary supplements, a literature search was conducted using the SciFinder data base for "*Acacia* species and their biological activities". An analysis of the references found indicated that the name of *Acacia nilotica* had been changed to *Vachellia nilotica*, even though the name of the genus *Acacia* originated from its original name. This review briefly describes why and how the name of *A. nilotica* changed. Tannin has been analyzed using the Stiasny method when the tannin is used to make adhesives and the hide-powder method is used when the tannin is to be used for leather tanning. A simple UV method is also able to be used to estimate the values for both adhesives and leather tanning applications. The tannin content in bark can also be estimated using NIR and NMR. Tannin content estimations using pyrolysis/GC, electrospray mass spectrometry and quantitative ^{31}P-NMR analyses have also been described. Tannins consists mostly of polyflavanoids and all the compounds isolated have been updated. Antioxidant activities of the tannin relating to anti-tumor properties, the viability of human neuroblastoma SH-SY5Y cells and also anti-hypertensive effects have been studied. The antioxidant activity of proanthocyanidins was found to be higher than that of flavan-3-ol monomers. A total of fourteen papers and two patents reported the antimicrobial activities of wattle tannin. Bacteria were more susceptible to the tannins than the fungal strains tested. Several bacteria were inhibited by the extract from *A. mearnsii* bark. The growth inhibition mechanisms of *E. coli* were investigated. An interaction between extracts from *A. mearnsii* bark and antibiotics has also been studied. The extracts from *A. mearnsii* bark inhibit the growth of cyanobacteria. Wattle tannin has the ability to inactivate α-amylase, lipase and glucosidase. *In vivo* experiments on anti-obesity and anti-diabetes were also reported. Several patents relating to these enzymes for anti-diabetes and anti-obesity are in the literature. In addition, studies on *Acacia* bark extract regarding its antitermite activities, inhibition of itching in atopic dermatitis and anti-inflammatory effects have also been reported. The growth of bacteria was inhibited by the extract from *A. mearnsii* bark, and typical intestinal bacteria such as *E. coli*, *K. pneumoniae*, *P. vulgaris* and *S. marcescenes* was also inhibited in vitro by extracts. Based on these results, the *Acacia* bark extract may inhibit not only the growth of these typical intestinal bacteria but also the growth of other types of intestinal bacteria such as *Clostridium* and *Bacteroides*, a so-called "bad bacteria". If the tannin extract from *A. mearnsii* bark inhibits growth of these "bad bacteria" *in vivo* evaluation, the extracts might be usable as a new dietary supplement, which could control the human intestinal microbiome to keep the body healthy.

1. Introduction

The bark of *Acacia mearnsii* De Wild. (black wattle) contains significant amounts of water-soluble components, known as "wattle tannin", which has been used for producing tanned leather for more than one hundred years and for the manufacture of water-resistant and structural wood adhesives for more than fifty years. Based on the initial discovery of the extremely high superoxide scavenging activity (SOSA) of the hot water extract from the bark of *A. mearnsii* De Wild. in 2002 and following a series of toxicity, safety and biological tests of the wattle tannin, including inhibition of lipase and α-amylase, a wattle tannin dietary supplement was developed in 2007. Since then, a supplement for human health has been marketed as ACAPOLIA® in Japan [1].

In order to explore additional possibilities for the use of wattle tannin in dietary supplements, a literature search using the SciFinder database (produced by Chemical Abstracts Service) was undertaken. A total of 489 references was found when the keywords "*Acacia*" and "biological activity" were searched (search performed on 13 June 2017). After a careful reading of those references on *Acacia* species and their biological activities, an important event was recognized. In spite of the fact that the name of the genus *Acacia* was derived from the name of *Acacia nilotica*, in 2013 the name of this particular plant was changed to *Vachellia nilotica*. This name change is critical for anyone searching the literature for the biological properties of *A. nilotica* where apparently there has been nothing reported after 2013. The new *V. nilotica* species name must be used to obtain data published after 2013. Consequently, a literature search (performed on 29 August 2017) on *A. mearnsii* as a keyword was conducted resulting in a total of 369 found references. This review briefly describes the historical events of the species name change of *A. nilotica* and then the determinations of wattle tannin from *A. mearnsii* bark and its biological activities with a view to developing new dietary supplements.

2. Taxonomy of *Acacia*

2.1. Acacia Mearnsii and Acacia Nilotica (Origin of the Genus "Acacia")

A. mearnsii De Wild. (black wattle) belongs to the family Fabaceae (pea family) and is a fast-growing native tree, which occurs naturally in south-eastern Australia. The genus *Acacia* contains over 1000 species, just behind the largest genus in the Fabaceae family, *Astragalus* which contains over 3000 species [2].

According to Kew*science*, Plants of the World online [3], *A. nilotica* (now *V. nilotica*) was used in medicine during the early Egyptian dynasties some 3500 years ago. Pedanius Dioscorides (a Greek physician and 'father of botany', ca. 40 to 90 A.D.) described a preparation of extracts from the leaves and fruit pods of a plant in his book on "Medicinal Material" and he called it 'akakia', from which the name of the genus *Acacia* originated. *Acacia* was formally adopted by Miller [4] in a paper describing 24 African and American species. However, his generic concepts were so broad that a number of his species are no longer accepted as belonging to the genus *Acacia*. Prior to Miller, the name *Acacia* had been widely used in pre-Linnean literature [5]. Linnaeus [6] had placed 39 species in the genus *Mimosa* and two of these species were *Mimosa scorpioides* and *Mimosa nilotica*; these taxa were subsequently transferred to *Acacia* and *Acacia scorpioides* is now considered to be conspecific with *A. nilotica* [7].

There are some 1350 species of *Acacia* found throughout the world and approximately 1000 species found in Australia, where it is commonly known as "wattle". *Acacia* is the largest genus of vascular plants in Australia [8]. Based on morphological, palynological and biochemical characteristics, Pedley [9] in 1986 proposed that the genus *Acacia* could be divided into three genera: *Acacia* (161 species), *Senegalia* (231 species) and *Racosperma* (960 species). Although *A. nilotica* belongs to the smallest genus *Acacia*, since it was not only native to Africa but also named as the first *Acacia* species, South Africans believed that the name of "*Acacia*" should be retained to include *A. nilotica*. In contrast to this view, there are 960 species belonging to the genus *Racosperma* and most species are found in Australia. Australians believed wattles (*Acacia* species) to be an Australian icon, so that a proposal to keep the name *Acacia* instead of *Racosperma* for the Australian *Acacia* plants was made in

2003 [7,10]. The proposal was accepted at the 17th International Botanical Congress (IBC) in Vienna in July 2005. However, since then, argument and controversy on the change of genus name *Acacia* had not diminished and many arguments between African and Australian scholars have occurred [11]. In order to resolve this problem at the 18th IBC in Melbourne in July 2011, prior to the Congress, eight distinguished taxonomists published their pragmatic view on retypification of *Acacia* Mill. with an Australian type in Taxon [12] and finally the argument reached the conclusion that the proposed change in type and use of the name *Acacia* only for the Australian species were approved at the 18th IBC in Melbourne in July 2011. Following the IBC, South African scientists conducted phylogenetic studies on *Acacia sensu lato* including approximately 140 African species using details of the morphology and DNA sequence data. As a result from this study, two generic names were recognized as being able to accommodate the African taxa, namely *Senegalia* and *Vachellia*, in which the former *A. nilotica* is now named *V. nilotica*. This was due to the differences in not only taxonomical and phytochemical characteristics but also more decisively to differences in the genetic DNA sequences [13]. Tannin from the bark of the formerly known *A. nilotica* belongs to the hydrolysable tannins class, whilst tannin from *A. mearnsii* bark belongs to the condensed tannins [14]. New names for the African *Acacia* species were officially announced in 2014 [15,16].

2.2. Acacia Mearnsii De Wild.

The Belgian naturalist Émile Auguste Joseph De Wildeman first described *A. mearnsii* De Wild. in 1925 [17]. This species was first collected by E.A. Mearns from a cultivated specimen in East Africa [18]. *A. mearnsii* is native to south-eastern Australia and Tasmania, naturalized in Western Australia, India and the Hawaiian Islands and introduced into Africa, the Caribbean, East Asia, Europe, Sri Lanka, North America, New Zealand, South America and Southeast Asia [19]. *A. mearnsii* plantations covering ca. 300,000 ha have been established in South Africa, Brazil, China and Vietnam [20,21]. The bark of *A. mearnsii* contains significant amounts of water-soluble "wattle tannin" as has been noted previously [1].

3. Analyses Method of Wattle Tannin and Their Composition

3.1. Wattle Tannin Extracts and Tannin Analyses

Wattle tannins are composed of polyflavanoids and their precursors, which are the major components, together with other phenolic components and complex mixtures of carbohydrate gums, sugars and amino acids. Polyflavanoids consist of a large number of individual components, whose molecular masses may range from 300 for the monomeric compounds up to 3000 for the large polymers. Two methods of estimating the tannin contents in a sample are the Stiasny method and the hide-powder method. The principle of the Stiasny method is to estimate the amount of the polyflavanoid components in tannin extracts which react with formaldehyde in acid solution. This method is employed particularly when the tannin is used in the production of wood adhesives. The hide-powder method is based on the affinity of tannin components towards collagen. However, the true affinity of flavonoid compounds to proteins only becomes apparent from the triflavanoid level indicating that low molecular weight polyflavanoids with a molecular mass less than approximately 800 may not react with protein [22]. The hide-powder method is used for the application of wattle tannin to leather tanning.

3.1.1. Polyflavanoid Contents Analyzed Using the Stiasny Method for Wood Adhesives

The yield and quality of wattle tannin from a bark are economically extremely important. *A. mearnsii* was introduced into China in the 1950s, but was identified by the Chinese government as a promising species for tannin production only in early 1980. In 1985, the Australian Centre for International Agricultural Research (ACIAR) commenced research collaboration with the Chinese Academy of Forestry (CAF). One of the aims was to identify well-adapted, high tannin yielding

provenances of *A. mearnsii* in Australia. Special seed collections of *A. mearnsii* were made in Australia and at the same time bark samples from the twenty provenances were collected and the yield of tannin extract and polyflavanoids content for the application to wood adhesives were analyzed using the Stiasny method. Results from these analyses showed that the barks of *A. mearnsii* trees from samples provenances in both Victoria and Tasmania contained higher yield tannin and polyflavanoids than provenances in either New South Wales or South Australia [23].

3.1.2. Molecular Size Analysis of Wattle Tannin Extracts Using Ultrafiltration

Great variability in the growth rate, flowering periods, thickness of bark, the extent of gummosis and disease resistance appears among *A. mearnsii* trees in China. In addition, the quality of the extracts can be variable. In order to overcome the variable quality of extracts and also to assess the quality of extracts, an ultrafiltration method was developed, particularly for the application to wood adhesives. Two tannin extracts were commercially produced in China and South Africa and the aqueous (90 °C) extract of the barks from *A. mearnsii* trees (2–5 years old) was prepared at the CAF laboratory in Nanjing, China. On the basis of purity of polyflavanoids and also the preliminary viscosity for these wattle tannins, wattle tannin extracts from *A. mearnsii* bark in China can become a potential basis for wood adhesives production [24].

3.1.3. Tannin Content of Wattle Tannin Using Hide-Powder Method for Leather Tanning

In the middle 1980s in China, most of the tannin extracts obtained from barks of *Larix* and *Pinus* species had been used as tanning agents by leather manufacturers. The hide-powder method had been used for tannin analysis in the leather tanning industry [25] but it is labor intensive, whilst the Stiasny method is regarded as a rapid and reliable method. Therefore, the tannin contents of the bark samples from 18 of the 20 provenances were determined using both the hide-powder and the Stiasny methods. The results from the statistical analyses showed that although the correlation between tannin contents in the total solids and Stiasny values was marginally significant at $p = 0.05$, the Stiasny values were not able to be used to predict tannin contents for the treatment of leather [26].

3.1.4. Tannin Analyses Using UV, Stiasny and Hide-Powder Methods

Although the major components of wattle tannin extracts are polyflavanoids, which show strong absorption in the ultraviolet (UV) region at 250–280 nm, other phenolic compounds, which do not react with formaldehyde and/or protein also show strong absorptions in this UV region. Roux [27] developed a simple and extremely rapid UV method for tannin analysis for leather tannin. Consequently, the UV method was used to determine tannin contents of wattle tannin extracts which had been analyzed previously by both the Stiasny and the hide-powder methods. In addition, the relationships among the results obtained by these three methods were statistically analyzed with a desire to replace the laborious and time-consuming hide-powder and the Stiasny methods by the more rapid UV method. A Chinese wattle tannin, which had been previously analyzed [27] was fractionated into six fractions using an ultrafiltration technique and each fraction was analyzed by the hide-powder, the Stiasny and the UV methods. Since the ethyl acetate soluble fraction gave the highest values by both the Stiasny and the hide-powder methods, this was regarded as a standard tannin fraction. Consequently, these values (i.e., 108.9, 120.4 and 93.0 for the Stiasny, the UV and the hide-powder method, respectively) were used as standards for the three methods. The original values of wattle tannin were 95.4%, 105.3% and 81.1% for the Stiasny, the hide-powder and the UV methods were divided by these standard values, respectively, so that tannin contents calculated were 87.6, 87.5 and 87.2, respectively. Thus, the UV method is a quick and simple procedure which can be used to estimate both Stiasny values for wood adhesives and tannin contents for leather tanning [28].

3.2. Estimation of Tannin Contents in the Bark Using NIR and NMR

Near infrared (NIR) spectroscopy was previously investigated as an alternative to the traditional methods of bark analysis for *A. mearnsii* [29]. The availability of the bark samples studied together with the data obtained from the analyses using the hide-powder, the Stiasny and the UV methods provided an opportunity in investigate whether NIR spectroscopy could be used to estimate several parameters in a set of *A. mearnsii* bark samples. The analysis of two sets of *A. mearnsii* De Wild. samples by NIR spectroscopy were studied. Set 1 samples were characterized in terms of hot water extractives, Stiasny value and polyflavanoid content, whilst Set 2 samples were characterized by nine different parameters, including tannin content. Calibrations developed for hot water extractives and polyflavanoid content (Set 1) gave very good coefficients of determination and performed well in prediction. Set 2 calibrations were generally good with total and soluble solids, tannin content, Stiasny value-2 and UV-2. However, owing to the small number of Set 2 samples, no predictions were able to be made using the calibrations. The study concluded that NIR spectroscopy had considerable potential for the rapid assessment of the quality of extractives in *A. mearnsii* bark [30].

In order to obtain a direct estimation of the tannin content in *A. mearnsii* bark, the application of NIR spectroscopy together with multivariate calibration methods were studied on samples of barks which were natural non-treated, and also which had been dried and milled. Ten determinations per hour including the sample preparation procedures were claimed to be able to be completed using NIR with a time of twenty hours for each determination using the Standard (NBR 11131) method [31]. The NIR method has been further developed [32].

An analytical method based on the solid state ^{13}C-NMR spectrum of bark [33] has been reported. The solid state ^{13}C-NMR of ground *A. mearnsii* bark before and after tannin extraction were obtained. The signal intensities were normalized against the 173 ppm hemicellulose signal based on the assumption that hemicelluloses were not extracted. At least ca. 80% of the total tannin was extracted from the *A. mearnsii* bark. Thus, solid state ^{13}C-NMR offers the advantage of being applicable to source materials in their native state, and has potential applications in optimizing extraction processes, identification of tannin sources, and characterization of tannin content in cultivar yield improvement programs.

3.3. Proanthocyanidin Composition of Wattle Tannin from A. mearnsii Bark

Wattle tannin has been commercially produced by extracting *A. mearnsii* bark with hot water. The major components of wattle tannin are "condensed tannin" which consists of flavanoid units (mainly flavan-3-ols) condensed to varying degrees. The distinctive flavan-3-ols are fisetinidol, robinetinidol, catechin and gallocatechin. These flavanoid monomers are attached to one another by means of carbon-carbon linkages, so that polymeric flavonoids are formed by the 4-8 and the 4-6 bonds and four biflavanoids: fisetinidol-(4α-8)-catechin, robinetinidol-(4α-8)-catechin and robinetinidol-(4α-8)-gallocatechin (all trans stereochemistry) and fisetinidol-(4β-8)-catechin (2,3-*trans*-, 3,4-*cis*: 2′,3′-*trans*-stereochemistry) [34] and two triflavanoids: robinetinidol-(4α-8″)-robinetinidol (4′α-6″)-gallocatechin and robinetinidol-(4α-8″)-robinetinidol (4′α-6″)-catehin have been isolated and identified [35]. A study on wattle tannin from *A. mearnsii* bark in China isolated and identified three dimeric proanthocyanidins: robinetinidol-(4α-8)-catechin, fisetinidol-(4β-8)-catechin and robinetinidol-(4β-8)-catechin. The robinetinidol-(4β-8)-catechin isolated was found to be a new natural product [36].

As monomeric flavonoid compounds, wattle tannin from *A. mearnsii* bark contains leucofisetinidin, leucorobinetinidin, quercetin, myricetin, butin, butein, robtein, fisetinidol, robinetinidol, catechin, gallocatechin, fustin, dihydrorobinetin, fisetin and robinetin [37]. In addition, it contains as carbohydrates: pinitol, sucrose, glucose and fructose, and the amino acids pipecolic acid, 4-hydroxypipecolic acid, albizzine, proline, α-alanine, arginine, aspartic acid, glutamic acid and serine. A "steroid" alcohol, and a long-chain β-diketone have also been identified [38].

According to a recent phytochemical study, fractionation of *A. mearnsii* bark extract using a Diaion HP20SS column with water showed that the tannin consisted of 20.6% sugars and 72.4% polyflavonoid compounds from which sixteen compounds, including a new flavan-3-ol glycoside, 4′- *O*-methylrobinetinidol 3′-*O*-β-D-glucopyranoside and two new proanthocyanidin dimmers, fisetinidol-(4α-6)-gallocatechin and epirobinetinidol-(4β-8)-catechin were isolated and identified. In addition, the compounds robinetinidol, syringic acid, gallocatechin, catechin, taxifolin, butin, robinetinidol-(4α-8)-gallocatechin, robinetinidol-(4α-8)-catechin, fisetinidol-(4α-8)-catechin, 1,6-di-*O*-galloyl-β-D-glucose, 4-hydroxy-2-methoxyphenyl 1-*O*-β-D-glucopyranoside, 3,5-dimethoxy-4-hydroxybenzyl alcohol 4-*O*-β-D-glucopyranoside and multifidol glucoside were identified [39].

In order to determine the chemical structures of wattle tannin, small amounts (150–200 μg) of catechin, epicatechin, gallocatechin, catechin-(4α-8)-catechin and robinetinidol-(4α-8)-catechin were analyzed by pyrolysis/gas chromatography (GC). The results using this method established that pyrolysis/gas chromatography can give a rapid analysis of the degradation products. An acetone-water (70%) soluble condensed tannin extract from *A. mearnsii* bark was analyzed by using this pyrolysis/GC method and resorcinol and pyrogallol were found to be the main pyrolysis products with relatively small amounts of catechol, 4-methylcatechol and 5-methylpyrogallol. The ratio (P/C: mol/mol) of pyrogallol type B-ring to catechol type B-ring was found to be 4.21, which was consistent with that previously reported using the NMR method [40].

Since electrospray ionization (ESI) provides more reliable information on smaller molecules than matrix-assisted laser desorption ionization (MALDI) and also permits product and precursor ion investigations, a commercial wattle tannin from *A. mearnsii* bark was analyzed using a QTRAP 3200 triple-quadrupole mass spectrometer, coupled with an ESI source and the chemical composition of its proantocyanidins were determined. A total of 90.6% of the tannin extract was found to be proanthocyanidins, in which the compositions of dimers, trimers and tetramers are 42%, 40% and 8.6%, respectively. In addition, the analysis was able to provide detailed chemical structures of these proanthocyanidins [41].

Although ^{1}H- and ^{13}C-NMR spectroscopy has been used to elucidate the chemical structures of proanthocyanidins from bark extracts of *A. mearnsii*, particularly two-dimensional ^{13}C, ^{1}H-correlated (HSQC: Heteronuclear Single Quantum Correlation) spectroscopy, a new analytical method using ^{31}P-NMR has recently been developed for the quantitative determination of wattle tannin from *A. mearnsii* bark. All labile hydrogens (aliphatic, phenolic hydroxys and carboxylic acid hydroxyl groups) of a commercial wattle tannin were labeled with a phosphorus-containing reagent, 2-chloro-4,4,5,5-tetramethyl-1,3,2dioxaphospholane (Cl-TMDP) and were analyzed by quantitative ^{31}P-NMR and HSQC spectroscopy. The results showed that the ratio of pyrogallol to catechol was 6.8 to 1 in B-ring, whilst the A-ring substitution showed a phlorogrucinol to resorcinol ratio of 3 to 2. However, the calculated proanthocyanidins content of the sample was only 49% [42].

4. Biological Activities of Wattle Tannin

4.1. Antioxidant

The antioxidant activity of wattle tannin from *A. mearnsii* bark was first discovered in 2001 and reported in a patent publication in 2004 [1] but scientific papers on wattle tannin and its antioxidant activity have been published more recently.

In 2007, Liu et al. [43] reported a relationship between antioxidant activity of *A. mearnsii* bark extract and anti-tumor activity. Radical scavenging ability assays indicated that the proanthocyanidins crude products from the extract had a strong antioxidant activity. An anti-tumor test of the proanthocyanidins on human cancer cells cultured in vitro showed that the proanthocyanidins had a medium effect on promyelocytic cell line, weak effect on human stomach adenocarcinoma and human hepatocellular carcinoma. In 2010, Shen et al. [44] showed that free-radical scavenging activity of the proanthocyanidins from the bark of *A. mearnsii* was measured by the DPPH method and

found that the proanthocyanidins product had a strong radical scavenging ability. In addition, it was also found that the proanthocyanidins had better anti-tumor activities than those from the bark of *Pinus massoniana*, and interestingly, the proanthocyanidins obtained from the ethyl acetate fraction of the wattle tannin had better anti-tumor activities than those from the water fraction. Huang et al. [45] reported also in 2010 on a relationship between antioxidant activity of *A. mearnsii* extract and viability of human neuroblastoma SH-SY5Y cells and indicated that a galloyl dimer prorobinetinidin from *A. mearnsii* De Wild. robinetinidol-(4β-8)-epigallocatechin 3-*O*-gallate (REO), has antioxidant properties and could protect the brain against acrolein-induced oxidative damage. The REO protects neurons from the deleterious effects of acrolein via the attenuation of oxidative stress. In 2017, a study on the comparison of the antioxidant activity between proanthocyanidins' dimer from *A. mearnsii* De Wild. bark powders and catechins was made and showed that the antioxidant activity of the proanthocyanidin, procyandin-(4,6)-prorobinetinidin was higher than that of catechin and epigallocatechin gallate (EGCG) [46].

In 2018, Ikarashi et al. [47] reported the anti-hypertensive effects of the extracts from bark of *A. mearnsii*. Spontaneously hypertensive rats (SHR) with hypertension and control Wistar Kyoto rats (WKY) were fed food containing the extracts or control food for 4 weeks. The systolic blood pressure of the SHR treated with the extracts for 4 weeks were found to have decreased from the first week of treatment when compared to the systolic blood pressure of the controls. The decrease depended on the dose of the extracts. Diastolic blood pressure showed similar results. Additionally, blood SOD activity in SHR was significantly higher in the extracts group than in the control group. The anti-hypertensive effects of the extracts may be related to the anti-oxidative effects of increased blood SOD activity.

In 2004, the first patent entitled "Active oxygen scavenger prepared from Acacia plant bark, and composition made from the same" was published [48]. The superoxide sucavenging activity (SOSA) values of hot water extract from *A. mearnsii bark*, both ethanol and methanol soluble fractions from the hot water extract, vitamin C, and catechin were found to be 1900, 2400, 2100, 360, and 340 ($\times 10^3$ unit/g), respectively. It suggested that the antioxidant activity of the extract from *A. mearnsii* was extremely high. A patent was applied for in 2006 entitled "Antioxidant composition containing component originating in the bark of tree belonging to the genus *Acacia*" [49] and another patent relating to antitumor applications in 2006 entitled "Composition for preventing and/or treating tumor containing component originating in the bark of tree belonging to the genus *Acacia*" was applied for [50]. Then in 2009, a patent entitled "Anti-oxidant compositions" was published. The specification of the patent described that an extract from the bark of *A. mearnsii* may be used as an anti-oxidant in animal feeds and in the raw materials of feeds, as well as in the prevention of the oxidation and depletion of vitamins therein and in vivo [51].

4.2. Antimicrobial Activity

It has been reputed that *A. mearnsii* bark extract have been used as a medicinal plant for the treatment of microbial infections in Africa. Antimicrobial effects of wattle tannin from *A. mearnsii* bark have been studied and the results are summarized in Table 1.

4.2.1. Antifungal Activity

In 1994, Ohara et al. [52] studied the effects of 70% acetone/water extract from *A. mearnsii* bark on wood rotting fungi. Results of antifungal activities of the ethyl acetate-soluble fraction (EA) and water-soluble fraction (AW) on white rot fungus, *Coriolus versicolor*, showed that AW had no antifungal activity at 0.01–0.25% concentrations, and EA had very mild activities at 0.1–0.25% concentrations. Similar tendencies have been observed with brown rot fungus, *Tyromyces palustris*.

The antimicrobial activity of a crude acetone extract of *A. mearnsii* stem bark was also evaluated. Fungal isolates are shown in Table 1. The Minimum Inhibitory Concentration (MIC) values for fungal isolates were 625–5000 µg/mL. The antibiosis determination showed that the extract was more fungicidal (66.67%) than fungistatic (33.33%) [53]. Cristiane et al. [54] reported that *A. mearnsii* extract

tannin showed antimicrobial activity. Inhibition activities of *Aspergillus niger* ATCC 9642 (fungus) and *Candida sp.* ATCC 14053 (yeast) were weak.

The toxicity of the tannin extract from *A. mearnsii* bark was also evaluated with *Saccharomyces cerevisiae*, Wild-type strain BY4741 and Δ*gsh1* strain which lacks the glutathione enzyme. In the poisoner quantitative drop test, both strains showed growth at concentrations of 2.10 mg/L, which is comparable with the control (0.0 mg/L). However, it was observed that toxic effects on the both strains became apparent at a concentration of 4.20 mg/L. This result showed that *A. mearnsii* extract could be toxic on yeast if the extract concentrations were sufficiently high [55].

A Brazilian patent [56] filed in 2007 entitled "Antifungal composition based on plant extracts for the treatment of green wood" describes the antifungal composition which comprises 10–70% tannins: extracts from *A. mearnsii*, *Quebracho colorado*, *Caesalpinia spinosa*, *Caesalpinia coriaria*, *Rhus coriaria*, etc. and 5–30% anionic surfactant prepared in situ by neutralization of sulfonic acids with agents in aqueous solution. A Chinese patent specification [57] filed in 2007 entitled "Compounded bacteriostatic agent containing plant polyphenol" also describes agents composed of tannins from valonia, larch and/or *A. mearnsii*, *Radix glycyrrhizae* powder, *Ginkgo biloba* leaf powder and baicalein.

4.2.2. Antibacterial Activity

Smith et al. [58] reported that the growth of *Escherichia coli* was inhibited by wattle tannin extract only when the tannins were exposed to oxygen. This is bacause tannins autoxidize and a substantial amount of hydrogen peroxide is generated when they are added to an aerobic medium.

Zoetendal et al. [59] found that when *E. coli* was grown with tannin extract from *A. mearnsii* bark under anaerobic conditions, its growth was not inhibited. One of the mechanisms whereby the cells of gram-negative bacteria was protected was believed to be related to genes such as the cell envelope stress protein gene *spy* and the multidrug transporter-encoding operon *mdt*ABCD, both of which are controlled by the BaeSR two-component regulatory system. Since the growth of *E. coli* mutant, which lacks the BaeSR system, was found to be inhibited by wattle tannin under anaerobic conditions, the BaeSR system may also play a prominent role.

Scientific validation of the antifungal and antibacterial activities have been reported, and these results support the use of *A. mearnsii* in traditional medicine for the treatment of microbial infections [53,60]. Olajuyigbe et al. [60] found antibacterial potentials of crude methanolic extract of the stem bark of *A. mearnsii* against some bacteria of clinical importance in shigellosis. Bacteria used in the study are shown in Table 1. The MIC values for gram-negative bacteria were 0.0391–0.3125 mg/mL while for Gram-positive bacteria they were 0.0781–0.625 mg/mL. The antimicrobial activity of a crude acetone extract of *A. mearnsii* stem bark was also evaluated. Bacterial isolates are shown in Table 1. The MIC values for Gram-positive bacteria were 78.1–312.5 µg/mL and for Gram-negative bacteria 39.1–625 µg/mL. The bacteria were more susceptible to the tannins than the fungal strains tested. The antibiosis determination showed that the extract was more (75%) bactericidal than bacteriostatic (25%) [53]. The results also showed that there was no significant differences between the MIC values of methanol extract and those of acetone extract against Gram-negative and Gram-positive bacteria.

The cytotoxicity activity of an acetone extract was observed between the concentration range 31.25 µg/mL and 500 µg/mL. The LC_{50} value 112.36 µg/mL indicated that the extract was nontoxic in the brine shrimp lethality assay ($LC_{50} > 100$ µg/mL) [53].

A number of additional investigations on the antimicrobial activity of tannin extracts has been reported. Cristiane et al. [54] reported that *A. mearnsii* extract tannin showed antimicrobial activity. Inhibition activities of *Staphylococcus aureus* (gram-positive) were strong. Tannins from *A. mearnsii* were encapsulated using sol-gel methods silicate route, and the hybrid materials had good antimicrobial activities, which were similar to those exhibited by the neat tannins.

The influences of acetone, methanol and aqueous extracts of *A. mearnsii* on the ultrastructures, protein and lipid leakages of five different bacteria were investigated. The bacteria used in the study are shown in Table 1. The extracts caused significant ultrastructural changes, protein and lipid leakages.

While an aqueous extract was the most effective in causing protein leakages, the methanol extract was the leading cause of lipid leakages [61].

Interactions between the methanol extract of *A. mearnsii* bark and eight antibiotics were investigated by MIC, agar diffusion and checkerboard assays. Bacteria used in the study are shown in Table 1. The MICs of all the antibiotics ranged between 0.020 and 500 µg/mL while that of the the extract varied between 0.156 and 1.25 mg/mL. The checkerboard assays showed synergistic interaction (61.25%), additivity/indifference (23.75%) and antagonistic (15%) effects. Differences in the resultant synergistic, indifferent and antagonistic interactions observed in this test were due to the elevated MIC values obtained from the resistance of these bacteria to some of the antibiotics [62]. The antibacterial activities of the acetone extract from *A. mearnsii* bark and its interactions with antibiotics against some resistant bacterial strains were evaluated. The bacteria used in the study are shown in Table 1. The antibacterial combinations were mainly antagonistic than synergistic in the agar diffusion assay. Although the antibacterial combinations in agar diffusion assay were mostly antagonistic interactions, the microbroth dilution assay showed the extract and the antibiotics exerted a variable degree of inhibitory effects on the test organisms. The in vitro antibacterial activities of these antibiotics and their combinations were further assessed with the checkerboard assay to determine the fractional inhibitory concentration (FIC) index. From the checkerboard assay, the antibacterial combinations showed a variety of degrees of interactions including synergism, additive, indifference and antagonism interactions. While antagonistic and additive interactions were 14.44%, indifference interaction was 22.22% and synergistic interaction was 37.78% of the antibacterial combinations against the test isolates [63].

Commercially available tannin-based products were studied as natural sanitizers. Lettuce is often involved in foodborne outbreaks caused by pathogenic *E. coli*. Klug et al. [64] compared the efficacy of tannin extracts and chlorine treatments on the reduction of *E. coli* ATCC 25922 adhering to lettuce leaves. The treatment with tannin extracts from black wattle (1%, *v*/*v*) reduced the *E. coli* adhering to and under any biofilm formation on lettuce leaves and its effect was similar to that found with chlorine solutions.

4.2.3. Inhibitory Effects on Cyanobacteria

Algal bloom control by black wattle extract has been studied in China. Zhou et al. [65] showed that in a short-term test, 3–4 mg/L black wattle extract inhibited the growth of *Microcystis aeruginosa* and reduced the algal cell density in one week, whereas serious algal blooms occurred in the untreated control mesocosm. More importantly, a long-term test suggested that black wattle extract played a significant role in plankton structure optimization at the lower concentrations of 1–2 mg/L. This study provided a novel natural plant agent, which not only had positive effects on algal bloom control but also restored the aquatic ecosystem. Luo et al. [66] indicated that *A. mearnsii* extracts increased the membrane permeability of *M. aeruginosa* by damaging the ultrastructure of the algal cells, leading to a decrease in the number of algal cells and chlorophyll-a. Liu et al. [67] suggested that both the photosynthetic systems and membranes of *M. aeruginosa* were potentially damaged by the *A. mearnsii* extract. That *A. mearnsii* extract can significantly increase cell membrane permeability and Ca^{2+}/Mg^{2+}-ATPase activity on the membrane was demonstrated. A long-term exposure of *A. mearnsii* extract at 20 ppm led to algal cell membrane leakage or even lysis. A comparison of expression of three photosynthesis-related genes (*rbc*L, *psa*B and *psb*D) in *M. aeruginosa* with and without plant extract treatment revealed that their expression was remarkably reduced in the presence of the extract. This could indicate the inhibition of the photosynthetic process.

Table 1. Antimicrobial effects of wattle tannin from *A. mearnsii* bark.

No.	Extracts	Tested Bacterial Isolates	Growth or Inhibition	Reference
1 *	Water soluble fraction (AW) from 70% acetone-water soluble extract	*Coriolus versicolor* *Tyromyces palustris*	No antifungal activity at 0.01–0.25% concentrations	[52]
	Ethyl acetate soluble fraction (EA) from 70% acetone-water soluble extract	*C. versicolor* *T. Palustris*	Very mild activities at 0.1–0.25% concentration	
	Crude acetone extract	*Candida krusei* *Candida albicans* *Candida rugosa* *Candida glabrata* ATCC 2001 *Absidia corymbifera* *Fusarium sporotrichioides* *Trichophyton tonsurans* *Trichophyton mucoides* ATCC 201382 *Aspergillus niger* *Aspergillus terreus* *Aspergillus flavus*	MIC values were fungal isolates (625–5000) µg/mL	[53]
	Tannins	*A. niger* ATCC 9642 *Candida* sp. ATCC 14053	Weak inhibition activity	[54]
2 *	Aqueous extract	*Saccharomyces cerevisiae* BY4741 *S. cerevisiae* Δ gsh1	In the poisoner quantitative drop test, toxicological effects from a concentration of 4.20 mg/L	[55]
	Crude acetone extract	*Escherichia coli* ATCC 25922 *Bacillus cereus* ATCC 10702 *Proteus vulgaris* KZN *Serratia marcescens* ATCC 9986 *Pseudomonas aeruginosa* ATCC 19582 *Enterococcus faecalis* KZN *Klebsiella pneumoniae* ATCC 10031 *P. vulgaris* CSIR 0030 *Bacillus pumilus* ATCC 14884 *K. pneumoniae* KZN *Staphylococcus aureus* OK1 *Salmonella typhi* ATCC 13311	MIC values were Gram-positive bacteria (78.1–312.5) µg/mL, Gram-negative bacteria (39.1–625) µg/mL	[53]
	Tannins	*S. aureus*	Strong inhibition activity	[54]
	Aqueous extract	*E. coli* BW13711 *E. coli* TA4131	No growth in 0.1% wattle tannin extract medium	[58]
		E. coli WTT1 *E. coli* TA4110	No growth in 0.15% wattle tannin extract medium	
	Aqueous extract	*E. coli* BW13711 *E. coli* Δ*Bae*SR13711	Growth of the *E. coli* ΔBaeSR mutant reached behind stationary phase compared to that of *E. coli* BW13711 in the presence of tannins	[59]
	Crude methanol extract	*E. coli* ATCC 8739 *K. pneumoniae* ATCC 10031 *B. pumilus* ATCC 14884 *P. vulgaris* ATCC 6830 *Acinetobacter calcoaceticus* *A. calcoaceticus* anitratis CSIR *P. vulgaris* CSIR 0030 *Shigella flexneri* KZN *S. typhi* ATCC 13311 *Micrococcus luteus* *E. faecalis* KZN *S. aureus* OK2b *S. aureus* OK1 *S. aureus* OK3	Minimum inhibitory concentration (MIC) values were gram-negative (0.0391–0.3125) mg/mL and gram-positive bacteria (0.0781–0.625) mg/mL	[60]
	Acetone, methanol and aqueous extracts	*E. coli* *S. aureus* *B. pumilus* *P. vulgaris* *S. flexneri*	Extracts caused the disruption of the cytoplasmic membranes of the bacterial cells.	[61]

Table 1. *Cont.*

No.	Extracts	Tested Bacterial Isolates	Growth or Inhibition	Reference
	Methanol extract	*S. aureus* ATCC 6538 *E. faecalis* ATCC 29212 *E. faecalis* ATCC 29212 *E. coli* ATCC 25922 *Bacillus subtilis* KZN *P. vulgaris* KZN *E. faecalis* KZN *Enterobacter cloacae* ATCC 13047 *K. pneumoniae* (ATCC 10031) *P. vulgaris* ATCC 6830 *Shigella sonnei* ATCC 29930	Synergetic, indifferent and antagonistic interactions were differences depending on combination between bacterial types and antibiotics agent types with the extract	[62]
	Acetone extract	*E. coli* ATCC 25922 *B. cereus* ATCC 10702 *P. aeruginosa* ATCC 19582 *S. marcescens* ATCC 9986 *E. faecalis* KZN *S. aureus* ok1 *S. flexneri* KZN *M. luteus* *P. vulgaris* CSIR 0030 *S. typhi* ATCC 13311	Synergetic, additive, indifference and antagonism interactions were differences depending on combination between bacterial types and antibiotics agent types with the extract	[63]
	Tannin extract	*E. coli* ATCC 25922	Tannin extract is capable of reducing the counts of *E. coli* adhered to and under biofilm formation on lettuce leaves.	[64]
3 *	Aqueous extract	*Microcystis aeruginosa*	Black wattle extract inhibits algal blooms in a short-term test and the extract maintains water quality and prevents algal blooms in a long-term test.	[65]
	Extract	*M. aeruginosa*	Extract damage to the ultrastructure of the algal cell and decrease algal cells and chlorophyll-a.	[66]
	Aqueous extract	*M. aeruginosa*	Expression of photosynthesis-related genes was remarkably reduced in the presence of the extract.	[67]

1 *: Antifungal activity, 2 *: Antibacterial activity, 3 *: Inhibitory effect on cyanobacteria.

4.3. Inhibition of Enzymes

The protein-adsorbing capacities of various kinds of tannin fractions can be determined by the formation of precipitates with bovine serum albumin. Ohara et al. [53] indicated that the protein-adsorbing capacities of low-molecular weight proanthocyanidins were weaker than those of proanthocyanidin polymers. Since enzymes are protein molecules in cells, proanthocyanidins polymers are very likely able to adsorb these proteins resulting in the deactivation of the enzymes. Several studies on the enzyme inhibitions of *A. mearnsii* extract have been reported.

Takagi et al. reported the tyrosinase inhibition effects of aqueous acetone (70%) extracts of *A. mearnsii* bark, which showed high flavanol contents and strong tyrosinase inhibition, whilst the quebracho extracts inhibited tyrosinase activity only slightly despite its high flavanol content. The relation between the phenolic hydroxylation pattern and tyrosinase inhibition suggested that the proanthocyanidins with a 5,7-dihydroxyphenyl structure in the A-ring and a 3,4,5-trihydroxyphenyl structure in the B-ring have potent tyrosinase inhibitory activity [68]. Before these results were reported in the scientific journal in 2003, a patent entitled "Preparation for external use for skin/Novel use of extract isolated from bark of larch, acacia or duramen of *Schinopsis lorentsii* as skin whitening agent" was published in 1998 [69]. The patent describes that an extract from bark of *A. mearnsii* has an inhibition effect on the tyrosinase activity and can be used for producing an external preparation for skin whitening. More recently, a Chinese patent "Skin deep-clean facial cream for suppressing

tyrosinase and decomposing melanin" was published in 2017 [70]. The title facial cream comprises (by wt %): *A. mearnsii* bark proanthocyanidins 0.01–0.5%.

Other studies on the inhibition of digestive enzymes such as lipase, α-amylase and glucosidase have been reported. Kusano et al. [40] indicated that the bark extract from *A. mearnsii* showed strong lipase and α-amylase inhibition. Active substances responsible for the inhibition were found to be proanthocyanidins oligomers, which are mainly composed of 5-deoxyflavan-3-ol units with pyrogallol- and catechol-type B-rings. Mariano et al. [71] showed that a condensed tannin from *A. mearnsii* was an effective inhibitor of both human salivary and porcine pancreatic α-amylase. Similarly, the extract from pinhão (*Araucaria angustifolia*) seed coat was also effective in diminishing the post-prandial glycemic levels in rats after starch administration. Matsuo et al. [72] showed that the extent of the strength of α-amylase inhibitory activity depended on the B-ring's structures of the proanthocyanidins. The spectroscopic results clearly indicated that fractions with strong inhibitory activity contained proanthocyanidins oligomers with catechol-type B-rings rather than pyrogallol-type B-rings. HPLC analysis of the pyrolysis products showed peaks for pyrocatechol were only observed in the mixtures obtained from the fractions with high inhibitory activities. Kato et al. [73] indicated that the human salivary α-amylase was more strongly inhibited by hydrolysable tannin than by condensed tannin with the concentrations for 50% inhibitory concentration (IC_{50}) being 47.0 and 285.4 μM, respectively. The inhibitory capacities of both tannins on the pancreatic α-amylase were also different, with IC_{50} values being 141.1 μM for the hydrolysable tannin and 248.1 μM for the condensed tannin. Xiong et al. [74] compared the anti-inflammatory and digestive enzymes (α-glucosidase and α-amylase) inhibitory activities of the polyphenols isolated from *A. mearnsii* bark crude extract and fractions (Fr.1–Fr.7) obtained by high-speed counter-current chromatography (HSCCC). Fractions B4, B5, B6, B7 (total phenolics 850.3, 983.0, 843.9, and 572.5 mg/g, respectively) showed significant activities against reactive oxygen species (ROS), nitric oxide (NO) production, and expression of pro-inflammatory genes interleukin-1β (IL-1β) and inducible nitric oxide synthase (iNOS) in a lipopolysaccharide-stimulated mouse macrophage cell line RAW 264.7 (a mouse macrophage cell line ATCC TIB-71). All of the crude extract and the fractions suppressed α-glucosidase and α-amylase activities.

4.4. Anti-Obesity and Anti-Diabetes

Wattle tannin from *A. mearnsii* bark has been studied as a functional substance. Ikarashi et al. [75] investigated the anti-obesity/anti-diabetic effects of the extracts from the bark of *A. mearnsii* using obese diabetic KKAy mice. Increases in body weight, plasma glucose and insulin were significantly suppressed for the extract groups. The mRNA expression of energy expenditure-related genes (PPARα, PPARδ, CPT1, ACO and UCP3) in skeletal muscle increased, and the protein expressions of CPT1, ACO and UCP3 also increased. However, the expression of fat acid synthesis-related genes (SREBP-1c, ACC and FAS) in the liver decreased. The mRNA expression of adiponectin increased while the TNF-α in white adipose tissue decreased. These results indicated that the anti-obesity actions of the extract of *A. mearnsii* bark are attributable to increased expression of energy expenditure-related genes in skeletal muscle, and decreased fatty acid synthesis and fat intake in the liver.

Another mechanism for the anti-obesity and anti-diabetes, reduction in the intestinal absorption of lipids and carbohydrates has been reported by Ikarashi et al. [76]. In an in vitro study, the inhibitory activity of extracts from the bark of *A. mearnsii* on lipase and glucosidase was measured. The effects of the extracts on absorption of orally administered olive oil, glucose, maltose, sucrose and starch solution in mice were evaluated. The concentration of the extracts were found to inhibit the activity of lipase, maltase and sucrase with IC_{50}s of 0.95, 0.22 and 0.60 mg/mL, respectively. When oral administration of the extract solutions was used on ICR mice, the extracts significantly inhibited the increase in plasma triglyceride concentration after olive oil loading. The extracts also significantly inhibited the increase in plasma glucose concentration after maltose, sucrose or glucose loading. These results suggested that the extracts inhibited lipase and glucosidase activities, which lead to a reduction in the intestinal

absorption of lipids and carbohydrates. The inhibition of glucose uptake via a sodium-dependent glucose transporter (SGLT) and glucose transporter (GLUT) may be attributable to the extracts.

Before the use of proanthocyanidins as anti-obesity and anti-diabetes materials was reported in the scientific literature, two patents were filed. The first was published in 2006 [77] entitled "Hypoglycemic composition containing component originating in the bark of tree belonging to the genus *Acacia*", while the other entitled "An anti-obesity composition extracted from bark of trees belonging to *Acacia*" was filed in 2006 [78]. This patent specification describes polyphenols from bark of *A. mearnsii* De Wild. having effects in preventing and treating obesity, hypertension, diabetes, fatty liver, arteriosclerosis, cerebral infarction, hyperlipidemia, peripheral blood vessel dysfunction and ischemic heart disease, and the polyphenols could be incorporated into food, animal feed or pharmaceuticals, or used as an external use medicine.

4.5. Other Biological Activities

The aqueous-soluble fraction (AW) and the ethyl acetate-soluble fraction (EA) from the 70% acetone-water soluble extract from *A. mearnsii* bark described in Section 4.2.1 were considered to be promising naturally occurring termiticides because they had the ability to deactivate some insect enzymes. Results from termite tests showed that the EA and AW had remarkable anti-termite activities. Therefore, Ohara et al. [54] suggested that toxicities of proanthocyanidins as phenolic compounds might be involved in the anti-termite activities of the substances. In 2006, a patent [79] entitled "Aqueous extract to repel or exterminate termites" was published. The invention was aimed at the development of an aqueous solution based on a modified aqueous vegetable extract of tannins that could repel or exterminate termites. Active ingredients were based on aqueous organic sources such as tannins from the black wattle tree (*A. mearnsii* De Wild). In 2008, another patent entitled "*Acacia* mearnsii bark extract as insecticide" was published. The extract from *A. mearnsii* bark had been found to be an insecticide suitable for the control of *Aedes aegypti*, *Culex quinquefasciatus* and *Simulium pertinax* [80].

In 2012, the effect of the extract from *A. mearnsii* bark on skin was studied. By using HR-1 mice with atopic dermatitis (AD), an improvement in atopic dermatitis symptoms was observed when the mice were fed the extract. A ceramide expression in the skin was not changed in the *Acacia* group despite a decrease in the AD group. The mRNA expression of ceramidase was found to decrease in the *Acacia* group compared to the AD group. The extract from *A. mearnsii* bark appeared to inhibit itching in atopic dermatitis by preventing the skin from drying. The mechanism by which this occurred involved the inhibition of increased ceramidase expression associated with atopic dermatitis [81]. In 2001, a patent entitled "Histamine liberation suppressing agent/Histamine release inhibitor containing plant extracts for relieving inflammation and preventing periodontitis" was filed. The patent specification described a safe histamine release inhibitor comprising wattle bark (bark of *A. mearnsii*). This could be formulated into cosmetics and pharmaceuticals for relieving inflammation, or formulated into dentifrice or oral drug for preventing periodontitis [82]. In 2006, the patent "Composition for preventing and/or treating itching containing component originating in the bark" was published [83].

Xiong et al. [74] showed that polyphenols could be isolated from a crude extract of *A. mearnsii* bark and evaluated their anti-inflammatory effects. The study showed that the crude extract could significantly decrease the non-mitochondrial oxidative burst that is often associated with an inflammatory response in human monocytic macrophages.

5. Conclusions

Even though the name of the genus *Acacia* was derived from *Acacia nilotica*, the name of the species originally known as *Acacia nilotica* was recently changed to *Vachellia nilotica*, whilst the name of *Acacia mearnsii* has remained.

In order to determine the amount of active compounds in wattle tannin for a specific application, a number of analytical methods are in use. When tannin is to be used for the production of a wood

adhesive, the Stiasny method is used; however when the tannin is to be used in the tanning of hides, the hide-powder method is usedA simple UV method has been found to estimate values found using both the Stiasny and hide-powder methods. The tannin contents in bark can also be estimated using NIR and NMR, although these techniques require data from wet chemistry.

The chemical composition of wattle tannin has been determined using traditional organic chemistry techniques such as isolation and identification of compounds. Tannin consists of polyflavanoids whose molecular masses which may range from 300 to 3000 with flavanoid units such as fisetinidol, robinetinidol, catechin and gallocatechin. All the chemical compounds isolated from wattle tannin have been updated. More detailed chemical composition information can be obtained using pyrolysis/GC analysis, electrospray mass spectrometry investigation and quantitative ^{31}P-NMR and HSQC analyses.

Studies on the relationships between antioxidant and anti-tumor activity of wattle tannin, viability of human neuroblastoma SH-SY5Y cells and the anti-hypertensive effects have been studied. Robinetinidol-(4β-8)-epigallocatechin 3-*O*-gallate was found to have antioxidant properties and could protect brain cells against acrolein-induced oxidative damage.

The antioxidant activity of proanthocyanidins from tannin was higher than that of flavan-3-ols monomers such as catechin and epigallocatechin gallate. As there are many reports on the relationship between antioxidant and a number of biological activities, the possibilities exist for making use of these properties of proanthocyanidins.

A total of fourteen papers and two patents reported the antimicrobial activities of wattle tannin. Generally, bacteria were more susceptible to the tannins than the fungal strains tested. Several bacteria were inhibited by the extract from *A. mearnsii* bark. The growth inhibition mechanisms of *E. coli* were investigated. An interaction between extracts from *A. mearnsii* bark and antibiotics have also been studied. The extracts from *A. mearnsii* bark inhibit the growth of cyanobacteria.

The proanthocyanidins from wattle tannin have the ability to inactivate digestive enzymes such as α-amylase, lipase and glucosidase. In vivo experiments on anti-obesity and anti-diabetes have also been reported. Several patents describing the behavior of these digestive enzymes in anti-diabetes and anti-obesity studies have been reported. There have been reports on the use of *Acacia* bark extract as an antitermite material, on the inhibition of itching in atopic dermatitis and anti-inflammatory effects.

In conclusion, the growth of bacteria was inhibited by the extract from *A. mearnsii* bark, and a typical intestinal bacterium such as *E. coli*, *K. pneumoniae*, *P. vulgaris* and *S. marcescenes* was also inhibited by extracts. Based on these results, the *Acacia* bark extract may inhibit not only the growth of *E. coli*, *K. pneumoniae*, *P. vulgaris* and *S. marcescenes* but also the growth of other types of intestinal bacteria such as *Clostridium* and *Bacteroides*, the so-called "bad bacteria" If tannin extract from *A. mearnsii* bark inhibits growth of these "bad bacteria" in vivo evaluation, the extracts might be able to be used as a new dietary supplement, which could control the human intestinal microbiome to keep the body healthy.

References

1. Yazaki, Y. Utilization of Flavonoid Compounds from Bark and Wood: A Review. *Nat. Prod. Commun.* **2015**, *10*, 513–520. [PubMed]
2. Stevens, P.F. "Fabaceae". Available online: http://www.mobot.org/MOBOT/Research/APweb/orders/fabalesweb.htm#Fabaceae (accessed on 17 January 2018).
3. Kewscience. Plants of the World online (/). Available online: http://www.plantsoftheworldonline.org/taxon/urn:lsid:ipni.org:names:77089275-1 (accessed on 17 January 2018).

4. Miller, P. The Gardeners Dictionary, 4th ed.London, UK, 1754.

5. Ross, J.H. A survey of some of the pre-Linnean history of the genus *Acacia*. *Bothalia* **1980**, *13*, 95–110. [CrossRef]

6. Linnaeus, C. *Species Plantarum*, 1st ed.; Laurentius Salvius: Stockholm, Sweden, 1753.

7. Orchard, A.E.; Maslin, B.R. Proposal to conserve the name *Acacia* (*Leguminosae*: *Mimosoideae*) with a new type. *Taxan* **2003**, *52*, 362–363. [CrossRef]

8. Wattles-genus *Acacia*. Available online: http://www.anbg.gov.au/Acacia/ (accessed on 17 January 2018).

9. Pedley, L. Derivation and dispersal of *Acacia* (Leguminosae), with particular reference to Australia, and the recognition of *Senegalia* and *Racosperma*. *Bot. J. Linn. Soc.* **1986**, *92*, 219–254. [CrossRef]

10. Maslin, B.R.; Orchard, A.E.; West, J.G. Nomenclatural and classification history of *Acacia* (Leguminosae: Momosaoideae), and the implications of generic subdivision. Available online: http://worldwidewattle. com/infogallery/taxonomy/nomen-class.pdf (accessed on 17 January 2018).

11. Carruthers, J.; Robin, L. Taxonomic imperialism in the battles for *Acacia*: Identity and science in South Africa and Australia. *Trans. R. Soc. S. Afr.* **2010**, *65*, 48–64. [CrossRef]

12. Thiel, K.R.; Funk, V.A.; Iwatsuki, K.; Morat, P.; Peng, C.-I.; Raven, P.H.; Sarukhán, J.; Seberg, O. The controversy over the retypification of *Acacia* Mill. with an Australian type: A pragmatic view. *Taxon* **2011**, *60*, 194–198.

13. Kyalangalilwa, B.; Boatwright, J.S.; Daru, B.H.; Maurin, O.; Van der Bank, M. Phylogenetic position and revised classification of *Acacia s.l.* (Fabaceae: Mimosoideae) in Africa, including new combinations in *Vachellia* and *Senegalia*. *Bot. J. Linn. Soc.* **2013**, *172*, 500–523. [CrossRef]

14. Rather, L.J.; Shahid-ul-Islam; Mohammad, F. *Acacia nilotica* (L.): A review of its traditional uses, phytochemistry, and pharmacology. *Sustain. Chem. Pharm.* **2015**, *2*, 12–30. [CrossRef]

15. Dyer, C. New names for the African *Acacia* species in *Vachellia* and *Senegalia*. *Southern For. J. For. Sci.* **2014**, *76*. [CrossRef]

16. Boatwright, J.S.; Van der Bank, M.; Maurin, O. Name changes in African *Acacia* species. *VELD FLORA* **2014**, *100*, 33.

17. De Wildeman, E.A.J. Vascular Plants APNI—Australian Plant Name Index. Available online: https://biodiversity.org.au/nsl/services/APNI?publication=Wildeman%2C+E.A.J.+De+%281925%29% 2C+Plantae+Bequaertianae+3&search=true&advanced=true&display=apni (accessed on 17 January 2018).

18. Tame, T.; Kodela, P.; Conn, B.; Hill, K. Available online: http://plantnet.rbgsyd.nsw.gov.au/cgi-bin/euctax. pl?/PlantNet/wattle=&name=Acacia+mearnsii (accessed on 17 January 2018).

19. World Wide Wattle. *Acacia mearnsii* De Wild. Available online: http://worldwidewattle.com/speciesgallery/ species-intro.php?id=17958 (accessed on 17 January 2018).

20. Wiersum, K.F. *Acacia mearnsii* De Wild. In *Plant Resources of South-East Asia No. 3. Dye and Tannin-producing Plants*; Lemmens, R.H.M.J., Wulijarni-Soetjipto, N., Eds.; Pudoc/Prosea: Wageningen, The Netherlands, 1991; pp. 41–45.

21. Turnbull, J.W.; Midgley, S.J.; Cossaltar, C. Tropical *Acacias* planted in Asia: An overview. In *Recent Developments in Acacia Planting, Proceedings of the Third International Acacia Workshop, Hanoi, Vietnam, 27–31 October 1997*; Turnbull, J.W., Compton, H.R., Pinyopusarerk, K., Eds.; Fores Science Institute of Vietnam: Hanoi, Vietnam.

22. Roux, D.G. Study of the affinity of black wattle extract constituents. Part I. Affinity of polyphenols for swollen collagen and cellulose in water. *J. Soc. Leather Trades' Chem.* **1955**, *39*, 80–91.

23. Yazaki, Y.; Zheng, G.; Searle, S.D. Extractives Yields and Polyfavanoid Contents of *Acacia mearnsii* Barks in Australia. *Aust. For.* **1990**, *53*, 148–153. [CrossRef]

24. Zheng, G.; Lin, Y.; Yazaki, Y. Comparing Molecular Size Distribution of Tannin Extracts from *Acacia mearnsii* Bark from Different Countries. *Holzforshung* **1988**, *42*, 407–408.

25. Anon. *Official Method of Analysis*, 4th ed.; Society of Leather Trades' Chemists: Hertfordshire, UK, 1965.

26. Zheng, G.; Lin, Y.; Yazaki, Y. Bark tannin contents of *Acacia mearnsii* provenances and the relationship between the hide-powder and the Stiasny methods of estimation. *Aust. For.* **1991**, *54*, 209–211.

27. Roux, D.G. Photometric methods of tannin analysis for black wattle tannin. *J. Soc. Leather Technol. Chem.* **1951**, *35*, 322–337.

28. Yazaki, Y.; Gu, R.; Lin, Y.; Chen, W.; Nguyen, N.K. Analyses of Black Wattle (*Acacia mearnsii*) Tannins-Relationships Among the Hide-Powder, the Stiasny and the Ultra-Violet (UV) Methods. *Holzforschung* **1993**, *47*, 57–61. [CrossRef]

29. Donkin, M.J.; Pearce, J. Tannin analysis by near infrared spectroscopy. *J. Soc. Leather Technol. Chem.* **1995**, *79*, 8–11.

30. Schimleck, L.R.; Yazaki, Y. Analysis of Black Wattle (*Acacia mearnsii* De Wild.) Bark by Near Infrared Spectroscopy. *Holzforschung* **2003**, *57*, 527–532. [CrossRef]

31. Menezes, C.M.; Ben da Costa, A.; Renner, R.R.; Bastos, L.F.; Ferrão, M.F.; Dressler, V.L. Direct determination of tannins in *Acacia mearnsii* bark using near-infrared spectroscopy. *Anal. Methods* **2014**, *6*, 8299–8305. [CrossRef]

32. Grasel, F.S.; Marcelo, M.C.A.; Ferrão, M.F. Development of an inexpensive, practical and non-destructive methodology based on digital images from a scanner for the classification of commercial tannins from *Acacia mearnsii*. *Anal. Methods* **2017**, *9*, 3977–3982. [CrossRef]

33. Reid, D.G.; Bonnet, S.L.; Kemp, G.; van der Westhuizen, J.H. Analysis of commercial proanthocyanidins. Part 4: solid state ^{13}C-NMR as a tool for *in situ* analysis of proanthocyanidin tannins, in heartwood and bark of *Quebracho* and *Acacia*, and related species. *Phytochemistry* **2013**, *94*, 243–248. [CrossRef] [PubMed]

34. Botha, J.J.; Ferreira, D.; Roux, D.G. Condensed Tannins: Direct Synthesis, Structure, and Absolute Configuration of Four Biflavonoids from Black Wattle Bark ('Mimosa') Extract. *J. Chem. Soc. Chem. Commun.* **1978**, 700–702. [CrossRef]

35. Botha, J.J.; Ferreira, D.; Roux, D.G. Condensed Tannins: Condensation Mode and Sequence during Formation of Synthetic and Natural Triflavonoids. *J. Chem. Soc. Chem. Commun.* **1979**, 510–512. [CrossRef]

36. Shen, Z.; Yu, Q.; Chen, X.; Shen, H.; Xiao, Z. Study on black wattle tannins. III. Isolation and identification of proanthocyanidins and their ^{13}C-NMR characteristics. *Linchan Huaxue Yu Gongye* **1991**, *11*, 85–95.

37. Roux, D.G. Review Article: Recent advances in the chemistry and chemical utilization of the natural condensed tannins. *Phytochemistry* **1972**, *11*, 1219–1230. [CrossRef]

38. Saayman, H.M.; Roux, D.G. The origins of tannins and flavonoids in black-wattle barks and heartwoods, and their associated "non-tannin" components. *Biochem. J.* **1965**, *97*, 794–801. [CrossRef] [PubMed]

39. Kusano, R.; Ogawa, S.; Matsuo, Y.; Tanaka, T.; Yazaki, Y.; Kouno, I. α-Amylase and lipase inhibitory activity and structural characterization of *Acacia* bark proantocyanidins. *J. Nat. Prod.* **2011**, *74*, 119–128. [CrossRef] [PubMed]

40. Ohara, S.; Yasuta, Y.; Ohi, H. Structure elucidation of condensed tannins from barks by pyrolysis/gas chromatography. *Holzforschung* **2003**, *57*, 145–149. [CrossRef]

41. Venter, P.B.; Senekal, N.D.; Kemp, G.; Amra-Jordaan, M.; Khan, P.; Bonnet, S.L.; van der Westhuizen, J.H. Analysis of commercial proanthocyanidins. Part 3: The chemical composition of wattle (*Acacia mearnsii*) bark extract. *Phytochemistry* **2012**, *83*, 153–167. [CrossRef] [PubMed]

42. Crestini, C.; Lange, H.; Bianchetti, G. Detailed chemical composition of condensed tannins via quantitative (31) P NMR and HSQC analyses: *Acacia catechu*, *Schinopsis balansae*, and *Acacia mearnsii*. *J. Nat. Prod.* **2016**, *79*, 2287–2295. [CrossRef] [PubMed]

43. Liu, X.; Wang, F. Investigation on biological activities of proanthocyanidins from black wattle bark. *Chem. Ind. For. Prod.* **2007**, *27*, 43–48.

44. Shen, X.; Wang, Y.; Wang, F. Characterisation and biological activities of proanthocyanidins from the barks of *Pinus massonian* and *Acacia mearnsii*. *Nat. Prod. Res.* **2010**, *24*, 590–598. [CrossRef] [PubMed]

45. Huang, W.; Niu, H.; Xue, X.; Li, J.; Li, C. Robinetinidol-(4β→8)-epigallocatechin 3-*O*-gallate, a galloyl dimer prorobinetinidin from *Acacia mearnsii* De Wild, effectively protects human neuroblastoma SH-SY5Y cells against acrolein-induced oxidative damage. *J. Alzheimer's Dis.* **2010**, *2*, 493–506. [CrossRef] [PubMed]

46. Zhou, M.; Liu, G.; He, L.; Wang, F. Preparation and antioxidant activity of proanthocyanidins dimers from *Acacia mearnsii* De Willd. *Chem. Ind. For. Prod.* **2017**, *37*, 135–140.

47. Ikarashi, N.; Toda, T.; Hatakeyama, Y.; Kusunoki, Y.; Kon, R.; Mizukami, N.; Kaneko, M.; Ogawa, S.; Sugiyama, K. Anti-Hypertensive Effects of Acacia Polyphenol in Spontaneously Hypertensive Rat. *Int. J. Mol. Sci.* **2018**, *19*, 700. [CrossRef] [PubMed]

48. Nakamoto, Y.; Tsunoda, T.; Ono, K.; Yazaki, Y.; Tongi, L.Y.; Lawson, F.; Uhlherr, P.H.T. Active Oxygen Scavenger Prepared from *Acacia* Plant Bark, and Composition Made from the Same. Jp. Patent 2004352639, 16 December 2004.

49. Nakamoto, Y.; Ono, K. Antioxidant Composition Containing Component Originating in the Bark of Tree Belonging to the Genus *Acacia*. Jp. Patent 2006306803, 9 November 2006.

50. Nakamoto, Y.; Ono, K. Composition for Preventing and/or Treating Tumor Containing Component Originating in the Bark of Tree Belonging to the Genus *Acacia*. Jp. Patent 2006306801, 9 November 2006.

51. Wiid, M.N. Anti-Oxidant Compositions. WO Patent 2009126976, 15 October 2009.

52. Ohara, S.; Suzuki, K.; Ohira, T. Condensed tannins from *Acacia mearnsii* and their biological activities. *Mokuzai Gakkaishi.* **1994**, *40*, 1363–1374.

53. Olajuyigbe, O.O.; Afolayan, A.J. Pharmacological assessment of the medicinal potential of *Acacia mearnsii* De Wild.: antimicrobial and toxicity activities. *Int. J. Mol. Sci.* **2012**, *13*, 4255–4267. [CrossRef] [PubMed]

54. Dos Santos, C.; Vargas, Á.; Fronza, N.; dos Santos, J.H.Z. Structural, textural and morphological characteristics of tannins from *Acacia mearnsii* encapsulated using sol-gel methods: Applications as antimicrobial agents. *Colloids Surf. B: Biointerfaces* **2017**, *151*, 26–33. [CrossRef] [PubMed]

55. Timotheo, C.A.; Lauer, C.M., Jr. Toxicity of vegetable tannin extract from *Acacia mearnsii* in *Saccharomyces cerevisiae*. *Int. J. Environ. Sci. Technol.* **2017**, *15*, 659–664. [CrossRef]

56. Morandi, L.A.P.; Morandi, J.L.P. Antifungal Composition Based on Plant Extracts for Treatment of Green Wood. Br. Patent 2006001476, 18 December 2007.

57. Zhang, L.; Li, J.; Liu, Y. Compounded Bacteriostatic Agent Containing Plant Polyphenol. Cn. Patent 1957697, 9 May 2007.

58. Smith, A.H.; Imlay, J.A.; Mackie, R.I. Increasing the oxidative stress response allows *Escherichia coli* to overcome inhibitory effects of condensed tannins. *Appl. Environ. Microbiol.* **2003**, *69*, 3406–3411. [CrossRef] [PubMed]

59. Zoetendal, E.G.; Smith, A.H.; Sundset, M.A.; Mackie, R.I. The BaeSR two-component regulatory system mediates resistance to condensed tannins in *Escherichia coli*. *Appl. Environ. Microbiol.* **2008**, *74*, 535–539. [CrossRef] [PubMed]

60. Olajuyigbe, O.O.; Afolayan, A.J. In vitro antibacterial and time-kill assessment of crude methanolic stem bark extract of *Acacia mearnsii* De Wild against bacteria in shigellosis. *Molecules* **2012**, *17*, 2103–2118. [CrossRef] [PubMed]

61. Olajuyigbe, O.O.; Afolayan, A.J. A comparative effect of the alcoholic and aqueous extracts of *Acacia mearnsii* De Wild on protein leakage, lipid leakage and ultrastructural changes in some selected bacterial strains as possible mechanisms of antibacterial action. *J. Pure Appl. Microbiol.* **2014**, *8*, 1243–1257.

62. Olajuyigbe, O.O.; Afolayan, A.J. Synergistic interactions of methanolic extract of *Acacia mearnsii* De Wild. with antibiotics against bacteria of clinical relevance. *Int. J. Mol. Sci.* **2012**, *13*, 8915–8932. [CrossRef] [PubMed]

63. Olajuyigbe, O.O.; Coopoosamy, R.M. Influence of first-line antibiotics on the antibacterial activities of acetone stem bark extract of *Acacia mearnsii* De Wild. against drug-resistant bacterial isolates. *Evid. Based Complement. Alternat. Med* **2014**, *2014*, 423751. [CrossRef] [PubMed]

64. Klug, T.V.; Novello, J.; Laranja, D.C.; Aguirre, T.A.S.; de Oliveira Rios, A.; Tondo, E.C.; dos Santos, R.P.; Bender, R.J. Effect of tannin extracts on biofilms and attachment of *Escherichia coli* on lettuce leaves. *Food Bioprocess Technol.* **2016**, *10*, 275–283. [CrossRef]

65. Zhou, L.; Bi, Y.; Jiang, L.; Wang, Z.; Chen, W. Effect of black wattle (*Acacia mearnsii*) extract on blue-green algal bloom control and plankton structure optimization: a field mesocosm experiment. *Water Env. Res.* **2012**, *84*, 2133–2142. [CrossRef]

66. Luo, K.; Liu, D.; Zhou, L.; Chen, W. Allelopathic inhibitory effect of the *Acacia mearnsii* extracts on *Microcystis aeruginosa*. *J. Shenzhen Univ. Sci. Eng.* **2014**, *31*, 205–209. [CrossRef]

67. Liu, Z.; Zhou, L.; Liu, D.; Zhu, Q.; Chen, W. Inhibitory mechanisms of *Acacia mearnsii* extracts on the growth of *Microcystis aeruginosa*. *Water Sci. Technol.* **2015**, *71*, 856–861. [CrossRef] [PubMed]

68. Takagi, K.; Mitsunaga, T. Tyrosinase inhibitory activity of proanthocyanidins from woody plants. *J. Wood Sci.* **2003**, *49*, 461–465. [CrossRef]

69. Abe, I.; Mitsunaga, T.; Takagi, K.; Shimomura, K. Preparation for External Use for Skin/Novel Use of Extract Isolated from Bark of Larch, Acacia or Duramen of *Schinopsis lorentsii* as Skin Whitening Agent. Jp. Patent 10025238, 27 January 1998.

70. Cuirong, L. Skin Deep-Clean Facial Cream for Suppressing Tyrosinase and Decomposing Melanin. Cn. Patent 106963681, 21 July 2017.

71. Da Silva, S.M.; Koehnlein, E.A.; Bracht, A.; Castoldi, R.; de Morais, G.R.; Baesso, M.L.; Peralta, R.A.; de Souza, C.G.M.; de Sá -Nakanishi, A.B.; Peralta, R.M. Inhibition of salivary and pancreatic α-amylases by a pinhão coat (*Araucaria angustifolia*) extract rich in condensed tannin. *Food Res. Int.* **2014**, *56*, 1–8. [CrossRef]

72. Matsuo, Y.; Kusano, R.; Ogawa, S.; Yazaki, Y.; Tanaka, T. Characterization of the α-amylase inhibitory activity of oligomeric proanthocyanidins from *Acacia mearnsii* Bark Extract. *Nat. Prod. Commun.* **2016**, *11*, 1851–1854.

73. Kato, C.G.; de Almeida Gonçalves, G.; Peralta, R.A.; Seixas, F.A.V.; de Sá-Nakanishi, A.B.; Bracht, L.; Comar, J.F.; Bracht, A.; Peralta, R.M. Inhibition of α-amylases by condensed and hydrolysable tannins: focus on kinetics and hypoglycemic actions. *Enzyme Res.* **2017**, *3*, 1–12. [CrossRef] [PubMed]

74. Xiong, J.; Grace, M.H.; Esposito, D.; Komarnytsky, S.; Wang, F.; Lila, M.A. Polyphenols isolated from *Acacia mearnsii* bark with anti-inflammatory and carbolytic enzyme inhibitory activities. *Chin. J. Nat. Med.* **2017**, *15*, 816–824. [CrossRef]

75. Ikarashi, N.; Toda, T.; Okaniwa, T.; Ito, K.; Ochiai, W.; Sugiyama, K. Anti-obesity and anti-diabetic effects of Acacia polyphenol in obese diabetic KKAy mice fed high-fat diet. *Evid.-Based Complement. Alternat. Med.* **2011**, *2011*, 952031. [CrossRef] [PubMed]

76. Ikarashi, N.; Takeda, R.; Ito, K.; Ochiai, W.; Sugiyama, K. The inhibition of lipase and glucosidase activities by Acacia polyphenol. *Evid.-Based Complement. Alternat. Med.* **2011**, *2011*, 272075. [CrossRef] [PubMed]

77. Nakamoto, Y.; Ono, K. Hypoglycemic Composition Containing Component Originating in the Bark of Tree Belonging to the Genus *Acacia*. Jp. Patent 2006232781, 7 September 2006.

78. Nakamoto, Y.; Ono, K. Antiobesity Composition Containing Component Originating in the Bark of Tree Belonging to the Genus *Acacia*. Jp. Patent 2006232782, 7 September 2006.

79. Fava, F.J.; Monteiro De Barros, N.; Stumpp, E.; Ramao Marceli, F., Jr. Aqueous Extract to Repel or Exterminate Termites. WO Patent 2006021064, 2 March 2006.

80. Fermandes, R.M., Jr.; Fava, F.J.; Gobatto, V.; Monteiro de, B.N.; Specht, A. *Acacia mearnsii* Bark Extract as Insecticide. Br. Patent 2006002039, 8 January 2008.

81. Ikarashi, N.; Sato, W.; Toda, T.; Ishii, M.; Ochiai, W.; Sugiyama, K. Inhibitory effect of polyphenol-rich fraction from the bark of *Acacia mearnsii* on itching associated with allergic dermatitis. *Evid.-Based Complement. Alternat. Med.* **2012**, *2012*, 120389. [CrossRef] [PubMed]

82. Tada, T.; Hattori, F.; Ito, S.; Yamada, S.; Takagi, K.; Shimomura, K. Histamine Liberation Suppressing Agent/Histamine Release Inhibitor Containing Plant Extracts for Relieving. Jp. Patent 2001048766, 20 February 2001.

83. Nakamoto, Y.; Ono, K. Composition for Preventing and/or Treating Itching Containing Component Originating in the Bark of Trees Belonging to *Acacia*. Jp. Patent 2006306802, 9 November 2006.

Article

Different Inhibitory Potencies of Oseltamivir Carboxylate, Zanamivir, and Several Tannins on Bacterial and Viral Neuraminidases as Assessed in a Cell-Free Fluorescence-Based Enzyme Inhibition Assay

Stefanie Quosdorf [1], Anja Schuetz [2,†] and Herbert Kolodziej [1,*,†]

1   Institute of Pharmacy, Freie Universität Berlin, Königin-Luise-Str. 2+4, 14195 Berlin, Germany;
    stquosdorf@gmail.com
2   Max-Delbrück-Centrum for Molecular Medicine, Helmholtz Protein Sample Production Facility,
    Robert-Rössle-Str. 10, 13125 Berlin, Germany; anja.schuetz@mdc-berlin.de
*   Correspondence: kolpharm@zedat.fu-berlin.de; Tel.: +49-30-838-53731
†   These authors share last authorship.

Abstract: Neuraminidase is a key enzyme in the life cycle of influenza viruses and is present in some bacterial pathogens. We here assess the inhibitory potency of plant tannins versus clinically used inhibitors on both a viral and a bacterial model neuraminidase by applying the 2′-(4-methylumbelliferyl)-α-D-N-acetylneuraminic acid (MUNANA)-based activity assay. A range of flavan-3-ols, ellagitannins and chemically defined proanthocyanidin fractions was evaluated in comparison to oseltamivir carboxylate and zanamivir for their inhibitory activities against viral influenza A (H1N1) and bacterial *Vibrio cholerae* neuraminidase (VCNA). Compared to the positive controls, all tested polyphenols displayed a weak inhibition of the viral enzyme but similar or even higher potency on the bacterial neuraminidase. Structure–activity relationship analyses revealed the presence of galloyl groups and the hydroxylation pattern of the flavan skeleton to be crucial for inhibitory activity. The combination of zanamivir and EPs® 7630 (root extract of *Pelargonium sidoides*) showed synergistic inhibitory effects on the bacterial neuraminidase. Co-crystal structures of VCNA with oseltamivir carboxylate and zanamivir provided insight into bacterial versus viral enzyme-inhibitor interactions. The current data clearly indicate that inhibitor potency strongly depends on the biological origin of the enzyme and that results are not readily transferable. The therapeutic relevance of our findings is briefly discussed.

Keywords: neuraminidase; inhibition; tannins; oseltamivir carboxylate; zanamivir; crystal structure; molecular interactions

1. Introduction

Influenza is an acute viral infection of the respiratory tract, afflicting millions of individuals each year. Due to the imminent threat of epidemics and pandemics in human population and the alarming emergence of drug-resistant influenza virus strains, there is an urgent need for new and effective anti-influenza drugs.

The influenza virus employs two key enzymes located on the surface, hemagglutinin (HA) and neuraminidase (NA), to initiate viral fusion and subsequent budding of progeny virions from the infected cell [1]. In the virus infection life cycle, HA binds to terminally linked sialic acid receptors on target cells, thus facilitating entry of the virus into the host cell. NA plays a key role not only

in the release of virions from infected host cells by cleaving terminal sialic acid residues but also in preventing self-aggregation of the released influenza viruses, thereby allowing continuous and efficient viral replication.

Annual vaccination has been the main global strategy for preventing influenza infections, but frequent virus antigenic drifts present a permanent challenge in the development of effective vaccines. Antiviral drugs offer an alternative therapeutic option. Currently, there are two classes of anti-influenza drugs available, matrix-2 (M2) protein ion channel blockers and neuraminidase inhibitors (NAIs). The therapeutic efficacy of M2 ion channel blockers such as amantadine and rimantadine is limited to influenza A viruses. These therapeutics are also associated with the rapid emergence of drug resistance and have the disadvantage of side effects. At present, the approved NAIs oseltamivir, zanamivir, peramivir, and laninamivir are first choice antiviral drugs for the treatment of influenza A and B virus infections. Until the season 2007/2008, NAI-resistance to the first introduced NA-targeting drugs has been reported only sporadically [2]. Over the years, the emergence of oseltamivir-resistant strains is a cause for concern. Nevertheless, NAIs are currently considered to be the most promising drugs for combating influenza A and B. Despite their considerable therapeutic potential, the number of approved competitive inhibitors of the influenza NA is rather limited to date. Taking into account the serious problem of resistance development from antigenic shifts or drifts, there is a persistent demand to develop new NAIs.

A successful modus operandi for finding promising antiviral agents involves the exploration of plants and their chemical constituents. The plant kingdom has been recognized as an inestimably rich source of metabolites for target-oriented drug discovery. In particular, various plant polyphenols that have a broad spectrum of other biological activities have been identified to possess viral NA inhibitory activities [3–5]. Although isolated pure products have been preferentially elucidated for this bioactivity, some plant extracts, in particular traditional Chinese medicines have been subjected to anti-influenza activity studies [6–9].

NAs are also present in other biological systems [10], for example bacteria, and these non-influenza NAs are critical virulence factors in many pathogenic organisms including *Streptococcus pneumoniae*, *Pseudomonas aeruginosa*, and *Vibrio cholerae* [5,11,12]. Bacterial sialidases have been suggested to promote microbial survival and to contribute to microbe–host interactions [13]. Their function in pathogenesis remains to be clarified. However, bacterial NA activity has been shown to contribute to respiratory tract infections in a mouse model [14]. Taking into account the demonstrated synergism between influenza virus and bacterial pathogens in pulmonary infectious conditions resulting from the exposure of pneumococcal receptors [15], bacterial NAs may be an appealing target to prevent microbial colonization.

Established functional assays to assess NA inhibitory activities are based on either fluorescence or chemiluminescence and are reported to be compared to culture-based assays, more predictive in terms of their in vivo susceptibility [3]. The in vitro NA inhibition assays work with both viral and bacterial NAs, because the enzymes recognize the applied substrates independent of their biological origin [16]. The use of commercially available bacterial or viral NA-based test systems may be beneficial for a given pathogenic condition. In addition, bacterial NA-based setups are less expensive and are used for antiviral activity studies in laboratories. To date, however, comparative studies on the effect of tannins on bacterial and viral NAs are lacking. These comparisons could allow for the evaluation of the therapeutic significance of bacterial enzyme inhibition data in the identification of anti-viral substances [3].

To fill this gap, we here disclose results for the inhibition of both a viral and a bacterial model NA by various tannins. In addition to a range of flavan-3-ols and ellagitannins, highly purified and chemically defined proanthocyanidin fractions of different composition were included to gain insight into structure–activity relationships for this group of polyphenols. To provide a rationale for differential inhibition of bacterial and viral NAs, we additionally performed X-ray crystallographic analyses of NAs in complex with the synthetic reference compounds oseltamivir carboxylate and zanamivir.

2. Results

Preliminary experiments in our research group have indicated differential inhibition of bacterial and viral NAs by some polyphenolic substances [17] and have prompted the present more detailed study. We here explore the structure–activity relationship of a range of polyphenolic NAIs using the well-established 2′-(4-methylumbelliferyl)-α-D-N-acetylneuraminic acid (MUNANA)-based activity assay [18]. The assay is based on the NA-catalyzed hydrolysis of the substrate MUNANA and quantification of the released fluorochrome 4-methylumbelliferone (Figure 1). The established NAIs oseltamivir carboxylate (active form of oseltamivir) and zanamivir were included as reference compounds.
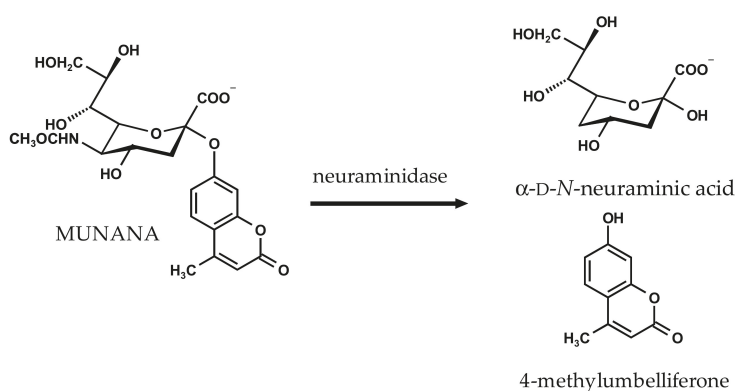
Figure 1. Neuraminidase-catalyzed hydrolysis of 2′-(4-methylumbelliferyl)-α-D-N-acetylneuraminic acid (MUNANA).

2.1. Inhibition of Viral Influenza a Neuraminidase and Bacterial Vibrio Cholerae Neuraminidase by the Reference Compounds

To validate our assay conditions, we first assessed the inhibitory potency of the reference NAIs oseltamivir carboxylate and zanamivir (Figure 2) against both the viral influenza A/California/04/2009 (H1N1) neuraminidase (H1N1-NA) and the bacterial *Vibrio cholerae* neuraminidase (VCNA). With IC_{50} values (the inhibitor concentration that is required for 50% inhibition) of around 10 nM, oseltamivir carboxylate and zanamivir are very active against the viral H1N1-NA. The bacterial VCNA, on the other hand, is only moderately inhibited by the reference compounds, displaying IC_{50} values of 144 μM for oseltamivir carboxylate and 52 μM for zanamivir. These IC_{50} values are comparable to other NA inhibition data [19,20], although modified assay conditions were used.
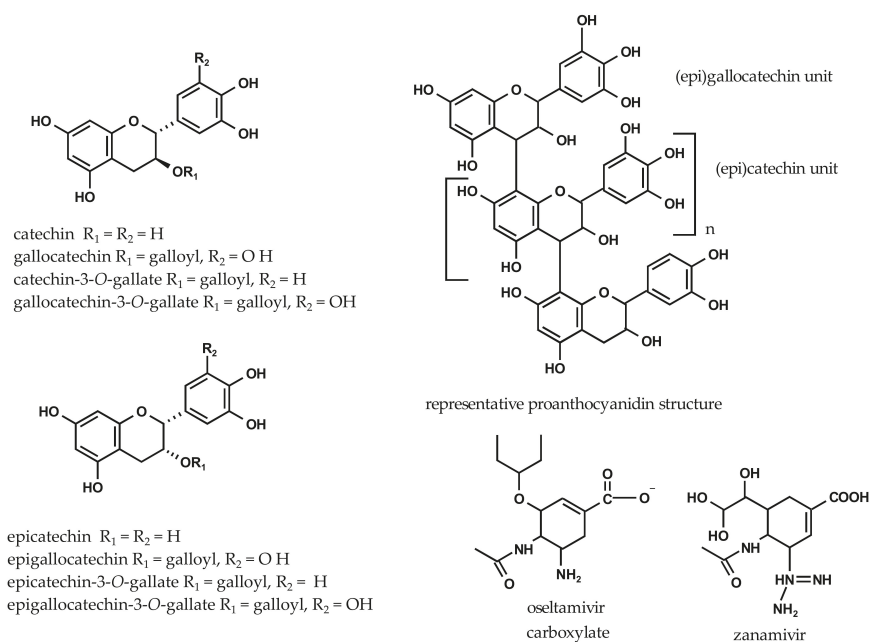
Figure 2. Chemical structures of tested flavan-3-ols, proanthocyanidins, oseltamivir carboxylate, and zanamivir.

2.2. Inhibition of Viral H1N1-NA and Bacterial VCNA by Flavan-3-ols

The inhibitory potencies of a series of flavan-3-ols are shown in Table 1, revealing markedly different inhibitory activities towards the bacterial and viral NAs. All tested flavan-3-ols (Figure 2) display only moderate to very weak inhibitory activities against the viral H1N1-NA when compared to the synthetic reference inhibitors. The IC_{50} values range from 0.3 to 0.9 mM, and gallocatechin-3-*O*-gallate is the most active compound within this series. This finding is consistent with modest inhibitory activities (>100 µM) reported for (*epi*)catechin [3].

Table 1. IC_{50} values for the inhibition of viral influenza A (H1N1) neuraminidase (H1N1-NA) and bacterial *Vibrio cholerae* neuraminidase (VCNA) by flavan-3-ols.

Test Substance	IC_{50} (Viral) µg/mL µM		IC_{50} (Bacterial) µg/mL µM	
Positive control				
oseltamivir carboxylate	2.9 ± 0.2 [1]	0.01 ± 0.001	41 ± 1	144 ± 1
zanamivir	3.7 ± 0.4 [1]	0.01 ± 0.001	17 ± 1	52 ± 2
Flavan-3-ols				
catechin	312 ± 21	1076 ± 75	595 ± 25	2050 ± 87
gallocatechin	547 ± 23	1787 ± 74	603 ± 61	1969 ± 199
catechin-3-*O*-gallate	862 ± 2	1949 ± 4	24 ± 2	55 ± 4
gallocatechin-3-*O*-gallate	181 ± 3	396 ± 7	11 ± 1	25 ± 2
epicatechin	305 ± 19	1053 ± 64	670 ± 29	2186 ± 99
epigallocatechin	532 ± 41	1739 ± 135	598 ± 57	1955 ± 185
epicatechin-3-*O*-gallate	845 ± 24	1910 ± 55	93 ± 8	211 ± 19
epigallocatechin-3-*O*-gallate	717 ± 63	1565 ± 137	29 ± 1	64 ± 3

IC_{50} values are expressed as mean ± standard deviation (SD) (*n* = 3–6 independent experiments); [1] data are in ng/mL.

In contrast, these compounds are effective inhibitors of the bacterial VCNA. The flavan-3-ols gallocatechin-3-*O*-gallate (IC$_{50}$ = 25 µM), catechin-3-*O*-gallate (IC$_{50}$ = 55 µM), and epigallocatechin-3-*O*-gallate (IC$_{50}$ = 64 µM) have comparable or greater potency compared to the reference compounds (Table 1). All tested non-galloylated flavan-3-ols, on the other hand, show comparatively weak inhibitory activities, indicating that a 3-*O*-galloyl group is crucial for pronounced inhibition of VCNA by polyphenols. The enhanced inhibitory activity of the 2,3-*trans* galloylated flavan-3-ols compared with their 2,3-*cis* analogues suggests that the relative 2,3-configuration is, to some extent, an additional structural feature contributing to the inhibition of the bacterial NA.

2.3. Inhibition of Viral H1N1-NA and Bacterial VCNA by Ellagitannins

We next evaluated the inhibitory potency of a series of ellagitannins (Figure 3), including members of dehydroellagitannins and *C*-glycosidic ellagitannins. All ellagitannins inhibit bacterial VCNA with an IC$_{50}$ value of 15–236 µM. The most potent compounds, which were even more effective than zanamivir, are paeonianin C (IC$_{50}$ = 15 µM) and terchebin (IC$_{50}$ = 31 µM). In tests with the viral H1N1-NA, the inhibition is also in the µM range, but terchebin showed a 3.5-fold higher inhibitory potency compared to paeonianin C (Table 2). Overall, the ellagitannins are less effective against the viral compared to the bacterial NA. It is also worth mentioning that the only moderately effective VCNA ellagitannin inhibitors are still as potent as the reference compound oseltamivir carboxylate.

A structural element characteristic of dehydroellagitannins is the presence of at least one dehydrohexahydroxydiphenoyl (DHHDP) unit in addition to a varying number of galloyl groups on the glucose core. Structure–activity relationship analyses indicate that the inhibitory activity of the tested compounds depends in part on the degree of galloylation. As shown in Table 2, inhibition decreased in the order of terchebin > geraniin > carpinusin > granatin A (IC$_{50}$ values of 31, 135, 138 and 158 µM), corresponding to three, one, and no galloyl groups. Further examination of the structures revealed that the presence of additional 1′,6′- or 3′,6′-hexahydroxydiphenoyl (HHDP) residue (Figure 3) results in significantly weaker inhibitory activities, possibly due to steric effects.
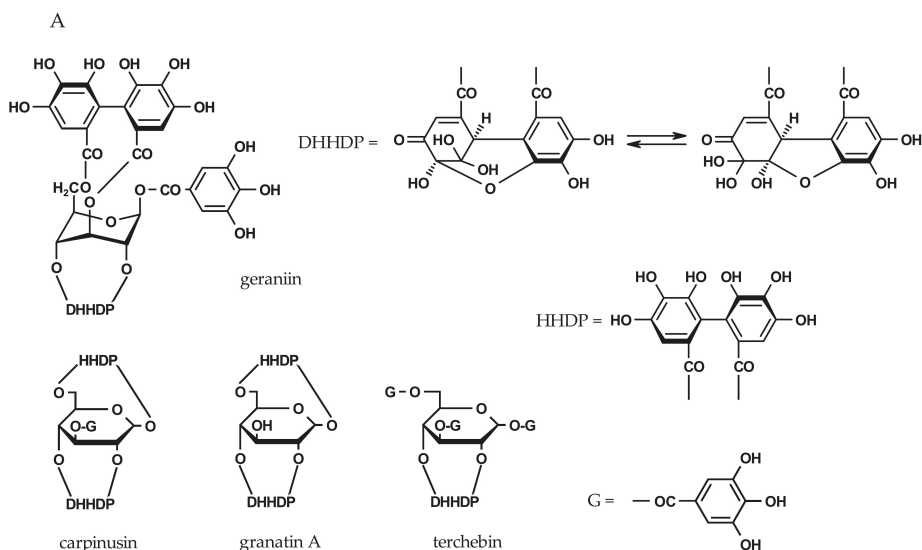
Figure 3. *Cont.*
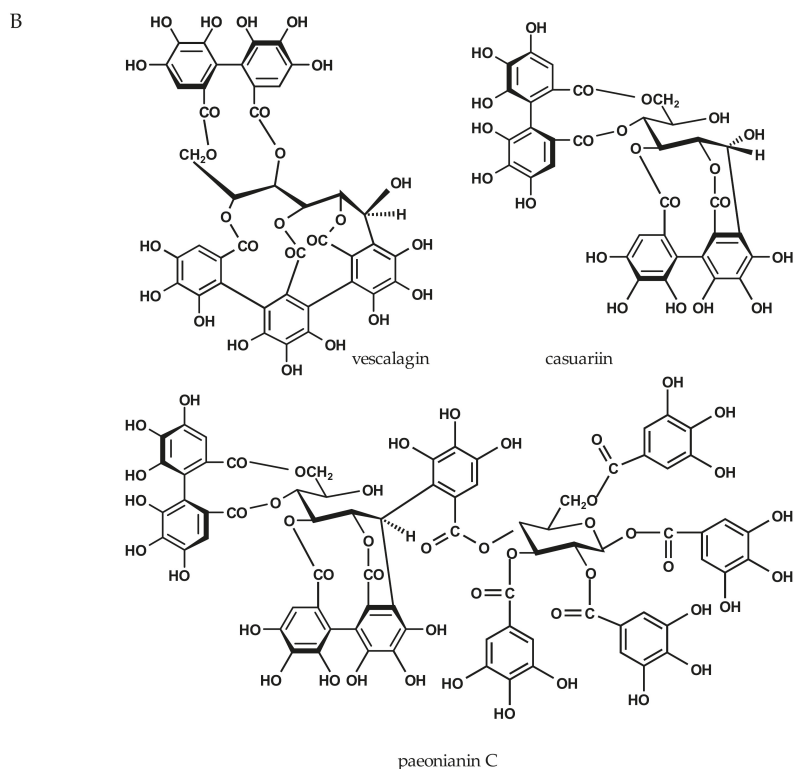
Figure 3. Chemical structures of ellagitannins. (**A**) Dehydroellagitannins and (**B**) *C*-glycosidic members (DHHDP = dehydrohexahydroxydiphenoyl; HHDP = hexahydroxydiphenoyl).

Table 2. IC_{50} values for the inhibition of viral H1N1-NA and bacterial VCNA by ellagitannins.

Test Substance	IC_{50} (Viral) μg/mL μM		IC_{50} (Bacterial) μg/mL μM	
Positive control				
oseltamivir acid	2.9 ± 0.2 [1]	0.01 ± 0.001	41 ± 1	144 ± 1
zanamivir	3.7 ± 0.4 [1]	0.01 ± 0.001	17 ± 1	52 ± 2
Ellagitannins				
dehydroellagitannin members				
geraniin	-	-	128 ± 2	135 ± 2
granatin A	-	-	124 ± 2	158 ± 4
carpinusin	-	-	131 ± 5	138 ± 5
terchebin	97 ± 2	101 ± 3	29 ± 2	31 ± 2
C-glycosidic members				
casuariin	-	-	185 ± 4	236 ± 5
vescalagin	-	-	125 ± 11	73 ± 11
paeonianin C	587 ± 24	344 ± 14	25 ± 2	15 ± 1

IC_{50} values are expressed as mean $\pm$ SD (n = 3–6 independent experiments); [1] data are in ng/mL.

Although the number of tested *C*-glycosidic ellagitannins was limited, some structural features determining inhibitory potency were evident. Paeonianin C, possessing a 1C-penta-*O*-galloyl glucose moiety, was significantly more potent (IC_{50} = 15 μM) than vescalagin (IC_{50} = 73 μM), having a 4,6-HHDP and a 2,3,5-flavogalloyl unit, and casuariin (IC_{50} = 236 μM), which lacks the

5-*O*-galloyl residue as part of the flavogalloyl group. The inhibition correlates with the number of pyrogallol elements. More information is needed to decide between galloyl-derived structural variants. However, it appears that the conformation of these molecules with bulky substituents plays a significant role and more *C*-glycosidic ellagitannins need to be tested to fully understand the structure–activity relationships.

2.4. Inhibition of Viral H1N1-NA and Bacterial VCNA by Plant-Derived Fractions

Proanthocyanidins are oligomeric flavan-3-ols and represent another group of plant tannins. Extensive structural variations and challenges in the isolation and purification of chemically defined proanthocyanidins prompted the evaluation of well-characterized plant fractions. Table 3 lists the main component of the composite fractions and the resulting IC_{50} values for both viral H1N1-NA and bacterial VCNA inhibition. Most of the tannin fractions inhibit the bacterial VCNA significantly better than the reference compounds. The inhibition of viral H1N1 is reduced by a factor of 6–10 compared to the clinically used inhibitors, leaving potential for further optimization.

Table 3. IC_{50} values for the inhibition of viral H1N1-NA and bacterial VCNA by tannin fractions.

Tested Substance	Constituent Flavanyl Units	IC_{50} (Viral) µg/mL	IC_{50} (Bacterial) µg/mL
Positive control			
oseltamivir acid		2.9 ± 0.2 [1]	41 ± 1
zanamivir		3.7 ± 0.4 [1]	17 ± 1
Tannin fractions			
Diospyros kaki	galloylated flavan-3-ols	20 ± 1	0.5 ± 0.04
EPs® 7630 [2]	(*epi*)gallocatechin/(*epi*)catechin	61 ± 2	1.7 ± 0.1
Nelia meyeri	epicatechin	29 ± 1	3.2 ± 0.1
Salix ssp.	catechin	32 ± 3	4.4 ± 0.2
Potentilla erecta	epicatechin/catechin	-	9.2 ± 1
Betula spp.	epicatechin/catechin	-	13 ± 1
Rhus leptodictya	fisetinidol	-	25 ± 1

IC_{50} values are expressed as mean $\pm$ SD (n = 3–6 independent experiments); [1] data are in ng/mL; [2] proportion of polyphenols ca. 40%. EPs® 7630 (root extract of *Pelargonium sidoides*).

For both NAs, the *Diospyros kaki* sample is the most active fraction, suggesting that pyrogallol B-ring elements (prodelphinidin units) and 3-*O*-galloylation are preferred structural determinants for NA inhibition. In line with this, weaker inhibitory activity is found for the prodelphinidin-rich but mainly ungalloylated extract of *Pelargonium sidoides* EPs® 7630 extract. The trend continues for the *Nelia meyeri* and *Salix* spp. fractions, which comprise either homogeneous 2,3-*cis* or 2,3-*trans* proanthocyanidins composed of non-galloylated dimers to hexamers in similar proportions. Interestingly, fractions with mixed 2,3-*trans* and 2,3-*cis* constituent flavanyl units obtained from *Potentilla erecta* and *Betula* spp. are less potent than preparations dominated by compounds with the homogeneously linked building blocks. Increasing proportions of 2,3-*cis* entities as in the *Betula* fraction apparently reduces the inhibitory activity (Table 3). More studies with fractions of defined 2,3-*cis*/2,3-*trans* ratios and a focus on the impact of the molecular weight are fruitful avenues for future research.

The data additionally show the relatively poor activity of 5-deoxy analogues, such as the compounds in the *Rhus leptodictya* fraction. The profisetinidins with characteristic resorcinol A-rings show the weakest inhibition within the series of tested proanthocyanidin fractions. The hydroxylation pattern on the two aromatic rings of the flavan skeleton thus proves to be an important structural feature.

2.5. Combined Effect of Zanamivir and EPs® 7630 on VCNA Activity

Possible beneficial effects of combination therapy include synergistic activity, reduced dosage with decrease of side effects, and delay or prevention of development of drug resistance. Indeed, previous reports have stated advantages of synthetic NAI combinations over single-drug influenza treatment [21–24]. Additionally, drug–herb combinations such as the Manuka honey constituent methylglyoxal along with oseltamivir [25] as well as also some entirely herbal-based combinations [26] proved to be effective anti-influenza NAIs.

Recent work indicates that bacterial NAs play a role in the pathogenesis of respiratory tract infections [14]. However, little information is available on natural products inhibiting bacterial NA activity. We thus examined the hitherto less studied drug–herb combination approach and determined the combined effect of zanamivir and EPs® 7630 on bacterial VCNA using the median-plot effect analysis [27,28]. Selection of EPs® 7630 was based on its VCNA-inhibition potential demonstrated in this study and its approval for the treatment of acute bronchitis [29]. The clinically used drug zanamivir was chosen because it is more effective against VCNA than oseltamivir carboxylate against VCNA.

The enzyme was treated with zanamivir and EPs® 7630 either individually over a range of concentrations or in combination at different weight ratios (1:10, 1:5, 1:1, 5:1, or 10:1) (Table 4). The median–effect concentration (D_m, a parameter analogous to the IC_{50} value indicating potency), the slope of the concentration–effect relationship (m, the dynamic order or the shape of dose–effect curve), and the linear regression correlation coefficient (r, a measure of data quality) were determined from the median–effect plots. The parameter r of the median–effect plots exceeds 0.95 (data not shown), showing the conformity of the data to the median–effect principle. The calculated D_m values indicate an enhanced VCNA inhibition with increasing amounts of EPs® 7630 (ratio of 1:5 and 1:10, $D_m = 1.4$) as compared to zanamivir alone ($D_m = 17$).

Table 4. Concentration–effect relationship parameters and mean combination index (CI) values of zanamivir and EPs® 7630 alone and in combinations for the inhibition of the bacterial VCNA.

Compound	Concentration–Effect Parameters		CI Values at				CI$_{wt}$	Combined Effect
	D_m	m	IC_{50}	IC_{75}	IC_{90}	IC_{95}		
zanamivir	17.0 ± 1	0.9	-	-	-	-	-	-
EPs® 7630	1.7 ± 0.1	1.4	-	-	-	-	-	-
Ratio of Zanamivir and EPs® 7630								
5:1	7.8 ± 0.6	1.1	1.1	0.7	0.5	0.4	0.5	synergistic
10:1	9.1 ± 0.4	1.7	0.9	0.7	0.6	0.5	0.6	synergistic
1:1	7.8 ± 0.6	1.7	2.3	1.8	1.5	1.3	1.6	antagonistic
1:5	1.4 ± 0.1	1.2	0.7	0.8	1.0	1.1	1.0	additive
1:10	1.4 ± 0.2	1.0	0.7	0.8	0.8	0.9	0.8	moderate synergistic

The parameters D_m (antilog of the x-intercept) and m (slope) are derived from the median effect plot and are used to calculate the CI values (n = 3–4 experiments). IC_{50}, IC_{75}, IC_{90} and IC_{95} are the concentrations (µg/mL) that achieve 50%, 75%, 90% and 95% inhibition of VCNA. The weighted CI (CI$_{wt}$) is calculated on the basis of these representative CI values at effect levels $f_a > 0.5$.

We calculated the combination index (CI) values that offer a quantitative definition for an additive effect (CI = 1), synergism (CI < 1), and antagonism (CI > 1) in drug combinations [27,28]. CI values were determined at IC_{50}, IC_{75}, IC_{90}, and IC_{95}, indicating the concentrations required to achieve 50%, 75%, 90% or 95% inhibition of VCNA activity. It should be noted that only CIs of higher effect levels (fraction affected values, $f_a > 0.5$) are considered relevant for therapeutic applications [30]. The f_a-CI plots for various zanamivir/EPs® 7630 combinations are shown in Figure 4. The CI values are concentration-dependent and are generally higher with lower sample concentrations. The tendency of combined effects moving from antagonism towards additivity and synergism as effect levels increase, appears to be a common phenomenon. Indeed, antagonism is restricted to the region of lower f_a values in our study. For higher effect levels, CI values move to synergism except for the 1:1 combination,

exhibiting continuously antagonistic effects (Figure 4). The combined effect (CI_{wt}) was calculated on the basis of selected average CI values including IC_{50}, IC_{75}, IC_{90} and IC_{95} at four representative effect levels ($f_a > 0.5$). The most effective combinations include drug–herb ratios of 10:1, 5:1, and, surprisingly, 1:10, with CIs ranging between 0.5 and 0.8, indicative of synergism. For the zanamivir/EPs® 7630 combination with a ratio of 1:5, the CI revealed additivity.
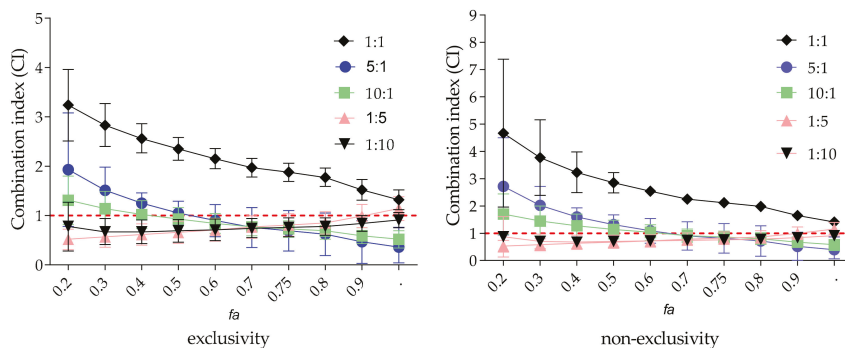
Figure 4. Fraction affected (f_a)–CI-plot for VCNA activity measurements by zanamivir/EPs® 7630-combinations. The vertical bars indicate 95% confidence intervals ($n = 3$–4 independent experiments).

Differences in the slopes of the median effect plots for EPs® 7630 ($m > 1$, sigmoidal) and zanamivir ($m < 1$, flat sigmoidal) alone and for the tested combinations (all $m > 1$) indicate possible different binding sites for each compound. Therefore, the data were reanalyzed with an assumption of non-exclusivity for the calculations of CI values of the tested combinations (Table S1). However, the overall combined effects (CI_{wt}) are very similar for all the tested combinations, whether the calculation was based on exclusivity or non-exclusivity. Further analyses of the complex EPs® 7630 extract composition [29,31] might be beneficial, but are beyond the scope of this work.

2.6. Molecular Basis of NA-Inhibitor Interactions as Assessed by Crystallographic Analyses

The in vitro studies presented here unambiguously show the different inhibitory potency of tannins against bacterial and viral NAs. To better understand the differential NA–tannin interactions at the molecular level and to assess the specificity of tannin binding, we aimed at solving the crystal structures of various NA–flavan-3-ol complexes. These attempts, however, remained unsuccessful. Instead, we solved the crystal structures of bacterial VCNA in complex with the reference compounds oseltamivir carboxylate and zanamivir at 1.87 and 1.75 Å resolution (Figure S1), allowing a comparative analysis of bacterial versus viral enzyme-inhibitor interactions for these synthetic substances. Data collection and refinement statistics are reported in Table 5.

The uncomplexed crystal structures of influenza A H1N1-NA and bacterial VCNA have been previously published. The enzymes have different overall structural topologies. The viral enzyme is a mushroom-like shaped homotetramer, while the bacterial NA is a monomer with two flanking lectin-like domains [32–34]. Both enzymes share the canonical six-blade β-propeller fold of the catalytic NA domain, despite exhibiting a relatively low amino acid sequence identity of only 12% as revealed by structure-based sequence alignment (Figure S2). Co-crystal structures of H1N1-NA in complex with zanamivir and oseltamivir carboxylate are publicly available (Protein Data Bank (PDB) ID codes 3TI5 and 3TI6) [19], and were used for the following detailed comparison of protein–ligand interactions with the herein determined new bacterial VCNA complex structures.

Table 5. Data collection and refinement statistics for determined VCNA-inhibitor complex structures.

	Oseltamivir Carboxylate	Zanamivir
Data Collection		
Space group	$P2_12_12_1$	$C121$
Cell dimension		
a, b, c (Å)	71.76, 77.86, 163.48	190.55, 50.34, 86.09
α, β, γ (°)	90, 90, 90	90, 107.24, 90
Resolution (Å)	44.33–1.87 (1.94–1.87) *	46.00–1.75 (1.81–1.75)
R_{merge} (%)	10.1 (49.6)	4.4 (47.8)
$<I/\sigma(I)>$	10.2 (2.4)	14.7 (1.8)
Completeness (%)	99.2 (97.9)	97.8 (96.8)
Multiplicity	3.7 (3.5)	2.3 (2.2)
Refinement		
Resolution (Å)	44.33–1.87	46.00–1.75
No. reflections	282260	176727
R_{work}/R_{free} (%)	16.31/20.44	16.69/20.29
No. atoms	6632	6569
Protein	5834	5852
Ligand/ion	42	57
Water	756	660
Average B-factor (Å^2)		
Overall	24.3	32.0
Protein	23.4	31.3
Ligand/ion	22.7	36.0
Water	31.9	38.0
R.m.s. deviations		
Bond lengths (Å)	0.010	0.007
Bond angles (°)	1.18	1.05

One single-crystal was used to collect a complete dataset for every structure. * Highest resolution shell is shown in parenthesis.

A common feature of viral and bacterial inhibitor binding is the electrostatic and hydrogen bonding interaction of the carboxylic acid group of oseltamivir carboxylate or zanamivir to a cluster of three positionally conserved arginine residues (Arg224, Arg635, and Arg712 in VCNA; Arg118, Arg292, and Arg371 in H1N1-NA) (Figure 5, Tables S2 and S3). Notably, Arg224 of VCNA belongs to the bacterially conserved RIP/RLP motif and Arg118 of H1N1-NA belongs to the corresponding REP motif of viral NAs [35]. A second common structural feature is the electrostatic and hydrogen bonding interaction of the 5-amino group of oseltamivir carboxylate or the 4-guanidino moiety of zanamivir with an electronegative binding pocket within the active site (Glu243, Arg 245, Asp250 and Asp292 in VCNA; Glu119, Asp151, and Glu227 in H1N1-NA) (Figure 5, Tables S2 and S3). Notable differences between viral and bacterial inhibitor complexes are observed in the surrounding region of the acetamido moiety of oseltamivir carboxylate and zanamivir. In viral H1N1-NA, the side chain of Arg152 is hydrogen bonded to the acetamido moiety of the inhibitors, an interaction that is missing in the bacterial complexes (Figure 5). Moreover, the acetamido binding cavity in bacterial VCNA is sterically constrained by the short amino acid stretch of Gln317 and Asn318 that extends into the active site. Another steric restriction in the bacterial VCNA active site is seen in the microenvironment around the 5-amino group of oseltamivir carboxylate and the 4-guanidino moiety of zanamivir. Glu243 and Arg245 extend further into the active site compared to Leu134 and Arg156 of the influenza enzyme, thereby reducing the available space in that subpocket. Thus, oseltamivir carboxylate and zanamivir fit much better into the active site of influenza H1N1-NA than that of bacterial VCNA, consistent with their relative inhibitory potencies (Table 1). Taken together, the structural differences between H1N1-NA and VCNA inhibitor complexes contribute to the observed differential inhibition of viral and bacterial NA by oseltamivir carboxylate and zanamivir.
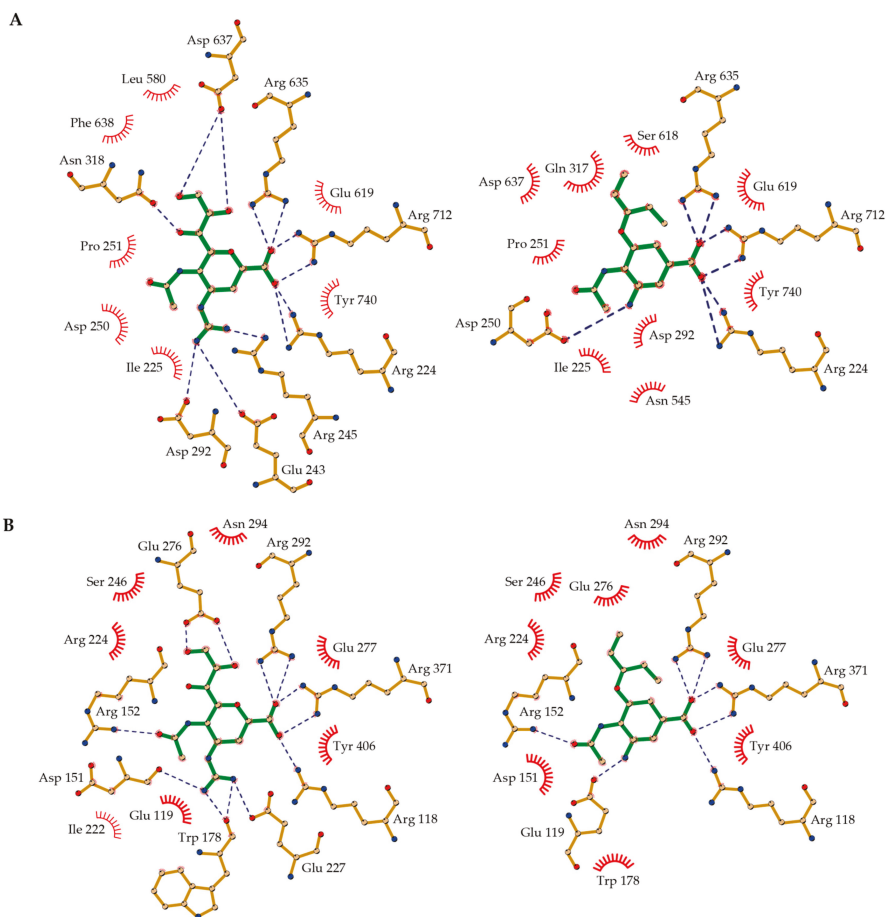
Figure 5. Binding modes of zanamivir (left, green stick model) and oseltamivir carboxylate (right, green stick model) in the active site of (**A**) VCNA, determined in this study (Protein Data Bank (PDB) codes 6EKU and 6EKS); and (**B**) H1N1-NA (PDB codes 3TI5 and 3TI6) [19]. Hydrogen bonds are depicted with dashed blue lines and hydrophobic interactions are shown as red arcs. The figures were prepared with LIGPLOT+ [36].

To rationalize the observed increased inhibitory activity of zanamivir over oseltamivir carboxylate for bacterial VCNA (IC$_{50}$ of 52 μM versus 144 μM, Table 1), we compared the inhibitor interactions in the determined VCNA complex structures. The interaction network differs most in those regions where the chemical structure of the inhibitors is different. The 4-guanidino group of zanamivir, for example, forms electrostatic and hydrogen bonding interactions with Glu243, Arg245, and Asp292, whereas the 5-amino group of oseltamivir carboxylate interacts with Arg250 only (Figure 5, Table S3). The hydrophilic 6-(1′,2′,3′)-trihydroxypropyl group of zanamivir hydrogen bonds with Asn318 and Asp637, the corresponding 3-(1′-ethylpropoxy) group of oseltamivir carboxylate, however, interacts only hydrophobically. Furthermore, the oxygen within the 5,6-dihydro-4*H*-pyran ring of zanamivir forms a hydrogen bond with the side chain of Tyr740, while the cyclohex-1-ene entity of oseltamivir carboxylate interacts exclusively hydrophobically (Figure 5, Table S3). Summarizing, the elevated

number of hydrogen bonds in the zanamivir complex likely explains the increased potency of zanamivir over oseltamivir carboxylate for bacterial VCNA inhibition.

3. Discussion

The current data clearly indicate a differential inhibition of the viral H1N1-NA and bacterial VCNA by the various tested tannins and the reference compounds. While oseltamivir carboxylate and zanamivir showed pronounced inhibition of the viral H1N1-NA, the polyphenolic substances were more effective against bacterial VCNA. Thus, IC_{50} values obtained from a fluorometric activity assay using neuraminidases of different biological origin are not readily comparable and it is therefore advisable to select viral NAs when screening compounds for their anti-influenza potencies, and bacterial NAs when the testing is aimed at targeting bacterial pathogens.

Previous structure–activity relationship analyses of various groups of flavonoids revealed that the presence of the 4-keto function and the C2–C3 double bond are relevant structural elements for potent viral NA inhibition [3,37]. These chemical features are "missing" in flavan-type molecules such as the flavan-3-ols tested in this study, consistent with their weak viral inhibitory activity. In contrast, oligomeric flavan-3-ols (proanthocyanidins) show more promise as antiviral candidates. A computational virtual screening recorded proanthocyanidins within the top ranked plant metabolites selected from ligand databases, but detailed chemical information is lacking [38]. We demonstrate that pure fractions of proanthocyanidins are only 6–10 times less potent compared with the viral-specific reference NA inhibitors. Given the bioactive potential of proanthocyanidins, compositional extract optimization and structural modifications may improve their ability to inhibit viral NAs. Proanthocyanidins may furthermore be sufficiently active against influenza by different modes of action. Targets other than NAs could well provide more potent antiviral effects as exemplarily reported for EPs® 7630 [39].

Next to possible antiviral effects, tannins may also be beneficial for treating bacterial infections. Importantly, NAs of many bacterial, respiratory pathogens play a key role in early stages of pulmonary infection by forming biofilms that contribute to initial colonization of the respiratory tract [14]. Bacterial NAs may additionally be involved in the pathogenesis of enteric bacterial infections [40]. Modulation of bacterial NAs by, for example, secondary plant products thus presents an appealing approach to prevent bacterial infection of the respiratory tract and to maintain gut homeostasis. We analyzed the inhibitory potential of a series of flavan-3-ols and chemically defined proanthocyanidin fractions on the bacterial NA from *Vibrio cholerae*. Compared to the reference NAIs, the proanthocyanidin samples are significantly more potent. We demonstrate that the hydroxylation pattern of the flavan skeleton of the inhibitors and the presence of a 3-*O*-galloyl group is a key structural feature for effective VCNA inhibition. Moreover, inhibitor potency is correlated with the number of molecular interactions within the active site as shown by our crystal structure analysis of VCNA complexes with zanamivir and oseltamivir carboxylate. Within the series of ellagitannins, paeonianin C and terchebin show superior VCNA inhibitory activities compared to zanamivir and oseltamivir carboxylate, a finding that deserves further attention. Overall, tannins exhibit remarkable VCNA inhibitory potencies, a stimulus for similar studies on other bacterial NAs.

The impact of oseltamivir carboxylate and zanamivir on the activity of other bacterial NAs has been reported in previous publications [41–43]. The *Streptococcus pneumoniae* NA NanA, for example, has a K_i value of 1.77 μM for oseltamivir carboxylate and 0.72 mM for zanamivir [41]. Also the *Ruminococcus gnavus* NA is more effectively inhibited by oseltamivir carboxylate than by zanamivir (IC_{50} of 30 μM versus 11.89 mM) [42]. In contrast, we observed an increased inhibitory activity of zanamivir over oseltamivir carboxylate for bacterial VCNA (IC_{50} of 52 μM versus 144 μM, Table 1), consistent with recent findings [44]. This highlights the difficulties in translating structure-based drug developments even between bacterial NAs of different origin, though NAs share a similar fold in their active sites [43].

Another important finding of our study is that the drug–herb combination zanamivir and EPs®
7630 is a more potent inhibitor of bacterial VCNA than either compound alone, suggesting promising
benefits of similar combinatory therapies. Clinical studies are needed to approve the therapeutic
potential. The fact that herbal medicines are increasingly used as an adjuvant treatment of both
bacterial and viral infections makes this field a promising but challenging research in the future.

Finally, absorption, distribution in tissues, and metabolism are important efficacy-influencing
parameters. The intestine and its microbiota play a crucial role in this process. Further research is
needed to clarify the impact of microbial degradation of tannins and their metabolites on health effects.

4. Materials and Methods

4.1. Chemicals

4-Methylumbelliferone, 2′-(4-methylumbelliferyl)-α-D-*N*-acetylneuraminic acid (MUNANA),
and 2-(*N*-morpholino) ethanesulfonic acid (MES) were purchased from Sigma Aldrich
(Taufkirchen Germany). Sources of NAIs: Oseltamivir carboxylate (5-*N*-acetyl-3-(1-ethylpropyl-
1-cyclohexene-1-carboxylic acid), the active form of oseltamivir, was kindly supplied by Hoffmann La
Roche (Basel, Switzerland) and zanamivir (2,4-dideoxy-2,3-didehydro-4-guanidino- *N*-acetylneuraminic
acid) by GlaxoSmithKline (Brentford, Middlesex, UK). All flavan-3-ols (purity > 95%) were commercially
obtained (catechin, Roth, Germany; gallocatechin and catechin-3-*O*-gallate, Sigma Aldrich, Taufkirchen,
Germany; gallocatechin-3-*O*-gallate and epicatechin, Fluka, Switzerland; epigallocatechin, Alfa Aesar,
Germany; epicatechin-3-*O*-gallate, AppliChem, Darmstadt, Germany; epigallocatechin-3-*O*-gallate,
Tocris Bioscience, Bristol, UK), while the ellagitannins are generous gifts from Prof. T. Yoshida,
Okayama University, Japan. The highly purified proanthocyanidin fractions obtained from *Nelia meyeri*,
Salix spp., *Betula* spp., *Potentilla erecta*, *Rhus leptodictya*, and *Diospyros kaki* were available in our research
group. The preparation and characterization of the oligomeric proanthocyanidin mixtures are described
elsewhere [45–50]. The root extract of *Pelargonium sidoides* (EPs® 7630, an aqueous-ethanolic extract),
was obtained from Dr. Willmar Schwabe Pharmaceuticals (Karlsruhe, Germany).

4.2. NA Inhibition Assay

To assess NA activity, a fluorometric NA inhibition assay using MUNANA as a substrate and
commercially available *Vibrio cholerae* NA was performed [18]. VCNA (Hoffmann La Roche, Basel,
Switzerland) (1 U stock) was diluted 1:10 in MES-buffer (34.8 μM MES-NaOH pH 6.5, 4 mM CaCl$_2$)
and stored at −22 °C in aliquots, while the viral NA (influenza virus strain/California/04/2009;
H1N1; BioTrend, Köln, Germany) in Tris-buffer (20 mM Tris-HCl pH 7.4, 500 mM NaCl, 10% glycine)
was adjusted to 80–120 mU/mL with distilled water and kept in aliquots at −80 °C until use. Stock
solutions (0.1–10 mg/mL) of the test substances were prepared in MES-buffer, aqueous ethanol or
DMSO/H$_2$O (1:5 v/v) and serially diluted in MES-buffer for measurements.

To quantify enzyme activity, 60 μL of MES-buffer and 10 μL of diluted VCNA were mixed with
10 μL of varying concentrations of the test substance in black 96-well plates. For analyses of the viral
NA, half of the volumes were used. After agitating gently and incubating for 2 min at 37 °C, 20 μL
of the substrate MUNANA (1 mM stock solution) was added, and the fluorescence measured over
the course of 14 min at an excitation wavelength of 360 nm and an emission wavelength of 465 nm.
Appropriate controls were included in the measurements. All assays were at least performed in
triplicates (n = 3–6) and IC$_{50}$ values for each substance were calculated from fitting curves to data
points (percentage of inhibition vs. concentration) using GraphPad Prism version 6.0 for Windows
(GraphPad Software, La Jolla, CA, USA, www.graphpad.com).

IC$_{50}$ values are expressed as mean values ± standard deviation for n = 3–6 experiments.
For normally distributed data, first the variance homogeneity test (F-test) was applied, followed
by the *t*-test. For data with non-normal distributions, the Welch-modified *t*-test was used. Analysis

of variance (ANOVA) followed by the Bonferonni's multiple comparison test was used to evaluate differences between tests. *p*-values < 0.05 were considered statistically significant.

4.3. Drug Combination Analysis

The combined effect of zanamivir and EPs® 7630 on VCNA was determined using the diagonal constant ratio combination method designed by Chou and Talalay [27]. VCNA was incubated with zanamivir or EPs® 7630 individually and in combination at weight ratios of zanamivir to EPs® 7630 (10:1, 5:1, 1:1, 1:5, and 1:10) as described in Section 4.2. The concentration–efficiency curves of the test samples were transformed into the double-logarithmic mean action diagram (shape (*m*), intercepts and regression coefficients were used to determine the median effect dose D_m).

$$D_m = 10^{-\left(\frac{b}{m}\right)}$$

Fraction affected (f_a) and fraction unaffected (f_u) by the concentration D were calculated by the median effect equation [27]:

$$\frac{f_a}{f_u} = \left(\frac{D}{D_m}\right)^m$$

D_m is the concentration required to produce the median effect.

The CI for quantification of synergism, additive effects, or antagonism was calculated as follows:

$$\text{CI} = \frac{D_1}{(D_x)_1} + \frac{D_2}{(D_x)_2} \; (\text{exclusivity}) \tag{1}$$

$$\text{CI} = \frac{D_1}{(D_x)_1} + \frac{D_2}{(D_x)_2} + \frac{D_1 \times D_2}{(D_x)_1 \times (D_x)_2} \; (\text{non} - \text{exclusivity}) \tag{2}$$

Due to the therapeutic significance of the high degrees of effects, the weighted average CI values were calculated as

$$\text{CI}_{\text{wt}} = \frac{\text{CI}_{50} + 2 \times \text{CI}_{75} + 3 \times \text{CI}_{90} + 4 \times \text{CI}_{95}}{10} \tag{3}$$

4.4. Expression and Purification of Recombinant VCNA

The expression vector pET30b(+) that produces *Vibrio cholerae* serotype O1 (strain ATCC 39315/E1 Tor Inaba N165961) NA was a gift from Prof. G. Taylor, University of St. Andrews, Scotland. VCNA was produced according to a previously reported method with the following modifications [51]. VCNA was expressed in *E. coli* Rosetta™ 2 (DE3) (Merck KGaA, Darmstadt, Germany) using an LEX ultra-high-throughput bench-top bioreactor (Epiphyte3 Inc., Toronto, ON, Canada). Cells were grown at 37 °C in Terrific Broth medium to an optical density at 600 nm (OD$_{600}$) of about 2.0–2.5, cooled to 17 °C, and induced with 0.5 mM isopropyl β-D-1-thiogalactopyranoside (IPTG). Cultures were then left shaking overnight, and cells were collected by centrifugation.

For purification, cells were resuspended in 20 mM Tris–HCl pH 7.6 supplemented with cOmplete™ ethylenediamine tetra-acetic acid (EDTA)-free protease inhibitor cocktail (Merck KGaA, Darmstadt, Germany), and lysed by sonication (SONOPULS HD 2200, Bandelin Electronic GmbH & Co. KG, Berlin, Germany). The purification procedure comprised initial ammonium sulfate precipitation (50% *w*/*v*), desalting on a 26/10 HiPrep Desalting column (GE Healthcare, Munich, Germany) equilibrated with 10 mM Tris-HCl pH 7.6 and 150 mM NaCl, a Source 30Q anion exchange column, and a final size-exclusion chromatography on a Superdex 200 prep grade column (XK 26 × 60, GE Healthcare, Munich, Germany). Purified protein was concentrated to about 6 mg/mL in a buffer containing 20 mM Tris-HCl, pH 7.6, 0.15 M NaCl, and 10 mM CaCl$_2$.

4.5. VCNA Crystallization and Structure Determination

The VCNA-inhibitor complexes were crystallized using the sitting-drop vapor-diffusion method at 20 °C by mixing equal volumes (200 nL) of purified protein (see Section 4.4) and reservoir solution, with a reservoir volume of 75 μL in 96-well plates. VCNA (in 20 mM Tris-HCl pH 7.6, 0.15 M NaCl, 10 mM $CaCl_2$) was complexed with a 20 mM inhibitor (oseltamivir, zanamivir) and concentrated to 6–7 mg/mL. The VCNA–oseltamivir complex was crystallized using 20% (*w/v*) polyethylene glycol (PEG) 3350 and 0.2 M lithium acetate as reservoir solution. For the VCNA–zanamivir complex, the reservoir solution contained 20% (*w/v*) PEG 3350 and 0.2 M sodium fluoride. Before flash-freezing in liquid nitrogen, the crystals were transferred into a cryoprotectant consisting of reservoir solution supplemented with 30% (*v/v*) glycerol.

X-ray diffraction data were collected at beamline BL14.1 at the Helmholtz-Zentrum Berlin [52] at a wavelength of 0.9184 Å and a temperature of 100 K. Data were processed with the program XDSAPP [53]. The structure was solved by molecular replacement using the program PHASER [54] and uncomplexed VCNA as search model (PDB entry 1KIT) [34]. Structure refinement was done with the PHENIX program suite [55]. The graphics program COOT was used for manual model building and visualization [56]. PRODRG was used for generation of ligand restraint parameters [57]. Data collection and refinement statistics are reported in Table 5. Coordinates and structure factors for the VCNA-inhibitor complex structures have been deposited in the Protein Data Bank under accession codes 6EKS and 6EKU.

4.6. Multiple Sequence Alignment

The structure-based sequence alignment was performed with PDBeFold [58] using the PDB entries 1W0O (VCNA) and 3NSS (H1N1-NA). The aligned amino-acid sequences were transferred to the Clustal Omega server [59] to generate the input file for TEXshade [60], which was used for final visualization. The Uniprot accession numbers for *Vibrio cholerae* NA and influenza virus H1N1 A/California/04/2009 NA are P0C6E9 and C3W5S3.

Author Contributions: S.Q., A.S., and H.K. conceived and designed the experiments; S.Q. performed the inhibition assays and X-ray structure analysis; A.S. performed the VCNA protein production, the protein crystallization, the X-ray data collection, the structure determination, and the X-ray structure analysis; S.Q., A.S. and H.K. analyzed the data; H.K. and A.S. wrote and H.K. finalized the manuscript.

Conflicts of Interest: The authors declare no conflict of interest.

References

1. Matrosovich, M.N.; Matrosovich, T.Y.; Gray, T.; Roberts, N.A.; Klenk, H.D. Neuraminidase is important for the initiation of influenza virus infection in human airway epithelium. *J. Virol.* **2004**, *78*, 12665–12667. [CrossRef] [PubMed]
2. Nguyen, H.T.; Fry, A.M.; Gubareva, L.V. Neuraminidase inhibitor resistance in influenza viruses and laboratory testing methods. *Antivir. Ther.* **2012**, *17*, 159–173. [CrossRef] [PubMed]
3. Grienke, U.; Schmidtke, M.; von Grafenstein, S.; Kirchmair, J.; Liedl, K.R.; Rollinger, J.M. Influenza neuraminidase: A druggable target for natural products. *Nat. Prod. Rep.* **2012**, *29*, 11–36. [CrossRef] [PubMed]

4. Rakers, C.; Schwerdtfeger, S.M.; Mortier, J.; Duwe, S.; Wolff, T.; Wolber, G.; Melzig, M.F. Inhibitory potency of flavonoid derivatives on influenza virus neuraminidase. *Bioorg. Med. Chem. Lett.* **2014**, *24*, 4312–4317. [CrossRef] [PubMed]

5. Song, J.M.; Lee, K.H.; Seong, B.L. Antiviral effect of catechins in green tea on influenza virus. *Antivir. Res.* **2005**, *68*, 66–74. [CrossRef] [PubMed]

6. Wang, X.; Jia, W.; Zhao, A. Anti-influenza agents from plants and traditional Chinese medicine. *Phytother. Res.* **2006**, *20*, 335–341. [CrossRef] [PubMed]

7. Ge, H.; Wang, Y.F.; Xu, J.; Gu, Q.; Liu, H.B.; Xiao, P.G.; Zhou, J.; Liu, Y.; Yang, Z.; Su, H. Anti-influenza agents from traditional Chinese medicine. *Nat. Prod. Rep.* **2010**, *27*, 1758–1780. [CrossRef] [PubMed]

8. Droebner, K.; Ehrhardt, C.; Poetter, A.; Ludwig, S.; Planz, O. CYSTUS052, a polyphenol-rich plant extract, exerts anti-influenza virus activity in mice. *Antivir. Res.* **2007**, *76*, 1–10. [CrossRef] [PubMed]

9. Ehrhardt, C.; Hrincius, E.R.; Korte, V.; Muzur, I.; Droebner, K.; Poetter, A.; Dresschers, S.; Schmolke, M.; Planz, O.; Ludwig, S. A polyphenol-rich plant extract, CYSTUS=52, exerts anti influenza virus activity in cell culture without toxic side effects or the tendency to induce viral resistance. *Antivir. Res.* **2007**, *76*, 38–47. [CrossRef] [PubMed]

10. Schwerdtfeger, S.M.; Melzig, M.F. Sialidases in biological systems. *Pharmazie* **2010**, *65*, 551–561. [PubMed]

11. Kelly, R.T.; Farmer, S.; Greiff, D. Neuraminidase activities of clinical isolates of *Diplococcus pneumoniae*. *J. Bacteriol.* **1967**, *84*, 272–273.

12. Pettigrew, M.M.; Fennie, K.P.; York, M.P.; Daniels, J.; Ghaffar, F. Variation in the presence of neuraminidase genes among *Streptococcus pneumoniae* isolates with identical sequence types. *Infect. Immun.* **2006**, *74*, 3360–3365. [CrossRef] [PubMed]

13. Lewis, A.L.; Lewis, W.G. Host sialoglycans and bacterial sialidases: A mucosal perspective. *Cell. Microbiol.* **2012**, *14*, 1174–1182. [CrossRef] [PubMed]

14. Soong, G.; Muir, A.; Gomez, M.I.; Waks, J.; Reddy, B.; Planet, P.; Singh, P.K.; Kaneko, Y.; Wolfgang, M.C.; Hsiao, Y.S.; et al. Bacterial neuraminidase facilitates mucosal infection by participating in biofilm production. *J. Clin. Investig.* **2006**, *116*, 2297–2305. [CrossRef] [PubMed]

15. McCullers, J.A.; Bartmess, K.C. Role of neuraminidase in lethal synergism between influenza virus and *Streptococcus pneumoniae*. *J. Infect. Dis.* **2003**, *187*, 1000–1009. [CrossRef] [PubMed]

16. Mann, M.C.; Thomson, R.J.; Dyason, J.C.; McAtamney, S.; von Itzstein, M. Modelling, synthesis and biological evaluation of novel glucuronide-based probes of *Vibrio cholerae* sialidase. *Med. Chem.* **2006**, *14*, 1518–1537. [CrossRef] [PubMed]

17. Potier, M.; Mameli, L.; Belisle, M.; Dallaire, L.; Melancon, S. Fluorometric assay of neuraminidase with a sodium (4-methylumbelliferyl-α-D-*N*-acetylneuraminate) substrate. *Anal. Biochem.* **1979**, *94*, 287–296. [CrossRef]

18. Quosdorf, S.J.; Kolodziej, H. The potential of flavan-3-ols and their oligomers as neuraminidase inhibitors and limitation of a fluorescence-based assay. In Proceedings of the 8th ISANH Congress on Polyphenols Applications, Lisbon, Portugal, 5–6 June 2014; p. 237.

19. Vavricka, C.J.; Li, Q.; Wu, Y.; Qi, J.; Wang, M.; Liu, Y.; Gao, F.; Liu, J.; Feng, E.; He, J. Structural and functional analysis of laninamivir and its octanoate prodrug reveals group specific mechanisms for influenza NA inhibition. *PLoS Pathog.* **2011**, *7*, e1002249. [CrossRef] [PubMed]

20. Nishikawa, T.; Shimizu, K.; Tanaka, T.; Kuroda, K.; Takayama, T.; Yamamoto, T.; Hanada, N.; Hamada, Y. Bacterial neuraminidase rescues influenza virus replication from inhibition by a neuraminidase inhibitor. *PLoS ONE* **2012**, *7*, e45371. [CrossRef] [PubMed]

21. Govorkova, E.A.; Fang, H.B.; Tan, M.; Webster, R.G. Neuraminidase inhibitor-rimantadine combinations exert additive and synergistic anti-influenza virus effects in MDCK Cells. *Antimicrob. Agents Chemother.* **2004**, *48*, 4855–4863. [CrossRef] [PubMed]

22. Ilyushina, N.A.; Bovin, N.V.; Webster, R.S.; Govorkan, E.A. Combination chemotherapy, a potential strategy for reducing the emergence of drug-resistant influenza A variants. *Antivir. Res.* **2006**, *70*, 121–131. [CrossRef] [PubMed]

23. Ilyushina, N.A.; Hoffmann, E.; Salomon, R.; Webster, R.S.; Govorkan, E.A. Amantadine-oseltamivir combination therapy for H5N1 influenza virus infection in mice. *Antivir. Ther.* **2007**, *12*, 363–370. [PubMed]

24. Ilyushina, N.A.; Hay, A.; Yilmaz, N.; Boon, A.C.; Webster, R.S.; Govorkan, E.A. Oseltamivir-ribavirin combination therapy for highly pathogenic H5N1 influenza virus infection in mice. *Antimicrob. Agents Chemother.* **2008**, *52*, 3889–3897. [CrossRef] [PubMed]

25. Charyasriwong, S.; Watanabe, K.; Rahmasari, R.; Matsunaga, A.; Haruyama, T.; Kobayashi, N. In vitro evaluation of synergistic inhibitory effects of neuraminidase inhibitors and methylglyoxal against influenza virus infection. *Arch. Med. Res.* **2015**, *46*, 8–16. [CrossRef] [PubMed]

26. Haidari, M.; Ali, M.; Casscells, S.W.; Madjid, M. Pomegranate (*Punica granatum*) purified extracts inhibits influenza virus and has a synergistic effect with oseltamivir. *Phytomedicine* **2009**, *16*, 1127–1136. [CrossRef] [PubMed]

27. Chou, T.; Talalay, P. Quantitative analysis of dose-effect relationships: The combined effects of multiple drugs or enzyme inhibitors. *Adv. Enzym. Regul.* **1984**, *22*, 27–55. [CrossRef]

28. Chou, T. Theoretical basis, experimental design, and computerized simulation of synergism and antagonism in drug combination studies. *Pharmacol. Rev.* **2006**, *58*, 621–681. [CrossRef] [PubMed]

29. Kolodziej, H. Fascinating metabolic pools of *Pelargonium sidoides* and *Pelargonium reniforme*, traditional and phytomedicinal sources of the herbal medicine Umckaloabo®. *Phytomedicine* **2007**, *14* (Suppl. VI), 18–26. [CrossRef] [PubMed]

30. Bijnsdorp, I.V.; Giovannetti, E.; Peters, G.J. Analysis of drug interactions. *Methods Mol. Biol.* **2011**, *731*, 421–434. [PubMed]

31. Schoetz, K.; Erdelmeier, C.; Germer, S.; Hauer, H. A detailed view on the constituents of EPs® 7630. *Planta Med.* **2008**, *74*, 667–674. [CrossRef] [PubMed]

32. Varghese, J.; Lawer, W.; Coleman, P.M. Structure of the influenza virus glycoprotein antigen neuraminidase at 2.9 Å resolution. *Nature* **1983**, *303*, 35–40. [CrossRef] [PubMed]

33. Colman, P.M.; Varghese, J.N.; Laver, W.G. Structure of the catalytic and antigenic sites in influenza virus neuraminidase. *Nature* **1983**, *303*, 41–44. [CrossRef] [PubMed]

34. Crennell, S.; Garman, E.; Laver, G.; Vimr, E.; Taylor, G. Crystal structure of *Vibrio cholerae* neuraminidase reveals dual lectin-like domains in addition to the catalytic domain. *Structure* **1994**, *2*, 535–544. [CrossRef]

35. Taylor, G. Sialidases: Structures, biological significance and therapeutic potential. *Curr. Opin. Struct. Biol.* **1996**, *6*, 830–837. [CrossRef]

36. Laskowski, R.A.; Swindells, MB. LigPlot+: Multiple ligand–protein interaction diagrams for drug discovery. *J. Chem. Inf. Model.* **2011**, *51*, 2778–2786. [CrossRef] [PubMed]

37. Liu, A.L.; Wang, H.D.; Lee, S.M.Y.; Wang, Y.T.; Du, G.H. Structure–activity relationships of flavonoids as influenza virus neuraminidase inhibitors and their in vitro antiviral activities. *Bioorg. Med. Chem.* **2008**, *16*, 7141–7147. [CrossRef] [PubMed]

38. Sharma, A.; Tendulkar, A.V.; Wangikar, P.P. Drug discovery against H1N1 virus (influenza virus) via computational virtual screening approach. *Med. Chem. Res.* **2011**, *20*, 1445–1449. [CrossRef]

39. Kolodziej, H. Antimicrobial, antiviral and immunomodulatory activity studies of *Pelargonoium sidoides* (EPs® 7630) in the context of health promotion. *Pharmaceuticals* **2011**, *4*, 1295–1314. [CrossRef] [PubMed]

40. Juge, N.; Tailford, L.; Owen, C.D. Sialidases from gut bacteria: A mini-review. *Biochem. Soc. Trans.* **2016**, *44*, 166–175. [CrossRef] [PubMed]

41. Gut, H.; Xu, G.; Taylor, G.L.; Walsh, M.A. Structural basis for *Streptococcus pneumoniae* NanA inhibition by influenza antivirals zanamivir and oseltamivir carboxylate. *J. Mol. Biol.* **2011**, *408*, 498–503. [CrossRef] [PubMed]

42. Tailford, L.E.; Owen, C.D.; Walshaw, J.; Crost, E.H.; Hardy-Goddard, J.; le Gall, G.; de Vos, W.M.; Taylor, G.L.; Juge, N. Discovery of intramolecular *trans*-sialidases in human gut microbiota suggests novel mechanisms of mucosal adaptation. *Nat. Commun.* **2015**, *6*, 7624. [CrossRef] [PubMed]

43. Owen, C.D.; Lukacik, P.; Potter, J.A.; Sleator, O.; Taylor, G.L.; Walsh, M.A. *Streptococcus pneumoniae* NanC—Structural insights into the specificity and mechanism of a sialidase that produces a sialidase inhibitor. *J. Biol. Chem.* **2015**, *290*, 27736–27748. [CrossRef] [PubMed]

44. Richter, M.; Schumann, L.; Walther, E.; Hoffmann, A.; Braun, H.; Grienke, U.; Rollinger, J.M.; von Grafenstein, S.; Liedl, K.R.; Kirchmair, J.; et al. Complementary assays helping to overcome challenges for identifying neuraminidase inhibitors. *Future Virol.* **2015**, *10*, 77–88. [CrossRef]

45. Kolodziej, H. Ocurrence of procyanidins in *Nelia meyeri*. *Phytochemistry* **1984**, *23*, 1745–1752. [CrossRef]

46. Kolodziej, H. Oligomeric flavan-3-ols from medicinal willow bark. *Phytochemistry* **1990**, *29*, 955–960. [CrossRef]
47. Schleep, S.; Kolodziej, H. Phenolic metabolites from *Potentilla erecta*. *Phytochemistry (Life Sci. Adv.)* **1992**, *11*, 87–92.
48. Kolodziej, H. Procyanidins from medicinal birch: Bonding patterns and sequence of units in triflavanoids of mixed stereochemistry. *Phytochemistry* **1989**, *28*, 3487–3492. [CrossRef]
49. Viviers, P.; Kolodziej, H.; Young, D.; Ferreira, D.; Roux, D. Synthesis of condensed tannins. Part 11. Intramolecular enantiomerism of the constituent units of tannins from the anacardiaceae: Stoicheiometric control in direct synthesis: Derivation of ^{1}H-nuclear magnetic resonance parameters applicable to higher oligomers. *J. Chem. Soc. Perkin Trans. 1* **1983**, 527–533. [CrossRef]
50. Li, C.; Leverence, R.; Trombley, J.D.; Xu, S.; Yang, J.; Tian, Y.; Reed, J.D.; Hagerman, A.E. High molecular weight persimmon (*Diospyros kaki* L.) proanthocyanidin: A highly galloylated, A-linked tannin with an unusual flavonol terminal unit, myricetin. *J. Agric. Food Chem.* **2010**, *58*, 9033–9042. [CrossRef] [PubMed]
51. Moustafa, I.; Connaris, H.; Taylor, M.; Zaitsev, V.; Wilson, J.C.; Kiefel, M.J.; Itzstein, M.; Taylor, G. Sialic acid recognition by *Vibrio cholerae* neuraminidase. *J. Biol. Chem.* **2004**, *279*, 40819–40826. [CrossRef] [PubMed]
52. Mueller, U.; Darowski, N.; Fuchs, M.R.; Förster, R.; Hellmig, M.; Paithankar, K.S.; Pühringer, S.; Steffien, M.; Zocher, G.; Weiss, M.S. Facilities for macromolecular crystallography at the Helmholtz-Zentrum Berlin. *J. Synchrotron Radiat.* **2012**, *19*, 442–449. [CrossRef] [PubMed]
53. Sparta, K.M.; Krug, M.; Heinemann, U.; Mueller, U.; Weiss, M.S. XDSAPP2.0. *J. Appl. Cryst.* **2016**, *49*, 1085–1092. [CrossRef]
54. McCoy, A.J.; Grosse-Kunstleve, R.W.; Storoni, L.C.; Read, R.J. Likelihood-enhanced fast translation functions. *Acta Crystallogr. Sect. D* **2005**, *61*, 458–464. [CrossRef] [PubMed]
55. Adams, P.D.; Afonine, P.V.; Bunkóczi, G.; Chen, V.B.; Davis, I.W.; Echols, N.; Headd, J.J.; Hung, L.W.; Kapral, G.J.; Grosse-Kunstleve, R.W.; et al. PHENIX: A comprehensive Python-based system for macromolecular structure solution. *Acta Crystallogr. Sect. D* **2010**, *66*, 213–221. [CrossRef] [PubMed]
56. Emsley, P.; Lohkamp, B.; Scott, W.G.; Cowtan, K. Features and development of Coot. *Acta Crystallogr. Sect. D* **2010**, *66*, 486–501. [CrossRef] [PubMed]
57. Schüttelkopf, A.W.; van Aalten, D.M.F. PRODRG: A tool for high-throughput crystallography of protein-ligand complexes. *Acta Crystallogr. Sect. D* **2004**, *60*, 1355–1363. [CrossRef] [PubMed]
58. Krissinell, E.; Henrick, K. Secondary-structure matching (SSM), a new tool for fast protein structure alignment in three dimensions. *Acta Crystallogr. Sect. D* **2004**, *60*, 2256–2268. [CrossRef] [PubMed]
59. Sievers, F.; Wilm, A.; Dineen, D.; Gibson, T.J.; Karplus, K.; Li, W.; Lopez, R.; McWilliam, H.; Remmert, M.; Söding, J.; et al. Fast, scalable generation of high-quality protein multiple sequence alignments using Clustal Omega. *Mol. Syst. Biol.* **2011**, *7*, 539. [CrossRef] [PubMed]
60. Beitz, E. TEXshade: Shading and labeling of multiple sequence alignments using LATEX2 epsilon. *Bioinformatics* **2000**, *16*, 135–139. [CrossRef] [PubMed]

Sample Availability: Not available.

Simultaneous Quantification of Ellagitannins and Related Polyphenols in *Geranium thunbergii* Using Quantitative NMR

Februadi Bastian [1], **Yurie Ito** [1], **Erika Ogahara** [2], **Natsuki Ganeko** [1], **Tsutomu Hatano** [2] **and Hideyuki Ito** [1,2,*]

[1]   Faculty of Health and Welfare Science, Okayama Prefectural University, 111 Kuboki, Soja, Okayama 719-1197, Japan; februadi@unhas.ac.id (F.B.); yurieng8@icloud.com (Y.I.); ganeko@fhw.oka-pu.ac.jp (N.G.)

[2]   Division of Pharmaceutical Sciences, Okayama University Graduate School of Medicine, Dentistry, Pharmaceutical Sciences, 1-1-1 Tsushima-naka, Kita-ku, Okayama 700-8530, Japan; fraaaan.1441@gmail.com (E.O.); hatano-t@cc.okayama-u.ac.jp (T.H.)

*   Correspondence: hito@fhw.oka-pu.ac.jp; Tel.: +81-866-94-2086

check for
updates

Abstract: Compared to commonly employed liquid chromatography-based methods, quantitative nuclear magnetic resonance (qNMR) is a recently developed method for accurate quantification of natural compounds in extracts. The simultaneous quantification of ellagitannins and the related polyphenols of *Geranium thunbergii* were studied using qNMR after a short-term and long-term decoction. The qNMR fingerprint for quantifying ellagitannin was presented in this work. Geraniin was observed in the short-term decoction as a major component while corilagin was the major component of the long-term decoction. An aqueous acetone extract of *G. thunbergii* after long-term decoction was extracted with diethyl ether, ethyl acetate, and *n*-butanol. Corilagin was found as a major constituent in the ethyl acetate and *n*-butanol extracts. Furthermore, the contents of these polyphenols in *G. thunbergii* from six locations in Japan and three locations in China were quantified. The contents of geraniin and corilagin in *G. thunbergii* from Japan were higher than those from China. Our finding raised the possibility that qNMR can be effectively employed as a simple, accurate, and efficient method for quantification of ellagitannins in medicinal plants.

1. Introduction

Nuclear magnetic resonance (NMR) has become the leading analytical tool for chemical structure elucidation in numerous fields of industrial and academic research. One advantage for using NMR is that the technique is non-destructive, enabling compound detection from both pure and impure samples without compromising the initial sample [1–3]. NMR has the potential to simultaneously provide both qualitative and quantitative information.

Since 1963, NMR spectroscopy has been described as a quantitative measurement [4]. Quantitative nuclear magnetic resonance (qNMR) is founded on the principle that signal intensities of a given NMR spectrum are directly proportional to the molar amount of that nucleus in the sample, so that qNMR can be a simple and absolute quantification method able to determine the purities of compounds or the absolute content of a compound in the natural source with unit traceability. The past decade has seen an increasing amount of literature on the usefulness of qNMR. The survey by Pauli and co-workers showed that quantification using NMR on pharmaceutical, chemical, and food fields has significantly increased in recent years [5,6]. The usefulness of qNMR is further accelerated by additional advantages, such as the lack of calibration curve requirements, the non-destructive character of the NMR technique,

for the lack of special sample preparation requirements, relatively short measurement times, and the possibility of simultaneously quantifying multiple compounds in crude extracts [5–10].

The accuracy of a qNMR measurement is one of the key reasons for why this method was employed. Previous studies have established no significant difference between the accuracy of assays conducted using qNMR and other methods, such as HPLC. Huo et al. measured the content of avermectin using HPLC and qNMR. They reported no significant difference between the assay results of these two methods [10]. Similarly, Napolitano et al. plotted the concentration of catechin obtained by HPLC-MS/MS against values obtained using qNMR. Both methods yielded similarly good linear regression correlations of $R^2 > 0.999$. No significant difference between HPLC-MS/MS and qNMR methods was found [3]. For these reasons, combined with numerous additional advantages, qNMR might be a powerful tool for the quantification of natural products.

Ellagitannins belong to the class of hydrolysable tannins. They have shown potential health benefits, such as the prevention of advanced glycation end products formation [11], anti-inflammatory effects [12,13], anti-diabetic effects [14], anti-fungal effects [15], and antioxidant effects [16,17]. It is now well established from a variety of studies that over 500 ellagitannins have been discovered [18,19]. *Geranium thunbergii,* a member of the *Geranium* genus, is well known to contain large amounts of ellagitannins. The dried weight of *G. thunbergii* leaves can contain up to 10% of ellagitannins, including geraniin and corilagin. Geraniin contains the typical acyl groups found in ellagitannins, such as galloyl, hexahydroxydiphenolyl (HHDP), and dehydrohexahydroxydiphenolyl (DHHDP) units [20]. Therefore, we selected a suitable candidate for the present study.

Geraniin is the major ellagitannin in *G. thunbergii*, which has long been used as a remedy for intestinal disorders in Japan [20,21]. Geraniin has also been reported to have various biological activities [22]. *G. Thunbergii* is traditionally known in Japan as *gennoshoko* [20]. There are two ways to use *G. thunbergii* medicinally. The dried aerial parts can be brewed with hot water (making a tea) or the dried plant can be boiled in water for one hour. The resulting concoctions are used for the treatment of constipation and diarrhea, respectively.

To the best of our knowledge, no study has yet investigate the quantity of ellagitannin in *G. thunbergii* using qNMR. Most researchers quantifying ellagitannin have utilized chromatographic methods, such as HPLC, UHPLC, and LC-MS/MS [23–25]. Analytical methods using HPLC require pure standards for drawing the calibration curve. It is well known that obtaining commercially pure native standards of specific ellagitannins is difficult. For HPLC and other chromatographic studies, an initial purification of the specific ellagitannin is generally required for use in further quantification processes. In addition, large ellagitannin oligomers are more difficult to purify than monomers [26]. In this study, we investigated the application of qNMR to assay the main ellagitannin and the related polyphenol contents (Figure 1) in the short-term and long-term extracts of *G. thunbergii*. The present study also explored the main polyphenol contents in *G. thunbergii* plants cultivated in Japan and China. The contents of the targeted compounds were calculated from the integral of the characteristic anomeric or aromatic proton signals against that of an internal standard.
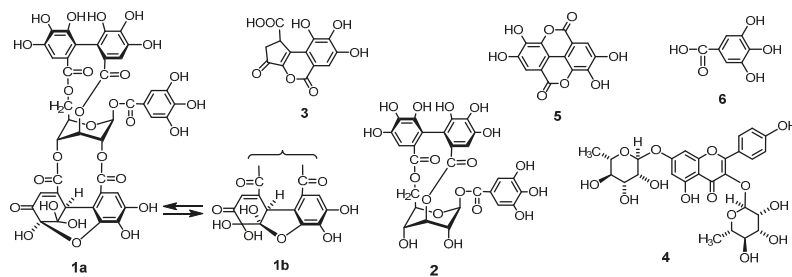
Figure 1. Structures of the main ellagitannins and related polyphenols in *G. thunbergii*.

2. Results

2.1. HPLC Analysis of Geraniin and the Related Polyphenols in G. thunbergii

Quantification of geraniin using HPLC has several weaknesses. Geraniin, belonging to the dehydroellagitannin family, usually forms an equilibrium mixture of six- and five-membered hemiacetal forms (**1a** and **1b,** respectively) in aqueous solutions. Thus, methanol adducts with methoxyl groups at hemiacetal in geraniin were produced in methanol solution subjected to HPLC resulted in showing multiple or broad peaks in HPLC profile. [27,28].

In this study, problems of coelution on HPLC during the analysis of geraniin were found. The HPLC profiles of *G. thunbergii* extracts after brewing in hot water showed the geraniin (**1**) peak. After boiling for 1 h, geraniin was completely hydrolyzed to corilagin (**2**), brevifolincarboxylic acid (**3**), ellagic acid (**5**), and gallic acid (**6**). However, after boiling for 1 h, selected signals at the same retention time to geraniin remained on the chromatograph in normal phase HPLC, implying that other compounds overlapped with the retention time signal corresponding to geraniin (Figure 2). Furthermore, ellagic acid, gallic acid, and brevifolincarboxylic acid elute closely on normal phase HPLC. The reversed phase HPLC profile also revealed that brevifolincarboxylic acid, geraniin, and corilagin all eluted close together. This HPLC coelution phenomenon is one of the reasons why we began to explore other methods to quantify ellagitannins and the related polyphenols.
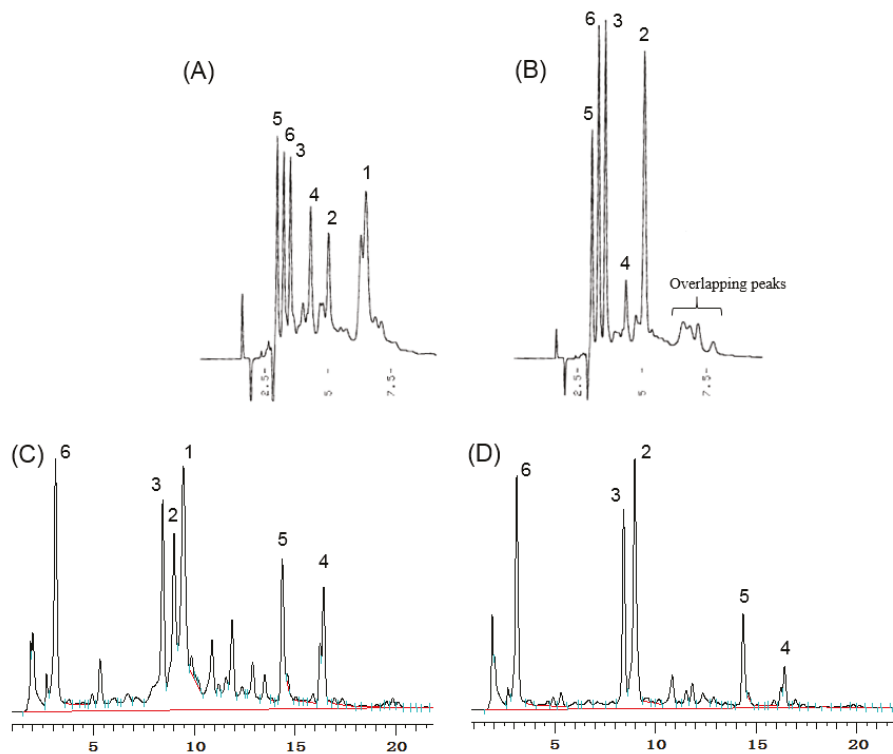
Figure 2. HPLC profiles for the extracts of *G. thunbergii*: (**A**) short-term decoction on normal phase HPLC; (**B**) long-term decoction on normal phase HPLC; (**C**) short-term decoction on reversed phase HPLC; and (**D**) long-term decoction on reversed phase HPLC.

2.2. ^{1}H-NMR Fingerprint

There are two critical issues for determining the type of solvent to employ: the ability to dissolve the compounds of interest and signal separation. Dimethyl sulfoxide (DMSO)-d_6 was a very good choice for solvating ellagitannins, but it did not provide sufficient ^{1}H-NMR signal separation.

Despite the addition of CF_3COOD-D_2O and employing variable temperature techniques, sufficient peak separation could not be obtained. Alternatively, acetone-d_6 could provide adequate ^{1}H-NMR signal separation, but it was inadequate at dissolving some of the target compounds. We could not obtain valuable data in the solvent with good solubility such as methanol-d_4, since necessary signals corresponding to some of candidate compounds were overlapped with a signal of HDO in the solvent. On the other hand, acetone-d_6 has less area overlapping with HDO. Furthermore, a small amount of D_2O was added to raise the solubility and CF_3COOD was added to provide sharp signals due to polyphenols. With peak separation being the most important factor in qNMR analysis, acetone-d_6 was selected and D_2O and CF_3COOD were added to obtain a final ratio of 70:25:5, respectively. This solvent ratio resulted in good ^{1}H-NMR peak separation.

To develop the ^{1}H-NMR fingerprints indicative of geraniin and its metabolites, sugar, and organic acids, ^{1}H-NMR spectrum analyses of the individual compounds were carried out. The indicative signals of the candidate compounds for qNMR are presented in Table 1 and Figure 3. Based on the integrations of these signals, the contents of ellagitannin, and the related compounds, in various extracts of *G. thunbergii* were quantified by the method described in Section 4.4.

Table 1. Specific ^{1}H-NMR data of main ellagitannins and the other compound of *G. thunbergii* for quantitative nuclear magnetic resonance (qNMR) analysis {600 MHz, acetone-d_6-CF_3COOD-D_2O (70:25:5)}.

Compounds	MW	^{1}H-NMR Data
Geraniin (**1**)	952	δ 6.54 (**1a** form glucose H-1; 1H, br s) δ 6.51 (**1b** form glucose H-1; 1H, br s)
Corilagin (**2**)	634	δ 6.30 (glucose H-1; 1H, br s)
Brevifolincarboxylic acid (**3**)	292	δ 7.36 (aromatic proton; 1H, s)
Kaempferitrin (**4**)	578	δ 7.78 (B-ring H-2′,6′; 2H, d, *J* = 9.0 Hz)
Ellagic acid (**5**)	302	δ 7.55 (2H, s)
Gallic acid (**6**)	170	δ 7.04 (2H, s)
Glucose	180	δ 4.52 (β-form H-1; 1H, d, *J* = 8.4 Hz) δ 5.11 (α-form H-1; 1H, d, *J* = 3.6 Hz)
Malic acid	134	δ 4.44 (1H, dd, *J* = 4.2, 7.2 Hz)
Citric acid	210	δ 2.85 (1H, d, *J* = 15.6 Hz)

2.3. Short-Term and Long-Term Decoctions

Based on the selected peaks for qNMR in Table 1, we evaluated the composition differences of the target polyphenols in *G. thunbergii* obtained from extraction in both short-term and long-term decoctions. Extraction by short-term decoction showed geraniin as the predominant ellagitannin and the related polyphenols (62.0% of the total polyphenols). In contrast, corilagin (corresponding to the hydrolysate of geraniin) was a major extraction compound from long-term decoction. During short-term decoction, the amount of corilagin was only 13.2%. After long-term decoction, the amount of corilagin increased to 49.0% (Table 2). Additionally, the percentages of gallic acid, ellagic acid, and brevifolincarboxylic acid also increased. However, geraniin was not detected and no significant difference was found between the amount of kaempferitrin before and after long-term decoction. These results indicate that geraniin was hydrolyzed to corilagin, gallic acid, ellagic acid, and brevifolincarboxylic acid after 1 h of decoction.
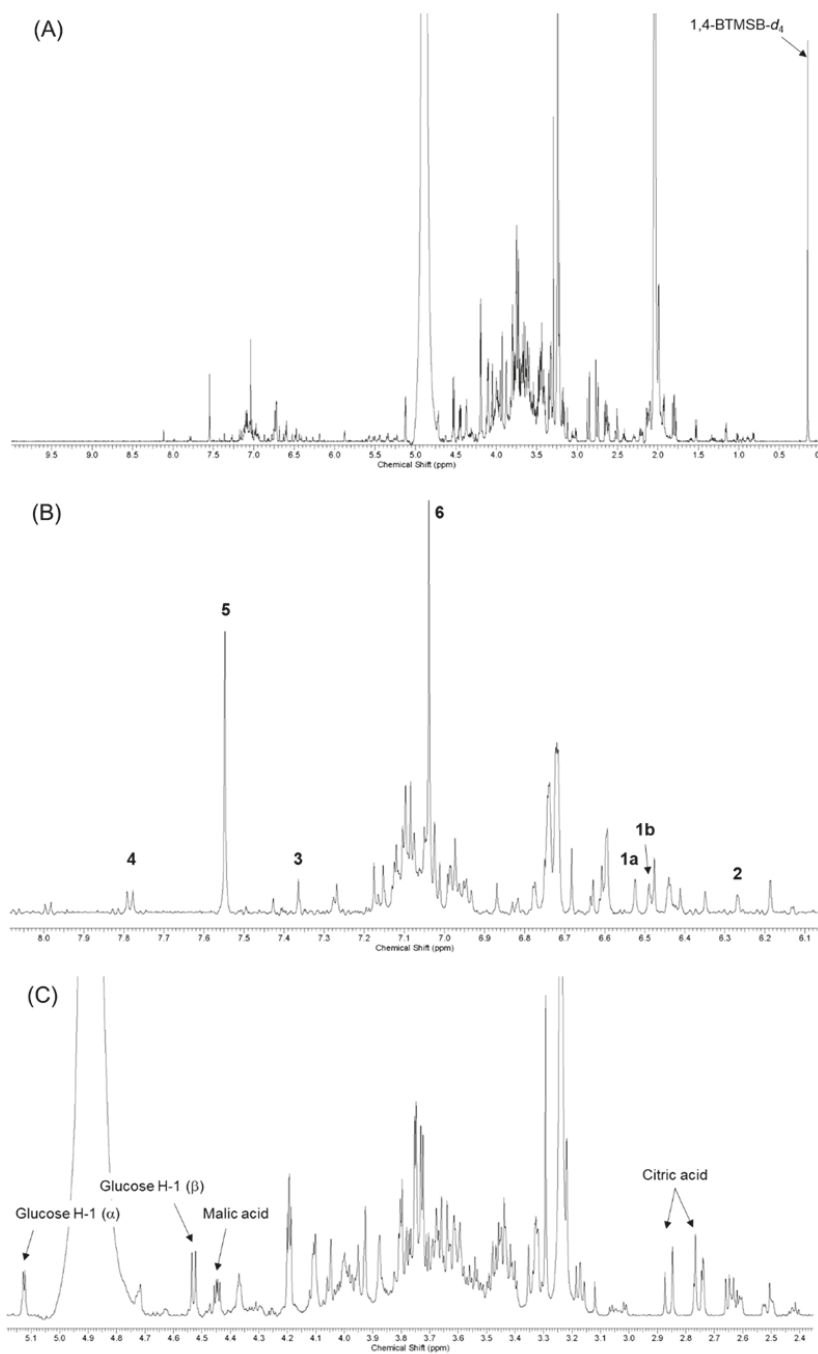
Figure 3. ^{1}H-NMR spectra {600 MHz, acetone-d_6-CF$_3$COOD-D$_2$O (70:25:5)} of the short-term decoction of *G. thunbergii*: (**A**) entire spectrum; (**B**) expansion of the low-field region; and (**C**) expansion of the high-field region.

Figure 4 presents a graph of the change in main polyphenol content during 50 min of decoction. Geraniin was found to increase until 10 min into decoction; thereafter, it decreased sharply. In contrast, the amount of corilagin increased steadily over the entire 50 min decoction [29]. The amounts of brevifolincarboxylic acid, gallic acid, and ellagic acid also increased steadily.

Table 2. % composition relative to the amount of total polyphenols in the short-term and long-term decoction extracts of *G. thunbergii*.

Main Polyphenols	Contents (%)	
	Short-Term Decoction	**Long-Term Decoction**
Geraniin (**1**)	62.0	0.0
Corilagin (**2**)	13.2	49.0
Brevifolincarboxylic acid (**3**)	5.1	13.1
Kaempferitrin (**4**)	6.0	5.4
Ellagic acid (**5**)	6.5	16.1
Gallic acid (**6**)	7.2	16.4
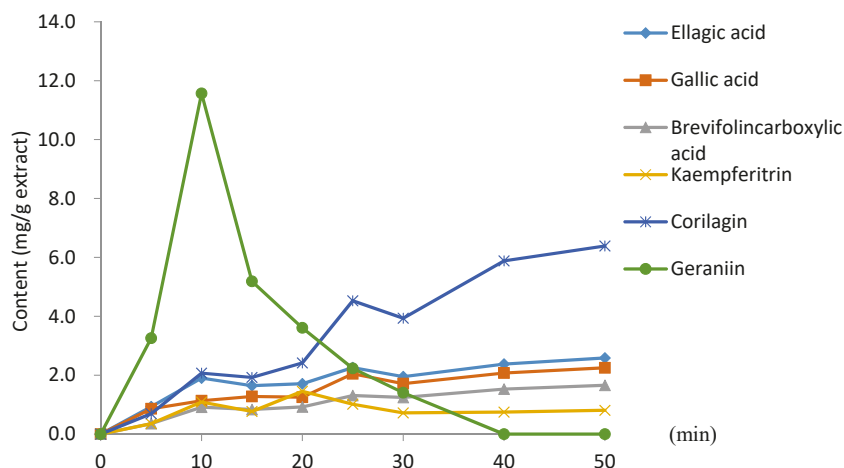
Figure 4. Change in main polyphenol content during *G. thunbergii* decoction.

2.4. The Main Polyphenol Contents in each Extract of G. thunbergii

Next, the extract obtained from long-term decoction of *G. thunbergii* was successively extracted with diethyl ether, ethyl acetate, and water-saturated *n*-butanol. The ether, ethyl acetate, *n*-butanol, and water-soluble extracts were measured for main polyphenols and organic acid content using the qNMR method. The ether extract contained gallic acid exclusively. Gallic acid was also found in the ethyl acetate extract and *n*-butanol extract. Corilagin accounted for half of the extracts in ethyl acetate and *n*-butanol. (Figure 5). These data indicate that ellagitannins, such as corilagin, could be effectively extracted by ethyl acetate and *n*-butanol.
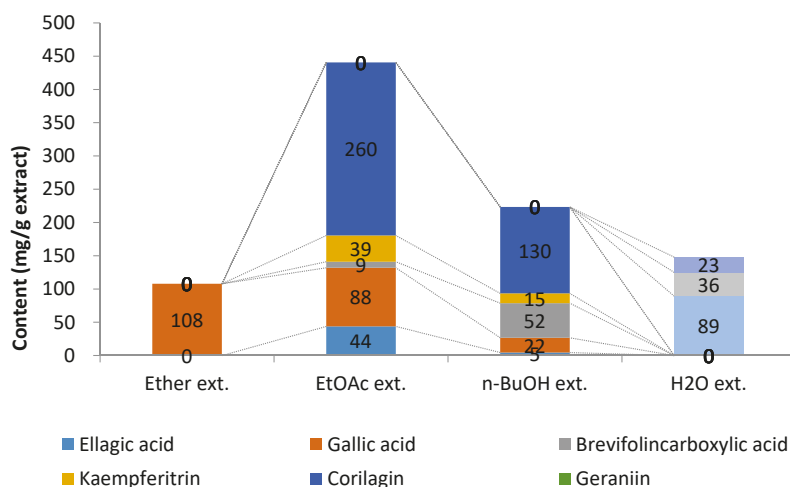
Figure 5. The main polyphenol and organic acid contents in each extract from the long-term decoction of *G. thunbergii*.

2.5. Amount of Main Polyphenols in G. thunbergii Cultivated in Japan and China

We estimated the amount of main polyphenols in *G. thunbergii* from nine cultivates in Japan and China using our qNMR method. All samples were extracted with 70% aqueous acetone. As shown in Table 3, *G. thunbergii* in Japan contained geraniin in the range of 3.49 to 7.41 mg/g (average: 5.21 mg/g) whereas geraniin content in *G. thunbergii* from Zhejiang province in China was in the range of 0.44 to 2.82 mg/g (average: 1.61 mg/g). The amounts of corilagin, gallic acid, ellagic acid, and brevifolincarboxylic acid were very similar between the Japanese and Zhejiang cultivates. However, kaempferitrin was found in the Japan cultivates in the range of 0.13 to 0.56 mg/g (average: 0.2 mg/g) while the three cultivates from Zhejiang did not contain kaempferitrin.

Table 3. The amounts of main polyphenols in *G. thunbergii* cultivated in Japan and China (mg/g dried weight).

Polyphenols	Japan						China		
	Fukushima	Nagano 1	Nagano 2	Nagano 3	Hyogo	Miyazaki	Zhejiang 1	Zhejiang 2	Zhejiang 3
Geraniin (**1**)	3.49	4.15	4.23	3.57	8.65	7.14	2.82	1.57	0.44
Corilagin (**2**)	0.65	0.43	0.61	0.23	0.53	0.43	0.49	0.23	0.17
Brevifolincarboxylic acid (**3**)	0.17	0.14	0.25	0.07	0.22	0.09	0.12	0.06	0.05
Kaempferitrin (**4**)	0.13	0.25	0.56	0.12	0.36	0.35	0.00	0.00	0.00
Ellagic acid (**5**)	0.33	0.37	0.41	0.23	0.47	0.30	0.28	0.13	0.12
Gallic acid (**6**)	0.21	0.23	0.31	0.21	0.23	0.03	0.14	0.08	0.09

3. Discussion

We developed ^{1}H-NMR fingerprints for quantifying ellagitannins, especially in *G. thunbergii* extract. Several specific proton signals from these ellagitannins were identified for geraniin, corilagin, corilagin, ellagic acid, brevifolincarboxylic acid, and organic acids, such as malic acid and citric acid. Table 1 and Figure 3 show the chemical shift used for further quantifying the *G. thunbergii* extracts in this study.

Furthermore, we evaluated the quantification of polyphenols using our qNMR assay in short-term and long-term decoctions of *G. thunbergii*. Geraniin was the major compound (62.0%) in the short-term decoction extract and corilagin was the major compound (49.0%) from the long-term decoction extract

(Table 2). The amount of geraniin reached a maximum after 10 min of extraction. Geraniin was not observed by 40 min thereafter due to hydrolysis. Instead, corilagin became the dominant compound.

In Japan, there are two methods of using *G. thunbergii* as a folk medicine. The short and long decoctions are used for treating constipation and diarrhea, respectively. Our findings suggested that both geraniin and corilagin possess the ability to treat gastrointestinal diseases, but that they may show distinct functions. It might be speculated that geraniin has an ability to treat constipation while corilagin plays a key role in diarrhea treatment.

Fractionation of the long-term decoction showed that corilagin was obtained in the ethyl acetate and *n*-butanol fractions. Based on our qNMR method, corilagin was the major compound in both fractions, obtained at 59% and 58% in ethyl acetate and *n*-butanol, respectively. Among the solvents tested (diethyl ether, ethyl acetate, *n*-butanol, and water), ethyl acetate and *n*-butanol were found suitable for extraction of the main ellagitannin. In addition, our data indicated that only gallic acid could be extracted by diethyl ether. Malic acid, citric acid, and glucose were all obtained in the water-soluble portion (Figure 5).

The main ellagitannin contents of *G. thunbergii* extracts from plants cultivated in Japan and Zhejiang province in China are presented in Table 3. We found that the *G. thunbergii* cultivates from Japan contained higher levels of geraniin and corilagin than those from Zhejiang. Overall, the polyphenol content of cultivates from Japan were higher than those from Zhejiang. Furthermore, the six cultivates of *G. thunbergii* from Japan contained kaempferitrin, whereas the three cultivates from Zhejiang did not contain kaempferitrin. Differences in the content of these polyphenols in *G. thunbergii* may be affected by soil and weather conditions.

All samples were directly quantified using qNMR after the extracting solvents were removed. The advantages of qNMR include: accuracy, simplicity, and speediness. This is because the initial separation of target analytes into pure compounds is unnecessary. Therefore, further research should be undertaken to investigate other specific chemical shifts from other ellagitannins to enrich the number of unique qNMR ellagitannin identifier peaks.

4. Materials and Methods

4.1. Plant Material

Japanese pharmacopoeia standard products *G. thunbergii* (*gennoshoko*) cultivated in Japan and China were purchased from Japanese companies, Kokumin, Konishi, Kojuma, Daiko, Eidai, Matsuura, Japan Health, and Uchida.

4.2. HPLC Analysis

The normal phase HPLC system consisted of a pump (Jasco PU-980), UV-Vis detector (Shimadzu SPD-6A, Kyoto, Japan), and a column (YMC-Pack SIL A-003, 4.6 mm I.D × 250 mm). The mobile phase consisted of oxalic acid (450 mg/L) in *n*-hexane:methanol:tetrahydrofuran:formic acid (55:33:11:1, $v/v/v/v$, respectively). The extract (5 μL) was injected into the HPLC and delivered at a flow rate of 1.5 mL/min. The detection wavelength was set to 280 nm. The reversed phase HPLC system consisted of pump (Hitachi L-2130, Tokyo, Japan) equipped with a diode array detector (Hitachi L-7455). The separation employed an Intersustain C18 column (GL Science, 5μm, 4.6 mm I.D. × 150 mm) at 40 °C. The mobile phase consisted of eluent A (H_2O:acetonitrile:formic acid, 90:5:5 $v/v/v$) and eluent B (H_2O:acetonitrile:formic acid, 50:45:5, $v/v/v$). The eluent was programmed as follows: 0 min 0% B; 30 min. 100% B; 30.1–45 min 0% B. The flow rate of the mobile phase was set at 1.0 mL/min.

4.3. NMR Spectroscopy

All NMR analyses were carried out on a Varian NMR System 600PS (Palo Alto, CA, USA) operating at 600 MHz for ^{1}H-NMR. The measurement parameters were as follows: pulse flip angle,

90°; number of acquisitions, 8; acquisition time, 4 s; number of points, 48,077; delay time, 60 s; spin, off; temperature, room temperature.

4.4. qNMR Analysis

70% aqueous acetone extracts of the short-term and long-term decoction (20 mg) of *G. thunbergii* were dissolved in acetone-d_6:D$_2$O:CF$_3$COOD (70:25:5, $v/v/v$) (1 mL) + 1,4-BTMSB-d_4 (0.1 mg) (Fujifilm, Wako Pure Chemical Corporation, Tokyo, Japan). 1,4-BTMSB-d_4 (99.9% purity) was used as an internal standard. Sample quantification was performed according to Equation (1):

$$P_{sample} = \frac{I_{sample}/H_{sample}}{I_{1,4-BTMSB-d4}/H_{1,4-BTMSB-d4}} \times \frac{M_{sample}/W_{sample}}{M_{1,4-BTMSB-d4}/W_{1,4-BTMSB-d4}} \times P_{1,4-BTMSB-d4} \tag{1}$$

where: P_{sample} = purity of desired compound; $P_{1,4\text{-}BTMSB\text{-}d4}$ = 99.9%; I_{sample} = area measured by integration of the desired compound on the ^{1}H-NMR spectrum; $I_{1,4\text{-}BTMSB\text{-}d4}$ = 100; H_{sample} = number of hydrogen(s) of the desired signal of compound; $H_{1,4\text{-}BTMSB\text{-}d4}$ = 18; M_{sample} = molar mass of the desired compound; $M_{1,4\text{-}BTMSB\text{-}d4}$ = 226.5; W_{sample} = weight of sample (20 mg); $W_{1,4\text{-}BTMSB\text{-}d4}$ = 0.1 mg. To determine the weight of the compound ($m_{compound}$) in the sample, an absolute equation was used (Equation (2)):

$$m_{compound} = \frac{P_{sample}}{P_{1,4-BTMSB-d4}} \times W_{sample} \tag{2}$$

4.5. Short-Term and Long-Term Decoction

The short-term decoction was performed by brewing 10 g of dried *G. thunbergii* in 600 mL of boiling water for 1 min. The mixture was then filtered and the obtained liquid was concentrated to dryness on a rotary evaporator to obtain 2.2 g of dried filtrate. The long-term decoction was performed by boiling 10 g of dried *G. thunbergii* in 600 mL water until the water was reduced to 300 mL. After filtration, the filtrate was dried on a rotary evaporator to obtain 0.34 g of extract. These methods imitated the traditional Japanese methods used to treat gastrointestinal diseases with *G. thunbergii*.

The long-term decoction fractionation was carried out by extracting 2.2 g of the dried extract sequentially using diethyl ether, ethyl acetate, *n*-butanol, and water (250 mL for each solvent). The extracts obtained from each solvent were: diethyl ether, 44.6 mg; ethyl acetate, 173.1 mg; *n*-butanol, 269.1 mg; and water 1.72 g.

5. Conclusions

Our data indicated that the qNMR method can be used to perform accurate, simple, and rapid analysis of target analyte content without the need for intricate separation steps or authentic materials for calibration. qNMR is a powerful tool for quantification of ellagitannins that have an anomeric center or can equilibrate in solution. Therefore, extensive research on various ellagitannins in medicinal plants and food sources is necessary to enrich the qNMR database of unique marker signals for ellagitannin quantification.

Author Contributions: H.I. conceived and designed the experiments; F.B., Y.I, N.G., and E.O. extracted of *G. thunbergii* and performed HPLC analyses and the qNMR experiments; H.I. and T.H. contributed reagents, materials, analysis tools; F.B. wrote the paper.

Conflicts of Interest: The authors declare no conflicts of interest.

References

1. Weber, M.; Hellriegel, C.; Rueck, A.; Wuethrich, J.; Jenks, P. Using high-performance ^{1}H-NMR (HP-qNMR$^®$) for the certification of organic reference materials under accreditation guidelines—Describing the overall process with focus on homogeneity and stability assessment. *J. Pharm. Biomed. Anal.* **2014**, *93*, 102–110. [CrossRef] [PubMed]

2. Rituerto, E.L.; Cabredo, S.; Lopez, M.; Avenoza, A.; Busto, J.H.; Peregrina, J.M. A thorough study on the use of quantitative ^{1}H-NMR in rioja red wine fermentation processes. *J. Agric. Food Chem.* **2009**, *57*, 2112–2118. [CrossRef] [PubMed]

3. Napolitano, J.G.; Godecke, T.; Lankin, D.C.; Jaki, B.U.; McAlpine, J.B.; Chen, S.N.; Pauli, G.F. Orthogonal analytical methods for bionical standardization: Determination of green tea catechins by qNMR and LC-MS/MS. *J. Pharm. Biomed. Anal.* **2014**, *93*, 59–67. [CrossRef] [PubMed]

4. Jungnickel, L.; Forbes, J.W. Quantitative measurement of hydrogen types by integrated nuclear magnetic resonance intensities. *Anal. Chem.* **1963**, *35*, 938–942. [CrossRef]

5. Pauli, G.F.; Jaki, B.U.; Lankin, D.C. Quantitative ^{1}H-NMR: Development and potential of a method for natural product analysis. *J. Nat. Prod.* **2005**, *68*, 133–149. [CrossRef] [PubMed]

6. Pauli, G.F.; Godecke, T.; Jaki, B.U.; Lankin, D.C. Quantitative ^{1}H-NMR. Development and potential of an analytical method: An update. *J. Nat. Prod.* **2012**, *75*, 834–851. [CrossRef] [PubMed]

7. Malz, F.; Jancke, H. Validation of quantitative NMR. *J. Pharm. Biomed. Anal.* **2005**, *38*, 813–823. [CrossRef] [PubMed]

8. Godecke, T.; Yao, P.; Napolitano, J.G.; Nicolic, D.; Dietz, B.M.; Bolton, J.L.; Breemen, R.B.; Farnsworth, N.R.; Chen, S.N.; Lankin, D.C.; et al. Integrated standardization concept for Angelica botanicals using quantitative NMR. *Fitoterapia* **2012**, *83*, 18–32. [CrossRef] [PubMed]

9. Tanaka, R.; Shibata, H.; Sugimoto, N.; Akiyama, H.; Nagatsu, A. Appication of a quantitative ^{1}H-NMR method for determination of paenol in moutan cortex, Hachimijiogan and Keishibukuryogan. *Nat. Med.* **2016**, *70*, 797–802. [CrossRef] [PubMed]

10. Hou, Z.; Liang, X.; Du, L.; Su, F.; Su, W. Quantitative determination and validation of avermectin B1a in commercial products using quantitative nuclear magnetic resonance spectroscopy. *Magn. Reson. Chem.* **2014**, *52*, 480–485. [CrossRef] [PubMed]

11. Ito, H.; Li, P.; Koreishi, M.; Nagatomo, A.; Nishida, N.; Yoshida, T. Ellagitannin oligomers and a neolignan from pomegranate arils and their inhibitory effects on the formation of advanced glycation end products. *Food Chem.* **2014**, *152*, 323–330. [CrossRef] [PubMed]

12. Ismail, T.; Sestili, P.; Akhtar, S. Pomegranate peel and fruit extracts: A review of potential anti-inflammatory and anti-infective effects. *J. Ethnopharm.* **2012**, *143*, 397–405. [CrossRef] [PubMed]

13. Piwowarski, J.P.; Granica, S.; Zwierzynska, M.; Stefanska, J.; Schopohl, P.; Melzig, M.F.; Kiss, A.K. Role of human gut microbiota metabolism in the anti-inflammatory effect of traditionally used ellagitannin-rich plant materials. *J. Ethnopharm.* **2014**, *155*, 801–809. [CrossRef] [PubMed]

14. Kashchenko, N.I.; Chirikova, N.K.; Olennikov, D.N. Agrimoniin, an active ellagitannin from *Comarum palustre* Herb with anti-α-glucosidase and antidiabetic potential in streptozotocin-induced diabetic rats. *Molecules* **2017**, *22*, 73. [CrossRef] [PubMed]

15. Valdes, J.A.; Burboa, E.; Carbo, A.F.A.; Aparicio, M.; Schmidt, R.P.; Rodriguez, R.; Aguilar, C.V. Antifungal ellagitannin isolated from *Euphorbia antisyphilitica* Zucc. *Asian Pac. J. Trop. Biomed.* **2013**, *3*, 41–46. [CrossRef]

16. Kaneshima, T.; Myoda, T.; Nakata, M.; Fujimori, T.; Toeda, K.; Nishizawa, M. Antioxidant activity of *C*-Glycosidic ellagitannins from the seeds and pell of camu-camu (*Myrciaria dubia*). *LWT-Food Sci. Technol.* **2016**, *69*, 76–81. [CrossRef]

17. Kahkonen, M.; Kylli, P.; Ollilainen, V.; Salminen, J.P.; Heinonen, M. Antioxidant activity of isolated ellagitannin from red raspberries and cloudberries. *J. Agric. Food Chem.* **2012**, *60*, 1167–1174. [CrossRef] [PubMed]

18. Okuda, T.; Yoshida, T.; Hatano, T.; Ito, H. Ellagitannins renewed the concept of tannin. In *Chemistry and Biology of Ellagitannin: An Underestimated Class of Bioactive Plant Polyphenols*, 1st ed.; Quideau, S., Ed.; World Scientific: Singapore, 2009; pp. 1–54.

19. Okuda, T.; Ito, H. Tannin of constant structure in medical and food plants-hydrolyzable tannin and polyphenols related to tannins. *Molecules* **2011**, *16*, 2191–2217. [CrossRef]

20. Okuda, T.; Yoshida, T.; Hatano, T. Constituents of *Geranium thunbergii* Sieb. *et* Zucc. Part 12. Hydrated stereostructure and equilibration of geraniin. *J. Chem. Soc. Perkin Trans.* **1982**, *1*, 9–14. [CrossRef]
21. Ito, H.; Hatano, T.; Namba, O.; Shirono, T.; Okuda, T.; Yoshida, T. Constituents of *Geranium thunbergii* SIEB. et ZUCC. XVI) Modified dehydroellagitannins, geraniinic Acids B and C, and phyllanthusiin F. *Chem. Pharm. Bull.* **1999**, *47*, 1148–1151. [CrossRef]
22. Graca, V.C.; Ferreira, I.C.F.R.; Santos, P.F. Phytochemical composition and biological activities of *Geranium robertianum* L.: A review. *Ind. Crops Prod.* **2016**, *87*, 363–378. [CrossRef]
23. Fischer, U.A.; Carle, R.; Kammerer, D.R. Identification and quantification of phenolic compounds from pomegranate (*Punica granatum* L.). *Food Chem.* **2011**, *127*, 807–821. [CrossRef] [PubMed]
24. Pinto, M.S.; Lajolo, F.M.; Genovese, M.I. Bioactive compounds and quantification of total ellagic acid in strawberries (*Fragaria x ananasa* Duch.). *Food Chem.* **2008**, *107*, 1629–1635. [CrossRef]
25. Moilanen, J.; Koskinen, P.; Salminen, J.P. Distribution and content of ellagitannin in Finnish plant species. *Phytochemistry* **2015**, *116*, 188–197. [CrossRef] [PubMed]
26. Baert, N.; Karonen, M.; Salminen, J.P. Isolation, characterization and quantification of the main oligomeric macrocyclic ellagitannin in *Epilobium angustifolium* by ultra-high performance chromatography with diode array detection and electrospray tandem mass spectrometry. *J. Chromatogr. A* **2015**, *1419*, 26–36. [CrossRef] [PubMed]
27. Hatano, T.; Yoshida, T.; Okuda, T. Chromatography of tannins, III. Multiple peaks in high-performance liquid chromatography of some hydrolyzable tannins. *J. Chromatogr.* **1988**, *435*, 285–295. [CrossRef]
28. Okuda, T.; Yoshida, T.; Hatano, T. New methods of analyzing tannins. *J. Nat. Prod.* **1989**, *52*, 1–31. [CrossRef]
29. Okuda, T.; Mori, K.; Ishino, M. Constituents of *Geranium thunbergii* SIEB. et ZACC. VIII. Transformation of geraniin upon decoction. *Yakugaku Zasshi* **1979**, *99*, 505–509. [CrossRef] [PubMed]

Sample Availability: Samples of the compounds are not available from the authors.

MDPI

Article

Stability of Principal Hydrolysable Tannins from *Trapa taiwanensis* Hulls

Ching-Chiung Wang [1,2], Hsyeh-Fang Chen [3], Jin-Yi Wu [3] and Lih-Geeng Chen [3,*]

[1] School of Pharmacy, College of Pharmacy, Taipei Medical University, Taipei 11031, Taiwan; crystal@tmu.edu.tw

[2] Traditional Herbal Medicine Research Center, Taipei Medical University Hospital, Taipei 11031, Taiwan

[3] Department of Microbiology, Immunology and Biopharmaceuticals, College of Life Sciences, National Chiayi University, Chiayi 60004, Taiwan; snowfang@ccpc.com.tw (H.-F.C.); jywu@mail.ncyu.edu.tw (J.-Y.W.)

* Correspondence: lgchen@mail.ncyu.edu.tw; Tel.: +886-5-2717798

check for updates

Abstract: The fruit and hulls of the water caltrop (*Trapa taiwanensis* Nakai) are used as hepatoprotective herbal tea ingredients in Taiwan. The stability of hydrolysable tannins in herbal drinks has rarely been reported. In the present study, two hydrolysable tannins, tellimagrandin II (TGII) and 1,2,3,4,6-pentagalloylglucopyranose (PGG), were isolated from water caltrop hulls. The stability of the two compounds was evaluated by treatment with various pH buffer solutions, simulated gastric fluid and intestinal fluid, different temperatures, and photo-irradiation at 352 nm in different solvents. Results showed that TGII and PGG were more stable in a pH 2.0 buffer solution (with 91.88% remaining) and in a water solution with 352 nm irradiation (with 95% remaining). TGII and PGG were more stable in methanol or ethanol solutions (with >93.69% remaining) than in an aqueous solution (with <43.52% remaining) at 100 °C. In simulated gastric fluid, more than 96% of the hydrolysable tannins remained after incubation at 37 °C for 4 h. However, these hydrolysable tannins were unstable in simulated intestinal fluid, as after incubation at 37 °C for 9 h, the content of TGII had decreased to 31.40% and of PGG to 12.46%. The synthetic antioxidants, butyl hydroxy anisole (BHA), di-butyl hydroxy toluene (BHT), and propyl gallate, did not exhibit photoprotective effects on these hydrolysable tannins. However, catechin, a natural antioxidant, displayed a weak photoprotective effect. Ascorbic acid had a short-term thermal-protective effect but not a long-term protective effect. The different stability properties of hydrolysable tannins in solutions can be used in the development of related herbal teas in the future.

Keywords: *Trapa taiwanensis* Nakai; hydrolysable tannin; stability; gallotannin; ellagitannin

1. Introduction

Tannins belong to water-soluble polyphenols and are present in many vegetables and herbal teas [1]. They can be classified into hydrolysable, condensed, and complex tannins [1]. Recently, herbal teas with several health benefits, such as antioxidative, hepatoprotective, and hypolipidemic activities, have become popular in Taiwan [2]. Catechins, hydrolysable tannins, flavonoids, anthocyanins, and chlorogenic acid derivatives are the major active ingredients in herbal teas. For convenience, bottled herbal tea drinks are popular and are being produced worldwide. The contents of bioactive polyphenols influence the shelf-life of drinks. However, the stability of these polyphenols in aqueous solution has rarely been reported [3,4].

Water caltrop (*Trapa taiwanensis* Nakai, Trapaceae), a floating plant that grows in shallow water, is widely used in folk medicine for treating diarrhea and dysentery. Hot water decoctions of water caltrop fruit or hulls are used as herbal drinks with hepatoprotective effect in Taiwan [5]. Tea bags

containing water caltrop hulls are also commercially available in Taiwan. Water caltrop was reported to have hepatoprotective, antioxidative, antibacterial, anti-inflammatory, hypoglycemic, and other healthy functions [5–22]. Hydrolysable tannins are regarded as the active compounds in water caltrop hulls [5,8,11,21,22]. Hulls of *T. taiwanensis* have the potential to be developed as herbal tea drink ingredients.

In the present study, we isolated two major hydrolysable tannins components, tellimagrandin II (TGII) and 1,2,3,4,6-pentagalloylglucopyranose (PGG) from water caltrop hulls, which are respectively classified as ellagitannin and gallotannin. These two hydrolysable tannins were subjected to different pH solutions, simulated gastric and intestinal fluids, different temperatures, and photo-irradiation, and the protective effects of antioxidants were evaluated to determine the stabilities of these two hydrolysable tannins in aqueous solutions.

2. Results

2.1. Isolation of Hydrolysable Tannins from T. taiwanensis Hulls

Two major hydrolysable tannins, TGII and PGG, were isolated from the ethyl acetate (EtOAc) fraction of T. taiwanensis hulls, and their structures are shown in Figure 1 (Figure S1). Both compounds have a galloyl ester linkage with glucose. We used the two compounds to estimate their stability in different pH solutions, in simulated gastric fluid and intestinal fluid, and when subjected to various light and thermal conditions.
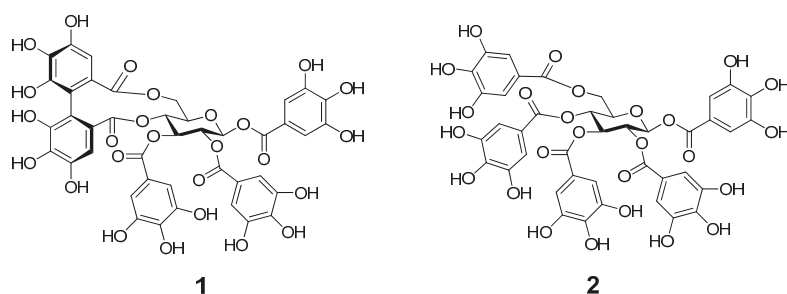
Figure 1. Two hydrolysable tannins, tellimagrandin II (TGII, **1**) and 1,2,3,4,6-pentagalloylglucopyranose (PGG, **2**), isolated from *Trapa taiwanensis* hulls.

2.2. The Stability of Hydrlysable Tannins in Different pH Solutions

TGII and PGG were dissolved in pH 0.1 M buffer solutions to give a final concentration of 1.0 mg/mL and incubated in a dry bath for 24 h. Results are shown in Figure 2 (Table S1). These hydrolysable tannins were more stable in strongly acidic conditions (pH 2.0 and 4.0) than in weakly acidic, neutral, and basic conditions (pH 6.0, 7.0, 8.0, and 10.0). TGII was more unstable than PGG. After 3 h of incubation in a pH 10.0 buffer solution, TGII had totally degraded, but 20% of PGG remained. TGII and PGG were more stable in a pH 2.0 buffer solution (with 91.88% remaining).

2.3. The Stability of Hydrlysable Tannins in Simulated Gastric Fluid and Intestinal Fluid

TGII and PGG were dissolved in simulated gastric fluid and intestinal fluid to a final concentration of 1.0 mg/mL and were then incubated in a dry bath for 4 and 9 h. These incubation times respectively mimicked the physiological condition of food retention times in the stomach and intestines. Results are shown in Figure 3. TGII and PGG were more stable in simulated gastric fluid (pH 1.2) than simulated intestinal fluid (pH 7.5). After 4 h of incubation in simulated gastric fluid, more than 96% of TGII and PGG remained (Figure 3A, Table S2). However, in simulated intestinal fluid TGII and PGG quickly

degraded. After 9 h of incubation in simulated intestinal fluid, only 31.40% and 12.46% of TGII and PGG remained, respectively (Figure 3B, Table S2).

(**A**) (**B**)
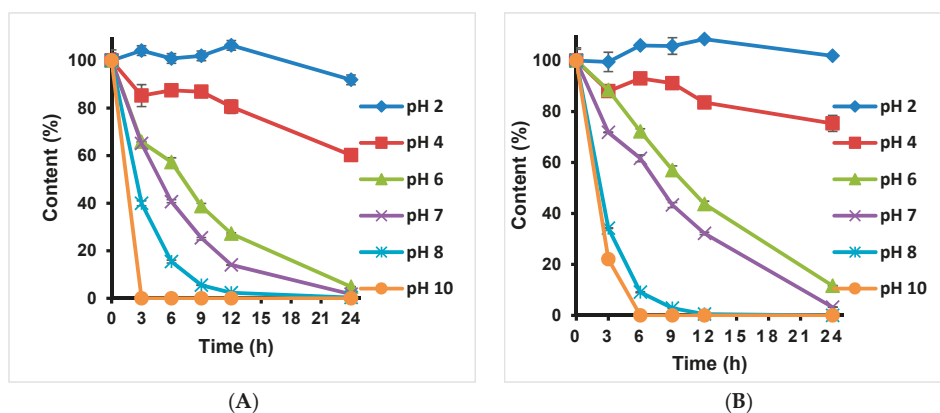
Figure 2. The pH stability test of hydrolysable tannins of TGII (**A**) and PGG (**B**), respectively. These hydrolysable tannins were treated with various pH values. $n = 3$; values are presented as the mean ± standard deviation.

(**A**) (**B**)
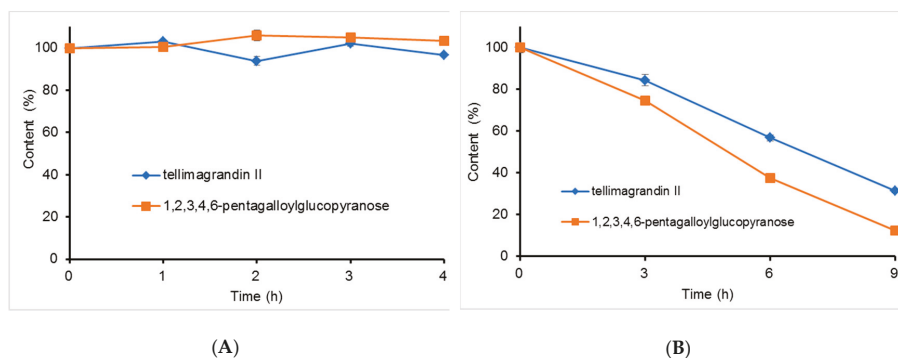
Figure 3. Simulated gastric fluid (**A**) and simulated intestinal fluid (**B**) stability tests of the hydrolysable tannins of TGII and PGG. $n = 3$; values are presented as the mean ± standard deviation.

2.4. The Photostability of Hydrlysable Tannins

TGII and PGG were dissolved in different solvents (1.0 mg/mL) and placed in a photochemical reactor for irradiation with an ultraviolent (UV) lamp at 352 nm (8 W × 16 = 128 W) for 4 h. Results are shown in Figure 4 (Table S3). These hydrolysable tannins were more stable in water (with 95% remaining) than methanol or ethanol. PGG was more stable than TGII. These hydrolysable tannins dissolved in ethanol (EtOH) were more sensitive to UV irradiation. After 4 h, 60.98% of TGII and 72.74% of PGG remained. Four antioxidants (butyl hydroxy anisole (BHA), di-butyl hydroxy toluene (BHT), propyl gallate, and catechin) were individually added to the sample solution to test their light protective effects. Only propyl gallate and catechin showed weak irradiation protective effects for PGG (Table 1).
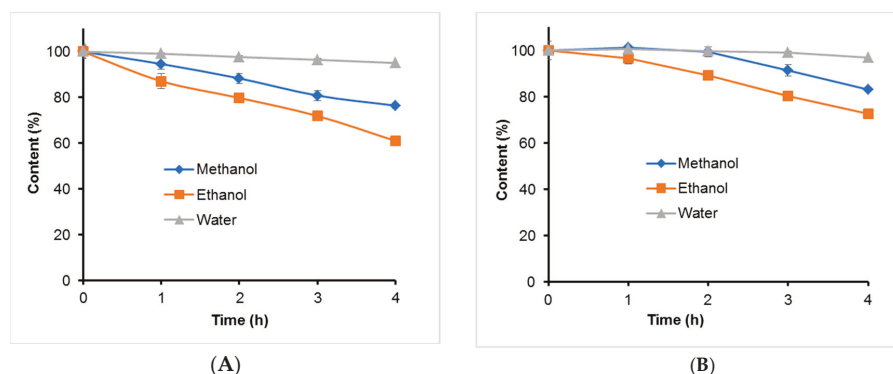
Figure 4. Photostability test of hydrolysable tannins of (**A**) TGII and (**B**) PGG. The sample solution was irradiated with an ultraviolent lamp of a photochemical reactor (8 W × 16 = 128 W) at 352 nm and a distance of about 3.2 cm for 4 h. $n = 3$; values are presented as the mean ± standard deviation.

Table 1. Protective effects of various antioxidants against irradiation with UV light at 352 nm.

Irradiation time (h)	Content (%)	
	0	**4**
TGII	100.00 ± 0.08	66.02 ± 1.60
TGII + BHA	100.00 ± 0.11	63.27 ± 0.37
TGII + BHT	100.00 ± 0.19	64.64 ± 0.15
TGII + propyl gallate	100.00 ± 1.16	51.62 ± 0.54 **
TGII + catechin	100.00 ± 0.44	57.12 ± 0.30 **
PGG	100.00 ± 3.15	70.79 ± 2.92
PGG + BHA	100.00 ± 0.41	66.40 ± 0.91
PGG + BHT	100.00 ± 4.27	52.80 ± 1.03
PGG + propyl gallate	100.00 ± 0.08	78.91 ± 2.20 **
PGG + catechin	100.00 ± 0.28	77.43 ± 2.17 **

These hydrolysable tannins were dissolved in ethanol EtOH (1.0 mg/mL), and the final concentration of each antioxidant was 1.0 mg/mL. $n = 3$; values are represented as the mean ± standard deviation. BHA: butyl hydroxy anisole; BHT: di-butyl hydroxy toluene. ** $p < 0.01$ compared to the untreated sample.

2.5. The Thermal Stability of Hydrlysable Tannins

TGII and PGG dissolved in methanol, ethanol, or water (1.0 mg/mL) were incubated at different temperatures in a dry bath for 4 h. Results are shown in Figure 5 (Table S4). These hydrolysable tannins were more stable in the methanol or ethanol solution than in the aqueous solution at temperatures from 70 to 100 °C. When the temperature increased in the aqueous solution, the hydrolysable tannins were more unstable. PGG was more stable than TGII in the aqueous solution. TGII and PGG were more stable in the methanol and ethanol solutions (with >93.69% remaining) than in the aqueous solution (with <43.52% remaining) at 100 °C.

2.6. Protective Effect of Ascorbic Acid on Thermal Stability

Different concentrations of ascorbic acid (0~1000 µg/mL) were added to the sample solution to evaluate the protective effect on hydrolysable tannins in 100 °C aqueous solutions. Ascorbic acid protected TGII and PGG from thermal degradation (Figure 6, Table S5). When a high concentration of ascorbic acid (1 mg/mL) was added to a TGII solution and incubated at 100 °C for 4 h, the content increased from 51.28% (without ascorbic acid) to 85.55%. However, when a high concentration of ascorbic acid (1 mg/mL) was added to a PGG solution and incubated at 100 °C for 4 h, the content moderately increased from 54.29% (without ascorbic acid) to 65.95%. Long-term storage with ascorbic

acid was evaluated at different temperatures (4 °C and 25 °C) for 4 weeks. Results are shown in Table 2. When aqueous solutions of hydrolysable tannins were stored at 4 °C for 4 weeks, the contents of TGII and PGG moderately decreased. However, when stored at 25 °C, contents of TGII and PGG significantly decreased.
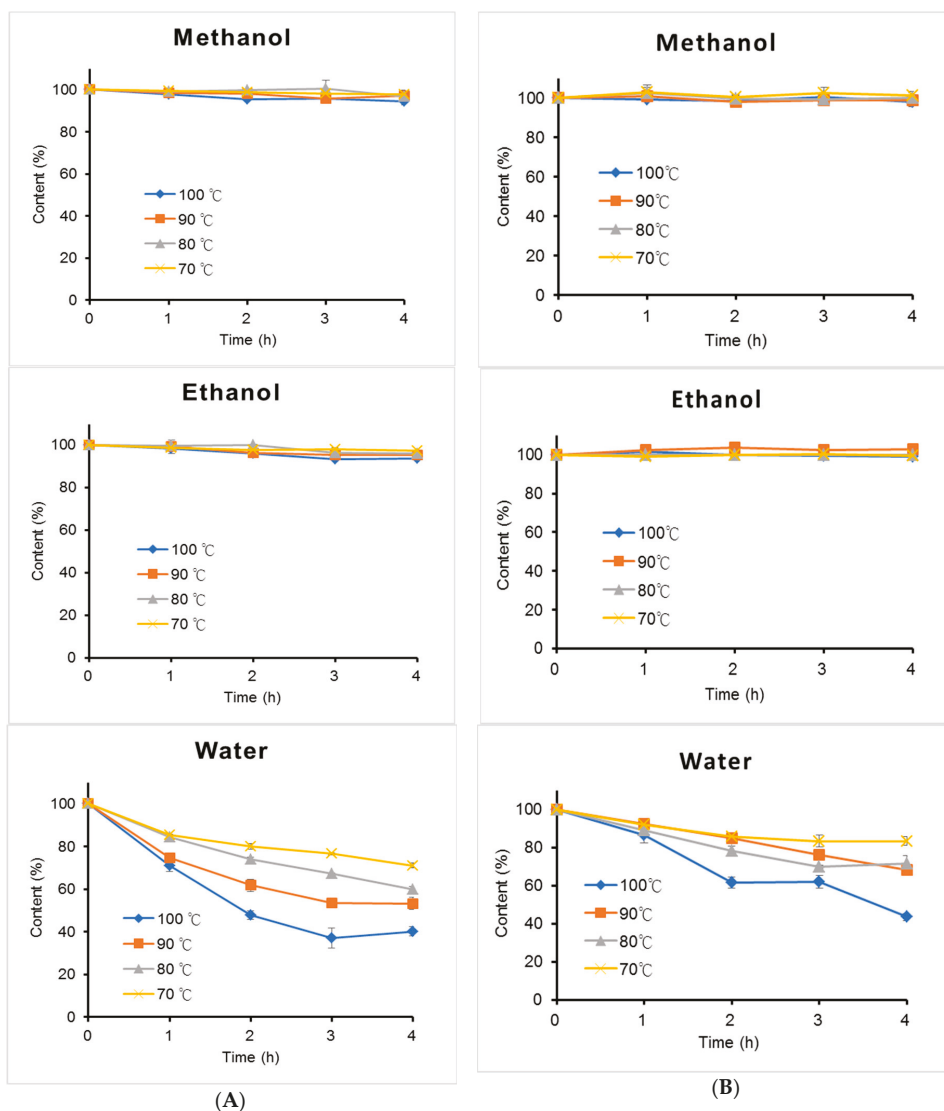
Figure 5. Thermal stability test of hydrolysable tannins of (**A**) TGII and (**B**) PGG in methanol, ethanol, and water solutions. Sample solutions were placed in a dry bath at 70, 80, 90, and 100 °C for 4 h. *n* = 3; values are presented as the mean ± standard deviation.
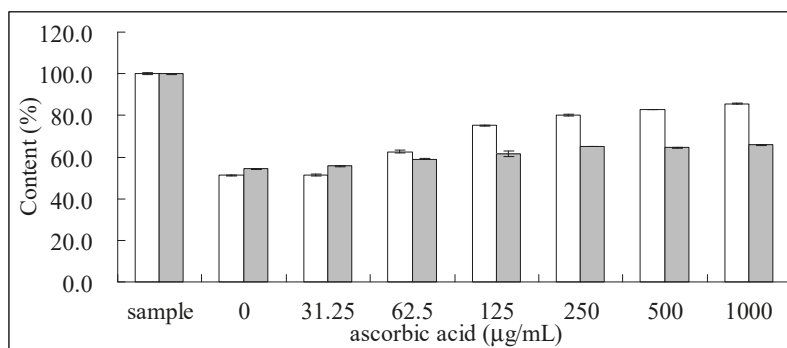
Figure 6. Protective effects of different concentrations of ascorbic acid on TGII (□) and PGG (■) in a dry bath at 100 °C for 4 h. *n* = 3; values are presented as the mean ± standard deviation.

Table 2. Protective effects of ascorbic acid on TGII and PGG during storage at 4 and 25 °C.

	TGII Content (%) [1]			
Ascorbic Acid (mg/mL)	4 °C		25 °C	
	0	1.0	0	1.0
Time (week)				
0	100.00 ± 1.02	100.00 ± 0.26	100.00 ± 1.02	100.26 ± 0.26
1	101.15 ± 0.35	98.31 ± 0.19	85.24 ± 0.69	83.75 ± 0.73
2	100.05 ± 0.80	95.78 ± 0.50	77.37 ± 1.57	75.56 ± 0.66
3	97.07 ± 0.71	92.88 ± 0.13	71.86 ± 0.84	68.18 ± 0.91
4	96.41 ± 1.51	90.92 ± 0.47	74.29 ± 0.60	52.54 ± 0.49
	PGG Content (%) [1]			
Ascorbic Acid (mg/mL)	4 °C		25 °C	
	0	1.0	0	1.0
Time (week)				
0	100.00 ± 0.66	100.00 ± 0.25	100.00 ± 0.66	100.00 ± 0.25
1	100.30 ± 0.50	97.83 ± 0.06	95.89 ± 1.42	73.76 ± 0.31
2	100.13 ± 0.57	92.93 ± 0.81	93.47 ± 0.85	73.23 ± 0.47
3	100.35 ± 0.74	91.89 ± 0.74	86.82 ± 0.69	44.57 ± 0.11
4	104.18 ± 1.37	97.50 ± 0.43	91.82 ± 15.1	58.05 ± 0.47

[1] These hydrolysable tannins were dissolved in an aqueous solution (1.0 mg/mL). *n* = 3; values are presented as the mean ± standard deviation.

3. Discussion

The structures of hydrolysable tannins contain several ester linkages which are easily cleaved when in a basic solution or at higher temperatures. In the present study, we found two types of hydrolysable tannins that were more resistant in an acidic solution than a basic solution. Gallotannins are more stable than ellagitannins in acidic or basic solutions. Tuominen and Sundman reported that hydrolysable tannins were unstable in a basic condition, and the degradation products were formed by hydrolysis, deprotonation, and oxidation [4]. Ellagic acid can also be formed by gallotannins in a basic condition [4]. Ellagitannin metabolites, urolithins, with potent antioxidative activities, were found in plasma after the oral administration of geraniin and other ellagitannin-rich plant leaves to animals [1]. Urolithin B was more stable than urolithin A and ellagic acid in simulated gastrointestinal fluid and fecal fermentation [3]. Ellagitannins are hydrolyzed to produce ellagic acid in the small intestine, and then ellagic acid is metabolized to urolithins by intestinal bacterial fermentation.

Beverages and bottled herbal tea drinks are becoming more popular worldwide. Such drinks are stored in transparent plastic bottles and sold in convenience stores. People do not need to waste time preparing herbal decoctions themselves. However, herbal teas in a liquid state are more unstable than in tea bags or as a powder. UV radiation can be classified into UVA (320~400 nm), UVB (280~320 nm), and UVC (100~280 nm) according to different wavelengths [23]. UVA can be divided into UVA-1 (340~400 nm) and UVA-2 (320~340 nm). The ability of UVA-1 to penetrate is stronger than that of UVB or UVC. In the present study, a 352-nm UV lamp belonging to UVA-1 region was used to study the photoprotective effect of antioxidants [23]. UV can generate radicals which degrade hydrolysable tannins. The synthetic antioxidants, BHA, BHT, and propyl gallate, have free radical-scavenging effects which can protect compounds from oxidation and are widely used in processed food products. However, as shown in Table 1, BHA, BHT, and propyl gallate did not exert photoprotective effects on hydrolysable tannins. But catechin, a natural antioxidant, displayed a weak photoprotective for PGG but not TGII. Therefore, UV irradiation may cause cleavage of chemical bonds of hydrolysable tannins which cannot be prevented by antioxidants.

Ascorbic acid was used in the aqueous solution as an antioxidant. In Figure 6, the short-term thermal protective effect of ascorbic acid was significant for both hydrolysable tannins. However, in Figure 2, the long-term protective effect of ascorbic acid was not significant. The ascorbic acid concentrations that remained in the two temperature conditions (data not shown) significantly differed. Ascorbic acid in the 4 °C solution was higher than that in the 25 °C solution. After 4 weeks of storage at 4 and 25 °C, ascorbic acid concentrations in the two solutions were 866~815 and 28~24 µg/mL, respectively. It was interesting that ascorbic acid was exhausted at the high temperature and enhanced degradation of the hydrolysable tannins (Table 2). The reason may have been oxidative stress produced by the oxidized ascorbic acid. These results indicated that adding ascorbic acid to hydrolysable tannin-rich herbal teas to prevent oxidation is not effective. Adjusting the pH to be mildly acidic, protecting hydrolysable tannin-rich herbal teas from light, and storing them at 4 °C can improve their shelf life. The different stability properties of TGII and PGG can be used for developing related herbal drinks in the future.

4. Materials and Methods

4.1. General

^{1}H (500 MHz) and ^{13}C nuclear magnetic resonance (NMR) (125 MHz) spectra were measured on a Bruker Avance DRX 500 instrument (Bruker, Billerica, MA, USA). The chemical shifts were calibrated by the actone-d_6 solvent signal and are given in δ (ppm) values. Acetonitrile, L-ascorbic acid, sodium carbonate, sodium chloride, and sodium hydroxide were purchased from J.T. Baker (Phillipsburg, NJ, USA). (+)-Catechin, butyl hydroxy anisole (BHA), di-butyl hydroxy toluene (BHT), boric acid, hydrochloric acid, potassium chloride, potassium biphthalate, pancreatin from porcine pancreas, and pepsin were purchased from Sigma-Aldrich (St. Louis, MO, USA). *n*-Propyl 3,4,5-trihydroxybenzoate (propyl gallate) and trifluoroacetic acid (TFA) were purchased from Alfa Aesar (Tewksbury, MA, USA). Ultrapurified water (>18 mΩ·cm) was produced by EASYpure LF (Barnstead, Dubuque, IA, USA). Column chromatography was carried out on Diaion HP-20 gel (Mitsubishi Chemical Industry, Tokyo, Japan) and LiChroprep RP-18 gel (40~63 µm, Merck, Darmstadt, Germany).

4.2. Plant Material

The fruit of *T. taiwanensis* was purchased in December 2006 at Guantian, Tainan. Hulls of *T. taiwanensis* were separated and air blow-dried below 40 °C. A voucher specimen was deposited in the Department of Microbiology, Immunology and Biopharmaceuticals, College of Life Sciences, National Chiayi University (Chiayi, Taiwan).

4.3. Isolation of Hydrolysable Tannins from T. taiwanensis Hulls

Dried hulls of *T. taiwanensis* (2.0 kg) were pulverized and macerated with methanol (20 L × 5) at room temperature. After being concentrated, the methanol extract (318 g) was dissolved in water and extracted with EtOAc. The EtOAc layer (45 g) was used to separate TGII and PGG. The EtOAc layer was chromatographed on a Diaion HP-20 column (9 cm i.d. × 40 cm) sequentially eluted with H_2O (5 L), 20% MeOH (5 L), 40% MeOH (10 L), 60% MeOH (5 L), and 100% MeOH (5 L). A portion (9.2 g) of the Diaion HP-20 column 40% MeOH eluate was purified on a LiChroprep RP-18 column (2.5 cm i.d. × 50 cm) eluted with 0.05% TFA-CH_3CN (85:15) to obtain TGII (4.95 g, yield 0.25%) and PGG (2.23 g, yield 0.11%).

TGII. ^{1}H-NMR (500 MHz, acetone-d_6) δ: 7.12 (2H, s, galloyl H), 7.01 (2H, s, galloyl H), 6.97 (2H, s, galloyl H), 6.66 (1H, s), 6.48 (1H, s), 6.20 (1H, d, *J* = 8.4 Hz, Glc H-1), 5.84 (1H, t, *J* = 9.6Hz, Glc H-3), 5.60 (1H, dd, *J* = 8.4, 9.6 Hz, Glc H-2), 5.36 (1H, dd, *J* = 6.6, 13.4 Hz, Glc H-6), 5.22 (1H, t, *J* = 9.6 Hz, H-4), 4.55 (1H, dd, *J* = 6.2, 9.6 Hz, Glc H-5), 3.89 (1H, d, 13.4 Hz, Glc H-6). ^{13}C-NMR (125 MHz, acetone-d_6) δ: 167.3, 166.9, 165.5, 164.9, 164.2 (C=O), 145.3, 145.1, 144.9, 144.4, 144.3, 143.6, 138.9, 138.5, 138.3, 135.7, 135.5, 125.6, 125.0, 119.6, 119.5, 118.9, 114.9, 114.8, 109.4, 0.9.3, 109.2, 107.3, 107.0, 92.8 (Glc C-1), 72.4 (Glc C-3), 72.2 (Glc C-5), 71.0 (Glc C-2), 69.9 (Glc C-4), 62.2 (Glc C-6).

PGG. ^{1}H-NMR (500 MHz, acetone-d_6) δ: 7.17, 7.11, 7.05, 7.01, 6.97 (each 2H, galloyl-H), 6.33 (1H, d, *J* = 8.3 Hz, Glc H-1), 6.01 (1H, t, *J* = 9.7 Hz, Glc H-3), 5.65 (1H, t, *J* = 9.7 Hz, Glc H-4), 5.62 (1H, dd, *J* = 8.3, 9.7 Hz, Glc H-2), 4.56 (1H, m, Glc H-5), 4.53 (1H, brd, *J* = 12.0 Hz, Glc H-6), 4.40 (1H, dd, *J* = 5.0, 12.0 Hz, Glc H-6). ^{13}C-NMR (125 MHz, acetone -d_6) δ: 166.5, 166.0, 165.8, 165.7, 165.1 (C=O), 146.3, 146.1, 146.1, 146.1, 146.0 (galloyl C-3, 5), 139.9, 139.4, 139.4, 139.2, 139.1 (galloyl C-4), 121.5, 120.8, 120.7, 120.0 (galloyl C-1), 110.5, 110.4, 110.3, 110.2 (galloyl C-2, 6), 93.4 (Glc C-1), 74.0 (Glc C-3), 73.4 (Glc C-5), 71.8 (Glc C-2), 69.4 (Glc C-4), 62.9 (Glc C-6).

4.4. Stability Studies

4.4.1. Preparation of Solutions

TGII and PGG were dissolved in purified water to a final concentration of 2 mg/mL as stock solutions. The 0.2 M buffered solutions at pH 2, 4, 6, 7, 8, and 10 were prepared according USP38 [24].

4.4.2. Stability of pH

TGII and PGG stock solutions were dissolved in an equal volume of different pH aqueous buffer solutions to a final concentration of 1 mg/mL. The solution was dispensed in a 2-mL glass vial and kept in a 37 °C dry bath for 24 h. Vials were taken every 3 h and analyzed by high-performance liquid chromatography (HPLC) to calculate the content.

4.4.3. Simulated Gastric Fluid Stability

Simulated gastric fluid (pH 1.2) was prepared by dissolving 2.0 g NaCl, 3.2 g pepsin, and 7.0 mL of 37% HCl in 1 L of purified water [24]. TGII and PGG stock solutions were dissolved in an equal volume of simulated gastric fluid or simulated intestinal fluid to a final concentration of 1 mg/mL. The solution (1 mL) was dispensed in a 2-mL glass vial and kept in a 37 °C dry bath for 4 h. Vials were taken every 1 h, and 0.5 mL 0.2 N Na_2CO_3 was added to neutralize the solution. The neutralized solution was passed through a Sep-Pak® Plus C18 cartridge (55~105 µm, Waters, Milford, MA, USA) washed with 10 mL water and then eluted with 10 mL MeOH. The MeOH eluate was analyzed by HPLC to calculate the content.

4.4.4. Simulated Intestinal Fluid Stability

Simulated intestinal fluid was prepared by dissolved 6.8 g KH_2PO_4, 190 mL of a 0.2 N NaOH solution, and 10 g pancreatin in 650 mL of purified water. The pH was adjusted with 0.2 N NaOH to 7.5 ± 0.1, and water was added to a final volume of 1 L [24]. TGII and PGG stock solutions were dissolved in an equal volume of simulated intestinal fluid to a final concentration of 1 mg/mL. The solution (1 mL) was dispensed in a 2-mL glass vial and kept in a 37 °C dry bath for 9 h. Vials were taken every 3 h, and 0.5 mL of water was added. The solution was passed through a Sep-Pak Plus C18 cartridge (55~105 μm, Waters) washed with 10 mL water and then eluted with 10 mL MeOH. The MeOH eluate was analyzed by HPLC to calculate the content.

4.4.5. Photostability

The hydrolysable tannins (1 mg/mL) were dissolved in different solvents (methanol, ethanol, and water) in a quartz glass test tube (1 cm i.d.) and then treated with a 352-nm UV lamp of a photochemical reactor (8 W × 16 = 128 W) at a distance of about 3.2 cm for 4 h. An aliquot of the solution was taken every 1 h and analyzed by HPLC to calculate the content. Four antioxidants (BHA, BHT, propyl gallate, and catechin) were added to the sample solution (1 mg/mL EtOH) to test the light protective effect.

4.4.6. Temperature Stability

The hydrolysable tannins (1 mg/mL) were dissolved in different solvents (methanol, ethanol, and water) and placed in a dry bath at different temperatures (70, 80, 90, and 100 °C) for 4 h. All data were from triplicate confirmation tests. An aliquot of the solution was taken and analyzed by HPLC to calculate the content.

4.4.7. Protective Effect of Ascorbic Acid Against Thermal Degradation

Ascorbic acid (0~1000 μg/mL) was added to the sample solution to evaluate the protective effect on aqueous solutions of the hydrolysable tannins at 100 °C. Long-term storage with ascorbic acid was evaluated at different temperatures (4 and 25 °C) for 4 weeks.

4.5. HPLC analysis of TGII and PGG

HPLC equipment was composed of a Waters 1525 binary HPLC pump, an in-line degasser AF, a 2487 dual l absorbance detector, a 717 plus autosampler, and Millennium 32 vs. 3.20 software (Milford, MA, USA). The LiChrospher RP-18e column (4.0 mm i.d. × 250 mm, 5 μm, Merck) was used for the HPLC analysis. The mobile phase consisted of water with 0.05% TFA-acetonitrile (85:15). The flow rate was 1.0 mL/min, and 10 μL was injected into the column. The column temperature was maintained at 40 °C. Chromatograms were detected by absorbance at 280 nm. Three replicates were performed. The retention times for TGII and PGG were 9.91 and 11.47 min, respectively. The peak area of the compound at 0 h of treatment was regarded as a content of 100%.

4.6. Statistical Evaluation

Data are presented as mean ± standard deviation. Student's *t*-test was used to compare different contents between treated and untreated samples.

5. Conclusions

In conclusion, we investigated the stability of TGII and PGG in solutions of various conditions. Both hydrolysable tannins were quite stable in a pH 2.0 buffer solution and unstable in neutral or basic buffer solutions. In simulated gastric (pH 1.2) and intestinal fluids (pH 7.5), the two hydrolysable tannins also presented similar pH stability properties. The photostability test displayed that the two hydrolysable tannins dissolved in water were stable under UV 352 nm irradiation for 4 h but unstable in methanol and ethanol solutions. The photodegradation of PGG was slightly prevented by propyl

gallate and catechin. As to the thermal stability of the two hydrolysable tannins, the contents decreased as the storage temperature increased. Their thermal degradation at 100 °C for 4 h was prevented by ascorbic acid. At room temperature or at refrigerated conditions, adding ascorbic acid did not inhibit the degradation effect. We hope the above results are helpful for the future production of herbal tea drinks.

Supplementary Materials: The following are available online, Figure S1: The HPLC chromatograms of TGII (A) and PGG (B). Table S1: The pH stability test of hydrolysable tannins of TGII and PGG. These hydrolysable tannins were treated with various pH values. Table S2: Simulated gastric fluid and simulated intestinal fluid stability tests of the hydrolysable tannins of TGII and PGG. Table S3: Photostability test of hydrolysable tannins of TGII and PGG. Table S4: Thermal stability test of hydrolysable tannins of TGII and PGG in methanol, ethanol, and water solutions. Table S5: Protective effects of different concentrations of ascorbic acid on TGII and PGG in a dry bath at 100 °C for 4 h.

Author Contributions: Conceptualization, C.-C.W. and L.-G.C.; Data curation, H.-F.C.; Methodology, L.-G.C., H.-F.C., and J.-Y.W.; Validation, H.-F.C. and L.-G.C.; Formal analysis, H.-F.C.; Investigation, H.-F.C.; Writing-original draft preparation, C.-C.W. and L.-G.C.; Writing-review and editing, L.-G.C.; Visualization, L.-G.C.; Supervision, L.-G.C.; Project administration, L.-G.C.; Funding acquisition, L.-G.C.

Conflicts of Interest: The authors declare no conflict of interest.

References

1. Okuda, T.; Ito, H. Tannins of Constant Structure in Medicinal and Food Plants—Hydrolyzable Tannins and Polyphenols Related to Tannins. *Molecules* **2011**, *16*, 2191–2217. [CrossRef]

2. Chung, K.T.; Wong, T.Y.; Wei, C.I.; Huang, Y.W.; Lin, Y. Tannins and Human Health: A Review. *Crit. Rev. Food Sci. Nutr.* **1998**, *38*, 421–464. [CrossRef] [PubMed]

3. Mena, P.; Dall'Asta, M.; Calani, L.; Brighenti, F.; Del Rio, D. Gastrointestinal stability of urolithins: An in vitro approach. *Eur. J. Nutr.* **2017**, *56*, 99–106. [CrossRef] [PubMed]

4. Tuominen, A.; Sundman, T. Stability and oxidation products of hydrolysable tannins in basic conditions detected by HPLC/DAD-ESI/QTOF/MS. *Phytochem. Anal.* **2013**, *24*, 424–435. [CrossRef] [PubMed]

5. Wang, S.H.; Kao, M.Y.; Wu, S.C.; Lo, D.Y.; Wu, J.Y.; Chang, J.C.; Chiou, R.Y. Oral administration of *Trapa taiwanensis* Nakai fruit skin extracts conferring hepatoprotection from CCl₄-caused injury. *J. Agric. Food Chem.* **2011**, *59*, 3686–3692. [CrossRef] [PubMed]

6. Hussain, T.; Subaiea, G.M.; Hussain, T.; Firdous, H. Hepatoprotective evaluation of *Trapa natans* against drug-induced hepatotoxicity of antitubercular agents in rats. *Pharm. Mag.* **2018**, *14*, 180–185. [CrossRef] [PubMed]

7. Xia, J.; Yang, C.; Wang, Y.; Yang, Y.; Yu, J. Antioxidant and antiproliferative activities of the leaf extracts from *Trapa bispinosa* and active components. *S. Afr. J. Bot.* **2017**, *113*, 377–381. [CrossRef]

8. Lee, D.; Lee, O.H.; Choi, G.; Kim, J.D. Antioxidant and anti-adipogenic activities of *Trapa japonica* shell extract cultivated in Korea. *Prev. Nutr. Food Sci.* **2017**, *22*, 327–334. [CrossRef]

9. Kim, Y.-S.; Kim, E.-K.; Hwang, J.-W.; Seo, I.-B.; Jang, J.-H.; Son, S.; Jeong, J.-H.; Moon, S.-H.; Jeon, B.-T.; Park, P.-J. Characterization of the antioxidant fraction of *Trapa japonica* pericarp and its hepatic protective effects in vitro and in vivo. *Food Funct.* **2016**, *7*, 1689–1699. [CrossRef]

10. Yu, H.; Shen, S. Phenolic composition, antioxidant, antimicrobial and antiproliferative activities of water caltrop pericarps extract. *LWT-Food Sci. Technol.* **2015**, *61*, 238–243. [CrossRef]

11. Kim, Y.S.; Hwang, J.W.; Han, Y.K.; Kwon, H.J.; Hong, H.; Kim, E.H.; Moon, S.H.; Jeon, B.T.; Park, P.J. Antioxidant activity and protective effects of *Trapa japonica* pericarp extracts against tert-butylhydroperoxide-induced oxidative damage in Chang cells. *Food Chem. Toxicol.* **2014**, *64*, 49–56. [CrossRef] [PubMed]

12. Shindo, K.; Kuroki, E.; Toyoda, M. Antioxidative compounds contained in the seed with hard shell of *Trapa japonica* Flerov. and its herbal tea. *Nippon Kasei Gakkaishi* **2013**, *64*, 353–359.

13. Malviya, N.; Jain, S.; Jain, A.; Jain, S.; Gurjar, R. Evaluation of in vitro antioxidant potential of aqueous extract of *Trapa natans* L. fruits. *Acta Pol. Pharm.* **2010**, *67*, 391–396. [PubMed]

14. Chiang, P.-Y.; Ciou, J.-Y. Effect of pulverization on the antioxidant activity of water caltrop (*Trapa taiwanensis* Nakai) pericarps. *LWT-Food Sci. Technol.* **2009**, *43*, 361–365. [CrossRef]

15. Chiang, P.-Y.; Ciou, J.-Y.; Hsieh, L.-C. Antioxidant activity of phenolic compounds extracted from fresh and dried water caltrop pulp (*Trapa taiwanensis* Nakai). *J. Food Drug Anal.* **2008**, *16*, 66–73.

16. Ciou, J.Y.; Wang, C.R.; Chen, J.C.; Chiang, P.Y. Total Phenolics content and antioxidant activity of extracts from dried water caltrop (*Trapa Taiwanensis* Nakai) hulls. *J. Food Drug Anal.* **2008**, *16*, 41–47.

17. Radojevic, I.D.; Vasic, S.M.; Dekic, M.S.; Radulovic, N.S.; Delic, G.T.; Durdevic, J.S.; Comic, L.R. Antimicrobial and Antibiofilm Effects of Extracts from *Trapa Natans* L. Evaluation of total phenolic and flavonoid contents and GC-MS Analysis. *Acta Pol. Pharm.* **2016**, *73*, 1565–1574.

18. Rahman, M.M.; Mosaddik, M.A.; Wahed, M.I.I.; Haque, M.E. Antimicrobial activity and cytotoxicity of *Trapa bispinosa*. *Fitoterapia* **2000**, *71*, 704–706. [CrossRef]

19. Kim, Y.-S.; Hwang, J.-W.; Jang, J.-H.; Son, S.; Seo, I.-B.; Jeong, J.-H.; Kim, E.-H.; Moon, S.-H.; Jeon, B.-T.; Park, P.-J. *Trapa japonica* pericarp extract reduces LPS-induced inflammation in macrophages and acute lung injury in mice. *Molecules* **2016**, *21*, 392. [CrossRef]

20. Kim, B.; Kim, J.E.; Choi, B.-K.; Kim, H.-S. Anti-inflammatory effects of water chestnut extract on cytokine responses via nuclear factor-κB-signaling pathway. *Biomol. Ther.* **2015**, *23*, 90–97. [CrossRef]

21. Huang, H.C.; Chao, C.L.; Liaw, C.C.; Hwang, S.Y.; Kuo, Y.H.; Chang, T.C.; Chao, C.H.; Chen, C.J.; Kuo, Y.H. Hypoglycemic constituents isolated from *Trapa natans* L. Pericarps. *J. Agric. Food Chem.* **2016**, *64*, 3794–3803. [CrossRef] [PubMed]

22. Kharbanda, C.; Sarwar Alam, M.; Hamid, H.; Bano, S.; Haider, S.; Nazreen, S.; Ali, Y.; Javed, K. Trapa natans L. root extract suppresses hyperglycemic and hepatotoxic effects in STZ-induced diabetic rat model. *J. Ethnopharmacol.* **2014**, *151*, 931–936. [CrossRef] [PubMed]

23. Damiani, E.; Rosati, L.; Castagna, R.; Carloni, P.; Greci, L. Changes in ultraviolet absorbance and hence in protective efficacy against lipid peroxidation of organic sunscreens after UVA irradiation. *J. Photochem. Photobiol. B Biol.* **2006**, *82*, 204–213. [CrossRef] [PubMed]

24. *U.S. Pharmacopeia National Formulary USP38 NF33*; The United States Pharmacopeial Convention: Rockviie, MD, USA, 2015; Volume 1, pp. 1884–1889, ISBN 978-1-936424-32-0.

Sample Availability: Samples of the compounds are available from the authors.

molecules

MDPI

Characterization of Proanthocyanidin Oligomers of *Ephedra sinica*

Joanna Orejola, Yosuke Matsuo, Yoshinori Saito and Takashi Tanaka *

Department of Natural Product Chemistry, Graduate School of Biomedical Sciences, Nagasaki University,
1-14 Bunkyo-machi, Nagasaki 852-8521, Japan; jjorejola@up.edu.ph (J.O.); y-matsuo@nagasaki-u.ac.jp (Y.M.);
saiyoshi@nagasaki-u.ac.jp (Y.S.)
* Correspondence: t-tanaka@nagasaki-u.ac.jp; Tel.: +81-95-819-2432

Abstract: *Ephedra sinica*, an important plant in Chinese traditional medicine, contains a complex mixture of proanthocyanidin oligomers as major constituents; however, only the minor components have been chemically characterized. In this study, oligomers with relatively large molecular weights, which form the main body of the proanthocyanidin fractions, were separated by adsorption and size-exclusion chromatography. Acid-catalyzed degradation in the presence of mercaptoethanol or phloroglucinol led to the isolation of 18 fragments, the structures of which were elucidated from their experimental and TDDFT-calculated ECD spectra. The results indicated that (−)-epigallocatechin was the main extension unit, while catechin, the A-type epigallocatechin–gallocatechin dimer, and the A-type epigallocatechin homodimer, were identified as the terminal units. Among the degradation products, thioethers of gallocatechin with 3,4-*cis* configurations, a B-type prodelphinidin dimer, a prodelphinidin trimer with both A- and B-type linkages, and a prodelphinidin dimer with an α-substituted A-type linkage were new compounds. In addition, a phloroglucinol adduct of an A-type prodelphinidin dimer, a doubly-linked phloroglucinol adduct of epigallocatechin, and a unique product with a flavan-3-ol skeleton generated by the rearrangement of the aromatic rings were also isolated.

Keywords: *Ephedra sinica*; proanthocyanidin; oligomer; thiolysis; phloroglucinolysis; TDDFT; ECD

1. Introduction

Ephedra sinica Stapf (Fam. *Ephedraceae*) is one of the most important plants in traditional medicine, and is used as a diuretic, antipyretic, diaphoretic, and for relieving a cough and asthma [1]. As the crude drug, it has an official monograph in both the Chinese and Japanese Pharmacopoeias, where it is standardized against the major alkaloids, ephedrine and pseudoephedrine [2]. Thus, the main emphasis is conventionally given to its alkaloidal content, despite the fact that this only constitutes about 0.7–0.8% of the whole plant [3,4]. Clearly, the motivation for this is the proven clinical effects of these alkaloids on the respiratory, central nervous, and cardiovascular systems [5]. However, many species of *Ephedra* have also been shown to contain significant amounts of proanthocyanidins [6]. Recently, many health benefits of foods and medicinal plants have been attributed to proanthocyanidins [7], and some of their biological activities, including hypotensive and vasorelaxant effects [8,9], improvement of the airway microenvironment in asthma [10], and the inhibition of inflammation and remodeling in murine models of chronic asthma [11], are responsible for the aforementioned activities of *E. sinica*, especially its respiratory and cardiovascular effects. A number of studies have shown that *Ephedra* spp. also display other biological activities that are not attributed to alkaloids, including antimicrobial [12,13], antioxidant [14], anti-inflammatory [15,16], immunosuppressive [17], antiviral [18], anti-invasive, antiangiogenic, antitumor [19], and cytotoxic [20] properties. The dimeric proanthocyanidins of *E. sinica* show cytotoxic activity against the tumor cell

lines SGC-7901, HepG2, and HeLa [21]. In addition, a decrease in the uremic toxin parameters of rats was reportedly induced by the administration of proanthocyanidin oligomers of *E. sinica* [22,23].

As for the composition of the proanthocyanidins of *E. sinica*, monomeric flavan-3-ols [12,24] and dimeric proanthocyanidins with A-type linkages have been isolated [12,21,25–28]. The presence of prodelphinidin trimers and tetramers with A- and B-type linkages has also been shown [12]. However, these flavan-3-ols and proanthocyanidins are minor components of the total polyphenol content, and our preliminary HPLC and TLC analysis of the extract suggested that the main body of the polyphenols was a complex mixture of oligomers, detected as a broad hump on the HPLC baseline and at the origin of the TLC plate (Figure 1a). Thus, the present study aimed at characterizing these proanthocyanidin oligomers by acid-catalyzed degradation in the presence of nucleophilic agents, that is, 2-mercaptoethanol or phloroglucinol. The degradation involved the cleavage of the interflavan bonds under acidic conditions, generating flavan-3-ols from the terminal units and flavanyl-4 cations from the extension units, which were trapped by nucleophilic agents (Scheme 1) [29].
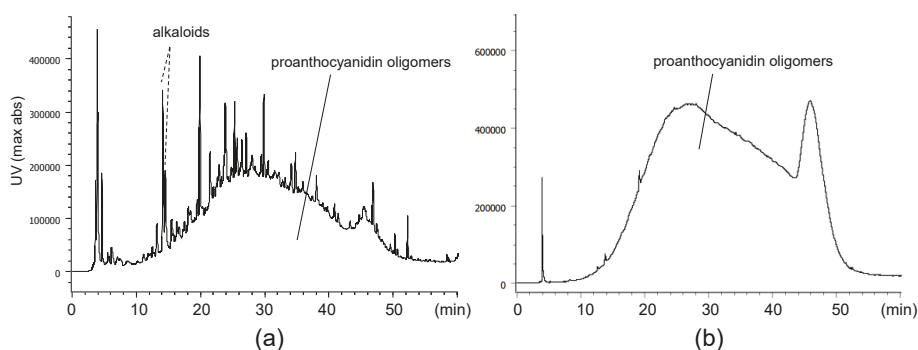
Figure 1. HPLC profiles of 60% EtOH extract of *E. sinica* (**a**) and proanthocyanidin oligomer fraction (**b**).
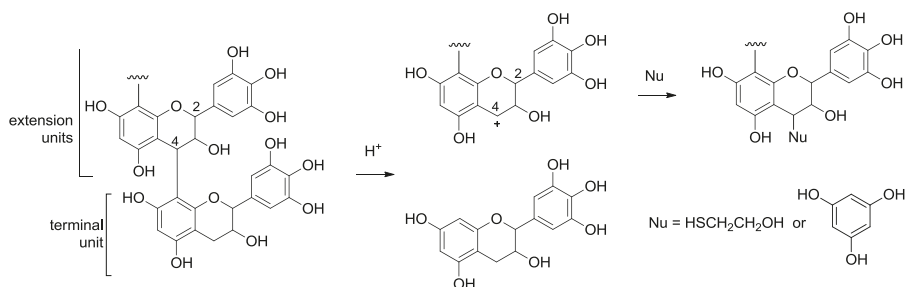
Scheme 1. Reaction mechanism of the acid-catalyzed cleavage of the interflavan bond in the presence of nucleophiles (Nu).

2. Results and Discussion

2.1. Composition of the Intact Proanthocyanidin Oligomer

The dried aerial parts of *E. sinica* were extracted with aqueous acetone and fractionated by a series of chromatographic separation methods, including size-exclusion chromatography [30]. The fractions containing only oligomeric proanthocyanidins accounted for 2.7% of the dried plant material, and the HPLC profile showed a broad hump on the baseline (Figure 1b). The ^{13}C-NMR spectrum of the oligomer fraction in DMSO-d_6 (Figure 2) showed signals characteristic of proanthocyanidins [31]. Based on a comparison with the literature data [11], the signals at δ_C 77 and δ_C 70–73, which were

attributable to flavan C-ring C-2 and C-3 methine carbons, respectively, suggested the occurrence of B-type linkages. The chemical shifts also indicated that the 2,3-*cis* configuration was more abundant than 2,3-*trans* [32,33]. The signals in the range of δ_C 27–31 were attributable to the C-4 carbons of A-type proanthocyanidin extension units [12] and of terminal units [34,35]. The prominent aromatic signals observed at δ_C 106, 130, 132, and 145 suggested the predominance of pyrogallol-type B-rings over catechol-type B-rings (δ_C 115–120).
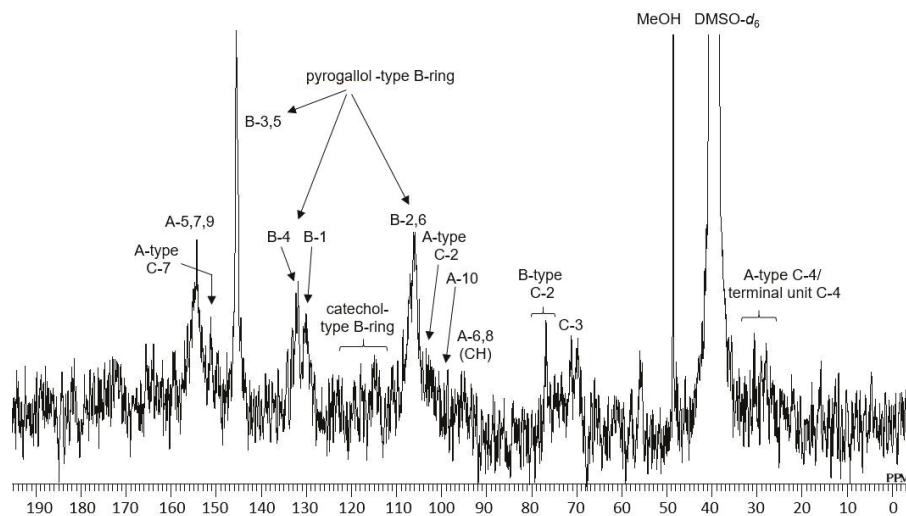
Figure 2. ^{13}C-NMR spectrum of the proanthocyanidin oligomers from *E. sinica*, measured at 100 MHz in DMSO-d_6.

2.2. Acid-Catalyzed Degradation Products

2.2.1. Identification of Known Products

Thiol degradation was performed according to the previously described method [35] with modifications of the reaction time and temperature, and 10 compounds (**1–10**) were isolated and characterized (Figure 3a). Acid-catalyzed degradation with phloroglucinol [29,36] yielded a different set of 10 products (**5**, **8**, **11–18**), among which two products (**5** and **8**) were identical to those obtained by thiol degradation (Figure 3b).

Based on a comparison of the ^{1}H- and ^{13}C-NMR data with those published [12,33], four products were identified as (+)-catechin (**4**), (−)-epigallocatechin-(4β→8,2→*O*→7)-(+)-gallocatechin (**5**), (−)-epigallocatechin-(4β→8,2→*O*→7)-(+)-catechin (**8**), and (−)-epigallocatechin-(4→8,2→*O*→7)-(−)-epigallocatechin (**17**) (Figure 4). These products originated from the terminal units. As depicted in the HPLC profile of the reaction mixture (Figure 3), the peaks attributable to the terminal units were very small compared with those of the extension units, suggesting a high degree of polymerization. The major degradation products of thiolysis **6** and of phloroglucinolysis **12** were identified as epigallocatechin–nucleophile adducts [33,37], indicating that epigallocatechin was the major extension unit of the oligomer. The ^{1}H- and ^{13}C-NMR spectra of **9**, **10**, **11**, **15**, and **18** were found to be consistent with those previously reported for (−)-epigallocatechin-(4→8,2→*O*→7)-(−)-epigallocatechin-4-(2-hydroxyethyl)-thioether, (−)-epicatechin-4-(2-hydroxyethyl)-thioether, (+)-gallocatechin-4-phloroglucinol, (−)-epicatechin-4-phloroglucinol, and (+)-catechin-4-phloroglucinol, respectively [33,37,38].
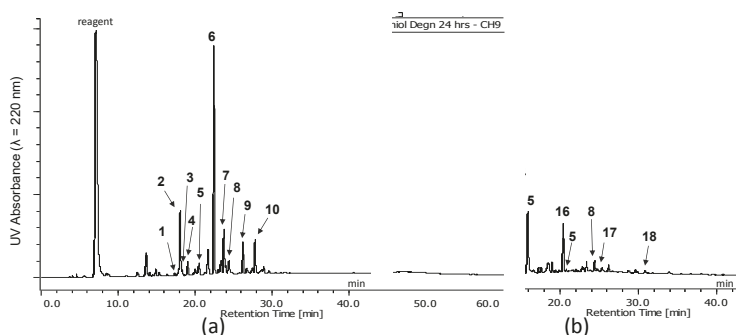
Figure 3. HPLC profiles of thiol degradation products (**a**) and phloroglucinolysis products (**b**).

4: R$_1$= H	R$_2$= ▬OH	R$_3$= H
6: R$_1$= OH	R$_2$= ▪▪▪OH	R$_3$= ▬ SCH$_2$CH$_2$OH
10: R$_1$= H	R$_2$= ▪▪▪OH	R$_3$= ▬ SCH$_2$CH$_2$OH
11: R$_1$= OH	R$_2$= ▬OH	R$_3$= ▪▪▪▪ P
12: R$_1$= OH	R$_2$= ▪▪▪OH	R$_3$= ▬ P
15: R$_1$= H	R$_2$= ▪▪▪OH	R$_3$= ▬ P
18: R$_1$= H	R$_2$= ▬OH	R$_3$= ▪▪▪ P

5: R$_1$= OH	R$_2$= ▪▪▪OH	R$_3$= H
8: R$_1$= H	R$_2$= ▪▪▪OH	R$_3$= H
9: R$_1$= OH	R$_2$= ▬OH	R$_3$= ▪▪▪▪ SCH$_2$CH$_2$OH
17: R$_1$= OH	R$_2$= ▬OH	R$_3$= H
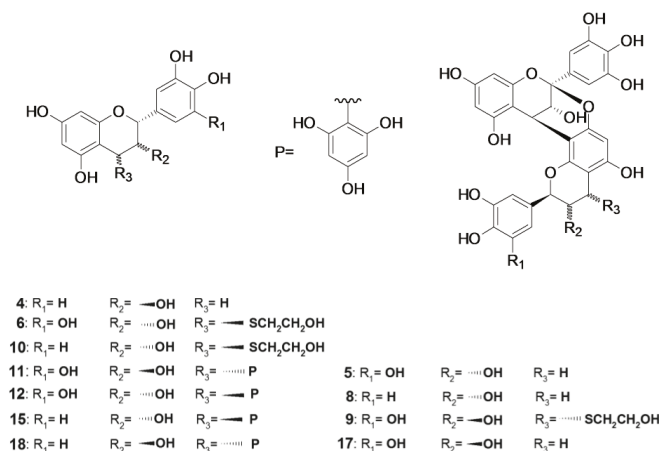
Figure 4. Structures of known degradation products.

2.2.2. Structure Elucidation of New Degradation Products

Among the 18 isolated products, **1**, **2**, **3**, **7**, **13**, **14**, and **16** are reported here for the first time. Their structures are shown in Figure 5 and the ^{1}H- and ^{13}C-NMR spectroscopic data are summarized in Tables 1 and 2.

The molecular formula of **1** was shown to be C$_{32}$H$_{30}$O$_{15}$S based on the [M + H]$^+$ peak at m/z 687.1382 in HRFABMS, indicating that **1** was a mercaptoethanol adduct of a prodelphinidin dimer with a B-type linkage. This was confirmed by the appearance of two intense signals at δ_H 6.57 and δ_H 6.67 (each 2H) arising from two pyrogallol-type B-rings and two methine proton signals attributable to C-ring H-2 in the ^{1}H-NMR signals (Table 1). In the HSQC spectrum, the C-ring H-2 signal at δ_H 4.34 (*J* = 9.4 Hz) was correlated to a carbon signal at δ_C 83.2, while the other F-ring H-2 (Figure 6) at δ_H 5.31 (br s) was found to be connected to the carbon that resonated at δ_C 75.05. The former indicated a 2,3-*trans* configuration and the latter, a 2,3-*cis* configuration [33]; thus, the dimer was composed of gallocatechin and epigallocatechin. The ^{1}H-^{1}H COSY and HMBC correlations (Figure 6) allowed the determination of the connectivity of the two catechin units and hydroxyethylthiol group. The strong NOESY correlations between C-ring H-2 and H-4 (Figure 6), and between -SCH$_2$- and F-ring H-3, confirmed the configuration of the C- and F-rings [39,40]. A linkage between C-ring C-4 and D-ring C-8 was deduced from the NOESY correlation between aromatic E-ring H-2, 6 and C-ring H-4 [41,42].
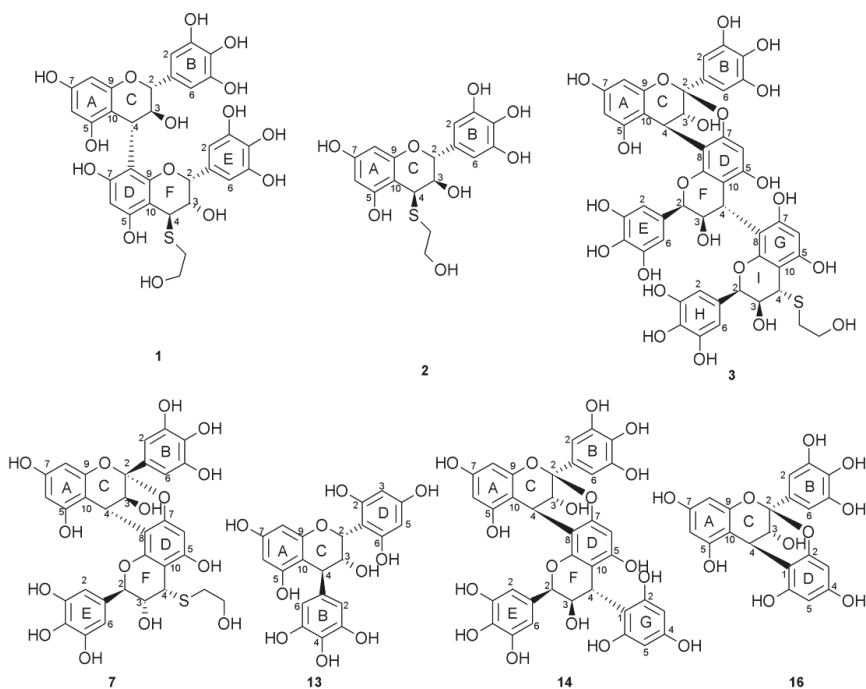
Figure 5. Structures of the new products obtained by the thiolysis and phloroglucinolysis of *E. sinica* proanthocyanidin oligomers.

Table 1. ^{1}H- (500 MHz) and ^{13}C- (125 MHz) NMR data of **1**, **2**, **3**, and **7** in acetone-d_6.

Position		**1** δ_H	(*J* in Hz)	δ_C	**2** δ_H	(*J* in Hz)	δ_C	**3** δ_H	(*J* in Hz)	δ_C	**7** δ_H	(*J* in Hz)	δ_C
C	2	4.34	d (9.5)	83.19	4.77	d(9.7)	78.77			99.91			100.07
	3	4.50	dd (7.8, 9.5)	73.26	4.07	dd(9.7, 4.4)	71.59	4.20	d (3.4)	67.31	4.15	d (3.6)	66.82
	4	4.68	d (7.8)	38.11	4.36	d(4.4)	44.90	4.38	d (3.4)	28.68	4.17	d (3.6)	28.47
A	5			158.27			157.51			156.59			156.04
	6	5.82	s	97.04	6.00	d(2.3)	96.67	5.85	d (2.4)	97.58	5.89	d (2.3)	97.62
	7			157.15			159.14			157.69			157.88
	8	5.82	d (1.7)	95.82	5.78	d(2.3)	94.96	6.05	s	96.00	6.02	d (2.3)	96.12
	9			156.93			155.88			151.65			153.76
	10			106.09			102.14			103.92			103.38
B	1			131.56			130.36			131.50			130.96
	2	6.57	s	107.94	6.50	s	108.19	6.77	s	107.23	6.74	s	107.23
	3			146.16			146.08			145.63			145.64
	4			133.28			133.49			133.74			133.81
	5			146.16			146.08			145.63			145.64
	6	6.57	s	107.94	6.50	s	108.19	6.77	s	107.23	6.74	s	107.23
F	2	5.31	br s	75.05				5.31	br s	78.02	4.99	d (9.8)	79.57
	3	4.04	d (1.1)	71.95				3.95	d (2.2)	72.84	4.21	dd (9.8, 4.3)	71.02
	4	4.05	d (1.1)	43.67				4.79	d (2.2)	36.21	4.39	d (4.3)	44.43
D	5			156.49						155.74			155.74
	6	6.04	s	97.69				6.05	s	96.00	6.13	s	96.92
	7			156.49						153.78			153.02
	8			108.15						106.13			105.98
	9			154.34						151.31			149.62
	10			98.91						104.48			104.33
E	1			130.97						130.62			129.08
	2	6.67	s	106.11				6.56	s	106.42	6.64	s	108.00
	3			145.94						146.27			146.32
	4			132.60						133.08			134.05
	5			145.94						146.27			146.32
	6	6.67	s	106.11				6.56	s	106.42	6.64	s	108.00
I	2							5.29	br s	75.06			
	3							4.14	d (2.3)	71.18			
	4							4.12	d (2.3)	43.83			

Table 1. *Cont*.

Position		1 δH	(J in Hz)	δC	2 δH	(J in Hz)	δC	3 δH	(J in Hz)	δC	7 δH	(J in Hz)	δC
G	5									156.77			
	6							5.96	s	97.45			
	7									157.05			
	8									106.91			
	9									153.90			
	10									99.96			
H	1									130.93			
	2							6.70	s	106.42			
	3									146.14			
	4									132.74			
	5									146.14			
	6							6.70	s	106.42			
CH$_2$OH-		3.73–3.89	m	62.65	3.68–3.88	m	62.68	3.73–3.94	m	62.72	3.73–3.84	m	62.47
SCH$_2$-		2.75–2.96	m	34.95	2.75–3.11	m	37.22	2.78–2.99	m	35.14	2.77–3.09	m	37.54

Table 2. ^{1}H- (500 MHz) and ^{13}C- (125 MHz) NMR data of **13** in methanol-d_4, **14** and **16** in acetone-d_6.

Position		13 δH	(J in Hz)	δC	14 δH	(J in Hz)	δC	16 δH	(J in Hz)	δC
C	2	5.53	br s	70.22			99.97			100.21
	3	4.05	dd (2.4,1.0)	74.27	4.22	d (3.5)	67.26	4.15	d (3.6)	66.99
	4	4.06	br s	45.70	4.38	d (3.5)	28.66	4.25	d (3.6)	28.74
A	5			158.59			156.60			155.32
	6	5.95	d (2.4)	96.59	5.84	d (2.4)	97.58	6.04	d (1.5)	97.21
	7			158.05			157.65			157.69
	8	5.94	d (2.4)	95.24	6.04	d (2.4)	96.17	6.07	br s	96.21
	9			157.76			153.79			153.96
	10			102.49			104.06			104.26
B	1			135.98			131.53			131.23
	2	6.19	s	108.50	6.78	s	107.29	6.53	s	107.32
	3			146.47			145.62			145.62
	4			132.19			133.73			133.76
	5			146.47			145.62			145.62
	6	6.19	s	108.50	6.78	s	107.29	6.53	s	107.32
F	2				5.32	br s	78.12			
	3				3.95	d (2.3)	72.61			
	4				4.63	d (2.3)	36.24			
D	1			104.59						106.96
	2			158.59						153.81
	3	5.79	s	95.95				5.96	d (1.5)	96.01
	4			159.52						158.18
	5	5.79	s	95.95			156.16	6.03	d (1.5)	97.19
	6			158.59	6.02	s	95.63			154.23
	7						151.54			
	8						105.79			
	9						157.65			
	10						104.58			
E	1						130.96			
	2				6.58	s	106.42			
	3						146.27			
	4						133.02			
	5						146.27			
	6				6.58	s	106.42			
G	1						106.90			
	2						151.31			
	3				6.05	s	95.96			
	4						155.43			
	5				6.05	s	95.96			
	6						151.31			
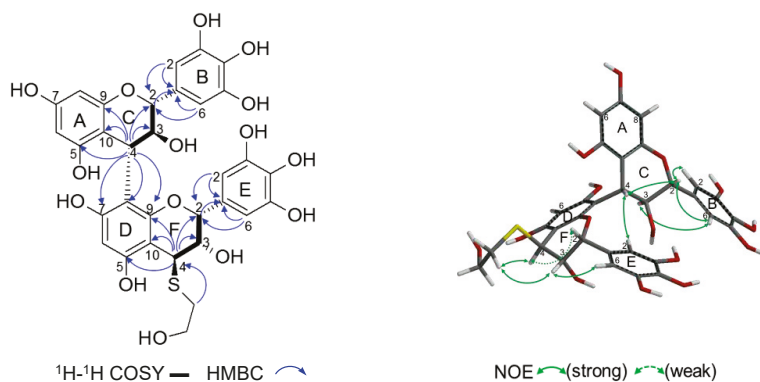
Figure 6. HMBC, ^{1}H-^{1}H COSY, and NOESY correlations of **1**.

ECD spectroscopy allowed the determination of the absolute configuration at C-4. The ^{1}H coupling constants of the C-ring indicated that the B-ring was in an equatorial position (*E*-conformer). Taking this observation into account, the negative Cotton effect at 218 nm implied an α-orientation of the terminal unit at C-4 [40]. Thus, the extension unit was concluded to be (+)-gallocatechin. The establishment of the absolute configuration of the epigallocatechin unit relied on the Cotton effect at the ^{1}L$_b$ band (280 nm) rather than the ^{1}L$_a$ band (220–240 nm) [40]. Here, the negative Cotton effect at 288 nm, in addition to the predominance of *E*-conformers, both led to the conclusion that the pyrogallol E-ring had an α-orientation relative to the F-2 carbon. The terminal unit was thereby designated as (−)-epigallocatechin. Furthermore, the ECD spectrum for **1** showed a close resemblance to those of procyanidins B-4 previously observed by Barrett and colleagues [43]. Accordingly, **1** was concluded to be (+)-gallocatechin-(4→8)-(−)-epigallocatechin-4-(2-hydroxyethyl)thioether.

Product **2** showed the [M + H]$^+$ peak at *m/z* 383.0801 in HRFABMS, confirming the molecular formula as C$_{17}$H$_{18}$O$_8$S. The ^{1}H-NMR spectrum (Table 1) showed a doublet signal at δ$_H$ 4.77 (*J* = 9.6 Hz), indicating the 2,3-*trans* configuration characteristic of gallocatechin. The C-ring H-4 resonated as a doublet at δ$_H$ 4.36 (*J* = 4.3 Hz), which indicated the 3,4-*cis* configuration [31]. This was further confirmed by the appearance of a strong NOESY correlation between H-3 and H-4, and the absence of NOE between H-2 and H-4 (Figure 7). As for the absolute configuration, a negative Cotton effect at 284 nm in the ECD spectrum, which was similar to that of (+)-catechin [43], suggested *P*-helicity for the flavan A- and B-rings. Based on these results, **2** was concluded to be (+)-gallocatechin-4-(2-hydroxyethyl)thioether.
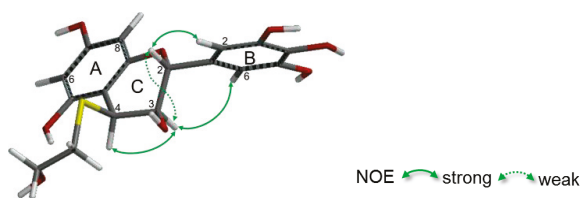
Figure 7. NOE correlations of **2**.

Compound **3** was found to have the molecular formula C$_{47}$H$_{40}$O$_{22}$S based on the [M + Na]$^+$ peak at *m/z* 1011.1639 in HRFABMS. This implied that **3** was a thioether of a prodelphinidin trimer involving both A-type and B-type linkages. In the ^{1}H-NMR spectrum (Table 1), three intense aromatic singlets at δ$_H$ 6.77, δ$_H$ 6.70, and δ$_H$ 6.56 (each 2H) indicated the presence of three pyrogallol-type

B-rings. The presence of two B-type linkages was apparent from the two C-ring H-2 signals resonating at δ_H 5.31 and δ_H 5.29 with small $J_{2,3}$ values (<2 Hz). This again indicated that the two units were epigallocatechin. These spectroscopic features suggested a close relationship between **3** and the epigallocatechin trimer isolated from *E. sinica* with A- and B-type linkages [12]. In the HMBC spectrum of **3** (Figure 8), the ketal carbon C-2 (δ_C 99.91) of the A-type linkage was correlated to C-ring H-4 (δ_H 4.38, J = 3.4 Hz), which was in turn correlated to a D-ring C-9 (δ_C 151.31) of the middle unit. Another benzylic methine H-4 of the middle unit F-ring (δ_H 4.79, J = 2.2 Hz) showed an HMBC correlation to the D-ring C-9 and terminal unit G-ring C-9 (δ_C 153.90). This indicated that an A-type linkage was involved between the top and middle units. The ^{13}C-NMR chemical shift for F-ring C-4 at δ_C 36.21 was consistent with its involvement in a B-type linkage at this position [12,33,44], and the I-ring C-4 at a lower field (δ_C 43.83) was indicative of a thioether at this position [38]. The F-ring H-4 and I-ring H-4 were observed as doublet signals with coupling constants of J = 2.3 Hz and J = 2.4 Hz, respectively, indicating that both flavan rings adopted a 3,4-*trans* configuration [31]. This was further supported by the absence of a NOESY correlation between H-2 and H-4 in both the F-ring and the I-ring (Figure 8). The linkage between rings C and D was established as 4→8, 2→*O*→7 by the presence of a NOESY correlation between E-ring H-2,6 and C-ring H-4 [41]. The connection between the F-ring and the G-ring was also determined to be from C-4 to C-8 based on the NOESY cross peaks of H-ring H-2,6 with F-ring H-4 and H-3.
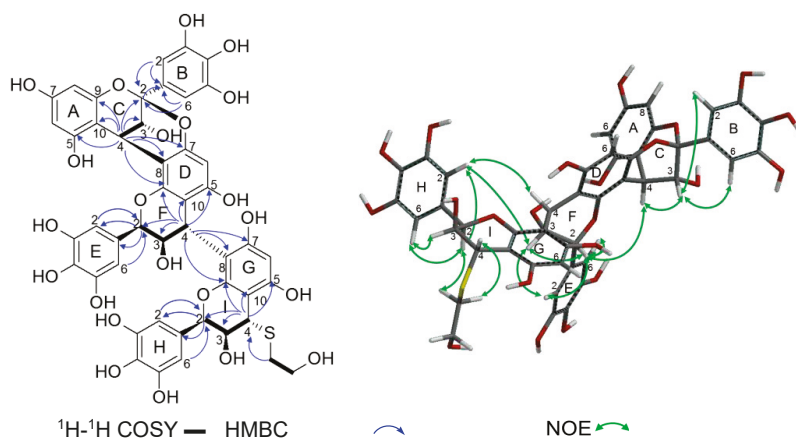
Figure 8. ^{1}H-^{1}H COSY and HMBC correlations (**left**) and NOESY correlations (**right**) of **3**.

The ECD spectrum of **3** showed a strong positive Cotton effect at 233 nm, reflecting the configuration at C-ring C-4, thereby establishing the top extension unit as (−)-epigallocatechin; however, the configuration of the middle and bottom epigallocatechin units could not be determined from the ECD data. Prodelphinidin oligomers with (+)-epigallocatechin units were previously isolated from the same plant source [12]; therefore, the absolute configuration of **3** was established by TDDFT calculations of the ECD spectra for four stereostructures: (**a**) (−)-epigallocatechin-(−)-epigallocatechin-(−)-epigallocatechin, (**b**) (−)-epigallocatechin-(+)-epigallocatechin-(−)-epigallocatechin, (**c**) (−)-epigallocatechin-(−)-epigallocatechin-(+)-epigallocatechin, and (**d**) (−)-epigallocatechin-(+)-epigallocatechin-(+)-epigallocatechin (Figure 9). The experimental ECD spectrum of **3** (Figure 9**e**) showed a positive Cotton effect at 233 nm and a negative Cotton effect at 218 nm, similar to the Cotton effects observed in the calculated ECD spectra **a** and **c**. This comparison of calculated and experimental spectra revealed that the absolute structure of the upper and middle units in **3** was (−)-epigallocatechin. Moreover, the experimental spectrum **e** contained a weak negative Cotton effect at 250–300 nm, similar to the negative Cotton effect in the calculated ECD spectrum **a**. Therefore, **3** was established

as (−)-epigallocatechin-(4β→8,2→*O*→7)-(−)-epigallocatechin-(4β→8)-(−)-epigallocatechin-4-(2-hydroxyethyl)thioether.
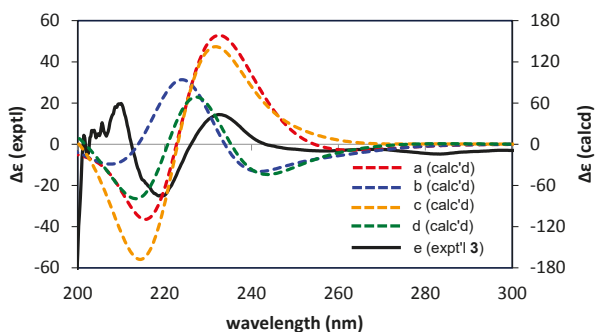
Figure 9. Calculated (a–d) and experimental (e) ECD spectra of prodelphinidin trimer thioether (**3**).

Compound **7** was characterized as an A-type prodelphinidin dimer with a mercaptoethanol substituent, and its molecular formula was determined as $C_{32}H_{28}O_{15}S$ from the $[M + Na]^+$ peak at *m/z* 707.1043 in HRFABMS. The presence of an A-type linkage was apparent from the signal at δ_C 100.07, attributable to the C-ring C-2 ketal carbon [12,42]. The large coupling constant (*J* = 9.8 Hz) of the H-2 at δ_H 4.99 indicated the 2,3-*trans* configuration of the lower unit F-ring. The coupling constants of the C-ring H-4 at δ_H 4.17 (*J* = 3.6 Hz) and F-ring H-4 at δ_H 4.39 (*J* = 4.3 Hz), which were similar to the values observed in **2**, suggested the 3,4-*cis* configuration of these rings. A comparison of the ^{1}H- and ^{13}C-NMR data with those in the literature suggested that the dimer was composed of epigallocatechin and gallocatechin [12,37]. This was supported by a strong NOE between F-3 and F-4, and weak NOE between F-2 and F-3 (Figure 10). The linkage between the C- and D-rings was established to be 4→8 by the observation of a NOESY correlation between C-ring H-4 and E-ring H-2,6. The absolute configuration at the C-ring C-4 was established by ECD spectroscopy, where the strong negative Cotton effect at 228 nm indicated that the extension unit was (+)-epigallocatechin. The terminal unit was designated as (+)-gallocatechin based on a comparison of the ECD spectrum with that of compound **2**, which also had a negative Cotton effect, of a lesser amplitude, at 284 nm. Compound **7** was thereby established as (−)-epigallocatechin-(4α→8,2→*O*→7)-(+)-gallocatechin-4-(2-hydroxyethyl)thioether.
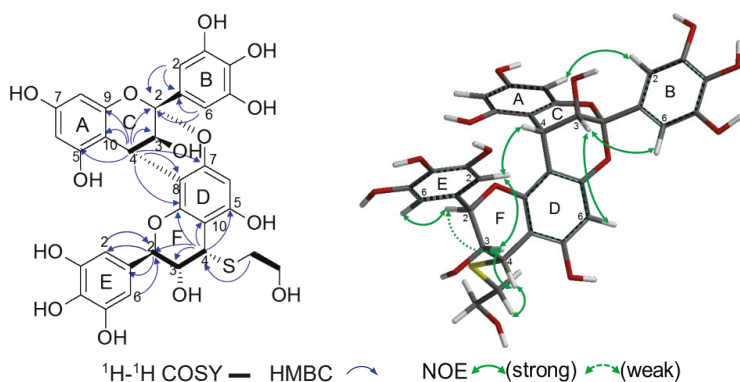
Figure 10. ^{1}H-^{1}H COSY, HMBC, and NOESY correlations of **7**.

Compound **13** was obtained as a product of phloroglucinolysis, and the HRFABMS peak (m/z 431.0979 [M + H]$^+$) confirmed the molecular formula as $C_{21}H_{18}O_{10}$, the same as that of **11** and **12**. Because of overlapping C-ring proton signals in the ^{1}H-NMR spectrum measured in acetone-d_6, the 2D NMR spectra were measured in methanol-d_4 (Table 2). The resulting ^{1}H-NMR spectrum showed signals attributable to pyrogallol (δ_H 6.19, 2H) and phloroglucinol (δ_H 5.79, 2H) rings, as well as mutually *meta*-coupled A-ring H-6 and H-8 (δ_H 5.94 and 5.95, J = 2.4 Hz), which were related to those observed in the spectra of **11** and **12** [12,37,42]. In the ^{1}H-^{1}H COSY spectrum (Figure 11), a broad aliphatic singlet signal at δ_H 5.53 was correlated to a methine signal at δ_H 4.05 (J = 2.4, 1.0 Hz), and these signals were attributed to C-ring H-2 and H-3, respectively. The small coupling constant suggested the 2,3-*cis* configuration [33]. Another aliphatic methine signal at δ_H 4.06 was assigned to C-ring H-4 based on its HMBC correlations to A-ring C-5, 9 and 10 (Figure 11). H-4 also showed HMBC correlations with pyrogallol H-2,6 (δ_H 6.19), indicating that the pyrogallol ring was attached to C-4. This was further supported by the long-range ^{1}H-^{1}H coupling between C-ring H-4 and pyrogallol B-ring H-2,6 in the ^{1}H-^{1}H COSY spectrum and the HMBC cross peak between C-ring H-3 and pyrogallol C-1 [45]. The remaining moiety, i.e., the phloroglucinol ring with a symmetrical structure, was shown to be located at C-ring C-2 by the HMBC correlation of C-ring H-2 to the phloroglucinol C-1, 2, and 6. The 2,3-*cis*-3,4-*trans* configuration was inferred by a comparison of the coupling constants with those in the literature [31], and this was further supported by the absence of NOE between H-2 and H-4 and occurrence of the strong NOE between C-ring H-2 and pyrogallol B-ring H-2,6 (Figure 11). The weak correlation observed between the C-ring H-2 and A-ring H-8 protons suggested that H-2 was at the axial position, thereby implying that the C-ring adopted the *E*-conformation. From the positive Cotton effect at 227 nm, the absolute configuration at C-4 was determined to be *S* [31]. Accordingly, **13** was concluded to be 2-(2,4,6-trihydroxyphenyl)-4-(3,4,5-trihydroxyphenyl)-3,4-dihydro-2*H*-1-benzopyran-3,5,7-triol (2*R*,3*R*,4*S*). This compound was a byproduct of phloroglucinolysis, and a plausible production mechanism is proposed in Scheme 2.
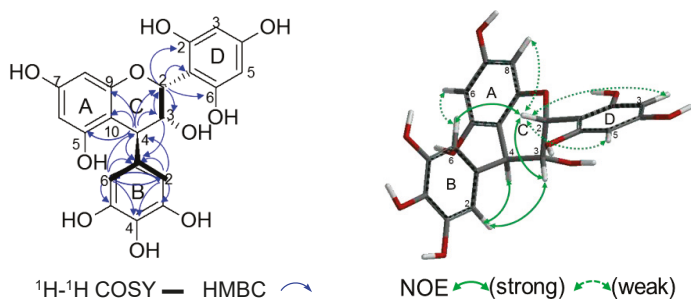
Figure 11. ^{1}H-^{1}H COSY, HMBC, and NOESY correlations of **13**.
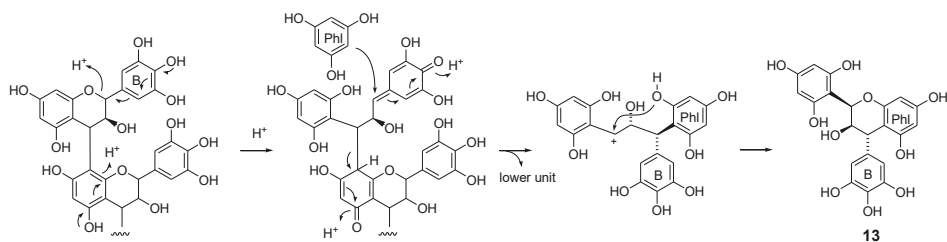
Scheme 2. A possible production mechanism of **13**.

Compound **14** was determined to have the molecular formula $C_{36}H_{28}O_{17}$ (m/z 733.1406, $[M + H]^+$), identifying it as a phloroglucinol adduct of a prodelphinidin dimer involving an A-type linkage. The signals in the ^1H- and ^{13}C-NMR spectra were related to those of the epigallocatechin–epigallocatechin dimer [12] and the procyanidin A2–phloroglucinol adduct [46], and their assignments (Table 2) were based on a comparison with the reported data. The signal of F-ring H-2 (δ_H 5.32) was observed as a singlet, indicating the 2,3-*cis* configuration of the F-ring [33]. In addition, the coupling constant of the F-ring H-4 (δ_H 4.63, J = 2.3 Hz) was consistent with the 3,4-*trans* configuration [31]. This was confirmed by the NOESY spectrum, which displayed a strong correlation between F-ring H-3 and H-4, but no NOE between H-2 and H-4 (Figure 12). The 4→8 linkage between the C- and D-rings was established by the NOE between E-ring H-2,6 and C-ring H-4. Furthermore, the strong positive Cotton effect at 232 nm established that the upper unit was (−)-epigallocatechin [12]. On the basis of previous studies of compound **7**, by Nam et al. [42] and Barrett et al. [43], and considering the weak positive Cotton effect at 220–240 nm of **12**, the lower unit was deduced to be (−)-epigallocatechin. It was therefore concluded that compound **14** was (−)-epigallocatechin-(4β→8,2→*O*→7)-(−)-epigallocatechin-4-phloroglucinol.
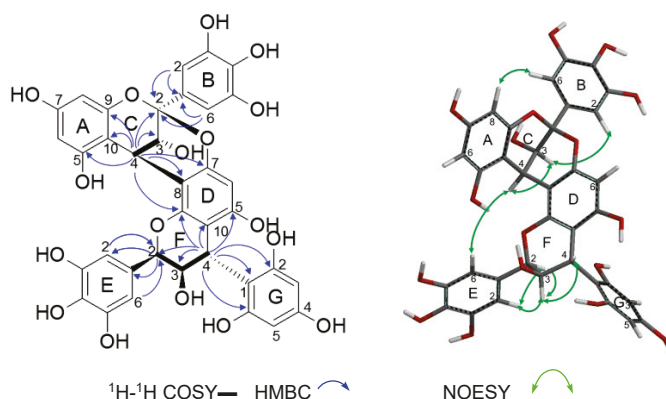
Figure 12. ^1H-^1H COSY, HMBC, and NOESY correlations of **14**.

Product **16** showed the $[M + H]^+$ peak at m/z 429.0818 in HRFABMS, indicating the molecular formula $C_{21}H_{16}O_{10}$. An unambiguous assignment of the ^1H- and ^{13}C-NMR signals was achieved by ^1H-^1H COSY, HSQC, HMBC, and NOESY spectroscopy. The absence of a C-2 proton signal and appearance of a C-2 carbon signal at δ_C 100.21 confirmed the presence of an A-type linkage [12,44,46]. The HMBC cross peaks (Figure 13) between C-ring H-4 and D-ring C-1,2,6 indicated the linkage of the phloroglucinol moiety to C-ring C-4. The NOE cross peaks between H-3 and B-ring H-2,6 indicated the 3,4-*trans* configuration [47]. Furthermore, the ECD spectrum showed a positive Cotton effect at 220–240 nm, indicating a β- configuration at C-4. Accordingly, **16** was established to be (−)-epigallocatechin-(4β→1,2→*O*→2)-phloroglucinol. Compound **16** was regarded as a byproduct of phloroglucinolysis involving the oxidation of the pyrogallol-type B-ring (Scheme 3) [45].
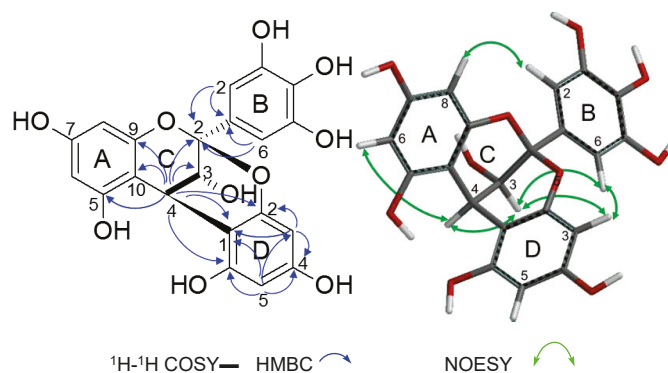
Figure 13. ^{1}H-^{1}H COSY, HMBC, and NOESY correlations of **16**.
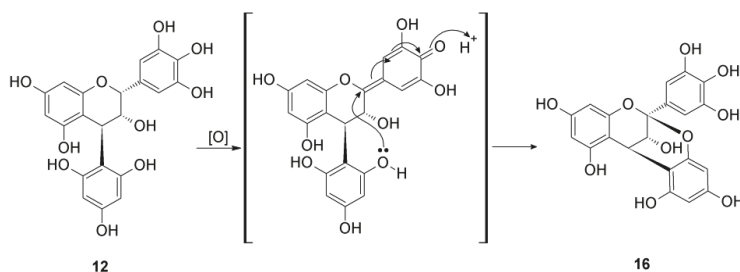
Scheme 3. Formation of **16** by oxidative hydride abstraction.

3. Materials and Methods

3.1. General

NMR spectra were recorded in acetone-d_6 (Wako Pure Chem. Ind. Ltd., Osaka, Japan), methanol-d_4 (Kanto Chem. Co., Inc., Tokyo, Japan), and DMSO-d_6 (Kanto Chemical Co., Inc., Tokyo, Japan) with a Varian Unity Plus 500 spectrometer (Palo Alto, CA, USA) operating at 500 MHz for ^{1}H and 125 MHz for ^{13}C, and with a JEOL JNM-AL 400 spectrometer (JEOL Ltd, Tokyo, Japan) at 400 MHz for ^{1}H and 100 MHz for ^{13}C. HRFABMS spectra were recorded on a JMS 700N spectrometer (JEOL Ltd., Tokyo, Japan) in positive ion mode, with glycerol or *m*-nitrobenzyl alcohol, with or without NaCl, as the matrix. UV spectra were recorded in MeOH with a Jasco V-560 UV/Vis spectrometer (Jasco Co. Ltd., Tokyo, Japan). The same solvent was used for the ECD spectroscopic analysis using a Jasco-725N spectrometer (Jasco Co. Ltd., Tokyo, Japan), and optical rotation measurement using a Jasco P-1020 (Jasco Co. Ltd., Tokyo, Japan). IR spectra were recorded using a Jasco FT/IR-410K (Jasco Co. Ltd., Tokyo, Japan). Column chromatography was performed using a Sephadex LH-20 (25–100 mm, GE Healthcare UK Ltd., Buckinghamshire HP7 9NA, UK), a Diaion HP20SS (Mitsubishi Chemical Co., Tokyo, Japan), and a Chromatorex ODS (Fuji Silysia Chemical Ltd., Kasugai, Japan). TLC was performed on 0.25-mm thick, precoated silica gel 60 F$_{254}$ (Merck, Darmstadt, Germany) with toluene–ethyl formate–formic acid (1:7:1, *v/v*) as the solvent system. Spots were detected by illumination under a short wavelength UV (254 nm) followed by spraying with 2% ethanolic FeCl$_3$. Analytical HPLC was performed with gradient elution from 4–30% (39 min), 30–75% (15 min), 75–95% (6 min) acetonitrile (Kanto Chemical Co., Inc., Tokyo, Japan) in 50 mM phosphoric acid (Kishida Chemical Co., Osaka, Japan) on a Cosmosil 5C$_{18}$-ARII 4.6 × 250 mm column (Nacalai Tesque, Inc., Kyoto, Japan) at a flow rate of 0.8 mL/min, using an HPLC system composed of a Jasco DG-2080-53

Plus degasser, Jasco PU-2080 Plus pump, Jasco AS-2055 Plus autosampler, Jasco CO-2065 Plus column oven (maintained at 35 °C), and Jasco MD-2018 Plus PDA detector (Jasco Co. Ltd., Tokyo, Japan).

3.2. Plant Material

Dried aerial parts of *Ephedra sinica* were purchased from Uchida Wakanyaku Ltd., Tokyo, Japan.

3.3. Extraction and Isolation

The dried aerial parts (500 g) of *E. sinica* were extracted with 70% acetone (3 L) at room temperature overnight, three times. The extracts were combined and concentrated by rotary evaporation under reduced pressure at 40 °C. The resulting aqueous solution was charged into a Sephadex LH-20 (5 cm × 19 cm) and eluted with H_2O-MeOH (0–100%, 20% stepwise gradient) and 60% acetone to give two fractions: Fr. 1 and 2 (Figure S1). The first fraction eluted with H_2O was acidified with trifluoroacetic acid and loaded into a Diaion HP20SS column (5 cm × 30 cm). After washing out sugars and inorganic substances with H_2O, the column was eluted with 0–100% MeOH (10% stepwise gradient) and then 60% acetone to give Fr. 1-1 (9.16 g) containing proanthocyanidin oligomers and Fr. 1-2 (14.57 g) containing oligomers and low-molecular weight proanthocyanidins. A portion (5 g) of Fr. 1-2 was separated by size-exclusion column chromatography using a Sephadex LH-20 (4 cm × 45 cm) with a mixture of acetone and 7 M urea (3:2, *v/v*, containing conc. HCl 5 mL/L) to afford Fr. 1-2-1 containing oligomers and Fr. 1-2-2 containing low-molecular weight polyphenols. After the removal of acetone by evaporation, the resulting aqueous solution of Fr. 1-2-1 was subjected to Diaion HP20SS (3 cm × 19 cm) column chromatography, and urea and HCl were washed out by elution with H_2O. Subsequent elution of the column with 0–100% MeOH (10% stepwise gradient) yielded Fr. 1-2-1-1 (1.11 g) containing oligomeric proanthocyanidins. Separately, Fr. 2 was subjected to size-exclusion chromatography in a manner similar to that described for Fr. 1-2 to give three fractions. The resulting Fr. 2-2 was loaded into a Diaion HP20SS column to remove urea and HCl, yielding oligomeric proanthocyanidins (Fr. 2-2-2, 3.36 g).

3.4. Thiolysis

Thiol degradation was performed according to the method of Kusano et al. [35] with modifications. Proanthocyanidin oligomers (Fr. 1-1, 1.0 g) were dissolved in 60% EtOH (200 mL) containing mercaptoethanol (10 mL) (Kanto Chemical Co. Inc., Tokyo, Japan) and concentrated HCl (0.5 mL) (Kishida Chemical Co., Osaka, Japan). The reaction mixture was then heated at 70 °C for 22 h. The reaction mixture was then analyzed by HPLC and was further fractionated. Fr. 2-2-2 (1.0 g) was also subjected to thiolysis in the same manner. The reaction mixture of Fr. 1-1 was first concentrated to remove EtOH. The resulting aqueous solution was subjected to Sephadex LH-20 chromatography (3 cm × 24 cm), and mercaptoethanol was washed out with H_2O. Further elution of the column with increasing proportions of MeOH in H_2O (0–50%, 5% stepwise gradient; 50–100%, 10% stepwise gradient) gave eight fractions. Fr 1-1-5 (0.35 g) was loaded into a Diaion HP20SS (3 cm × 22 cm) with H_2O-MeOH to furnish five subfractions. Purification of Fr. 1-1-5-4 (41.9 mg) by Sephadex LH-20 chromatography (3 cm × 25 cm) with a systematic stepwise gradient of EtOH-H_2O-acetone (1:0:0, 9:1:0, 8:2:0, 6:4:0, 54:36:10, 48:32:20, 36:24:40, 0:50:50, *v/v*) enabled the isolation of **10** (19.5 mg). Separation of Fr. 1-1-5-3 (178.7 mg) with the same chromatographic procedure afforded compounds **4** (4.9 mg) and **6** (60.8 mg). Fr. 1-1-5-2 (72.9 mg) was separated by Chromatorex ODS chromatography (3 cm × 17 cm) with H_2O-MeOH and a Sephadex LH-20 (2.5 cm × 13 cm) with H_2O-MeOH to afford **6** (21.0 mg), **1** (5.2 mg), and **2** (21.3 mg). Separation of Fr. 1-1-7 by Diaion HP20SS chromatography (2 × 17 cm) with H_2O-MeOH afforded six subfractions, and Fr. 1-1-7-3 (104.3 mg) was further separated by Chromatorex ODS chromatography (2 cm × 16 cm) with H_2O-MeOH to give **3** (21.2 mg), **7** (19.3 mg), and **9** (9.0 mg). The thiol degradation products of the other oligomers, Fr. 2-2-2, were also fractionated in the same manner as described for Fr. 1-1 to give seven subfractions. Fr. 2-2-2-6 (241.5 mg) was separated by Diaion HP20SS column chromatography (3 cm × 16 cm) with H_2O-MeOH (0–100%,

20% stepwise gradient). Among the six subfractions obtained, the separation of Fr. 2-2-2-6-3 (74.5 mg) by a Chromatorex ODS (2.5 cm × 15 cm) with H_2O-MeOH yielded **5** (0.6 mg), **7** (36.2 mg), and **9** (10.0 mg). The same chromatographic procedure using a Chromatorex ODS was applied to the separation of Fr. 2-2-2-6-4 (49.3 mg), which yielded **9** (21.0 mg) and a crude crop of **8**. The latter was purified by Sephadex LH-20 (2 cm × 16 cm) and a system of increasing MeOH concentration in H_2O (0–40%, 20% stepwise gradient; 40–100%, 5% stepwise gradient), which led to the isolation of **8** (8.8 mg).

(+)-Gallocatechin-(4α→8)-(−)-epigallocatechin-4-(2-hydroxyethyl)thioether (**1**): yellowish brown amorphous powder; $[\alpha]_D^{16}$ −105.9 (*c* = 0.10, MeOH); UV (MeOH) λ_{max} (log ε) 270 (3.61), 239 (4.41), 214 (5.00) nm; CD (MeOH) $\Delta\varepsilon_{218}$ −33.1, $\Delta\varepsilon_{288}$ −2.3; IR ν_{max} 3311, 1609, 1449, 1541, 1449 cm^{-1}; HRFABMS *m/z* 687.1382 [M + H]$^+$ (calcd for $C_{32}H_{31}O_{15}S$, 687.1378); ^{1}H- and ^{13}C-NMR data, see Table 1.

(+)-Gallocatechin-4-(2-hydroxyethyl)thioether (**2**): pale brown amorphous powder; $[\alpha]_D^{16}$ +29.9 (*c* = 0.13, MeOH); UV (MeOH) λ_{max} (log ε) 273 (3.17), 235 (4.42), 209 (4.72) nm; CD (MeOH) $\Delta\varepsilon_{220}$ −2.8, $\Delta\varepsilon_{249}$ +2.2, $\Delta\varepsilon_{284}$ −0.4; IR ν_{max} 3344, 1621, 1537, 1515, 1455, 1345 cm^{-1}; HRFABMS *m/z* 383.0801 [M + H]$^+$ (calcd for $C_{17}H_{19}O_8S$, 383.0795); ^{1}H- and ^{13}C-NMR data, see Table 1.

(−)-Epigallocatechin-(4β→8,2→O→7)-(−)-epigallocatechin-(4α→8)-(−)-epigallocatechin-4-(2-hydroxyethyl) thioether (**3**): reddish brown amorphous powder; $[\alpha]_D^{20}$ −17.2 (*c* = 0.11, MeOH); UV (MeOH) λ_{max} (log ε) 270 (3.83), 241 (4.65), 205 (5.31) nm; CD (MeOH) $\Delta\varepsilon_{218}$ −25.0, $\Delta\varepsilon_{233}$ +14.2, $\Delta\varepsilon_{284}$ −4.3; IR ν_{max} 3276, 1615, 1541, 1445, 1348 cm^{-1}; HRFABMS *m/z* 1011.1639 [M + Na]$^+$ (calcd for $C_{47}H_{40}O_{22}SNa$, 1011.1624); ^{1}H- and ^{13}C-NMR data, see Table 1.

(+)-Epigallocatechin-(4α→8,2α→O→7)-(+)-gallocatechin-4-(2-hydroxyethyl)thioether (**7**): pale brown amorphous powder; $[\alpha]_D^{17}$ −50.1 (*c* = 0.15, MeOH); UV (MeOH) λ_{max} (log ε) 270 (3.55), 247 (4.32), 208 (5.00) nm; CD (MeOH) $\Delta\varepsilon_{228}$ −25.6, $\Delta\varepsilon_{252}$ +3.7, $\Delta\varepsilon_{284}$ −3.0; IR ν_{max} 3389, 1612, 1537, 1502, 1447, 1333 cm^{-1}; HRFABMS *m/z* 707.1043 [M + Na]$^+$ (calcd for $C_{32}H_{28}O_{15}SNa$, 707.1041); ^{1}H- and ^{13}C-NMR data, see Table 1.

3.5. Phloroglucinolysis

Fr. 1-1 was subjected to phloroglucinolysis according to the method reported by Kennedy and Jones and Bautista-Ortin and colleagues [18,36], with a few modifications. Fr. 1-1 (2.0 g) was dissolved in MeOH (200 mL) and then mixed with phloroglucinol reagent (200 mL). This phloroglucinol reagent was a methanolic solution containing phloroglucinol (20 g) (Sigma Chemical Co., St. Louis, MO, USA), ascorbic acid (4 g) (Kishida Chemical Co., Osaka, Japan), and concentrated HCl (2.92 mL). The mixture was heated at 50 °C for 60 min, and the reaction was then terminated by the addition of 0.2 M sodium acetate (800 mL). The reaction mixture was concentrated in vacuo to remove MeOH and acidified to pH 4 prior to fractionation. The aqueous solution was loaded into a Sephadex LH-20 column (3 cm × 24 cm) and eluted with H_2O containing increasing proportions of MeOH to give 10 fractions. Fr. 1-1-5 (810.7 mg) was separated by Diaion HP 20SS column chromatography (3 cm × 21 cm) with H_2O-MeOH to yield **12** (84.2 mg), **16** (103.7 mg), and five subfractions. Fr. 1-1-5-3 (454.4 mg) was successively separated by a Sephadex LH-20 (H_2O-MeOH) and a Chromatorex ODS (H_2O-MeOH) to afford **11** (24.4 mg). From Fr. 1-1-5-5 (59.8 mg), **17** (6.8 mg) was isolated by Chromatorex ODS chromatography (H_2O-MeOH). Purification of 1-1-6 (102.3 mg) by Diaion HP20SS column chromatography (3 cm × 26 cm) with 0–100% MeOH in H_2O yielded **13** (10.7 mg). Fractionation of 1-1-7 (120 mg) on a Diaion HP20SS (2 cm × 17 cm) with H_2O-MeOH gave **5** (9.3 mg) and nine subfractions. Purification of Fr. 1-1-7-2 (6.3 mg) and Fr. 1-1-7-7 (11.4 mg) by a Chromatorex ODS (H_2O-MeOH) furnished **13** (1.2 mg) and **17** (3.2 mg), respectively. Fr. 1-1-8 (210.7 mg) was separated by Diaion HP20SS chromatography to yield **8** (16.3 mg) and five subfractions, and subfraction 1-1-8-1 (59.4 mg) was further subjected to purification using a Sephadex LH 20 (2 cm × 16 cm) with EtOH-H_2O-acetone (1:0:0, 9:1:0, 8:2:0, 6:4:0, 54:36:10, 48:32:20, 36:24:40, 0:50:50, *v/v*) and then a Chromatorex ODS (H_2O-MeOH)

to give **14** (39.6 mg). Purification of Fr. 1-1-9 (204.8 mg) by Diaion HP 20SS chromatography (2 × 17 cm) with H_2O-MeOH resulted in the isolation of **18** (11.4 mg).

2-(2,4,6-Trihydroxyphenyl)-4-(3,4,5-trihydroxyphenyl)-3,4-dihydro-2H-1-benzopyran-3,5,7-triol (2R,3R,4S) (**13**): pale brown amorphous powder; $[\alpha]_D^{20}$ −15.0 (*c* = 0.11, MeOH); UV (MeOH) λ_{max} (log *ε*) 270 (3.50), 234 (4.40), 210 (4.85) nm; CD (MeOH) $\Delta\varepsilon_{227}$ +0.8, $\Delta\varepsilon_{267}$ +1.2; IR ν_{max} 3333, 1614, 1522, 1462, 1328 cm^{-1}; HRFABMS *m/z* 431.0979 [M + H]$^+$ (calcd for $C_{21}H_{19}O_{10}$, 431.0973); ^{1}H- and ^{13}C-NMR data, see Table 2.

(−)-Epigallocatechin-(4β→8,2→O→7)-(−)-epigallocatechin-4-phloroglucinol (**14**): pale brown amorphous powder; $[\alpha]_D^{19}$ +53.1 (*c* = 0.14, MeOH); UV (MeOH) λ_{max} (log *ε*) 270 (3.62), 235 (4.39), 214 (4.84) nm; CD (MeOH) $\Delta\varepsilon_{232}$ +18.9, $\Delta\varepsilon_{270}$ +1.5, $\Delta\varepsilon_{283}$ −1.2; IR ν_{max} 3297, 1625, 1476, 1347 cm^{-1}; HRFABMS *m/z* 733.1406 [M + H]$^+$ (calcd for $C_{36}H_{29}O_{17}$, 733.1399); ^{1}H- and ^{13}C-NMR data, see Table 2.

(−)-Epigallocatechin-(4β→1,2→O→2)-phloroglucinol (**16**): pale yellow amorphous powder; $[\alpha]_D^{19}$ −6.6 (*c* = 0.14, MeOH); UV (MeOH) λ_{max} (log *ε*) 270 (3.62), 235 (4.39), 214 (4.84) nm; CD (MeOH) $\Delta\varepsilon_{216}$ +4.2, $\Delta\varepsilon_{246}$ +1.2, $\Delta\varepsilon_{270}$ −1.6; IR ν_{max} 3297, 1625, 1476, 1347 cm^{-1}; HRFABMS *m/z* 429.0818 [M + H]$^+$ (calcd for $C_{21}H_{17}O_{10}$, 429.0816); ^{1}H- and ^{13}C-NMR data, see Table 2.

3.6. Calculations of ECD Spectra

A conformational search was performed using the Monte Carlo method with the MMFF94 force field using Spartan'14 (Wavefunction, Irvine, CA, USA). The resulting low-energy conformers within 6 kcal/mol of the global minimum were optimized at the B3LYP-SCRF/6-31G(d,p) level in MeOH (PCM). The vibrational frequencies were also calculated at the same level to confirm that they were true minima, and no imaginary frequencies were found. The energies, oscillator strengths, and rotational strengths of the low-energy conformers with Boltzmann populations greater than 1% were calculated using TDDFT at the CAM-B3LYP-SCRF/6-31G(d,p) level in MeOH (PCM). The ECD spectra were simulated by overlapping Gaussian functions with a 0.3 eV exponential half-width, and red-shifted by 25 nm. The calculated data for each conformer were averaged according to the Boltzmann distribution theory at 298 K based on their relative Gibbs free energies. All DFT calculations were performed using Gaussian 09 [48].

4. Conclusions

The proanthocyanidins of *E. sinica* are mainly composed of oligomers, and in this study, the oligomers were separated and chemically characterized for the first time. Acid-catalyzed degradation with mercaptoethanol and phloroglucinol afforded 18 products, among which seven were previously unreported compounds. Epigallocatechin was the major extension unit, and catechin and A-type prodelphinidin dimers were identified as terminal units. The new compounds were characterized by spectroscopic analyses, and the stereochemistry of the trimeric products was determined with the aid of TDDFT calculations of the ECD spectra. Since *E. sinica* is one of the most important crude drugs in East Asia, and proanthocyanidins are major constituents with a comparable abundance to alkaloids, our results provide important insights into the molecular basis of traditional medicine.

Author Contributions: T.T. and Y.M. conceived and designed the experiments, and analyzed the data; J.O. performed the experiments and analyzed the data. Y.M. performed the calculation and analyzed the ECD spectra of compound **3**. J.O., Y.M., Y.S., and T.T. all wrote the paper.

Conflicts of Interest: The authors declare no conflict of interest.

References

1. Zhu, Y. *Chinese Materia Medica: Chemistry, Pharmacology and Applications*; Harwood Academic Publisher: Amsterdam, Netherlands, 1998; pp. 48–51, ISBN 90-5702-285-0.
2. World Health Organization. *WHO Monographs on Selected Medicinal Plants*; World Health Organization: Geneva, Switzerland, 1999; Volume 1, pp. 145–153, ISBN 9241545178.
3. Wang, L.; Kakiuchi, N.; Mikage, M. Studies of *Ephedra* plants in Asia. Part 6: Geographical changes of anatomical features and alkaloids content of *Ephedra sinica*. *J. Nat. Med.* **2009**, *64*, 63–69. [CrossRef] [PubMed]
4. Liu, Y.; Sheu, S.; Chiou, S.; Chang, H.; Chen, Y. A comparative study of commercial samples of *Ephedrae herba*. *Planta Med.* **1993**, *59*, 376–378. [CrossRef] [PubMed]
5. Westfall, T.; Westfall, D. Adrenergic agonists and antagonists. In *Goodman & Gilman's the Pharmacological Basis of Therapeutics*, 12th ed.; Brunton, L., Chabner, B., Knollman, B., Eds.; McGraw-Hill Medical: New York, NY, USA, 2011; pp. 277–333, ISBN 978-0-07-162442-8.
6. Caveney, S.; Charlet, D.; Freitag, H.; Maier-Stolte, M.; Starratt, A. New observations on the secondary chemistry of world *Ephedra* (*Ephedraceae*). *Am. J. Bot.* **2001**, *88*, 1199–1208. [CrossRef] [PubMed]
7. De Bruyne, T.; Pieters, L.; Delstra, H.; Vlietinck, A. Condensed vegetable tannins: Biodiversity in structure and biological activities. *Biochem. Syst. Ecol.* **1999**, *27*, 445–459. [CrossRef]
8. Magos, G.; Mateos, J.; Páez, E.; Fernández, G.; Lobato, C.; Márquez, C.; Enríquez, R. Hypotensive and vasorelaxant effects of the procyanidin fraction from *Guazuma ulmifolia* bark in normotensive and hypertensive rats. *J. Ethnopharm.* **2008**, *117*, 58–68. [CrossRef] [PubMed]
9. Sanz, M.; Terencio, M.; Paya, M. Isolation and hypotensive activity of a polymeric procyanidin fraction from *Pistacia lentiscus* L. *Pharmazie* **1992**, *47*, 466–467. [PubMed]
10. Zeng, X.; Ma, Y.; Gu, H.; Gu, Y.; Huang, M. The effect of oligomeric proanthocyanidin on airway microenvironment in asthma. *Eur. Respir. J.* **2016**, *48* (Suppl. S60). [CrossRef]
11. Zhou, D.; Fang, S.; Zou, C.; Zhang, Q.; Gu, W. Proanthocyanidin from grape seed extract inhibits airway inflammation and remodeling in a murine model of chronic asthma. *Nat. Prod. Commun.* **2015**, *10*, 257–262. [PubMed]
12. Zang, X.; Shang, M.; Xu, F.; Liang, J.; Wang, X.; Mikage, M.; Cai, S. A-Type proanthocyanidins from the stems of *Ephedra sinica* (*Ephedraceae*) and their antimicrobial activities. *Molecules* **2013**, *18*, 5172–5189. [CrossRef] [PubMed]
13. Bagheri-Gavkosh, S.; Bigdeli, M.; Shams-Ghahfarokhi, M.; Razzaghi-Abyaneh, M. Inhibitory effects of *Ephedra major* host on *Aspergillus parasiticus* growth and aflatoxin production. *Mycopathologia* **2009**, *168*, 249–255. [CrossRef] [PubMed]
14. Okawa, M.; Kinjo, J.; Nohara, T.; Ono, M. DPPH (1,1-diphenyl-2-picrylhydrazyl) radical scavenging activity of flavonoids obtained from some medicinal plants. *Biol. Pharm. Bull.* **2001**, *24*, 1202–1205. [CrossRef] [PubMed]
15. Kim, I.; Park, Y.J.; Yoon, S.; Lee, H. Ephedrannin A and B from roots of *Ephedra sinica* inhibit lipopolysaccharide-induced inflammatory mediators by suppressing nuclear factor-kB activation in RAW 264.7 macrophages. *Int. Immunopharmacol.* **2010**, *10*, 1616–1625. [CrossRef] [PubMed]
16. Kim, S.; Son, K.; Chang, H.; Kang, S.; Kim, H. Inhibitory effects of plant extracts on adjuvant-induced arthritis. *Arch. Pharm. Res.* **1997**, *20*, 313–317. [CrossRef] [PubMed]
17. Chen, R.; Zhu, G.; Xu, Z. Effect of different extracts from Ephedra on cell immunity. *J. Nanjing Univ. Tradit. Chin. Med.* **2001**, *4*, 15.
18. Li, L.; Yu, C.; Ying, H.; Yu, J. Antiviral effects of modified Dingchuan decoction against respiratory syncytial virus infection in vitro and in an immunosuppressive mouse model. *J. Ethnopharm.* **2013**, *147*, 238–244. [CrossRef] [PubMed]
19. Nam, N.; Lee, C.; Hong, D.; Kim, H.; Bae, K.; Ahn, B. Antiinvasive, antiangiogenic and antitumor activity of *Ephedra sinica* extract. *Phytother. Res.* **2003**, *17*, 70–76. [CrossRef] [PubMed]

20. Lee, M.; Cheng, W.; Che, C.; Hsieh, D. Cytotoxicity assessment of Ma-huang (*Ephedra*) under different conditions of preparation. *Toxicol. Sci.* **2000**, *56*, 424–430. [CrossRef] [PubMed]

21. Tao, H.; Wang, L.; Cui, Z.; Zhao, D.; Liu, Y. Dimeric proanthocyanidins from the roots of *Ephedra sinica*. *Planta Med.* **2008**, *74*, 1823–1825. [CrossRef] [PubMed]

22. Yokozawa, T.; Fujioka, K.; Oura, H.; Tanaka, T.; Nonaka, G.; Nishioka, I. Decrease in uremic toxins, a newly found beneficial effect of Ephedrae Herba. *Phytother. Res.* **1995**, *9*, 382–384. [CrossRef]

23. Wang, G.Z.; Hikokichi, O. Experimental study in treating chronic renal failure with dry extract and tannins of Herba Ephedra. *Zhongguo Zhong Xi Yi Jie He Za Zhi* **1994**, *14*, 485–488. [PubMed]

24. King, F.; Clark-Lewis, J.; Forbes, W. The chemistry of extractives from hardwoods. Part XXV. (—)-*epi*Afzelechin, a new member of the catechin series. *J. Chem. Soc.* **1955**, 2948–2956. [CrossRef]

25. Hikino, H.; Takahashi, M.; Konno, C. Structure of ephedrannin A, a hypotensive principle of *Ephedra* roots. *Tetrahedron Lett.* **1982**, *23*, 673–676. [CrossRef]

26. Hikino, H.; Shimoyama, N.; Kasahara, Y.; Takahashi, M.; Konno, C. Structures of mahuannin A and B, hypotensive principles of *Ephedra* roots. *Heterocycles* **1982**, *19*, 1381–1384. [CrossRef]

27. Kasahara, H.; Hikino, H. Structure of mahuannin D, a hypotensive principle of *Ephedra* roots. *Heterocycles* **1983**, *20*, 1953–1956. [CrossRef]

28. Nonaka, G.; Morimoto, S.; Kinjo, J.; Nohara, T.; Nishioka, I. Tannins and related compounds L. Structures of proanthocyanidin A-1 and related compounds. *Chem. Pharm. Bull.* **1987**, *35*, 149–155. [CrossRef]

29. Kennedy, J.; Jones, G. Analysis of proanthocyanidin cleavage products following acid-catalysis in the presence of excess phloroglucinol. *J. Agric. Food Chem.* **2001**, *49*, 1740–1746. [CrossRef] [PubMed]

30. Yanagida, A.; Shoji, T.; Shibusawa, Y. Separation of proanthocyanidins by degree of polymerization by means of size-exclusion chromatography and related techniques. *J. Biochem. Biophys. Methods* **2003**, *56*, 311–322. [CrossRef]

31. Kolodziej, H. ^{1}H NMR spectral studies of procyanidin derivatives: Diagnostic ^{1}H NMR parameters applicable to the structural elucidation of oligomeric procyanidins. In *Plant Polyphenols-Synthesis, Properties, Significance*; Hemingway, R., Laks, P.E., Eds.; Plenum Press: New York, NY, USA, 1992; pp. 295–319, ISBN 978-1-4615-3476-1.

32. Porter, L.; Newman, R.; Foo, L.; Wong, H.; Hemingway, R. Polymeric proanthocyanidins. ^{13}C-NMR studies of procyanidins. *J. Chem. Soc. Perkin Trans. 1* **1982**, 1217–1221. [CrossRef]

33. Foo, L.; Newman, R.; Waghorn, G.; McNabb, W.; Ulyatt, M. Proanthocyanidins from *Lotus corniculatus*. *Phytochemistry* **1996**, *41*, 617–624. [CrossRef]

34. Chai, W.; Shi, Y.; Feng, H.; Qiu, L.; Zhou, H.; Deng, Z.; Yan, C.; Chen, X. NMR, HPLC-ESI-MS, and MALDI-TOF MS analysis of condensed tannins from *Delonix regia* (Bojer ex Hook.) Raf. and their bioactivities. *J. Agric. Food Chem.* **2012**, *60*, 5013–5022. [CrossRef] [PubMed]

35. Kusano, R.; Ogawa, S.; Matsuo, Y.; Tanaka, T.; Yazaki, Y.; Kouno, I. α-amylase and lipase inhibitory activity and structural characterization of acacia bark proanthocyanidins. *J. Nat. Prod.* **2011**, *74*, 119–128. [CrossRef] [PubMed]

36. Bautista-Ortin, A.; Molero, N.; Marín, F.; Ruiz-García, Y.; Gómez-Plaza, E. Reactivity of pure and commercial grape skin tannins with cell wall material. *Eur. Food Res. Technol.* **2015**, *240*, 645–654. [CrossRef]

37. Tanaka, T.; Takahashi, R.; Kouno, I.; Nonaka, G. Chemical evidence for the de-astringency (insolubilization of tannins) of persimmon fruit. *J. Chem. Soc. Perkin Trans. 1* **1994**, 3013–3022. [CrossRef]

38. Tanaka, T.; Kondou, K.; Kouno, I. Oxidation and epimerization of epigallocatechin in banana fruits. *Phytochemistry* **2000**, *53*, 311–316. [CrossRef]

39. Steynberg, J.; Brandt, E.; Hoffman, M.; Ferreira, D. Conformations of proanthocyanidins. In *Plant Polyphenols-Synthesis, Properties, Significance*; Hemingway, R., Laks, P.E., Eds.; Plenum Press: New York, NY, USA, 1992; pp. 501–519, ISBN 978-1-4615-3476-1.

40. Slade, D.; Ferreira, D.; Marais, J.P.J. Circular dichroism, a powerful tool for the assessment of absolute configuration of flavonoids. *Phytochemistry* **2005**, *66*, 2177–2215. [CrossRef] [PubMed]

41. Esatbeyoglu, T.; Jaschok-Kentner, B.; Wray, V.; Winterhalter, P. Structure elucidation of proanthocyanidin oligomers by low-temperature ^{1}H NMR spectroscopy. *J. Agric. Food Chem.* **2011**, *59*, 62–69. [CrossRef] [PubMed]

42. Nam, J.W.; Phansaklar, R.S.; Lankin, D.C.; McAlpine, J.B.; Leme-Kraus, A.A.; Vidal, C.M.; Gan, L.S.; Bedran-Russo, A.; Chen, S.N.; Pauli, G.F. Absolute configuration of native oligomeric proanthocyanidins with dentin biomodification potency. *J. Org. Chem.* **2017**, *82*, 1316–1329. [CrossRef] [PubMed]

43. Barrett, M.; Klyne, W.; Scopes, P.; Fletcher, A.; Porter, L.; Haslam, E. Plant proanthocyanidins. Part 6. Chiroptical studies. Part 95. Circular dichroism of procyanidins. *J. Chem. Soc. Perkin Trans. 1* **1979**, 2375–2377. [CrossRef]

44. Yu, R.J.; Liu, H.B.; Yu, Y.; Liang, L.; Xu, R.; Liang, C.; Tang, J.S.; Yao, X.S. Anticancer activities of proanthocyanidins from the plant *Urceola huaitingii* and their synergistic effects in combination with chemotherapeutics. *Fitoterapia* **2016**, *112*, 175–182. [CrossRef] [PubMed]

45. Burger, J.; Kolodziej, H.; Hemingway, R.; Steynberg, J.; Young, D.; Ferreira, D. Oligomeric flavonoids. Part 15a. Base-catalyzed pyran rearrangements of procyanidin B-2, and evidence for the oxidative transformation of B- to A-type procyanidins. *Tetrahedron* **1990**, *46*, 5733–5740. [CrossRef]

46. Koerner, J.; Hsu, V.; Lee, J.K. Determination of proanthocyanidin A2 content in phenolic polymer isolates by reversed-phase high-performance liquid chromatography. *J. Chromatogr. A* **2009**, *1216*, 1403–1409. [CrossRef] [PubMed]

47. Cronjé, A.; Burger, J.; Brandt, E.; Kolodziej, H.; Ferreira, D. Assessment of 3,4-*trans* and 3,4-*cis* relative configurations in the A-series of 4,8-linked proanthocyanidins. *Tetrahedron Lett.* **1990**, *31*, 3789–3792. [CrossRef]

48. Frisch, M.J.; Trucks, G.W.; Schlegel, H.B.; Scuseria, G.E.; Robb, M.A.; Cheeseman, J.R.; Scalmani, G.; Barone, V.; Mennucci, B.; Petersson, G.A.; et al. *Gaussian 09, Revision D.01*; Gaussian, Inc.: Wallingford, CT, USA, 2013.

Sample Availability: Samples of compounds **1**–**18** are all available from the authors.

Relationships between Structures of Condensed Tannins from Texas Legumes and Methane Production During In Vitro Rumen Digestion

Harley Naumann [1], Rebecka Sepela [2], Aira Rezaire [2], Sonia E. Masih [2], Wayne E. Zeller [3], Laurie A. Reinhardt [3], Jamison T. Robe [3], Michael L. Sullivan [3] and Ann E. Hagerman [2,*]

[1] Division of Plant Sciences, University of Missouri, 110 Waters, Columbia, MO 65211, USA; naumannhd@missouri.edu

[2] Department of Chemistry & Biochemistry, Miami University, Oxford, OH 45056, USA; rjsepela@ucdavis.edu (R.S.); aira.rezaire@gmail.com (A.R.); masihse@miamioh.edu (S.E.M.)

[3] USDA-ARS, U.S. Dairy Forage Research Center, Madison, WI 53706, USA; wayne.zeller@ars.usda.gov (W.E.Z.); laurie.reinhardt@ars.usda.gov (L.A.R.); jamison.robe@ars.usda.gov (J.T.R.); michael.sullivan@ars.usda.gov (M.L.S.)

* Correspondence: hagermae@miamioh.edu; Tel.: +1-513-529-2827

check for updates

Abstract: Previous studies showed that a series of purified condensed tannins (CTs) from warm-season perennial legumes exhibited high variability in their modulation of methane production during in vitro rumen digestion. The molecular weight differences between these CTs did not provide correlation with either the in vitro CH_4 production or the ability to precipitate bovine serum albumin. In an effort to delineate other structure-activity relationships from these methane abatement experiments, the structures of purified CTs from these legumes were assessed with a combination of methanolysis, quantitative thiolysis, ^{1}H-^{13}C HSQC NMR spectroscopy and ultrahigh-resolution MALDI-TOF MS. The composition of these CTs is very diverse: procyanidin/prodelphinidin (PC/PD) ratios ranged from 98/2 to 2/98; cis/trans ratios ranged from 98/2 to 34/66; mean degrees of polymerization ranged from 6 to 39; and % galloylation ranged from 0 to 75%. No strong correlation was observed between methane production and the protein precipitation capabilities of the CT towards three different proteins (BSA, lysozyme, and alfalfa leaf protein) at ruminal pH. However, a strong non-linear correlation was observed for the inhibition of methane production versus the antioxidant activity in plant sample containing typical PC- and PD-type CTs. The modulation of methane production could not be correlated to the CT structure (PC/PD or cis/trans ratios and extent of galloylation). The most active plant in methane abatement was *Acacia angustissima*, which contained CT, presenting an unusual challenge as it was resistant to standard thiolytic degradation conditions and exhibited an atypical set of cross-peak signals in the 2D NMR. The MALDI analysis supported a 5-deoxy flavan-3-ol-based structure for the CT from this plant.

Keywords: proanthocyanidins; condensed tannins; thiolysis; NMR spectroscopy; ultrahigh-resolution negative mode MALDI-TOF mass spectrometry; antioxidant; ORAC assay; *Acacia*; forage legume

1. Introduction

Condensed tannins (CTs, proanthocyanidins) consist of oligomers and polymers of flavan-3-ol subunits. Variations in hydroxylation patterns, *cis*- and *trans*-configuration of C-ring substituents, interflavan bond connections, mean degree of polymerization (mDP), and extent of esterification have been described for natural condensed tannins from various plants [1] (Figure 1).
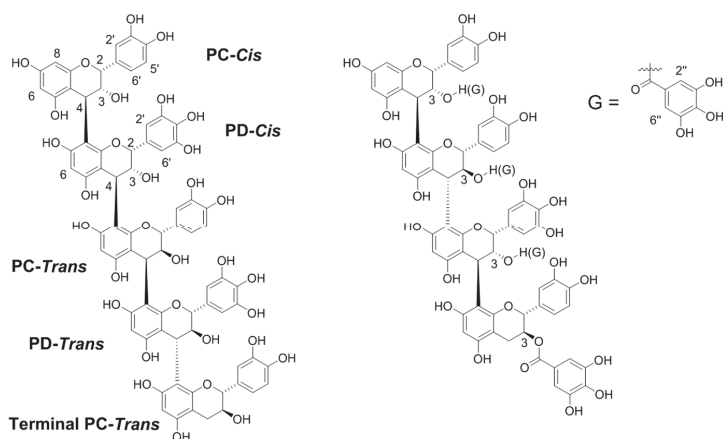
Figure 1. Common representation of condensed tannin structures. Left structure: PC = procyanidin; catechin (*trans* isomer) or epicatechin (*cis* isomer). PD = Prodelphinidin; gallocatechin (*trans* isomer) or epigallocatechin (*cis* isomer). In addition, hydroxyl groups, particularly on the C-3 hydroxyl, may be esterified with a galloyl (G) group (structure on the right). Carbons 2, 3, and 4 of the C ring, 2′ and 6′ of the B ring, 6 and 8 of the A ring, and 2″ and 6″ of the D ring are labeled.

Condensed tannins in human foods and beverages, including berries, cocoa, and wine, have been described in detail [2] but less is known about the CTs found in natural forages. Early studies on tannin-rich forages focused on diminished nitrogen utilization associated with protein binding by tannins during digestion [3] but more recent studies have revealed beneficial effects of tannins on domestic ruminants. For example, consumption of CT-containing feedstuffs can protect forage/microbial-generated protein during digestion and result in higher nitrogen utilization [4], improved meat and milk quality [5] and increased wool production [6]. Additional biological effects associated with CT-rich feeds include the mitigation of intestinal nematode proliferation [7], and the reduction in the incident of bloat [8] and abatement of methane production during digestion [9]. Ruminant animals contribute significantly to the production of methane during rumination and this greenhouse gas contributes to the increase of global temperatures [10]. Production of methane translates into lost energy which can negatively affect ruminant productivity [11], so identification of feeds that reduce methane production is economically favorable as well as environmentally beneficial.

Tannin-rich plants diminish ruminal methane production both in vitro [12,13] and in vivo [14–16]. Adding crude tannin to tannin-free forage also reduces methane production [17,18]. Notably, meta-analysis of the effects of tannin on methane production identified a significant relationship between level of tannin and methane production [9]. This analysis suggested that there is a broad-based tannin effect on methane production since studies that used both hydrolyzable and condensed tannins were included in the dataset. The authors noted that supplementing a diet with exogenous tannin may not be as effective as supplying a tannin-containing feed, presumably because the tannin is released at different rates and in different forms from natural vs. amended feeds. It is important to develop models that predict the relationship between tannin content of feeds and methane production because high levels of tannin in the diet can be detrimental to the animals [19]. Furthermore, the costs of detoxifying tannin and other natural products can outweigh the economic benefits of reducing methanogenesis [20]. Attempts to develop models have had limited success to date due to lack of data linking chemical details to bioactivity [21,22].

Although both hydrolyzable and condensed tannins appear to have a role in limiting methane production during rumination, the current study is focused only on CTs because of their widespread distribution among forages suitable for domestic ruminants [8]. Most of the studies to date provide limited dose-response information, and almost no information on tannin structure or chemical properties. In one

quantitative in vitro study that examined a variety of CT-rich species, Naumann et al. showed that total condensed tannins vs. methane production gave a correlation of $R^2 = 0.44$, suggesting that only 44% of the reduction in methane production is explained by total CT [23]. Other authors have proposed tentative relationships between methane production and CT structural features such as the degree of hydroxylation of the B ring, the *cis/trans* isomer ratio, or the molecular weight of the CT [24–27], but a strong predictive model has not been developed.

Tannins have several potent bioactivities that could be responsible for their role in ruminant nutrition. In addition to their well-known role as protein precipitating/binding agents [28], tannins are antioxidants [29]. Relatively few studies have attempted to correlate tannin bioactivity with suppression of methane production, although weak relationships between protein binding activity and methanogenesis have been reported in a few systems [30,31]. Studies correlating antioxidant activity of polyphenols to methane production have not been published to date.

In this study, we explore the role of CT structure on methane production in a model rumen system using a collection of CT-rich dryland legume species (Table 1) that have a range of abilities to diminish methane production in an in vitro model rumen [23]. We used several methods to evaluate the tannin structure, including degradation to anthocyanidins, quantitative thiolysis, ultrahigh-resolution negative mode MALDI-TOF MS, and 2D NMR spectroscopy of purified CTs from these legumes. We used the oxygen radical absorbance capacity test (ORAC) method to establish the antioxidant activity of each isolated CT [32] and correlated that activity to the methane production data from earlier studies [23]. We extended protein precipitation studies with CTs in this series of forage legumes to include not only bovine serum albumin, but also lysozyme and alfalfa leaf protein with assays conducted at ruminal pH.

Table 1. Dry land Texas legumes (*Fabaceae*) used in this study.

Plant	Subfamily	Subtribe	λ_{max} in HCl-Methanol (nm)	Methane Production [1] (g/kg DM)
Desmodium paniculatum	Papilionoideae	-	543	7.9
Lespedeza stuevei	Papilionoideae	-	543	4.9
Lespedeza cuneata	Papilionoideae	-	547	15.1
Mimosa strigillosa	Mimosoideae	Mimoseae	547	7.6
Desmanthus illinoensis	Mimosoideae	Mimoseae	547	24.9
Neptunia lutea	Mimosoideae	Mimoseae	547	19.7
Leucaena retusa	Mimosoideae	Mimoseae	538	40.7
Acacia angustissima STP5	Mimosoideae	Acacieae	508	0.6
Acacia angustissima STX	Mimosoideae	Acacieae	505	0.8

[1] Data from in vitro fermentations, in g methane per kg dry matter (DM) [23].

2. Results

2.1. Degradative and NMR Analysis of Purified CTs

Table 1 contains data from the acidic methanolysis to yield anthocyanidins, a classic method for estimating the composition of condensed tannins [33]. The λ_{max} of the mixture of reaction products provides general information about the predominance of subunits yielding delphinidin (λ_{max} 548 nm), cyanidin (λ_{max} 538 nm) or other anthocyanidins. For typical CT, acid methanolysis breaks the interflavan bond and any ester bonds, so that cyanidin is produced from catechin, epicatechin, and (epi)catechin gallate extender units while delphinidin is produced from (epi)gallocatechin and (epi)gallocatechin gallate [34]. The CT from these plants is categorized as prodelphinidin (PD) (*Lespedeza cuneata, Mimosa, Desmanthus, Neptunia*), procyanidin (PC) (*Leucaena*), or mixed (λ_{max} intermediate between 548 nm and 538 nm) (*Desmodium, Lespedeza stuevei*) (Table 1). The CT from *Acacia* was neither PC- nor PD-based, but produced small amounts of an anthocyanidin with λ_{max} typical of guibourtinidin, a 5-deoxy anthocyanidin (Table 1).

Thiolysis is a degradative method of analysis that provides more structural detail than acid methanolysis (Tables 2 and S1). The data provide quantitative procyanidin:prodelphinidin (PC/PD) ratios [25] that complement and extend the methanolysis results. The CTs identified as PD by methanolysis contain less than 15% of the cyanidin-type subunits, while the PC from *Leucaena* contains < 2% delphinidin-type units (Table 2). The mixed CTs (*Desmodium*, *Lespedeza stuevei*) contain similar amounts of both subunits (Table 2).

Table 2. Comparison of structural information obtained from thiolysis and ^{1}H-^{13}C HSQC NMR.

Plant Sample	PC/PD Ratio		cis/trans			% Galloyl			mDP	
	Thiol	NMR	Thiol	NMR H/C-4	NMR H/C-2	Thiol	NMR H/C-4	NMR H/C-2′,5′	Thiol	NMR
Desmodium paniculatum	55/45	52.5/47.5	90/10	87.8/12.2	84.2/15.8	None	None	None	18.6	ND [1]
Lespedeza stuevei	42/58	41.4/58.6	44/56	34.8/65.2	33.9/66.1	3	2.4	1.0	9.3	6.7
Lespedeza cuneata	8/92	4.3/95.7	80/20	82.1/17.9	75.4/24.6	None	ND [2]	5.3	10.6	9.1
Mimosa strigillosa	15/85	15.3/84.7	89/11	ND [3]	ND [4]	40	50.8	ND [5]	7.6	6.1
Desmanthus illinoensis	3/97	1.8/98.2	98/2	ND [3]	96.2/3.8	75	76.2	87.5	6.0	5.97
Neptunia lutea	12/88	8.2/91.8	93/7	ND [3]	91.5/8.5	32	34.4	25.6	11.5	8.1
Leucaena retusa	99/1	98.6/1.4	98/2	ND [3]	ND [4]	29	21.3	34.3	39.2	6.3

ND, not determined. [1] Low signal to noise ratio on terminal C-H cross-peak signal. [2] Low signal to noise ratio for H/C-4 cross-peak signal. [3] Due to galloylation of the CT sample, *cis/trans* assignments become ambiguous using H/C-4 cross-peaks. [4] Low signal to noise ratio for the *trans* H/C-2 cross-peak signal. [5] Integration of peaks indicated > 100 mol % galloylation.

The thiol products retain the original stereochemistry at C2 and C3, so *cis/trans* ratios for the CT can be calculated from thiolysis data. For these plants, *cis* stereochemistry (epicatechin pattern) is dominant (Table 2). Furthermore, thiolysis does not cleave the gallate ester bond so % galloylation can be determined from thiolysis data [34]. A predominance of the CT subunits are galloylated in the CT from *Desmanthus* while there are essentially no galloyl esters in *Desmodium* or the two *Lespedeza* species (Table 2).

Previous studies have shown that significant CT structural information (PC/PD and *cis/trans* ratios) can be obtained through integration of corresponding cross-peaks (Tables S4 and S5) in the ^{1}H-^{13}C HSQC NMR spectra of purified CT samples and highly corroborate results obtained via thiolytic degradation [35]. Analysis of the ^{1}H-^{13}C HSQC NMR spectra for these CTs showed that all the samples were of high purity indicated by the absence of significant non-CT component cross-peaks (Figures S1–S7). Detailed analysis of the information derived from ^{1}H-^{13}C HSQC NMR spectra is provided in the supplemental section (Tables S4 and S5, Figures S1–S9).

For the most part, the structural information obtained from thiolysis and NMR was very consistent. For PC:PD ratios, thiolytic and ^{1}H-^{13}C HSQC NMR analyses were no more than 4% different (Table 2). The *cis/trans* ratios were consistent within 10% (Table 2), and the % galloylation was consistent within 15%.

The mean degree of polymerization (mDP) for CT can be estimated through integration of the cross-peak volumes in NMR or from the peak area ratios for the extender and terminal units from thiolysis (Table 2). The two methods proved to be very consistent for all of the plants, except *Leucaena* (Table 2). In general, the CT from the plants in this study had mDP ranging from about 6 (*Desmanthus*) to about 20 (*Desmodium*). *Leucaena* was an exception, with a very high mDP (39) estimated by thiolysis, although NMR suggested a more typical mDP of about 6. The thiolysis data can overestimate mDP if the terminal units are heterogeneous leading to underestimation of some minor terminal units, but close inspection of the chromatograms from *Leucaena* did not provide any indication of minor terminal units. If the tannin preparation is contaminated with monomeric flavan-3-ols, the thioloysis method can underestimate mDP, but we eliminate this potential problem by running control samples of unthiolyzed tannin that reveal the presence of free flavan-3-ols. Similar to thiolysis, the NMR method does not always provide a useful measure of mDP. In some cases, the cross-peak signals of the terminal methylene C-H bonds suffer from low signal-to-noise ratios, increasing inherent error in mDP determination as mDP values increase. In these cases, no estimate of mDP was made based on

2D NMR data (*Desmodium*, Figure S1). In other cases, the signal arising from the terminal methylene C-H bonds is disrupted by the neighboring solvent (DMSO) peak, as exemplified by the spectrum for *Lespedeza cuneata* (Figure S3). In this case, we integrated the unperturbed, more downfield cross-peaks, and adjusted the formula for the mDP calculation to account for this modification.

The tannin from *Acacia* could not be analyzed by thiolysis. The reaction product chromatograms were dominated by a large peak characteristic of undegraded tannin, indicating that the reaction conditions are not sufficiently vigorous to degrade this CT. We tentatively concluded that the *Acacia* CT mainly comprises 5-deoxy flavan-3-ols (robinetinidol, fisetinidol, and/or guibourtinidol), based on the acid methanolysis data and the resistance of the *Acacia* CT to degradation [36–38]. This conclusion is supported by the 2D NMR spectral data. First, the H/C-6/8 set of cross-peaks arising from the A-ring of PC and PD subunits has a diminished presence relative to other NMR cross-peaks indicating that the phloroglucinol substitution pattern of the A-ring is not present to an appreciable extent. Second, cross-peaks typically assigned to a *para*-substitued phenolic B-ring, appear at 6.4/128 ppm in the NMR spectra of the *Acacia* CTs, indicating the guibourtinidol or afzelechin subunit substitution pattern. Lastly, the H/C-4 cross-peaks arising from extender subunits of the CT appear at chemical shifts that do not coincide with those of CTs composed of PC/PD subunits. In addition, the 2D NMR spectra exhibited a series of unusual and previously undocumented cross-peak signals, with the most unusual peaks found in the region where aliphatic signals, such as alpha carbonyl or allylic C-H, are usually observed (Figures S8 and S9). This may be due to an alkyl modification of the general CT structure. These cross-peaks are present even after multiple isolation and sequential purification attempts, so we believe that they do not arise from impurities co-eluting during the purification steps.

2.2. MALDI-TOF Mass Spectrometric Analysis

MALDI-TOF MS has been widely used to assess the composition of high molecular weight CTs with complex structural subunits [39,40]. In most previous studies, the data were collected in the positive ion mode using lower resolution instruments, and interpretation relied on finding intervals in the spectra characteristic of different types of subunits. An interval of 288 indicates (epi)catechin subunits (PC) while an interval of 304 is characteristic of (epi)gallocatechin subunits (PD) [40]. For the plants in this study, the intervals in the spectra (Figure 2, Table 3) confirm the CT compositions obtained by thiolysis and NMR. For example, the spectrum of *Desmanthus* is dominated by intervals of 304 and 152 mass units, consistent with the highly galloylated PD-type tannin identified by thiolysis and NMR. In addition to the major intervals, clusters of peaks separated by intervals of 16 mass units are clearly seen in each spectrum, consistent with different degrees of hydroxylation (catechin vs. gallocatechin, etc.). Although PC and PD subunits are easily distinguished by mass spectrometry, stereochemical differences are not detected so MALDI cannot be used to calculate the *cis*/*trans* ratios or other stereochemical features of CT.

Table 3. Interval between clusters of peaks in MALDI spectra [1].

Flavan-3-ol 5-Deoxy Flavan-3-ol Plant Sample	- Guibourtinidol 256.07	(Epi)afzelechin Fisetinidol 272.07	(Epi)catechin Robinetinidol 288.06	Epi(gallocatechin) - 304.06	Gallate Ester 152.01
Desmodium paniculatum	-	-	++	++	-
Lespedeza stuevei	-	-	++	++	+
Lespedeza cuneata	-	-	+	++	-
Desmanthus illinoensis	-	-	+	++	++
Neptunia lutea	-	+	+	++	+
Leucaena retusa	-	-	++	-	+
Acacia angustissima [2]	+	++	+	-	+

[1] CT from *Mimosa strigillosa* was not available when the analysis was performed. [2] Both ecotypes of *Acacia* had the same peaks on MALDI-MS.

Interpretation of positive ion mode MS data can be complicated by the ambiguity of protonated vs. metallated (Na^+, K^+) forms of the analyte [41,42]. In this study, we used Fourier transform ion

cyclotron resonance (FT-ICR) ultrahigh-resolution negative ion MALDI-TOF MS analysis, which not only eliminates the ambiguity of the cation species but also provides absolute identification of subunit composition by exact mass (Table 4). For example, *Desmanthus* CT comprises molecules with up to one gallate per flavan-3-ol subunit while *Neptunia* CT had only 0.2 gallate per favan-3-ol (Table 4). Unlike thiolysis or NMR, MALDI does not provide an accurate DP for the polymers, because ionization of higher molecular weight species is less efficient than that of smaller molecules. For the CT in this study, signals in the 3000 (DP ~10) to 4000 (DP ~14) were easily detected for all the plants except *Acacia*. For example, the predicted mean molecular weight of *Desmanthus* CT (mDP 6) is about 2500, consistent with the pattern of strong MALDI signals between 500 and 4000 mass units (Figure 2). The MALDI data for *Leucaena* has a peak distribution from about 500 to 4000 mass units similar to that of *Desmanthus*, suggesting the NMR estimate of mDP 6 is more accurate than the thiolysis estimate of mDP 39 for this CT (Table 2).

The ultrahigh-resolution MALDI-TOF data were particularly useful for the *Acacia* CT that was resistant to analysis by NMR or thiolysis. Intervals of 272 and 152 dominated the spectrum for this CT, consistent with a structure based on the 5-deoxy flavan-3-ol fisetinidol with a moderate degree of galloylation (Figure 2, Table 3). Using exact masses we identified CT fragments comprised of fisetinidol and small amounts of guibourtinidol with gallate esters (Table 4). Thus, the MALDI analysis is consistent with the hypothesis that the unique CT of *Acacia* is a 5-deoxy CT.
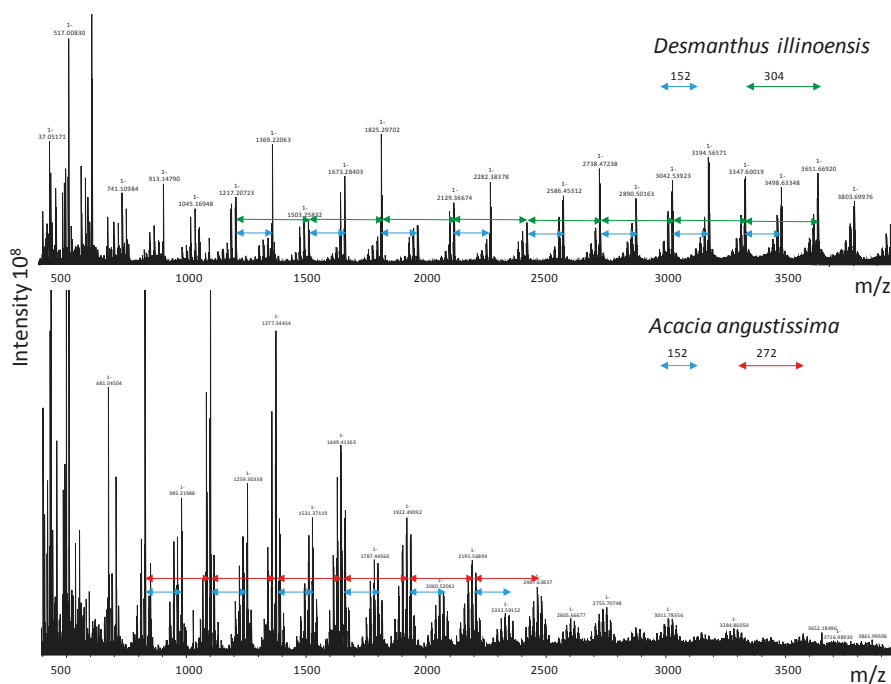
Figure 2. Representative ultrahigh resolution negative mode MALDI-MS data for CT. The top spectrum was obtained with CT from *Desmanthus illinoensis* and the bottom spectrum with CT from *Acacia angustissima*. The mass intervals between the clusters of peaks represent the characteristic subunits for the CT, with an interval of 304 typical of (epi)gallocatechin, an interval of 272 typical of fisetinidol, and an interval of 152 typical of gallate ester modification.

Table 4. Selected MALDI signals and their exact assignments. The polymers comprise the flavan-3-ol subunits (epi)catechin (cat), (epi)gallocatechin (gallocat); the 5-deoxy flavan-3-ol subunits guibourtinidol (gui), fisetinidol (fis) and, in some cases, gallate esters (gallate) [1].

Plant Sample	Observed Mass	Formula	Exact Mass	Error (ppm)	Interpretation
Desmodium paniculatum	2065.43585	$C_{105}H_{85}O_{45}$	2065.43630	0.22	cat_4-$gallocat_3$
Lespedeza stuevei	1473.31433	$C_{75}H_{61}O_{32}$	1473.31461	0.19	cat_3-$gallocat_2$
Lespedeza cuneata	1825.36676	$C_{90}H_{73}O_{42}$	1825.35766	4.99	$gallocat_6$
Desmanthus illinoensis	1369.22063	$C_{66}H_{49}O_{33}$	1369.21562	3.66	$gallocat_3$-$gallate_3$
Neptunia lutea	3025.55520	$C_{135}H_{125}O_{80}$	3025.55958	1.45	cat-$gallocat_8$-$gallate_2$
Leucaena retusa	1745.34814	$C_{89}H_{69}O_{38}$	1745.34670	0.83	cat_5-$gallate_2$
Acacia angustissima [2]	1241.29289	$C_{67}H_{53}O_{24}$	1241.29269	0.17	cat-gui-fis_2-gallate

[1] CT from *Mimosa strigillosa* was not available when the analysis was performed. [2] Both ecotypes of *Acacia* had the same peaks on MALDI-MS.

2.3. Antioxidant Activity

The ORAC method estimates the hydrogen atom transfer (HAT) potential of the putative antioxidant [43] by comparing the activity of the material to the well-known standard antioxidant Trolox [32]. For this set of plants, Trolox equivalents (TE) per g of CT ranged from 0.3 TE/g (*Neptunia*) to 1.5 TE/g (*Desmodium*) (Table S2). We excluded the poorly characterized *Acacia* CT from the analysis and attempted to correlate the molecular features of the CT (PC:PD ratio, % trans, % galloyl, mDP) to the antioxidant activity. Although previous studies found that galloylation increased the antioxidant activity of flavan-3-ols [44], we did not find strong relationships between any structural feature and antioxidant activity for these CT (Supplemental Files). Although there were no correlations between CT structure and antioxidant activity, there was a strong nonlinear correlation ($R^2 = 0.90$) between antioxidant activity (TE per g of plant tissue) and methane production (g CH_4 per kg of plant tissue) when the *Acacia* CT was excluded (Figure 3). The *Acacia* is exceptional because it is a very effective inhibitor of methane production despite its moderate antioxidant activity (Figure 3).
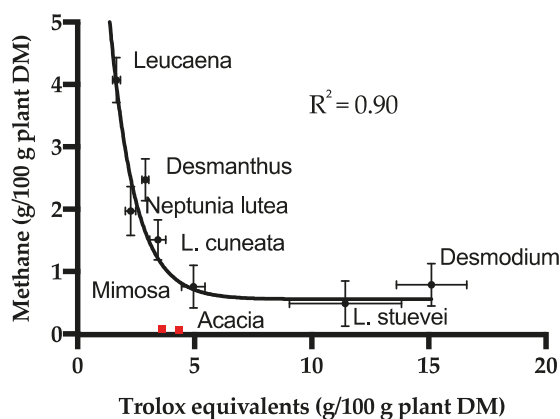
Figure 3. Relationship between methane production [23] and antioxidant activity for the forages. The non-linear exponential fit ($Y = 11.64(\exp(-0.772X)) + 0.6433$) does not include the *Acacia* CT data (red markers). The points are average for the ORAC method ($n = 3$) and the in vitro gas production ($n = 3$) and the error bars indicate standard deviations.

2.4. Protein Precipitation Activity

In previous studies, we examined the protein precipitation capabilities of the purified CTs from Texas legumes using bovine serum albumin (BSA) in acetate buffer at pH 4.9 [45], and found no relationship between precipitation, CT molecular weight, and methane abatement. To determine whether the use of the

model protein BSA biased this conclusion, we performed additional protein precipitation assays using model proteins, lysozyme, and alfalfa leaf protein at pH 6.5 (rumen pH) [46] (Figure S10a–f, Table S3). We did not find a clear correlation of the protein precipitation capacity and the level of methane inhibition (Figure S11a–f). Thus, we conclude that the ability of the CT to precipitate forage protein is not a major driving force relative to the inhibition of methane production.

In our analysis we compared methane production during in vitro digestion of intact tissue to chemical characteristics of extracted, soluble CT. Plant tissue may contain insoluble and cell wall-bound CT and other chemical (e.g., alkaloids) and physiochemical (e.g., lignified cell walls) attributes unrelated to CT content. Our correlation analysis can provide insights into possible mechanisms of methane abatement but does not provide proof of activity for the components tested. Earlier workers have noted that natural feeds more effectively inhibit methane production than tannin-amended feeds [9], suggesting that features of the intact tissue help to inhibit excess methanogenesis.

3. Discussion

3.1. Methods to Determine CT Structure

The three high-resolution methods were used to establish CT structure. Data obtained from the three methods were complementary and yielded very consistent results. Each method has strengths and weaknesses. Thiolysis is the most accessible of the methods, since HPLC with DAD is highly available and the chemical degradation method is simple. Thiolysis is very sensitive, requiring only a few milligrams of sample. It can be carried out on purified CT, unpurified CT extracts, or directly on plant tissue [47], making it particularly useful for screening plant collections. Unfortunately, a commercial library of standards is not available, making it necessary for individual laboratories to use methods such as HPLC-MS and published CT compositions to develop an internal library. Thiolytic analysis has traditionally been limited to B-type CT with 4- > 8 or 4- > 6 interflavan bonds [48], but has recently been modified to analyze A-type crosslinked CT [49]. Thiolysis is not useful for the chemically-resistant 5-deoxy CT [37], such as the *Acacia* CT in this study.

NMR spectroscopy is particularly useful because it is nondestructive and not dependent on derivatization. Samples can be recovered after analysis, and the method does not suffer from potential differences in the rates of derivatization among substrates or the production of side-products under derivatization conditions. CT samples must be reasonably pure (>70%) to avoid inclusion of overlapping cross-peaks from non-CT components interfering with integration values. The relative purity of sample can be rapidly assessed by the observations of presence or absence of non-CT cross-peaks, providing a definite advantage over both thiolysis and MALDI-TOF analyses. In cases where the measurement of a minor component present is desired, small signal-to-noise ratios of the cross-peaks of minor components undergoing analysis can lead to increasing the inherent error in the measurement. Both ^{13}C and ^{1}H-^{13}C HSQC NMR experiments require several hours or overnight acquisitions which limits access on multi-user instruments. NMR techniques are not as sensitive as thiolysis and mass spectrometry and require more sample for analysis on common instruments.

MALDI-TOF analysis is generally available only through a mass spectrometry facility, making it less accessible than thiolytic degradation. Positive-mode MALDI-TOF MS has been used in several other studies of CT structure to confirm data from other analytical methods [40,42]. Here, we used ultrahigh-resolution (15T Bruker SolariXR FT-ICR, Bruker Corp., Billerica, MA, USA) negative-mode MALDI MS and were able to confirm details of CT chemical formulae that were previously inaccessible. The ultrahigh resolution of the MALDI analysis allowed us to assign exact structures to the peaks noted in the spectra. For example, we calculated the stoichiometric ratio for ester groups on the galloylated CTs from the exact structures established by MALDI analysis. The 1:1 galloyl:flavan-3-ol ratio typical of species in the highly-modified *Desmanthus* CT is much larger than the ratios (0.2:1, 0.4:1) obtained for the less highly esterified CT from *Neptunia* or *Leucaena*. For each species, the galloyl:flavan-3-ol ratio from the exact structure is consistent with the % galloyl determined by thiolysis or NMR (Tables 2

and 4). Similarly, the PC/PD ratios determined by thiolysis or NMR reflect the exact structures determined by MALDI, as illustrated by the cat$_4$-gallocat$_5$ exact structure identified in *Desmodium* CT, which has a PC:PD ratio of about 55:45 (Tables 2 and 4).

Most importantly, MALDI analysis of the *Acacia* CT allowed us to establish structural information that was not available from thiolysis or NMR. The *Acacia* tannin is structurally diverse, with three types of subunits and a stoichiometric ratio of one galloyl ester per four flavan-3-ols corresponding to 25% galloylation (Table 4). As suggested by its recalcitrance to thiolysis, most of the subunits in the *Acacia* CT are 5-deoxy flavan-3-ols, but the individual structures identified from the exact mass data suggested that catechin was always the terminal unit of the 5-deoxy CTs.

Based on this direct comparison of methods to determine structures of CT, we conclude that thiolysis and NMR provide very similar information but that MALDI FT-ICR MS provides unique structural information about these complex natural products. While thiolysis and NMR yield quantitative composition and unambiguous stereochemical assignments based on bulk CT properties, ultrahigh resolution MALDI can be used to assign structures of specific molecular species. It is still not possible to purify CT to single molecular species, but, as demonstrated here, the pure polydisperse mixtures of CT purified by Sephadex LH-20 chromatography [50] can be described in detail using a combination of chemical and spectroscopic tools. Thiolysis and NMR provide information about average degree of polymerization of CT, but methods for obtaining more accurate information about molecular size and heterodispersity of CT are needed to further advance our knowledge of CT structure.

3.2. Chemotaxonomy

The legumes (family Fabaceae) analyzed here represent three taxonomic groupings [51] (Table 1). Similarities in secondary chemistry are often found within taxonomic groups, reflecting genetic similarities in enzymology and metabolic regulation [52]. Chemotaxonomic trends have previously been noted for polyphenols including flavonoids and tannins [47,53,54]. In this study, the CT from plants in the subfamily Papilionoideae are not galloylated, while CT from the Mimosoidae contain > 20% galloylation (Tables 2 and 4). Plants from the Papilionoideae are more likely to have mixed PC/PD, while Mimosoidae are more likely to have PD-type CT. Interestingly, *Lespedeza cuneata*, which has PD-type CT, is quite distinct from the closely related species *Lespedeza stuevei* or *Desmodium*, which contain mixed PC/PD CT (Tables 1 and 2).

Acacia is distinguished taxonomically from the other Mimosoidae (Table 1) and is also chemically distinct. *Acacia* CT is unique compared to the other plants in our set because of it is predominantly comprised of 5-deoxy flavan-3-ol subunits (Tables 3 and 4, Figure 2). The widespread occurrence of 5-deoxy flavonoid derivatives in *Acacia* was reported in many early surveys of the genus [51], and more recent studies have reported 5-deoxy CTs in *A. mangium* and *A. mearnsii* bark extracts [55,56]. One conflicting report found that CTs from leaves of *A. karroo* and *A. grandicornuta* were simple prodelphinidins or procyanidins, respectively, with no 5-deoxy-type subunits [57]. Our new structural analysis provides key information for the polyphenols from this important group of plants. In particular, the MALDI analysis shows that the CT is predominantly profistetinidin-based, with 25% galloylation. The *Acacia* CT does contain catechin units, which may serve as the terminal units of the 5-deoxy flavan-3-ol polymers. New methods of NMR and HSQC analysis that utilize phosphate-labeled CT offer promise for providing additional details about the structure of *Acacia angustissima* foliage CT [58].

3.3. Methane Abatement

Many studies have demonstrated that forage plants with diverse natural products decrease gas production by ruminants, including methane emissions [59]. Previous studies have identified *Mimosa* spp. and *Acacia mearnsii* as tannin-rich legumes that decrease methane production, but mechanisms of action have not been established [15,19,60]. Biological activities of tannins are often attributed to their characteristic ability to bind and precipitate protein, but our data suggest that the ability of the CT to

precipitate forage protein is not directly related to the inhibition of methane production. For the plants studied here there is a strong nonlinear correlation between radical quenching activity and methane production, suggesting that CT, or other antioxidants contained in the forages may affect rumen microbial populations and their ability to carry out redox chemistry required for methane production.

The CT from the plants in this study that were most effective at reducing methane production in vitro (*Desmodium, Lespedeza stuevei, Mimosa, Acacia*) do not have any single common functional or structural feature. Condensed tannins from two of the plants that reduced methane production, *Desmodium* and *Lespedeza stuevei*, have similar compositions. Both CT have mixed PC and PD composition and trace levels of galloylation, features not previously identified as important in the context of methanogenesis. Earlier proposals that higher molecular weight CTs more effectively inhibit methane production were based on work with CT with apparent chain lengths ranging from about 15 to 70 [25]. It is difficult to compare that work to our CT with chain lengths from 6 to 20, although *Desmodium* CT (mDP 20) had high methane abatement activity. *Leucaena* had a very high mDP based on thiolysis data, but a much lower mDP based on NMR and MALDI analysis, and had little effect on methane production.

Mimosa CT is predominantly PD, has a moderate chain length, and an intermediate level of galloylation. Several earlier studies have noted a relationship between PD-type CT and diminished methane production [24,26]. The trihydroxy substitution pattern of PD-type tannins may confer particular reactivity that disrupts methanogenesis.

In our work, *Acacia* stands out for its high potential to abate methane production (Table 1) [23]. Based on the structural data obtained so far, we propose that the activity of *Acacia* CT in the rumen is at least in part a consequence of its chemical structure and characteristics. The interflavan bond in a typical CT is susceptible to attack because the 5-hydroxyl group adjacent to the bond is able to electronically contribute to the stabilization of the transient cation/quinone methide intermediate arising from acid catalyzed interflavan bond cleavage. CT comprised of 5-deoxy flavan-3-ol subunits lack this hydroxyl group and are less chemically susceptible to acid-catalyzed interflavan bond cleavage than typical CT [37]. We suggest that, relative to PC/PD CTs, *Acacia angustissima* tannins may have an unusually long lifetime in the rumen because of their chemical stability. A priority for future research is a more detailed determination of the structure of the *Acacia* CT and tests of its chemical stability under rumen conditions. Persistent, long-lived CT in the rumen may serve as a selective toxin that eliminates methanogens [61,62]. In addition to direct toxicity, the metal binding activity of tannins [7,63] could alter the availability of essential or toxic metals to rumen microbes especially if the CT has a long lifetime in the rumen. We propose that tannins modulate the rumen microbiome and as a consequence control methane production, and that *Acacia* tannins are especially active in the rumen because of their chemical stability and prolonged life times. Further studies using "omics" tools to explore the rumen microbiome under the influence of chemically well-defined tannins will be required to test this hypothesis.

4. Materials and Methods

4.1. Chemicals

The 2,5-dihydroxybenzoic acid was purchased from Hewlett Packard (Palo Alto, CA, USA, MALDI Quality Matrix Solutions). Sephadex LH-20, bovine serum albumin and chicken egg white lysozyme were from Sigma (St. Louis, MO, USA) and anthocyanidin chlorides from Chromadex (Irvine, CA, USA). Fluorescein (FLNA) was obtained from Spectrum (Stamford, CT, USA), Trolox (97%) from Acros (Bridgewater, NJ, USA), and 2,2′azobis(2-amidinopropane) HCl (AAPH) from Polysciences Inc., (Warrington, PA, USA). Solvents were HPLC grade and all other chemicals were reagent grade.

4.2. Tannin Purification

The harvesting and preparation of these North American native warm-season perennial legume samples (Table 1) have been previously described [23]. The plants included representatives of subfamily Papilionoideae (*Desmodium paniculatum* (panicledleaf ticktrefoil), *Lespedeza stuevei* (tall lespedeza), and *Lespedeza cuneata* (sericea lespedeza)), subfamiliy Mimosoideae subtribe Mimoseae [*Leucaena retusa* (littleleaf leadtree), *Desmanthus illinoensis* (Illinois bundleflower), *Mimosa strigillosa* (powderpuff), *Neptunia lutea* (yellowpuff)], and subfamily Mimosoideae subtribe Acacieae (*Acacia angustissima var. hirta* (prairie acacia)). Two ecotypes of *Acacia* were analyzed, one originating in the South Texas Plains (AA-STX) and the other from the Cross Timbers ecosystem (AA-STP5). All leaves were dried at 55 °C in a forced air oven for 48 h before grinding the samples to pass a 1 mm screen in a sheer mill and storing at −40 °C.

Tannin was prepared by standard methods [50]. Lipids were removed from the leaves with diethyl ether before extracting total polyphenols with 70% (v/v) acetone:water. Acetone was removed by rotary evaporation and the material was applied to a Sephadex LH-20 column equilibrated with methanol. After eluting small phenolics and nonphenolics with methanol, the column was washed with 70% acetone to recover the condensed tannins. The acetone was removed from the eluate by rotary evaporation and the tannin was freeze dried and stored at −40 °C [45]. The extinction coefficient ($E_{280}{}^{1\,\text{mg/mL}}$) was determined for each purified tannin using serial dilutions of 1.500 mg/mL aqueous solutions.

4.3. Anthocyanidins

The anthocyanidins produced by heating in alcoholic methanol were determined for each tannin by dissolving about 1 mg of the tannin in 200 μL of 6.25% HCl:methanol (v/v) and incubating the solution on a heating block at 70 °C for 30 min. The products were diluted with 200 μL methanol and analyzed directly by UV–VIS spectrometry (Agilent 8453, Santa Clara, CA, USA) to obtain the λ_{max} of the mixture of products. The spectral features of samples were compared to commercial standards of the six most common anthocyanidins (delphinidin, cyanidin, pelargonidin, robetinidin, fisetinidin, and guibourtinidin) [64].

4.4. Thiolysis

Purified CTs were analyzed by thiolysis according to published procedures [39,47]. Briefly, approximately 1 mg of tannin was dissolved in 200 μL of methanol containing 30 μL of the HCl reagent (32% (v/v) HCl in methanol) and 72 μL of the thiol reagent (5% (v/v) toluene-α-thiol in methanol) and incubated at 40 °C for 30 min. The thiolytic degradation products were analyzed by HPLC using an Agilent 1100 HPLC with ChemStation Rev. A.09.03 software (Agilent, Santa Clara, CA, USA). The column was an Agilent Zorbax PR-8 column (Agilent, Santa Clara, CA, USA), 4.6 mm × 150 mm with 5 μM packing. The gradient program employed 0.13% (v/v) trifluoroacetic acid in water and 0.10% (v/v) TFA in acetonitrile [47]. Reaction products were detected at 220 nm and were identified by their retention times and spectral characteristics compared to authentic standards [39,47]. Products were quantitated based on peak areas and converted to moles of extender and moles of terminal units. The chromatograms from control samples that did not contain the reagents were used to confirm that all of the tannin was degraded by thiolysis, and to confirm that the tannin did not contain any flavan-3-ol contamination that would interfere with terminal unit determination.

4.5. NMR Spectroscopy

^{1}H, ^{13}C, and ^{1}H-^{13}C HSQC NMR spectra were recorded at 27 °C on a BrukerBiospin DMX-500 (^{1}H 500.13 MHz, ^{13}C 125.76 MHz, Bruker Corp., Billerica, MA, USA) instrument equipped with TopSpin 3.5 software (Bruker Corp., Billerica, MA, USA) and a cryogenically cooled 5-mm TXI ^{1}H/^{13}C/^{15}N gradient probe in inverse geometry. Spectra were recorded in DMSO-d_6 and were referenced to the

residual signals of DMSO-d_6 (2.49 ppm for ^{1}H and 39.5 ppm for ^{13}C spectra). ^{13}C-NMR spectra were obtained using 1K scans (acquisition time 56 min). For ^{1}H-^{13}C HSQC experiments, spectra were obtained using between 200 and 620 scans (depending on sample size and instrument availability) obtained using the standard Bruker pulse program (hsqcetgpsisp.2) with the following parameters: Acquisition: TD 1024 (F2), 256 (F1); SW 16.0 ppm (F2), 165 ppm (F1); O1 2350.61 Hz; O2 9431.83 Hz; D1 = 1.50 s; CNST2 = 145. Acquisition time: F2 channel, 64 ms, F1 channel 6.17 ms. Processing: SI = 1024 (F2, F1), WDW = QSINE, LB = 1.00 Hz (F2), 0.30 Hz (F1); PH_mod = pk; Baseline correction ABSG = 5 (F2, F1), BCFW = 1.00 ppm, BC_mod = quad (F2), no (F1); Linear prediction = no (F2), LPfr (F1). Sample sizes used for these spectra ranged from 3–10 mg providing NMR sample solutions with concentrations of 6–20 mg/mL.

4.6. MALDI-TOF Mass Spectrometry

Solutions of purified CT samples were prepared (15 mg/mL) using reagent grade methanol. The CT sample (1 μL) was mixed with 10 μL of DHB matrix solution (0.1 M in acetonitrile:water, 1:1, containing 0.1% formic acid). A 1 μL aliquot of this sample-analyte mixture was deposited on the plate and allowed to dry before inserting in the Bruker 15T FR-ICR MALDI-MS. Calibration was run on a standard peptide mix (Bruker Daltonics, Billerica, MA, USA) in the negative ion mode. Typically, 20% of the Yag/Nd (351 nm) laser power was used for the spectral acquisition.

4.7. Antioxidant Activity

The ORAC assay was used to evaluate antioxidant potential [32]. Fluorescein (30 nM) was prepared in 75 mM phosphate pH 7 (PBS) and stored in the dark at 4 °C. The Trolox stock solution (5 mM in reagent grade methanol) was stored in the dark at 4 °C and diluted ten-fold in PBS for use. A 60 mM solution of the radical initiator (AAPH) was prepared immediately before use. Tannin samples were dissolved in water and diluted to an appropriate working concentration (0.1–10 μg/mL based on the absorbance at 280 nm and the extinction coefficients described above) after preliminary ORAC analyses to establish the correct concentration range for each tannin. The reactions were performed in triplicate in 96 well plates, with each 400 μL sample containing 25 nM fluorescein, an appropriate concentration of the antioxidant, and 5 mM AAPH. Immediately after adding the AAPH to the samples the plate was inserted into the plate reader (Biotek, Winooski, VT, USA) and the kinetics of fluorescence decay were recorded with excitation at 685 nm and emission at 520 nm. A standard curve with 0–8.3 μM Trolox was run with every set of samples. At the end of the 1.5 h reaction, the area under the curve was calculated for each reaction and the antioxidant activity of the tannin sample was calculated as Trolox equivalents.

4.8. Protein Precipitation

Bovine serum albumin (BSA) and chicken egg white lysozyme (LYS) were dissolved in 50 mM MES (2-[*N*-morpholino]ethanesulfonic acid), pH 6.5 (with NaOH) to a concentration of 5 mg/mL. Protein concentration of the desalted alfalfa leaf extract [46] was determined using the Pierce 660 nm Protein Assay Reagent (Thermo Fisher Scientific, Waltham, MA, USA) with BSA as the standard. Small aliquots (<1 mL) of the protein solutions were flash frozen in liquid nitrogen and stored at −80 °C until needed.

A master stock solution of each CT fraction was prepared by weighing out approximately 10 mg of purified CT and dissolving to a final concentration of 12 mg/mL in 50 mM MES, pH 6.5. Further working stock solutions were prepared from the master stock to give 8.00, 6.00, 4.00, 3.00, 2.50, 2.00, 1.50, 1.00, 0.75, 0.625, 0.50, 0.375, 0.25, and 0 mg/mL solutions. For each protein tested, 20 μL of each CT working stock solution (or buffer control for no CT) was pipetted into 1.7 mL microfuge tube containing buffer in duplicate. Previously frozen protein stock solutions were thawed and added to the CT in each tube to give a final reaction volume of 100 μL and a final protein concentration of 1 mg/mL (20 μL for BSA or LYS or ALF). The precipitation reactions were incubated for 30 min then centrifuged for 5 min at

10,000× *g*. Protein present in the supernatant was determined by adding 750 µL Pierce 660 nM protein assay reagent to a supernatant aliquot (50 µL) and measuring absorbance at 660 nm using a Beckman DU800 spectrophotometer (Beckman-Coulter, Brea, CA, USA). Background absorbance due to reaction of the CT with the reagent was recorded. Protein precipitation data were fitted to estimate PP50 defined as the mg of CT for precipitation of 50% of maximal protein precipitated (sometimes referred to as *b* values). After averaging duplicate points, replicate (*n* = 2) experiments of each tannin/protein combination were fit to an inhibitor dose-response curve (log [tannin concentration] versus response with variable slope) model:

$$\log y = A + [(B - A)/(1 + ((X^{Hillslope})/(PP50^{Hillslope})))] \tag{1}$$

using Prism (GraphPad Software, La Jolla, CA, USA). The fitted curves had R^2 values of > 0.92 (BSA), > 0.98 (LYS), and > 0.95 (ALF).

Supplementary Materials: Table S1. Detailed thiolysis data for the CT used in this study. Table S2. ORAC data for antioxidant capacity for CT used in this study. Table S3. Protein precipitation data for CT used in this study. Tables S4 and S5. Ranges of cross peak NMR signals. Figures S1–S7. NMR spectra for the CT used in this study. Figures S8 and S9. NMR spectra for the *Acacia* CT. Figure S10. Protein precipitation data for the CT used in this study. Figure S11. Protein precipitation versus methane production correlation graphs.

Author Contributions: Conceptualization: H.N., W.E.Z., and A.E.H.; data curation: W.E.Z. and A.E.H.; formal analysis: H.N., W.E.Z., and A.E.H.; funding acquisition: A.E.H.; investigation: R.S., A.R., S.E.M., L.A.R., J.T.R., and M.L.S.; writing—original draft: H.N., W.E.Z. and A.E.H.; writing—review and editing: L.A.R.

Conflicts of Interest: The authors declare no conflict of interest.

References

1. Quideau, S.; Deffieux, D.; Douat-Casassus, C.; Pouysegu, L. Plant polyphenols: Chemical properties, biological activities, and synthesis. *Angew. Chem. Int. Ed.* **2011**, *50*, 586–621. [CrossRef] [PubMed]
2. Cheynier, V. Phenolic compounds: From plants to foods. *Phytochem. Rev.* **2012**, *11*, 153–177. [CrossRef]
3. Hanley, T.A.; Robbins, C.T.; Hagerman, A.E.; McArthur, C. Predicting digestible protein and digestible dry matter in tannin containing forages consumed by ruminants. *Ecology* **1992**, *73*, 537–541. [CrossRef]
4. Min, B.R.; Barry, T.N.; Attwood, G.T.; McNabb, W.C. The effect of condensed tannins on the nutrition and health of ruminants fed fresh temperate forages: A review. *Anim. Feed Sci. Technol.* **2003**, *106*, 3–19. [CrossRef]
5. Rochfort, S.; Parker, A.J.; Dunshea, F.R. Plant bioactives for ruminant health and productivity. *Phytochemistry* **2008**, *69*, 299–322. [CrossRef] [PubMed]
6. Doran-Browne, N.; Behrendt, R.; Kingwell, R.; Eckard, R. Modelling the potential of birdsfoot trefoil (*Lotus corniculatus*) to reduce methane emissions and increase production on wool and prime lamb farm enterprises. *Anim. Prod. Sci.* **2015**, *55*, 1097–1105. [CrossRef]
7. Naumann, H.D.; Tedeschi, L.O.; Zeller, W.E.; Huntley, N.F. The role of condensed tannins in ruminant animal production: Advances, limitations and future directions. *Rev. Bras. Zootec.* **2017**, *46*, 929–949. [CrossRef]
8. Mueller-Harvey, I. Unravelling the conundrum of tannins in animal nutrition and health. *J. Sci. Food Agric.* **2006**, *86*, 2010–2037. [CrossRef]
9. Jayanegara, A.; Leiber, F.; Kreuzer, M. Meta-analysis of the relationship between dietary tannin level and methane formation in ruminants from in vivo and in vitro experiments. *J. Anim. Physiol. Anim. Nutr.* **2012**, *96*, 365–375. [CrossRef] [PubMed]

10. Kumar, S.; Choudhury, P.K.; Dolores Carro, M.; Griffith, G.W.; Dagar, S.S.; Puniya, M.; Calabro, S.; Ravella, S.R.; Dhewa, T.; Upadhyay, R.C.; et al. New aspects and strategies for methane mitigation from ruminants. *Appl. Microbiol. Biotechnol.* **2014**, *98*, 31–44. [CrossRef] [PubMed]

11. Johnson, K.A.; Johnson, D.E. Methane emissions from cattle. *J. Anim. Sci.* **1995**, *73*, 2483–2492. [CrossRef] [PubMed]

12. Bhatta, R.; Baruah, L.; Saravanan, M.; Suresh, K.P.; Sampath, K.T. Effect of medicinal and aromatic plants on rumen fermentation, protozoa population and methanogenesis in vitro. *J. Anim. Physiol. Anim. Nutr.* **2013**, *97*, 446–456. [CrossRef] [PubMed]

13. Tiemann, T.T.; Lascano, C.E.; Wettstein, H.R.; Mayer, A.C.; Kreuzer, M.; Hess, H.D. Effect of the tropical tannin-rich shrub legumes *Calliandra calothyrsus* and *Flemingia macrophylla* on methane emission and nitrogen and energy balance in growing lambs. *Animal* **2008**, *2*, 790–799. [CrossRef] [PubMed]

14. Ramirez-Restrepo, C.A.; Barry, T.N. Alternative temperate forages containing secondary compounds for improving sustainable productivity in grazing ruminants. *Anim. Feed Sci. Technol.* **2005**, *120*, 179–201. [CrossRef]

15. Bhatta, R.; Enishi, O.; Yabumoto, Y.; Nonaka, I.; Takusari, N.; Higuchi, K.; Tajima, K.; Takenaka, A.; Kurihara, M. Methane reduction and energy partitioning in goats fed two concentrations of tannin from *Mimosa* spp. *J. Agric. Sci.* **2013**, *151*, 119–128. [CrossRef]

16. Moreira, G.D.; Lima, P.D.T.; Borges, B.O.; Primavesi, O.; Longo, C.; McManus, C.; Abdalla, A.; Louvandini, H. Tropical tanniniferous legumes used as an option to mitigate sheep enteric methane emission. *Trop. Anim. Health Prod.* **2013**, *45*, 879–882. [CrossRef] [PubMed]

17. Pellikaan, W.F.; Stringano, E.; Leenaars, J.; Bongers, D.J.G.M.; Van Laar-van Schuppen, S.; Plant, J.; Mueller-Harvey, I. Evaluating effects of tannins on extent and rate of in vitro gas and CH4 production using an automated pressure evaluation system (APES). *Anim. Feed Sci. Technol.* **2011**, *166–167*, 377–390. [CrossRef]

18. Hassanat, F.; Benchaar, C. Assessment of the effect of condensed (acacia and quebracho) and hydrolysable (chestnut and valonea) tannins on rumen fermentation and methane production in vitro. *J. Sci. Food Agric.* **2013**, *93*, 332–339. [CrossRef] [PubMed]

19. Grainger, C.; Clarke, T.; Auldist, M.J.; Beauchemin, K.A.; McGinn, S.M.; Waghorn, G.C.; Eckard, R.J. Potential use of *Acacia mearnsii* condensed tannins to reduce methane emissions and nitrogen excretion from grazing dairy cows. *Can. J. Anim. Sci.* **2009**, *89*, 241–251. [CrossRef]

20. White, R.G.; Lawler, J.P. Can methane suppression during digestion of woody and leafy browse compensate for energy costs of detoxification of plant secondary compounds? A test with muskoxen fed willows and birch. *Comp. Biochem. Physiol. A Mol. Integr. Physiol.* **2002**, *133*, 849–859. [CrossRef]

21. Patra, A.K.; Saxena, J. Exploitation of dietary tannins to improve rumen metabolism and ruminant nutrition. *J. Sci. Food Agric.* **2011**, *91*, 24–37. [CrossRef] [PubMed]

22. Tedeschi, L.O.; Ramirez-Restrepo, C.A.; Muir, J.P. Developing a conceptual model of possible benefits of condensed tannins for ruminant production. *Animal* **2014**, *8*, 1095–1105. [CrossRef] [PubMed]

23. Naumann, H.D.; Tedeschi, L.O.; Muir, J.P.; Lambert, B.D.; Kothmann, M.M. Effect of molecular weight of condensed tannins from warm-season perennial legumes on ruminal methane production in vitro. *Biochem. Syst. Ecol.* **2013**, *50*, 154–162. [CrossRef]

24. Hatew, B.; Carbonero, C.H.; Stringano, E.; Sales, L.F.; Smith, L.M.J.; Mueller-Harvey, I.; Hendriks, W.H.; Pellikaan, W.F. Diversity of condensed tannin structures affects rumen in vitro methane production in sainfoin (*Onobrychis viciifolia*) accessions. *Grass Forage Sci.* **2015**, *70*, 474–490. [CrossRef]

25. Hatew, B.; Stringano, E.; Mueller-Harvey, I.; Hendriks, W.H.; Carbonero, C.H.; Smith, L.M.J.; Pellikaan, W.F. Impact of variation in structure of condensed tannins from sainfoin (*Onobrychis viciifolia*) on in vitro ruminal methane production and fermentation characteristics. *J. Anim. Physiol. Anim. Nutr.* **2016**, *100*, 348–360. [CrossRef] [PubMed]

26. Huyen, N.T.; Fryganas, C.; Uittenbogaard, G.; Mueller-Harvey, I.; Verstegen, M.W.A.; Hendriks, W.H.; Pellikaan, W.F. Structural features of condensed tannins affect in vitro ruminal methane production and fermentation characteristics. *J. Agric. Sci.* **2016**, *154*, 1474–1487. [CrossRef]

27. Saminathan, M.; Sieo, C.C.; Abdullah, N.; Wong, C.; Ho, Y.W. Effects of condensed tannin fractions of different molecular weights from a *Leucaena leucocephala* hybrid on in vitro methane production and rumen fermentation. *J. Sci. Food Agric.* **2015**, *95*, 2742–2749. [CrossRef] [PubMed]

28. Hagerman, A.E. Fifty years of polyphenol-protein complexes. *Rec. Adv. Polyphen. Res.* **2012**, *3*, 71–97.

29. Hagerman, A.E.; Riedl, K.M.; Rice, R.E. Tannins as biological antioxidants. In *Plant Polyphenols 2: Chemistry, Biology, Pharmacology, Ecology*; Gross, G.G., Hemingway, R.W., Yoshida, T., Eds.; Kluwer Academic/Plenum: New York, NY, USA, 1999; pp. 495–505.

30. Huang, X.D.; Liang, J.B.; Tan, H.Y.; Yahya, R.; Khamseekhiew, B.; Ho, Y.W. Molecular weight and protein binding affinity of *Leucaena* condensed tannins and their effects on in vitro fermentation parameters. *Anim. Feed Sci. Technol.* **2010**, *159*, 81–87. [CrossRef]

31. Jayanegara, A.; Goel, G.; Makkar, H.P.S.; Becker, K. Divergence between purified hydrolysable and condensed tannin effects on methane emission, rumen fermentation and microbial population in vitro. *Anim. Feed Sci. Technol.* **2015**, *209*, 60–68. [CrossRef]

32. Ishimoto, H.; Tai, A.; Yoshimura, M.; Amakura, Y.; Yoshida, T.; Hatano, T.; Ito, H. Antioxidative properties of functional polyphenols and their metabolites assessed by an ORAC assay. *Biosci. Biotech. Biochem.* **2012**, *76*, 395–399. [CrossRef] [PubMed]

33. Joslyn, M.A.; Goldstein, J.L. Conversion of leucoanthocyanins into corresponding anthocyanidins. *Science* **1964**, *143*, 954–955. [CrossRef] [PubMed]

34. Prieur, C.; Rigaud, J.; Cheynier, V.; Moutounet, M. Oligomeric and polymeric procyanidins from grape seeds. *Phytochemistry* **1994**, *36*, 781–784. [CrossRef]

35. Zeller, W.E.; Ramsay, A.; Ropiak, H.M.; Fryganas, C.; Mueller-Harvey, I.; Brown, R.H.; Drake, C.; Grabber, J.H. H-1-C-13 HSQC NMR spectroscopy for estimating procyanidin/prodelphinidin and *cis/trans*-flavan-3-ol ratios of condensed tannin samples: Correlation with thiolysis. *J. Agric. Food Chem.* **2015**, *63*, 1967–1973. [CrossRef] [PubMed]

36. Roux, D.G.; Evelyn, S.R. Condensed tannins: A study of complex leuco-anthocyanins present in condensed tannins. *Biochem. J.* **1958**, *69*, 530–538. [CrossRef] [PubMed]

37. Steynberg, P.J.; Bezuidenhoudt, B.C.B.; Ferreira, D.; Steynberg, J.P. Cleavage of the interflavanyl bond in 5-deoxy (A-ring) proanthocyanidins. *J. Chem. Soc. Chem. Comm.* **1994**, 31–32. [CrossRef]

38. Steynberg, P.J.; Steynberg, J.P.; Bezuidenhoudt, B.C.B.; Ferreira, D. Oligomeric flavonoids. Part 19. Reductive cleavage of the interflavanyl bond in proanthocyanidins. *J. Chem. Soc. Perk. Trans.* **1995**, *1*, 3005–3012. [CrossRef]

39. Li, C.; Leverence, R.; Trombley, J.D.; Xu, S.; Yang, J.; Tian, Y.; Reed, J.D.; Hagerman, A.E. High molecular weight persimmon (*Diospyros kaki* L.) proanthocyanidin: A highly galloylated, A-linked tannin with an unusual flavonol terminal unit, myricetin. *J. Agric. Food Chem.* **2010**, *58*, 9033–9042. [CrossRef] [PubMed]

40. Monagas, M.; Quintanilla-Lopez, J.E.; Gomez-Cordoves, C.; Bartolome, B.; Lebron-Aguilar, R. MALDI-TOF MS analysis of plant proanthocyanidins. *J. Pharm. Biomed. Anal.* **2010**, *51*, 358–372. [CrossRef] [PubMed]

41. Krueger, C.G.; Vestling, M.M.; Reed, J.D. Matrix-assisted laser desorption/ionization time-of-flight mass spectrometry of heteropolyflavan-3-ols and glucosylated heteropolyflavans in sorghum [*Sorghum bicolor* (L.) Moench]. *J. Agric. Food Chem.* **2003**, *51*, 538–543. [CrossRef] [PubMed]

42. Stringano, E.; Cramer, R.; Hayes, W.; Smith, C.; Gibson, T.; Mueller-Harvey, I. Deciphering the complexity of sainfoin (*Onobrychis viciifolia*) proanthocyanidins by MALDI-TOF mass spectrometry with a judicious choke of isotope patterns and matrixes. *Anal. Chem.* **2011**, *83*, 4147–4153. [CrossRef] [PubMed]

43. Schaich, K.M.; Tian, X.; Xie, J. Hurdles and pitfalls in measuring antioxidant efficacy: A critical evaluation of ABTS, DPPH, and ORAC assays. *J. Funct. Food.* **2015**, *14*, 111–125. [CrossRef]

44. Cai, Y.Z.; Sun, M.; Xing, J.; Luo, Q.; Corke, H. Structure-radical scavenging activity relationships of phenolic compounds from traditional Chinese medicinal plants. *Life Sci.* **2006**, *78*, 2872–2888. [CrossRef] [PubMed]

45. Naumann, H.D.; Hagerman, A.E.; Lambert, B.D.; Muir, J.P.; Tedeschi, L.O.; Kothmann, M.M. Molecular weight and protein-precipitating ability of condensed tannins from warm-season perennial legumes. *J. Plant. Interact.* **2014**, *9*, 212–219. [CrossRef]

46. Zeller, W.E.; Sullivan, M.L.; Mueller-Harvey, I.; Grabber, J.H.; Ramsay, A.; Drake, C.; Brown, R.H. Protein precipitation behavior of condensed tannins from *Lotus pedunculatus* and *Trifolium repens* with different mean degrees of polymerization. *J. Agric. Food Chem.* **2015**, *63*, 1160–1168. [CrossRef] [PubMed]

47. Scioneaux, A.N.; Schmidt, M.A.; Moore, M.A.; Lindroth, R.L.; Wooley, S.C.; Hagerman, A.E. Qualitative variation in proanthocyanidin composition of *Populus* species and hybrids: Genetics is the key. *J. Chem. Ecol.* **2011**, *37*, 57–70. [CrossRef] [PubMed]

48. Gu, L.; Kelm, M.A.; Hammerstone, J.F.; Beecher, G.; Holden, J.; Haytowitz, D.; Prior, R.L. Screening of foods containing proanthocyanidins and their structural characterization using LC-MS/MS and thiolytic degradation. *J. Agric. Food Chem.* **2003**, *51*, 7513–7521. [CrossRef] [PubMed]

49. Gao, C.; Cunningham, D.G.; Liu, H.Y.; Khoo, C.; Gu, L.W. Development of a thiolysis HPLC method for the analysis of procyanidins in cranberry products. *J. Agric. Food Chem.* **2018**, *66*, 2159–2167. [CrossRef] [PubMed]

50. Hagerman, A.E.; Butler, L.G. Condensed tannin purification and characterization of tannin-associated proteins. *J. Agric. Food Chem.* **1980**, *28*, 947–952. [CrossRef] [PubMed]

51. Seigler, D.S. Phytochemistry of Acacia—*Sensu lato*. *Biochem. Syst. Ecol.* **2003**, *31*, 845–873. [CrossRef]

52. Hadacek, F. Secondary metabolites as plant traits: Current assessment and future perspectives. *Crit. Rev. Plant Sci.* **2002**, *21*, 273–322. [CrossRef]

53. Okuda, T.; Yoshida, T.; Hatano, T.; Iwasaki, M.; Kubo, M.; Orime, T.; Yoshizaki, M.; Naruhashi, N. Hydrolysable tannins as chemotaxonomic markers in the rosaceae. *Phytochemistry* **1992**, *31*, 3091–3096. [CrossRef]

54. Harborne, J.B. Flavonoids and the evolution of the angiosperms. *Biochem. Syst. Ecol.* **1977**, *5*, 7–72. [CrossRef]

55. Hoong, Y.B.; Pizzi, A.; Tahir, P.M.; Pasch, H. Characterization of *Acacia mangium* polyflavonoid tannins by MALDI-TOF mass spectrometry and CP-MAS ^{13}C NMR. *Eur. Polym. J.* **2010**, *46*, 1268–1277. [CrossRef]

56. Venter, P.B.; Senekal, N.D.; Kemp, G.; Amra-Jordaan, M.; Khan, P.; Bonnet, S.L.; Van der Westhuizen, J.H. Analysis of commercial proanthocyanidins. Part 3: The chemical composition of wattle (*Acacia mearnsii*) bark extract. *Phytochemistry* **2012**, *83*, 153–167. [CrossRef] [PubMed]

57. Hattas, D.; Julkunen-Tiitto, R. The quantification of condensed tannins in African savanna tree species. *Phytochem. Lett.* **2012**, *5*, 329–334. [CrossRef]

58. Crestini, C.; Lange, H.; Bianchetti, G. Detailed Chemical Composition of Condensed Tannins via Quantitative P-31 NMR and HSQC Analyses: *Acacia catechu*, *Schinopsis balansae*, and *Acacia mearnsii*. *J. Nat. Prod.* **2016**, *79*, 2287–2295. [CrossRef] [PubMed]

59. Durmic, Z.; Moate, P.J.; Eckard, R.; Revell, D.K.; Williams, R.; Vercoe, P.E. In vitro screening of selected feed additives, plant essential oils and plant extracts for rumen methane mitigation. *J. Sci. Food Agric.* **2014**, *94*, 1191–1196. [CrossRef] [PubMed]

60. Carulla, J.E.; Kreuzer, M.; Machmuller, A.; Hess, H.D. Supplementation of *Acacia mearnsii* tannins decreases methanogenesis and urinary nitrogen in forage-fed sheep. *Aust. J. Agric. Res.* **2005**, *56*, 961–970. [CrossRef]

61. Tavendale, M.H.; Meagher, L.P.; Pacheco, D.; Walker, N.; Attwood, G.T.; Sivakumaran, S. Methane production from in vitro rumen incubations with *Lotus pedunculatus* and *Medicago sativa*, and effects of extractable condensed tannin fractions on methanogenesis. *Anim. Feed Sci. Technol.* **2005**, *123*, 403–419. [CrossRef]

62. Getachew, G.; Makkar, H.P.S.; Becker, K. Tannins in tropical browses: Effects on in vitro microbial fermentation and microbial protein synthesis in media containing different amounts of nitrogen. *J. Agric. Food Chem.* **2000**, *48*, 3581–3588. [CrossRef] [PubMed]

63. Zhang, L.; Liu, R.; Gung, B.W.; Tindall, S.; Gonzalez, J.M.; Halvorson, J.J.; Hagerman, A.E. Polyphenol-aluminum complex formation: Implications for aluminum tolerance in plants. *J. Agric. Food Chem.* **2016**, *64*, 3025–3033. [CrossRef] [PubMed]

64. Andersen, O.M.; Jordheim, M. Chemistry of flavonoid-based colors in plants. In *Comprehensive Natural Products II: Chemistry and Biology*; Liu, H., Ed.; Elsevier: Amsterdam, The Netherlands, 2010; Volume 3, pp. 547–614.

Exploiting Compositionally Similar Grape Marc Samples to Achieve Gradients of Condensed Tannin and Fatty Acids for Modulating In Vitro Methanogenesis

Josh L. Hixson [1,*], Zoey Durmic [2], Joy Vadhanabhuti [2], Philip E. Vercoe [2,3], Paul A. Smith [1,†] and Eric N. Wilkes [1]

[1] The Australian Wine Research Institute, P.O. Box 197, Glen Osmond SA 5064, Australia;
paul.smith@wineaustralia.com (P.A.S.); eric.wilkes@awri.com.au (E.N.W.)

[2] School of Agriculture and Environment, The University of Western Australia M085, 35 Stirling Hwy,
Crawley WA 6009, Australia; zoey.durmic@uwa.edu.au (Z.D.); joy.vadhanabhuti@uwa.edu.au (J.V.);
philip.vercoe@uwa.edu.au (P.E.V.)

[3] Institute of Agriculture, The University of Western Australia M085, 35 Stirling Hwy,
Crawley WA 6009, Australia

[*] Correspondence: josh.hixson@awri.com.au; Tel.: +61-8-8313-6600

[†] Current address: Wine Australia, P.O. Box 660, Kent Town SA 5071, Australia.

Abstract: Ruminants produce large amounts of the greenhouse gas, methane, which can be reduced by supplementing feed with products that contain anti-methanogenic compounds, such as the solid winemaking by-product, grape marc. The aim of this study was to exploit compositional differences in grape marc to better understand the roles of condensed tannin and fatty acids in altering methanogenesis in a ruminant system. Grape marc samples varying in tannin extractability, tannin size and subunit composition, and fatty acid or tannin concentrations were selected and incubated in rumen fluid using an in vitro batch fermentation approach with a concentrate-based control. Four distinct experiments were designed to investigate the effects on overall fermentation and methane production. Generally, fatty acid concentration in grape marc was associated with decreased total gas volumes and volatile fatty acid concentration, whereas increased condensed tannin concentration tended to decrease methane percentage. Smaller, extractable tannin was more effective at reducing methane production, without decreasing overall gas production. In conclusion, fatty acids and tannin concentration, and tannin structure in grape marc play a significant role in the anti-methanogenic effect of this by-product when studied in vitro. These results should be considered when developing strategies to reduce methane in ruminants by feeding grape marc.

Keywords: condensed tannin; bioactivity; methanogenesis; grape marc; fatty acids; in vitro batch fermentation

1. Introduction

Methane is inherently produced in ruminant livestock systems, but there are options for limiting the emissions of this greenhouse gas (GHG). Changes to feeding systems and the addition of ruminant dietary supplements can alter digestion away from high methane production and towards capturing more energy for the animal with lower GHG emissions [1–4]. With an increasing global need for food, and finite resources on which to draw, agricultural by-products are a valuable input into feeding systems [5], especially when these can also have positive effects on GHG emissions. Diet supplementation with feed containing condensed tannins (CTs) has shown promise in reducing

methane emissions from livestock, and the link between tannin-containing feed and reductions in methane intensity have been noted previously [6]. The CTs are a diverse class of compounds, and more recent attention has turned away from the concentration-dependent model of CT dosing and focused more closely on the structure, composition, and extractability of CT to better understand the observed responses, be it for methanogenesis [7,8], protein binding capacity [9,10], or exploiting anthelmintic properties [11].

Grape marc, a solid material remaining after wine making, contains significant proportions of CT [12], and has been the topic of some interest in supplementing a ruminant diet [13–19]. The CT found in this winemaking by-product has been extensively surveyed and varies in both concentration and subunit composition [12]. While the concentration CT is dependent on the natural variability in the wine grape from which it is derived, the processing that grape marc is exposed to is also key in determining the concentration and extractability of CT that remains. For example, red grape marc that is present during alcoholic fermentation undergoes a higher level of extraction than white grape marc, and subsequent thermal treatments at processing plants can further decrease CT concentrations. Grape marc contains very small amounts of extractable tannin, if any, and mainly contains tannin that is loosely bound to cell walls [20]. Many studies linking CT to methanogenesis have exploited either CT-containing extracts, or a whole plant material that contains CT [6–8]. Very little work has focused on by-product feeding where the soluble CT has been largely removed, and the CT under investigation is bound in some way to cell wall material. In addition to variable CT concentration and composition, a considerable proportion of grape marc dry matter (DM) contains seed-derived fatty acids [12], which have also been widely implicated in reducing methanogenesis [13,21,22]. In grape marc this component is commonly referred to as "crude fat" or simply "fat" [13,23]; however, it will herein be referred to as fatty acid (FA) concentration to avoid confusion.

Winemaking and subsequent processing steps result in grape marc with a highly varied composition [12]. As such, establishing the role that CT or FA from grape marc plays in methanogenesis over another component may be difficult to determine by simply comparing individual grape marc samples. An alternative experimental approach is to study single compounds through the addition or removal of those components and generate samples that are varied in the desired species. However, many compounds of interest in grape marc are not readily extractable and are well incorporated into cell wall fibers. As such, additive studies can produce systems that fail to mimic naturally occurring interaction with cell wall material. Conversely, extractive removal of a suspected bioactive can affect numerous compounds. For grape marc, this methodology may not accurately replicate these species in a natural state.

This study aimed to identify grape marc samples that differ specifically in CT or FA concentration, or CT composition, but are otherwise compositionally similar. After identifying these samples, the aim was to produce blends or comparisons that result in changes of the single, desired variable, allowing for simplified investigations of key grape marc components with respect to methanogenesis. This approach was used to determine how the extractability, composition, or concentration of tannin, as well as the concentration of FA, affects the overall microbial fermentability and production of methane in an in vitro batch fermentation system.

2. Results and Discussion

2.1. Selection and Profile of Grape Marc Samples

Five grape marc samples (GM1, GM6, GM14, GM18, GM20) and a commercial enological tannin (GT) were selected for in vitro fermentation experiments based on their CT and FA concentrations, and CT compositional profiles (Table 1). To study the impact of CT extractability on methanogenesis grape marc 6 (GM6), a post-steam distillation mixture of red and white grape marc, was selected. This sample displayed moderate amounts of both CT and FA, and contained no water extractable tannin (WET). The addition of commercially available extractable tannin (GT) to this marc provided a

comparison of native, loosely-bound tannin with exogenous, extractable tannin on methane abatement (Experiment 1).

Much like the observed changes in CT extractability due to processing, the origin of CT is similarly important for determining CT composition. Skins and seeds from fresh grapes both provide structurally distinct CT [24,25], which is also the case for grape marc-derived CT [12]. Skin-derived CT is generally larger and consists of more subunits (higher mean degree of polymerization, mDP), is higher in both subunit cis/trans ratio (cis/trans) and percentage of prodelphinidin subunits (%PD), and lower in the extent of gallic acid substitution (%Gall). Conversely, seed-derived CT is compositionally opposed for these factors (lower mDP, %PD and cis/trans, and higher %Gall) (Figure 1). However, simply blending skin and seed samples does not isolate CT composition as a sole variable, as the desired CT compositional changes occur alongside FA concentration changes that inherently exist for skin- versus seed-derived samples [12].

CT variable	Information	Calculation
CT	Total CT content	Sum of all subunits (**1-7**)
mDP	Average CT chain length	Function of number of terminal (**1-3**) divided by total number (**1-7**) of subunits
cis/trans	Ratio of 2,3-stereochemisty	Molar ratio of 2,3-*cis* (**2,3,5-7**) versus 2,3-*trans* (**1,4**) subunit)
%PD	Proportion of prodelphinidin subunits	Prodelphinidin subunits (**6**) as a molar percentage of all subunits (**1-7**)
%Gall	Proportion of subunits with gallic acid substitution	Galloylated subunits (**3,7**) as a molar percentage of all subunits (**1-7**)

Figure 1. Acid-catalyzed depolymerization of a condensed tannin chain followed by reaction with phloroglucinol to yield identifiable subunits that are found in grape-derived CT, and subunits involved in calculating CT variables from phloroglucinolysis.

To overcome this, GM20, derived from grape stalk, was selected as it showed a unique composition with low FA concentrations (like marc skin), but also a seed-like CT composition. Therefore, blending a marc skin-derived sample, GM18, with GM20 provided a gradient in CT composition, specifically mDP, cis/trans ratio, and %Gall, without substantial changes in total CT concentration or FA (Experiment 2).

GM20 also provided an appropriate comparison against marc seed (GM14), as the relatively similar CT concentration and composition allowed for comparison of high- and low-FA grape marc samples, and for examination of differing FA concentrations on methane production (Experiment 3). Conversely, the impact of tannin and/or FA on methanogenesis was investigated by keeping the FA concentrations similar and varying the CT concentration. The extent of processing that created GM1 resulted in a very low CT concentration, without significantly impacting on FA content. A blend from GM14 to GM1 created a gradient of CT concentration, while FA concentration was held relatively constant (Experiment 4).

These selected grape marc samples and blends were incubated in sheep rumen fluid using an in vitro batch fermentation approach and compared against a concentrate-based control substrate. More detailed information of each treatment and resulting composition can be found in the Supplementary Material (Table S1).

Table 1. Key compositional information for selected grape marc samples (upper panel), as determined by Hixson et al. (2016) [12], and relative compositional change between grape marc samples being compared in this work (lower panel).

Sample	Type	CT (g/kg DM)	Tannin Composition				WET (g/kg DM)	FA (g/kg DM)	CP (%DM)	ADF (%DM)	NDF (%DM)	ME (MJ/kg)	Comments
			mDP	cis/trans	%PD	%Gall							
GM1	Steam distilled, dried	20.05	N/A				0	115.9	12.1	56.1	61.4	6.61	Low CT, high FA
GM6	Red/white spent	78.36	10.00	10.16	14.3%	9.1%	0	67.1	12.7	34.9	42.6	10.25	Typical processed marc
GM14	White seed	126.13	6.87	8.27	6.1%	16.1%	47.32	152.1	11.5	41.1	51.3	9.41	High CT, high FA
GM18	Red skin	120.74	32.55	26.00	24.7%	3.9%	0	14.0	8.3	16.4	19.4	11.72	High CT (large), low FA
GM20	Red stalk	114.79	9.98	9.22	20.0%	6.1%	40.65	5.2	3.2	26.3	34.1	9.20	High CT (small), low FA
Grap'tan PC (GT)	Grape-derived tannin extract	574.39	5.92	5.17	5.5%	16.0%							
Relative composition change between samples for comparison													
GM20/GM18		95.1	30.7	35.5	80.9	155.9	N/A	37.3	38.6	160.4	175.8	78.6	
GM14/GM20		109.9	68.8	89.6	30.3	265.0	116.4	2907.5	359.4	156.3	150.4	102.3	
GM14/GM1		629.1	N/A	N/A	N/A	N/A	N/A	131.2	95.0	73.3	83.6	142.4	

Numbers shown in red indicate desired compositional change to be achieved in the experiment. CT (condensed tannin concentration, as determined by phloroglucinoysis); mDP, mean degree of polymerization; %PD, percentage of prodelphinidin-type subunits; %Gall, percentage of subunits with gallic acid substitution; WET, water extractable tannin; CP, crude protein; ADF, acid detergent fiber; NDF, neutral detergent fiber; ME, metabolizable energy; DM, dry matter.

2.2. Experiment 1—Extractability of CT and Methanogenesis

Inclusion of GM6 had no effect on the total gas production and volatile fatty acid (VFA) concentration (Table 2), although there was a significant reduction in methane volume ($p < 0.05$) compared with the control. Inactivating the CT by addition of polyethylene glycol (GM6 + PEG) gave a slight recovery in gas volume, and the methane volume increased back to that of the control, suggesting that the slight reductions observed could be attributed to the presence of CT. The addition of extractable tannin (GM6 + GT) provided slight reductions in methane percentage (mL/100 mL of total gas) compared with GM6, without having a significant effect on overall fermentation. The addition of PEG (GM6 + GT + PEG) only recovered the gas volume to that observed for GM6, and not back to that of the control, bringing into question the impact of PEG on completely inhibiting CT in this treatment. The addition of extractable tannin provided the lowest methane production (volume and percentage) without affecting the total gas volume, although these changes were not statistically different from that observed with loosely bound CT present in GM6.

The investigation into the role of CT extractability in methanogenesis also inherently explored tannin composition. The extractability of grape-derived tannin changes with tannin size, as larger CT interacts more strongly with cell wall material, removing it from solution [26]. As a result, the distribution of tannin remaining in solution becomes skewed towards smaller CT. Due to the correlation between grape marc CT variables, modulation in tannin size (mDP) inherently favors CT of a lower cis/trans ratio and %PD, and higher %Gall. As such, any changes in methanogenesis observed in Experiment 1 may relate to compositional changes (i.e., smaller CT) in addition to the level of extractability.

Experiment 1 showed inconsistencies in the inhibition of CT by PEG, especially when both extractable and cell wall-bound tannin were present. Initially, it was concluded that the extractable CT present bound with all the PEG, leaving none available to interact with the loosely bound CT portion. In this study, PEG additions were made at 350 mg per ferment, which in the case of GM6 + GT + PEG (with a total of 34.9 mg of CT) represented a ratio of 10:1 (*w/w* PEG:CT). This was equivalent to the ratio used in previous work with extractable tannin [7], but much less than in experiments exploiting native CT in whole plant material (between 100:1 and 1000:1) [8,27].In one study it was also noted that the fermentation response derived from CT inactivation by PEG was not as expected [8]. As such, the role of PEG in ferments containing both extractable tannin and cell wall-bound tannin is unclear, and warrants further investigation. In this study, however, the behavior of PEG may have been a response to the low rate of PEG addition, and higher concentrations may be required for cell wall-bound CT than extractable CT.

2.3. Experiment 2—Composition of CT and Methanogenesis

The inclusion of GM18 into the control did not produce a significant reduction in gas production, VFA concentration, or methane variables. However, as the inclusion was moved across a gradient from GM18 to GM20, significant fermentation changes were observed, most notably for methane volume with GM18 + GM20 at 1:2 ratio (Table 3). While reductions in total gas volume across this gradient also occurred, the same effect was not seen for VFA concentration. Moving from treatment GM18 to GM20, a trend for reductions in methane percentage was seen with decreasing mDP and cis/trans ratio. Treatments that contained higher proportions of GM20 also possessed higher concentrations of WET (Table 1). This experiment likely mirrors Experiment 1 in exploiting CT extractability as well as composition, a relationship that cannot be uncoupled.

Here, minimal variation in the %PD was created across the grape marc gradient (20–24.7%PD), a factor that has previously been linked with CT-derived reductions in methanogenesis [7,8]. Reported in vitro batch fermentation assessment of grape marc samples have ranged from 3.9 to 33.0%PD [23], and %PD has been observed as high as 48.4% for CT from skin-only marc [12]. Comparatively, when %PD has been linked to methanogenesis, the CT assessed ranged from 3.3 to 99.2%PD in one study [7], and 52.7 to 94.8%PD in the second [8]. As such, even if isolation of %PD in grape marc CT as a sole variable was achievable, the range available may not provide a high enough %PD required to generate comparative reductions in methane.

Molecules **2018**, *23*, 1793

Table 2. In vitro fermentation parameters for Experiment 1; grape marc samples of differing tannin extractability.

Treatment	Description	Gas Volume (mL/g DM)	CH₄ Volume (mL/g DM)	CH₄% (mL/100 mL Total Gas)	VFA (mmol/L)	Ac:Pr	NH₃ (mg/L)
Control	Control	290.8 ± 6.1	39.60 ± 1.31 [a]	13.62 ± 0.17 [a]	90.46 ± 2.33 [a]	2.997 ± 0.006 [a]	160.4 ± 6.2 [a]
GM6	Loosely bound CT	264.4 ± 19.4	33.03 ± 2.54 [b]	12.45 ± 0.08 [a,b]	84.02 ± 0.61 [a,b]	3.123 ± 0.012 [b,c]	142.8 ± 0.0 [c]
GM6 + PEG	Removal of CT	288.8 ± 3.4	38.83 ± 1.65 [a]	13.46 ± 0.64 [a]	84.31 ± 2.12 [a,b]	3.057 ± 0.025 [a,b]	152.8 ± 1.8 [a,b]
GM6 + GT	Addition of extractable CT	267.4 ± 0.8	32.43 ± 1.00 [a]	11.89 ± 0.34 [b]	81.44 ± 1.26 [b]	3.153 ± 0.060 [c]	114.8 ± 2.5 [d]
GM6 + GT + PEG	Removal of CT	269.6 ± 8.9	34.73 ± 2.84 [a,b]	12.58 ± 0.66 [a,b]	80.42 ± 4.29 [b]	3.107 ± 0.025 [b,c]	150.0 ± 1.2 [b,c]
SEM		13.78	2.738	0.609	3.374	0.0436	4.29
p		0.0217	0.0018	0.0037	0.0045	0.001	<0.0001

Data expressed as mean value ± standard deviation of triplicates. Values in the same column within each experiment with different superscript letters were significantly different ($p < 0.05$). GM, grape marc; PEG, polyethylene glycol; GT, Grap'tan extractable tannin; CT (condensed tannin concentration, as determined by phloroglucinoysis), VFA, volatile fatty acid; Ac:Pr, molar ratio of acetate to propionate; DM, dry matter.

Table 3. In vitro fermentation parameters for Experiment 2; gradient of grape marc samples with differing tannin composition.

Treatment	Description	Gas Volume (mL/g DM)	CH₄ Volume (mL/g DM)	CH₄% (mL/100 mL Total Gas)	VFA (mmol/L)	Ac:Pr	NH₃ (mg/L)
Control	Control	290.8 ± 6.1 [a,b]	39.60 ± 1.31 [a]	13.62 ± 0.17 [a]	90.46 ± 2.33	2.997 ± 0.006 [a]	160.4 ± 6.2 [a]
GM18	High mDP and cis/trans CT	295.9 ± 3.5 [a]	38.23 ± 1.16 [a]	12.91 ± 0.28 [a,b]	84.49 ± 6.82	2.780 ± 0.036 [b]	112.0 ± 3.9 [b]
GM18 + GM20 (2:1)	Medium-high mDP and cis/trans CT	296.7 ± 2.1 [a]	37.87 ± 0.29 [a,b]	12.75 ± 0.03 [a,b]	85.17 ± 2.51	2.800 ± 0.026 [b]	105.2 ± 3.7 [b,c]
GM18 + GM20 (1:2)	Medium-low mDP and cis/trans CT	275.9 ± 11.3 [b]	33.57 ± 3.14 [b]	12.06 ± 0.63 [b]	82.97 ± 2.04	2.840 ± 0.070 [b]	96.0 ± 3.2 [c]
GM20	Low mDP and cis/trans CT	288.3 ± 2.5 [a,b]	35.37 ± 1.10 [a,b]	12.23 ± 0.42 [b]	85.56 ± 5.74	2.823 ± 0.021 [b]	95.6 ± 9.7 [c]
SEM		8.39	2.310	0.505	5.99	0.0526	8.00
p		0.0125	0.008	0.0031	0.3502	0.0003	<0.0001

Data expressed as mean value ± standard deviation of triplicates. Values in the same column within each experiment with different superscript letters were significantly different ($p < 0.05$). GM, grape marc; mDP, mean degree of polymerization; CT (condensed tannin concentration, as determined by phloroglucinoysis); VFA, volatile fatty acid; Ac:Pr, molar ratio of acetate to propionate; DM, dry matter.

2.4. Experiment 3 and 4—CT and/or FA Concentration and Methanogenesis

Separating the effect of tannin and FA on methanogenesis was achieved in two separate experiments, one comparing high-CT samples with differing FA content (Experiment 3), and another blending high-FA samples across a gradient of increasing CT concentration (Experiment 4).

In Experiment 3, a 30% inclusion of GM20 yielded similar gas production and VFA concentration to the control, but gave a significant reduction in both methane volume and percentage (Table 4). The addition of PEG (GM20 + PEG) provided no recovery in methane production, suggesting either that tannin is not as anti-methanogenic as previously thought, or as noted in Experiment 1, that the mechanism of action of PEG with grape marc CT is not as simple as previously suggested. The inclusion of GM14 (high FA sample) resulted in a significant reduction in the gas volume and VFA concentration from the control, which is consistent with earlier results that high-FA grape marc retards fermentation, specifically gas production [23]. The addition of PEG (GM14 + PEG) had no significant effect on gas volume and VFA concentration, while methane percentage was closer to that of the control. These results suggest that CT are more heavily impacting methane production, and the reductions observed in total gas production are due to the presence of FA. The comparison between GM20 (high CT, low FA) and GM14 (high CT, high FA) showed a similar trend, as methane percentage was not significantly affected by the increase in FA, unlike overall gas volume and methane volume.

In Experiment 4, as well as the gradient in CT, the blend of GM1 and GM14 in this experiment also provided an increase in ME and a slight increase in FA content (see Table 1). All grape marc inclusions gave significant reductions in gas volume and VFA production from the control (Table 5), which aligned with previous results in this study and others using grape marc containing high levels of fatty acids [23]. There was no obvious increase in gas production or VFA concentration with increasing ME across the gradient. However, the significant drop in methane percentage observed from the control to GM1 provided evidence for the anti-methanogenic property of FA. In the case of ruminant digestion, reductions in methane gas production may be beneficial as this represents an energy loss to the system that could be directed into animal performance, rather than lost as gaseous emissions [4]. However, here the fermentations that contained high FA grape marc samples (GM1 and GM14) also resulted in lower VFA concentrations, suggesting that it may not be a redirection of energy, but rather just a reduction in the extent of fermentation and a net loss of energy to the system. Shifting the inclusion towards GM14 and higher CT concentrations yielded significant reductions in methane volume and percentage, while gas production and VFA concentration remained relatively steady. This again, highlighted the anti-methanogenic properties of CT without yielding a negative effect on the extent of fermentation.

2.5. The Grape Marc Blending Methodology

The use of compositionally similar grape marc samples to understand how individual components alter in vitro methanogenesis in these experiments has provided some clarity despite the complexity of grape marc composition. In our previous compositional survey of grape marc [12], principal component analysis of the analytical outcomes produced a model containing 42 variables that were significant in contributing to the difference between those 20 samples, many of which were co-correlated. Table 6 outlines the relationship between key compositional parameters of those 20 samples that were of consequence here, either the bioactive compounds of interest (CT and FA), or other metrics that were expected to heavily influence fermentation parameters, such as fiber composition, fermentable sugars, and metabolizable energy.

Table 4. In vitro fermentation parameters for Experiment 3; grape marc samples of differing fatty acid concentrations.

Treatment	Description	Gas Volume (mL/g DM)	CH$_4$ Volume (mL/g DM)	CH$_4$% (mL/100 mL Total Gas)	VFA (mmol/L)	Ac:Pr	NH$_3$ (mg/L)
Control	Control	290.8 ± 6.1 [a]	39.60 ± 1.31 [a]	13.62 ± 0.17 [a]	90.46 ± 2.33 [a]	2.997 ± 0.006 [a]	160.4 ± 6.2 [a,b]
GM20	High CT, low FA	288.3 ± 2.5 [a]	35.37 ± 1.10 [b]	12.23 ± 0.42 [b,c]	85.56 ± 5.74 [a,b]	2.823 ± 0.021 [b]	95.6 ± 9.7 [c]
GM20 + PEG	Removal of CT, FA effect only	295.2 ± 2.1 [a]	36.47 ± 0.75 [b]	12.35 ± 0.17 [b,c]	87.63 ± 0.63 [a]	2.767 ± 0.015 [b]	105.6 ± 3.6 [c]
GM14	High CT, high FA	266.5 ± 2.4 [b]	31.40 ± 0.76 [c]	11.76 ± 0.18 [b]	79.40 ± 2.11 [b]	3.030 ± 0.046 [a]	145.2 ± 3.6 [a]
GM14 + PEG	Removal of CT, FA effect only	271.5 ± 3.5 [b]	34.47 ± 0.55 [b]	12.67 ± 0.20 [c]	78.03 ± 1.06 [b]	2.963 ± 0.055 [a]	174.8 ± 6.2 [b]
SEM		4.99	1.280	0.339	4.084	0.0468	8.58
p		<0.0001	<0.0001	0.339	0.0019	0.0468	<0.0001

Data expressed as mean value ± standard deviation of triplicates. Values in the same column within each experiment with different superscript letters were significantly different ($p <$ 0.05). GM, grape marc; PEG, polyethylene glycol; FA, fatty acids; CT (condensed tannin concentration, as determined by phloroglucinoysis); VFA, volatile fatty acid; Ac:Pr, molar ratio of acetate to propionate; DM, dry matter.

Table 5. In vitro fermentation parameters for Experiment 4; gradient of grape marc samples with differing condensed tannin concentration.

Treatment	Description	Gas Volume (mL/g DM)	CH$_4$ Volume (mL/g DM)	CH$_4$% (mL/100 mL Total Gas)	VFA (mmol/L)	Ac:Pr	NH$_3$ (mg/L)
Control	Control	290.8 ± 6.1 [a]	39.60 ± 1.31 [a]	13.62 ± 0.17 [a]	90.46 ± 2.33 [a]	2.997 ± 0.006 [a]	160.4 ± 6.2 [a]
GM1	Low CT, high FA	268.1 ± 4.6 [b]	34.23 ± 0.95 [b]	12.72 ± 0.23 [b]	78.03 ± 3.26 [b]	3.077 ± 0.046 [a,b]	156.8 ± 6.6 [a,b]
GM1 + GM14 (2:1)	Medium-low CT, high FA	269.3 ± 7.1 [b]	32.97 ± 0.25 [b,c]	12.21 ± 0.23 [c,d]	76.68 ± 4.04 [b]	3.113 ± 0.012 [b]	152.0 ± 3.7 [a,b]
GM1 + GM14 (1:2)	Medium-high CT, high FA	270.1 ± 0.9 [b]	33.30 ± 0.26 [b,c]	12.30 ± 0.06 [b,c]	78.51 ± 0.66 [b]	3.050 ± 0.026 [a,b]	146.8 ± 3.5 [b]
GM14	High CT, high FA	266.5 ± 2.4 [b]	31.40 ± 0.76 [c]	11.76 ± 0.18 [d]	79.40 ± 2.11 [b]	3.030 ± 0.046 [a,b]	145.2 ± 3.6 [b]
SEM		6.59	1.115	0.250	3.741	0.0438	6.72
p		0.0006	<0.0001	<0.0001	0.0006	0.011	0.0157

Data expressed as mean value ± standard deviation of triplicates. Values in the same column within each experiment with different superscript letters were significantly different ($p <$ 0.05). GM, grape marc; CT (condensed tannin concentration, as determined by phloroglucinoysis); VFA, volatile fatty acid; Ac:Pr, molar ratio of acetate to propionate; DM, dry matter.

Table 6. Pearson correlation coefficients (r) for grape marc compositional variables, with *p*-value shown in parentheses, using data for twenty grape marc samples taken from Hixson et al., 2016 and re-assessed to give correlations within the sample set.

Variable	CT	mDP	cis/trans	%PD	%GalI	FA	ADF	NDF	NFC	ESC	ME
mDP	0.14 (0.5624)										
cis/trans	−0.04 (0.886)	0.94 (<0.0001)									
%PD	0.17 (0.476)	0.70 (0.0009)	0.59 (0.0084)								
%GalI	−0.03 (0.9157)	−0.70 (0.0009)	−0.69 (0.0011)	−0.71 (0.0006)							
FA	0.00 (0.9915)	−0.58 (0.0086)	−0.58 (0.0091)	−0.62 (0.0045)	0.93 (<0.0001)						
ADF	0.05 (0.8262)	−0.73 (0.0004)	−0.72 (0.0005)	−0.64 (0.0035)	0.81 (<0.0001)	0.82 (<0.0001)					
NDF	0.04 (0.8744)	−0.74 (0.0003)	−0.74 (0.0003)	−0.67 (0.0017)	0.88 (<0.0001)	0.87 (<0.0001)	0.97 (<0.0001)				
NFC	0.10 (0.6837)	0.73 (0.0004)	0.70 (0.0008)	0.70 (0.0008)	−0.87 (<0.0001)	−0.87 (<0.0001)	−0.96 (<0.0001)	−0.98 (<0.0001)			
ESC	0.14 (0.5633)	0.66 (0.0022)	0.65 (0.0027)	0.55 (0.014)	−0.74 (0.0003)	−0.70 (0.0008)	−0.90 (<0.0001)	−0.90 (<0.0001)	0.93 (<0.0001)		

Table 6. *Cont.*

Variable	CT	mDP	cis/trans	%PD	%Gall	FA	ADF	NDF	NFC	ESC	ME
ME	−0.26 (0.273)	0.52 (0.0212)	0.57 (0.0117)	0.37 (0.1189)	−0.70 (0.0009)	−0.66 (0.0021)	−0.77 (0.0001)	−0.80 (<0.0001)	0.68 (0.0014)	0.62 (0.0048)	
Lignin	0.09 (0.7108)	−0.60 (0.0062)	−0.59 (0.0072)	−0.61 (0.0052)	0.86 (<0.0001)	0.93 (<0.0001)	0.94 (<0.0001)	0.93 (<0.0001)	−0.92 (<0.0001)	−0.78 (0.0001)	−0.74 (0.0003)

CT (condensed tannin concentration, as determined by phloroglucinoysis), mDP, mean degree of polymerization; %PD, percentage of prodelphinidin-type subunits; %Gall, percentage of subunits with gallic acid substitution; FA, fatty acid; ADF, acid detergent fiber; NDF, neutral detergent fiber; NFC, non-fiber carbohydrate; ESC, ethanol soluble carbohydrate; ME, metabolizable energy; DM, dry matter.

It has already been stated that grape marc CT compositional variables are well correlated, and further investigation of compositional correlations show that many other parameters are also significantly correlated. For example, the size of CT (mDP) correlates with most other parameters with a high level of statistical significance. This creates an inability to select multiple samples that display differences in a single variable as there exists an inherent difference in many other key fermentation-relevant variables. It appears the processing differences that create compositional change in grape marc, in addition to the natural variation that is observed in CT, makes grape marc an unsuitable candidate for this simplified methodology.

3. Materials and Methods

3.1. Grape Marc and Grape-Derived Tannin

Five different grape marc samples were selected from a pool of 20 diverse grape marc samples that had been thoroughly characterized [12]. Samples were chosen based on their tannin and fatty acid content; these were a steam-distilled and flash-dried marc (GM1), a steam-distilled mix of red and white marc (GM6), a seed-only sample from fresh white marc (GM14), a skin-only sample from fresh red marc (GM18), and a grape stalk-only sample (GM20). Grape marc collection, storage, and preparation were as previously described. Grape marc sample identifiers were consistent with previous work on these same samples [12,23]. Extractable grape-derived tannin, Grap'tan PC (GT), was obtained commercially (EnolTech, Angaston, South Australia, Australia) and used as supplied.

3.2. Chemical Analysis

All grape marc samples were analyzed for tannin chemistry, nutritive value, and a range of other important factors as previously described [12], with all sample identifiers matching those used in previous publications. Only key analytical outcomes (tannin, fatty acids, energy) have been re-published here. Extractable grape-derived CT (Grap'tan PC) was analyzed for CT subunit concentration and composition by phloroglucinolysis as previously described [24]. The composition of GM blends submitted to fermentation was calculated from the individual composition, and either the mass ratio of substrates used for concentration-based components (CT, FA, ME etc.), or using the mass ratio of CT for CT compositional variables (mDP, cis/trans, %PD and %Gall). The full composition of each treatment used in this work can be seen in Supplementary Material (Table S1), along with the fatty acid profiles (Table S2).

3.3. In Vitro Fermentation

The use of donor animals was approved by the Animal Ethics Committee of The University of Western Australia, Approval number RA3/100/1424. The in vitro batch fermentation experiments were run as previously described, with some modifications [28]. In brief, the control fermentation substrate was a commercial pellet (Milne Standard Pellets, Milne Feed, Welshpool, Western Australia, Australia) that contained barley (350 g/kg), oats (200 g/kg), wheat (200 g/kg), lupins (60 g/kg), straw (100 g/kg), mill mix (50 g/kg), and minerals (40 g/kg); and had nutritive value of dry matter (DM) 910 g/kg DM, acid detergent fiber 156 g/kg DM, neutral detergent fiber 282 g/kg DM, starch 310 g/kg DM, crude protein 145 g/kg DM, and crude fat 12 g/kg DM. Pellet material was ground to pass a 1 mm screen prior to inclusion in the assay.

Each treatment was tested in triplicate. Fermentation substrate (control, 0.5 g) was weighed into specialized anaerobic culturing vials (100 mL serum bottle, Cat. No. W012465I Wheaton, Millville, NJ 08332, USA) and transferred into an anaerobic chamber (Coy Vinyl Anaerobic Chamber; Coy Laboratory Products Inc., Grace Lake, MI, USA, maintained at 39 °C and supplied with 800 mL/L N_2, 100 mL/L CO_2 and 100 mL/L H_2). The rumen fluid was collected on the day of the experiment 3 h after feeding to obtain a sample with a maximal microbial activity from three ruminally cannulated adult Merino wethers (mean body weight 65.4 ± 2.0 kg) that were fed a diet consisting of 1 kg oaten

chaff, 250 g lupins, and 25 g mineral mix for 2 weeks before sampling. Rumen fluid was pooled, strained, buffered using McDougall buffer (1:1.5 v/v), and the pH adjusted to between 7.1 and 7.3 using citric acid. Each tube was filled with 50 mL of this buffered rumen fluid. For grape marc treatments, 0.35 g of a control substrate was mixed with 0.15 g of grape marc or grape marc blend. Where extractable tannin was used, 10 mg was added, and polyethylene glycol-containing treatments were supplemented with 350 mg of PEG 8000. Tubes were stoppered, crimped, and incubated with shaking for 24 h. At the end of the incubation period, gas and methane volume and methane concentrations in the headspace gas expressed as mL/g dry matter incubated (DMi), as well as concentrations of volatile fatty acids (VFA), ammonia, and acetate:propionate ratios were measured as described previously [28]. Gas production was measured using a pressure transducer (Greisinger Electronic GmbH, Regenstauf, Germany), and methane production was determined by gas chromatography with Thermal Conductivity Detector (Bruker-450 GC, Bruker Technologies, Melbourne, Australia) equipped with Compass CDS Acquisition software (Bruker Technologies, Australia), using a Hayesep Q 0.25 mm × 10 m column with He as carrier gas flow at 30 mL/min. Data shown are an average of triplicate ferments, results from individual replicates can be found in Supplementary Material (Table S3).

3.4. Statistical Analyses

Values shown in the text are the average of triplicates. Analysis of variance ($p = 0.05$) was performed using Tukey's multiple comparison test (GraphPad Prism, GraphPad Software, La Jolla, CA, USA). Pearson correlation coefficients and corresponding *p*-values were determined from data taken from Hixson et al. (2016) [12] using an X-Y correlation analysis (GraphPad Prism).

4. Conclusions

The methodology used here provided a preliminary insight into the compounds present in grape marc that are responsible for modulating methanogenesis. We have investigated the role that grape marc CT and FA play in methanogenesis. In general, treatments containing high FA concentrations resulted in significant reductions in gas production and VFA concentration, and any reductions in methane volume were largely attributed to this drop in overall gas production. When considering CT, a trend for smaller, more extractable tannin being more effective at reducing methanogenesis was observed.

Author Contributions: J.L.H. conceived the experiments; J.L.H., E.N.W., Z.D., and P.E.V. designed the experiments; J.V. and Z.D. performed the in vitro batch fermentation experiments; J.L.H., P.A.S., Z.D., and P.E.V. analyzed and interpreted the data; J.L.H. drafted the manuscript; all authors provided critical assessment and editing on the manuscript.

References

1. Knapp, J.R.; Laur, G.L.; Vadas, P.A.; Weiss, W.P.; Tricarico, J.M. Invited review: Enteric methane in dairy cattle production: Quantifying the opportunities and impact of reducing emissions. *J. Dairy Sci.* **2014**, *97*, 3231–3261. [CrossRef] [PubMed]
2. Gerber, P.J.; Hristov, A.N.; Henderson, B.; Makkar, H.; Oh, J.; Lee, C.; Meinen, R.; Montes, F.; Ott, T.; Firkins, J.; et al. Technical options for the mitigation of direct methane and nitrous oxide emissions from livestock: A review. *Animal* **2013**, *7* (Suppl. 2), 220–234. [CrossRef] [PubMed]
3. Hristov, A.N.; Ott, T.; Tricarico, J.; Rotz, A.; Waghorn, G.; Adesogan, A.; Dijkstra, J.; Montes, F.; Oh, J.; Kebreab, E.; et al. Special topics—Mitigation of methane and nitrous oxide emissions from animal operations: III. A review of animal management mitigation options. *J. Anim. Sci.* **2013**, *91*, 5095–5113. [CrossRef] [PubMed]
4. Patra, A. Enteric methane mitigation technologies for ruminant livestock: A synthesis of current research and future directions. *Environ. Monit. Assess.* **2012**, *184*, 1929–1952. [CrossRef] [PubMed]
5. Mirzaei-Aghsaghali, A.; Maheri-Sis, N. Nutritive value of some agro-industrial by-products for ruminants—A review. *World J. Zool.* **2008**, *3*, 40–46.
6. Jayanegara, A.; Leiber, F.; Kreuzer, M. Meta-analysis of the relationship between dietary tannin level and methane formation in ruminants from in vivo and in vitro experiments. *J. Anim. Physiol. Anim. Nutr.* **2012**, *96*, 365–375. [CrossRef] [PubMed]
7. Huyen, N.T.; Fryganas, C.; Uittenbogaard, G.; Mueller-Harvey, I.; Verstegen, M.W.A.; Hendriks, W.H.; Pellikaan, W.F. Structural features of condensed tannins affect in vitro ruminal methane production and fermentation characteristics. *J. Agric. Sci.* **2016**, *154*, 1474–1487. [CrossRef]
8. Hatew, B.; Hayot Carbonero, C.; Stringano, E.; Sales, L.F.; Smith, L.M.J.; Mueller-Harvey, I.; Hendriks, W.H.; Pellikaan, W.F. Diversity of condensed tannin structures affects rumenin vitromethane production in sainfoin (*Onobrychis viciifolia*) accessions. *Grass Forage Sci.* **2015**, *70*, 474–490. [CrossRef]
9. Kraus, T.E.; Yu, Z.; Preston, C.M.; Dahlgren, R.A.; Zasoski, R.J. Linking chemical reactivity and protein precipitation to structural characteristics of foliar tannins. *J. Chem. Ecol.* **2003**, *29*, 703–730. [CrossRef] [PubMed]
10. Lorenz, M.M.; Alkhafadji, L.; Stringano, E.; Nilsson, S.; Mueller-Harvey, I.; Uden, P. Relationship between condensed tannin structures and their ability to precipitate feed proteins in the rumen. *J. Sci. Food Agric.* **2014**, *94*, 963–968. [CrossRef] [PubMed]
11. Mueller-Harvey, I.; Bee, G.; Dohme-Meier, F.; Hoste, H.; Karonen, M.; Külliker, R.; Lüscher, A.; Niderkorn, V.; Pellikaan, W.F.; Salminen, J.-P.; et al. Benefits of condensed tannins in forage legumes fed to ruminants: Importance of structure, concentration and diet composition. *Crop Sci.* **2017**. [CrossRef]
12. Hixson, J.L.; Jacobs, J.L.; Wilkes, E.N.; Smith, P.A. Survey of the Variation in Grape Marc Condensed Tannin Composition and Concentration and Analysis of Key Compositional Factors. *J. Agric. Food Chem.* **2016**, *64*, 7076–7086. [CrossRef] [PubMed]
13. Moate, P.J.; Williams, S.R.; Torok, V.A.; Hannah, M.C.; Ribaux, B.E.; Tavendale, M.H.; Eckard, R.J.; Jacobs, J.L.; Auldist, M.J.; Wales, W.J. Grape marc reduces methane emissions when fed to dairy cows. *J. Dairy Sci.* **2014**, *97*, 5073–5087. [CrossRef] [PubMed]
14. Abarghuei, M.J.; Rouzbehan, Y.; Alipour, D. The influence of the grape pomace on the ruminal parameters of sheep. *Livest. Sci.* **2010**, *132*, 73–79. [CrossRef]
15. Besharati, M.; Taghizadeh, A. Evaluation of dried grape by-product as a tanniniferous tropical feedstuff. *Anim. Feed Sci. Technol.* **2009**, *152*, 198–203. [CrossRef]
16. Basalan, M.; Gungor, T.; Owens, F.N.; Yalcinkaya, I. Nutrient content and in vitro digestibility of Turkish grape pomaces. *Anim. Feed Sci. Technol.* **2011**, *169*, 194–198. [CrossRef]
17. Spanghero, M.; Salem, A.Z.M.; Robinson, P.H. Chemical composition, including secondary metabolites, and rumen fermentability of seeds and pulp of Californian (USA) and Italian grape pomaces. *Anim. Feed Sci. Technol.* **2009**, *152*, 243–255. [CrossRef]
18. Molina-Alcaide, E.; Moumen, A.; Martín-García, A.I. By-products from viticulture and the wine industry: Potential as sources of nutrients for ruminants. *J. Sci. Food Agric.* **2008**, *88*, 597–604. [CrossRef]
19. Greenwood, S.L.; Edwards, G.R.; Harrison, R. Short communication: Supplementing grape marc to cows fed a pasture-based diet as a method to alter nitrogen partitioning and excretion. *J. Dairy Sci.* **2012**, *95*, 755–758. [CrossRef] [PubMed]

20. Hixson, J.L.; Bindon, K.A.; Smith, P.A. Evaluation of direct phloroglucinolysis and colorimetric depolymerization assays and their applicability for determining condensed tannins in grape marc. *J. Agric. Food Chem.* **2015**, *63*, 9954–9962. [CrossRef] [PubMed]

21. Rasmussen, J.; Harrison, A. The Benefits of Supplementary Fat in Feed Rations for Ruminants with Particular Focus on Reducing Levels of Methane Production. *ISRN Vet. Sci.* **2011**, *2011*, 10. [CrossRef] [PubMed]

22. Beauchemin, K.A.; McGinn, S.M.; Benchaar, C.; Holtshausen, L. Crushed sunflower, flax, or canola seeds in lactating dairy cow diets: Effects on methane production, rumen fermentation, and milk production. *J. Dairy Sci.* **2009**, *92*, 2118–2127. [CrossRef] [PubMed]

23. Russo, V.M.; Jacobs, J.L.; Hannah, M.C.; Moate, P.J.; Dunshea, F.R.; Leury, B.J. In vitro evaluation of the methane mitigation potential of a range of grape marc products. *Anim. Prod. Sci.* **2017**, *57*. [CrossRef]

24. Kennedy, J.A.; Jones, G.P. Analysis of proanthocyanidin cleavage products following acid-catalysis in the presence of excess phloroglucinol. *J. Agric. Food Chem.* **2001**, *49*, 1740–1746. [CrossRef] [PubMed]

25. Bindon, K.A.; Smith, P.A.; Holt, H.; Kennedy, J.A. Interaction between Grape-Derived Proanthocyanidins and Cell Wall Material. 2. Implications for Vinification. *J. Agric. Food Chem.* **2010**, *58*, 10736–10746. [CrossRef] [PubMed]

26. Bindon, K.A.; Smith, P.A.; Kennedy, J.A. Interaction between Grape-Derived Proanthocyanidins and Cell Wall Material. 1. Effect on Proanthocyanidin Composition and Molecular Mass. *J. Agric. Food Chem.* **2010**, *58*, 2520–2528. [CrossRef] [PubMed]

27. Alipour, D.; Rouzbehan, Y. Effects of ensiling grape pomace and addition of polyethylene glycol on in vitro gas production and microbial biomass yield. *Anim. Feed Sci. Technol.* **2007**, *137*, 138–149. [CrossRef]

28. Durmic, Z.; Moate, P.J.; Eckard, R.; Revell, D.K.; Williams, R.; Vercoe, P.E. In vitro screening of selected feed additives, plant essential oils and plant extracts for rumen methane mitigation. *J. Sci. Food Agric.* **2014**, *94*, 1191–1196. [CrossRef] [PubMed]

Sample Availability: Samples of the grape marcs used in this work, and the extractable tannin are available from the authors.

Characterization of Condensed Tannins from Purple Prairie Clover (*Dalea purpurea* Vent.) Conserved as either Freeze-Dried Forage, Sun-Cured Hay or Silage

Kai Peng [1,2,3]**, Qianqian Huang** [4]**, Zhongjun Xu** [2]**, Tim A. McAllister** [2]**, Surya Acharya** [2]**, Irene Mueller-Harvey** [5]**, Christopher Drake** [5]**, Junming Cao** [1]**, Yanhua Huang** [1]**, Yuping Sun** [1]**, Shunxi Wang** [3] **and Yuxi Wang** [2]**,***

[1]   Key Laboratory of Animal Nutrition and Feed Science (South China) of Ministry of Agriculture, Guangdong Key Laboratory of Animal Breeding and Nutrition, Institute of Animal Science, Guangdong Academy of Agricultural Science, Guangzhou 510640, China; pengkai1016@126.com (K.P.); junmcao@163.com (J.C.); huangyh111@126.com (Y.H.); sunnyxrdragon@sohu.com (Y.S.)

[2]   Agriculture and Agri-Food Canada, Lethbridge Research and Development Centre, Lethbridge, AB T1J 4B1, Canada; zhongjun.xu@agr.gc.ca (Z.X.); tim.mcallister@agr.gc.ca (T.A.M.); surya.acharya@agr.gc.ca (S.A.)

[3]   College of Engineering, China Agriculture University, Beijing 100083, China; wsx68@cau.edu.cn

[4]   College of Animal Science and Technology, Yangzhou University, Yangzhou 225009, China; huangq0315@126.com

[5]   Chemistry and Biochemistry Laboratory, School of Agriculture, Policy and Development, University of Reading, Reading RG6 6AT, UK; i.mueller-harvey@reading.ac.uk (I.M.-H.); chrsdrake@googlemail.com (C.D.)

*   Correspondence: yuxi.wang@agr.gc.ca; Tel.: +1-403-317-3498; Fax: +1-403-317-2182

Abstract: Conservation methods have been shown to affect forage nutrient composition and value, but little information is available about the effect of forage conservation on plant condensed tannins (CT). The objective of this study was to assess the effects of conservation method on the concentration, chemical composition and biological activity of CT. Whole-plant purple prairie clover (PPC, *Dalea purpurea* Vent.) was harvested at full flower and conserved as freeze-dried forage (FD), hay (HAY) or silage (SIL). Concentration of CT in conserved PPC was determined by the butanol-HCl-acetone method. Structural composition, protein-precipitation capacity and anti-bacterial activity of CT isolated from conserved forage were determined by in situ thiolytic degradation followed by HPLC-MS analysis, a protein precipitation assay using bovine serum albumin and ribulose 1,5-disphosphate carboxylase as model proteins and by an *Escherichia coli* (*E. coli*) growth test, respectively. Conservation method had no effect on concentration of total CT, but ensiling decreased ($p < 0.001$) extractable CT and increased ($p < 0.001$) protein- and fiber-bound CT. In contrast, hay-making only increased ($p < 0.01$) protein-bound CT. Regardless of conservation method, epigallocatechin (EGC), catechin (C) and epicatechin (EC) were the major flavan-3-ol units, and gallocatechin (GC) was absent from both terminal and extension units of PPC CT. The SIL CT had the lowest ($p < 0.001$) EGC, but the highest ($p < 0.01$) EC in the extension units. Similarly, SIL CT exhibited a lower ($p < 0.001$) mean degree of polymerization (mDP), but higher ($p < 0.001$) procyanidins (PC) than FD or HAY CT. The protein-precipitating capacity of CT in conserved PPC ranked ($p < 0.001$) as FD > HAY > SIL. *E. coli* growth n M9 medium was inhibited by 25–100 μg/mL of CT isolated from FD, HAY and SIL ($p < 0.05$), but preservation method had no effect on the ability of CT to inhibit bacterial growth. The results demonstrated that ensiling decreased the extractability and protein-precipitating capacity of CT by increasing the proportions of PC. Purple prairie clover conserved as hay retained more biologically active CT than if it was conserved as silage.

Keywords: tannin composition; purple prairie clover; conservation method; protein precipitation; *Escherichia coli*

1. Introduction

Condensed tannins (CT) are a group of naturally occurring phenolic compounds that are widely present in plants including a number of common forages. Condensed tannins are oligomeric or polymeric flavonoids consisting of flavan-3-ol units that commonly include catechin (C), epicatechin (EC), gallocatechin (GC) and epigallocatechin (EGC) with the relative proportions of these flavonoids differing among plant types. Condensed tannins exhibit various antimicrobial, anti-parasitic, anti-oxidant, and anti-inflammatory activities and as a result are seen as a promising natural alternative to in-feed antibiotics [1]. It has been shown that concentration and composition of CT in a plant are affected by the growing conditions, phenological growth stage as well as tissue type [2–5]. Ensiling and hay-making are two common methods used to conserve forage as silage or hay for ruminant livestock. It is generally recognized that these conservation methods alter the nutrient composition of forage, leading to changes in the feed value of conserved forages [6]. For example, excessive proteolysis can occur during ensiling, decreasing protein nutritive value [7]. Although studies have found that forage conservation methods also reduce the extractability of CT [6], their effects on the structural nature and specific biological activity of CT have not been examined. Research in this area is needed because the biological activities of CT in forage are closely associated with their concentrations and chemical structures [8].

Purple prairie clover (PPC; *Dalea purpurea* Vent.) is a native legume that is widely distributed in the North America prairie and contains high concentrations of CT (up to 94 g/kg DM). It has been shown that CT in PPC possess strong anti-*Escherichia coli* activity [9–12]. In addition, PPC CT cause greater precipitation of bovine serum albumin (BSA) and spinach ribulose 1,5-disphosphate carboxylase (Rubisco) [5,9] than CT from other plant sources. Huang et al. [6] suggested that the biological activity of CT in PPC conserved as hay was higher than that in silage because more of the CT remained in an extractable form. However, the chemical composition of the extractable CT in these conserved forages was not determined. The objective of this study was to assess the effects of PPC conservation method on the concentration, chemical composition and biological activity of CT.

2. Results

2.1. Characteristics of PPC Conserved as FD, HAY and SIL

Although organic matter (OM) and crude protein (CP) were not affected by forage conservation method (Table 1), PPC conserved as FD had lower ($p < 0.01$) concentrations of neutral detergent fibre (NDF) and acid detergent fibre (ADF) than HAY or SIL.

Table 1. Chemical composition (g/kg DM) of whole-plant purple prairie clover conserved as freeze-dried forage (FD), hay (HAY) or silage (SIL) ($n = 3$).

Item	FD	HAY	SIL	SEM	*p*-Value
Organic matter	924	923	913	3.96	0.174
Crude protein (N × 6.25)	158	157	165	2.20	0.058
Neutral detergent fibre	439 [b]	497 [a]	480 [a]	5.74	0.001
Acid detergent fibre	405 [b]	422 [a]	417 [a]	2.38	0.006
Acid detergent lignin	79.8 [b]	98.3 [a]	90.1 [a,b]	2.79	0.009
Water-soluble carbohydrate	25.4 [a]	11.5 [b]	2.4 [c]	0.34	<0.001
Total phenols [1]	66.2 [a]	51.4 [b]	28.6 [c]	0.95	<0.001
Condensed tannins (CT)					
Extractable CT	70.2 [a]	64.1 [a]	27.4 [b]	1.53	<0.001
Fibre-bound CT	5.2 [b]	5.6 [b]	7.1 [a]	0.17	<0.001
Protein-bound CT	9.0 [c]	12.4 [b]	44.3 [a]	0.17	<0.001
Total CT	84.5	82.2	78.9	1.45	0.083

[1] Determined as tannic acid equivalent. [a, b, c] Means with different letters differ within rows ($p < 0.05$). SEM, standard error of the mean.

The acid detergent lignin (ADL) content of FD was lower ($p < 0.01$) than HAY. Contents of NDF, ADF and ADL were similar ($p > 0.05$) between HAY and SIL. The water-soluble carbohydrate (WSC) concentration in conserved forages ranked as FD > HAY > SIL ($p < 0.001$). Among the conserved forages, SIL contained the lowest ($p < 0.001$) level of total phenolics, followed by HAY and FD, respectively. Similarly, SIL exhibited lower ($p < 0.001$) extractable CT than FD or HAY. However, SIL had greater ($p < 0.001$) concentrations of fiber-bound and protein-bound CT than FD or HAY. Protein-bound CT were also greater ($p < 0.001$) in HAY than in FD. Conservation method had no effect on the concentration of total CT ($p > 0.05$).

2.2. CT Terminal and Extension Units

Regardless of conservation method, the terminal units of PPC CT were composed of C and EC only, and no GC or EGC was detected.

Following thiolytic degradation, two flavan-3-ols (i.e., C and EC), were detected in terminal units as well as EGC-benzyl mercaptan (BM), C-BM and EC-BM adducts in extension units in all samples, regardless of conservation method (Figure 1). Terminal units accounted on average for 5–8% of all flavan-3-ol units in tannins. The extension units (92–95%) contained three flavanols, i.e., EGC (19–28%), C (2–4%) and EC (64–69%), but lacked GC (Table 2).

Table 2. Flavan-3-ol composition (% molar percentages) in condensed tannins of whole-plant purple prairie clover conserved as freeze-dried forage (FD), hay (HAY) or silage (SIL).

	Terminal Units (%)				Extension Units (%)			
	GC [1]	EGC	C	EC	GC-BM [2]	EGC-BM	C-BM	EC-BM
FD	0	0	1.56 [a]	4.26 [b]	0	23.50 [b]	2.42 [b]	68.26 [a]
HAY	0	0	1.26 [b]	4.13 [b]	0	27.97 [a]	2.19 [b]	64.45 [b]
SIL	0	0	1.29 [b]	6.94 [a]	0	19.17 [c]	3.78 [a]	68.82 [a]
SEM	-	-	0.063	0.282	-	0.928	0.164	0.743
p-value	-	-	0.008	<0.001	-	<0.001	<0.001	0.002

[1] GC = gallocatechin, EGC = epigallocatechin, C = catechin, EC = epicatechin. [2] Extension units as BM-adducts: EGC-BM = epigallocatechin, C-BM = catechin, EC-BM = epicatechin, where BM = benzyl mercaptan. [a,b,c] Means with different letters differ within columns ($p < 0.05$). SEM, standard error of the mean.

Condensed tannins present in HAY had greater ($p < 0.001$) proportion of EGC, but lower ($p < 0.01$) EC in the extension units than FD and SIL. In contrast, CT from SIL had lower ($p < 0.001$) EGC, but a greater ($p < 0.001$) proportion of C as compared to FD.

The average polymer size of CT, ranged from 12.4 to 18.6 of mean degree polymerization (mDP) in conserved PPC (Table 3). The mDP was lower ($p < 0.001$) in SIL as compared to FD or HAY.
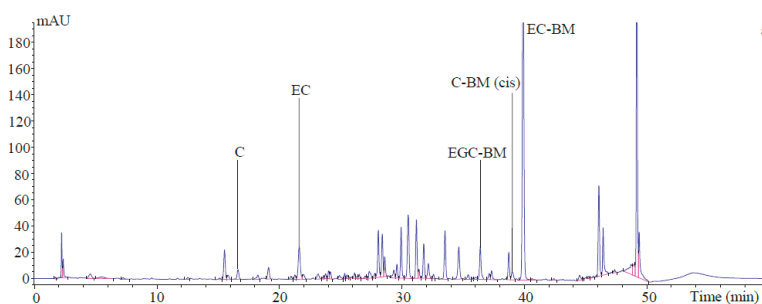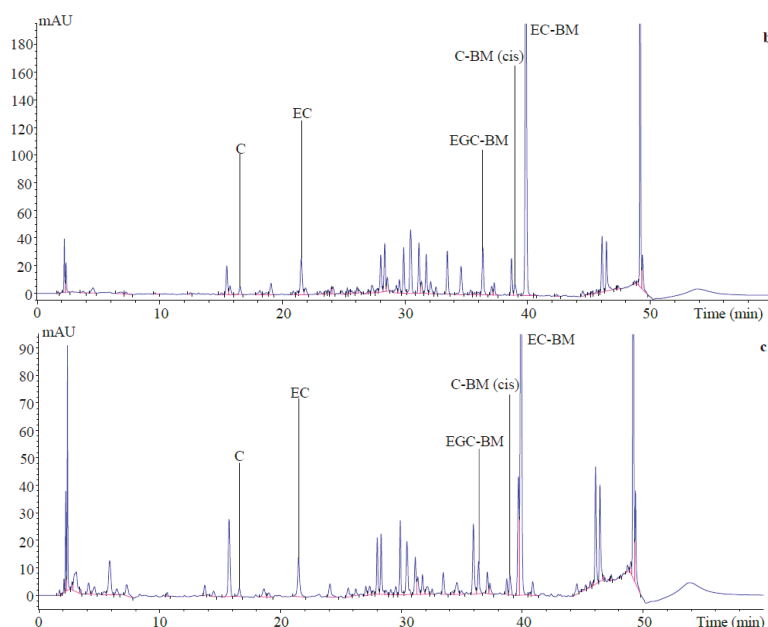

Figure 1. *Cont.*

Figure 1. HPLC chromatograms (280 nm) of thiolysis reaction products that were obtained from (**a**) freeze-dried; (**b**) hay and (**c**) silage of whole-plant purple prairie clover. Terminal units: C = catechin, EC = epicatechin; Extension units as BM-adducts: EGC-BM = epigallocatechin, C-BM = catechin, EC-BM = epicatechin, where BM = benzyl mercaptan.

Table 3. Structural composition of condensed tannins from whole-plant purple prairie clover conserved as freeze-dried forage (FD), hay (HAY) or silage (SIL).

	mDP [1]	PC (%) [2]	PD (%)	*Cis* (%) [3]	*Trans* (%)
FD	17.3 [a]	76.5 [b]	23.5 [b]	96.0 [a]	4.0 [b]
HAY	18.6 [a]	72.0 [c]	28.0 [a]	96.6 [a]	3.4 [b]
SIL	12.4 [b]	80.8 [a]	19.2 [c]	94.9 [b]	5.1 [a]
SEM	0.66	0.93	0.93	0.20	0.20
p-value	<0.001	<0.001	<0.001	<0.001	<0.001

[1] mDP = mean degree of polymerization; [2] PC = procyanidin tannins (C + EC); PD = prodelphinidin tannins (GC + EGC); [3] *cis* = *cis* isomers of flavan-3-ol subunits (EC + EGC); *trans* = *trans* isomers of flavan-3-ol subunits (C + GC); [a, b, c] Means in a column with different letters differ within columns (*p* < 0.05). SEM, standard error of the mean.

Similarly, CT in SIL had a lower (*p* < 0.001) proportion of prodelphinidins (PD; i.e., GC + EGC), but a higher (*p* < 0.001) proportion of procyanidins (PC; i.e., C + EC) than FD and HAY. In contrast, CT in HAY had a higher (*p* < 0.001) proportion of PD but lower (*p* < 0.001) proportion of PC than FD PPC. Irrespective of conservation method, PPC CT were dominated by the *cis*-isomers (i.e., EC + EGC). SIL had a lower (*p* < 0.001) proportion of *cis*-isomers and higher (*p* < 0.001) proportion of *trans*-isomers than in FD or HAY. There was no difference (*p* > 0.05) in *cis*- and *trans*-isomers between FD and HAY.

2.3. Protein-Precipitating Capacities of CT in PPC Conserved as FD, HAY and SIL

Bovine serum albumin was completely precipitated by ≥1000 µg PPC CT (Figure 2a), whereas Rubisco was completely precipitated by ≥750 µg PPC CT (Figure 2b). The protein-precipitating capacity of CT in the conserved PPC ranked in the order of FD > HAY > SIL (*p* < 0.001) for both BSA

and Rubisco proteins. Condensed tannins from PPC, consistently exhibited a lower ($p < 0.001$) ability to precipitate BSA than Rubisco, irrespective of conservation method (Table 4).
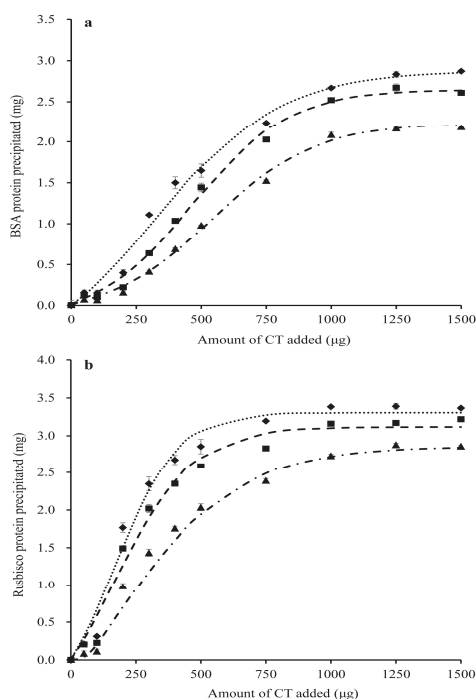

Figure 2. Precipitation of bovine serum albumin (BSA; **a**) and spinach ribulose 1,5-disphosphate carboxylase (Rubisco; **b**) by condensed tannins (CT) isolated from freeze-dried purple prairie clover (◆FD), or conserved as hay (■HAY) or silage (▲SIL). The dash lines relate to corresponding CT data which were fitted to a SigmaPlot curve as described under statistical analysis. Bars indicate standard error and where not visible, fall within symbols.

Table 4. Precipitating capacities of condensed tannins from purple prairie clover conserved as freeze-dried forage (FD), hay (HAY) or silage (SIL).

Protein [1]	Parameters [2]	FD	HAY	SIL	SEM	*p*-Value
BSA	$a_0 + a$	3.1 [a]	2.9 [b]	2.4 [c]	0.01	<0.001
	b	323 [b]	467 [a]	541 [a]	0.01	<0.001
	c	244 [a]	185 [b]	200 [b]	7.72	0.004
	PP	124 [c]	172 [b]	223 [a]	2.57	<0.001
Rubisco	$a_0 + a$	3.4 [a]	3.3 [b]	3.0 [c]	0.02	<0.001
	b	173	166	152	11.10	0.428
	c	120 [b]	152 [b]	242 [a]	17.14	0.006
	PP	62 [c]	70 [b]	97 [a]	1.08	<0.001

[a,b,c] Means within a row followed by different letters differ ($p < 0.05$). [1] BSA = bovine serum albumin; Rubisco = ribulose 1, 5-disphosphate carboxylase. [2] Parameters were obtained by fitting the amount of precipitated protein (mg) and amount of CT (µg) incubated with the equation: $y = a_0 + a/(1 + \exp(-(x-b)/c))$, where y = mg of protein (BSA or Rubisco) precipitated, x = µg of CT incubated, $a_0 + a$ = estimated maximal amount (mg) of protein (BSA or Rubisco) precipitated, b = sigmoidal centre (µg of CT at the 50% of maximal protein precipitation), and c = sigmoidal width. *PP*: protein-precipitating capacity, expressed as µg CT required to precipitate 1 mg of protein. SEM, standard error of the mean.

2.4. Growth of E. coli Affected by CT in PPC Conserved as FD, HAY and SIL

Compared to the control and irrespective of conservation method, growth of *E. coli* 25922 and 35281 was inhibited ($p < 0.001$) at all concentrations of CT tested (Table 5). The maximal growth rate (μ) of strain *E. coli* 25922 decreased ($p < 0.001$) as the CT increased from 25 to 100 µg/mL, whereas no difference was observed at CT < 100 µg/mL for *E. coli* 35281. Lag times (L) increased with increasing CT concentrations for both *E. coli* 25922 ($p < 0.001$) and 35281 ($p < 0.05$).

Table 5. Effects of condensed tannins in purple prairie clover conserved as freeze-dried forage (FD), hay (HAY) or silage (SIL) on the growth of the *Escherichia coli* 25922 and 35218.

Strain	Parameter	Conservation Method	Tannin Concentration (µg/mL)				SEM	*p*-Value
			0	25	50	100		
E. coli 25922	μ	FD	1.24 [a]	1.06 [B,b]	1.06 [b]	0.91 [c]	0.032	<0.001
		HAY	1.23 [a]	1.12 [A,b]	1.02 [c]	0.98 [c]	0.018	<0.001
		SIL	1.25 [a]	1.15 [A,b]	1.00 [c]	0.94 [c]	0.016	<0.001
		SEM	0.014	0.014	0.03	0.03		
		p-value	0.598	0.008	0.368	0.250		
	L	FD	0.52 [b]	0.59 [A,b]	0.85 [a]	0.82 [a]	0.028	<0.001
		HAY	0.53 [b]	0.49 [B,b]	0.86 [a]	0.89 [a]	0.011	<0.001
		SIL	0.52 [b]	0.51 [B,b]	0.82 [a,b]	0.95 [a]	0.073	0.006
		SEM	0.004	0.012	0.030	0.085		
		p-value	0.422	0.003	0.659	0.570		
E. coli 35281	μ	FD	1.04 [a]	0.92 [b]	0.92 [b]	0.91 [b]	0.014	<0.001
		HAY	1.06 [a]	0.91 [b]	0.90 [b]	0.86 [b]	0.015	<0.001
		SIL	1.05 [a]	0.89 [b]	0.91 [b]	0.91 [b]	0.016	<0.001
		SEM	0.011	0.018	0.015	0.016		
		p-value	0.572	0.583	0.747	0.133		
	L	FD	0.32 [b]	0.32 [b]	0.33 [b]	0.41 [A,a]	0.016	0.011
		HAY	0.32 [b]	0.30 [b]	0.32 [b]	0.39 [B,a]	0.007	<0.001
		SIL	0.31 [c]	0.34 [b,c]	0.35 [a,b]	0.38 [B,a]	0.006	<0.001
		SEM	0.008	0.016	0.011	0.005		
		p-value	0.530	0.310	0.158	0.032		

Note: The values were obtained by fitting the OD_{600} to the modified Gompertz equation, $\ln (OD_t/OD_0) = A \times \exp\{-\exp((\mu \times e/A) \times (L - t) + 1)\}$, where A is the logarithmic increase of bacterial population, μ is maximum growth rate (per hour), L is the lag time, t is the time (in hours), and OD_t and OD_0 are the optical densities obtained at time t and at zero hour, respectively. Means with different letters differ ($p < 0.05$). [A, B] Capital letters show differences between conservation methods. [a, b, c] Lowercase show differences between tannin concentrations. SEM, standard error of the mean.

The maximal growth rate of *E. coli* 25922 did not differ among conservation methods with the exception of CT at 25 µg/mL. Strain *E. coli* 25922 exposed to 25 µg/mL of FD CT had a greater ($p < 0.01$) L, but a lower ($p < 0.01$) μ than that exposed to HAY or SIL CT. In contrast, μ and the L of *E. coli* 35218 were not affected by the source or concentration of CT, excepting that 100 µg/mL of CT from HAY and SIL decreased ($p < 0.05$) L as compared to CT from FD.

3. Discussion

3.1. Effect of Conservation Method on the Compositions of PPC

The chemical composition of PPC forage conserved as FD, HAY and SIL was similar to the report by Huang et al. [6]. The concentrations of extractable, protein-bound and fiber-bound CT were also comparable with previous reports [6,13,14]. In this study, the higher NDF concentration in HAY and SIL compared with FD suggests that hay-making or ensiling increased the fibre concentration of PPC. The increased NDF in SIL reflects the microbial fermentation of soluble nutrients during ensiling as shown by the lower WSC content of SIL PPC compared to FD PPC. A significant increase in the post-ensiling NDF content of alfalfa was also observed by Broderick [15]. Although the increase of NDF in HAY may also reflect plant and microbial utilization of WSC during drying and post-baling, it is also a result of the loss of leaves, which lowers the leaf-to-stem ratio. As stems contain more

NDF than leaves, it also increases the NDF content of the conserved forage [16]. Loss of leaves during hay-making is one of the major factors that contribute to differences in the nutritive value between hay and other forage conservation methods [17]. Enoh et al. [18] also reported that hay-making increased NDF content of *Brachiaria* as compared to green forage.

Similar concentration of extractable CT in HAY and FD PPC suggests that sun-drying had minimal effect on biological activity of CT in PPC. Similar results were also reported for PPC [6] and sainfoin (*Onobrychis viciifolia* Scop.) hay [19–21]. On the contrary, other studies have observed that extractable CT in sun-cured sericea lespedeza (*Lespedeza cuneate* (Dum. Cours.) G. Don) and sainfoin hay was lower than that in the fresh forage [22,23]. The discrepancy among these studies is likely due to variations in drying conditions and forage type. Scharenberg et al. [20] dried sainfoin in a closed system at 30 °C, while Lorenz et al. [21] wilted sainfoin to a moisture level of 50%, while the PPC in the present study was wilted in the field under hot and windy conditions.

It is interesting to note that ensiling reduced extractable, but increased protein-bound and fiber-bound CT, with no effect on total CT. This result indicates that a portion of extractable CT has been transformed into protein-bound and fiber-bound during ensiling. A shift from extractable to bound CT during the ensiling of PPC was also observed by Huang et al. [6]. It is likely that partial disruption of plant cells as a result of physical chopping before ensiling and microbial fermentation during ensiling enables CT to react with other plant fractions, increasing the bound CT fraction [24]. Ensiling sainfoin (*Onobrychis viciifolia* Scop.) also decreases extractable and increases bound CT [19,20]. Because biological activity of CT in the plant depends on both chemical structure as well as the concentration of the extractable CT [8,25], the reduced extractability of CT in PPC silage suggests that this is the primary factor responsible for the reduced biological activity of PPC CT.

3.2. Effects of Forage Conservation Method on the Structure and Chemical Composition of PPC CT

Although it has been found that conservation methods affect the concentration of CT in forage [6,24], there is no information available about the effects of forage conservation on the chemical structure of CT. To our knowledge, this is the first study that demonstrates that ensiling and hay-making alters the structural characteristics of CT in conserved forage.

The flavan-3-ol composition of PPC in this study was consistent with that of CT extracted from various phenological PPC tissues, with epicatechin (average 72.2%) and epigallocatechin (average 24.2%) being the dominant monomers and gallocatechin being noticably absent from both terminal and extension units [5]. This is comparable to *Lotus corniculatus* CT, which contained about 67% epicatechin and lacked gallocatechin in both terminal and extension units [26,27]. However, the structural composition of CT in PPC also differs from some other forage sources. For examples, epigallocatechin was the principal monomer (≈64%) in *Lotus pedunculatus* [27] and sainfoin CT (52–63%) [28]. In addition, PPC CT in the present study contained more PC than PD, which was consistent with our previous study with PPC [5] but differing from sainfoin CT, which contain more PD than PC [28–31]. Consistent with most sources of CT, both sainfoin and PPC CT contained more *cis* than *trans* units. These results indicate that the structural composition of CT are plant species specific, which probably also contributes to the varying biological activity of different CT.

Compared to altering the extractability of CT, forage conservation method had a relatively minor impact on the structural composition of CT in PPC. Those minor alterations that were noticeable included an increase in PC with ensiling and PD with hay-making. Ensiling apparently decreased mDP and the proportion of *cis*-isomers, whereas hay-making did not affect these parameters. This suggests that ensiling had a greater effect on the composition of CT than hay-making. The reason that ensiling decreased mDP are unknown, but may be attributed to the higher proportion of PC in the ensiled PPC. It has been reported that CT with higher PC tend to have lower mDP and lower extractable CT concentrations [32–34]. Vidal et al. [35] and Tharayil et al. [36] also observed that mild acidic conditions could cleave interflavanic bonds, reducing the degree of polymerization of CTs. In the present study, the pH of PPC declined to 4.8 after one week and remained at this level throughout 10

weeks of storage. Therefore, the mild acidic conditions of the ensiling process may have contributed to a decline in mDP of CT in silage. Whether microbial activity during ensiling had any effect on this response is unknown, although there are significant CT-microbe interactions during ensiling [37]. As compared with ensiling, results indicated that hay-making by sun-curing under the conditions in this study had little effect on CT composition as demonstrated by the similar mDP and proportions of *cis*- and *trans*-isomers of FD and HAY samples.

3.3. Effect of Forage Conservation Method on the Protein-Precipitating Capacity of PPC CT

Previous studies have reported that the protein-precipitating capacities of PPC CT in different phenological tissues of differing maturity is a reflection of the chemical composition of CT [5]. The fact that the protein-precipitating capacity of CT decreased in the order of FD > HAY > SIL indicates that both ensiling and hay-making decreased protein-precipitating capacity, with this response being greater for silage. Binding and precipitating proteins is a common characteristic of CT and is the principal factor responsible for their biological activity [38]. The capacity of CT to bind proteins is determined by their chemical traits including chain length, molecular weight, PC/PD ratio, number of potential hydrogen and hydrophobic bonding sites and conformation [26,39,40]. Therefore, the decreased protein-precipitating capacity of CT by hay-making and ensiling in this study is likely due to alterations in their chemical structure. It has been demonstrated that the affinity of CT for proteins decreases with decreasing mDP [41–45] and proportions of PD [46–48]. Moreover, De Freitas and Mateus [49] found that the number of active sites that were able to bind proteins increased with the number of *cis*-flavanol units. Therefore, the decreased protein-precipitating capacity of CT after ensiling is likely attributable to the decline in mDP, proportions of PD and cis-flavanol units. However, the decrease in the protein-precipitating capacity of CT in HAY as compared to FD PPC cannot be explained by these factors as they did not differ between these two methods of forage conservation. This suggests that the protein-binding capacity may not only be related to mDP or the proportions of PD proportion or *cis*-flavanol units, but also due to the comprehensive effect of flavanol units or the spatial distribution of these monomers within CT [50]. Additional studies have indicated that CT with higher molecular weight (MW) exhibit stronger protein-binding capacities [51–54] as CT with higher MW contain a larger number of hydroxyl groups that promote the formation of cross-links with proteins [55]. It is also possible that the lower protein-precipitating capacities of ensiled CTs as compared to those from hay may reflect a reduction in the MW of CT during ensiling, but this was not determined in this study. Further research is needed to confirm this.

3.4. Effect of Forage Conservation Method on Anti-E. coli Activity of PPC CT

Condensed tannins in PPC have been shown to possess strong anti-*E. coli* activity both in vitro [9,10,56] and in vivo [12,13]. Results of the present study were consistent with these previous observations. Furthermore, this study demonstrated that although ensiling and hay-making altered the structural composition and protein-precipitating capacity to a degree, they did not affect the anti-*E. coli* activity of the PPC CT. This suggests that in addition to protein-precipitating ability, other factors may also be responsible for the involved in anti-*E. coli* activity of PPC CT. This is conceivable given the fact that protein-precipitation is a universal property of CT, but only CT from certain plant sources (e.g., *Acacia catechu*, *Holarrhena antidysenterica*, *Quercus infectoria*, *Uncaria gambir*, *Walsura robusta*, *Vaccinium macrocarpon*, PPC) have known anti-*E. coli* activity [10,57–62]. Liu et al. [9] reported that the anti-*E. coli* activity of PPC CT is attributable to their high affinity for proteins and ability to cause cell aggregation. This destabilizes the bacterial outer membrane (OM) and commensurately causes an alteration in its fatty acid composition [10]. Flavan-3-ol monomers, such as catechins in green tea (*Camellia sinensis*), have also been reported to express anti-*E. coli* activity by directly binding peptides of bacterial origin [63], damaging the liquid bilayer and increasing OM permeability [64,65]. It should be noted that although anti-*E. coli* actity of CT isolated from SIL and HAY did not differ to that from FD PPC, the actual anti-*E. coli* activity would be reduced because of a reduction in the extractibility of

CT from the whole plant. Conservation method, especially ensiling, decreased the extractability of CT. Therefore further study is needed to elucidate the mechanisms by which forage conservation method affect biological activity of CT.

4. Materials and Methods

4.1. Conservation of PPC as Freeze-Dried, Hay or Silage

Whole-plant PPC was harvested at full-bloom from three irrigated plots (approximately 0.25 acre each) of the Swinton silt loam soil (Orthic Brown Chernozem) [66] at the Lethbridge Research and Development Centre (Lethbridge, AB, Canada). Harvested forage from each plot was divided into three equal lots to be conserved as FD, HAY, or SIL. The lot for FD was frozen at −40 °C immediately after harvest and then lyophilized. The FD was used to simulate green chopped forage and therefore its CT content was considered to represent that of freshly harvested forage. HAY was allowed to sun cure in the field to <15% moisture, and was subsequently baled in approximately 20-kg square bales (90 × 50 × 30 cm; 3 bales) and stored in an enclosed shed at ambient temperature for 120 d. Subsamples from at least 3 locations of each bales were collected, composited and lyophilized. Forage for SIL was wilted in the field to ≈30% DM and chopped to a theoretical chop length of 1.0 cm using a paper cutter (X-ACTO 26612, Westerville, OH, USA). Chopped PPC was then packed (≈2.7 kg) into three PVC laboratory silos (10 × 35.5 cm) and compacted with a hydraulic press to achieve a packing density of approximately 890 kg (fresh weight)/m^3. Silos were sealed at both ends with rubber lids and metal bands, with one lid fitted with a 7.0-cm-long rubber tube as a vent. Laboratory silos were stored indoors at 22 °C and were opened after 76 d of ensiling. Upon opening, silage within 5.0 cm at both ends was discarded, and the remaining content of each silo was thoroughly hand mixed and subsamples taken. The subsamples from the three silos of each plot were composited, frozen at −40 °C and immediately lyophilized.

All forage samples were ground to pass 1.0 mm screen using a Thomas Wiley Cutting Mill (Arthur H. Thomas Co., Philadelphia, PA, USA) and stored in amber glass containers for chemical analyses. Subsamples of each type of preserved forages were also composited across the three plots to form a single sample for CT extraction, estimation of protein precipitating capacity and anti-*E. coli* activity.

4.2. Chemical Analysis

Conserved forage samples were analyzed for DM, OM and acid detergent lignin using AOAC method [67], NDF and ADF using an ANKOM 200 system (ANKOM Technology Corp., Fairport, NY, USA) with sodium sulfite and α-amylase added for NDF analysis. Samples were ball-ground in a planetary micro mill (Retsch Inc., Newtown, PA, USA) for measurement of total nitrogen (N) by flash combustion analysis using a NA1500 Nitrogen Analyzer (Carlo Erba Instruments, Milan, Italy). For WSC, 15 g subsamples from conserved forage were combined with 135 g of deionized H_2O and blended in a homogenizer (Osterizer, Sunbeam, Fontana, CA, USA) for 30 s. The homogenate was strained through four layers of cheesecloth and the supernatant was sampled and analyzed for WSC as described by Zahiroddini et al. [68]. Conserved PPC samples were analyzed for total phenolic compounds by the Folin-Ciocalteu method [69] with tannic acid (Sigma, St. Louis, MO, USA) as the standard and were expressed as tannic acid equivalents. The concentrations of extractable, protein-bound and fibre-bound CT were determined using the method of Terrill et al. [70] with CT purified from whole PPC plants as a standard.

4.3. In Situ Thiolysis of PPC Tannins and HPLC Analysis of Thiolysis Products

Condensed tannins were degraded with BM as described previously [31]. The resulting flavan-3-ols (terminal subunits) and their BM-adducts (extension subunits) were identified by HPLC-MS analysis [71,72] and quantified using peak areas at 280 nm in conjunction with published flavan-3-ol response factors against taxifolin [31,73]. This yielded data on the mean degree of CT

polymerization, molar percentages of PC and PD within CT, and molar percentages of *cis*- and *trans*-flavan-3-ols [73].

4.4. Determination of the Protein Precipitation Capacities of CT from Freeze-Dried, Silage or Hay PPC

Condensed tannins from PPC conserved as FD, HAY and SIL were extracted and purified as described by Wang et al. [74]. The purified CT were stored in a sealed amber glass bottle at $-20\ ^\circ$C and the same batch of each CT were used in all assays. The protein precipitation capacities of these purified CT were determined using a modified precedure described by McAllister et al. [75]. Bovine serum albumin and Rubisco (MW 557) from spinach (Sigma-Aldrich) were used as model proteins for determining the relative capacities of the extracted CT to bind protein. The BSA was dissolved (3 mg/mL) in 0.2 M acetate buffer (pH = 5.0) containing 0.17 M NaCl, and the Rubisco was dissolved (4 mg/mL) in 1 M 2-amino-2-(hydroxymethyl)-1, 3-propanediol hydrochloride (Tris HCl; pH = 7.8). One milliliter of each protein solution was combined with 0.5 mL of aqueous solutions containing 0, 50, 100, 200, 300, 400, 500, 750, 1000, 1250 or 1500 µg of CT from each source. Each mixture was vortexed, allowed to stand at room temperature for 30 min and centrifuged ($15,600\times$ *g*, 10 min). The CT remaining in a 1-mL subsample of supernatant were removed by adding 0.5 mL of aqueous polyethylene glycol (Sigma-Aldrich; MW 6000; 12 mg/mL) followed by centrifugation. Protein remaining in solution was quantified colorimetrically (OD_{595}) using a Dye Reagent Concentrate Kit (BioRad Laboratories, Mississauga, ON, Canada) against an original freshly prepared solution of BSA or Rubisco protein as a standard. Each assay consisted of six replicates for each dose of CT and the assay was repeated three times over a 1-week period.

The amount of protein precipitated was calculated as the difference between added protein and that present in the supernatant after CT addition. Data were fitted to a sigmoidal curve using nonlinear regression in SigmaPlot for Windows (version 13.0; Systat Software Inc., Santa Jose, CA, USA):

$$y \ = \ a_0 \ + \ a/(1 \ + \ \exp(-(x \ - \ b)/c))$$

where y = mg of protein (BSA or Rubisco) precipitated, x = µg of CT incubated, $a_0 + a$ = estimated maximum amount (mg) of protein (BSA or Rubisco) precipitated, b = sigmoidal centre (mg of CT at the 50% of maximal protein precipitation), and c = sigmoidal width. The protein-precipitating capacity (*PP*) of each CT was expressed as the amount (µg) of the CT required to precipitate 1.0 mg of BSA or Rubisco protein.

4.5. Determination of CT from Freeze-Dried, Silage or Hay PPC on the Growth of E. coli

Two generic *E. coli* strains (ATCC 25922 and ATCC 35281) were obtained from the Lethbridge Research and Development Centre culture collection. Both strains of bacteria were grown at 37 $^\circ$C with shaking (175 rpm, 16 h) for pre-incubation prior to being used as inoculants. An in vitro pure culture experiment was conducted using glass tubes (13 $\times$ 100 mm) with M9 medium including (g/L) M9 minimal salt (11.28), casamino acids (5), glucose (4.5), $MgSO_4 \cdot 7H_2O$ (0.239) and $CaCl_2$ (0.011). Prepared M9 medium (500 mL) was transferred into 1.0-L serum vials and sterilized by autoclaving. After cooling, each of pre-incubated bacterial cultures (30 µL) were added to a 200 mL of M9 medium and cultures were adjusted to identical densities (OD_{600} value was approximately 0.01) by diluting with M9 medium. Immediately after inoculation, 30 µL of filter-sterilized solutions of each purified CT (FD, HAY and SIL) at the concentrations of 0, 2, 500, 5000 and 10,000 µg/mL were added to the bacterial culture (3 mL), yielding 0, 25, 50 or 100 µg CT/mL in inoculated cultures. Triplicate vials were prepared for each bacterial strain and CT concentration. Triplicate vials for each CT concentration, but without bacterial inoculum were also prepared as blank controls. All glass tubes were incubated aerobically with shaking (175 rpm) at 37 $^\circ$C and assessed for bacterial growth after 0, 4, 6, 8, 12 and 24 h of incubation by measuring optical density at 600 nm (UltraSpec Plus 4054; Pharmacia, Baie, QC, Canada). Optical densities were corrected for the blank controls and the culture was diluted with M9

medium so that all OD_{600} were within the range of 0–0.5. The OD_{600} values were then fitted to the following modified Gompertz equation [76]:

$$\ln{(OD_t/OD_0)} = A \times \exp{\{-\exp[(\mu \times e/A) \times (L - t) + 1]\}}$$

where A is the logarithmic increase of bacterial population, μ is maximum growth rate (per hour), L is the lag time, t is the time (in hours), and OD_t and OD_0 are the optical densities obtained at times t and zero, respectively.

4.6. Statistical Analysis

All data were subjected to analysis of variance as a completely randomized design using the PROC MIXED procedure of SAS [77]. Conservation method was the fix effect for all determinations and plot where the original forage was obtained was the random effect for chemical and CT structural data analysis, whereas repeated run was the random effect for protein precipitating capacity data analysis. Data from *E. coli* strains were originally analyzed as a 3×4 factorial design with individual glass tube as a random factor. This revealed a CT level $\times$ conservation method interaction over the incubation period. Therefore, data were re-analyzed as a randomized complete block design for each conservation method of each *E. coli* strain. When CT level or CT level $\times$ conservation method interactions were significant (i.e., $p < 0.05$), means of the conservation methods were compared at each CT level. Differences among treatments were determined using LSMEANS with PDIFF function and adjusted by a Tukey's test in SAS with significance declared at $p < 0.05$.

5. Conclusions

Ensiling and hay-making both impacted CT extractability, structural composition and protein-precipitating capacity with the effect being greater for silage than for hay. Ensiling decreased the extractability of CT and reduced *cis*-isomers, mDP and protein-precipitating capacity of extractable CT. However, conservation methods did not affect the anti-*E. coli* activity of CT isolated from conserved forage. Overall, purple prairie clover preserved as hay conserved the biological activity of CT via preserving extractable CT more than silage.

Author Contributions: Y.W. conceived and designed the experiments; K.P., Q.H. and Z.X. performed the experiments; C.D. and I.M.-H. analyzed structure information of condensed tannins; K.P., Y.W. and Y.S. analyzed the data; Y.W., T.A.M., S.A. and S.W. contributed reagents/materials/analysis tools; K.P., Y.W., T.A.M., J.C. and Y.H. wrote the paper.

Conflicts of Interest: The authors declare no conflict of interest.

References

1. Huang, Q.; Liu, X.; Zhao, G.; Hu, T.; Wang, Y. Potential and challenges of tannins as an alternative to in-feed antibiotics for farm animal production. *Anim. Nutr.* **2018**, in press. [CrossRef]
2. Azuhnwi, B.N.; Boller, B.; Dohme-Meier, F.; Hess, H.D.; Kreuzer, M.; Stringano, E.; Mueller-Harvey, I. Exploring variation in proanthocyanidin composition and content of sainfoin (*Onobrychis viciifolia*). *J. Sci. Food Agric.* **2013**, *93*, 2102–2109. [CrossRef] [PubMed]
3. Lorenz, M.; Alkhafadji, L.; Stringano, E.; Nilsson, S.; Mueller-Harvey, I.; Uden, P. Relationship between condensed tannin structures and their ability to precipitate feed proteins in the rumen. *J. Sci. Food Agric.* **2014**, *94*, 963–968. [CrossRef] [PubMed]
4. Hatew, B.; Stringano, E.; Mueller-Harvey, I.; Hendriks, W.H.; Cabonero, C.H.; Smith, L.M.J.; Pellikaan, W.F. Impact of variation in structure of condensed tannins from sainfoin (*Onobrychis viciifolia*) on in vitro ruminal

methane production and fermentation characteristics. *J. Anim. Physiol. Anim. Nutr.* **2016**, *100*, 348–360. [CrossRef] [PubMed]

5. Huang, Q.; Hu, T.M.; Xu, Z.; Jin, L.; McAllister, T.A.; Acharya, S.; Zeller, W.; Hardcastle, E.; Drake, C.; Wang, Y. Structural composition and protein precipitation capacity of condensed tannins from purple prairie clover (*Dalea purpurea* Vent.). *J. Anim. Sci.* **2017**, *95* (Suppl. 4), 141–142. [CrossRef]

6. Huang, Q.Q.; Jin, L.; Xu, Z.; Acharya, S.; McAllister, T.A.; Hu, T.M.; Peng, K.; Iwaasa, A.; Schellenberg, M.; Wang, Y. Effects of conservation method on condensed tannin content, ruminal degradation, and in vitro intestinal digestion of purple prairie clover (*Dalea purpurea* Vent.). *Can. J. Anim. Sci.* **2016**, *96*, 524–531. [CrossRef]

7. Wang, Y.; Barbieri, L.R.; Berg, B.P.; McAllister, T.A. Effects of mixing sainfoin with alfalfa on ensiling, ruminal fermentation and total tract digestion of silage. *Anim. Feed Sci. Technol.* **2007**, *135*, 296–314. [CrossRef]

8. Waghorn, G. Beneficial and detrimental effects of dietary condensed tannins for sustainable sheep and goat production-Progress and challenges. *Anim. Feed Sci. Technol.* **2008**, *147*, 116–139. [CrossRef]

9. Liu, X.L.; Hao, Y.Q.; Jin, L.; Xu, Z.J.; McAllister, T.A.; Wang, Y. Anti-*Escherichia coli* O157:H7 properties of purple prairie clover and sainfoin condensed tannins. *Molecules* **2013**, *18*, 2183–2199. [CrossRef] [PubMed]

10. Wang, Y.; Jin, L.; Ominski, K.H.; He, M.; Xu, Z.; Krause, D.O.; Acharya, S.N.; Wittenberg, K.M.; Liu, X.L.; Stanford, K.; et al. Screening of condensed tannins from Canadian prairie forages for anti-*Escherichia coli* O157:H7 with an emphasis on purple prairie clover (*Dalea purpurea* Vent.). *J. Food Prot.* **2013**, *76*, 560–567. [CrossRef] [PubMed]

11. Jin, L.; Wang, Y.; Iwaasa, A.D.; Xu, Z.; Li, Y.; Schellenberg, M.P.; Liu, X.L.; McAllister, T.A.; Stanford, K. Purple prairie clover (*Dalea purpurea* Vent.) reduces fecal shedding of *Escherichia coli* in pastured cattle. *J. Food Prot.* **2015**, *78*, 1434–1441. [CrossRef] [PubMed]

12. Huang, Q.Q.; Jin, L.; Xu, Z.; Barbieria, L.R.; Acharyaa, S.; Hu, T.M.; Stanford, K.; McAllister, T.A.; Wang, Y. Effects of purple prairie clover (*Dalea purpurea* Vent.) on feed intake, nutrient digestibility and faecal shedding of *Escherichia coli* O157:H7 in lambs. *Anim. Feed Sci. Technol.* **2015**, *207*, 51–61. [CrossRef]

13. Jin, L.; Wang, Y.; Iwaasa, A.D.; Xu, Z.; Schellenberg, M.P.; Zhang, Y.G.; Liu, X.L.; McAllister, T.A. Effect of condensed tannins on ruminal degradability of purple prairie clover (*Dalea purpurea* Vent.) harvested at two growth stages. *Anim. Feed Sci. Technol.* **2012**, *176*, 17–25. [CrossRef]

14. Li, Y.; Iwaasa, A.D.; Wang, Y.; Jin, L.; Han, G.; Zhao, M. Condensed tannins concentration of selected prairie legume forages as affected by phenological stages during two consecutive growth seasons in western Canada. *Can. J. Plant Sci.* **2014**, *94*, 817–826. [CrossRef]

15. Broderick, G.A. Performance of lactating dairy cows fed either alfalfa silage or alfalfa hay as the sole forage. *J. Dairy Sci.* **1995**, *78*, 320–329. [CrossRef]

16. Griffin, J.L.; Jung, G.A. Leaf and stem forage quality of big bluestem and switchgrass. *Agron. J.* **2003**, *75*, 723–726. [CrossRef]

17. Wilkins, R.J. The Preservation of Forages. In *Feed Science*; Orskov, E.R., Ed.; Elsevier: Amsterdam, The Netherlands, 1988; pp. 231–255.

18. Enoh, M.B.; Kijora, C.; Peters, K.J.; Tanya, V.N.; Fonkem, D.; Mbanya, J. Investigation on change of forage quality at harvesting, during hay making and storage of hay harvested at different growth stages in the Adamawa plateau of Cameroon. *Livest. Res. Rural Dev.* **2005**, *17*, 1–6.

19. Scharenberg, A.; Arrigo, Y.; Gutzwiller, A.; Soliva, C.R.; Wyss, U.; Kreuzer, M.; Dohme, F. Palatability in sheep and in vitro nutritional value of dried and ensiled sainfoin (*Onobrychis viciifolia*) birdsfoot trefoil (*Lotus corniculatus*), and chicory (*Cichorium intybus*). *Arch. Anim. Nutr.* **2007**, *61*, 481–496. [CrossRef] [PubMed]

20. Scharenberg, A.; Arrigo, Y.; Gutzwiller, A.; Wyss, U.; Hess, H.D.; Kreuzer, M.; Dohme, F. Effect of feeding dehydrated and ensiled tanniferous sainfoin (*Onobrychis viciifolia*) on nitrogen and mineral digestion and metabolism of lambs. *Arch. Anim. Nutr.* **2007**, *61*, 390–405. [CrossRef] [PubMed]

21. Lorenz, M.M.; Eriksson, T.; Uden, P. Effect of wilting, silage additive, PEG treatment and tannin content on the distribution of N between different fractions after ensiling of three different sainfoin (*Onobrychis viciifolia*) varieties. *Grass Forage Sci.* **2010**, *65*, 175–184. [CrossRef]

22. Terrill, T.H.; Windham, W.R.; Evans, J.J.; Hoveland, C.S. Condensed tannins in sericea lespedeza: Effect of preservation method on tannin concentration. *Crop Sci.* **1990**, *30*, 219–224. [CrossRef]

23. Aufrère, J.; Dudilieu, M.; Poncet, C. In vivo and in situ measurements of the digestive characteristics of sainfoin in comparison with lucerne fed to sheep as fresh forages at two growth stages and as hay. *Animal* **2008**, *2*, 1331–1339. [CrossRef] [PubMed]

24. Wang, Y.; McAllister, T.A.; Acharya, S. Condensed tannins in sainfoin: Composition, concentration, and effects on nutritive and feeding value of sainfoin forage. *Crop Sci.* **2015**, *55*, 13–22. [CrossRef]

25. Mueller-Harvey, I. Unravelling the conundrum of tannins in animal nutrition and health. *J. Sci. Food Agric.* **2006**, *86*, 2010–2037. [CrossRef]

26. Foo, L.Y.; Newman, R.; Waghorn, G.; McNabb, W.C.; Ulyatt, M.J. Proanthocyanidins from *Lotus corniculatus*. *Phytochemistry* **1996**, *41*, 617–624. [CrossRef]

27. Foo, L.Y.; Lu, Y.; Mcnabb, W.C.; Waghorn, G.; Ulyatt, M.J. Proanthocyanidins from *Lotus pedunculatus*. *Phytochemistry* **1997**, *45*, 1689–1696. [CrossRef]

28. Koupai-Abyazani, M.R.; Mccallum, J.; Muir, A.D.; Bohm, B.A.; Towers, G.H.N.; Gruber, M.Y. Developmental changes in the composition of proanthocyanidins from leaves of sainfoin (*Onobrychis viciifolia* Scop.) as determined by HPLC analysis. *J. Agric. Food Chem.* **1993**, *41*, 613–621. [CrossRef]

29. Foo, L.Y.; Jones, W.T.; Porter, L.J.; Williams, V.M. Proanthocyanidin polymers of fodder legumes. *Phytochemistry* **1982**, *21*, 933–935.

30. Marais, J.P.; Mueller-Harvey, I.; Brandt, E.V.; Ferreira, D. Polyphenols, condensed tannins, and other natural products in *Onobrychis viciifolia* (Sainfoin). *J. Agric. Food Chem.* **2000**, *48*, 3440–3447. [CrossRef] [PubMed]

31. Gea, A.; Stringano, E.; Brown, R.H.; Mueller-Harvey, I. In situ analysis and structural elucidation of sainfoin (*Onobrychis viciifolia*) tannins for high-throughput germplasm screening. *J. Agric. Food Chem.* **2011**, *59*, 495–503. [CrossRef] [PubMed]

32. Kommuru, D.S.; Barker, T.; Desai, S.; Burke, J.M.; Ramsay, A.; Mueller-Harvey, I.; Miller, J.E.; Mosjidis, J.A.; Kamisetti, N.; Terrill, T.H. Use of pelleted sericea lespedeza (*Lespedeza cuneata*) for natural control of coccidia and gastrointestinal nematodes in weaned goats. *Vet. Parasitol.* **2014**, *204*, 191–198. [CrossRef] [PubMed]

33. Laaksonen, O.A.; Salminen, J.P.; Makila, L.; Kallio, H.P.; Yang, B. Proanthocyanidins and their contribution to sensory attributes of black currant juices. *J. Agric. Food Chem.* **2015**, *63*, 5373–5380. [CrossRef] [PubMed]

34. Mueller-Harvey, I.; Bee, G.; Dohme-Meier, F.; Hoste, H.; Karonen, M.; Kölliker, R.; Lüscher, A.; Niderkorn, V.; Pellikaan, W.; Salminen, J.P.; Skot, L.; Smith, L.; Thamsborg, S.; et al. Benefits of condensed tannins in forages fed to ruminants: Importance of structure, concentration and diet. *Crop Sci.* **2018**, in press.

35. Vidal, S.; Cartalade, D.; Souquet, J.M.; Fulcrand, H.; Cheynier, V. Changes in proanthocyanidin chain length in winelike model solutions. *J. Agric. Food Chem.* **2002**, *50*, 2261–2266. [CrossRef] [PubMed]

36. Tharayil, N.; Suseela, V.; Triebwasser, D.J.; Preston, C.M.; Gerard, P.D.; Dukes, J.S. Changes in the structural composition and reactivity of Acer rubrum leaf litter tannins exposed to warming and altered precipitation: Climatic stress-induced tannins are more reactive. *New Phytol.* **2011**, *191*, 132–145. [CrossRef] [PubMed]

37. Peng, K.; Jin, L.; Niu, D.; Huang, Q.; McAllister, T.A.; Yang, H.E.; Denise, H.; Xu, Z.; Acharya, S.; Wang, S.; et al. Condensed tannins affect bacterial and fungal microbiomes and mycotoxin production during ensiling and upon aerobic exposure. *Appl. Environ. Microbiol.* **2018**, *84*, e02274-17. [CrossRef] [PubMed]

38. Haslam, E. *Plant Polyphenols, Vegetable Tannins Revisited*; Cambridge University Press: Cambridge, UK, 1989.

39. Hagerman, A.E.; Butler, L.G. The specificity of proanthocyanidin-protein interactions. *J. Biol. Chem.* **1981**, *256*, 4494–4497. [PubMed]

40. Hagerman, A.E.; Rice, M.E.; Ritchard, N.T. Mechanisms of protein precipitation for two tannins, pentagalloyl glucose and epicatechin16 (4→8) catechin (procyanidin). *J. Agric. Food Chem.* **1998**, *46*, 2590–2595. [CrossRef]

41. Horigome, T.; Kumar, R.; Okamoto, K. Effects of condensed tannins prepared from leaves of fodder plants on digestive enzymes in vitro and in the intestine of rats. *Br. J. Nutr.* **1988**, *60*, 275–285. [CrossRef] [PubMed]

42. Theodoridou, K.; Aufrère, J.; Andueza, D.; Pourrat, J.; Morvan, A.L.; Stringano, E.; Mueller-Harvey, I.; Baumont, R. Effects of condensed tannins in fresh sainfoin (*Onobrychis viciifolia*) on in vivo and in situ digestion in sheep. *Anim. Feed Sci. Technol.* **2010**, *160*, 23–38. [CrossRef]

43. Theodoridou, K.; Aufrère, J.; Niderkorn, V.; Andueza, D.; Morvan, A.L.; Picard, F.; Baumont, R. Effect of plant development during first and second growth cycle on chemical composition, condensed tannins and nutritive value of three sainfoin (*Onobrychis viciifolia*) varieties and lucerne. *Grass Forage Sci.* **2011**, *66*, 402–414. [CrossRef]

44. Harbertson, J.F.; Kilmister, R.L.; Kelm, M.A.; Downey, M.O. Impact of condensed tannin size as individual and mixed polymers on bovine serum albumin precipitation. *Food Chem.* **2014**, *160*, 16–21. [CrossRef] [PubMed]

45. Ropiak, H.M.; Lachmann, P.; Ramsay, A.; Green, R.J.; Mueller-Harvey, I. Identification of structural features of condensed tannins that affect protein aggregation. *PLoS ONE* **2017**, *12*, e0170768. [CrossRef] [PubMed]

46. Jones, W.T.; Broadhurst, R.B.; Lyttleton, J.W. The condensed tannins of pasture legume species. *Phytochemistry* **1976**, *15*, 1407–1409. [CrossRef]

47. Mangan, J.L. Nutritional effects of tannins in animal feeds. *Nutr. Res. Rev.* **1988**, *1*, 209–231. [CrossRef] [PubMed]

48. Guimarães-Beelen, P.M.; Berchielli, T.T.; Beelen, R.; Filho, J.A.; Oliveira, S.G. Characterization of condensed tannins from native legumes of the Brazilian northeastern semi-arid. *Sci. Agric.* **2006**, *63*, 150–153.

49. De Freitas, V.; Mateus, N. Structural features of procyanidin interactions with salivary proteins. *J. Agric. Food Chem.* **2001**, *49*, 940–945. [CrossRef] [PubMed]

50. Rosales, R.B. Condensed Tannins in Tropical Forage Legumes: Their Characterization and Study of Their Nutritional Impact from the Standpoint of Structure-Activity Relationships. Ph.D Thesis, University of Reading, Reading, UK, 1999.

51. Kumar, R.; Horigome, T. Fractionation, characterization and protein precipitating capacity of the condensed tannins from *Robinia pseudoacacia* (L.) leaves. *J. Agric. Food Chem.* **1986**, *34*, 487–489. [CrossRef]

52. Osborne, N.J.T.; McNeill, D.M. Characterisation of *Leucaena* condensed tannins by size and protein precipitation capacity. *J. Sci. Food Agric.* **2001**, *81*, 1113–1119. [CrossRef]

53. Huang, X.D.; Liang, J.B.; Tan, H.Y.; Yahya, R.; Khamseekhiew, B.; Ho, Y.W. Molecular weight and protein binding affinity of *Leucaena* condensed tannins and their effects on in vitro fermentation parameters. *Anim. Feed Sci. Technol.* **2010**, *159*, 81–87. [CrossRef]

54. Huang, X.D.; Liang, J.B.; Tan, H.Y.; Yahya, R.; Long, R.; Ho, Y.W. Protein-binding affinity of Leucaena condensed tannins of differing molecular weights. *J. Agric. Food Chem.* **2011**, *59*, 10677–10682. [CrossRef] [PubMed]

55. Bacon, J.R.; Rhodes, M.J.C. Binding affinity of hydrolyzable tannins to parotid saliva and to proline-rich proteins derived from it. *J. Agric. Food Chem.* **2000**, *48*, 838–843. [CrossRef] [PubMed]

56. Wang, Y.; McAllister, T.A.; Iwaasa, A. Effects of condensed tannins from purple prairie clover on the growth of *E. coli* O157:H7. *J. Anim. Sci.* **2009**, *87*, 31.

57. Foo, L.Y.; Yinrong, L.; Howell, A.B.; Vorsa, N. A-type proamthocyanidin trimers from cranberry that inhibit adherence of uropathogenic P-fimbricated *Escherichia coli*. *J. Nat. Prod.* **2000**, *63*, 1225–1228. [CrossRef] [PubMed]

58. Voravuthikunchai, S.; Lortheeranuwat, A.; Jeeju, W.; Sririrak, T.; Phongpaichit, S.; Supawita, T. Effective medicinal plants against enterohaemorrhagic *Escherichia coli* O157:H7. *J. Ethnopharm.* **2004**, *94*, 49–54. [CrossRef] [PubMed]

59. Vattem, D.A.; Lin, Y.T.; Labbe, R.G.; Shetty, K. Antimicrobial activity against select food-borne pathogens by phenolic antioxidants enriched in cranberry pomace by solid-state bioprocessing using the food grade fungus *Rhizopus oligosporus*. *Process Biochem.* **2004**, *39*, 1939–1946. [CrossRef]

60. Puupponen-Pimia, R.; Nohynek, L.; Hartmann-Schmidlin, S.; Kahkonen, M.; Heinonen, M.; Maatta-Riihinen, M.; Oksman-Caldentey, K.M. Berry phenolics selectively inhibit the growth of intestinal pathogens. *J. Appl. Microbiol.* **2005**, *98*, 991–1000. [CrossRef] [PubMed]

61. Min, B.R.; Pinchak, W.E.; Anderson, R.C.; Callaway, T.R. Effect of tannins on the in vitro growth of *Escherichia coli* O157:H7 and in vivo growth of generic *Escherichia coli* excreted from steers. *J. Food Prot.* **2007**, *70*, 543–550. [CrossRef] [PubMed]

62. Kim, T.J.; Weng, W.L.; Stojanovic, J.; Lu, Y.; Jung, Y.S.; Silva, J.L. Antimicrobial effect of water-soluble muscadine seed extracts on *Escherichia coli* O157:H7. *J. Food Prot.* **2008**, *71*, 1465–1468. [CrossRef] [PubMed]

63. Shimamura, T.; Zhao, W.H.; Hu, Z.Q. Mechanism of action and potential for use of tea catechin as an anti-infective agent. *Anti-Infect. Agents Med. Chem.* **2007**, *6*, 57–62. [CrossRef]

64. Ikigai, H.; Nakae, T.; Hara, Y.; Shimamura, T. Bactericidal catechins damage the lipid bilayer. *Biochem. Biophys. Acta* **1993**, *1147*, 132–136. [CrossRef]

65. Tsuchiya, H. Stereospecificity in membrane effects of catechins. *Chem.-Biol. Interact.* **2001**, *134*, 41–54. [CrossRef]

66. Ayres, K.W.; Acton, D.F.; Ellis, J.G. *The Soils of Swift Current Map Area 725 Saskatchewan, Publ. 56*; University of Saskatchewan: Saskatoon, SK, Canada, 1985; p. 226.

67. AOAC. *Official Methods of Analysis of the Association of Official Agricultural Chemists*, 16th ed.; AOAC International: Gaithersburg, MD, USA, 1999.

68. Zahiroddini, H.; Baah, J.; Absalom, W.; McAllister, T.A. Effect of an inoculant and hydrolytic enzymes on fermentation and nutritive value of whole crop barley silage. *Anim. Feed Sci. Technol.* **2004**, *117*, 317–330. [CrossRef]

69. Makkar, H.P.S.; Blummel, M.; Borowy, N.K.; Becker, K. Gravimetric determination of tannins and their correlations with chemical and protein precipitation methods. *J. Sci. Food Agric.* **1993**, *61*, 161–165. [CrossRef]

70. Terrill, T.; Rowan, A.; Douglas, G.; Barry, T. Determination of extractable and bound condensed tannin concentrations in forage plants, protein concentrate meals and cereal grains. *J. Sci. Food Agric.* **1992**, *58*, 321–329. [CrossRef]

71. Williams, A.R.; Fryganas, C.; Ramsay, A.; Mueller-Harvey, I.; Thamsborg, S.M. Direct anthelmintic effects of condensed tannins from diverse plant sources against *Ascaris suum*. *PLoS ONE* **2014**, *9*. [CrossRef] [PubMed]

72. Desrues, O.; Mueller-Harvey, I.; Pellikaan, W.F.; Enemark, H.L.; Thamsborg, S.M. Condensed tannins in the gastrointestinal tract of cattle after sainfoin (*Onobrychis viciifolia*) intake and their possible relationship with anthelmintic effects. *J. Agric. Food Chem.* **2017**, *65*, 1420–1427. [CrossRef] [PubMed]

73. Ropiak, H.M.; Ramsay, A.; Mueller-Harvey, I. Condensed tannins in extracts from European medicinal plants and herbal products. *J. Pharm. Biomed. Anal.* **2016**, *121*, 225–231. [CrossRef] [PubMed]

74. Wang, Y.; Xu, Z.; Bach, S.J.; McAllister, T.A. Sensitivity of *Escherichia coli* to seaweed *(Ascophyllum nodosum)* phlorotannins and terrestrial tannins. *Asian-Aust. J. Anim. Sci.* **2009**, *22*, 238–245. [CrossRef]

75. McAllister, T.A.; Martinez, T.; Bae, H.D.; Muir, A.D.; Yanke, L.J.; Jones, G.A. Characterization of condensed tannins purified from legume forages: Chromophore production, protein precipitation, and inhibitory effects on cellulose digestion. *J. Chem. Ecol.* **2005**, *31*, 2049–2068. [CrossRef] [PubMed]

76. Dalgaard, P.; Koutsoumanis, K. Comparison of maximum specific growth rates and lag times estimated from absorbance and viable count data by different mathematical models. *J. Microbiol. Methods* **2001**, *43*, 183–196. [CrossRef]

77. SAS Institute Inc. *SAS Online Doc*® *9.1.3*; SAS Institute Inc.: Cary, NC, USA, 2012.

Sample Availability: Samples of the PPC CT are available from the authors.

Chemical Composition, Antibacterial and Antifungal Activities of Crude *Dittrichia viscosa* (L.) Greuter Leaf Extracts

Wafa Rhimi [1,2], **Issam Ben Salem** [2,*], **Davide Immediato** [3], **Mouldi Saidi** [2], **Abdennacer Boulila** [4] **and Claudia Cafarchia** [3]

[1] Faculté des Sciences de Bizerte, Université de Carthage, 7021 Zarzouna, Tunisia; wafa_Rhimi@hotmail.com
[2] Laboratory of Biotechnology and Nuclear Technolog, National Centre of Nuclear Science and Technology (CNSTN), Sidi Thabet Technopark, 2020 Ariana, Tunisia; official@cnstn.rnrt.tn
[3] Dipartimento di Medicina Veterinaria, Università degli Studi di Bari, 70010 Valenzano, Italy; direzione.veterinaria@uniba.it (D.V.); claudia.cafarchia@uniba.it (C.C.)
[4] Laboratory of Natural Substances LR10INRAP02, National Institute of Research and Physico-chemical Analyses, Biotechpole of Sidi Thabet, 2020 Ariana, Tunisia; abdennacer.boulila@inrap.rnrt.tn
* Correspondence: issam.bensalem@cnstn.rnrt.tn; Tel.: +216-71-537-410

Abstract: The small amount of data regarding the antifungal activity of *Dittrichia viscosa* (L.) Greuter against dermatophytes, *Malassezia* spp. and *Aspergillus* spp., associated with the few comparative studies on the antimicrobial activity of methanolic, ethanolic, and butanolic extracts underpins the study herein presented. The total condensed tannin (TCT), phenol (TPC), flavonoid (TFC), and caffeoylquinic acid (CQC) content of methanol, butanol, and ethanol (80% and 100%) extracts of *D. viscosa* were assessed and their bactericidal and fungicidal activities were evaluated. The antibacterial, anti-*Candida* and anti-*Malassezia* activities were evaluated by using the disk diffusion method, whereas the anti-*Microsporum canis* and anti-*Aspergillus fumigatus* activities were assessed by studying the toxicity effect of the extracts on vegetative growth, sporulation and germination. The methanolic extract contained the highest TPC and CQC content. It contains several phytochemicals mainly caffeoylquinic acid derivatives as determined by liquid chromatography with photodiode array and electrospray ionisation mass spectrometric detection (LC/PDA/ESI-MS) analysis. All extracts showed an excellent inhibitory effect against bacteria and *Candida* spp., whereas methanolic extract exhibited the highest antifungal activities against *Malassezia* spp., *M. canis* and *A. fumigatus* strains. The results clearly showed that all extracts, in particular the methanolic extract, might be excellent antimicrobial drugs for treating infections that are life threatening (i.e., *Malassezia*) or infections that require mandatory treatments (i.e., *M. canis* or *A. fumigatus*).

Keywords: *Dittrichia viscosa*; antifungal activities; *Candida* spp.; *Malassezia* spp.; *Microsporum canis*; *Aspergillus fumigates*

1. Introduction

The growing worldwide concern about the alarming increase in the rate of human and animal infections caused by antibiotic-resistant microorganisms have spurred the interest of the scientific community in developing alternative methods for their control [1]. Many kinds of natural extracts from medicinal plants containing phenolic and flavonoid compounds have excellent biological properties and are used as alternative therapies. Among the large variety of Mediterranean folkloric herbs, *Dittrichia viscosa* belonging to the Asteraceae family, has proven to be a source of natural products forming the basis for alternative medicine and natural therapies [2–4]. *Dittrichia viscosa* was studied

against antibiotic-resistant microorganisms, antibacterial activity and anti-fungal activity against *Candida albicans* and *Fusarium* species [5,6]. To the best of our knowledge, reports on antifungal activity of *D. viscosa* against dermatophytes, *Malassezia* spp. and *Aspergillus* spp. are scant or limited to *Microsporum canis*. In particular, dermatophytes are a group of fungi which have the ability to invade the keratinized tissues (skin, hair, nails) causing cutaneous infections in humans and animals commonly known as dermatophytosis [7]. They are distributed worldwide and some of them are considered zoonotic, being transmitted from animals to humans [8]. The treatment of infections is mandatory due to the contagious and the zoonotic nature and usually requires long antifungal therapy with azoles [9]. In addition, these treatments are not usually performed in food producing animals since they are more expensive, and treated animals need long withholding before using in food processing industry [10].

The fungal genus *Malassezia* is part of the normal skin microbiota. These yeasts cause human and animal skin disorders in immune-competent hosts and systemic infections in immune- compromised patients which usually require prolonged treatment with and/or high doses of antifungal agents [11,12]. In addition, recent studies clearly show that the same species within the genus of *Malassezia furfur* and *Malassezia pachydermatis* are characterized by high minimal inhibitory concentration (MIC) values against all azole drugs commonly employed in the treatment of the infections.

Finally, *Aspergillus* species are found worldwide in humans and in almost all domestic animals and birds as well as in many wild species, causing a wide range of diseases from localized infections to fatal disseminated diseases, as well as allergic responses to inhaled conidia [13]. Some prevalent forms of animal *aspergillosis* are invasive fatal infections and are difficult to treat. In addition, the environmental diffusion of *A. fumigatus* strains presenting azole resistant phenomena is worldwide reported [13].

Thus, this study aimed to: (i) quantify the phenolic and flavonoids content of *D. viscosa* leaf extract with different solvents; (ii) evaluate their activities against gram positive and negative bacteria, and against *Candida* spp. (i.e., *Candida albicans*, *Candida krusei*, *Candida prapsilos*); and (iii) to assess their activities against *Malassezia* spp. (*Malassezia pachydermatis* and *Malassezia furfur*), *Aspergillus fumigatus* and *Microsporum canis*.

2. Results and Discussion

2.1. Phytochemical Screening

The total condensed tannin (CTC), phenol (TPC), flavonoid (TFC), and caffeoylquinic acid (CQC) content of different *D. viscosa* extracts are reported in Table 1. They are expressed as mg catechin equivalent (CE), mg gallic acid equivalent, mg quercetin equivalent (QE) and mg of chlorogenic acid equivalent (ChlA E) per g dry extract, respectively.

The CTC amounts varied from 7.05 ± 1.6 to 27.15 ± 2.21 mg CE/g, being the highest in the methanolic extract (Table 1). The TPC ranged from 75.34 ± 1.30 to 123.39 ± 1.22 mg GAE/g, the highest content retrieved in methanolic and 80% ethanolic extracts (Table 1).

The CQC amounts of *D. viscosa* extracts ranged from 57.11 ± 0.98 to 87.61 ± 1.06 mg ChlA E/g (Table 1) and the highest amount of CQC was registered in methanolic extract. The TFC varied from 30.86 ± 1.28 to 58.03 ± 1.85 mg QE/g and the highest content was registered in butanolic extract (Table 1). The methanolic extract contains the highest CTC, TPC and CQC values while the butanolic extract contained the highest amount of TFC.

The results of this study clearly indicate that phenolic and flavonoids content of *D. viscosa* crude extracts vary according to the solvent extraction procedure. In particular, this study reports for the first time the presence of condensed tannins in this plant species. Indeed, no previous studies have evaluated CTC in *D. viscosa* leaves, but results herein indicate that the amount within methanolic extracts are in the same range as those of some *Asteraceae* species such as *Artemisia* genus [14]. On the contrary, the TPC values of Tunisian *D. viscosa* extracts were in same range or slightly lower than

those reported from Turkish or Moroccan samples [4,15], thus suggesting that TPC values of *D. viscosa* does not vary accordingly to plant origin. Accordingly, the TPC amounts depend on the polarity of the solvent, and it was highest when the solvent polarity increased. Similar results were reported by Negi and Jayaprakasha when studying methanol extracts of *Punica granatum* peel [16]. However, a high value of TFC in our extracts was detected in butanolic extract, suggesting that the flavonoid composition of *D. viscosa* might comprise of substances with a high solubility in butanol, like luteolin derivatives [17,18].

Table 1. Condensed tannins, total polyphenols, total flavonoids, and caffeoylquinic acid content of different *D. viscosa* leaf extracts.

Polyphenols and Flavonoids Content	Ethanolic	Ethanolic 80%	Butanolic	Methanolic
CTC(mgCAE/g extract)	14.29 ± 1.30 [a]	7.05 ± 1.6 [b]	16.86 ± 1.62 [c]	27.15 ± 2.21 [d]
TPC (mgGAE/g extract)	117.58 ± 1.29 [a]	123.39 ± 1.22 [b]	75.34 ± 1.30 [c]	123.07 ± 1.69 [b]
TFC (mgQE/g extract)	57.79 ± 1.76 [a]	49.23 ± 1.039 [b]	58.03 ± 1.85 [a]	30.86 ± 50 [c]
CQC (mgCGAE/g extract)	71.85 ± 0.35 [a]	73.13 ± 1.06 [a]	57.11 ± 0.98 [b]	87.61 ± 1.06 [c]

Values followed by the same letter along the row are not significantly different ($p < 0.05$).

2.2. Phenolic Profile of D. viscosa Extracts

The HPLC-PDA/ESI-MS analysis allowed us to tentatively identify 18 phenolic compounds in the methanolic *D. viscosa* extract (Figure 1). The phenolic fraction of methanolic *D. viscosa* extract was dominated by caffeoylquinic acid derivatives such as chlorogenic acid, dicaffeoylquinic acid isomers, and caffeoyl glucose as it shown in Table 2. Other hyhydroxycinnamic acids like coumaric acid and caffeic acid derivatives were also detected.
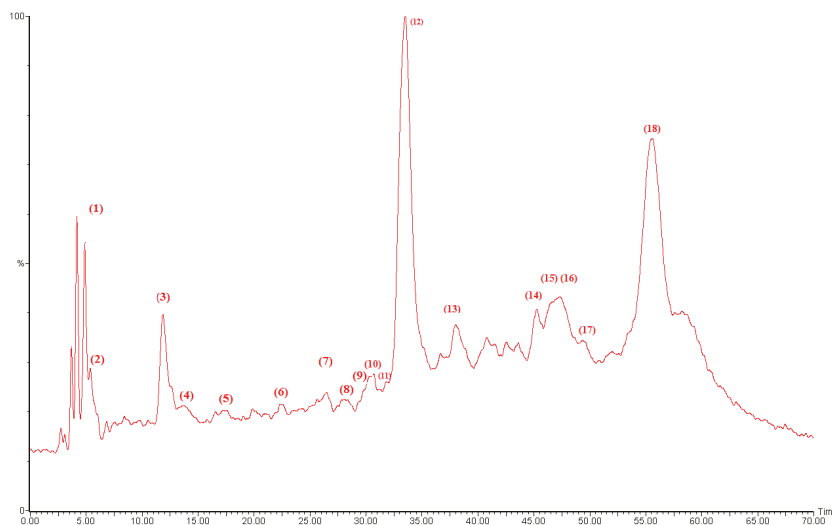

Figure 1. Chemical characterization of methanolic extract of *D. viscosa* leaves by HPLC-PDA-ESI-S. The peaks are numbered and assignments are given in Table 2.

Some flavonoid compounds were also detected. They were represented exclusively by quercetin derivatives (e.g., quercetin-*O*-hexoside, quercetin glucuronide, quercetin dimethyl ether isomers), and the flavonol catechin glucoside. The identification of phenolic compounds by HPLC-PDA-ESI-MS as shown in Table 2 confirmed our photochemical screening findings about the richness of *D. viscosa*

extract in caffeoylquinic acid derivatives, and in agreement with previous reports from Israel, Turkey and Tunisia [4,15,19]. From these results, it emerges that *D. viscosa* might be advised as potential source of bioactive components especially caffeoylquinic acid derivatives.

Table 2. Retention time (RT), wavelengths of maximum absorption (λmax), mass spectral data, relative occurrence, and tentative identification of phenolic compounds in methanolic extract of *D. viscosa* leaves.

Compound	RT (min)	λmax	$[M − H]^-$	Fragment Ions	Proposed Structure	Occurrence
1	4.856	292sh–322	377	341 (100), 179, 119	Caffeic acid hexoside	++
2	5.346	292sh–322	341	191 (100), 137, 128	3-Caffeoylquinic acid	++
3	11.876	292sh–322	353	191 (100), 161	Chlorogenic acid	+++
4	13.856	292sh–322	353	191, 161 (100)	4-Caffeoylquinic acid isomer	+
5	17.222	293–310	467	163 (100)	Coumaric acid derivative	+
6	22.365	-	429	267 (100), 173, 161	Feruloyl caffeolglycerol	+
7	27.982	360, 262	463	301 (100), 331, 255	Quercetin hexoside	+
8	28.007	293sh–321	463	301(100)	Hydroxyluteolin hexoside	+
9	30.452	293sh–354	477	301 (100)	Quercetin glucuronide	+
10	30.714	294sh–354	477	301 (100), 161	Quercetin glucuronide	+
11	32.888	292sh–322	353	191 (100), 179, 161	5-Caffeoylquinic acid	+
12	33.463	292sh–322	353	191 (100), 179 (32)	Dicaffeoylquinic acid isomer	++++
13	37.98	292–322	353	191 (78), 179 (100), 161 (80)	Caffeoylquinic acid isomer	+++
14	44.561	290, 320	339	135 (100)	Caffeoyl glucose	+++
15	47.234	253–349	329	314 (100), 299 (80), 285 (70), 271 (53), 243 (50)	Quercetin-dimethyl ether isomer	+++
16	47.395	253–349	329	314 (100), 299 (85) 271 (75), 241 (40)	Quercetin-dimethyl ether isomer	+++
17	49.315	253–349	329	314 (100), 299 (85), 285, 243	Quercetin-dimethyl ether isomer	+
18	55.566	278	493	289 (40), 165 (100), 139 (80)	Catechin glucoside	+++

+: low in abundance; ++: moderate in abundance; +++: high in abundance); ++++: very high in abundance.

2.3. Antibacterial, Anti-Candida and Antifungal Activity of D. viscosa Extracts

Table 3 shows the inhibitory effects of *D. viscosa* extracts against Gram positive (i.e., *Staphylococcus aureus*, *Enterococcus feacium*, *Streptococcus agalactiae*) and Gram negative bacteria (i.e., *Escherichia coli* and *Salmonella typhimurium*) with the inhibition halo ranging from 9.5 to 34.5 mm. No statistically significant differences were recorded between different extracts. The highest antimicrobial activity was observed against *Enterococcus feacium* (G+) and *Streptococcus agalactiae* (G+) with inhibition zones of 34.5 ± 0.7 mm and 29 ± 1.41 mm, respectively.

Table 3. Antibacterial properties of extracts under study, expressed as diameter of inhibition halo (in mm) versus several strains.

Bacterial spps.	Concentration (mg/mL)	Ethanol	Ethanol 80%	Butanol	Methanol
Eshershia coli	50	12±1.41 [a]	11.5 ± 0.70 [a]	12.5 ± 0.70 [a]	12 ± 0.70 [a]
	10	11 ± 1.41 [a]	10 ± 0.0 [a]	10.5 ± 0.0 [a]	10 ± 0.0 [a]
Sal Salmonella typhimurium	50	10.5 ± 0.70 [a]	9.5 ± 0.70 [a]	10.5 ± 0.70 [a]	10 ± 0.0 [a]
	10	9.5 ± 0.70 [a]	0 ± 0.0 [b]	9.5 ± 0.70 [a]	9.5 ± 0.0 [a]
Enterococcus feacium	50	34 ± 1.41 [a]	28.5 ± 0.0 [b]	34.5 ± 0.70 [a]	34.5 ± 0.7 [a]
	10	30 ± 0.0 [a]	25 ± 0.0 [b]	28 ± 0.0 [c]	29 ± 0.0 [d]
Streptococcus agalactiae	50	28 ± 1.41 [a]	28 ± 1.41 [a]	29 ± 1.41 [a]	29 ± 1.41 [a]
	10	18.5 ± 0.70 [a]	17 ± 0.0 [a]	21.5 ± 1.41 [b]	18 ± 1.14 [a]
Staphylococus aureus	50	25 ± 0.0 [a]	25 ± 0.0 [a]	22.5 ± 0.70 [b]	20 ± 0.0 [c]
	10	13.5 ± 0.70 [a]	10 ± 0.0 [b]	13 ± 1.41 [a]	11 ± 0.0 [c]

Values followed by the same superscript along the row are not significantly different ($p < 0.05$).

The results of anti-*Candida* and anti-*Malassezia* activities are reported in Table 4. The diameter halo ranged from 7 to 14.5 mm according to extract concentration. No significant differences were recorded among the activity of different extracts against *Candida* species.

Table 4. *Anti-Candida* and *Anti-Malassezia* properties of extracts under study, expressed as diameter of inhibition halo (in mm) versus several strains.

Candida and *Malassezia* spp.	Concentration (mg/mL)	Ethanol	Ethanol 80%	Butanol	Methanol
Candida prapsilosis **ATCC 22019**	50	10.25 ± 0.58 [a]	9.66 ± 1.52 [a]	8.75 ± 1.73 [a]	10.75 ± 0.95 [a]
	10	8.66 ± 1.73 [a]	8.5 ± 1.73 [a]	8.66 ± 1.73 [a]	10 ± 0.95 [a]
Candida krusei **ATCC 6258**	50	10 ± 1.41 [a]	10.5 ± 0.57 [a]	10 ± 1 [a]	10 ± 0.0 [a]
	10	9.5 ± 0.7 [a]	10 ± 0.0 [a]	9 ± 0.82 [a]	10 ± 0.0 [a]
Candida albicans **ATCC 10231**	50	13.5 ± 0. 70 [a]	13.5 ± 0.70 [a]	14.5 ± 0.70 [a]	14.5 ± 0.70 [a]
	10	12 ± 0.0 [a]	11.5 ± 0.70 [a]	13 ± 0.00 [a]	12 ± 1.41 [a]
Candida albicans **CD 1358**	50	10.5 ± 0.57 [a]	11 ± 0.00 [a]	10.25 ± 0.5 [a]	10 ± 2.0 [a]
	10	10.25 ± 0.5 [a]	10 ± 0.57 [a]	9.5 ± 0.57 [a]	9.5 ± 2.0 [a]
Candida albicans **CD 1378**	50	10.25 ± 0.5 [a]	11.0 ± 0 [b]	10 ± 0.0 [a]	10 ± 0.81 [a]
	10	10 ± 0.5 [a]	10.33 ± 0.0 [a]	10 ± 0.5 [a]	10 ± 0.0 [a]
Candida albicans **CD 140**	50	10.66 ± 0 [a]	10.33 ± 1.89 [a]	10.75 ± 0.5 [a]	11 ± 0.81 [a]
	10	10 ± 0.5 [a]	8.25 ± 1.89 [a]	10.33 ± 0.57 [a]	9.66 ± 0.57 [a]
Candida albicans **CD 1408**	50	9.5 ± 1.91 [a]	10.5 ± 0.57 [a]	10.75 ± 0.5 [a]	11 ± 0.81 [a]
	10	7 ± 1.15 [a]	10 ± 0.57 [a]	6.66 ± 0.57 [a]	9.66 ± 0.57 [a]
Malassezia pachydermatis **CBS1879**	50	10 ± 0.0 [a]	10 ± 0.0 [a]	10.33 ± 0.57 [a]	11 ± 00 [a]
	10	9.33 ± 1.15 [a]	9.33 ± 0.57 [a]	9.66 ± 1.52 [a]	9.33 ± 0.57 [a]
Malassezia pachydermatis **CD 112**	50	10.33 ± 0.57 [a]	10.66 ± 0.57 [a]	9.33 ± 1.15 [a]	10.66 ± 0.57 [a]
	10	7.66 ± 0.57 [a]	7.66 ± 0.57 [a]	7 ± 0.97 [a]	10.33 ± 0.57 [b]
Malassezia pachydermatis **CD 90**	50	10.33 ± 1.55 [a]	10.33 ± 0.57 [a]	9.66 ± 0.57 [a]	9.66 ± 0.57 [a]
	10	0 ± 0.0 [a]	7.66 ± 0.57 [b]	7.33 ± 0.57 [b]	9.33 ± 0.57 [c]
Malassezia furfur **CBS1978**	50	10.66 ± 1.54 [a]	10.33 ± 1.52 [a]	8.33 ± 0.57 [a]	9.66 ± 1.15 [a]
	10	0 ± 0.0 [a]	7 ± 0.0 [b]	0 ± 0.0 [a]	8 ± 1.0 [b]
Malassezia furfur **CD 1006**	50	9.33 ± 0.57 [a]	9.66 ± 1.52 [a]	8.33 ± 1.52 [a]	9 ± 1.73 [a]
	10	0 ± 0.0 [a]	0 ± 0.0 [a]	0 ± 0.0 [a]	8 ± 1.0 [b]
Malassezia furfur **CD 1029**	50	8 ± 1.0 [a]	9 ± 0.0 [a]	0 ± 0.0 [b]	9 ± 1.0 [a]
	10	0 ± 0.0	0 ± 0.0	0 ± 0.0	0 ± 0.0

Regarding the biological activity, the results herein are not only confirmed existing data about the antibacterial activities of crude extracts of *D. viscosa*, but are extended our knowledge on the

antifungal activities against different *Candida* spp. (i.e., *C. parapsilosis* and *C. krusei*), *Malassezia* and *A. fumigatus* strains.

All the extracts investigated exhibited antibacterial and anti-*Candida* activities which are independent of the extraction solvent, but dependent on the extract concentrations, suggesting that both flavonoid and phenolic compounds might act as antibacterial and anti-*Candida* drugs [20]. It is well known, that luteolin derivatives, isorhamnetin and in particular 3′-di-*O*-methylquercetin and 3-*O*-methyquercetin from Jordanian *D. viscosa* have an excellent inhibitory efects against *B. cereus*, *S. typhimurium* and *S. aureus*. Phenolic compounds such as hydroxycinnamic acids derivatives (caffeoylquinic acid and chlorogenic acid) or *p*-coumaric acid are also potent inhibitors of *E. coli*, *K. pneumoniae*, *B. cereus* and *C. albicans* [20,21]. Both phenolic and flavonoid compounds provoke damage in bacterial or yeast cell walls and cytoplasmic membranes [21,22]. Interestingly, the gram-positive bacteria tested were significantly more sensitive to *D. viscosa* extracts than gram-negative bacteria, most likely due to the presence of a lipopolysaccharide (LPS) membrane in Gram-negative bacteria, being more resistant to the foreign agents [23]. The absence of these LPS in membrane cell of *Candida* spp. makes them vulnerable against foreign agents.

The anti-*Malassezia* inhibition zone ranged from 0 to 11 mm. Among the yeast populations tested in this study, *Malassezia* species present a susceptibility profile varying according to the species and strain (Table 4). In particular, all extracts showed good broad-spectrum action against *M. pachydermatis* from dog otitis/dermatitis whereas the lowest effectiveness against *Malassezia furfur* isolated from human blood stream infections. These results are not surprising since similar trends were observed when the susceptibility of *M. pachydermatis* and *M. furfur* to azoles was compared due to the variability of the cell wall chemical composition of *Malassezi*a yeasts [24]. The anti-*Malassezia* activity of our extracts not only varied according to *Malassezia* species, but also to the solvent used for extraction with methanol extract most active against *M. furfur* (Table 4). Indeed, the extracts prepared with the high polarity solvents (methanol) were more effective against *Malassezia* species including *M. furfur* than those using low polarity solvents. Similar trends have been observed using chloroformic extract of *Lawsonia inermis* leaves or aqueous extracts of *Allium cepa* and *Allium sativum* against *Malassezia furfur* [25]. The anti-*Malassezia* activities of *D. viscosa* extracts may be explained by the high TFC and CQC content identified in methanol extracts thus confirming previous results with *I. paraguariensis* extracts [26].

Toxicity assays and the effect on fungal germination of extracts against *M. canis* and *A. fumigatus* are reported in Tables 5 and 6, respectively. The germination and sporulation were expressed as mean values (±standard deviation) of Log10 of colony forming units (CFU)/mL and vegetative growth as mean value (±standard deviation) of colony diameters (Ø) of three independent experiments. All *D. viscosa* extracts were able to completely inhibit the germination of *M. canis* at concentration higher than 1 mg/mL. The germination of *A. fumigatus* was completely inhibited at concentrations higher than 10 mg/mL. *D. viscosa* extracts affect both *M. canis* vegetative growth and sporulation, being non-toxic for *M. canis* CD 1279 and *M. canis* CD 1447 only when ethanolic and 80% ethanolic of *D. viscosa* extracts were used at 1 mg/mL (Table 5). All *D. viscosa* extracts are toxic to *A. fumigatus*, except for the strains CD 1435 and CD 1441. In particular, all *D. viscosa* extracts at a concentration of 1 mg/mL are non-toxic for CD 1435, with the exception of 80% ethanolic extract which is not toxic for the *A. fumigatus* CD 1441 at this concentration.

Table 5. Effects of *D. viscosa* extracts on conidia germination, vegetative growth and sporulation of *M. canis*. Degree of toxicity (*T* value) was also reported.

Strains	[C] mg/mL	Ethanol Germination (Log₁₀ CFU/mL)	Growth (Ø cm)	Sporulation (Log₁₀ CFU/mL)	T Value	Ethanol 80% Germination (Log₁₀ CFU/mL)	Growth (Ø cm)	Sporulation (Log₁₀ CFU/mL)	T Value	Butanol Germination (Log₁₀ CFU/mL)	Growth (Ø cm)	Sporulation (Log₁₀ CFU/mL)	T Value	Methanol Germination (Log₁₀ CFU/mL)	Growth (Ø cm)	Sporulation (Log₁₀ CFU/mL)	T Value
CD 1279	50	0	0	0	0	0	0	0	0	0	0	0	0	0	0	0	0
	10	0	0	0	0	0	0	0	0	0	0	0	0	0	0	0	0
	5	0	2.4 ± 0.3	3.54 ± 0.1	14.71	0	2.55 ± 0.1	4.06 ± 0.1	23.08	0	2.5 ± 0.1	3.47 ± 0.1	14.54	0	1.8 ± 0.1	2.97 ± 0.1	9.31
	1	3.72 ± 0.1	3.65 ± 0.4	4.79 ± 0.1	77.78	3.87 ± 0.1	3.85 ± 0.1	4.77 ± 0.1	76.91	3.56 ± 0.2	3.5 ± 0.1	4.58 ± 0.1	53.55	3.49 ± 0.1	2.55 ± 0.1	4.43 ± 0.1	38.45
	Control	4.30 ± 0.1	5.45 ± 0.1	4.91 ± 0.1	100	4.30 ± 0.2	5.45 ± 0.1	4.91 ± 0.1	100	4.30 ± 0.2	5.45 ± 0.1	4.91 ± 0.1	100	4.3 ± 0.2	5.45 ± 0.1	4.91 ± 0.1	100
CD 1243	50	0	0	0	0	0	0	0	0	0	0	0	0	0	0	0	0
	10	0	0	0	0	0	0	0	0	0	0	0	0	0	0	0	0
	5	0	2.1 ± 0.14	3.13 ± 0.1	10.62	0	2.25 ± 0.1	3.41 ± 0.04	13.85	0	1.85 ± 0.1	3.06 ± 0.1	9.52	0	1.85 ± 0.1	2.86 ± 0.1	8.61
	1	3.73 ± 0.1	2.55 ± 0.1	4.22 ± 0.2	48.97	3.81 ± 0.1	2.85 ± 0.1	4.22 ± 0.02	45.41	3.24 ± 0.1	2.85 ± 0.1	3.79 ± 0.1	25.71	3.24 ± 0.1	2.35 ± 0.1	3.43 ± 0.1	15.11
	C	4.18 ± 0.1	5.55 ± 0.1	4.51 ± 0.1	100	4.18 ± 0.1	5.55 ± 0.1	4.51 ± 0.1	100	4.18 ± 0.1	5.55 ± 0.1	4.51 ± 0.1	100	4.18 ± 0.1	5.55 ± 0.1	4.51 ± 0.1	100
CD 1447	50	0	0	0	0	0	0	0	0	0	0	0	0	0	0	0	0
	10	0	0	0	0	0	0	0	0	0	0	0	0	0	0	0	0
	5	0	2.5 ± 0.1	3.36 ± 0.2	16.58	0	2.85 ± 0.1	3.55 ± 0.2	21.12	0	2.45 ± 0.1	3.81 ± 0.1	14.77	0	1.65 ± 0.1	2.81 ± 0.1	9.16
	1	3.85 ± 0.1	3.45 ± 0.1	4.43 ± 0.1	66.31	3.88 ± 0.3	3.8 ± 0.1	4.26 ± 0.1	17.19	2.52 ± 0.1	3 ± 0.1	4.29 ± 0.1	50.23	2.29 ± 0.3	2.65 ± 0.1	4.26 ± 0.1	46.31
	C	4.46 ± 0.1	4.15 ± 1	4.61 ± 0.1	100	4.46 ± 0.1	4.15 ± 0.1	4.61 ± 0.2	100	4.46 ± 0.1	4.15 ± 0.1	4.61 ± 0.1	100	4.46 ± 0.1	4.15 ± 0.1	4.61 ± 0.1	100

* *T* value = very toxic (0 ≤ *T* ≤ 30); toxic (31 ≤ *T* ≤ 45); moderately toxic (46 ≤ *T* ≤ 60); non-toxic (*T* > 60); [C]: Concentration (mg/mL); C: Control.

Table 6. Effects of *D. viscosa* extracts on conidia germination, vegetative growth and sporulation of *A. fumigatus*. Degree of toxicity (*T* value) was also reported.

Strains	[C] mg/mL	Ethanol Germination (Log₁₀ CFU/mL)	Growth (Ø cm)	Sporulation (Log₁₀ CFU/mL)	T Value	Ethanol 80% Germination (Log₁₀ CFU/mL)	Growth (Ø cm)	Sporulation (Log₁₀ CFU/mL)	T Value	Butanol Germination (Log₁₀ CFU/mL)	Growth (Ø cm)	Sporulation (Log₁₀ CFU/mL)	T Value	Methanol Germination (Log₁₀ CFU/mL)	Growth (Ø cm)	Sporulation (Log₁₀ CFU/mL)	T Value
CD 1435	50	0	1.25 ± 0.1	5.09 ± 0.2	2.88	0	1.55 ± 0.1	6.25 ± 0.2	4.71	0	1.35 ± 0.1	5.12 ± 0.2	3.11	0	1.15 ± 0.1	4.08 ± 0.3	2.59
	10	3.66 ± 0.1	2.35 ± 0.1	6.45 ± 0.2	7.13	3.51 ± 0.1	2.85 ± 0.1	6.81 ± 0.1	13.62	3.47 ± 0.3	3.35 ± 0.2	6.18 ± 0.1	8.56	3.46 ± 0.3	1.95 ± 0.1	5.08 ± 0.6	4.75
	5	4.06 ± 0.1	5.9 ± 0.1	6.72 ± 0.2	19.33	4.20 ± 0.1	6.25 ± 0.1	7.23 ± 0.0	29.86	4.03 ± 0.3	5.7 ± 0.14	6.51 ± 0.1	16.44	4.14 3 ± 0.1	5.35 ± 0.1	6.18 ± 0.3	14.45
	1	5.21 ± 0.2	7.85 ± 0.1	7.75 ± 0.1	73.53	5.03 ± 0.1	8.15 ± 0.1	7.79 ± 0.1	78.41	4.97 ± 0.1	8.15 ± 0.1	7.74 ± 0.1	73.71	4.7 ± 0.1	8.25 ± 0.1	7.66 ± 0.1	64.9
	C	5.24 ± 0.1	8.9 ± 1.0	7.91 ± 0.1	100	5.24 ± 0.1	8.9 ± 1.0	7.91 ± 0.6	100	5.24 ± 0.1	8.95 ± 1.0	7.91 ± 0.1	100	5.24 ± 0.1	8.95 ± 1.1	7.91 ± 0.1	100
CD 1441	50	0	1.2 ± 0.0	5.35 ± 0.2	2.86	0	1.65 ± 0.1	5.23 ± 0.2	3.85	0	1.2 ± 0	5.13 ± 0.3	2.81	0	1.1 ± 0.0	4. 67 ± 0.1	2.54
	10	3.55 ± 0.1	3.4 ± 0.3	6.59 ± 0.1	9.93	3.68 ± 0.1	3.4 ± 0.0	6.56 ± 0.1	9.8	3.19 ± 0.1	3.3 ± 0.5	6.17 ± 0. 2	8.33	2.67 ± 0.1	2.95 ± 0.1	5.64 ± 0.1	8.25
	5	4.07 ± 0.2	5.25 ± 0.1	6.96 ± 0.1	17.2	4.34 ± 0.1	5.4 ± 0.3	7.04 ± 0.10	18.78	3.95 ± 0.1	4.55 ± 0.2	6.84 ± 0.1	14.34	3.8 ± 0.1	4.4 ± 0.2	6.72 ± 0.1	13.1
	1	4.99 ± 0.1	7.55 ± 0.2	7.73 ± 0.1	47.5	5.06 ± 0.1	7.95 ± 0.1	7.9 ± 0.1	63.81	4.83 ± 0.1	7.4 ± 0.1	7.57 ± 0.1	38.74	4.66 ± 0.1	7.8 ± 0.1	7.47 ± 0.1	34.82
	C	5.35 ± 0.1	8.8 ± 0.1	8.15 ± 0.1	100	5.53 ± 0.1	8.8 ± 0.1	8.15 ± 0.1	100	5.35 ± 0.1	8.84 ± 0.1	8.15 ± 0.1	100	5.35 ± 0.1	8.8 ± 0.1	8.15 ± 0.1	100
CD 1438	50	0	1.25 ± 0.1	5.06 ± 0.1	2.84	0	1.6 ± 0.0	5.19 ± 1.1	3.83	0	2.95 ± 0.1	5.85 ± 0.1		0	1.2 ± 0.0	0.00	0
	10	4.3 ± 0.1	3.05 ± 0.2	5.76 ± 0.5	7.2	4.58 ± 0.1	3.8 ± 0.1	6.5 ± 0.2	9.72	2.67 ± 0.1	3.95 ± 0.1	6.84 ± 0.1	6.94	4.3 ± 0.1	2.55 ± 0.2	5.61 ± 0.1	5.97
	5	5.08 ± 0.1	5.55 ± 0.2	6.69 ± 0.1	14.37	5.19 ± 0.1	6.6 ± 0.1	7.78 ± 0.1	23.54	3.96 ± 0.1		7.78 ± 0.1	12.23	4.68 ± 0.1	3.6 ± 0.1	6.18 ± 0.2	8.84
	1	5.45 ± 0.1	7.65 ± 0.2	7.89 ± 0.1	49.38	5.76 ± 0.1	8.0 ± 0.3	7.78 ± 0.01	41.49	4.12 ± 0.1	7.62 ± 0.1		40.84	5.3 ± 0	7.55 ± 0.2	7.69 ± 0.1	40.73
	C	5.92 ± 0.1	8.95 ± 1.0	8.31 ± 0.2	100	5.92 ± 0.1	8.95 ± 1.0	8.31 ± 0.2	100	5.92 ± 0.1	8.95 ± 1.0	8.31 ± 0.2	100	5.92 ± 0.1	8.95 ± 1.0	8.31 ± 0.2	100

The present study shows that all *D. viscosa* extracts significantly decrease the vegetative growth, germination, conidia production of both *M. canis* and *A. fumigatus,* thus confirming previous results against dermatophytes or other fungal species (i.e., *Cladosporium cucumerinum*, *Botrytis cinerea*, *Pseudoperonospora cubensis*, *Phytophthora infestans*, *Erysiphe graminis* and *Puccinia helianthi* [5,22]. However, all extracts evinced a concentration-dependent inhibitory activity, which varies accordingly to fungal genus. In fact, the *A. fumigatus* strains seems to be less susceptible than *M. canis* as previously reported using acetone extracts of *Arctotis arctotoides* [22]. Additionally the highest antifungal activity was observed with methanol extracts in both fungal species, thus suggesting the efficacy of both TPC and CQA content as antifungal drugs [21,27]. The mechanism of action of phenolic compounds against fungi was previously explained by several studies and might be due to the membrane lipid perturbation. Sung and Lee (2010) [28] demonstrated that phenolic acids might cause disruption of ion transport, whereas Teodoro et al. (2015) [20] indicated that the hydroxyl group and carboxylic acid groups of pheonlic compounds plays an important role in destabilizing the fungal cytoplasmic membrane. Even if the low toxicity values of *D. viscosa* methanolic extract in one strain of *A. fumigatus* need to be confirmed, the herein obtained results, suggested that concentrations higher than 1 mg/mL should be employed in controlling *A. fumigatus* strains. The antifungal activity against *Malassezia* yeasts, *M. canis* and *A. fumigatus* is of interest since the control of these infections is the subject of debate in the scientific community. In particular, *Malassezia* yeast infections in animals, mainly dogs, may be unresponsive to antifungal therapy and the animals usually have recurrences thus requiring multiple drug regimens [24]. The treatment of *M. canis* infections in animals is mandatory because of the zoophilic nature of this fungus, but it is not always possible in animals used for food production [29].

Finally, the high azoles resistance phenomena registered in *Aspergillus* spp. strains also suggests the usefulness of studies on new antifungal drugs [30]. All these findings promote the employment of drugs of plant origin.

3. Materials and Methods

3.1. Chemical and Reagents

Vanillin ($C_3H_8O_3$), catechin ($C_{15}H_{14}O_6$), Folin-Ciocalteu reagent, sodium carbonate (Na_2CO_3), gallic acid ($C_7H_6O_5$), aluminum chloride ($AlCl_3$), potassium acetate ($C_2H_3KO_2$), rutin ($C_{27}H_{30}O_{16}$), quercetin ($C_{15}H_{10}O_7$), sodium molybdate dihydrate (Na_2MoO_4), dipotassium hydrogen phosphate (K_2HPO_4), potassium dihydrogen phosphate (KH_2PO_4), chlorogenic acid ($C_{16}H_{18}O_9$) were purchased from Sigma‑Aldrich® (Steinheim, Germany). Solvents of analytical and HPLC grade were purchased from Carlo Erba Reactif-CDS (Val de Reuil, France).

3.2. Plant Material

The leaves of the plants were collected in June 2015 from uncultivated land in Sidi Thabet, located in the North East of Tunisia (latitude 36°55′45″ N, longitude 10°06′02.10″ E, altitude 30 m).

3.3. Preparation of Extracts

Dried and ground leaves (10 g) were macerated in four different solvents (ethanol (80% and 100%), methanol and butanol) (10:100 *w/v*) for 48 h with shaking at room temperature. The extracts were filtered with Whatman No. 1 filter paper and the filtrate evaporated to dryness using a rotary evaporator. In order to test the antimicrobial activities, the samples were solubilized in dimethyl sulfoxide (DMSO) to obtain concentrations of 1, 5, 10 and 50 mg/mL.

3.4. Phytochemical Screening

3.4.1. Condensed Tannins Content (CTC)

The CTC was determined as previously described [31]. In particular, 0.5 mL of extract was condensed using 3 mL of vanillin at 4% in methanol and 1.5 mL of concentrated hydrochloric acid (HCl). The mixture was kept in the dark for 15 min at 20 °C and the CTC were measured using a Jenway 6300 spectrophotometer (Cole-Parmer, Staffordshire, UK) at absorbance of 500 nm. The CTC was calculated from calibration curve using catechin (CAE) as a standard and results were expressed as milligrams of catechin equivalent per gramm (g) of dry extract (mg CAE/g).

3.4.2. Total Phenol Content (TPC)

The TPC was determined using the Folin-Ciocalteu method [32]. Briefly, 0.5 mL of each dissolved extract was mixed with 2.5 mL of Folin-Ciocalteu reagent in each test tube. After 4 min, 2 mL of saturated sodium carbonate (Na_2CO_3) solution (7.5%) was added to the mixture. The reaction mixtures were incubated for 2 h. Methanol was used as the blank. All assays were conducted in triplicate and the results were averaged. The TPC was calculated from a calibration curve using gallic acid (GAE) as the standard and the results were expressed as milligrams of gallic acid equivalent per gram of extract (mg GAE/g).

3.4.3. Total Flavonoid Content (TFC)

The TFC was quantified using the aluminum chloride colorimetric assay with slight modifications [33]. In brief, 0.5 mL of each solution extract was mixed with 1.5 mL methanol, 0.1 mL of 10% aluminum chloride, 0.1 mL of 1 mol/L potassium acetate solution and 2.8 mL distilled water. The mixture was allowed to stand for 15 min, and absorbance was measured at 415 nm. All assays were conducted in triplicate and the results were averaged. The TFC was calculated from a calibration curve using quercetin (QE) as the standard, and the result was expressed as mg of quercetin equivalent per gram dry extract (mg QE/g).

3.4.4. Caffeoylquinic Acid (CQC) Content

The CQC content of extracts was quantified using the molybdate colorimetric method [34]. Sodium molybdate (16.5 g), dipotassium hydrogen (8.0 g) phosphate, and potassium dihydrogen phosphate (7.9 g) were dissolved in 1 liter of deionized water to prepare the molybdate reagent. For each *I. viscosa* extract solution 0.3 mL was mixed with 2.7 mL of molybdate reagent. The mixture was incubated at room temperature for 10 min. Absorbance was measured at 370 nm. All assays were conducted in triplicate and the results were averaged. The CQC was calculated from a calibration curve using chlorogenic acid (ChlA) as the standard and the result was expressed as mg of ChlA equivalent per g dry extract (mg ChlA/g).

3.5. Characterization of PhenolicCcompounds by HPLC-PDA-ESI-MS

The phenolic compounds present in methonolic extract were tentatively identified using the chromatographic separation method as previously reported [4].

Chromatographic separation was performed on an Alliance e2695 HPLC system (Waters, Bedford, MA, USA) equipped with a RP-xTerra MS column (150 × 4.6 mm i.d., 3.5 μm particle size), photodiode array detector (PDA) and interfaced with a triple quadruple mass spectrometer (MSD 3100, Waters) fitted with an ESI ion source. The sample (20 μL) was eluted through the column with a gradient mobile phase consisting of A (0.1% formic acid) and B (acetonitrile acidified with formic acid 0.1%) with a flow rate of 0.5 mL/min. The following multistep linear solvent gradient was used: 0–40 min: 14–26% B; 40–60 min: 15% B; 60–75: 0% B; 75–80 min: 14% B. The HPLC-PDA-ESI-MS chromatogram spectral

data were stored and processed with Masslynx 4.1 data system. Each peak in the chromatogram was accomplished in a single chromatographic run in order to be identified [35].

3.6. Antibacterial and Antifungal Activities

3.6.1. Bacterial Strains

Five reference bacterial strains, including Gram-positive (i.e., *Staphylococcus aureus* ATCC 6538, *Enterococcus feaciu*m ATCC 19434, *Streptococcus agalactiae* ATCC 12386), and Gram-negative (i.e., *Escherichia coli* ATCC 8739, 29212 and *Salmonella typhimurium* ATCC 14028), were used to assess the antibacterial properties of the extracts.

3.6.2. Fungal Strains

Candida spp.

Three references strains of *Candida* (i.e., *Candida krusei* ATCC 6258, *Candida parapsilosis* ATCC 22019, *Candida albicans* ATCC 10231), and four *Candida albicans* strains (i.e., CD 1358, CD 1378, CD 1407, CD 1408) isolated from cloaca of laying hens, were used to evaluate the anti-*Candida* activity of *I. viscosa* extracts. All strains were obtained from the fungal collection of the Department of Veterinary Medicine at the University of Bari (Aldo Moro, Italy).

Malassezia spp. Strains

A total of six *Malassezia* spp. strains (three *Malassezia pachydermatis* and three *Malassezia furfur*) were tested. Two reference strains (i.e., *M. pachydermatis* CBS1879 and *M. fufur* CBS1978), two strains isolated from dogs with dermatitis and/or otitis (i.e., *M. pachydermatis* CD 112 and CD 90), two *M. furfur* strains from human skin (i.e., *M. furfur* CD 1029), and one from a human blood stream infection (i.e., *M. furfur* CD 1006) were tested.

Aspergillus fumigatus strains

Three *A. fumigatus* strains (CD 1435, CD 1438 and CD 1441) were tested. All strains were isolated from the respiratory tract of critically ill human patients. All strains were obtained from the fungal collection of the Department of Veterinary Medicine at the University of Bari.

Microsporum canis strains

Three *M. canis* strains (CD 1243, CD 1447, and CD 1279), isolated with skin lesions from human, cat, and dog were tested, respectively. All strains were stored in the fungal collection of the Department of Veterinary Medicine at the University of Bari.

3.7. Determination of Antibacterial, Anti-Candida and Antifungal Activity of I. viscosa Extract

The antibacterial, anti-*Candida* and anti-*Malassezia* activities were evaluated by the disk diffusion method [36], whereas the antifungal activity of *I. viscosa* extracts against *M. canis* and *A. fumigatus* was assessed by studying the toxicity effect of the extract on vegetative growth and sporulation as well their effect on fungal germination.

3.7.1. Toxicity Assay

The antifungal activity of *D. viscosa* extracts against *M. canis* and *A. fumigatus* was assessed as previously reported [37]. In particular, the antifungal properties of extracts were assessed by applying the following mathematical model in order to evaluate the degree of toxicity:

$$T = 20[VG] + 80[SR]/100 \tag{1}$$

where: T is the degree of toxicity useful for the classification of the product; VG is the percentage of vegetative growth with respect to the control; SR is the percentage of sporulation with respect to the control. The product was classified, based on the T value, as: very toxic ($0 \leq T \leq 30$); toxic ($31 \leq T \leq 45$) moderately toxic ($46 \leq T \leq 60$); non-toxic (i.e., compatible) ($T > 60$) [36].

The *A. fumigatus* and *M canis* strains were sub-cultured onto PDA and incubated at 25 °C for 10 days before testing. Vegetative growth (VG) was measured by placing a mycelial plug (i.e., 5 mm in diameter) onto the center of a 90 mm Petri dish containing potato dextrose agar (PDA), with and without extract or DMSO (solvent control), and measuring the diameter of the colonies after incubation at 25 °C for 10 days. Sporulation was evaluated by collecting the spores from surface of fungi grown on the PDA with and without the extracts after 10 incubation days at 25 °C. Spores and mycelia were collected by scraping the surface of the plate with 4 mL of 20% tween 80 solution. The solution was filtered through sterile gauze to remove mycelia, and then centrifuged ($3000\ g \times 5$ min), washed twice in 1 mL of phosphate-buffered saline solution (PBS), and re-suspended in 1 mL of PBS. Numbers of spores were determined by quantitative plate counts of (CFU)/mL on PDA after incubation at 25 °C for 4 days [37].

3.7.2. Effect of *D. viscosa* Extract on Fungal Germination

The effect of *D. viscosa* extracts on *M. canis* and *A. fumigatus* germination was also measured, culturing fungi in SDA medium after 14 days at 25 °C and collecting spores and mycelia as reported above. The solution obtained was diluted in PBS to obtain an inoculum concentration of 10^7 conidia/mL which was evaluated by quantitative plate counts of CFU/mL in PDA. Finally, a total of 100 μL of the fungal spore suspensions were cultured in PDA with and without different extract concentrations. The number of germinated spores were determined by counts of CFU/mL on PDA [38]. All experiments were performed in duplicate and repeated three times on different days.

3.8. Statistical Analysis

The results of toxicity assay on vegetative growth, sporulation and fungal germination were expressed as mean values (±standard deviation (SD)) of the three independent experiments. Vegetative growth (VG) was expressed as mean value of colony diameters after incubation and the sporulation and germination as mean values of Log_{10} CFU/mL. Results were statistically analyzed using one way analysis of variance (ANOVA). Significant differences were set at $p < 0.05$.

4. Conclusions

The employment of these extracts might be useful to treat infections that are life threatening (i.e., *Malassezia*) or infections that require a mandatory treatment (i.e., *M. canis* or *A. fumigatus*), thus providing another commercial validation of this weed and working towards reducing the hazards associated with excessive use of chemical products.

Author Contributions: Rhimi Wafa and Davide Immediato conceived and performed the experiments; Abdennacer Boulila contributed to plant extraction and identification of phenolic compounds; Mouldi Saidi analysed and rechecked the manuscript; Claudia Cafarchia, Rhimi Wafa, Issam Ben Salem designed the experiments analyzed the data, and wrote this paper.

Conflicts of Interest: The authors declare no conflict of interest.

References

1. Rossolini, G.M.; Arena, F.; Pecile, P.; Pollini, S. Update on the antibiotic resistance crisis. *Curr. Opin. Pharmacol.* **2014**, *18*, 56–60. [CrossRef] [PubMed]
2. Çelik, T.A.; Aslantürk, Ö.S. Evaluation of cytotoxicity and genotoxicity of *Inula viscosa* leaf extracts with *Allium* test. *J. Biomed. Biotechnol.* **2010**, *2010*, 189252.

3. Parolin, P.; Scotta, M.I.; Bresch, I. Biology of *Dittrichia viscosa*, a Mediterranean ruderal plant. *φyton.* **2013**, *83*, 251–262.

4. Mahmoudi, H.; Hosni, K.; Zaouali, W.; Amri, I.; Zargouni, H.; Hamida, N.B.; Kaddour, R.; Hamrouni, L.; Nasri, M.B.; Ouerghi, Z. Comprehensive Phytochemical Analysis, Antioxidant and Antifungal Activities of *Inula viscosa* Aiton Leaves. *J. Food Saf.* **2015**, *36*, 77–88. [CrossRef]

5. Omezzine, F.; Daami-Remadi, M.; Rinez, A.; Ladhari, A.; Haouala, R. In vitro assessment of *Inula* spp. organic extracts for their antifungal activity against some pathogenic and antagonistic fungi. *Afr. J. Microbiol. Res.* **2011**, *5*, 3527–3531.

6. Assaf, A.M.; Amro, B.I.; Mashallah, S.; Haddadin, R.N. Antimicrobial and anti-inflammatory potential therapy for opportunistic microorganisms. *J. Infect. Dev. Ctries* **2016**, *10*, 494–505. [CrossRef] [PubMed]

7. Duek, L.; Kaufman, G.; Ulman, Y.; Berdicevsky, I. The pathogenesis of dermatophyte infections in human skin sections. *J. Infect.* **2004**, *48*, 175–180. [CrossRef] [PubMed]

8. Bender, J.B.; Shulman, S.A. Reports of zoonotic disease outbreaks associated with animal exhibits and availability of recommendations for preventing zoonotic disease transmission from animals to people in such settings. *J. Am. Vet. Med. Assoc.* **2004**, *224*, 1105–1109. [CrossRef] [PubMed]

9. Raad, I.I.; Graybill, J.R.; Bustamante, A.B.; Cornely, O.A.; Gaona-Flores, V.; Afif, C.; Graham, D.R.; Greenberg, R.N.; Hadley, S.; Langston, A.; et al. Safety of long-term oral posaconazole use in the treatment of refractory invasive fungal infections. *Clin. Infect. Dis.* **2006**, *42*, 1726–1734. [CrossRef] [PubMed]

10. Cafarchia, C.; Figueredo, L.A.; Otranto, D. Fungal diseases of horses. *Vet. Microbiol.* **2013**, *167*, 215–234. [CrossRef] [PubMed]

11. Cafarchia, C.; Figueredo, L.A.; Iatta, R.; Montagna, M.T.; Otranto, D. In vitro antifungal susceptibility of *Malassezia pachydermatis* from dogs with and without skin lesions. *Vet. Microbiol.* **2012**, *155*, 395–398. [CrossRef] [PubMed]

12. Cafarchia, C.; Figueredo, L.A.; Iatta, R.; Colao, V.; Montagna, M.T.; Otranto, D. In vitro evaluation of *Malassezia pachydermatis* susceptibility to azole compounds using E-test and CLSI microdilution methods. *Med. Mycol.* **2012**, *50*, 795–801. [PubMed]

13. Seyedmousavi, S.; Guillot, J.; Arn, P.; De Hoog, G.S.; Mouton, J.W.; Melchers, W.J.G.; Verweij, P.E. *Aspergillus* and aspergilloses in wild and domestic animals: A global health concern with parallels to human disease. *Med. Mycol.* **2015**, *53*, 765–797. [CrossRef] [PubMed]

14. Sefi, M.; Fetoui, H.; Makni, M.; Zeghal, N. Mitigating effects of antioxidant properties of *Artemisia campestris* leaf extract on hyperlipidemia, advanced glycation end products and oxidative stress in alloxan-induced diabetic rats. *Food Chem. Toxicol.* **2010**, *48*, 1986–1993. [CrossRef] [PubMed]

15. Trimech, I.; Weiss, E.K.; Chedea, V.S.; Marin, D.; Detsi, A.; Ioannou, E.; Roussis, V.; Kefalas, P. Evaluation of anti-oxidant and acetylcholinesterase activity and identification of polyphenolics of the invasive weed *Dittrichia viscosa*. *Phytochem. Anal.* **2014**, *25*, 421–428. [CrossRef] [PubMed]

16. Negi, P.S.; Jayaprakasha, G. Antioxidant and Antibacterial Activities of *Punica granatum* Peel Extracts. *J. Food Sci.* **2003**, *68*, 1473–1477. [CrossRef]

17. Geng, H.-M.; Zhang, D.-Q.; Zha, J.-P.; Qi, J.-L. Simultaneous HPLC Determination of Five Flavonoids in Flos Inulae. *Chromatographia* **2007**, *66*, 271–275. [CrossRef]

18. Naeem, I.; Saddiqe, Z.; Patel, A.; Hellio, C. Analysis of flavonoid and antimicrobial activity of extracts of *Hypericum perforatum*. *Asian J. Chem.* **2010**, *22*, 3596–3600.

19. Danino, O.; Gottlieb, H.E.; Grossman, S.; Bergman, M. Antioxidant activity of 1,3-dicaffeoylquinic acid isolated from *Inula viscosa*. *Food Res. Int.* **2009**, *42*, 1273–1280. [CrossRef]

20. Teodoro, G.R.; Ellepola, K.; Seneviratne, C.J.; Koga-Ito, C.Y. Potential use of phenolic acids as anti-*Candida* agents: A review. *Front. Microbiol.* **2015**, *6*, 1–11. [CrossRef] [PubMed]

21. Cushnie, T.P.T.; Lamb, A.J. Antimicrobial activity of flavonoids. *Int. J. Antimicrob. Agents* **2005**, *26*, 343–356. [CrossRef] [PubMed]

22. Otang, W.M.; Grierson, D.S.; Ndip, R.N. The effect of the acetone extract of *Arctotis arctotoides* (Asteraceae) on the growth and ultrastructure of some opportunistic fungi associated with HIV/AIDS. *Int. J. Mol. Sci.* **2011**, *12*, 9226–9235. [CrossRef] [PubMed]

23. Silhavy, T.J.; Kahne, D.; Walker, S. The bacterial cell envelope. *Cold Spring Harb. Perspect. Biol.* **2010**, *2*, 1–16. [CrossRef] [PubMed]

24. Velegraki, A.; Cafarchia, C.; Gaitanis, G.; Iatta, R.; Boekhout, T. *Malassezia.* Infections in Humans and Animals: Pathophysiology, Detection, and Treatment. *PLoS Pathog.* **2015**, *11*, e1004523. [CrossRef] [PubMed]
25. Berenji, F.; Rakhshandeh, H.; Ebrahimipour, H. In vitro study of the effects of henna extracts (*Lawsonia inermis*) on Malassezia species. *Jundishapur J. Microbiol.* **2010**, *3*, 125–128.
26. Filip, R.; Davicino, R.; Anesini, C. Antifungal activity of the aqueous extract of Ilex paraguariensis against malassezia furfur. *Phyther. Res.* **2010**, *24*, 715–719.
27. Von Nussbaum, F.; Brands, M.; Hinzen, B.; Weigand, S.; Häbich, D. Antibacterial natural products in medicinal chemistry–Exodus or revival? *Angew. Chem. Int. Ed.* **2006**, *45*, 5072–5129. [CrossRef] [PubMed]
28. Sung, W.S.; Lee, D.G. Antifungal action of chlorogenic acid against pathogenic fungi, mediated by membrane disruption. *Pure Appl. Chem.* **2010**, *82*, 219–226. [CrossRef]
29. Magwedere, K.; Hemberger, M.Y.; Hoffman, L.C.; Dziva, F. Zoonoses: A potential obstacle to the growing wildlife industry of Namibia. *Infect. Ecol. Epidemiol.* **2012**, *2*, 1–16. [CrossRef] [PubMed]
30. Tanwar, J.; Das, S.; Fatima, Z.; Hameed, S. Multidrug Resistance: An Emerging Crisis. *Interdiscip. Perspect. Infect. Dis.* **2014**, *2014*, 541340. [CrossRef] [PubMed]
31. Chavan, U.; Shahidi, F.; Naczk, M. Extraction of condensed tannins from beach pea (*Lathyrus maritimus* L.) as affected by different solvents. *Food Chem.* **2001**, *75*, 509–512. [CrossRef]
32. Meda, A.; Lamien, C.E.; Romito, M.; Millogo, J.; Nacoulma, O.G. Determination of the total phenolic, flavonoid and proline contents in Burkina Fasan honey, as well as their radical scavenging activity. *Food Chem.* **2005**, *91*, 571–577. [CrossRef]
33. Zheng, C.J.; Yoo, J.-S.; Lee, T.-G.; Cho, H.-Y.; Kim, Y.-H.; Kim, W.-G. Fatty acid synthesis is a target for antibacterial activity of unsaturated fatty acids. *FEBS Lett.* **2005**, *579*, 5157–5162. [CrossRef] [PubMed]
34. Chan, E.W.C.; Lim, Y.Y.; Ling, S.K.; Tan, S.P.; Lim, K.K.; Khoo, M.G.H. Caffeoylquinic acids from leaves of *Etlingera* species (Zingiberaceae). *LWT–Food Sci. Technol.* **2009**, *42*, 1026–1030. [CrossRef]
35. Nyau, V.; Prakash, S.; Rodrigues, J.; Farrant, J. HPLC-PDA-ESI-MS Identification of Polyphenolic Phytochemicals in Different Market Classes of Common Beans (*Phaseolus vulgaris* L.). *Int. J. Biochem. Res. Rev.* **2015**, *8*, 1–11. [CrossRef]
36. Dhouioui, M.; Boulila, A.; Jemli, M.; Schiets, F.; Casabianca, H.; Zina, M.S. Fatty Acids Composition and Antibacterial Activity of *Aristolochia longa* L. and *Bryonia dioïca* Jacq. Growing Wild in Tunisia. *J. Oleo Sci.* **2016**, *65*, 655–661. [CrossRef] [PubMed]
37. Immediato, D.; Aguiar, L.; Iatta, R.; Camarda, A.; Lira, R.; De Luna, N.; Giangaspero, A.; Brandão-filho, S.P.; Otranto, D.; Cafarchia, C. Veterinary Parasitology Essential oils and *Beauveria. bassiana* against *Dermanyssus gallinae* (Acari: Dermanyssidae): Towards new natural acaricides. *Vet. Parasitol.* **2016**, *229*, 159–165. [CrossRef] [PubMed]
38. Tamai, M.A.; Alves, S.B.; Lopes, R.B.; Faion, M.; Padulla, L.F.L. Toxicidade De Produtos Fitossanitários para Beauveria Bassiana (Bals.) Vuill. *Arq. Inst. Biol. (Sao Paulo)* **2002**, *69*, 65–69.

Sample Availability: Samples of the phenolic and flavonoid compounds are available from the authors.

Article

Green Tea Catechin Is an Alternative Immune Checkpoint Inhibitor that Inhibits PD-L1 Expression and Lung Tumor Growth

Anchalee Rawangkan [1,2], Pattama Wongsirisin [1,2], Kozue Namiki [1,2], Keisuke Iida [3], Yasuhito Kobayashi [4], Yoshihiko Shimizu [4], Hirota Fujiki [5] and Masami Suganuma [1,2,*]

[1] Graduate School of Science and Engineering, Saitama University, Saitama 338-8570, Japan; ewmedsci@gmail.com (A.R.); wongsiri.patt@gmail.com (P.W.); k.namiki1080@gmail.com (K.N.)

[2] Research Institute for Clinical Oncology, Saitama Cancer Center, Saitama 362-0806, Japan

[3] Molecular Chirality Research Center and Department of Chemistry, Graduate School of Science, Chiba University, Chiba 263-8522, Japan; kiida@chiba-u.jp

[4] Saitama Cardiovascular and Respiratory Center, Kumagaya, Saitama 360-0197, Japan; kobayashiyasuhito@yahoo.co.jp (Y.K.); shimizu.yoshihiko@pref.saitama.lg.jp (Y.S.)

[5] Faculty of Medicine, Saga University, Saga 849-8501, Japan; uv4h-fjk@asahi-net.or.jp

*   Correspondence: masami0306@mail.saitama-u.ac.jp; Tel.: +81-48-722-1111

check for updates

Abstract: The anticancer activity of immune checkpoint inhibitors is attracting attention in various clinical sites. Since green tea catechin has cancer-preventive activity in humans, whether green tea catechin supports the role of immune checkpoint inhibitors was studied. We here report that (−)-epigallocatechin gallate (EGCG) inhibited programmed cell death ligand 1 (PD-L1) expression in non–small-cell lung cancer cells, induced by both interferon (IFN)-γ and epidermal growth factor (EGF). The mRNA and protein levels of IFN-γ–induced PD-L1 were reduced 40–80% after pretreatment with EGCG and green tea extract (GTE) in A549 cells, via inhibition of JAK2/STAT1 signaling. Similarly, EGF-induced PD-L1 expression was reduced about 37–50% in EGCG-pretreated Lu99 cells through inhibition of EGF receptor/Akt signaling. Furthermore, 0.3% GTE in drinking water reduced the average number of tumors per mouse from 4.1 ± 0.5 to 2.6 ± 0.4 and the percentage of PD-L1 positive cells from 9.6% to 2.9%, a decrease of 70%, in lung tumors of A/J mice given a single intraperitoneal injection of 4-(methylnitrosamino)-1-(3-pyridyl)-1-butanone (NNK). In co-culture experiments using F10-OVA melanoma cells and tumor-specific CD3+ T cells, EGCG reduced *PD-L1* mRNA expression about 30% in F10-OVA cells and restored *interleukin-2* mRNA expression in tumor-specific CD3+ T cells. The results show that green tea catechin is an immune checkpoint inhibitor.

Keywords: (−)-epigallocatechin gallate; immune checkpoint; interferon-γ; epidermal growth factor; lung tumor

1. Introduction

Blockade of programmed cell death ligand 1 (PD-L1)/programmed cell death 1 (PD-1) immune checkpoints by monoclonal antibodies has shown measurable success in cancer therapy against a variety of tumor types, including non–small-cell lung cancer (NSCLC) [1,2]. PD-L1 is expressed on both tumor cells and immune cells, and PD-1 is predominantly expressed on activated T cells. Binding of PD-L1 to PD-1 inhibits T cell effector function by inducing exhaustion and apoptosis of T cells, resulting in an immunosuppressive state [3]. Expression of PD-L1 in tumor cells plays an important role in tumor

immune escape and cancer progression. Although immunotherapy targeting PD-L1/PD-1 signaling is being used for treatment of advanced lung cancers, the benefit is limited to the early stages, because antibody-based checkpoint inhibitors are associated with unique immune-related adverse effects and high costs [4]. Recently, bromodomain and extraterminal (BET) inhibitors have also been shown to be inhibitors of PD-L1 expression by directly targeting the *PD-L1* gene [5]. Apigenin, a phytochemical, also inhibits interferon (IFN)-γ–induced PD-L1 protein [6]. Development of small-molecule blocking PD-L1/PD-1 signaling is now being actively investigated.

Green tea and (−)-epigallocatechin gallate (EGCG), the main constituent of green tea catechins, are nontoxic, effective cancer preventives for humans [7]: drinking 10 cups (120 mL/cup) of green tea per day delayed cancer onset in a 10-year prospective cohort study in Japan, and also prevented colorectal adenoma recurrence in a double-blind randomized phase II clinical trials in Japan and Korea [7–10]. Recently we reported that human cancer stem cells (CSCs) are a target for cancer prevention using EGCG [7], based on evidence that EGCG generally inhibits the self-renewal of CSCs and the expression of epithelial-mesenchymal transition (EMT) phenotypes in human CSCs. Green tea catechins are tannins that can bind to various proteins and nucleic acids [11,12]. EGCG inhibits the binding of various ligands, tumor promoters, and epidermal growth factor (EGF) to their receptors in the cell membrane, which is called the "sealing effects" of EGCG. This is achieved by stiffening of the cell membrane after EGCG treatment [11]. Since EGCG inhibits metastasis of mouse B16 melanoma cells and enhances anticancer activity in combination with anticancer agents [13,14], we propose that EGCG may have additional clinical benefits through immunological interactions. The expression of PD-L1 on tumor cells is induced by EMT, IFN-γ, tumor necrosis factor-α (TNF-α), and EGF in the inflammatory tumor microenvironment [3,15,16]. Therefore, we hypothesize that EGCG will inhibit PD-L1, an immune checkpoint molecule, leading to enhancement of the antitumor immune response.

We first examined the effects of EGCG on PD-L1 expression induced by two factors, IFN-γ and EGF, in NSCLC cell lines in vitro. This is because IFN-γ is the strongest stimulator of PD-L1 expression, and EGF and EGF receptor (EGFR) mutations induce PD-L1 expression with lung cancer progression [1,2,16]. We then studied the relationship between inhibition of PD-L1 expression and lung tumor growth by giving water containing 0.3% green tea extract (GTE), a freeze-dried form of green tea infusion, to A/J mice treated with a tobacco-specific carcinogen, 4-(methylnitrosamino)-1-(3-pyridyl)-1-butanone (NNK), in vivo. In addition, to determine whether EGCG reverses the inhibitory effect of the PD-L1/PD-1 pathway on T cell activity, we conducted a co-culture experiment using F10-OVA mouse melanoma cells and tumor-specific CD3+ T cells isolated from the spleens of F10-OVA–immunized C57BL/6 mice.

In this study, we found that EGCG and GTE inhibited both IFN-γ– and EGF-induced PD-L1 expression by inhibiting two signaling pathways, JAK2/STAT1 and EGFR/Akt, in human NSCLC cell lines. In addition, oral administration of GTE reduced the percentage of PD-L1–positive cells in lung tumors and the average number of tumors per mouse in A/J mice treated with NNK. EGCG also reduced *PD-L1* mRNA expression in F10-OVA cells and partially restored *interleukin-2* (*IL-2*) mRNA expression in tumor-specific T cells in a co-culture experiment. This is the first report showing that EGCG and GTE have some activity as immune checkpoint inhibitors in lung cancer development.

2. Results

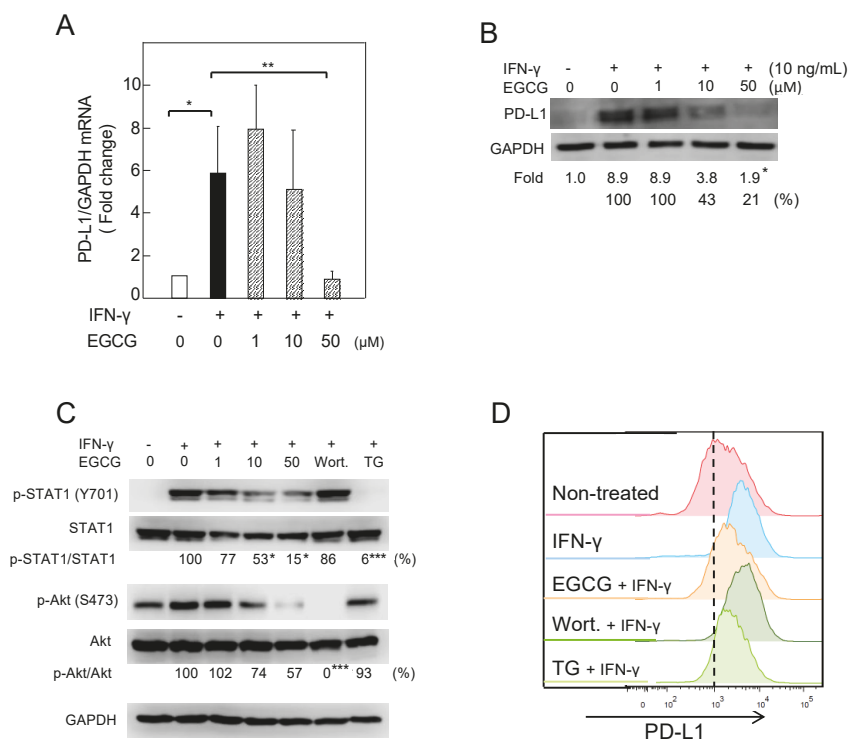### 2.1. Downregulation of IFN-γ–Induced PD-L1 Protein and Inhibition of STAT1 and Akt Phosphorylation in A549 Cells Treated with GTE and EGCG

It is well known that IFN-γ, produced by activated T cells, stimulates PD-L1 expression in the tumor microenvironment [1,2], so we first examined the effects of green tea catechins on IFN-γ–induced PD-L1 expression. Treatment with IFN-γ (10 ng/mL) increased the mRNA and protein of PD-L1 and cell-surface PD-L1 protein twofold in A549 cells (Supplementary Figure S1). GTE contains at least four catechins: EGCG, (−)-epicatechin gallate (ECG), (−)-epigallocatechin (EGC), and (−)-epicatechin (EC) [17]. Pretreatment of A549 cells with 50 or 100 μg/mL GTE reduced the levels of cell-surface

PD-L1 protein induced by IFN-γ (Figure 1A); cells pretreated with EGCG (10 and 50 μM), ECG (50 μM), or EGC (50 μM) reduced PD-L1 protein levels from 3.8 ± 0.3 median fluorescence intensity (MFI) to 2.8 ± 0.1 to 1.0 ± 0.2 MFI, a decrease of 40–80%. EC, an inactive catechin, had no effect on PD-L1 protein expression. EGCG showed the most potent inhibition among the green tea catechins (Figure 1B). Pretreatment of the cells with EGCG dose-dependently inhibited *PD-L1* mRNA and protein, and 50 μM EGCG decreased *PD-L1* mRNA by 86% (from 5.8-fold to 0.8-fold) and PD-L1 protein by 79% (Figure 2A,B). A similar reduction of IFN-γ–induced PD-L1 expression with EGCG was observed in H1299 cells (Supplementary Figure S2).

To clarify the inhibitory mechanisms of EGCG, we next studied the IFN receptor (IFNR) signaling pathway. Pretreatment with EGCG dose-dependently reduced the levels of p-STAT1 and p-Akt: 50 μM EGCG inhibited p-STAT1 and p-Akt by 85% and 43%, respectively, in A549 cells (Figure 2C). Furthermore, pretreatment of A549 with 1 μM TG-101348 (TG), a JAK2 inhibitor, reduced p-STAT1 by 94%, but did not affect p-Akt, and showed a strong reduction of cell-surface PD-L1 protein, as EGCG did (Figure 2C,D). However, wortmannin, a phosphoinositide 3-kinase (PI3K) inhibitor, inhibited p-Akt, but did not show any reduction of cell-surface PD-L1 (Figure 2C,D). These results indicate that EGCG reduced PD-L1 expression via inhibition of the JAK2/STAT1 signaling pathway.
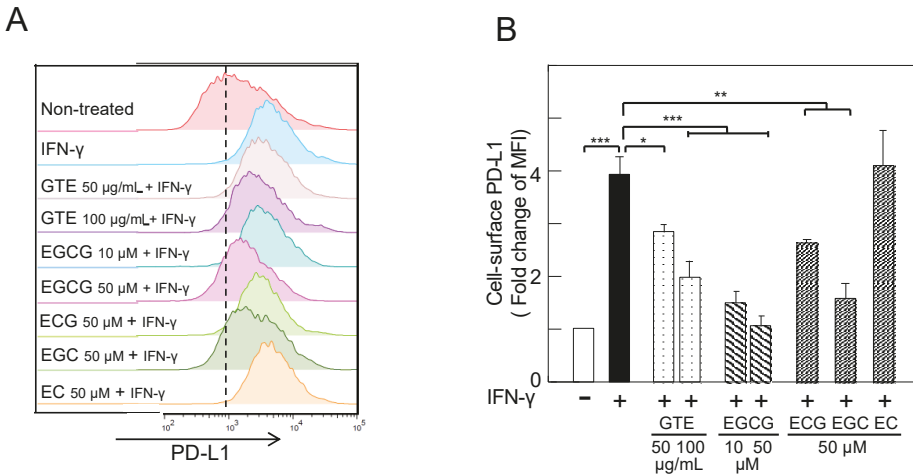
Figure 1. Inhibition of interferon (IFN)-γ–induced cell-surface programmed cell death ligand 1 (PD-L1) protein by green tea extract (GTE) and green tea catechins in A549 cells. (**A**) Cell-surface PD-L1, and (**B**) average of fold change of median fluorescence intensity (MFI). "−" and "+" indicate in the absence or presence of IFN-γ (10 ng/mL). * $p < 0.05$, ** $p < 0.01$, *** $p < 0.001$. EGCG, (−)-epigallocatechin gallate; ECG, (−)-epicatechin gallate; EGC, (−)-epigallocatechin; EC, (−)-epicatechin.

Figure 2. Downregulation of IFN-γ–induced PD-L1 protein and inhibition of STAT1- and Akt-phosphorylation in A549 cells treated with (−)-epigallocatechin gallate (EGCG). (**A**) *PD-L1* mRNA expression, (**B**) PD-L1 protein, (**C**) phosphorylation of STAT1 and Akt, and (**D**) cell-surface PD-L1. "−" and "+" indicate in the absence or presence of IFN-γ (10 ng/mL). Numbers indicate average percentage compared with IFN-γ–treated cells. * $p < 0.05$, ** $p < 0.01$, *** $p < 0.001$. GAPDH, glyceraldehyde-3-phosphate dehydrogenase.

2.2. Downregulation of EGF-Induced PD-L1 Protein and Inhibition of Akt Phosphorylation in Lu99 Cells Treated with EGCG

Activation of EGFR signaling by EGF and EGFR mutations also drove PD-L1 expression in NSCLC cells [16,18]. Treatment with 10 ng/mL EGF significantly increased *PD-L1* mRNA and protein expression 5.8-fold and 8.9-fold, respectively, and cell-surface PD-L1 about 2.7-fold in Lu99 cells (Supplementary Figure S1). Pretreatment with 50 μM EGCG for 3 h decreased the levels of *PD-L1* mRNA and protein in Lu99 cells by 50% and 37%, respectively (Figure 3A,B). It is important to note that EGCG inhibited the EGFR signaling pathway. Pretreatment with 50 μM EGCG decreased p-Akt by 35%, and pretreatment with 1 μM wortmannin reduced p-Akt and cell-surface PD-L1 levels more than EGCG did (Figure 3C,D). Although the effects of EGCG on the EGFR/Akt axis and cell-surface PD-L1 were not strong, EGCG inhibited the production of EGF-induced PD-L1. Overall, EGCG inhibited PD-L1 expression in NSCLC cells induced by two different factors via their specific receptors.
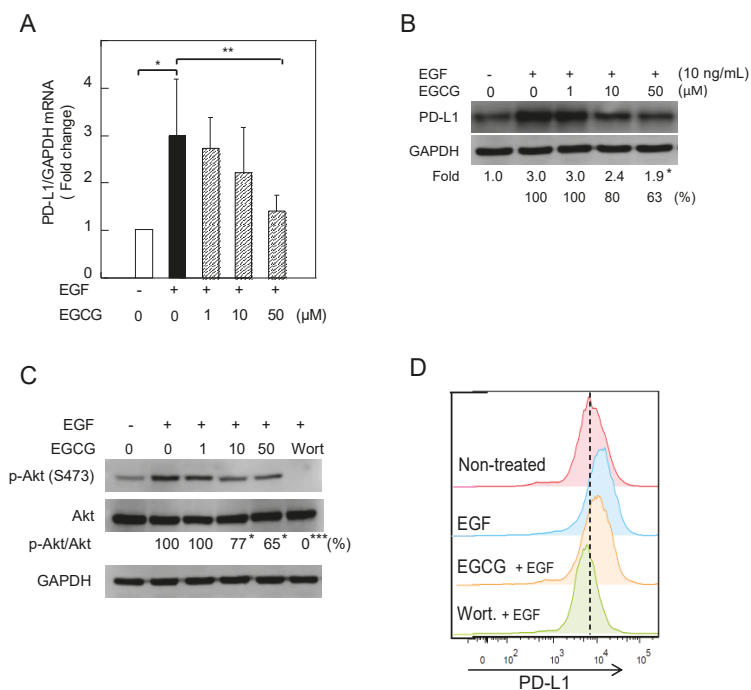
Figure 3. Downregulation of EGF-induced PD-L1 protein and inhibition of Akt phosphorylation in Lu99 cells treated with EGCG. (**A**) *PD-L1* mRNA expression, (**B**) PD-L1 protein, (**C**) phosphorylation of STAT1 and Akt, and (**D**) cell-surface PD-L1. "−" and "+" indicate in the absence or presence of EGF (10 ng/mL). Numbers indicate average percentage compared with EGF-treated cells. * $p < 0.05$, ** $p < 0.01$, *** $p < 0.001$.

2.3. Oral Administration of GTE Reduced PD-L1–Positive Cells and Inhibited Tumor Growth in the Lungs of NNK-Treated A/J Mice

Next, we conducted lung carcinogenesis experiments with female A/J mice. A single intraperitoneal injection of NNK produced lung tumors in 100% of the mice after 16 weeks. Oral administration of 0.3% GTE in drinking water reduced the average number of tumors per mouse from 4.1 ± 0.5 to 2.6 ± 0.4 at week 16, a decrease of 37% (Table 1). All tumors were adenomas 0.8 mm or more in diameter. Immunohistochemical analysis with anti–PD-L1 antibody showed PD-L1 protein on the plasma membrane and in the cytosol of lung tumor cells; cells with PD-L1 on the plasma membrane were counted as PD-L1–positive cells (Figure 4A). Figure 4B shows average percentage of PD-L1–positive cells in individual tumors in the NNK and NNK + GTE groups. The NNK group had an average of 9.6 ± 4.9% PD-L1–positive cells, while the NNK + GTE group had 2.9 ± 2.2%, a decrease of 70% (Figure 4B and Table 1). GTE significantly reduced PD-L1 protein in lung tumors in vivo, which was associated with inhibition of tumor development. It is important to note that a solution of 0.3% (3 g/L) GTE contains 0.85 g/L of catechins (14% EGCG, 8% ECG, 3% EGC, and 3.5% EC) and 0.1 g/L of caffeine, corresponding to the totals in green tea beverages in Japan [19].

Table 1. Oral administration of GTE reduced average number of lung tumors and percentage of PD-L1–positive cells in 4-(methylnitrosamino)-1-(3-pyridyl)-1-butanone (NNK)-treated A/J mice.

Group	Average No. ofTumors/Mouse $\pm$ SE (% of inhibition)	Percentage of PD-L1–Positive Cells $\pm$ SE (% of inhibition)
NNK	4.1 ± 0.5	9.6 ± 4.9
NNK + GTE	2.6 ± 0.4 (36.6) *	2.9 ± 2.2 (69.8) *

<div align="center">* $p < 0.05$.</div>
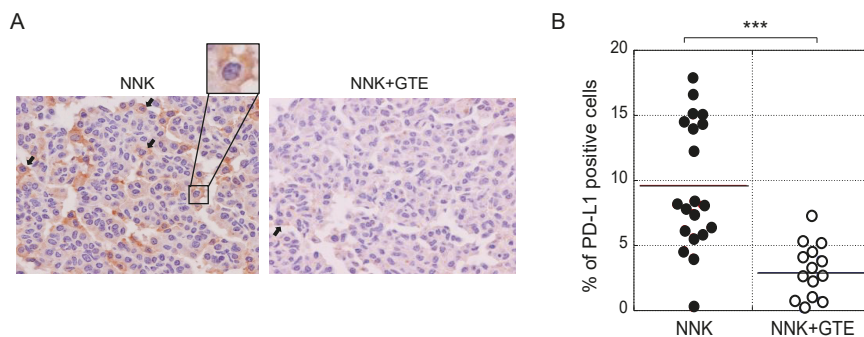
Figure 4. Oral administration of GTE reduced PD-L1–positive cells and inhibited tumor development in the lungs of NNK-treated A/J mice. (**A**) Representative immunohistochemical staining with anti–PD-L1 antibody. Black arrows indicate PD-L1–positive cells on the plasma membrane. (**B**) Average percentage of PD-L1–positive cells in individual tumors. *** $p < 0.001$.

2.4. EGCG Slightly Restored IL-2 mRNA Expression in Tumor-Specific CD3+ T Cells Co-cultured with Tumor Cells (F10-OVA)

We conducted a co-culture experiment using B16-F10 mouse melanoma cells expressing ovalbumin (F10-OVA) and tumor-specific mouse CD3+ T cells isolated from the spleens of F10-OVA-immunized C57BL/6 mice. The cell-surface *PD-L1* in F10-OVA cells increased twofold after co-culture with tumor-specific CD3+ T cells compared with F10-OVA cells alone (Figure 5A). Next, we found that EGCG (30 μM) reduced *PD-L1* mRNA expression approximately 30% in F10-OVA cells co-cultured with CD3+ T cells, but EGCG did not affect *PD-L1* mRNA level in F10-OVA cells not co-cultured (Figure 5B).

In addition, we measured *IL-2* mRNA expression in CD3+ T cells to determine T cell effector activity. After co-culture with F10-OVA cells for 48 h, *IL-2* mRNA expression was dramatically decreased by 24%. Treatment with EGCG (10 μM) recovered *IL-2* mRNA to approximately 40% (Figure 5C) and increased the number of T cells by 1.6-fold (Figure 5D) in CD3+ T cells co-cultured with F10-OVA cells, although EGCG did not affect *IL-2* mRNA expression or number of T cells in non–co-cultured CD3+ T cells. These results indicate that EGCG partially restored T cell activity by suppressing PD-L1/PD-1 signaling.
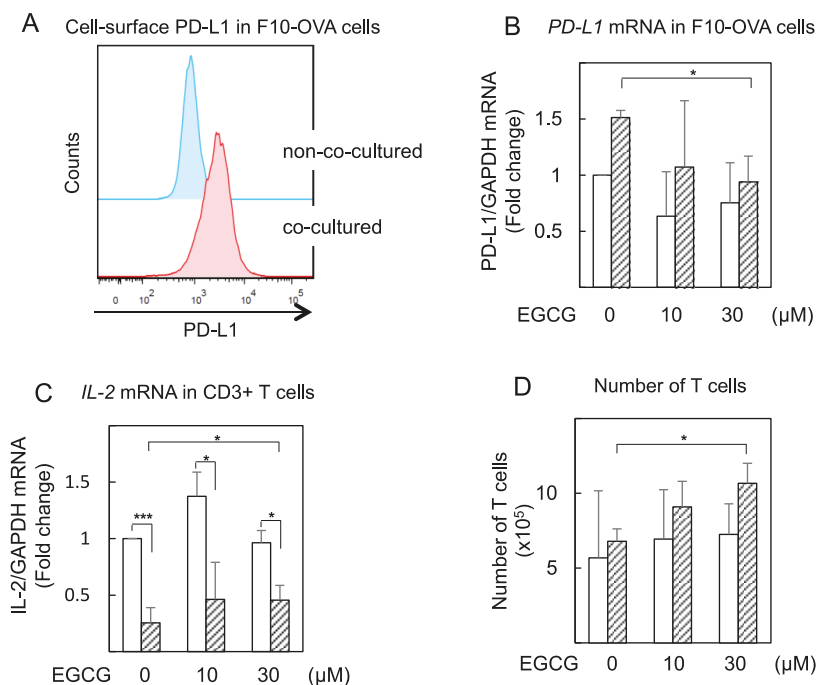
Figure 5. EGCG reduced *PD-L1* mRNA expression in co-cultured F10-OVA cells and restored *IL-2* mRNA expression in co-cultured tumor-specific CD3+ T cells. (**A**) Cell-surface PD-L1 and (**B**) *PD-L1* mRNA in F10-OVA cells alone (open bars) and cells co-cultured with CD3+ T cells (shaded bars). mRNA expression normalized by GAPDH in nontreated cells is expressed as 1 in (**B**) and (**C**). (**C**) *IL-2* mRNA in CD3+ T cells alone (open bars) and cells co-cultured with F10-OVA cells (shaded bars). (**D**) Number of T cells in CD3+ T cells alone (open bars) and cells co-cultured with F10-OVA cells (shaded bars) were counted by trypan blue exclusion method. * $p < 0.05$, *** $p < 0.001$.

3. Discussion

We showed, for the first time, that the main green tea catechin, EGCG, acts as an immune checkpoint inhibitor by inhibiting PD-L1 expression in tumor cells. For example, oral administration of GTE, which corresponds to green tea beverages consumed by Japanese people every day, reduced PD-L1 expression in lung tumors and the average number of tumors per mouse in A/J mice treated with NNK, so EGCG and GTE can probably reduce PD-L1 expression. In addition, results of co-culture experiments with F10-OVA tumor cells and tumor-specific CD3+ T cells support our conclusion that EGCG-mediated PD-L1 inhibition results in restoration of T cell activity.

Interestingly, EGCG inhibited both IFNR/JAK2/STAT1 and EGFR/Akt signaling pathways, suggesting that EGCG inhibits IFN-γ-IFNR and EGF-EGFR activation by inhibiting ligand-receptor binding [11]. The results are consistent with a recent report that EGCG increased the bending stiffness of artificial lipid membranes by adsorption of galloyl catechin aggregates to the lipid membrane surface [20]. We also reported that stiffening of cancer cell membranes with EGCG correlates well with inhibition of EMT, motility, and metastasis in lung cancer cells and B16-F10 mouse melanoma cells [11,21]. It is notable that Gimzewski's group reported that GTE increased cell stiffness of tumor cells isolated from the pleural effusions of various cancer patients, but it had no effect on normal mesothelial cells [22]. It is well known that membrane lipids such as cholesterol regulate T cell signaling and function [23]; whether EGCG directly enhances T-cell function or acts indirectly

will require further study. In addition to our results, EGCG was previously shown to suppress indoleamine 2,3-dioxygenase (IDO), which can enhance immune escape by blocking the IFN-γ–induced JAK/PKC/STAT1 signaling pathway in oral cancer cells [24]. These results strongly indicate that enhancing the effects of EGCG on adaptive immune cells will restrict the growth of tumor cells.

Based on results showing that the expression of *PD-L1* gene and cell-surface PD-L1 protein varied depending on the inducer and the cells, as shown in Supplementary Figure S1, we stimulated A549 cells with IFN-γ and Lu99 cells with EGF to induce PD-L1 expression. It is well known that PD-L1 protein in lung cancer cells is induced by activation of EGFR signaling through both overexpression and mutation of EGFR [16]. Lu99 cells showed high intrinsic PD-L1 levels and a strong response to EGF among the three lung cancer cell lines studied. This is probably because of high EGFR protein levels and a mutated T1025A in PI3K catalytic subunit α (PI3KCA) [25]. It has recently been reported that multiple microRNAs act as important regulators of PD-L1 expression directly or indirectly [26]. Since EGCG upregulates tumor suppressor microRNAs, it is important to determine whether alteration of microRNA levels regulated by EGCG inhibits *PD-L1* mRNA expression [27].

Phase III clinical trials recently reported that the combination of chemotherapy and immune checkpoint–targeted antibodies shows an effect superior to chemotherapy alone, indicating that the use of immune checkpoint inhibitors will be extended to cancer treatment [4]. We previously reported that the combination of EGCG and anticancer compounds showed synergistic enhancement of anticancer effects in numerous human cancer cell lines and xenograft mouse models, in vitro and in vivo [14,28]. Since EGCG and GTE act as immune checkpoint inhibitors, we think the combination of green tea catechins and checkpoint inhibitors will further increase the benefits of cancer therapy.

It is important to note that PD-L1 in tumor cells has functions other than as an immune checkpoint ligand, including stimulation of cancer progression, promotion of EMT, acquisition of tumor-initiating potential, and resistance to apoptosis [15]. As our previous experiments showed, EGCG and GTE inhibit EMT in lung cancer cells, increase cell stiffening, and inhibit self-renewal of cancer stem cells, leading to apoptosis of cancer cells [7,11,21].

4. Materials and Methods

4.1. Cell Lines and Chemicals

Human NSCLC cell lines A549, H1299 (American Type Culture Collection, Manassas, VA, USA), and Lu99 (Riken Bioresource Center, Tsukuba, Ibaraki, Japan) were cultured in RPMI 1640 supplemented with 10% fetal bovine serum (FBS) (Sigma-Aldrich, St. Louis, MO, USA). Mouse B16-F10 melanoma were kindly provided by Dr. Shun'ichiro Taniguchi at Shinshu University, Japan. EGCG (more than 99% purity) was purified from Japanese green tea leaves (*Camellia sinensis* L., O. Kuntze, Theaceae), and GTE was extracted by a similar procedure to make green tea infusion (sencha) as described previously [17,19]. Green tea leaves were cultivated at Saitama Prefectural Tea Institute, Saitama, Japan, and processed to make sencha. After brewing 2 kg of green tea leaves (sencha) in 70 L of hot water (85 °C) for 15 min, the green tea infusion was filtrated and freeze-dried. About 500 g of GTE was obtained. This GTE contained 14% EGCG, 8% ECG, 3% EGC, 3.5% EC, and 3.3% caffeine as analyzed by HPLC. ECG (>99%), EGC (>99%), and EC (>99%) were purchased from Funakoshi Co. Ltd., Tokyo, Japan. Anti-PD-L1 (Abcam, Cambridge, MA, USA), anti-STAT1, anti-phospho-STAT1 (BD Bioscience, NJ, USA), anti-Akt, anti-phospho-Akt (Cell Signaling Technology, Danvers, MA, USA) and anti- glyceraldehyde-3-phosphate dehydrogenase (GAPDH) (Trevigen, Gaithersburg, MD, USA) antibodies were used for the experiments. Recombinant human IFN-γ and human EGF were obtained from R&D Systems (Minneapolis, MN, USA) and PeproTech (Rocky Hill, London, UK), respectively. Wortmannin and TG-101348 were purchased from Sigma-Aldrich (St. Louis, MO, USA), and ChemScene (Monmouth Junction, NJ, USA), respectively.

4.2. Animals

Female A/J mice and C57BL/6 mice were obtained from Japan SLC Inc. (Hamamatsu, Japan) and Charles River Laboratories Japan Inc. (Yokohama, Japan), respectively. The animal experiments were performed in accordance with protocols approved by the Institutional Animal Care and Use Committee of the Research Institute for Clinical Oncology, Saitama Cancer Center (project identification code: 21-1) and the Saitama University Committee on Animal Research (project identification code: H29-A-1-12), under Fundamental Guidelines for Proper Conduct of Animal Experiments and Related Activities in Academic Research Institutions and Acts on Welfare and Management of Animals. All mice were housed at 23 ± 2 °C with a 12 h light-dark cycle. Mice were fed food and water *ad libitum*.

4.3. Establishment of Ovalbumin-Expressing B16-F10 (F10-OVA) Cells

F10-OVA cells were established by transfection of pcDNA3-OVA plasmid (Addgene, Cambridge, MA, USA) using Lipofectamine® 3000 Transfection reagent (Invitrogen, Thermo Fisher Scientific, Waltham, MA, CA, USA) to B16-F10 cells. F10-OVA cells were maintained with 2 mg/mL G418 sulfate in Dulbecco's Modified Eagle's medium (DMEM) containing 10% FBS. The F10-OVA clones were confirmed by ovalbumin gene expression using PCR.

4.4. Quantitative RT-PCR

Total RNA of the cells was extracted using ISOGEN (Nippon Gene Co. Ltd., Toyama, Japan). cDNA was synthesized from total RNA using Oligo(dT)$_{16}$ and MuLV reverse transcriptase (Thermo Fisher Scientific, Cambridge, MA, USA), and real-time PCR was conducted using SYBR Green I (LightCycler 480, Roche Lifescience, Basel, Switzerland), as described previously [29]. Primers used were as follows:

human PD-L1 forward primer	5′-GGACAAGCAGTGACCATCAAG-3′
human PD-L1 reverse primer	5′-CCCAGAATTTACCAAAGTGAGTCCT-3′
human GAPDH forward primer	5′-TGGTATCGTGGAAGGACTCATGAC-3′
human GAPDH reverse primer	5′-ATGCCACTCAGCTTCCCGTTCAGC-3′
mouse PD-L1 forward primer	5′-GGACAAGCAGTGACCATCAAG-3′
mouse PD-L1 reverse primer	5′-TGATCTGAAGGGCAGCATTTC-3′
mouse IL-2 forward primer	5′-TTGTCGTCCTTGTCAACAGC-3′
mouse IL-2 reverse primer	5′-CTGGGGAGTTTCAGGTTCCT-3′
mouse GAPDH forward primer	5′-T TTGTCGTCCTTGTCAACAGC-3′
mouse GAPDH reverse primer	5′-CTGGGGAGTTTCAGGTTCCT-3′

The *PD-L1 and IL-2* mRNA relative expressions were normalized by *glyceraldehyde-3-phosphate dehydrogenase (GAPDH)* mRNA expression as an internal control. Results were obtained from at least 3 independent experiments.

4.5. Western Blot Analysis

Whole cell lysates were obtained with radioimmunoprecipitation assay (RIPA) buffer containing 50 mM Tris-HCl (pH 7.4), 1% NP-40, 0.5% sodium deoxycholate, 0.1% sodium dodecyl sulfate (SDS), 150 mM sodium chloride, 2 mM ethylenediaminetetraacetic acid (EDTA), 10 µg/mL aprotinin, 10 µg/mL leupeptin, 1 mM phenylmethanesulfonyl fluoride, 2.5 mM sodium pyrophosphate, 1 mM sodium orthovanadate, and 2.5 mM sodium fluoride. Cell lysates were subjected to gel electrophoresis and then transferred onto a nitrocellulose membrane. After incubation with the primary antibody (1:1000) followed by an appropriate secondary antibody (1:2000), specific bands were detected by Immunostar LD (Wako Pure Chem. Japan Ind. Ltd., Osaka, Japan), using C-DiGit Chemiluminescent Western Blot Scanner (LI-COR Biosciences Inc., Lincoln, NE, USA) [29]. GAPDH was used as an internal control. The values are the average fold changes for nontreated cells obtained from at least 3 independent experiments.

4.6. Flow Cytometry

Cells were stained with anti–PD-L1 antibody (1:200) in phosphate-buffered saline (PBS) with 2% FBS and 0.02% EDTA for 30 min, and then incubated with Alexa Fluor® 488 goat anti-rabbit IgG (Invitrogen, Waltham, MA, USA) for 20 min on ice. Labeled cells were analyzed by flow cytometry (FACSCanto II, BD Biosciences, San Jose, CA, USA). The data were analyzed by FlowJo v.10 software (FlowJo, LLC, Ashland, OR, USA) and the levels of cell-surface PD-L1 protein were estimated by median fluorescence intensity (MFI). The experiments were performed at least 3 times.

4.7. Development of Lung Tumors

Female A/J mice 7 weeks old were given a single intraperitoneal injection of NNK (100 mg/kg body weight; Toronto Research Chemicals Inc., North York, ON, Canada), as described previously [28,30]. Two days later, 15 mice received drinking water containing 0.3% GTE and 20 mice received drinking water without GTE for 16 weeks. After sacrifice, the lungs were kept and tumor size was measured. Lung tumors measuring 0.8 mm or more in diameter were counted.

4.8. Immunohistochemical Staining

Lung sections were incubated with 3% H_2O_2 for 10 min and then subjected to antigen retrieval using pressure cooking in antigen-activating solution (pH 9, 98 °C). After blocking with Protein Block (Dako, Carpinteria, CA, USA) for 5 min at room temperature, the sections were immunostained with anti–PD-L1 antibody (1:200) for 40 min at 37 °C, followed by secondary antibody (N-Histofine Simple Stain MAX-PO (Multi), Nichirei Bioscience Inc., Tokyo, Japan) for 20 min at 37 °C, as described previously [31]. Cells showing positive for PD-L1 on the plasma membrane were independently counted by 3 investigators. Results are expressed as average percentage of PD-L1–positive cells ± standard error (SE).

4.9. Co-culture with Tumor-Specific CD3+ T Cells and F10-OVA Cells

Tumor-specific CD3+ T cells were generated as previously described [32]. Briefly, F10-OVA cells were treated with 25 μg/mL of mitomycin C in DMEM containing 10% FBS for 20 min at 37 °C in the dark, and washed with PBS. C57BL/6 mice were intraperitoneally injected with mitomycin C–treated F10-OVA cells, and 14 days later CD3+ T cells were isolated from the spleen using anti-CD3 antibody-coated magnetic microbeads (Miltenyi Biotec, GmbH, Bergisch Gladbach, Germany). Mitomycin C–treated F10-OVA cells were pretreated with EGCG for 3 h, and then co-cultured with CD3+ T cells at a 1:20 ratio in the presence of EGCG for 48 h.

4.10. Statistical Analysis

Statistical analyses were performed using one-way analysis of variance (ANOVA) followed by Dunnett's test. Each experiment was conducted independently at least three times, and values are expressed as mean ± standard deviation (SD). For the in vivo lung carcinogenesis experiment, Student's *t*-test and Wilcoxon–Mann–Whitney test were used, and values are expressed as mean ± SE. *p* value < 0.05 was considered statistically significant.

5. Conclusions

All our results suggest that EGCG partially restores T cell activity by inhibition of PD-L1/PD-1 signaling, resulting in inhibition of lung cancer growth. Thus, we present a new concept: green tea catechin acts as an immune checkpoint inhibitor, leading to cancer prevention and treatment.

Conflicts of Interest: The authors declare no conflict of interest.

References

1. Ribas, A.; Wolchok, J.D. Cancer immunotherapy using checkpoint blockade. *Science* **2018**, *359*, 1350–1355. [CrossRef] [PubMed]
2. Baumeister, S.H.; Freeman, G.J.; Dranoff, G.; Sharpe, A.H. Coinhibitory pathways in immunotherapy for cancer. *Annu. Rev. Immunol.* **2016**, *34*, 539–573. [CrossRef] [PubMed]
3. Dong, H.; Strome, S.E.; Salomao, D.R.; Tamura, H.; Hirano, F.; Flies, D.B.; Roche, P.C.; Lu, J.; Zhu, G.; Tamada, K.; et al. Tumor-associated B7-H1 promotes T-cell apoptosis: A potential mechanism of immune evasion. *Nat. Med.* **2002**, *8*, 793–800. [CrossRef] [PubMed]
4. Hendriks, L.E.; Besse, B. Windows open for cancer immunotherapy. *Nature* **2018**, *558*, 376–377. [CrossRef] [PubMed]
5. Zhu, H.; Bengsch, F.; Svoronos, N.; Rutkowski, M.R.; Bitler, B.G.; Allegrezza, M.J.; Yokoyama, Y.; Kossenkov, A.V.; Bradner, J.E.; Conejo-Garcia, J.R.; et al. BET bromodomain inhibition promotes anti-tumor immunity by suppressing PD-L1 expression. *Cell Rep.* **2016**, *16*, 2829–2837. [CrossRef] [PubMed]
6. Coombs, M.R.; Harrison, M.E.; Hoskin, D.W. Apigenin inhibits the inducible expression of programmed death ligand 1 by human and mouse mammary carcinoma cells. *Cancer Lett.* **2016**, *380*, 424–433. [CrossRef] [PubMed]
7. Fujiki, H.; Watanabe, T.; Sueoka, E.; Rawangkan, A.; Suganuma, M. Cancer prevention with green tea and its principal constituent, EGCG: From early investigations to current focus on human cancer stem cells. *Mol. Cells* **2018**, *41*, 73–82. [CrossRef] [PubMed]
8. Nakachi, K.; Matsuyama, S.; Miyake, S.; Suganuma, M.; Imai, K. Preventive effects of drinking green tea on cancer and cardiovascular disease: Epidemiological evidence for multiple targeting prevention. *Biofactors* **2000**, *13*, 49–54. [CrossRef] [PubMed]
9. Shimizu, M.; Fukutomi, Y.; Ninomiya, M.; Nagura, K.; Kato, T.; Araki, H.; Suganuma, M.; Fujiki, H.; Moriwaki, H. Green tea extracts for the prevention of metachronous colorectal adenomas: A pilot study. *Cancer Epidemiol. Biomarkers Prev.* **2008**, *17*, 3020–3025. [CrossRef] [PubMed]
10. Shin, C.M.; Lee, D.H.; Seo, A.Y.; Lee, H.J.; Kim, S.B.; Son, W.C.; Kim, Y.K.; Lee, S.J.; Park, S.H.; Kim, N.; et al. Green tea extracts for the prevention of metachronous colorectal polyps among patients who underwent endoscopic removal of colorectal adenomas: A randomized clinical trial. *Clin. Nutr.* **2018**, *37*, 452–458. [CrossRef] [PubMed]
11. Suganuma, M.; Takahashi, A.; Watanabe, T.; Iida, K.; Matsuzaki, T.; Yoshikawa, H.Y.; Fujiki, H. Biophysical approach to mechanisms of cancer prevention and treatment with green tea catechins. *Molecules* **2016**, *21*, 1566. [CrossRef] [PubMed]
12. Kuzuhara, T.; Sei, Y.; Yamaguchi, K.; Suganuma, M.; Fujiki, H. DNA and RNA as new binding targets of green tea catechins. *J. Biol. Chem.* **2006**, *281*, 17446–17456. [CrossRef] [PubMed]
13. Taniguchi, S.; Fujiki, H.; Kobayashi, H.; Go, H.; Miyado, K.; Sadano, H.; Shimokawa, R. Effect of (−)-epigallocatechin gallate, the main constituent of green tea, on lung metastasis with mouse B16 melanoma cell lines. *Cancer Lett.* **1992**, *65*, 51–54. [CrossRef]
14. Fujiki, H.; Sueoka, E.; Watanabe, T.; Suganuma, M. Synergistic enhancement of anticancer effects on numerous human cancer cell lines treated with the combination of EGCG, other green tea catechins, and anticancer compounds. *J. Cancer Res. Clin. Oncol.* **2015**, *141*, 1511–1522. [CrossRef] [PubMed]
15. Marcucci, F.; Rumio, C.; Corti, A. Tumor cell-associated immune checkpoint molecules-drivers of malignancy and stemness. *Biochim. Biophys. Acta.* **2017**, *1868*, 571–583. [CrossRef] [PubMed]
16. Akbay, E.A.; Koyama, S.; Carretero, J.; Altabef, A.; Tchaicha, J.H.; Christensen, C.L.; Mikse, O.R.; Cherniack, A.D.; Beauchamp, E.M.; Pugh, T.J.; et al. Activation of the PD-1 pathway contributes to immune escape in EGFR-driven lung tumors. *Cancer Discov.* **2013**, *3*, 1355–1363. [CrossRef] [PubMed]

17. Fujiki, H.; Okuda, T. (−)-Epigallocatechin gallate. *Drugs Future* **1992**, *17*, 462–464. [CrossRef]

18. Lastwika, K.J.; Wilson, W., III; Li, Q.K.; Norris, J.; Xu, H.; Ghazarian, S.R.; Kitagawa, H.; Kawabata, S.; Taube, J.M.; Yao, S.; et al. Control of PD-L1 expression by oncogenic activation of the AKT-mTOR pathway in non-small cell lung cancer. *Cancer Res.* **2015**, *76*, 227–238. [CrossRef] [PubMed]

19. Fujiki, H.; Suganuma, M.; Matsuyama, S.; Miyazaki, K. Cancer prevention with green tea polyphenols for the general population, and for patients following cancer treatment. *Curr. Cancer Ther. Rev.* **2005**, *1*, 109–114. [CrossRef]

20. Matsuzaki, T.; Ito, H.; Chevyreva, V.; Makky, A.; Kaufmann, S.; Okano, K.; Kobayashi, N.; Suganuma, M.; Nakabayashi, S.; Yoshikawa, H.Y.; et al. Adsorption of galloyl catechin aggregates significantly modulates membrane mechanics in the absence of biochemical cues. *Phys. Chem. Chem. Phys.* **2017**, *19*, 19937–19947. [CrossRef] [PubMed]

21. Takahashi, A.; Watanabe, T.; Mondal, A.; Suzuki, K.; Kurusu-Kanno, M.; Li, Z.; Yamazaki, T.; Fujiki, H.; Suganuma, M. Mechanism-based inhibition of cancer metastasis with (−)-epigallocatechin gallate. *Biochem. Biophys. Res. Commun.* **2014**, *443*, 1–6. [CrossRef] [PubMed]

22. Cross, S.E.; Jin, Y.S.; Rao, J.; Gimzewski, J.K. Nanomechanical analysis of cells from cancer patients. *Nature Nanotechnol.* **2007**, *2*, 780–783. [CrossRef] [PubMed]

23. Yang, W.; Bai, Y.; Xiong, Y.; Zhang, J.; Chen, S.; Zheng, X.; Meng, X.; Li, L.; Wang, J.; Xu, C.; et al. Potentiating the antitumour response of CD8+ T cells by modulating cholesterol metabolism. *Nature* **2016**, *531*, 651–655. [CrossRef] [PubMed]

24. Cheng, C.W.; Shieh, P.C.; Lin, Y.C.; Chen, Y.J.; Lin, Y.H.; Kuo, D.H.; Liu, J.Y.; Kao, J.Y.; Kao, M.C.; Way, T.D. Indoleamine 2,3-dioxygenase, an immunomodulatory protein, is suppressed by (−)-epigallocatechin-3-gallate via blocking of γ-interferon-induced JAK-PKC-δ-STAT1 signaling in human oral cancer cells. *J. Agric. Food Chem.* **2010**, *58*, 887–894. [CrossRef] [PubMed]

25. The Broad Institute of MIT & Harvard. Cancer cell line encyclopedia. Available online: https://portals. broadinstitute.org/ccle (accessed on 5 May 2018).

26. Wang, Q.; Lin, W.; Tang, X.; Li, S.; Guo, L.; Lin, Y.; Kwok, H.F. The roles of microRNAs in regulating the expression of PD-1/PD-L1 immune checkpoint. *Int. J. Mol. Sci.* **2017**, *18*, 2540. [CrossRef] [PubMed]

27. Sethi, S.; Li, Y.; Sarkar, F.H. Regulating miRNA by natural agents as a new strategy for cancer treatment. *Curr. Drug Targets.* **2013**, *14*, 1167–1174. [CrossRef] [PubMed]

28. Suganuma, M.; Saha, A.; Fujiki, H. New cancer treatment strategy using combination of green tea catechins and anticancer drugs. *Cancer Sci.* **2011**, *102*, 317–323. [CrossRef] [PubMed]

29. Oya, Y.; Mondal, A.; Rawangkan, A.; Umsumarng, S.; Iida, K.; Watanabe, T.; Kanno, M.; Suzuki, K.; Li, Z.; Kagechika, H.; et al. Down-regulation of histone deacetylase 4, -5 and -6 as a mechanism of synergistic enhancement of apoptosis in human lung cancer cells treated with the combination of a synthetic retinoid, Am80 and green tea catechin. *J. Nutr. Biochem.* **2017**, *42*, 7–16. [CrossRef] [PubMed]

30. Xu, Y.; Ho, C.T.; Amin, S.G.; Han, C.; Chung, F.L. Inhibition of tobacco-specific nitrosamine-induced lung tumorigenesis in A/J mice by green tea and its major polyphenol as antioxidants. *Cancer Res.* **1992**, *52*, 3875–3879. [PubMed]

31. Devanand, P.; Oya, Y.; Sundaramoorthy, S.; Song, K.Y.; Watanabe, T.; Kobayashi, Y.; Shimizu, Y.; Hong, S.A.; Suganuma, M.; Lim, I.K. Inhibition of TNFα-interacting protein α (Tipα)-associated gastric carcinogenesis by BTG2(/TIS21) via downregulating cytoplasmic nucleolin expression. *Exp. Mol. Med.* **2018**, *50*, E449. [CrossRef] [PubMed]

32. Barsoum, I.B.; Smallwood, C.A.; Siemens, D.R.; Graham, C.H. A mechanism of hypoxia-mediated escape from adaptive immunity in cancer cells. *Cancer Res.* **2014**, *74*, 665–674. [CrossRef] [PubMed]

Sample Availability: Not Available.

molecules

MDPI

Search of Neuroprotective Polyphenols Using the "Overlay" Isolation Method

Hiroshi Sakagami [1,*], Haixia Shi [1,2,*], Kenjiro Bandow [3], Mineko Tomomura [3], Akito Tomomura [3], Misaki Horiuchi [4], Tomohiro Fujisawa [4] and Takaaki Oizumi [4]

[1] Meikai University Research Institute of Odontology (M-RIO), 1-1 Keyakidai, Sakado, Saitama 350-0283, Japan

[2] Department of Traditional Chinese Medicine, Shanghai Ninth People's Hospital, Shanghai Jiaotong University School of Medicine, Shanghai 201900, China

[3] Divisions of Biochemistry, Department of Oral Biology and Tissue Engineering, Meikai University School of Dentistry, Saitama 350-0283, Japan; kbando@dent.meikai.ac.jp (K.B.); mineko-t@dent.meikai.ac.jp (M.T.); atomomu@dent.meikai.ac.jp (A.T.)

[4] Daiwa Biological Research Institute Co., Ltd., Kanagawa 213-0012, Japan; m_horiuchi@daiwaseibutsu.co.jp (M.H.); t_fujisawa@daiwaseibutsu.co.jp (T.F.); takaakio@daiwaseibutsu.co.jp (T.O.)

* Correspondence: sakagami@dent.meikai.ac.jp (H.Sa.); haixia.0101@163.com (H.Sh.); Tel.: +81-49-279-2758 (H.Sa.); +81-49-279-2787 (H.Sh.)

check for updates

Abstract: Previous studies of the neuroprotective activity of polyphenols have used ununiform culture systems, making it difficult to compare their neuroprotective potency. We have established a new and simple method for preparing differentiated PC12 cells by removing the toxic coating step. Cells were induced to differentiate with the nerve growth factor (NGF) in a serum-free medium, without a medium change, but with a one-time overlay supplementation of NGF. The optimal inoculation density of the cells was 6–12×10^3 cells/cm^2, and the presence of serum inhibited the differentiation. Neuroprotective activity could be quantified by the specific index (SI) value, that is, the ratio of the 50% cytotoxic concentration to the 50% effective concentration. Alkaline extract from the leaves of *Sasa senanensis* Rehder (SE), having had hormetic growth stimulation, showed the highest SI value, followed by epigallocatechin gallate. The SI value of curcumin and resveratrol was much lower. This simple overly method, that can prepare massive differentiated neuronal cells, may be applicable for the study of the differentiation-associated changes in intracellular metabolites, and the interaction between neuronal cells and physiological factors.

Keywords: neuroprotection; PC12; NGF; differentiation; amyloid-β peptide; taxanes; hormesis; polyphenol; bamboo leaf extract; overlay method

1. Introduction

Improvement in the daily nutritional supply and the living environment resulted in the prolongation of our life span, but necessarily increased the number of elderly populations having cognitive diseases [1–3]. Alzheimer's disease, the most common form of dementia, is characterized by the accumulation of amyloid-β (Aβ) in the brain. Since the neurotoxicity of Aβ has been well established [4,5], preventing the accumulation [6] and early oligomerization [7] of Aβ may be a promising cognitive behavioral therapy.

Platinum drugs such as cisplatin, carboplatin and oxaliplatin have been important parts of combination chemotherapy regimens to treat different types of solid tumors, but they can cause

serious neurotoxicity in the dorsal root ganglion by the formation of adducts to DNA [8]. Taxanes, such as paclitaxel and docetaxel, induce microtubule assembly, mitotic arrest, and finally apoptosis in cancer cells. However, they often induce painful peripheral neurotoxicity during treatment [9]. Patients who received both platinum and taxane treatment showed aggravated neuropathy [10].

Polyphenols—defined as substances that possess an aromatic ring bearing one or more hydroxyl substituents—have been reported to show neuroprotective activity. Polyphenols are roughly classified into the following three groups: Tannins; flavonoids; and, lignin-carbohydrate complexes (LCC) [11]. Tannins are classified into two large groups: Hydrolysable tannins (in which a polyalcohol is esterified with a polyphenolic carboxylic acid such as a galloyl, hexahydroxydiphenoyl, valoneoyl, or dehydrohexahydroxydiphenoyl group); and, condensed tannins (composed of flavan units, mostly catechin, epicatechin, or their analogs, condensed with each other via carbon–carbon bonds) [12]. Flavonoids are secondary metabolites synthesized from chalcones [13] and are categorized into flavonols, flavones, flavanones, isoflavones, pterocarpan and coumestan. Resveratrol is classified as a stilbenoid. Lignins are formed through phenolic oxidative coupling processes. Lignin macromolecules are formed by the dehydrogenative polymerization of three monolignols: *p*-coumaryl, *p*-conifery, and sinapyl alcohols. Some polysaccharides in the cell walls of lignified plants are linked to lignin, and recover as lignin-carbohydrate complex—after extraction with alkaline solution [14].

Previous studies have mostly used low-molecular-weight polyphenols, such as flavonoids and tannins, which manifest various health-promoting activities (antioxidant, anti-inflammatory, and antibacterial activity). This was due to the recent development of separation technology for elucidating their chemical structure [15,16]. On the other hand, the search for neuroprotective, high-molecular substances, such as lignin-carbohydrate complex, have been delayed due to their amorphous structures. They did, however, show prominent anti-HIV activity [17].

Most previous studies of neuroprotection have used rat pheochromocytoma 12 (PC12) [18] and human SH-SY5Y neuroblastoma cell lines [19,20], since these cell lines differentiate into neuronal cells with elongated neurites upon treatment with nerve growth factor (NGF) or retinoic acid.

However, there was no uniformity in the culture condition of PC12 and SH-SY5Y cells in previous investigations. The culture media used was: Dulbecco's modified Eagle's medium (DMEM); the minimum essential medium (MEM); RPMI1640; a mixture of DMEM and Ham's F12 (1:1); and, non-essential amino acids (NEAA), which were supplemented with fetal bovine serum (FBS), alone or together with, horse serum (HS) (column A in Table 1) [21–31]. Differentiated and undifferentiated cells (column B), inoculated at different cell densities, were exposed to considerably different concentrations of neurotoxic agents (column C) in uncoated, collagen, or poly-lysine-coated plates (Table 1). Most importantly, previous investigators have not presented the chemotherapeutic index (safety margin). Therefore, it was difficult to compare with previous data on the neuroprotective activity of polyphenols.

In order to investigate the interaction between neuroprotective substances and cells, it is best to use the medium that has the simplest components. We have recently reported that the addition of Ham's F-12 and non-essential amino acids did not increase, but rather, reduced the growth and amino acid consumption of both PC12 and SH-SY5Y cells [32]. During neuronal differentiation induced by NGF, a medium change (that removes numerous neurotrophic factors released from differentiating cells) at an early stage resulted in the poor attachment and low recovery of differentiated cells. If a fresh NGF-containing medium was supplemented by an overlay at the middle stage (without a medium change), comparable numbers of differentiated cells could be harvested after six or seven days, regardless of the types of plates, either non-coated or coated with collagen I or IV. To our surprise, due to its toxicity, the use of poly-lysine coated plates significantly reduced the yield of differentiated cells [33]. Based on these results, DMEM, supplemented with NGF, was adopted as a regular differentiation induction medium, which was added to the culture plates that were not coated with collagen I, IV, or poly-lysine.

Table 1. Culture system for PC12 cells used by previous researchers.

Cell	Culture Medium	Differentiation-Induction Medium	Cytotoxicity Induced by	Rescue System	Ref
	(A)	**(B)**	**(C)**	**(D)**	
PC12	RPMI1640 + 10%FBS + 5%HS	NGF (50 ng/mL) in serum-free RPMI1640 for 7 days	Aβ_{25-35} (5–10 µM)	Autophagy	[21]
PC12	RPMI1640 + 10%FBS + 5%HS	NGF (25 ng/mL) in RPMI1640 + 10%FBS + 5%HS in collagen-coated dish for 2 days	Aβ_{25-35} (10 µM)	HSP-70	[22]
PC12	RPMI1640 + 5%FBS + 10%HS	No treatment	Aβ_{1-42} (75 µM)	ROS reduction	[23]
PC12	DMEM + 10%FBS	No treatment	Aβ_{25-35} (20 µM)	JAK2/STAT5/Bcl-xL	[24]
PC12	DMEM + 10%FBS	No treatment	Aβ_{25-35} (20 µM)		[25]
SH-SY5Y	DMEM + 10%FBS	No treatment	Aβ_{1-42} (0.5 µM)	HO-1 CO	[26]
SH-SY5Y	DMEM/Ham's F-12 (1:1) + 10%FBS	All-trans-retinoic acid (10 µM) + 3%FBS for 7–8 days	Aβ_{25-35} (20 µM)		[27]
SH-SY5Y	DMEM/Ham's F-12 (1:1) + 10%FBS	No treatment	Aβ_{1-42} (1–50 µM)	Phospho HSP-20	[28]
SH-SY5Y	MEM/Ham's F-12 (1:1) + 10%FBS	No treatment	Aβ_{1-42} (20 µM)	Amyloid disaggregation	[29]
SH-SY5Y	DMEM/Ham's F-12 (1:1) + 10%FBS + 1%NEAA	No treatment	Aβ_{1-40} (10 µM)	KiSS overexpression	[30]
PC12	DMEM/Ham's F-12 (1:1) + 5%FBS + 10%HS	NGF (25 ng/mL) in RPMI1640 + 10%FBS + 5%HS in collagen-coated dish			[31]

FBS, fetal bovine serum; HS, horse serum; NEAA, non-essential amino acids.

Using PC12 cells prepared by the overlay method, we have re-investigated the neuroprotective activity of various polyphenols. This was compared with that of plant extracts and antioxidants, based on the specific index (SI) (defined as the ratio of 50% cytotoxic concentration (CC$_{50}$) to 50% protective concentration (EC$_{50}$)).

2. Results

2.1. Optimal Concentration of Ngf and Fbs for the Induction of PC12 Cell Differentiation

We first confirmed that NGF stimulated the growth of PC12 cells at the optimal concentration of 50 ng/mL in our assay system. The cell number increased up to day five, and thereafter, slightly declined, possibly due to it reaching the terminal differentiation (Figure 1A). NGF also stimulated the formation of neurite—the marker of neuronal differentiation. When differentiated cells were defined as the cells in which the extended neurite exceeds the longest diameter of each cell (Figure 1B), the percentage of differentiated cells reached a plateau at day five, with a maximum of 50 ng/mL NGF (Figure 1C).

2.2. FBS Inhibited the Differentiation of PC12 Cells

When PC12 cells were cultured in a serum-free medium, neuronal differentiation reached a maximum level. When inoculation of cell density was reduced to $3.125 \times 10^3/\text{cm}^2$, the incidence of cell death slightly increased (Figure 2), which suggests the importance of continuous nutritional supply from neighboring cells. It was unexpected that the maximum differentiation can be achieved in the absence of FBS, and the addition of 1% or 10% FBS inhibited the differentiation induction. Thus, the optimal inoculation of cell density was determined to be between 6 and $12 \times 10^3/\text{cm}^2$ in the absence of serum.
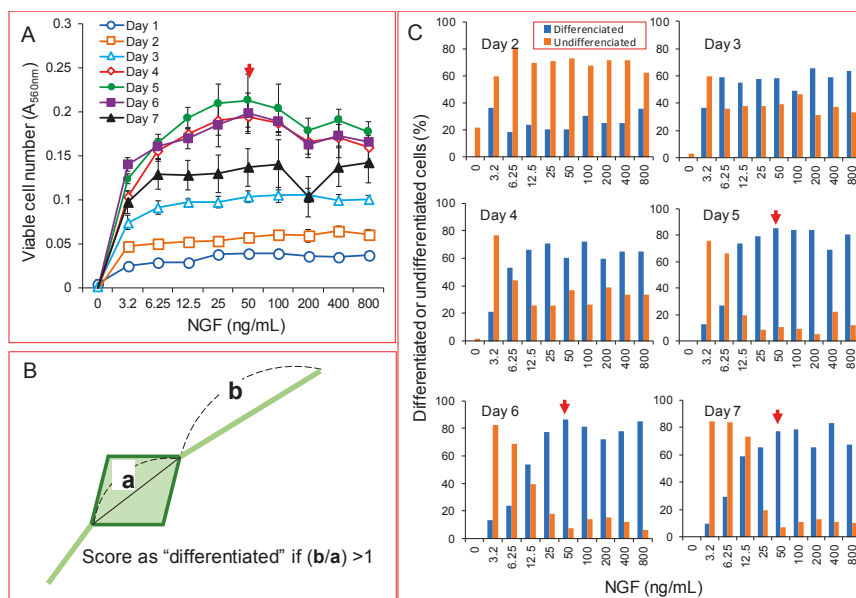
Figure 1. Stimulation of the growth and differentiation of PC12 cells by NGF. Cells were inoculated at 2×10^3/96-microwell plate (6.25×10^4/cm^2). After 24 h, the medium was replaced with a serum-free medium containing the indicated concentrations of NGF. At day three, additional NGF was supplemented on top of the medium. Viable cell number (**A**), and the percentage of differentiated cells, defined as in (**B**), and undifferentiated cells (counted after subtraction of differentiated cells and dead cells) (**C**), was then determined. In (**B**), (a) is the longest diameter of the cells, and (b) is the length of extended neurites. Each value represents the mean ± S.D. of 6 determinations.

2.3. Exploration of the Overlay Method

Based on this experimental data, we explored the overlay method to isolate differentiating PC12 cells. PC12 cells were incubated for a total of six or seven days in serum-free DMEM, containing 50 ng/mL NGF, with one more time overlay of NGF (Figure 3). The differentiated cells were well attached to the plate and were not detached by gentle pipetting.

2.4. Apoptosis-Inducing Activity of Neurotoxic Agents

We have previously reported that cisplatin showed potent cytotoxicity against differentiated PC12 cells [34], while taxanes (paclitaxel, docetaxel) and amyloid peptides (Aβ_{1-42}, Aβ_{25-35}) showed cytostatic effects [34,35]. A cell sorter analysis demonstrated that cisplatin induced the apoptosis, characterized by the accumulation of the subG$_1$ population (Figure 4). On the other hand, paclitaxel, Aβ_{1-42} and Aβ_{25-35} reduced the population of S-phase cells—reflecting their cytostatic growth inhibition—and accumulated the G2 + M phase cells, in accordance with the reported mitotic arrest by taxanes [36,37]. It was unexpected that differentiated cells were resistant to actinomycin D—a popular apoptosis inducer for various cancer cell lines.
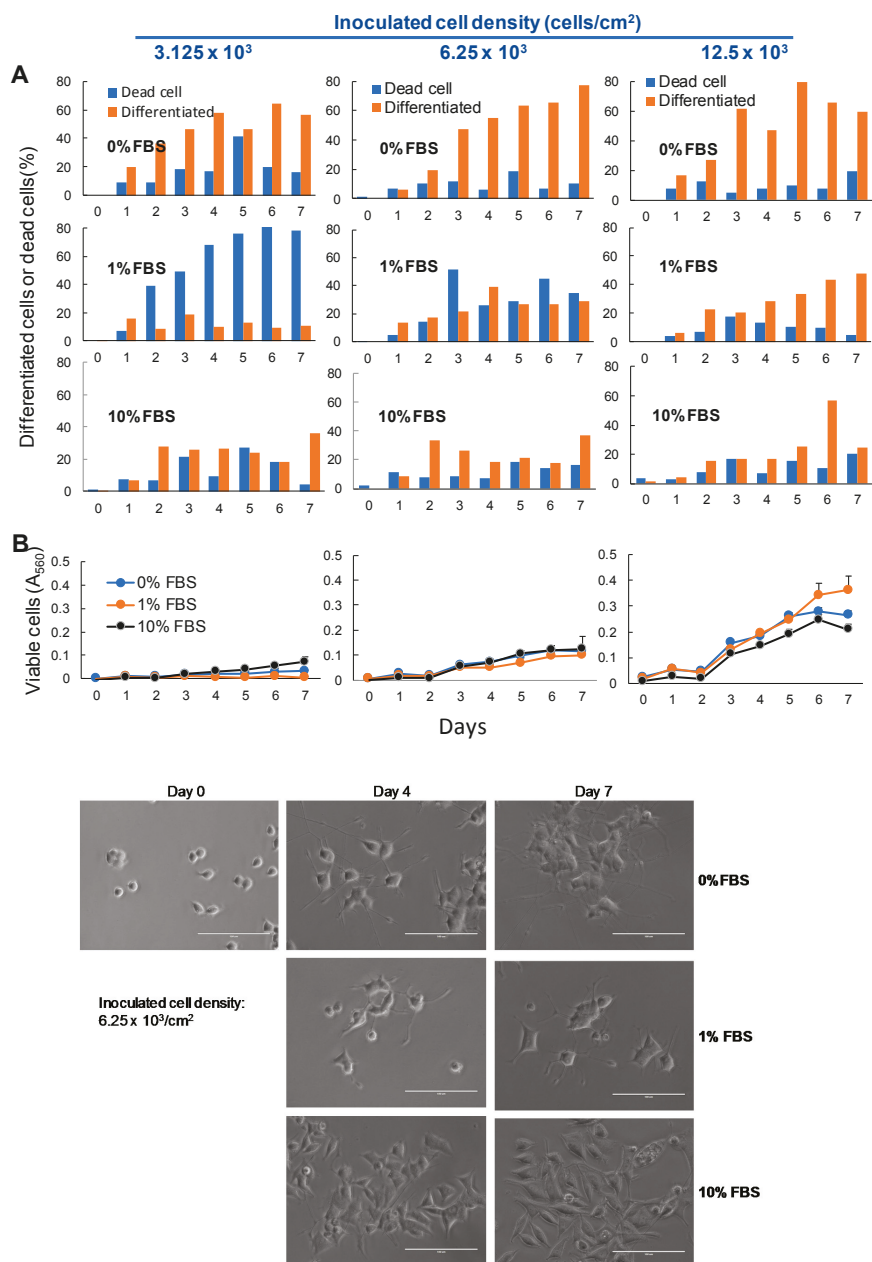
Figure 2. FBS reduced the neuronal differentiation of PC12 cells. PC12 cells were seeded at 3.125, 6.25 and 12.5 × 10^3/cm^2 into a 96-microwell plate. After 24 h, cells were replaced with DMEM supplemented with 0%, 1% or 10% FBS containing 50 ng/mL NGF, and were incubated for zero, four or seven days, with a one-time supplementation of NGF overlay at day three. The percentage of differentiated cells and undifferentiated cells (defined in the legend of Figure 1) (**A**), viable cell number (**B**) and morphological changes were monitored. To score the number of differentiated cells, the morphology of more than 100 cells were observed under the light microscope.
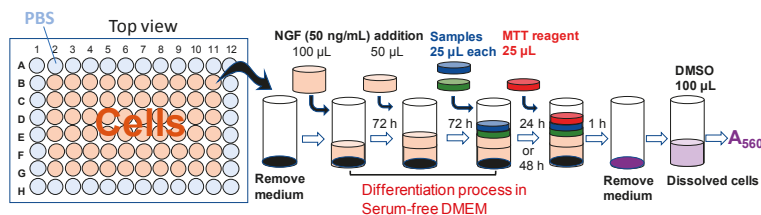
Figure 3. Schematic diagram of overlay method.

2.5. Neuroprotective Effects of Polyphenols

Alkaline extract from the leaves of *Sasa senanensis* Rehder (SE) protected the cytotoxicity induced by paclitaxel and $A\beta_{25-35}$, but not the cytotoxicity induced by cisplatin. Epigallocatechin gallate (EGCG) and curcumin showed some protective activity when induced by $A\beta_{25-35}$ (Figure 5A).
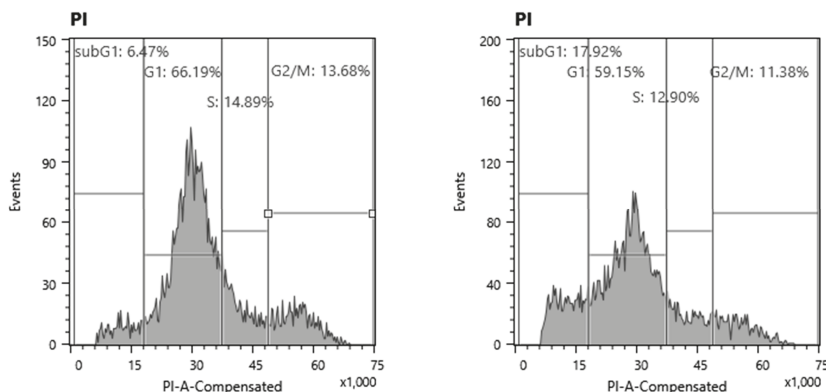
		Distribution of Each Cell Cycle Phase (%)									
		subG1			G1			S			G2 + M		
Control		8.1	±	1.4	67.6	±	1.2	14.2	±	0.6	11.3	±	2.1
Cisplatin	10 µM	11.8	±	0.8	69.6	±	1.0	12.9	±	0.5	7.0	±	0.2
	30 µM	13.3	±	0.6	69.7	±	0.3	11.9	±	0.6	6.3	±	0.4
	100 µM	18.3	±	0.3	59.7	±	0.7	12.3	±	0.5	11.0	±	0.5
Paclitaxel	0.1 µM	7.1	±	0.5	67.4	±	0.6	9.1	±	0.3	17.3	±	0.9
	0.3 µM	7.8	±	0.4	66.0	±	0.6	11.4	±	2.2	15.8	±	2.2
	1 µM	8.6	±	0.3	66.3	±	0.9	9.2	±	0.7	16.7	±	0.7
$A\beta_{1-42}$	36 nM	8.6	±	0.4	68.5	±	1.1	8.9	±	0.7	14.8	±	0.9
	100 nM	6.6	±	0.4	68.6	±	1.0	9.0	±	0.4	16.6	±	0.9
	360 nM	8.6	±	0.3	68.4	±	0.3	8.3	±	0.0	15.4	±	0.3
$A\beta_{25-35}$	143 nM	8.7	±	1.4	67.3	±	1.3	9.3	±	0.4	15.7	±	0.7
	429 nM	6.6	±	1.2	67.4	±	0.8	9.8	±	0.6	16.9	±	0.8
	1430 nM	7.5	±	1.0	67.7	±	0.6	9.3	±	0.5	16.4	±	0.5
Actinomycin D	1 µM	3.3	±	0.2	66.4	±	1.2	11.4	±	0.4	20.8	±	0.4
	2 µM	3.6	±	1.3	66.0	±	1.3	15.5	±	1.4	16.3	±	1.3

Figure 4. Cell cycle analysis of differentiated PC12 cells (day three) after treatment with neurotoxic agents. Each value represents the mean ± S.D. of triplicate assays.
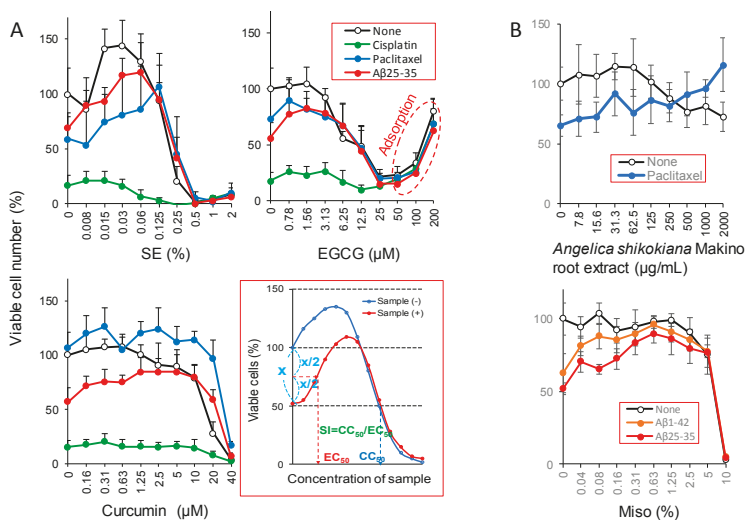
Figure 5. Neuroprotective effects of various polyphenols and plant extracts. Concentration of neurotoxic agents are: Aβ$_{25–35}$ (500 nM); cisplatin (50 μM); and, paclitaxel (50 nM).

Table 2 shows the SI (=CC$_{50}$/EC$_{50}$) value of polyphenols, plant extracts and antioxidants, calculated using the data from our original papers [33,35,38,39] and the present study (Table 2). The higher the SI value, the stronger the neuroprotective activity would be expected.

Table 2. Neuroprotective activity of polyphenols and plant extracts.

	Target Cell	FBS	Toxicant	Protective Substance	CC$_{50}$		EC$_{50}$		SI	Ref
Exp. 1	<Undifferentiated cell system>									
	SH-SY5Y Day 0	10%	Aβ$_{1–42}$	SE	4.19	%	0.11	%	37.2	[33]
			Aβ$_{1–42}$	SE	2.22	%	0.016	%	141.4	[33]
			Aβ$_{1–42}$	EGCG	66	μM	>400	μM	6.1	[33]
			Aβ$_{1–42}$	Resveratrol	387	μM	>400	μM	<1	[33]
			Aβ$_{1–42}$	Curcumin	46	μM	>200	μM	<1	
			Aβ$_{1–42}$	*p*-Coumaric acid	>400	μM	>400	μM	><1	
		10%	Aβ$_{25–35}$	SE	2.69	%	<0.21	%	>108	[33]
			Aβ$_{25–35}$	SE	2.22	%	>3.13	%	<1	[33]
			Aβ$_{25–35}$	EGCG	47.8	μM	>400	μM	<1	[33]
			Aβ$_{25–35}$	Resveratrol	>400	μM	>400	μM	><1	[33]
			Aβ$_{25–35}$	Curcumin	17.4	μM	>200	μM	<1	
			Aβ$_{25–35}$	*p*-Coumaric acid	>400	μM	>400	μM	><1	
	PC12 Day 0	10%	Aβ$_{1–42}$	SE	1.38	%	>1.56	%	<1	[33]
			Aβ$_{1–42}$	SE	0.71	%	0.1	%	7.1	[33]
			Aβ$_{1–42}$	EGCG	40.1	μM	>400	μM	<1	[33]
			Aβ$_{1–42}$	Resveratrol	326	μM	>400	μM	<1	[33]
			Aβ$_{1–42}$	Curcumin	19.1	μM	>200	μM	<1	
			Aβ$_{1–42}$	*p*-Coumaric acid	>400	μM	>400	μM	><1	
		10%	Aβ$_{25–35}$	SE	1.15	%	0.21	%	5.9	[33]
			Aβ$_{25–35}$	SE	0.71	%	0.13	%	5.4	[33]
			Aβ$_{25–35}$	EGCG	33.1	μM	>400	μM	<1	[33]
			Aβ$_{25–35}$	Resveratrol	370	μM	>400	μM	<1	[33]
			Aβ$_{25–35}$	Curcumin	60.2	μM	>200	μM	<1	
			Aβ$_{25–35}$	*p*-Coumaric acid	>400	μM	>400	μM	><1	

Table 2. *Cont.*

Target Cell		FBS	Toxicant	Protective Substance	CC$_{50}$		EC$_{50}$		SI	Ref
Exp. 2	<Differentiated cell system>									
PC12	Day 7	1%	Aβ$_{1-42}$	SE	0.55	%	0.012	%	45.8	[33]
		1%	Aβ$_{25-35}$	SE	0.55	%	0.0075	%	73.3	[33]
PC12	Day 6	0%	Aβ$_{25-35}$	SE	0.2	%	0.005	%	40.2	
		0%	Paclitaxel	SE	0.2	%	0.026	%	7.7	
		0%	Cisplatin	SE	0.2	%	>2	%	<1	
		0%	Aβ$_{25-35}$	EGCG	8.33	µM	0.78	µM	10.7	
		0%	Paclitaxel	EGCG	8.33	µM	0.55	µM	15.1	
		0%	Cisplatin	EGCG	8.33	µM	>25	µM	<1	
		0%	Cisplatin	Resveratrol	60.4	µM	>200	µM	<1	
		0%	Aβ$_{25-35}$	Curcumin	15.7	µM	0.91	µM	17.3	
		0%	Cisplatin	Curcumin	15.7	µM	>200	µM	<1	
Exp. 3				<Plant extracts>						
				Angelica shikokiana Makino root						
	Day 0	10%	Aβ$_{1-42}$	Leaf PBS extract	1472	µg/ml	417	µg/ml	3.5	[38]
				Root PBS extract	2686	µg/ml	107	µg/ml	25.1	[38]
				Seed PBS extract	2118	µg/ml	41.7	µg/ml	50.8	[38]
				Leaf NaHCO$_3$ extract	1827	µg/ml	4.71	µg/ml	387.9	[38]
				Root NaHCO$_3$ extract	2691	µg/ml	43.8	µg/ml	61.4	[38]
				Seed NaHCO$_3$ extract	2441	µg/ml	73.9	µg/ml	33	[38]
	Day 6	1%	Paclitaxel	Root PBS extract	>2000	µg/ml	107	µg/ml	>18.7	[38]
	Day 6		Aβ$_{1-42}$	Miso extract	6.83	%	0.039	%	175.1	[39]
	Day 6		Aβ$_{25-35}$	Miso extract	6.83	%	0.191	%	35.8	[39]
Exp. 4				<Antioxidants>						
	Day 5		Paclitaxel	Docosahexaenoic acid	0.017		>0.02		<1	[35]
				Acetyl-L-carnitine hydrochlorid	>10		0.07		142.9	[35]
				N-Acetyl-L-cysteine	>10		2.25		>4.4	[35]
				Sodium ascorbate	0.52		>1		<1	[35]

2.5.1. Neuroprotective Activity against Undifferentiated PC12 and SH-SY5Y Cells (Exp. 1)

The SE showed the highest neuroprotective activity (SI = 37.2, 141.4, >108, <1, <1, 7.1, 5.9, 5.4), followed by EGCG (SI = 6.1, <1, <1, <1). However, resveratrol (SI = <1, ><1, <1, <1), curcumin (SI = <1, <1, <1, <1) and *p*-coumaric acid (SI = ><1, ><1, ><1, ><1) showed no apparent neuroprotective activity [33].

2.5.2. Protective Activity against Differentiated PC12 Cells (Exp. 2)

SE showed the highest neuroprotective activity (SI = 45.8, 73.3, 40.2, 7.7, <1), followed by EGCG (SI = 10.7, 15.1, <1), and curcumin (SI = 17.3, <1). Resveratrol did not show any apparent protective activity (SI < 1). None of these substances were protective against cisplatin-induced neurotoxicity.

2.5.3. Neuroprotective Activity of Plant Extracts (Exp. 3)

Angelica shikokiana Makino extract [38] and the hot water extract of Miso—a traditional Japanese fermented food that has supported our diet for many years [39]—showed neuroprotective effects against paclitaxel and amyloid peptides (Figure 5B). Especially, a significant (*p* < 0.05) growth stimulation effect of Miso on Aβ$_{1-42}$ and Aβ$_{25-35}$-treated cells was observed above 0.04%.

2.6. Growth Stimulation by SE

There was a possibility that neuroprotective effects may be related to the growth stimulation against PC12 cells. To test this possibility, PC12 cells were cultured for 24 h in a serum-free medium containing various sample concentrations. The removal of serum from the cultured medium reduced the growth potential of PC12 cells to 10% of the control level (Figure 6). By the addition of SE,

the viability returned back to 40% of the control level, whereas the growth stimulation effects of EGCG, resveratrol, and curcumin was much less (Figure 6).
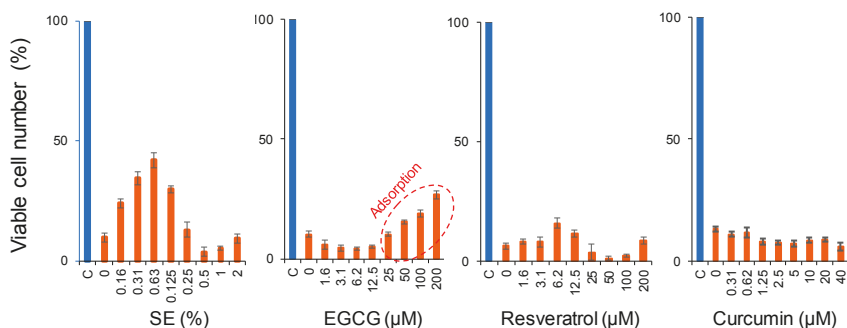
Figure 6. Growth stimulation activity of various polyphenols. PC12 cells were cultured for 24 h in DMEM, supplemented with 10% FBS (indicated by C (control) in blue), or without serum (red) in the presence of indicated concentrations of test samples. The viable cell number was then measured by 3-(4,5-dimethylthiazol-2-yl)-2,5-diphenyltetrazolium bromide (MTT) reagent, and expressed as a percentage of control (C). Each value represents the mean ± S.D. of six determinants.

3. Discussion

We have explored a new and simple method that enabled us to prepare differentiated neuronal cells by the repeated overlay of the NGF-containing medium without a medium change, omitting the use of expensive collagen-coated plates, or the toxic coating step. Using the overlay method, we re-investigated the neuroprotective activity of polyphenols.

SE, a group of three over-the-counter drugs, showed the highest neuroprotective activity against both undifferentiated and differentiated PC12 cells, as well as undifferentiated SH-SY5Y cells. This seems to be linked to growth stimulation at lower doses, known as hormesis [40], since we have experienced similar growth stimulation of SE towards human gingival epithelial fibroblast (HGEP) [41] and PC12 cells [33]. SE showed prominent anti-HIV [42] and anti-UV activity [43], like the lignin-carbohydrate complexes extracted with alkaline solution. The present study further adds that SE showed potent neuroprotective activity. SE contains the lignin-carbohydrate complex and the various degradation products, and thus not a purified material. The lignin-carbohydrate complex showed poor bioavailability [44], and its biological activity might be mediated through one of the pattern-recognition receptors (dectin-2) in the mucosa of oral cavities [45] and intestinal duct. We found that *p*-coumaric acid, one of the lignin precursors present in SE (unpublished data), has no neuroprotective activity. Further fractionation of SE is necessary to identify the neuroprotective substances present in SE.

EGCG, a main component of green tea, showed some neuroprotective activity. We found that higher concentrations of EGCG led to false-positive coloring with MTT reagent—indicated by the red circle in Figures 5 and 6—and were possibly due to the non-specific binding of tannin to protein [46,47]. Neuroprotective effects of EGCG may be mediated through cell-surface receptors [48] or by the direct binding to neurotoxic agents.

Curcumin showed some neuroprotective activity against differentiated PC12 cells, but not against undifferentiated cells. The fluctuation in the SI value of this compound may be due to its potent cytotoxicity, narrowing the chemotherapeutic range.

Food polyphenols, at low and nontoxic concentrations, slow down the progression of neurodegenerative diseases and therefore may be a promising approach [49]. It was unexpected that Miso extract also showed neuroprotective (Figure 5B) and growth promotion activity [38], further substantiating the possible link between neuroprotective activity and hormesis. Since Miso is a

daily food, it is very much meaningful to identify the active principle for the future research aiming at alleviating the neuronal diseases.

As a mechanism of neuronal protection, activation of the NF-E2 related factor 2 (Nrf2) pathway and the consequent upregulation of detoxification enzymes, such as heme-oxygenase-1 (HO-1), have been suggested [50,51]. However, we have recently reported that the neuroprotective activity of four antioxidants: Docosahexaenoic acid; acetyl-L-carnitine hydrochloride; *N*-acetyl-L-cysteine; and, sodium ascorbate, only partially protected PC12 cells from paclitaxel-induced toxicity [35]. Furthermore, it has recently been reported that neuronal protection caused by blackberry polyphenols is produced by mechanisms other than modulating reactive oxygen species (ROS) levels [52]. It is possible that both oxidative and other mechanisms, such as: Autophagy [21]; heat shock protein (HSP)-70 [22]; JAK2/STAT5/Bcl-xL [24]; phosphor HSP-20 [28]; amyloid disaggregation [29]; and, the overexpression of the *KiSS* gene [30], may be involved in the induction of neurotoxicity (column D in Table 1).

We have recently manufactured highly tumor-specific derivatives from the chromone core structure found in flavones, isoflavones and 2-styrylchromones, and discovered that their tumor-specificity was correlated with molecular shape and hydrophobicity [53,54]. By analogy, for searching new neuroprotective substances, it may be one way to introduce various functional groups to the core substance present in the natural kingdom, repeat the synthesis, and verify the process using QSAR analysis.

4. Materials and Methods

4.1. Materials

The following chemicals and reagents were obtained from the indicated companies: DMEM; human recombinant NGF; paclitaxel; propidium iodide (PI); actinomycin D (Act. D); 4% paraformaldehyde phosphate buffer solution; dimethyl sulfoxide (DMSO) (Wako Pure Chemical Ind., Ltd., Osaka, Japan); Nonidet P-40 (NP-40) (Nakalai Tesque Inc., Kyoto, Japan); FBS; 3-(4,5-dimethylthiazol-2-yl)-2; 5-diphenyltetrazolium bromide (MTT) (Sigma-Aldrich Inc., St. Louis, MO, USA); $A\beta_{1-42}$ and $A\beta_{25-35}$ (Cosmo Bio Co., Ltd., Tokyo, Japan); NGF (dissolved in water at 0.5 mg/mL); $A\beta_{1-42}$ (dissolved in DMSO at 1 mM); and, $A\beta_{25-35}$ (dissolved in water at 0.1 mM) were frozen at $-20\,°C$. The following 96-microwell plates were purchased from TPP (Techno Plastic Products AG, Trasadingen, Switzerland).

4.2. Cell Culture

PC12 cells were purchased from Riken Cell Bank (Tsukuba, Japan). These cells were cultured in DMEM and were supplemented with 10% FBS, 100 units/mL, penicillin G and 100 µg/mL streptomycin under a humidified 5% CO_2 atmosphere.

4.3. Determination of Viable Cell Numbers

To the culture medium, a fresh medium containing 3-(4,5-dimethylthiazol-2-yl)-2,5-dipheny ltetrazolium bromide (MTT) (final concentration: 0.1 mg/mL) with (for differentiated cells) or without (for non-differentiated cells) of 50 ng/mL NGF. The cells were incubated for 1 h, and the formazan precipitate was dissolved in DMSO to measure their absorbance at 560 nm with a plate reader (Infinite F 50 R, TECAN, Kawasaki, Japan).

4.4. Induction of Differentiation Toward Neurons

For the induction of differentiation, PC12 cells were incubated for the indicated times with a differentiating inducing medium (DMEM, supplemented with 0% or 1% FBS, 50 ng/mL NGF and antibiotics). Differentiated cells were defined as the cells in which the extended neuritis exceeded the

longest diameter of each cell, assessed under the light microscope (EVOS FL, ThermoFisher Scientific, Waltham, MA, USA) (Figure 1B).

4.5. Neuroprotection Assay

Undifferentiated (PC12, SH-SY5Y) and differentiated PC12 cells were pretreated for 1 h with test samples, and then neurotoxic agents were added (0.3 μM, Aβ_{1-42}, 2 μM Aβ_{25-35}, 50 μM cisplatin, 0.4 μM paclitaxel). After treatment for 24 or 48 h, viable cell numbers were determined, as described above. The 50% cytotoxic concentration (CC$_{50}$) was determined from the neurotoxicant-free culture, and the 50% effective concentration (EC$_{50}$) that reduced the neurotoxicant-induced cytotoxicity by 50% was calculated (Figure 5). The protective effect was quantified by the SI, using the following formula: SI = CC$_{50}$/EC$_{50}$ (Figure 5).

4.6. Cell Cycle Analysis

Cells (approximately 10^6) were harvested, fixed with a 1% paraformaldehyde in phosphate-buffered saline without calcium or magnesium ions [PBS($-$)]. Fixed cells were washed twice with PBS($-$), and then treated for 30 min with 400 μL of 0.2 mg/mL RNase A (preheated for 10 min at 100 $^\circ$C to deactivate DNase) to degrade RNA. Cells were then washed twice with PBS($-$) and stained for 15 min with 0.005% propidium iodide (PI) in the presence of 0.01% NP-40 in PBS($-$), which prevents cell aggregation. After filtering through Falcon® cell strainers (40 μM) (Corning Inc., Corning, NY, USA) to remove aggregated cells, PI-stained cells were subjected to a cell sorter (SH800 Series, SONY Imaging Products and Solutions Inc., Kanagawa, Japan). Cell cycle analysis was performed with the Cell Sorter Software version 2.1.2 (SONY Imaging Products and Solution Inc., Kanagawa, Japan).

4.7. Statistical Treatment

Experimental values are expressed as the mean $\pm$ standard deviation (SD) of triplicate or quadruplicate samples. Statistical analysis was performed using Student's *t*-test. A *p*-value of <0.05 was considered to be significant.

5. Conclusions

The present study demonstrated that plant extracts, having hormetic growth stimulation, showed higher neuroprotective activity than lower molecular weight polyphenols. The overlay method, that can prepare massive differentiated neuronal cells, may be applicable for the study of differentiation-associated changes in intracellular metabolites by metabolomics, and the interaction between neuronal cells and physiological factors.

References

1. Parra-Vidales, E.; Soto-Pérez, F.; Perea-Bartolomé, M.V.; Franco-Martín, M.A.; Muñoz-Sánchez, J.L. Online interventions for caregivers of people with dementia: A systematic review. *Actas Esp. Psiquiatr.* **2017**, *45*, 116–126. [PubMed]

2. Ostan, R.; Monti, D.; Gueresi, P.; Bussolotto, M.; Franceschi, C.; Baggio, G. Gender, aging and longevity in humans: An update of an intriguing/neglected scenario paving the way to a gender-specific medicine. *Clin. Sci.* **2016**, *130*, 1711–1725. [CrossRef] [PubMed]

3. Kroneman, M.; Boerma, W.; van den Berg, M.; Groenewegen, P.; de Jong, J.; van Ginneken, E. Netherlands: Health system review. *Health Syst. Transit.* **2016**, *18*, 1–240. [PubMed]

4. Aleksis, R.; Oleskovs, F.; Jaudzems, K.; Pahnke, J.; Biverstål, H. Structural studies of amyloid-β peptides: Unlocking the mechanism of aggregation and the associated toxicity. *Biochimie* **2017**, *140*, 176–192. [CrossRef] [PubMed]

5. Li, H.H.; Lin, C.L.; Huang, C.N. Neuroprotective effects of statins against amyloid β-induced neurotoxicity. *Neural Regen Res.* **2018**, *13*, 198–206. [CrossRef] [PubMed]

6. Reid, L.D.; Avens, F.E.; Walf, A.A. Cognitive behavioral therapy (CBT) for preventing Alzheimer's disease. *Behav. Brain Res.* **2017**, *334*, 163–177. [CrossRef] [PubMed]

7. Parsons, C.G.; Rammes, G. Preclinical to phase II amyloid beta (Aβ) peptide modulators under investigation for Alzheimer's disease. *Expert Opin. Investig. Drugs* **2017**, *26*, 579–592. [CrossRef] [PubMed]

8. Kanat, O.; Ertas, H.; Caner, B. Platinum-induced neurotoxicity: A review of possible mechanisms. *World J. Clin. Oncol.* **2017**, *8*, 329–335. [CrossRef] [PubMed]

9. Velasco, R.; Bruna, J. Taxane-Induced peripheral neurotoxicity. *Toxics* **2015**, *3*, 152–169. [CrossRef] [PubMed]

10. Hershman, D.L.; Till, C.; Wright, J.D.; Awad, D.; Ramsey, S.D.; Barlow, W.E.; Minasian, L.M.; Unger, J. Comorbidities and risk of chemotherapy-induced peripheral neuropathy among participants 65 years or older in southwest oncology group clinical trials. *J. Clin. Oncol.* **2016**, *34*, 3014–3022. [CrossRef] [PubMed]

11. Sakagami, H. Biological activities and possible dental application of three major groups of polyphenols. *J. Pharmacol. Sci.* **2014**, *126*, 92–106. [CrossRef] [PubMed]

12. Okuda, T.; Yoshida, T.; Hatano, T. Hydrolyzable tannins and related polyphenols. In *Fortschritte der Chemie Organischer Naturstoffe/Progress in the Chemistry of Organic Natural Products*; Springer: Vienna, Austria, 1995; pp. 1–117.

13. Nomura, T.; Hano, Y.; Fukai, T. Chemistry and biosynthesis of isoprenylated flavonoids from Japanese mulberry tree. *Proc. J. Acad.* **2009**, *85*, 391–408. [CrossRef]

14. Sakagami, H.; Hashimoto, K.; Suzuki, F.; Ogiwara, T.; Satoh, K.; Ito, H.; Hatano, T.; Takashi, Y.; Fujisawa, S. Molecular requirements of lignin-carbohydrate complexes for expression of unique biological activities. *Phytochemistry* **2005**, *66*, 2108–2120. [CrossRef] [PubMed]

15. Cendrowski, A.; Ścibisz, I.; Mitek, M.; Kieliszek, M.; Kolniak-Ostek, J. Profile of the phenolic compounds of *Rosa rugosa* petals. *J. Food Qual.* **2017**, *2017*, 7941347. [CrossRef]

16. Cendrowski, A.; Ścibisz, I.; Kieliszek, M.; Kolniak-Ostek, J.; Mitek, M. UPLC-PDA-Q/TOF-MS profile of polyphenolic compounds of liqueurs from Rose petals (*Rosa rugosa*). *Molecules* **2017**, *22*, 1832. [CrossRef] [PubMed]

17. Sakagami, H.; Sheng, H.; Yasui, T.; Fukuchi, K.; Oizumi, T.; Ohno, H.; Yamamoto, M.; Fukuda, T.; Kotohda, K.; Yoshida, H.; et al. Therapeutic potential of solubilized nanolignin against oral diseases. In *Nanostructures for Oral Medicine*; Elsevier: Amsterdam, The Netherlands, 2017; pp. 545–576.

18. Greene, L.A.; Tischler, A.S. Establishment of a noradrenergic clonal line of rat adrenal pheochromocytoma cells which respond to nerve growth factor. *Proc. Natl. Acad. Sci. USA* **1976**, *73*, 2424–2428. [CrossRef] [PubMed]

19. Biedler, J.L.; Helson, L.; Spengler, B.A. Morphology and growth, tumorigenicity, and cytogenetics of human neuroblastoma cells in continuous culture. *Cancer Res.* **1973**, *33*, 2643–2652. [PubMed]

20. Biedler, J.L.; Roffler-Tarlov, S.; Schachner, M.; Freedman, L.S. Multiple neurotransmitter synthesis by human neuroblastoma cell lines and clones. *Cancer Res.* **1978**, *38*, 3751–3757. [PubMed]

21. Xu, P.; Li, Z.; Wang, H.; Zhang, X.; Yang, Z. Triptolide Inhibited cytotoxicity of differentiated PC12 cells induced by amyloid-beta25-35 via the autophagy pathway. *PLoS ONE* **2015**, *10*, e0142719. [CrossRef] [PubMed]

22. Tsai, Y.C.; Lee, Y.M.; Lam, K.K.; Lin, J.F.; Wang, J.J.; Yen, M.H.; Cheng, P.Y. The role of heat shock protein 70 in the protective effect of YC-1 on β-amyloid-induced toxicity in differentiated PC12 cells. *PLoS ONE* **2013**, *8*, e69320. [CrossRef] [PubMed]

23. Muthaiyah, B.; Essa, M.M.; Chauhan, V.; Chauhan, A. Protective effects of walnut extract against amyloid beta peptide-induced cell death and oxidative stress in PC12 cells. *Neurochem. Res.* **2011**, *36*, 2096–2103. [CrossRef] [PubMed]

24. Ma, R.; Hu, J.; Huang, C.; Wang, M.; Xiang, J.; Li, G. JAK2/STAT5/Bcl-xL signalling is essential for erythropoietin-mediated protection against apoptosis induced in PC12 cells by the amyloid β-peptide Aβ25-35. *Br. J. Pharmacol.* **2014**, *171*, 3234–3245. [CrossRef] [PubMed]

25. Ai, Z.; Li, C.; Li, L.; He, G. Resveratrol inhibits β-amyloid-induced neuronal apoptosis via regulation of p53 acetylation in PC12 cells. *Mol. Med. Rep.* **2015**, *11*, 2429–2434. [CrossRef] [PubMed]

26. Hettiarachchi, N.; Dallas, M.; Al-Owais, M.; Griffiths, H.; Hooper, N.; Scragg, J.; Boyle, J.; Peers, C. Heme oxygenase-1 protects against Alzheimer's amyloid-β(1–42)-induced toxicity via carbon monoxide production. *Cell Death Dis.* **2014**, *5*, e1569. [CrossRef] [PubMed]

27. Zhang, Y.; Jiao, G.; Song, C.; Gu, S.; Brown, R.E.; Zhang, J.; Zhang, P.; Gagnon, J.; Locke, S.; Stefanova, R.; et al. An extract from shrimp processing by-products protects SH-SY5Y cells from neurotoxicity induced by Aβ25–35. *Mar Drugs.* **2017**, *15*, 83. [CrossRef] [PubMed]

28. Cameron, R.T.; Quinn, S.D.; Cairns, L.S.; MacLeod, R.; Samuel, I.D.; Smith, B.O.; Carlos Penedo, J.; Baillie, G.S. The phosphorylation of Hsp20 enhances its association with amyloid-β to increase protection against neuronal cell death. *Mol. Cell. Neurosci.* **2014**, *61*, 46–55. [CrossRef] [PubMed]

29. Wang, Q.; Yu, X.; Patal, K.; Hu, R.; Chuang, S.; Zhang, G.; Zheng, J. Tanshinones inhibit amyloid aggregation by amyloid-β peptide, disaggregate amyloid fibrils, and protect cultured cells. *ACS Chem. Neurosci.* **2013**, *4*, 1004–1015. [CrossRef] [PubMed]

30. Chilumuri, A.; Milton, N.G. The role of neurotransmitters in protection against amyloid-β toxicity by KiSS-1 overexpression in SH-SY5Y neurons. *ISRN Neurosci.* **2013**. [CrossRef] [PubMed]

31. Hattori, N.; Nomoto, H.; Mishima, S.; Inagaki, S.; Goto, M.; Sako, M.; Furukawa, S. Identification of AMP N1-oxide in royal jelly as a component neurotrophic toward cultured rat pheochromocytoma PC12 cells. *Biosci. Biotechnol. Biochem.* **2006**, *70*, 897–906. [CrossRef] [PubMed]

32. Sakagami, H.; Suzuki, R.; Shirataki, Y.; Iwama, S.; Nakagawa, M.; Suzuki, H.; Tanaka, K.; Tamura, N.; Takeshima, H. Re-evaluation of culture condition of PC12 and SH-SY5Y cells based on growth rate and amino acid consumption. *In Vivo* **2017**, *31*, 1089–1095. [PubMed]

33. Sakagami, H.; Tsuji, M.; Tomomura, M.; Masuda, Y.; Iwama, S.; Nakagawa, M.; Suzuki, H.; Tanaka, K.; Abe, T.; Tamura, N.; et al. Protection of differentiating neuronal cells from amyloid β peptide-induced injury by alkaline extract of leaves of *Sasa senanensis* Rehder. *In Vivo* **2018**, *32*, 231–239. [PubMed]

34. Sakagami, H.; Hara, Y.; Shi, H.; Iwama, S.; Nakagawa, M.; Suzuki, H.; Tanaka, K.; Abe, T.; Tamura, N.; Takeshima, H.; et al. Change in anticancer drug sensitivity during neuronal differentiation of PC12 Cells. *In Vivo* **2018**, *32*, 765–770. [CrossRef] [PubMed]

35. Hara, Y.; Sakagami, H.; Shi, H.; Abe, T.; Tamura, N.; Takeshima, H.; Horie, N.; Kaneko, T.; Shiratsuchi, H.; Kaneko, T. Partial protection of paclitaxel-induced neurotoxicity by antioxidants. *In Vivo* **2018**, *32*, 745–752. [CrossRef] [PubMed]

36. Lewis, C.W.; Jin, Z.; Macdonald, D.; Wei, W.; Qian, X.J.; Choi, W.S.; He, R.; Sun, X.; Chan, G. Prolonged mitotic arrest induced by Wee1 inhibition sensitizes breast cancer cells to paclitaxel. *Oncotarget* **2017**, *8*, 73705–73722. [CrossRef] [PubMed]

37. Ye, Q.F.; Zhang, Y.C.; Peng, X.Q.; Long, Z.; Ming, Y.Z.; He, L.Y. siRNA-mediated silencing of Notch-1 enhances docetaxel induced mitotic arrest and apoptosis in prostate cancer cells. *Asian Pac. J. Cancer Prev.* **2012**, *13*, 2485–2489. [CrossRef] [PubMed]

38. Saita, K.; Saita, S.; Yahata, Y.; Mitsuma, O.; Aoki, O.; Abylaiuly, Z.; Bolshakova, S.B.; Bogenbayeva, G.A.; Dalenov, E.D.; Fukuchi, K.; et al. Neuroprotective action and clinical effects of *Angelica shikokiana* Makino. *New Food Ind.* **2018**, *60*, 39–48.

39. Kojima, M.; Sano, A.; Suzuki, R.; Shirataki, Y.; Sakagami, H. Neuroprotective action of Miso. *New Food Ind.* **2018**, *60*, 79–83.

40. Calabrese, E.J. Biphasic dose responses in biology, toxicology and medicine: Accounting for their generalizability and quantitative features. *Environ. Pollut.* **2013**, *182*, 452–460. [CrossRef] [PubMed]

41. Sakagami, H.; Okudaira, N.; Masuda, Y.; Amano, O.; Yokose, S.; Kanda, Y.; Suguro, M.; Natori, T.; Oizumi, H.; Oizumi, T. Induction of apoptosis in human oral keratinocyte by doxorubicin. *Anticancer Res.* **2017**, *37*, 1023–1029. [PubMed]

42. Sakagami, H.; Fukuchi, K.; Kanamoto, T.; Terakubo, S.; Nakashima, H.; Natori, T.; Suguro-Kitajima, M.; Oizumi, H.; Yasui, T.; Oizumi, T. Synergism of alkaline extract of the leaves of *Sasa senanensis* rehder and antiviral agents. *In Vivo* **2016**, *30*, 421–426. [PubMed]

43. Sakagami, H.; Sheng, H.; Okudaira, N.; Yasui, T.; Wakabayashi, H.; Jia, J.; Natori, T.; Suguro-Kitajima, M.; Oizumi, H.; Oizumi, T. Prominent anti-UV activity and possible cosmetic potential of lignin-carbohydrate complex. *In Vivo* **2016**, *30*, 331–339. [PubMed]

44. Sakagami, H.; Asano, K.; Yoshida, T.; Kawazoe, Y. Organ distribution and toxicity of lignin. *In Vivo* **1999**, *13*, 41–44. [PubMed]

45. Feller, L.; Khammissa, R.A.; Chandran, R.; Altini, M.; Lemmer, J. Oral candidosis in relation to oral immunity. *J. Oral Pathol. Med.* **2014**, *43*, 563–569. [CrossRef] [PubMed]

46. Hatano, T.; Yasuhara, T.; Yoshihara, R.; Agata, I.; Noro, T.; Okuda, T. Effects of interaction of tannins with co-existing substances. VII. Inhibitory effects of tannins and related polyphenols on xanthine oxidase. *Chem. Pharm. Bull.* **1990**, *38*, 1224–1229. [CrossRef] [PubMed]

47. Okuda, T.; Mori, K.; Hatano, T. Relationship of the structures of tannins to the binding activities with hemoglobin and methylene blue. *Chem. Pharm. Bull.* **1985**, *33*, 1424–1433. [CrossRef] [PubMed]

48. Byun, E.B.; Kim, W.S.; Sung, N.Y.; Byun, E.H. Epigallocatechin-3-Gallate Regulates Anti-Inflammatory Action Through 67-kDa Laminin Receptor-Mediated Tollip Signaling Induction in Lipopolysaccharide-Stimulated Human Intestinal Epithelial Cells. *Cell Physiol. Biochem.* **2018**, *46*, 2072–2081. [CrossRef] [PubMed]

49. Silva, R.F.; Pogačnik, L. Food, polyphenols and neuroprotection. *Neural Regen. Res.* **2017**, *12*, 582–583. [PubMed]

50. Moosavi, F.; Hosseini, R.; Saso, L.; Firuzi, O. Modulation of neurotrophic signaling pathways by polyphenols. *Drug Des. Dev. Ther.* **2015**, *10*, 23–42.

51. Scapagnini, G.; Sonya, V.; Nader, A.G.; Calogero, C.; Zella, D.; Fabio, G. Modulation of Nrf2/ARE pathway by food polyphenols: A nutritional neuroprotective strategy for cognitive and neurodegenerative disorders. *Mol. Neurobiol.* **2011**, *44*, 192–201. [CrossRef] [PubMed]

52. Tavares, L.; Figueira, I.; Macedo, D.; McDougall, G.J.; Leitão, M.C.; Vieira, H.L.; Stwewart, D.; Alves, P.M.; Ferreira, R.B.; Santos, C.N. Neuroprotective effect of blackberry (*Rubus* sp.) polyphenols is potentiated after simulated gastrointestinal digestion. *Food Chem.* **2012**, *131*, 1443–1452. [CrossRef]

53. Sugita, Y.; Takao, K.; Uesawa, Y.; Sakagami, H. Search for new type of anticancer drugs with high tumor-specificity and less keratinocyte toxicity. *Anticancer Res.* **2017**, *37*, 5919–5924. [PubMed]

54. Sakagami, H.; Tomomura, M. Dental application of natural products. *Medicines* **2018**, *5*, 21. [CrossRef] [PubMed]

Sample Availability: Samples of the compounds are not available from the authors.

(−)-Epigallocatechin 3-Gallate Synthetic Analogues Inhibit Fatty Acid Synthase and Show Anticancer Activity in Triple Negative Breast Cancer

Joan Crous-Masó [1,2,†], Sònia Palomeras [1,†], Joana Relat [3,4], Cristina Camó [2],
Úrsula Martínez-Garza [3,4], Marta Planas [2,*], Lidia Feliu [2,*] and Teresa Puig [1,*]

[1] New Therapeutic Targets Laboratory (Targets Lab)-Oncology Unit, Department of Medical Sciences, University of Girona, Girona Institute for Biomedical Research, Emili Grahit 77, 17003 Girona, Spain; joan.crousmaso@gmail.com (J.C.-M.); sonia.palomeras@udg.edu (S.P.)

[2] LIPPSO, Department of Chemistry, University of Girona, Maria Aurèlia Capmany 69, 17003 Girona, Spain; cristina.camo@udg.edu

[3] Department of Nutrition, Food Sciences and Gastronomy, School of Pharmacy and Food Sciences, Food and Nutrition Torribera Campus, University of Barcelona, Prat de la Riba 171, 08921 Santa Coloma de Gramenet, Spain; jrelat@ub.edu (J.R.); ursula-mtz@hotmail.com (Ú.M.-G.)

[4] Institute of Nutrition and Food Safety of the University of Barcelona (INSA-UB), Prat de la Riba 171, 08921 Santa Coloma de Gramenet, Spain

* Correspondence: marta.planas@udg.edu (M.P.); lidia.feliu@udg.edu (L.F.); teresa.puig@udg.edu (T.P.); Tel.: +34-97-241-8274 (M.P.); +34-97-241-8959 (L.F.); +34-97-241-9628 (T.P.)

† These authors contributed equally to this work.

Abstract: (−)-Epigallocatechin 3-gallate (EGCG) is a natural polyphenol from green tea with reported anticancer activity and capacity to inhibit the lipogenic enzyme fatty acid synthase (FASN), which is overexpressed in several human carcinomas. To improve the pharmacological profile of EGCG, we previously developed a family of EGCG derivatives and the lead compounds G28, G37 and G56 were characterized in HER2-positive breast cancer cells overexpressing FASN. Here, diesters G28, G37 and G56 and two G28 derivatives, monoesters M1 and M2, were synthesized and assessed in vitro for their cytotoxic, FASN inhibition and apoptotic activities in MDA-MB-231 triple-negative breast cancer (TNBC) cells. All compounds displayed moderate to high cytotoxicity and significantly blocked FASN activity, monoesters M1 and M2 being more potent inhibitors than diesters. Interestingly, G28, M1, and M2 also diminished FASN protein expression levels, but only monoesters M1 and M2 induced apoptosis. Our results indicate that FASN inhibition by such polyphenolic compounds could be a new strategy in TNBC treatment, and highlight the potential anticancer activities of monoesters. Thus, G28, G37, G56, and most importantly M1 and M2, are anticancer candidates (alone or in combination) to be further characterized in vitro and in vivo.

Keywords: triple-negative breast cancer; fatty acid synthase; FASN inhibition; polyphenolic FASN inhibitors; (−)-epigallocatechin 3-gallate; synthetic analogues; apoptosis; anticancer activity

1. Introduction

Breast cancer is the most widespread cancer in women worldwide [1]. Although mortality has diminished in recent years owing to the programs of early diagnosis and to the improvement in treatment, this disease is still the first cause of death in women. Triple-negative breast cancer (TNBC) is a subtype of breast cancer in which the estrogen and the progesterone receptors are not expressed, and the human epidermal growth factor receptor 2 (HER2) is not amplified or overexpressed [2–5].

TNBC comprises about 15–20% of all breast cancers diagnosed. It tends to have an aggressive clinical course and to metastasize, resulting in early relapse and poor overall survival [2]. Patients with TNBC do not benefit from the targeted therapies used in other breast cancer subtypes, such as hormonal and anti-HER2 receptor therapies, thus leaving systemic cytotoxic chemotherapy as the sole treatment option [3–5]. The aggressiveness of this cancer and the scarcity of effective treatment options evidence the need of developing new therapeutic agents.

Metabolism deregulation is considered a hallmark of cancer [6,7]. In this sense, some metabolic enzymes such as fatty acid synthase (FASN) have been identified as valuable therapeutic targets for cancer treatment [8]. FASN is a homodimeric multienzymatic protein responsible for de novo fatty acid synthesis. It has a low or absent expression in normal tissues, but it is overexpressed and hyperactivated in many carcinomas such as breast cancer [8,9]. This overexpression correlates with a malignant phenotype and a poor disease prognosis. Therefore, the pharmacological inhibition of FASN is recognized as an attractive therapeutic approach. Blocking FASN activity triggers apoptosis in cancer cells and inhibits tumor growth in xenograft models [10], by disrupting lipid membrane synthesis, protein palmitoylation, and signalling of major oncogenic pathways [11,12]. Remarkably, FASN inhibition has minimal effect on non-malignant cells. Moreover, a recent study has shown that FASN is expressed in TNBC patient samples and that TNBC preclinical models benefit from FASN inhibition [13].

The most representative FASN inhibitors are cerulenin, its synthetic derivative C75, and orlistat [9,11]. Even though these compounds have proven effective at controlling the progression of breast cancer, they have limitations that restrict their clinical development. These include chemical instability, low bioavailability, and stimulation of carnitine palmitoyltransferase-1 (CPT-1), which causes the acceleration of fatty acid β-oxidation and undesirable side effects such as body weight loss. On the other hand, epigallocatechin-3-gallate (EGCG, Figure 1a), the main polyphenolic catechin of green tea, has been described to inhibit FASN, to induce apoptosis in vitro and to reduce tumor size, without parallel CPT-1 stimulation or weight loss [9,13–16]. Specifically, the antiproliferative effects of EGCG have been widely reported in MDA-MB-231 TNBC cells [13,17–19], and such effects have also been associated, besides to FASN inhibition, to β-catenin downregulation [17,20]. Nevertheless, EGCG displays low potency, poor bioavailability, and limited stability in physiological conditions [21,22].

Considering this profile, EGCG's structure inspired the design and synthesis of a novel collection of polyphenolic compounds, containing two galloyl moieties (3,4,5-trihydroxybenzoyl group) linked by a variable cyclic subunit (Figure 1b) [21,22]. The collection was screened for cytotoxicity and FASN inhibition against a HER2-positive human breast cancer cell line overexpressing FASN, and three lead compounds were identified, G28, G37, and G56 (Figure 1c), which improved the properties of their precursor molecule EGCG without affecting mice body weight [21–23]. G28 has been the most studied lead to date, proving effective in different HER2-positive breast cancer models, both in vivo and in vitro [10,24], and recently in TNBC in vitro models [25]. In addition, in vivo pharmacokinetic analyses have showed that G28 is hydrolyzed into two metabolites, M1 and M2 (Figure 1d) [23]. These compounds have already been tested for potential antibacterial activity [26] but, interestingly, not for anticancer activity. The purpose of the current study was to assess FASN inhibition by synthetic polyphenolic compounds as a potential therapeutic approximation for the clinically challenging TNBC. We synesized diesters G28, G37 and G56 together with G28-derived monoesters M1 and M2, and we evaluated their cytotoxicity and capacity to inhibit FASN activity and to induce apoptosis in the MDA-MB-231 TNBC cell model.
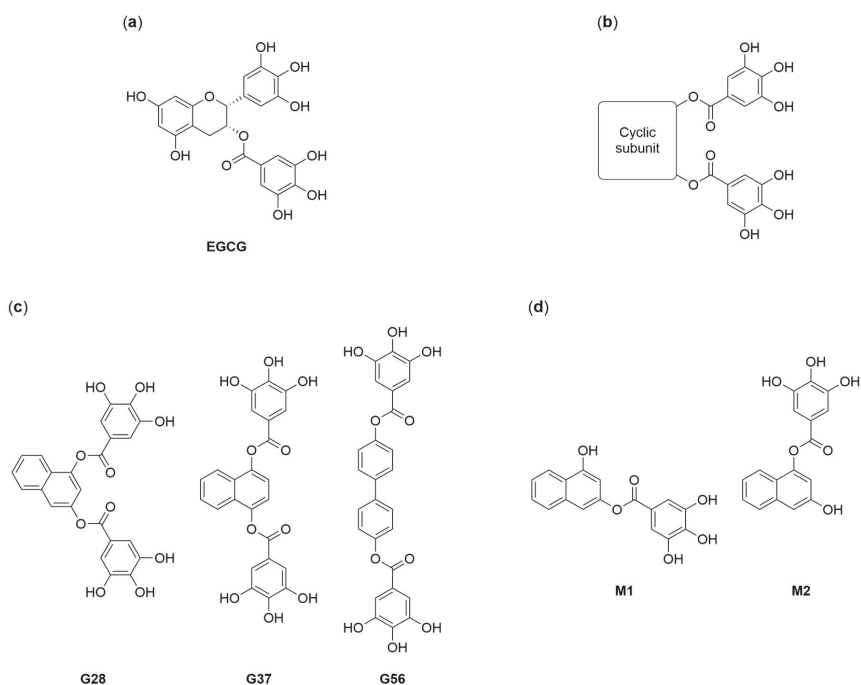
Figure 1. Structures of (−)-epigallocatechin 3-gallate (EGCG) (**a**), EGCG derivatives (**b**), the lead diesters (**c**) and the monoesters of G28 (**d**) [21,22,26].

2. Results

2.1. Synthesis of EGCG Analogues

The synthesis of diesters G28, G37 and G56 [21,22], and of monoesters M1 and M2 [26] was performed using procedures adapted from previously described protocols (Supplementary Materials) [23,26,27]. The synthesis encompassed the esterification of the corresponding aromatic diol with the conveniently protected acyl chloride derivative of gallic acid and the subsequent removal of the protecting groups. Diesters G28, G37 and G56 were obtained in 46, 65 and 61% overall yield, respectively, and monoesters M1 and M2 in 24 and 20% overall yield, respectively. All compounds were fully characterized by NMR and mass spectrometry. Additional NOESY and HMBC experiments allowed the unambiguous assignment of the regioisomeric monoesters M1 and M2.

2.2. Effect of EGCG Analogues on Cell Proliferation

The cytotoxic activity of G28, G37, G56 [21,22], M1 and M2 [26] was evaluated in the MDA-MB-231 human TNBC cell line. The IC_{50} values of compounds were determined from their dose-response curves (Table 1). This line has lower constitutive FASN expression levels than the SK-Br3 HER2-positive breast cancer cell line against which compounds were previously screened [21,22].

Diesters G28, G37 and G56 were more cytotoxic than their parent molecule EGCG (IC_{50} = 149 μM [13]), in particular being 1.9-, 1.4- and 3.3-fold more potent respectively. Monoesters M1 and M2 turned out to inhibit cell proliferation. In comparison to their parent compound G28 (77 μM), M2 exhibited the same cytotoxic activity (79 μM) and, interestingly, M1 doubled such cytotoxicity (41 μM).

Table 1. Cytotoxicity in MDA-MB-231 cancer cells of diesters and monoesters.

Compound	IC$_{50}$ (μM) [a]
EGCG	149.0 ± 6.7 [b]
G28 [c]	77.3 ± 3.4
G37 [c]	103.7 ± 1.9
G56 [c]	45.4 ± 3.4
M1 [d]	41.4 ± 1.5
M2 [d]	78.9 ± 4.6

[a] Data are mean ± SE from six independent experiments performed in triplicate. [b] Datum taken from [13]. [c] Compound described in [21,22]. [d] Compound described in [26].

2.3. Effect of EGCG Analogues on FASN Activity and on FASN Protein Expression

The capacity of G28, G37, G56 [21,22], M1 and M2 [26] to block FASN enzymatic activity in MDA-MB-231 cells was analyzed after a 48-h treatment with a concentration equal to the IC$_{50}$ value of each compound. The inhibition is represented as the percentage of remaining activity with respect to untreated cells (Figure 2). The previously reported FASN-specific inhibitor C75 (IC$_{50}$ = 46.6 ± 2.2 μM in MDA-MB-231 [13]) was used as a positive control.

Diesters G28, G37 and G56 significantly reduced FASN activity to 1.99 ± 0.27%, 2.39 ± 0.48%, and 0.86 ± 0.20% of untreated (control, CTRL) cells, respectively (all p = 0.000), to an equivalent extent as C75 (1.81 ± 0.39%). Monoesters M1 and M2, besides their cytotoxicity, were also able to reduce FASN activity in an even more powerful way than their parent G28. M1- and M2-treated cells displayed remaining FASN activities of 0.07 ± 0.01% and 0.04 ± 0.01%, respectively (both p = 0.000).
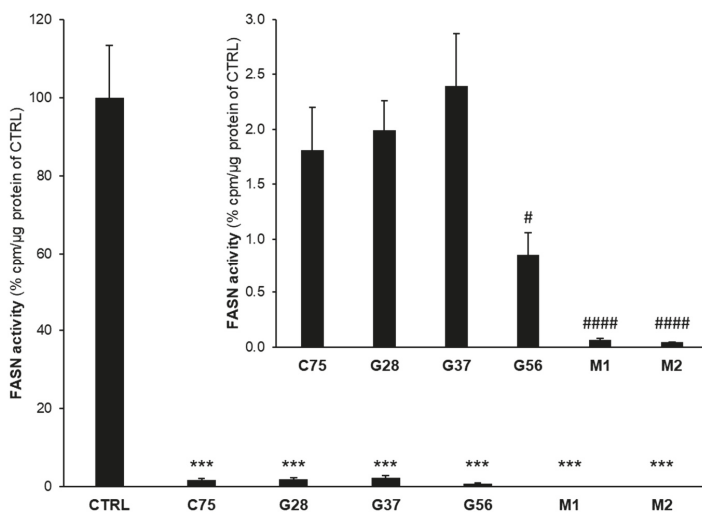
Figure 2. G28, G37, G56 [21,22], M1 and M2 [26] inhibit fatty acid synthase (FASN) activity in MDA-MB-231 TNBC cells. Cells were treated for 48 h with an IC$_{50}$ concentration of G28, G37, G56, M1, M2, C75 or with dimethyl sulfoxide (DMSO). FASN activity was assayed by counting radiolabelled fatty acids synthesized de novo. Bars represent the remaining activity as percentage in treated cells versus untreated (control, CTRL) cells considered 100% activity. Data are mean ± SE from at least 4 assay points per condition in 3 independent experiments. ***, p < 0.001 versus control cells (DMSO). #, p < 0.05; ####, p < 0.001 versus C75-treated cells. Statistics were performed through Student's t-test.

In parallel, in order to check whether the observed FASN activity decrease was related to changes in FASN protein levels, cells were treated with diesters and monoesters as described in the next Section 2.4 and FASN expression was analyzed by Western blot (Figure 3a). G37 and G56 did not modulate FASN protein levels, whereas G28 and its derivatives M1 and M2 displayed a tendency to reduce such levels (Figure 3b), which was more noticeable for M2.
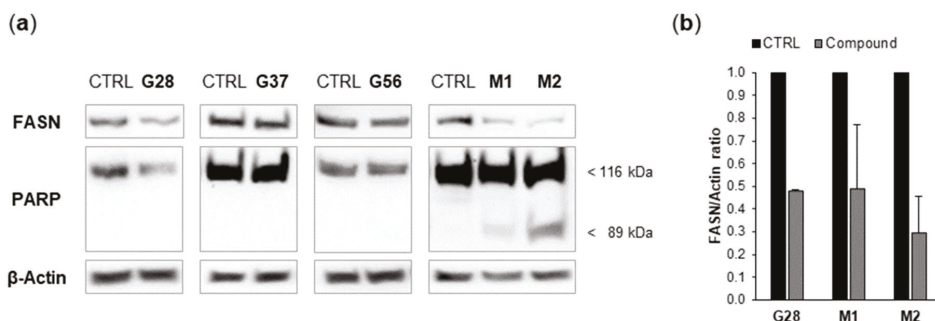
Figure 3. (**a**) G28, G37, G56 [21,22], M1 and M2 [26] differentially affect FASN protein expression in MDA-MB-231 TNBC cells, and only M1 and M2 induce apoptosis, as determined by poly(ADP-ribose) polymerase (PARP) cleavage. Cells were treated for 24 h with a 5-fold IC_{50} concentration of G28, G56, M1 and M2, a 2-fold IC_{50} concentration of G37, or with DMSO. Equal amounts of lysates were immunoblotted with anti-FASN and anti-PARP antibodies (the latter identified intact and cleaved PARP at 116 and 89 kDa, respectively). Blots were reproved for β-actin as loading control. Gels shown are equivalent to those obtained from two or three independent experiments. (**b**) G28, M1 and M2 downregulate FASN protein expression. FASN and β-actin immunoblot bands were quantified by densitometry and FASN/β-actin ratios of treatments are represented relative to those of controls. Data are mean ± SE from two or three independent experiments.

2.4. Effect of EGCG Analogues on Apoptosis

Our group previously reported in SK-Br3 cells the activation of the apoptotic cell death mechanism by EGCG and its new-generation derivatives [14–16,21,22]. Accordingly, diesters [21,22] and monoesters [26] were evaluated in MDA-MB-231 cells for their ability to induce caspase activity, which causes cleavage of poly(ADP-ribose) polymerase (PARP). Cells were incubated for 24 h with concentrations corresponding to five-fold the IC_{50} values of G28, G56, M1 and M2, and two-fold the IC_{50} value of G37, because of the mortality induced by G37 at higher IC_{50} multiples (data not shown). PARP cleavage was analyzed by Western blot (Figure 3a). Apoptosis induction was not detected under the assayed conditions for any of the three diesters G28, G37 and G56. In contrast and interestingly, it was detected for both monoesters M1 and M2, with M2 showing a more intense band of cleaved PARP (89 kDa).

3. Discussion

TNBC is an aggressive cancer lacking a targeted therapy [3–5]. FASN is overexpressed in a variety of human carcinomas [8,9], including TNBC [28], and its inhibition with polyphenolic compounds such as EGCG has been demonstrated to be a promising therapeutic strategy, alone and in combination, for TNBC [13]. In this study, we characterized the anticancer effects of the EGCG analogues G28, G37 and G56 [21,22], and the G28 derivatives M1 and M2 [26], in MDA-MB-231 cells.

Firstly, the cytotoxic activity of compounds was determined. Diesters G28, G37 and G56 [21,22] displayed moderate IC_{50} values of 77, 104 and 45 μM, respectively, at 48-h exposure. Our group has studied the reference FASN inhibitors C75 and EGCG in several cancer cell lines, including MDA-MB-231 [13], in which the IC_{50} values were 46.6 ± 2.2 and 149.0 ± 6.7 μM, respectively. Thus,

the three diesters are more potent than their parent molecule, as reported in SK-Br3 cells, and G56 is equally potent to C75. On the other hand, from the initial screening of EGCG analogues in SK-Br3 cells, some structure-activity relationships were inferred [22]. One of them was that cytotoxicity increases as the distance between the two galloyl moieties augments within the cyclic subunit. This could explain the superior cytotoxicity of G56, in which galloyl groups are in a relative 4,4′-position within a biphenyl system, further from each other than in the naphthalene ring of G28 and G37 (Figure 1c). Concerning monoesters M1 and M2 [26], which are metabolites of G28 in physiological conditions [23], they proved cytotoxic in MDA-MB-231 cells. M2 (IC_{50} = 79 μM) retained the activity of G28 while M1 (41 μM) enhanced that activity. This result raised the possibility that the in vivo antitumor efficacy of G28 is due, at least partially, to the two monoesters.

Beyond the obtained results, a positive correlation between the cytotoxic effects of the aforementioned inhibitors and cellular FASN expression has been reported [14,21–23], from the observation that compounds are less potent in MDA-MB-231 triple-negative cells, with low FASN levels, than in SK-Br3 HER2-positive cells, with high FASN levels. To support the correlation, it was demonstrated that the addition of exogenous palmitate, the end product of FASN, reduced the cytotoxicity of EGCG [14], and that the knockdown of FASN suppressed the cytotoxicity of G56 [22]. Hence, FASN inhibition plays a major role in the cytotoxicity of these polyphenolic compounds.

Secondly, the ability of the tested compounds [21,22,26] to block FASN activity was tackled. Compounds, at 48-h exposure, exerted a significant FASN activity reduction of 98.0%, 97.6% and 99.1% for diesters G28, G37 and G56, and of 99.93% and 99.96% for monoesters M1 and M2, respectively, as measured by an enzymatic radioassay. Moreover, G28 and its derivatives M1 and M2 also reduced FASN protein levels, unlike G37 and G56. Therefore, the observed FASN activity decrease in G28, M1 and M2 lysates could probably result not only from enzyme inhibition but also from diminished amounts of FASN protein. Our results show that, as for diesters [21,22], G56 is a more potent FASN inhibitor than G37 and G28, assuming that for G28 the remaining activity could be slightly higher in the absence of FASN downregulation (Figure 2). On the other hand, G28 stands out as the most effective diester due to its dual effect on FASN (activity and expression). Regarding monoesters [26], M1 and M2 affect FASN protein levels to a similar extent as G28 (Figure 3b) but, remarkably, both are better FASN inhibitors than G28 (Figure 2). These results indicate that the affinity for FASN of monoesters is greater than that of their parent molecule, being probably similar between the two monoesters.

In the original characterization, FASN inhibition values in SK-Br3 cells at 24-h exposure were 90 ± 4%, 69 ± 19% and 90 ± 5% for G28, G37 and G56, and 18% for EGCG, as measured by spectrophotometry, and FASN inhibition was not accompanied by downregulation of FASN expression [21,22]. These data evidence that diesters inhibit FASN more effectively than their parent molecule and agree with our results that G37 seems to be the less potent inhibitor. The observed FASN downregulation by G28 in MDA-MB-231 but not in SK-Br3 could be attributable to the concentration used, which was five-fold the IC_{50} value in our treatments against one-fold the IC_{50} value in the literature. Anyway, FASN downregulation has also been reported elsewhere, by C75 in A2780 ovarian cancer cells in a dose-dependent manner [29], and by EGCG, in A549 lung cancer cells [16] and in chemo-sensitive and -resistant MDA-MB-231 and HCC1806 TNBC cells [13]. A possible mechanism for this downregulation is that G28, apart from inhibiting FASN, could to some extent also inhibit the EGF receptor (EGFR), which is overexpressed in TNBC [30], thus impairing the downstream signalling that ends in FASN expression. This effect could occur at the transcriptional level, through PI3K and MAPK pathways activating the transcription factor SREBP-1c [31]; and at the translational level, through mTOR protein activating eIF4E and S6K [32]. Finally, FASN downregulation by monoesters M1 and M2 [26] is consistent with the result obtained for their parent molecule.

Beyond our results, in parallel to FASN inhibition and downregulation, EGCG and other polyphenols such as quercetin have also been described to reduce β-catenin protein expression [17,20,33,34]. β-catenin, when bound to E-cadherin complexes, functions as a cell-cell adhesion molecule, but when translocated to the nucleus acts as a key element in the Wnt signalling

pathway, activating the transcription of target genes related to cell proliferation and metastasis, thus contributing to breast cancer progression [17,33]. Therefore, forthcoming studies in our group will investigate whether diesters and monoesters are able to modulate β-catenin expression and its nuclear accumulation in TNBC.

This is the first study testing monoesters M1 and M2 as potential anticancer agents. However, both monoesters have already been tested in another setting, as synthetic inhibitors of bacterial cell division targeting the GTP-binding site of protein FtsZ [26]. In that study, the affinity for FtsZ of monoesters, competing with GTP, was one order of magnitude lower than that of diester G28, with the affinity of M2 being slightly higher than that of M1, as determined by K_b comparison. The affinity of EGCG was two orders of magnitude lower relative to that of G28. Thus, only G28 was included in further biochemical, structural and antibacterial characterization. In striking contrast, our results suggested that the affinity for FASN is larger for monoesters than for G28. Aiming to understand this differential affinity, a future perspective of our group will be to gain insights, through molecular docking analyses, in the potential binding modes of G28 and monoesters to their target FASN catalytic domains. These domains are probably the same as those targeted by EGCG, the NADPH-dependent domains ketoreductase (KR) [35] and enoyl reductase (ER) [36–39], which participate in the saturation of the growing fatty acid chain [40]. Interestingly, EGCG has been shown to compete with NADPH/NADH for binding to KR and ER [35–39]. Since both NADPH/NADH (FASN) and GTP (FtsZ) are nucleotides, it is worth noting that, in the FtsZ study, the galloyl groups and the naphthalene scaffold of G28 were predicted to replace the interactions by the phosphates and the nucleobase of the nucleotide, respectively [26]. This could also be true in the interaction of G28 with FASN.

Thirdly, the capacity of compounds [21,22,26] to activate apoptotic cell death was addressed. The superior activity of monoesters was reaffirmed since, at 24-h exposure, monoesters, more importantly M2, induced PARP cleavage whereas diesters did not have this effect, despite using IC_{50} multiples as concentration. In the original characterization of diesters in SK-Br3 cells, an IC_{50} concentration value was sufficient to perceive truncated PARP as early as 12 h [21,22]. An equal result was obtained for C75 and EGCG in SK-Br3 and A549 cells [14,16], and for EGCG in chemo-sensitive and -resistant MDA-MB-231 and HCC1806 cells [13]. In addition, apoptosis has also been reported for EGCG combined with cetuximab in TNBC xenograft models [13]; and for G28, in other HER2-positive breast cancer models both in vivo and in vitro, alone and combined with anti-HER drugs [10], and in several ovarian cancer models in a dose-dependent manner [41,42].

Considering the effect of EGCG and diesters in SK-Br3, it is surprising that only EGCG shows effect in MDA-MB-231. The above described correlation between cytotoxicity and cellular FASN levels implies that MDA-MB-231 cells are less reliant on FASN activity than SK-Br3 cells for their survival and aggressiveness. Then, a possible hypothesis is that inhibition of FASN activity and expression by diesters in MDA-MB-231 may not be enough to compromise cell survival and reach the threshold for apoptosis induction, a threshold that may be comparatively lower in SK-Br3. In contrast, the two monoesters have larger affinities for FASN than those of diesters and both affect FASN expression, thus being able to overcome the threshold in MDA-MB-231. On the other hand, EGCG has been described to bind targets other than FASN [43]. Therefore, it may induce apoptosis through FASN inhibition along with other mechanisms, and so apoptosis may be detected irrespective of the cellular dependence on FASN.

In summary, in this study we evaluated the previously described G28 derivatives M1 and M2 [26] for first time as anticancer agents and partially disclosed their pharmacological profile in a TNBC model. Monoesters M1 and M2 turned out to be equally or more cytotoxic and to have a larger affinity for FASN than their parent molecule, to affect FASN expression and to induce apoptosis, which suggests that they could individually contribute to the in vivo antitumor activity of G28 after it has been hydrolyzed. In order to confirm this hypothesis, a future decisive study will be conducted to compare the efficacy of each monoester with that of G28 in a TNBC xenograft model. On the other hand, in the same in vitro model, the previously designed EGCG-derived diesters G28, G37

and G56 [21,22] exhibited cytotoxicity and remarkable FASN inhibition. Diesters, and especially monoesters, hold promise as target-directed anticancer drugs, either alone or in combination, focused on TNBC treatment. Furthermore, this work constitutes a starting point in our group for the future synthesis and evaluation of other polyphenolic compounds, such as the monoesters of G37 and G56, or computationally optimized compounds derived from the three diesters.

4. Materials and Methods

4.1. Cell Culture

MDA-MB-231 breast carcinoma cells were obtained from the American Type Culture Collection (ATCC, Rockville, MD, USA). Cells were routinely grown in two-dimensional adherent conditions in Dulbecco's Modified Eagle's Medium (DMEM, Gibco, Waltham, MA, USA) supplemented with 10% heat-inactivated fetal bovine serum (FBS), 1% L-glutamine, 1% sodium pyruvate, 50 U/mL penicillin and 50 μg/mL streptomycin (HyClone Laboratories, Logan, UT, USA). Cells were maintained at 37 °C in a humidified atmosphere of 95% air and 5% CO_2. The absence of *Mycoplasma* in cultures was checked before experiments.

4.2. Inhibition of Cell Proliferation

Dose-response experiments were done by means of the standard colorimetric MTT (3-4,5-dimethylthiazol-2-yl-2,5-diphenyltetrazolium bromide) reduction assay. Cells were plated out at a density of 4×10^3 cells/well in 96-well microtiter plates and were incubated overnight for attachment. Then, cells were exposed for 48 h to fresh medium containing a range of concentrations of the corresponding EGCG derivative (10–140 μM) or were exposed to fresh medium alone. An influence of the vehicle dimethyl sulfoxide (DMSO) in the cytotoxicity of compounds was discarded. Following treatment, cells were incubated for 3 h with drug-free medium (100 μL/well) and 5 mg/mL MTT solution (Sigma-Aldrich, St. Louis, MO, USA; 10 μL/well). The formazan crystals formed by metabolically viable cells were solubilized in DMSO and their absorbance (Abs) was measured at 570 nm (Benchmark Plus microplate spectrophotometer, Bio-Rad Laboratories, Hercules, CA, USA). Using test (T) and control (C) average Abs values, the percentage of cell proliferation inhibition (CPI) at each concentration was calculated from the formula CPI = $100(1-T/C)$. By interpolation in the trendline of the resulting data points, the compound concentration that triggered 50% CPI (IC_{50} value) was determined. The assay was performed six times per compound.

4.3. Inhibition of Fatty Acid Synthase Activity

Cells were plated out at a density of 5×10^4 cells/well in 24-well plates. Following overnight cell adherence, the medium was replaced by DMEM supplemented with 1% lipoprotein-deficient FBS (Sigma-Aldrich) along with the corresponding concentrations of compounds or DMSO. Treatments were maintained for 48 h, and for the last 6 h (1,2-^{14}C) Acetic Acid Sodium salt (53.9 mCi/mmol, Perkin Elmer Biosciences, Waltham, MA, USA) was added to the medium (0.5 μCi/mL). The lipid extraction was done as previously described in [16]. Briefly, cells were harvested and washed twice with phosphate-buffered saline (PBS, HyClone Laboratories, Logan, UT, USA) and once with MeOH/PBS (2:3). Cells were then resuspended in 0.2 M NaCl and were lysed with freeze-thaw cycles. Lipids from cell debris were extracted with $CHCl_3$/phenol (2:1) and 0.1 M KOH, and the organic phase was washed with $CHCl_3$/MeOH/H_2O (3:48:47). After solvents evaporation, pellets were resuspended in EtOH and transferred to a vial for radioactive counting. The total protein content in cell debris was quantified by the Bradford assay (Sigma-Aldrich).

4.4. Immunoblot Analysis of Cell Lysates

After a 24-h exposure to the corresponding EGCG derivative or DMSO, culture appearance was observed under microscope and cells were harvested by treatment with trypsin-ethylenediaminetetraacetic

acid (EDTA) solution (Linus, Cultek, Madrid, Spain), together with supernatant cell debris. Cells plus debris were washed with PBS and lysed in ice-cold lysis buffer (Cell Signaling Technology, Danvers, MA, USA) supplemented with 2 mM phenylmethanesulfonyl fluoride (PMSF, Sigma-Aldrich) by vortexing every 5 min for 30 min. Particle-free lysates were obtained and their total protein content was determined by the Lowry-based DC Protein Assay (Bio-Rad Laboratories). Lysates' equal protein amounts (30 µg) were heated in LDS Sample Buffer with Sample Reducing Agent (Invitrogen, Waltham, MA, USA) for 10 min at 70 °C, were run on sodium dodecyl sulphate polyacrylamide gel electrophoresis (SDS-PAGE, 7.5% polyacrylamide) and were transferred onto nitrocellulose membranes (Thermo Scientific, Pierce Protein Biology, Waltham, MA, USA). Blots were incubated for 1 h at room temperature in blocking buffer [5% powdered skimmed milk in tris-buffered saline with Tween 20 (TBST; 10 mM Tris-HCl pH 8.0, 150 mM NaCl, 0.1% Tween 20)] to avoid non-specific antibody binding. Then, blot fragments were incubated overnight at 4 °C with the appropriate primary antibody diluted in blocking buffer. Primary antibodies were rabbit polyclonal antibodies against FASN (Assay Designs, Ann Arbor, MI, USA; 905-069; dilution 1:1500) and PARP (Cell Signaling Technology; #9542; dilution 1:1000), and the mouse monoclonal antibody against β-actin (Cell Signaling Technology; #3700; dilution 1:2500). β-actin was used as a control of protein loading and transfer. Next, blots were washed in TBST and were incubated for 1 h at room temperature with the corresponding horseradish peroxidase (HRP)-conjugated goat secondary antibody diluted in blocking buffer, against rabbit (Cell Signaling Technology; #7074; dilution 1:4000) or mouse (Merck Millipore, Darmstadt, Germany; #401215; dilution 1:5000) antibodies. Lastly, blots were washed again and revealed (ChemiDoc MP Imaging System, Bio-Rad Laboratories) employing a chemiluminescent HRP substrate [Immobilon Western (Merck Millipore) or SuperSignal West Femto (Thermo Scientific, Pierce Protein Biology)]. The immunoblot analysis for each compound was repeated two or three times and a representative result is shown. FASN and β-actin bands were quantified using ImageJ software (version 1.51j8, National Institutes of Health, Bethesda, MD, USA).

4.5. Statistical Analysis

All data are expressed as mean ± standard error (SE). FASN inhibition data were analyzed by Student's *t*-test and levels of statistical significance were $p < 0.001$ (***) versus control cells, and $p < 0.05$ (#), $p < 0.001$ (####) versus C75-treated cells.

References

1. DeSantis, C.E.; Lin, C.C.; Mariotto, A.B.; Siegel, R.L.; Stein, K.D.; Kramer, J.L.; Alteri, R.; Robbins, A.S.; Jemal, A. Cancer treatment and survivorship statistics, 2014. *CA Cancer J. Clin.* **2014**, *64*, 252–271. [CrossRef] [PubMed]
2. Qiu, J.; Xue, X.; Hu, C.; Xu, H.; Kou, D.; Li, R.; Li, M. Comparison of clinicopathological features and prognosis in triple-negative and non-triple negative breast cancer. *J. Cancer* **2016**, *7*, 167–173. [CrossRef] [PubMed]
3. Yao, H.; He, G.; Yan, S.; Chen, C.; Song, L.; Rosol, T.J.; Deng, X. Triple-negative breast cancer: Is there a treatment on the horizon? *Oncotarget* **2016**, *8*, 1913–1924. [CrossRef] [PubMed]

4. Bianchini, G.; Balko, J.M.; Mayer, I.A.; Sanders, M.E.; Gianni, L. Triple negative breast cancer: challenges and opportunities of a heterogeneous disease. *Nat. Rev. Clin. Oncol.* **2016**, *13*, 674–690. [CrossRef] [PubMed]

5. Denkert, C.; Liedtke, C.; Tutt, A.; von Minckwitz, G. Molecular alterations in triple-negative breast cancer-the road to new treatment strategies. *Lancet* **2016**, *389*, 2430–2442. [CrossRef]

6. Hanahan, D.; Weinberg, R.A. Hallmarks of cancer: The next generation. *Cell* **2011**, *144*, 646–674. [CrossRef] [PubMed]

7. Pavlova, N.N.; Thompson, C.B. The emerging hallmarks of cancer metabolism. *Cell Metab.* **2016**, *23*, 27–47. [CrossRef] [PubMed]

8. Menéndez, J.A.; Lupu, R. Fatty acid synthase and the lipogenic phenotype in cancer pathogenesis. *Nat. Rev. Cancer* **2007**, *7*, 763–777. [CrossRef] [PubMed]

9. Oliveras, G.; Blancafort, A.; Urruticoechea, A.; Campuzano, O.; Gómez-Cabello, D.; Brugada, R.; López-Rodríguez, M.L.; Colomer, R.; Puig, T. Novel anti-fatty acid synthase compounds with anticancer activity in HER2⁺ breast cancer. *Ann. N. Y. Acad. Sci.* **2010**, *1210*, 86–93. [CrossRef] [PubMed]

10. Puig, T.; Aguilar, H.; Cufí, S.; Oliveras, G.; Turrado, C.; Ortega-Gutiérrez, S.; Benhamú, B.; López-Rodríguez, M.L.; Urruticoechea, A.; Colomer, R. A novel inhibitor of fatty acid synthase shows activity against HER2+ breast cancer xenografs and is active in anti-HER2 drug-resistant cell lines. *Breast Cancer Res.* **2011**, *13*, R131. [CrossRef] [PubMed]

11. Jones, S.F.; Infante, J.R. Molecular pathways: Fatty acid synthase. *Clin. Cancer Res.* **2015**, *21*, 5434–5438. [CrossRef] [PubMed]

12. Ventura, R.; Mordec, K.; Waszczuk, J.; Wang, Z.; Lai, J.; Fridlib, M.; Buckley, D.; Kemble, G.; Heuer, T.S. Inhibition of de novo palmitate synthesis by fatty acid synthase induces apoptosis in tumor cells by remodelling cell membranes, inhibiting signalling pathways, and reprogramming gene expression. *EBioMedicine* **2015**, *2*, 806–822. [CrossRef] [PubMed]

13. Giró-Perafita, A.; Palomeras, S.; Lum, D.H.; Blancafort, A.; Viñas, G.; Oliveras, G.; Pérez-Bueno, F.; Sarrats, A.; Welm, A.L.; Puig, T. Preclinical evaluation of fatty acid synthase and EGFR inhibition in triple-negative breast cancer. *Clin. Cancer Res.* **2016**, *22*, 4687–4697. [CrossRef] [PubMed]

14. Puig, T.; Vázquez-Martín, A.; Relat, J.; Pétriz, J.; Menéndez, J.A.; Porta, R.; Casals, G.; Marrero, P.F.; Haro, D.; Brunet, J.; et al. Fatty acid metabolism in breast cancer cells: differential inhibitory effects of epigallocatechin gallate (EGCG) and C75. *Breast Cancer Res. Treat.* **2008**, *109*, 471–479. [CrossRef] [PubMed]

15. Puig, T.; Relat, J.; Marrero, P.F.; Haro, D.; Brunet, J.; Colomer, R. Green tea catechin inhibits fatty acid synthase without stimulating carnitine palmitoyltransferase-1 or inducing weight loss in experimental animals. *Anticancer Res.* **2008**, *28*, 3671–3676. [PubMed]

16. Relat, J.; Blancafort, A.; Oliveras, G.; Cufí, S.; Haro, D.; Marrero, P.F.; Puig, T. Different fatty acid metabolism effects of (−)-epigallocatechin-3-gallate and C75 in adenocarcinoma lung cancer. *BMC Cancer* **2012**, *12*. [CrossRef] [PubMed]

17. Hong, O.-Y.; Noh, E.-M.; Jang, H.-Y.; Lee, Y.-R.; Lee, B.K.; Jung, S.H.; Kim, J.-S.; Youn, H.J. Epigallocatechin gallate inhibits the growth of MDA-MB-231 breast cancer cells via inactivation of the β-catenin signaling pathway. *Oncol. Lett.* **2017**, *14*, 441–446. [CrossRef] [PubMed]

18. Chisholm, K.; Bray, B.J.; Rosengren, R.J. Tamoxifen and epigallocatechin gallate are synergistically cytotoxic to MDA-MB-231 human breast cancer cells. *Anticancer Drugs* **2004**, *15*, 889–897. [CrossRef] [PubMed]

19. Roy, A.M.; Baliga, M.S.; Katiyar, S.K. Epigallocatechin-3-gallate induces apoptosis in estrogen receptor-negative human breast carcinoma cells via modulation in protein expression of p53 and Bax and caspase-3 activation. *Mol. Cancer Ther.* **2005**, *4*, 81–90. [PubMed]

20. Amado, N.G.; Fonseca, B.F.; Cerqueira, D.M.; Neto, V.M.; Abreu, J.G. Flavonoids: potential Wnt/beta-catenin signaling modulators in cancer. *Life Sci.* **2011**, *89*, 545–554. [CrossRef] [PubMed]

21. Puig, T.; Turrado, C.; Benhamú, B.; Aguilar, H.; Relat, J.; Ortega-Gutiérrez, S.; Casals, G.; Marrero, P.F.; Urruticoechea, A.; Haro, D.; et al. Novel inhibitors of fatty acid synthase with anticancer activity. *Clin. Cancer Res.* **2009**, *15*, 7608–7615. [CrossRef] [PubMed]

22. Turrado, C.; Puig, T.; García-Cárceles, J.; Artola, M.; Benhamú, B.; Ortega-Gutiérrez, S.; Relat, J.; Oliveras, G.; Blancafort, A.; Haro, D.; et al. New synthetic inhibitors of fatty acid synthase with anticancer activity. *J. Med. Chem.* **2012**, *55*, 5013–5023. [CrossRef] [PubMed]

23. Turrado, C. Novel Inhibitors of Fatty Acid Synthase (FASN): Validation As a New Therapeutic Target for Breast Cancer Treatment. Ph.D. Thesis, Universidad Complutense de Madrid, Madrid, Spain, 2013.

24. Blancafort, A.; Giró-Perafita, A.; Oliveras, G.; Palomeras, S.; Turrado, C.; Campuzano, O.; Carrión-Salip, D.; Massaguer, A.; Brugada, R.; Palafox, M.; et al. Dual fatty acid synthase and HER2 signalling blockade shows marked antitumor activity against breast cancer models resistant to anti-HER2 drugs. *PLoS ONE* **2015**, *10*, e0131241. [CrossRef] [PubMed]

25. Giró-Perafita, A. Fatty Acid Synthase Expression and Inhibition in Triple-Negative Breast Cancer. Ph.D. Thesis, University of Girona, Girona, Spain, 2016.

26. Ruiz-Avila, L.B.; Huecas, S.; Artola, M.; Vergoñós, A.; Ramírez-Aportela, E.; Cercenado, E.; Barasoain, I.; Vázquez-Villa, H.; Martín-Fontecha, M.; Chacón, P.; et al. Synthetic inhibitors of bacterial cell division targeting the GTP-binding site of FtsZ. *ACS Chem. Biol.* **2013**, *8*, 2072–2083. [CrossRef] [PubMed]

27. Feldman, K.S.; Sambandam, A.; Bowers, K.E.; Appel, H.M. Probing the role of polyphenol oxidation in mediating insect-pathogen interactions. Galloyl-derived electrophilic traps for the Lymantria dispar nuclear polyhedrosis virus matrix protein polyhedrin. *J. Org. Chem.* **1999**, *64*, 5794–5803. [CrossRef]

28. Giró-Perafita, A.; Sarrats, A.; Pérez-Bueno, F.; Oliveras, G.; Buxó, M.; Brunet, J.; Viñas, G.; Puig, T. Fatty acid synthase expression and its association with clinico-histopathological features in triple-negative breast cancer. *Oncotarget* **2017**, *8*, 74391–74405. [CrossRef] [PubMed]

29. Grunt, T.W.; Wagner, R.; Grusch, M.; Berger, W.; Singer, C.F.; Marian, B.; Zielinski, C.C.; Lupu, R. Interaction between fatty acid synthase- and ErbB-systems in ovarian cancer cells. *Biochem. Biophys. Res. Commun.* **2009**, *385*, 454–459. [CrossRef] [PubMed]

30. Corkery, B.; Crown, J.; Clynes, M.; O'Donovan, N. Epidermal growth factor receptor as a potential therapeutic target in triple-negative breast cancer. *Ann. Oncol.* **2009**, *20*, 862–867. [CrossRef] [PubMed]

31. Yang, Y.A.; Morin, P.J.; Han, W.F.; Chen, T.; Bornman, D.M.; Gabrielson, E.W.; Pizer, E.S. Regulation of fatty acid synthase expression in breast cancer by sterol regulatory element binding protein-1c. *Exp. Cell Res.* **2003**, *282*, 132–137. [CrossRef]

32. Petroulakis, E.; Mamane, Y.; Le Bacquer, O.; Shahbazian, D.; Sonenberg, N. mTOR signalling: implications for cancer and anticancer therapy. *Br. J. Cancer* **2006**, *94*, 195–199. [CrossRef] [PubMed]

33. Sultan, A.S.; Khalil, M.I.M.; Sami, B.M.; Alkhuriji, A.F.; Sadek, O. Quercetin induces apoptosis in triple-negative breast cancer cells via inhibiting fatty acid synthase and β-catenin. *Int. J. Clin. Exp. Pathol.* **2017**, *10*, 156–172.

34. Srinivasan, A.; Thangavel, C.; Liu, Y.; Shoyele, S.; Den, R.; Selvakumar, P.; Lakshmikuttyamma, A. Quercetin regulates β-catenin signaling and reduces the migration of triple negative breast cancer. *Mol. Carcinog.* **2016**, *55*, 743–756. [CrossRef] [PubMed]

35. Wang, X.; Song, K.S.; Guo, Q.X.; Tian, W.X. The galloyl moiety of green tea catechins is the critical structure feature to inhibit fatty acid synthase. *Biochem. Pharmacol.* **2003**, *66*, 2039–2047. [CrossRef]

36. Zhang, Y.M.; Rock, C.O. Evaluation of epigallocatechin gallate and related plant polyphenols as inhibitors of the FabG and FabI reductases of bacterial type II fatty-acid synthase. *J. Biol. Chem.* **2004**, *279*, 30994–31001. [CrossRef] [PubMed]

37. Sharma, S.K.; Parasuraman, P.; Kumar, G.; Surolia, N.; Surolia, A. Green tea catechins potentiate triclosan binding to enoyl-ACP reductase from *Plasmodium falciparum* (PfENR). *J. Med. Chem.* **2007**, *50*, 765–775. [CrossRef] [PubMed]

38. Sharma, S.K.; Kumar, G.; Kapoor, M.; Surolia, A. Combined effect of epigallocatechin gallate and triclosan on enoyl-ACP reductase of *Mycobacterium tuberculosis*. *Biochem. Biophys. Res. Commun.* **2008**, *368*, 12–17. [CrossRef] [PubMed]

39. Narayanan, S.; Ramesh, K.V. Epigallocatechin gallate, a green tea polyphenol inhibits *Mycobacterium smegmatis*: In silico and in vitro studies. *Indian J. Pharm. Sci.* **2017**, *79*, 625–632. [CrossRef]

40. Maier, T.; Leibundgut, M.; Ban, N. The crystal structure of a mammalian fatty acid synthase. *Science* **2008**, *321*, 1315–1322. [CrossRef] [PubMed]

41. Veigel, D.; Wagner, R.; Stübiger, G.; Wuczkowski, M.; Filipits, M.; Horvat, R.; Benhamú, B.; López-Rodríguez, M.L.; Leisser, A.; Valent, P.; et al. Fatty acid synthase is a metabolic marker of cell proliferation rather than malignancy in ovarian cancer and its precursor cells. *Int. J. Cancer* **2015**, *136*, 2078–2090. [CrossRef] [PubMed]

42. Wagner, R.; Stübiger, G.; Veigel, D.; Wuczkowski, M.; Lanzerstorfer, P.; Weghuber, J.; Karteris, E.; Nowikovsky, K.; Wilfinger-Lutz, N.; Singer, C.F.; et al. Multi-level suppression of receptor-PI3K-mTORC1 by fatty acid synthase inhibitors is crucial for their efficacy against ovarian cancer cells. *Oncotarget* **2017**, *8*, 11600–11613. [CrossRef] [PubMed]

43. Colomer, R.; Sarrats, A.; Lupu, R.; Puig, T. Natural polyphenols and their synthetic analogues as emerging anticancer agents. *Curr. Drug Targets* **2017**, *18*, 147–159. [CrossRef] [PubMed]

Sample Availability: Samples of the compounds are not available from the authors.

Article

Direct Observation of Hydrangea Blue-Complex Composed of 3-*O*-Glucosyldelphinidin, Al³⁺ and 5-*O*-Acylquinic Acid by ESI-Mass Spectrometry

Takaaki Ito [1], Kin-ichi Oyama [2] and Kumi Yoshida [3,*]

[1] Graduate School of Information Sciences, Nagoya University, Chikusa, Nagoya 464-8601, Japan; ito.takaaki@b.mbox.nagoya-u.ac.jp

[2] Research Institute for Materials Science, Nagoya University, Chikusa, Nagoya 464-8602, Japan; oyama@cic.nagoya-u.ac.jp

[3] Graduate School of Informatics, Nagoya University, Chikusa, Nagoya 464-8601, Japan

* Correspondence: yoshidak@i.nagoya-u.ac.jp; Tel.: +81-052-789-5638

check for updates

Abstract: The blue sepal color of hydrangea is due to a metal complex anthocyanin composed of 3-*O*-glucosyldelphinidin (**1**) and an aluminum ion with the co-pigments 5-*O*-caffeoylquinic acid (**2**) and/or 5-*O*-*p*-coumaroylquinic acid (**3**). The three components, namely anthocyanin, Al³⁺ and 5-*O*-acylquinic acids, are essential for blue color development, but the complex is unstable and only exists in an aqueous solution. Furthermore, the complex did not give analyzable NMR spectra or crystals. Therefore, many trials to determine the detailed chemical structure of the hydrangea-blue complex have not been successful to date. Instead, via experiments mixing **1**, Al³⁺ and **2** or **3** in a buffered solution at pH 4.0, we obtained the same blue solution derived from the sepals. However, the ratio was not stoichiometric but fluctuated. To determine the composition of the complex, we tried direct observation of the molecular ion of the complex using electrospray-ionization mass spectrometry. In a very low-concentration buffer solution (2.0 mM) at pH 4.0, we reproduced the hydrangea-blue color by mixing **1**, **2** and Al³⁺ in ratios of 1:1:1, 1:2:1 and 1:3:1. All solution gave the same molecular ion peak at *m*/*z* = 843, indicating that the blue solution has a ratio of 1:1:1 for the complex. By using **3**, the observed mass number was *m*/*z* = 827 and the ratio of **1**, **3** and Al³⁺ was also 1:1:1. A mixture of **1**, 3-*O*-caffeoylquinic acid (**4**) and Al³⁺ did not give any blue color but instead was purple, and the intensity of the molecular ion peak at *m*/*z* = 843 was very low. These results strongly indicate that the hydrangea blue-complex is composed of a ratio of 1:1:1 for **1**, Al³⁺ and **2** or **3**.

Keywords: Aluminum ion; blue color development; 5-*O*-caffeoylquinic acid; 3-*O*-glucosyldelphinidin; *Hydrangea macrophylla*; ESI-mass; metal complex

1. Introduction

Hydrangea (*Hydrangea macrophylla*) originated from Japan, and what we consider to be its flower is not a true flower but a sepal. Its original sepal color is blue and very famous for its changes in hue with soil conditions, from red through purple to blue [1,2]. In the early 20th century, it was already known that hydrangea cultivated in acidic soil is blue [3,4]. In this condition, aluminum ion (Al³⁺) in soil becomes water-soluble and is absorbed from roots, followed by transport to sepal vacuoles to give a blue color [1,5,6]. In the mid-20th century, the sepal components were reported: colored sepals contained one anthocyanin component, 3-*O*-glucosyldelphinidin (Dp3G, **1**), and three co-pigment components: 5-*O*-caffeoyl-quinic acid (5CQ, **2**), 5-*O*-*p*-coumaroylquinic acid (5*p*CQ, **3**) and 3-*O*-caffeoylquinic acid (3CQ, **4**). These compounds can develop all of the reported sepal colors, red, purple and blue (Scheme 1) [5,7–10]. In the late 20th century, the different effects of the three

co-pigments on blue coloration were reported [11]. The 5-*O*-acylquinic acids (**2** and **3**) and Al^{3+} were revealed to be essential for blue coloration [11]. However, further investigation into the chemical structure and mechanism of blue color development was not performed.

3-*O*-glucosyl delphinidin (Dp3G, **1**)

R^1 = OH, R^2 = OH: 5-*O*-caffeoylquinic acid (5CQ, **2**)
R^1 = OH, R^2 = H: 5-*O*-*p*-coumaroylquinic acid (5*p*CQ, **3**)

3-*O*-caffeoylquinic acid (3CQ, **4**)
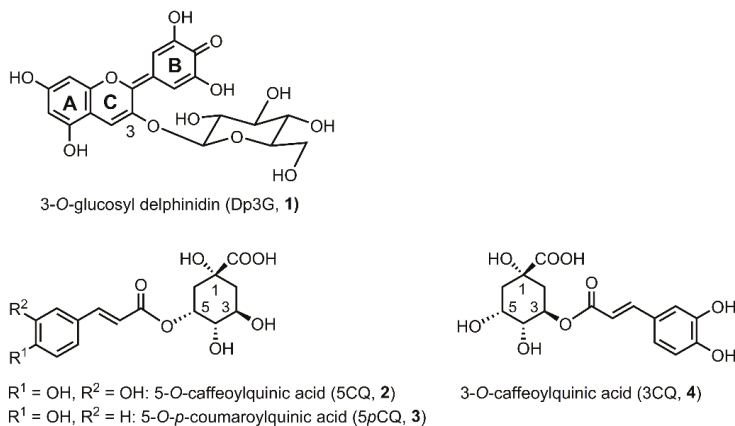
Scheme 1. Structures of pigment and co-pigments in hydrangea sepal.

We are interested in this phenomenon and have tried to reveal the chemical mechanisms of the color variation of hydrangea [12–16]. In 2003, we measured the vacuolar pH of colored sepal cells using the microelectrode method and reported that the pHv of the blue cells was 4.1, which is significantly higher than that of the red cells (pHv: 3.3) [12]. We next synthesized various natural and unnatural co-pigment derivatives and performed reproduction experiments by mixing **1**, co-pigments and Al^{3+}. As a result, the essential structure of co-pigment for blue coloration was clarified as the 1-OH, 1-COOH, 5-ester structure in quinic acid, and the aromatic acyl moiety had a stabilizing effect through a hydrophobic interaction with the anthocyanidin chromophore [13,14]. In 2009, quantitative analysis of **1–4** and Al^{3+} in blue and red sepal cells was performed, and it was clarified that the concentration of **1** in blue and red cells was not very different, but the molar ratio of **2** and **3** and Al^{3+} in blue cells was much higher than that of red cells [15]. However, neither the structure nor the ratio of the components in the blue colored pigment in hydrangea could be determined because the blue pigment can exist only in aqueous solutions and did not give an analyzable NMR spectrum.

We named the complex that develops blue color in hydrangea in sepals as "hydrangea blue-complex" and have performed experiments to elucidate its composition and chemical structure. Recently, we measured the ^{1}H-NMR spectrum of the hydrangea blue-complex by mixing **1**, **2** and Al^{3+} in a ratio of 1:2:1 in 6 M acetate buffer at pD 4.0 [17]. Analysis of the spectrum gave a partial structural information, indicating that in the hydrangea-blue complex, Dp3G (**1**) might exist in an equilibrium between chelating and non-chelating structures that have an interaction with 5CQ (**2**). Therefore, we proposed a schematic structure of the hydrangea blue-complex as a 1:1:1 complex of **1**, **2** and Al^{3+} [17]. However, the composition was not determined unambiguously.

For the mass analysis of such unstable metal complex anthocyanins, electrospray ionization is a very powerful tool. We determined the molecular weight of several metalloanthocyanins [16] such as commelinin [18], protocyanin [19], protodelphin [20] and cyanosalvianin [21]. Therefore, we applied this ionization method for determination of the composition of hydrangea blue-complex. In this study, we reproduced the blue color of hydrangea in very low concentrated buffer solution (2 mM) at pH 4.0, and the blue solution was analyzed using ESI-TOF Mass. We detected the molecular ion peak of hydrangea blue-complex for the first time.

2. Results and Discussion

2.1. Reproduction of Blue and Red Sepal Colors In Vitro

As previously reported [13,14,17], we performed reproduction experiments by mixing Dp3G (**1**), co-pigment and Al^{3+} in various buffer solutions at a concentration of 100 mM. For NMR measurements, we used an unusually concentrated buffer such as 6 M [17]. In both experiments, we obtained the same blue solution, with identical Vis and CD spectra to the hydrangea sepals and protoplast [13–15]. However, in ESI-Mass analysis with such a high concentrated salt solution, the molecular ion peak of the complex was hardly detected; only the molecular ion peaks attributable to the monomer anthocyanin and co-pigment were observed. This phenomenon, inhibition of ionization by co-existing salts, is usually observed in mass spectrometry. Therefore, we tried to reproduce the hydrangea blue-complex in very low mM salt solutions. Using preliminary experiments, it was found that the blue solution in an acetate buffer less than 5 mM gave a molecular ion peak for the hydrangea blue-complex, and therefore, we chose the concentration of the buffer as 2 mM.

Figure 1 shows the photos of reproduction experiments that mixed **1** (0.1 mM) and 1 eq. of Al^{3+} with 2 eq. of co-pigment (**2**–**4**) in buffer solutions at pH 4.0 (Panel A) and pH 3.2 (Panel B). At pH 4.0, a mixture of **1** and Al^{3+} without co-pigment exhibited a purple color, but the addition of 5CQ (**2**) or 5pCQ (**3**) gave blue solutions (Figure 1A). Contrasting with 5-*O*-acylquinic acids, 3CQ (**4**) gave a purple solution (Figure 1A). At pH 3.2, the solution of **1** with 1 eq. of Al^{3+} exhibited a red color. Two equivalents of 5CQ (**2**) gave a purple solution, and the addition of 2 eq. of 5pCQ (**3**) color led to a solution that became bluer than that of 5CQ. The solution with 3CQ showed a red solution similar to that without co-pigment (Figure 1B). Those results were the same as in our previous reproduction experiment in buffers with higher concentration.
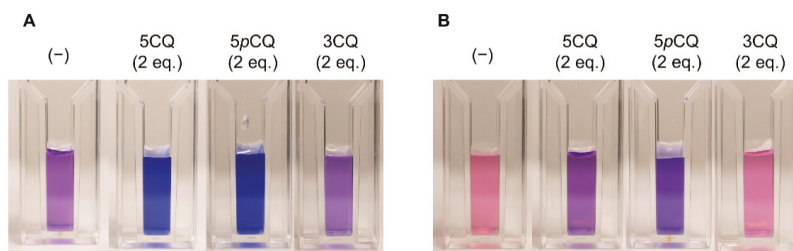
Figure 1. Color of reproduced solutions via mixing of Dp3G (**1**, 0.1 mM) and Al^{3+} (0.1 mM, 1 eq. to **1**) with 0.2 mM (2 eq. to **1**) of co-pigment, 5CQ (**2**), 5pCQ (**3**), or 3CQ (**4**) in buffered solutions of 2 mM. (**A**) Solutions mixed at pH 4.0. (**B**) Solutions mixed at pH 3.2.

Before reproduction experiments, we prepared the pressed juice of blue hydrangea sepals to compare the Vis and CD spectra of the reproduced solutions. Frozen blue sepals were crushed, then, the residues were centrifuged, and the supernatant was filtered to obtain the blue cell sap. Figure 2A shows Vis and CD spectra for the cell sap. In the Vis absorption spectrum, the λ_{vismax} was observed at 580 nm, and in CD, positive Cotton effects were observed near 600 nm, identical to our previous data [13–15]. Figure 2B–E show Vis and CD spectra of reproduced solutions by mixing **1** (0.1 mM) and 1 eq. of Al^{3+} with 0 to 3 eq. of co-pigment at pH 4.0 and 3.2, and the data are summarized in Table 1. As shown in Figure 2B, without a co-pigment, the mixture of **1** and Al^{3+} (1 eq.) gave a reddish-purple solution with λ_{vismax} at 566 nm. Upon addition of 5CQ, the solution color became deeper and bluer; the λ_{vismax} of the Vis spectrum shifted to 576 nm (1 eq.), 579 nm (2 eq.) and 581 nm (3 eq.), but the absorbance peaked with 2 eq. of 5CQ. In CD, when 5CQ was added, the positive Cotton effect near 600 nm appeared. These results indicated that the equivalent of co-pigments should affect λ_{vismax} and absorbance. However, it is difficult to determine the composition of the blue complex by only

UV-Vis and CD spectral experiments. The color was also affected by the concentration of pigments even if the ratio of the components was the same [13–15,17]. We though that this was because the blue complex is unstable in aqueous solutions and exist under equilibrium. Figure 2C shows the results of reproduction experiments in more acidic conditions, at pH 3.2. At pH 3.2, the mixture of **1** and Al^{3+} (1 eq.) gave a red solution with λ_{vismax} at 525 nm. The addition of 5CQ showed hyperchromic and bathochromic effects, but the λ_{vismax} was 543 nm (1 eq.), 567 nm (2 eq.) and 576 nm (3 eq.). Positive Cotton effects near 600 nm were small compared to those at pH 4.0.
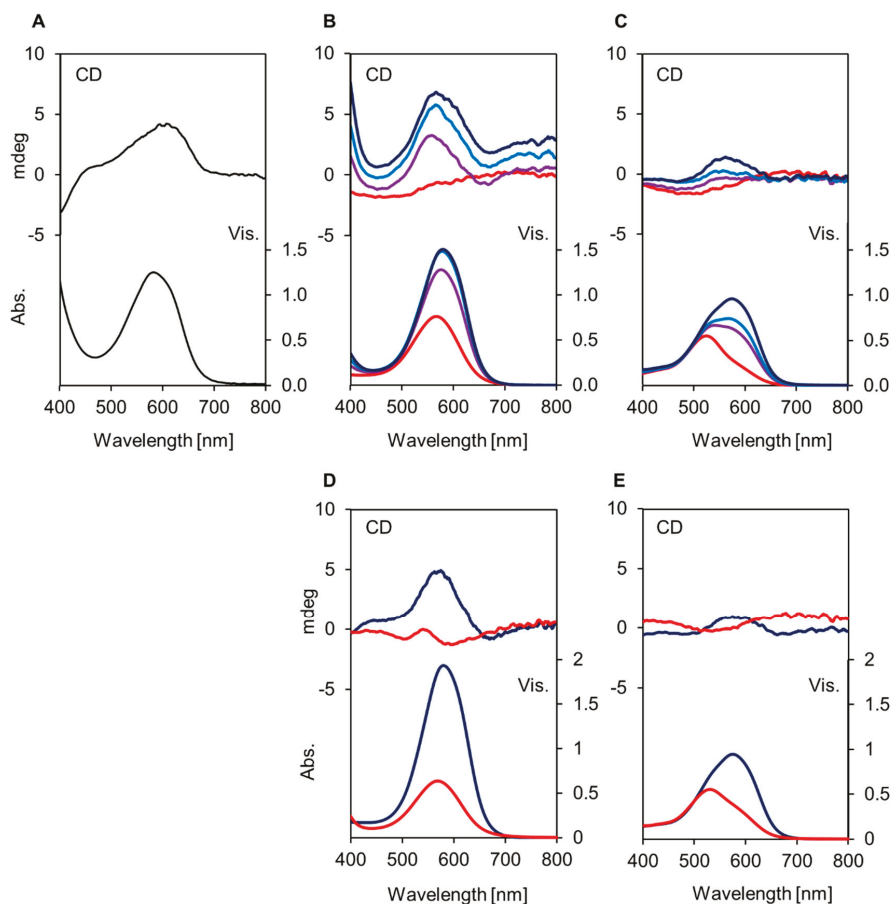
Figure 2. Visible and CD spectra of reproduced solutions by mixing **1** (Dp3G, 0.1 mM) and Al^{3+} (1 eq.) with 0-3 eq. of co-pigment, 5CQ (**2**), 5*p*CQ (**3**), or 3CQ (**4**) in buffered solutions of 2 mM. (**A**) Cell sap obtained from blue hydrangea sepals. (**B**) With 5CQ (**2**) at pH 4.0. —: 0 eq., —: 1 eq., —: 2 eq., —: 3 eq. (**C**) With 5CQ (**2**) at pH 3.2. —: 0 eq., —: 1 eq., —: 2 eq., —: 3 eq. (**D**) With 2 eq. of co-pigment, pH 4.0, —: 5*p*CQ (**3**), —: 3CQ (**4**). (**E**) With 2 eq. of co-pigment, pH 3.2, —: 5*p*CQ (**3**), —: 3CQ (**4**).

Figure 2D,E show the Vis and CD spectra of the reproduced solution obtained by the addition of 2 eq. of 5*p*CQ (**3**) and 3CQ (**4**) at pH 4.0 or 3.2, respectively. At pH 4.0, 2 eq. of 5*p*CQ gave a blue solution with λ_{vismax} at 580 nm, but 3CQ (**4**) gave a reddish-purple-colored solution with λ_{vismax} at 569 nm (Table 1, Figure S1). A positive Cotton effect near 600 nm also indicated that 5*p*CQ gave a similar blue complex to that of 5CQ. At pH 3.2, the λ_{vismax} of the solution of 5*p*CQ was 575 nm and that

of 3CQ was 530 nm. All results were identical to our previously reported data in which the hydrangea blue complex could be reproduced by mixing Dp3G (**1**), approximately 2 eq. of 5-*O*-acylquinic acid, and 1 eq. of Al^{3+} at pH 4.0 [13–15]. The hydrangea red color was reproduced by mixing Dp3G (**1**) and > 1 eq. 3CQ (**4**) w/wo Al^{3+} at pH 3.2 (Figure 2E, Table 1). Therefore, it was confirmed that even in very low-concentration buffer solutions, the blue and red colors of the hydrangea sepals could be reproduced. Comparing the color of the solution mixing with 2 eq. of co-pigment (5CQ or 5*p*CQ) to Dp3G (**1**, 0.1 mM) and Al^{3+} (1 eq.), 5*p*CQ (**3**) showed a bluer color at 575 nm than that of 5CQ (**2**) with λ_{vismax} at 567 nm (Table 1). By addition of 3 eq. of co-pigment, 5CQ and 5*p*CQ gave almost similar color, but the absorbance was much higher with 5*p*CQ than 5CQ (Table 1, Figure S1). This was because the catechol structure of the caffeoyl residue in 5CQ easily chelates to Al^{3+} to form a 5CQ-Al^{3+} complex and reduces the effective concentration of Al^{3+}, which can chelate to form the hydrangea blue–complex. In contrast, 5*p*CQ has no such structure, and therefore, the amount of free Al^{3+} may not decrease. Our previous experiments support this phenomenon. As shown in Figure S2, the addition of Al^{3+} to 5CQ (**2**) showed bathochromic shift of λ_{vismax}, but, no such color change was observed in the case of 5*p*CQ (**3**). Furthermore, the chelating position of 5-*O*-acylquinic acid to Al^{3+} in the hydrangea blue-complex is presumed to be 1-COOH, 1-OH and 5-ester [13,14]. At pH 3.2, the 1-COOH may be protonated, and therefore, the chelating efficiency of 1-COOH might be lowered and the dissociation of the blue complex might be promoted. In both pH, pH 4.0 and pH 3.2, 3CQ did not showed typical color change according to increase in co-pigment amount (Table 1). At pH 4.0 3CQ gave a purple colored solution with λ_{vismax} at 569 nm and at pH 3.2 it showed a red color with λ_{vismax} at 531 nm.

Table 1. λ_{vismax} and absorbance of reproduced solutions. Dp3G (**1**, 0.1 mM), Al^{3+} (0.1 mM, 1 eq.) in 2 mM buffer solution.

Co-Pigment	pH	λ_{max} (A_{max})			
		0 eq.	1 eq.	2 eq.	3 eq.
5CQ (**2**)			576 (1.28)	579 (1.49)	581 (1.51)
5*p*CQ (**3**)	4.0	566 (0.77)	578 (1.56)	580 (1.94)	582 (1.99)
3CQ (**4**)			569 (0.91)	569 (0.64)	569 (0.61)
5CQ (**2**)			543 (0.67)	567 (0.74)	576 (0.96)
5*p*CQ (**3**)	3.2	525 (0.55)	569 (0.73)	575 (0.95)	578 (1.22)
3CQ (**4**)			531 (0.54)	530 (0.55)	531 (0.58)

2.2. ESI-Mass Analysis of Reproduced Blue and Red Solutions

Using the reproduced blue solution in very low-concentration buffered solution (2 mM), the ESI-TOF-Mass spectra were measured. In Figure 3, the mass spectra of the solutions mixed with Dp3G (**1**, 0.1 mM), co-pigment (2 eq.) and Al^{3+} (1 eq.) at pH 4.0 are shown. With positive-ion mode detection, the blue solution mixed with 5CQ gave a molecular ion peak at m/z = 843.16 (Figure 3A). With negative-ion mode detection, the same solution gave a molecular ion peak at m/z = 841.14 (Figure S3A). Using high-resolution mass analysis (HR-MS), the molecular formula was determined to be $C_{37}H_{35}O_{21}Al$ (Figure S4A,B), suggesting that the ion is composed of 1:1:1 of Dp3G (**1**), 5CQ (**2**) and Al. When a blue solution obtained by the addition of 5*p*CQ (**3**) was measured, the molecular ion peak was shifted to m/z = 827.16 (Figure 3B), and with negative-mode detection, the molecular ion was observed at m/z = 825.14 (Figure S3B). HR-MS analysis gave the molecular formula as $C_{37}H_{35}O_{20}Al$ (Figure S4C, D). However, the reddish-purple solution obtained by 3CQ (**4**) gave a very small peak at m/z = 843.16 (Figure 3C). All three spectra showed an ion peak at m/z = 521.07 attributable to Dp3G (**1**, Figure 3). In the buffered solutions and/or during ionization, formation of pseudobase from Dp3G (**1**) by hydration followed by addition of potassium ion gave a pseudobase-potassium ion at m/z = 521.07 (calcd for $C_{21}H_{22}KO_{13}$ [Dp3G + OH + K]$^+$ 521.07). Potassium ion is known to be easily contaminated from calibration solution of pH meter.

To confirm the composition of each molecular ion peak obtained by mixing Dp3G, 5CQ or 5pCQ, and Al^{3+}, MS/MS analysis was performed (Figure S5). With positive-mode detection from the molecular ion peak at m/z = 843.16 (with 5CQ), an ion peak at m/z = 465.10 attributable to Dp3G (**1**), Al-complex with Dp3G (m/z = 489.06) and deglucosyl ion (m/z = 681.11) were observed (Figure S5A). With negative-mode detection from the ion of m/z = 841.15, an ion peak at m/z = 391.05 attributable to potassium adduct of 5CQ was observed (Figure S5B). The MS/MS analysis from the ion at m/z = 827.17 (with 5pCQ) also gave an ion peak at m/z = 465.10 attributable to Dp3G (**1**), and from the ion at m/z = 825.15, an ion peak at m/z =375.05 and potassium adduct of 5pCQ (**3**) were observed (Figure S5C,D). These results strongly suggested that in the blue solution representative of hydrangea blue sepal color, a complex composed of Dp3G, 5-*O*-acylquinic acid and Al^{3+} with the ratio of 1:1:1 should exist, even though the ratio of co-pigment in reproduced solution was 2 eq. to anthocyanin.
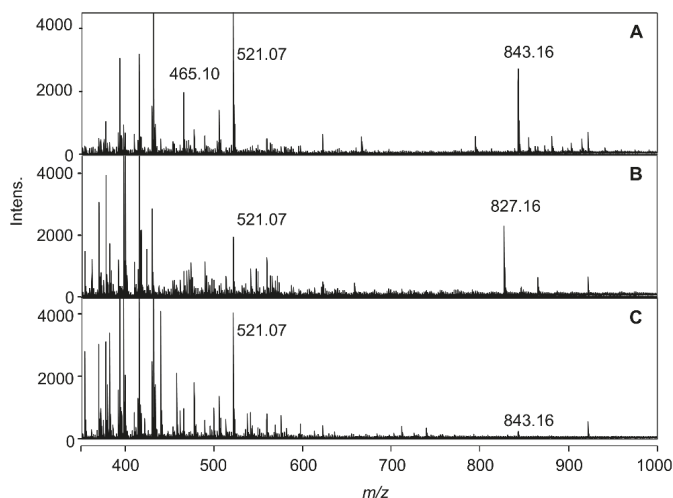
Figure 3. Positive detection ESI-TOF-Mass spectra of reproduced solutions formed by mixing **1** (Dp3G, 0.1 mM) and Al^{3+} (1 eq.) with 2 eq. of co-pigment, 5CQ (**2**), 5pCQ (**3**), or 3CQ (**4**) in buffered solutions at pH 4.0 (2 mM). (**A**) 5 CQ (**2**). (**B**) 5*p* CQ (**3**). (**C**) 3 CQ (**4**).

In Figure 4, the mass spectra of the solutions mixing at pH 3.2 are shown. The 5CQ and 3CQ did not give an obvious molecular ion peak at m/z = 843.15, but the solution with 5pCQ (2 eq.) gave a molecular ion peak at m/z = 827.16. The molecular formula of this ion peak was confirmed to be $C_{37}H_{36}O_{20}Al$ [M + H]$^+$, the same peak detected in Figure 3B. This might give evidence that at pH 3.2, some amount of blue-complex composed of Dp3G, 5pCQ and Al^{3+} at a ratio of 1:1:1 exists, though other co-pigments, such as 5CQ and 3CQ, did not produce the blue-colored complex in such conditions, as suggested from the Vis and CD spectra shown in Figure 2.

We also measured Mass using other reproduced blue solutions with different equivalents of 5CQ (1, 3 eq. to **1**) at pH 4.0 (Figure S6). In the mass spectra, the molecular ion peak at m/z = 843.16 was observed. During all the mass experiments with the mass range to 3500, no ion peak which was composed of Dp3G-5CQ-Al = 1:2:1 and 1:3:1, was detected. These results strongly suggested that in blue solutions reproduced with any ratio of the three components **1**, **2** and Al^{3+}, the complex composed of a ratio of 1:1:1 forms. As mentioned in 2.1, using Vis and CD experiments we could not determine the ratio of complex because the increase in equivalent of co-pigments to **1** increased absorbance at λ_{vismax}. This was because hydrangea blue-complex in buffered solutions was more unstable than other stoichiometric metal complex pigments such as commelinin and protocyanin [16]. This instability gave the characteristics of hydrangea sepal color being easy to change.
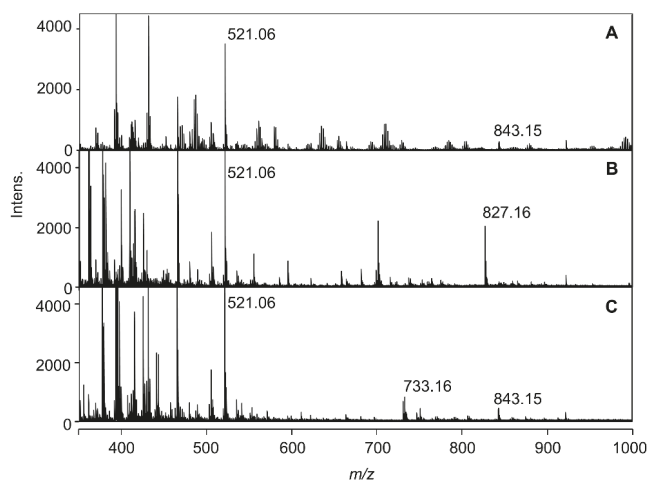
Figure 4. Positive detection ESI-TOF-Mass spectra of reproduced solutions formed by mixing **1** (Dp3G, 0.1 mM) and Al^{3+} (1 eq.) with 2 eq. of co-pigment, 5CQ (**2**), 5*p*CQ (**3**), or 3CQ (**4**) in buffered solutions at pH 3.2 (2 mM). (**A**) 5CQ (**2**). (**B**) 5*p*CQ (**3**). (**C**) 3CQ (**4**).

2.3. Chemical Structure of the Hydrangea Blue-Complex

Unfortunately, the direct mass analysis of cell sap did not give the ion, due to the high salt concentration; the conc. of K$^+$ was higher than 30 mM with ICP-AES analysis (Table S1). However, the results of ESI-TOF-Mass analysis of the reproduced blue-colored solution in a very low-concentration buffer solution gave a distinct molecular ion peak of the complex at $m/z = 843$ with 5CQ and at 827 with 5*p*CQ. This should give strong evidence that the hydrangea blue-complex was composed of Dp3G (**1**), 5CQ (**2**) or 5*p*CQ (**3**) and Al^{3+} in a 1:1:1 ratio. Combined with our previous reproduction experiment using unnatural co-pigments and NMR analysis in 6 M buffer [17], we confirmed the structure of the blue complex shown in Scheme 2. Al^{3+} chelates to the catechol at the B-ring of Dp3G (**1**) to produce quinonoidalbase anion in weakly acidic media, and the hydrangea blue color was developed. In addition, Al^{3+} chelates to the 1-COOH, 1-OH and 5-ester residues of co-pigments, 5CQ (**2**) and 5*p*CQ (**3**) [13,14]. This complex with six-coordination should give a relatively stable coordination structure of Al^{3+} and also stabilizes the anthocyanidin chromophore by hydrophobic interactions between aromatic acyl group of quinic acid ester. However, the coordination stability might not be so high, and thus, the hydrangea blue-complex may exist in equilibrium between the coordination and dissociation states of co-pigments. Therefore, the NMR spectrum of the blue solution may give both broad and unanalyzable signals of components in complex with sharp signals derived from free 5CQ.
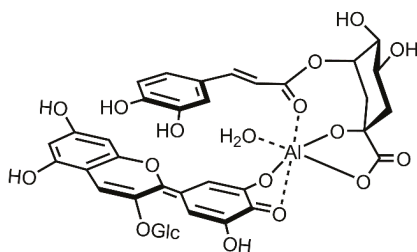
Scheme 2. Structure of hydrangea blue-complex.

3. Materials and Methods

3.1. Plant Materials

H. macrophylla cv. Narumi blue was donated by Okumura Farm (Toyoake, Aichi) and cultivated in the Botanical Garden, Nagoya University Museum.

3.2. Chemicals and Reagents

Dp3G (**1**) was purified from the seed coat of the scarlet bean, *Phaseolus coccineus*, according to our procedure [17]. The co-pigments 5CQ (**2**) and 5*p*CQ (**3**) were synthesized [17,22], and 3CQ (**2**) was purchased from WAKO. Formate buffer (pH 3.2) was prepared by mixing 5 mM formic acid (diluting of 88% Formic acid, WAKO, Osaka, Japan) and 5 mM sodium formate (dissolving of sodium formate, WAKO). Acetate buffer (pH 4.0) was prepared by mixing 5 mM acetic acid (diluting of 99% acetic acid, WAKO) and 5 mM sodium acetate (dissolving of sodium acetate, WAKO). Then, 1 mM aluminum solutions were prepared with $AlCl_3 \cdot 12H_2O$ (Kanto Kagaku, Tokyo, Japan) by dissolution in distilled water.

3.3. Cell Sap Preparation

Blue hydrangea sepals were frozen with liquid nitrogen in a mortar, crushed with a pestle, and centrifuged (4 °C, 48,000× g, 30 min) in a tube with himac CR21F (Hitachi, Tokyo, Japan). After centrifugation, the supernatant (cell sap) was collected by filtering with a cellulose acetate filter (0.45 μM, TOYO Roshi, Tokyo, Japan).

3.4. Reproduction of Hydrangea Blue Color

Stock solutions of Dp3G (**1**, 1 mM) and co-pigments 5CQ (**2**, 2 mM), 5*p*CQ (**3**, 2 mM), and 3CQ (**4**, 2 mM) were prepared just before reproduction experiments by dissolution in water. To a microtube with the volume of 1.5 mL, stock solutions of **1** (70 μL, 100 μM), aluminum solution (70–210 μL, 1–3 eq. to **1**), co-pigment (0–105 μL 0–3 eq.) and a buffer solution (2 mM, 280 μL) were added, and water was added to the mixture to a final solution volume of 700 μL. The solution was mixed, and the pH was measured with a D-21 pH meter (Horiba, Kyoto, Japan) and a LAQUA 9618S-10D electrode (Horiba).

3.5. Measurement of Vis and CD Spectra

Visible adsorption spectra (Vis) were recorded with a UV V-550 spectrometer (Jasco, Hachioji, Japan) from 400 to 800 nm with a scanning rate of 400 nm min^{-1} at 25 °C. CD spectra were measured with a CD J-720 spectrometer (Jasco) over the range of 400–800 nm with a scanning rate of 500 nm min^{-1} at 25 °C, and the mean of 4 trials was determined. The spectra of cell sap were measured in a quartz cell with a path length of 0.1 mm, and those of the reproduced solutions were tested in a quartz cell with a 10-mm path length.

3.6. ESI-TOF-Mass Analysis

After Vis and CD measurements, all samples were frozen and stored at −20 °C until mass analysis. The frozen samples were quickly melted under r.t., and the sample solutions were filtered using a cartridge filter (cellulose acetate, pore size: 0.45 μm, Toyo Roshi). These sample solutions were injected directly by syringe pump (flow rate: 180 μL/hr, KDS-100-CE (KD Scientific Inc., Holliston, MA, USA) without adding any flow-solvent. Electrospray ionization-time of flight mass spectrometry (ESI-TOF-Mass) analysis was performed using a micrOTOF-QII mass spectrometer (Bruker, Billerica, MA, USA) and analyzed using the included software. Mass measurement was performed over the mass range (m/z) from 100 to 3500. HR-MS was recorded by micrOTOF-QII, and calibration was performed with TuneMIX (Agilent Technologies, Santa Clara, CA, USA). The collision energy of the MS/MS analysis was set at 20 eV (positive detection) or 30 eV (negative detection).

4. Conclusions

In conclusion, we obtained the hydrangea blue-complex by mixing Dp3G (**1**), 5CQ (**1**) or 5*p*CQ (**3**) and Al^{3+} in very low-concentration buffer solutions at pH 4.0. By ESI-TOF-Mass analysis, we detected the molecular ion peak, which is attributable to the ratio of **1**, **2** or **3** and Al^{3+} of 1:1:1. Thus, we determined the structure of the complex responsible for the sepal blue coloration to be Dp3G-Al^{3+}-5-*O*-acylquinic acid.

Supplementary Materials: The following are available online: Figures S1–S6 and Table S1.

Author Contributions: K.Y. conceived and designed the experiments; T.I. and K.-i.O. performed the experiments; T.I. and K.-i.O. analyzed the data; T.I., K.-i.O. and K.Y. wrote the paper.

Conflicts of Interest: The authors declare no conflict of interest.

References

1. Ma, J.F.; Ryan, P.R.; Delhaize, E. Aluminium tolerance in plants and the complexing role of organic acids. *Trends Plant Sci.* **2001**, *6*, 273–278. [CrossRef]
2. Yoshida, K.; Ito, D.; Shinkai, Y.; Kondo, T. Change of color and components in sepals of chameleon hydrangea during maturation and senescence. *Phytochemistry* **2008**, *69*, 3159–3165. [CrossRef] [PubMed]
3. Chenery, E.M. The Problem of the blue hydrangea. *J. R. Hort. Soc.* **1937**, *62*, 604–620.
4. Allen, R.C. Influence of aluminum on the flower color of *Hydrangea macrophylla* DC. *Boyce Thompson Inst.* **1943**, *13*, 221–242.
5. Asen, S.; Siegelman, H.W. Effect of aluminum on absorption spectra of the anthocyanin and flavonols from sepals of *Hydrangea macrophylla* var. Merveille. *Proc. Am. Soc. Hort. Sci.* **1957**, *70*, 478–481.
6. Kinraide, T. Identity of the rhizotoxic aluminium species. *Plant Soil* **1991**, *134*, 167–178. [CrossRef]
7. Lawrence, W.J.C.; Price, J.R.; Robinson, G.M.; Robinson, R. CCXV. A survey of anthocyanins. V. *Biochem. J.* **1938**, *32*, 1661–1667. [CrossRef] [PubMed]
8. Robinson, G.M.; Robinson, R. The colloid chemistry of leaf and flower pigments and the precursors of the anthocyanins. *J. Am. Chem. Soc.* **1939**, *61*, 1606–1607. [CrossRef]
9. Hayashi, K.; Abe, Y. Studien über anthocyane, XXIII. Papier-chromatographische übersicht der anthocyane im pflanzeneich. I. *Misc. Rep. Res. Inst. Nat. Resour.* **1958**, *29*, 1–8.
10. Asen, S.; Siegelman, H.W.; Stuart, N.W. Anthocyanin and other phenolic compounds in red and blue sepals of *Hydrangea Macrophylla* var. Merveille. *Proc. Am. Soc. Hort. Sci.* **1957**, *69*, 561–569.
11. Takeda, K.; Yamashita, T.; Takahashi, A.; Timberlake, C.F. Stable blue complexes of anthocyanin-aluminium-3-*p*-coumaroyl- or 3-caffeoyl-quinic acid involved in the blueing of *Hydrangea* flower. *Phytochemistry* **1990**, *29*, 1089–1091. [CrossRef]
12. Yoshida, K.; Toyama-Kato, Y.; Kameda, K.; Kondo, T. Sepal color variation of *Hydrangea macrophylla* and vacuolar pH measured with a proton-selective microelectrode. *Plant Cell Physiol.* **2003**, *44*, 262–268. [CrossRef] [PubMed]
13. Kondo, T.; Toyama-Kato, Y.; Yoshida, K. Essential structure of co-pigment for blue sepal-color development of hydrangea. *Tetrahedron Lett.* **2005**, *46*, 6645–6649. [CrossRef]
14. Toyama-Kato, Y.; Kondo, T.; Yoshida, K. Synthesis of designed acylquinic acid derivatives involved in blue color development of hydrangea and their co-pigmentation effect. *Heterocylces* **2007**, *72*, 239–254. [CrossRef]
15. Ito, D.; Shinkai, Y.; Kato, Y.; Kondo, T.; Yoshida, K. Chemical studies on different color development in blue- and red-colored sepal cells of *Hydrangea macrophylla*. *Biosci. Biotechnol. Biochem.* **2009**, *73*, 1054–1059. [CrossRef] [PubMed]
16. Yoshida, K.; Mori, M.; Kondo, T. Blue flower color development by anthocyanins: From chemical structure to cell physiology. *Nat. Prod. Rep.* **2009**, *26*, 884–915. [CrossRef] [PubMed]
17. Oyama, K.-I.; Yamada, T.; Ito, D.; Kondo, T.; Yoshida, K. Metal-complex pigment involved in the blue sepal color development of hydrangea. *J. Agric. Food. Chem.* **2015**, *63*, 7630–7635. [CrossRef] [PubMed]

18. Kondo, T.; Ueda, M.; Yoshida, K.; Titani, K.; Isobe, M.; Goto, T. Direct observation of a small-molecule associated supramolecular pigment, commelinin, by electrospray ionization mass spectroscopy. *J. Am. Chem. Soc.* **1994**, *116*, 7457–7458. [CrossRef]

19. Kondo, T.; Ueda, M.; Tamura, H.; Yoshida, K.; Isobe, M.; Goto, T. Composition of protocyanin, a self-assembled supramolecular pigment form the blue cornflower *Centaurea cyanus. Angew. Chem. Int. Ed.* **1994**, *33*, 978–979. [CrossRef]

20. Kondo, T.; Oyama, K.; Yoshida, K. Chiral molecular recognition on formation of a metalloanthocyanin: A supramolecular metal complex pigment from blue flower of *Salvia patens. Angew. Chem. Int. Ed.* **2001**, *40*, 894–897. [CrossRef]

21. Mori, M.; Kondo, T.; Yoshida, K. Cyanosalvianin, a supramolecular blue metalloanthocyanin, from petals of *Salvia uliginosa. Phytochemistry* **2008**, *69*, 3151–3158. [CrossRef] [PubMed]

22. Oyama, K.-I.; Watanabe, N.; Yamada, T.; Suzuki, M.; Sekiguchi, Y.; Kondo, T.; Yoshida, K. Efficient and versatile synthesis of 5-*O*-acylquinic acids with a direct esterification using a *p*-methoxybenzyl quinate as a key intermediate. *Tetrahedron* **2015**, *71*, 3120–3130. [CrossRef]

Sample Availability: Samples of the compounds **1**–**3** are available from the authors.

Article

Convenient Synthesis and Physiological Activities of Flavonoids in *Coreopsis lanceolata* L. Petals and Their Related Compounds

Daisuke Nakabo, Yuka Okano, Naomi Kandori, Taisei Satahira, Naoya Kataoka, Junpei Akamatsu and Yoshiharu Okada *

Department of Biotechnology and Chemistry, Faculty of Engineering, Kindai University, Umenobe-1, Takaya, Higashi-hiroshima 739-2116 Japan; 1633850001b@hiro.kindai.ac.jp (D.N.); 1333850001@hiro.kindai.ac.jp (Y.O.); 1433850002@hiro.kindai.ac.jp (N.K.); 0910910069@hiro.kindai.ac.jp (T.S.); 1110910080@hiro.kindai.ac.jp (N.K.); 1410980093@hiro.kindai.ac.jp (J.A.)

* Correspondence: okadasan@hiro.kindai.ac.jp; Tel.: +81-82-434-7000

Abstract: Chalcones, flavanones, and flavonols, including 8-methoxybutin isolated from *Coreopsis lanceolata* L. petals, were successfully synthesized with total yields of 2–59% from *O*-methylpyrogallols using the Horner–Wadsworth–Emmons reaction as a key reaction. Aurones, including leptosidin, were also successfully synthesized with 5–36% total yields using the Aldol condensation reaction as a key reaction. Each chalcone, flavanone, flavonol, and aurone with the 3,4-dihydroxy groups in the B-ring showed high antioxidant activity. Additionally, each of the chalcones, flavanones, flavonols, and aurones with the 2,4-dihydroxy groups in the B-ring showed an excellent whitening ability.

Keywords: *Coreopsis lanceolata* L.; chalcone; flavanone; flavonol; aurone; Horner–Wadsworth–Emmons reaction

1. Introduction

Coreopsis lanceolata L. is a plant native to North America with a yellow flower that blooms from May to June in Japan. We previously reported the isolation and physiological activities of lanceolin (3,4,2′,4′-tetrahydroxy-3′-methoxychalcone-4′-glucoside), 8-methoxybutin (7,3′,4′-trihydroxy-8-methoxyflavanone), and leptosidin (6,3′,4′-trihydroxy-7-methoxyaurone) from *C. lanceolata* L. petals as shown in Figure 1 [1,2]. Koketsu et al. reported the isolation of lanceoletin (3,4,2′,4′-tetrahydroxy-3′-methoxychalcone), okanin (3,4,2′,3′,4′-pentahydroxychalcone), 4-methoxylanceoletin (3,2′,4′-trihydroxy-4,3′-dimethoxychalcone), 8-methoxybutin, leptosidin, and leptosin (6,3′,4′-trihydroxy-7-methoxyaurone-6-glucoside) from *C. lanceolata* L., and the antileukemic activity of 4-methoxylanceoletin [3]. In this paper, we report the synthesis of the several kinds of flavonoids including *C. lanceolata* L. petals and their analogs, and the relationship between structure and physiological activities.
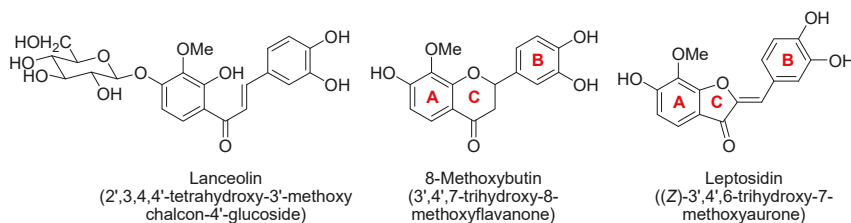
Figure 1. Isolated flavonoids from *Coreopsis lenceolata* L. petals.

2. Results and Discussion

2.1. Flavonoids Synthesis

The process used to synthesize the chalcones, flavanones, and flavonols is shown in Scheme 1. The protection of **1a,b** with chloromethyl methyl ether (MOMCl) produced compound **2a,b**. The lithiation at the 4-position of **2a,b** with *n*-BuLi, which was stabilized by the methoxymethoxy moiety and subsequent ethoxycarbonylation with ethyl chloroformate produced ethyl benzoates **3a,b** with 86 and 73% yields, respectively. The reaction of **3a,b** with dimethyl methylphosphonate in the presence of lithium diisopropylamide (LDA) produced β-keto phosphonates **4a,b** with 87 and 76% yields, respectively. The Horner–Wadsworth–Emmons (HWE) reaction, which is a key reaction in this process, of **4a,b** with aromatic aldehydes **5a–f** in the presence of 1,8-diazabicyclo[5.4.0]undec-7-ene (DBU) as a base produced the corresponding chalcone **6a–l** with 78–92% yields. Subsequently, the deprotection of **6a–l** with 3 M HCl at reflux produced the MOM group deprotected chalcones **7a–l** with 41–98% yields. The structures of **7a–l** were assigned based on their hydrogen and carbon nuclear magnetic resonance (^{1}H-NMR and ^{13}C-NMR) spectral data. The olefinic protons of **7a** were observed at δ 7.43 (d, *J* = 15.9 Hz) and δ 7.83 (d, *J* = 15.4 Hz), respectively. Therefore, the geometry of the double bond of **7a–l** was assigned as the (*E*)-form. A solution of **7a–l** in methanol containing potassium fluoride was heated at reflux to produce flavanones **8a–l** with 46–98% yields [4]. The ^{1}H-NMR spectrum of **8a** shows a signal for the methine proton (dd, *J* = 2.9 and 12.9 Hz) at δ 5.42 and two methylene protons (dd, *J* = 3.2 and 17.1 Hz) at δ 2.72 and (dd, *J* = 12.9 and 16.9 Hz) at δ 3.07, respectively. These coupling constants of 2.9 Hz and 12.9 Hz were the vicinal coupling constants assigned to two methylene protons and a methine proton, respectively. Therefore, the structures of **8a–l** were determined as flavanones. Treatment of **6a–k** with 1.5 M HCl at room temperature produced the chalcones **9a–k** with 65–95% yields, which the 2′-MOM groups activated by the close carbonyl groups, which were selectively deprotected. Treatment of **9a–k** and **7l** with basic H_2O_2 produced the corresponding flavonols **10a–l** with 17–65% yields [5]. ^{13}C-NMR spectrum of **10a** showed a signal for carbonyl carbon at δ 172.70. However, a similar signal for flavanone **8a** was observed at δ 193.21. The carbonyl carbon of **10a** shifted toward the upper field due to the influence of the double bond of flavonol. Therefore, the structures of **10a–l** were determined to be flavonols. Finally, the deprotection of the MOM groups of **10a–l** with 3 M HCl produced compounds **11a–l** with 38–98% yields.

The process used to synthesize the aurones is shown in Scheme 2. The Friedel–Crafts acylation of **1a,b** with chloroacetyl chloride produced compounds **12a,b** with 54 and 58% yields, respectively. The cyclization of **12b** with potassium hydroxide as a base produced benzofuranone **13b** with a low yield of 28% in a complex mixture since the intermolecular reaction of **12b** due to high basicity. Using sodium acetate instead of potassium hydroxide as a base resulted in an increase in the yield to 83%. A similar reaction of **12a** produced **13a** with a 77% yield. The protection of the hydroxyl group of **13a** with MOMCl produced compound **13c** with a 58% yield. The aldol condensation reaction, which is a key reaction in this process, of **13b,c** with aromatic aldehydes **5a–f** in the presence of aluminum oxide produced the corresponding aurones **14a–l** with 31–89% yields [6]. In this reaction, the use of **13a** resulted in decreasing yields. The structures of **14a–l** were classified on the basis of their ^{1}H-NMR and ^{13}C-NMR spectral data. The ^{1}H-NMR spectrum of **14a** showed a signal for an olefinic proton at δ 6.84 (s). The olefinic carbon was observed at δ 112.16. According to the ^{13}C-NMR study of the aurones, a signal for the olefinic carbon of the *Z*-isomer was observed at about 110 ppm, whereas that of *E*-isomer was observed at about 120 ppm [7]. Therefore, the structures of **14a–l** were classified as the (*Z*)-form. Finally, the deprotection of the MOM group of **14a–k** with 3 M HCl produced compounds **15a–k** with 51–97% yields.
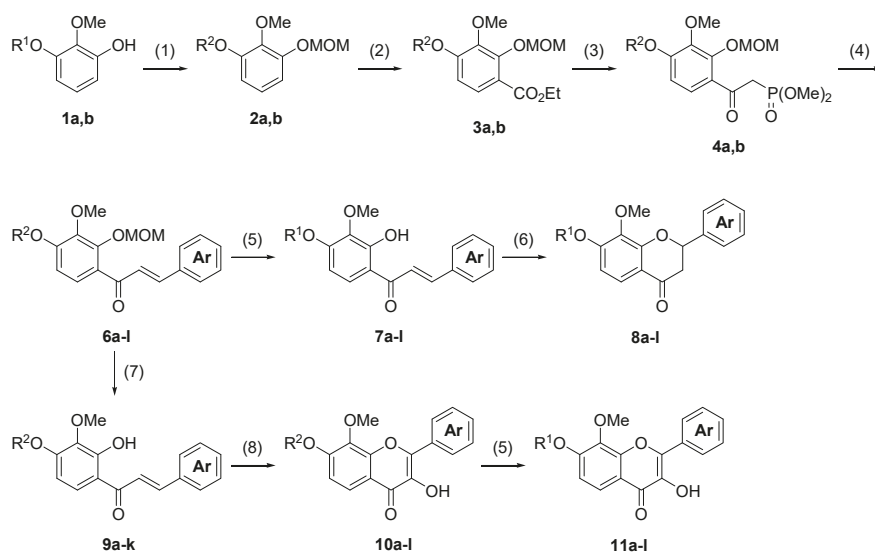
Reagents and conditions: (1) MOMCl, NaH, DMF, 0 °C to r.t.; (2) ^{n}BuLi, ClCO$_2$Et, THF, -70 °C to r.t.; (3) LDA, CH$_3$P(O)(OMe)$_2$, THF, -70 °C to r.t.; (4) DBU, ArCHO **5a-f**, THF, r.t.; (5) 3M HCl, THF, reflux; (6) KF, MeOH, reflux; (7) 1.5M HCl, THF, r.t.; (8) H$_2$O$_2$, 4M NaOH, MeOH, r.t.

Scheme 1. Synthesis of chalcones **7a–l**, flavanones **8a–l**, and flavonols **11a–l**.
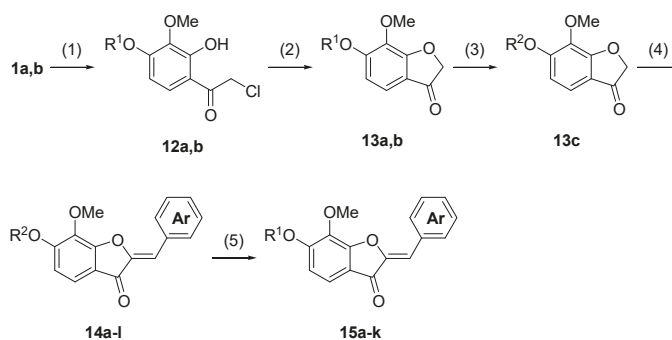
Reagents and conditions: (1) AlCl$_3$, ClCO$_2$Et, ClCH$_2$CH$_2$Cl, r.t.; (2) NaOAc, MeOH, reflux; (3) MOMCl, NaH, DMF, r.t.; (4) Al$_2$O$_3$, ArCHO **5a-f**, CH$_2$Cl$_2$, r.t.; (5) 3M HCl, THF, reflux.

Scheme 2. Synthesis of aurones **15a–k**.

2.2. Antioxidant and Tyrosinase Inhibitory Activity of the Synthesized Flavonoids

Next, the physiological activities of these synthesized compounds were investigated. The antioxidant activity and whitening effect were assessed based on the 2,2-diphenyl-1-picrylhydrazyl (DPPH) free radical scavenging assay [8] and tyrosinase inhibition assay [9], respectively. The results are summarized in Tables 1 and 3–4. The antioxidant activity was evaluated based on the scavenging rate of the DPPH radical under the condition where the final concentration of the samples and DPPH radical were prepared at 0.040 mM and 0.040 mM, respectively. A correlation was found between the physiological activity and

structures of the A-ring and B-ring of the chalcones, flavanones, flavonols, and aurones. On the chalcones, the hydroxyl group at the 4-position on the A-ring was confirmed to be important for the antioxidant activity since the chalcones **7g–l** with a methoxy group instead of a hydroxyl group at the 4-position displayed decreased activity. The flavanones **8a–f** showed lower antioxidant activity than chalcones **7a–f**, since the hydroxyl group at 2-position of the A-ring of chalcone was lost during the conversion into flavanone. For the aurones, **15g–k** with a methoxy substituent at the 6-position on the A-ring showed similar behavior. However, on the flavonols, the compounds **10l** and **11g–k** with methoxy groups at the 7-position on the A-ring showed a higher antioxidant activity than with hydroxyl groups. Each of the chalcones **7b,h**, flavanones **8b,h**, flavonols **11b,h**, and aurones **15b,h** with 3,4-dihydroxy groups on the B-ring had high antioxidant activity. In addition, each with a 4-hydroxy-3-methoxy placement on the B-ring (**7d,j**, **8d,j**, **11d,j**, and **15d,j**) had superior antioxidant effects compared with those with the 3-hydroxy-4-methoxy placement (**7e,k**, **8e,k**, **11e,k**, and **15e,k**). Moreover, the 4-hydroxyl group on the B-ring (**7j**, **8j**, **11j**, and **15j**) seemed to have more influence on the antioxidant activity than a hydroxyl group on the A-ring (**7f**, **8f**, **11f**, and **15f**). The flavanones and aurones showed low antioxidant activity; the correlation between the substitution groups and activity was recorded.

Although each of the chalcones **7c,i** and aurones **15c,i** with the 2,4-dihydroxy groups on the B-ring showed lower antioxidant activity, flavonols **11c,i** with those groups had a high activity due to an apparent enhancement by the hydroxyl group at the 3-position on the C-ring. Since flavanones showed lower radical scavenging activity overall, the double bond in the structure of the flavonoid was thought to strongly influence antioxidant activity. The antioxidant activity in decreasing order was flavonol, chalcone, aurone, and flavanone.

The whitening effect was evaluated by inhibition of tyrosinase activity under the condition where the final concentration of samples and tyrosinase were prepared in 0.10 mM and 20 units/mL, respectively. Each of chalcones **7b,h**, flavanones **8b,h**, flavonol **11h**, and aurones **15b,h** with 3,4-dihydroxy groups on the B-ring displayed a low inhibition rate. In addition, each with a 3-hydroxy-4-methoxy placement on the B-ring (**7e,k**, **8e,k**, **11e,k**, and **15e,k**) had a superior inhibition activity compared to those with the 4-hydroxy-3-methoxy placement (**7d,j**, **8d,j**, **11d,j**, and **15d,j**).

The chalcones **7c,i** and aurones **15c,i** bearing 2,4-dihydroxy groups on the B-ring demonstrated high inhibitory activity potential. Ramsden et al. explained that the reductive elimination and loss of copper atoms from the active site of tyrosinase via the resorcinol (1,3-dihydroxybenzene) moiety resulted in the inactivation of tyrosinase [10]. However, the flavonol **11c,i** bearing a similar group did not inhibit tyrosinase activity. This tendency could potentially be due to the steric hindrance of the hydroxyl group at the 3-position of the flavonol against the 2,4-dihydroxy groups on the B-ring. The whitening effect in decreasing order was chalcone, aurone. flavonol, and flavanone.

Table 1. The DPPH radical scavenging assay and tyrosinase inhibition activity assay of chalcones **7a–l**.
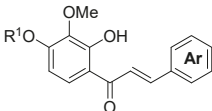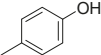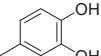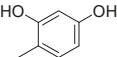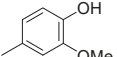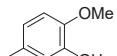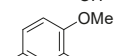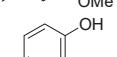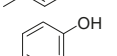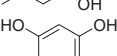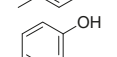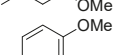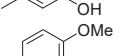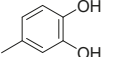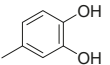
Entry	Compound	R¹	Ar	DPPH Radical Scavenging Assay	Tyrosinase Inhibition Activity Assay
				Scavenging Rate (%) [a]	Inhibition Rate (%) [b]
1	**7a**	H	OH	5.8	46.6
2	**7b**	H	OH OH	96.0	0.0

Table 1. *Cont.*

Entry	Compound	R^1	Ar	DPPH Radical Scavenging Assay	Tyrosinase Inhibition Activity Assay
				Scavenging Rate (%) [a]	Inhibition Rate (%) [b]
3	**7c**	H	HO⟮⟯OH (Me)	31.6	85.7
4	**7d**	H	OH, OMe	56.7	0.0
5	**7e**	H	OMe, OH	20.5	30.3
6	**7f**	H	OMe, OMe	11.4	5.1
7	**7g**	Me	OH	1.0	40.7
8	**7h**	Me	OH, OH	94.0	18.7
9	**7i**	Me	HO⟮⟯OH	6.9	80.3
10	**7j**	Me	OH, OMe	48.8	0.0
11	**7k**	Me	OMe, OH	0.1	22.5
12	**7l**	Me	OMe, OMe	4.2	7.2
13	Lanceolin			94.2 [c]	
14	α-Tocopherol			95.0	
15	Arbutin				9.3

[a] Final concentration: 0.040 mM; [b] Final concentration: 0.10 mM; [c] Tanimoto et al. [1].

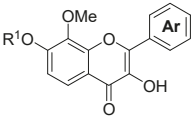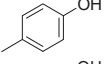**Table 2.** The DPPH radical scavenging assay and tyrosinase inhibition activity assay of flavanones **8a–l**.
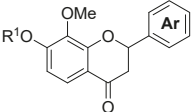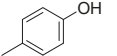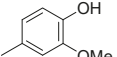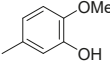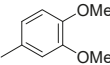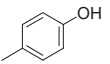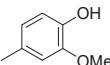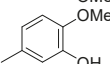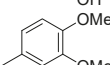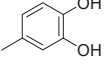
Entry	Compound	R^1	Ar	DPPH Radical Scavenging Assay	Tyrosinase Inhibition Activity Assay
				Scavenging Rate (%) [a]	Inhibition Rate (%) [b]
			R^1O⟮OMe, O, Ar, O⟯		
1	**8a**	H	OH	0.0	5.7
2	**8b**	H	OH, OH	68.4	0.0
3	**8d**	H	OH, OMe	20.3	0.0

Table 2. *Cont.*

Entry	Compound	R^1	Ar	DPPH Radical Scavenging Assay	Tyrosinase Inhibition Activity Assay
				Scavenging Rate (%) [a]	Inhibition Rate (%) [b]
4	**8e**	H	OMe / OH	16.2	0.0
5	**8f**	H	OMe / OMe	4.7	0.0
6	**8g**	Me	OH	0.6	27.4
7	**8h**	Me	OH / OH	94.2	23.1
8	**8j**	Me	OH / OMe	15.6	0.0
9	**8k**	Me	OMe / OH	7.2	0.0
10	**8l**	Me	OMe / OMe	0.0	1.8
11	8-Methoxybutin			94.3 [c]	
12	α-Tocopherol			95.0	
13	Arbutin				9.3

[a] Final concentration: 0.040 mM; [b] Final concentration: 0.10 mM; [c] Okada et al. [2].

Table 3. The DPPH radical scavenging assay and tyrosinase inhibition activity assay of flavonols **11a–l**.
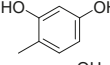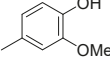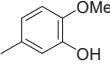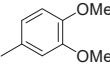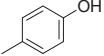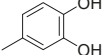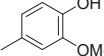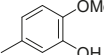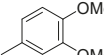
Entry	Compound	R^1	Ar	DPPH Radical Scavenging Assay	Tyrosinase Inhibition Activity Assay
				Scavenging Rate (%) [a]	Inhibition Rate (%) [b]
1	**11a**	H	OH	88.1	16.2
2	**11b**	H	OH / OH	66.5	48.4
3	**11c**	H	HO / OH	70.3	4.2
4	**11d**	H	OH / OMe	55.0 [c]	17.1
5	**11e**	H	OMe / OH	55.3	6.0
6	**11f**	H	OMe / OMe	53.6	4.7

Table 3. *Cont.*

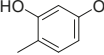| Entry	Compound	R[1]	Ar	DPPH Radical Scavenging Assay	Tyrosinase Inhibition Activity Assay
				Scavenging Rate (%) [a]	Inhibition Rate (%) [b]
7	**11g**	Me	OH	92.5	11.1
8	**11h**	Me	OH, OH	68.6	16.0
9	**11i**	Me	HO, OH	80.6	18.3
10	**11j**	Me	OH, OMe	81.5 [d]	2.7
11	**11k**	Me	OMe, OH	42.1	2.0
12	**10l**	Me	OMe, OMe	46.4	21.2
13	α-Tocopherol			95.0	
14	Arbutin				9.3

[a] Final concentration: 0.040 mM; [b] Final concentration: 0.10 mM; [c] Final concentration: 0.010 mM; [d] Final concentration: 0.020 mM.

**Table 4.** The DPPH radical scavenging assay and tyrosinase inhibition activity assay of aurones **14l** and **15a–k**.
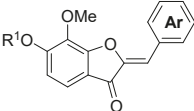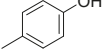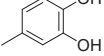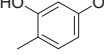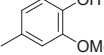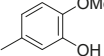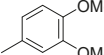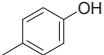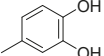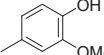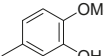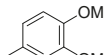
Entry	Compound	R[1]	Ar	DPPH Radical Scavenging Assay	Tyrosinase Inhibition Activity Assay
				Scavenging Rate (%) [a]	Inhibition Rate (%) [b]
1	**15a**	H	OH	4.8	32.5
2	**15b**	H	OH, OH	84.2	0.0
3	**15c**	H	HO, OH	42.8	74.6
4	**15d**	H	OH, OMe	47.4	0.0
5	**15e**	H	OMe, OH	0.0	41.9
6	**15f**	H	OMe, OMe	0.0	10.9
7	**15g**	Me	OH	0.2	46.8

Table 4. *Cont.*

Entry	Compound	R[1]	Ar	DPPH Radical Scavenging Assay	Tyrosinase Inhibition Activity Assay
				Scavenging Rate (%) [a]	Inhibition Rate (%) [b]
8	**15h**	Me		85.8	0.0
9	**15i**	Me		13.3	56.6
10	**15j**	Me		32.8	13.8
11	**15k**	Me		8.9	23.2
12	**14l**	Me		0.5	10.1
13	Leptosidin			93.4 [c]	
14	α-Tocopherol			95.0	
15	Arbutin				9.3

[a] Final concentration: 0.040 mM; [b] Final concentration: 0.10 mM; [c] Okada et al. [2].

3. Materials and Methods

3.1. General Methods

^{1}H-NMR and ^{13}C-NMR spectra were obtained on a JEOL JNM-EX400 (Tokyo, Japan) spectrometer in CDCl$_3$, CD$_3$OD, or dimethyl sulfoxide (DMSO)-d_6 operating at 400 MHz and 100 MHz, respectively, with Me$_4$Si as the internal standard. The absorbance was measured with a microplate reader Corona MTP-300 (Tokyo, Japan). The absorbance was recorded in the 200–600 nm range at room temperature with Jasco V630 (Tokyo, Japan). The mass spectra were obtained on a Shimadzu gas chromatograph mass spectrometer (GCMS)-QP5000 (Kyoto, Japan) with a column temperature of 240 °C, injection temperature of 200 °C, and interface temperature of 230 °C, with He as the carrier gas at a flow rate of 1.3 mL/min. Tetrahydrofuran (THF) was purified by distillation over benzophenone ketyl under an argon atmosphere before use. The melting points were measured in open capillary tubes and were uncorrected.

3.2. The General Procedure for the Protection of 2-O-Methylpyrogallol **1a,b** with Chloromethyl Methyl Ether
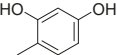
A solution of **1a,b** (100.0 mmol) in *N,N*-dimethylformamide (DMF) (50 mL) was added to a suspension of sodium hydride (60% in mineral oil, 9.60 g, 240.0 mmol or 4.80 g, 120.0 mmol) in DMF (150 mL) at 0 °C. After being stirred at room temperature for 30 min, chloromethyl methyl ether (15.2 mL, 200.0 mmol or 11.4 mL, 150.0 mmol) was added to the mixture at 0 °C. After being stirred at room temperature for 6 h, 100 mL Et$_2$O was added to the mixture. The reaction mixture was poured into ice water (400 mL). The mixture was extracted with Et$_2$O. The organic layer was washed with water and brine and dried over anhydrous MgSO$_4$. The solvent was evaporated in vacuo and the residue was chromatographed on silica gel with CHCl$_3$-Et$_2$O (9:1) to produce **2a,b**.

2-Methoxy-1,3-di(methoxymethoxy)benzene (**2a**): (22.14 g, 97.0 mmol, 97% yield); ^{1}H-NMR (CDCl$_3$) 3.52 (s, 6H, OCH$_3$), 3.89 (s, 3H, OCH$_3$), 5.22 (s, 4H, OCH$_2$), 6.85 (d, *J* = 8.1 Hz, 2H, H-4 and H-6), 6.95 (t, *J* = 8.3 Hz, 1H, H-5).

1,2-Dimethoxy-3-(methoxymethoxy)benzene (**2b**): (18.63 g, 94.0 mmol, 94% yield); ^{1}H-NMR (CDCl$_3$) 3.52 (s, 3H, OCH$_3$), 3.87 (s, 3H, OCH$_3$), 3.87 (s, 3H, OCH$_3$), 5.23 (s, 2H, OCH$_2$), 6.63 (d, *J* = 8.1 Hz, 1H, H-6), 6.80 (d, *J* = 7.6 Hz, 1H, H-4), 6.98 (t, *J* = 8.3 Hz, 1H, H-5).

3.3. The General Procedure for the Preparation of Ethyl Benzoates **3a,b**

n-BuLi (1.55 M hexane solution, 23.2 mL, 36.0 mmol) was added to a solution of **2a,b** (30.0 mmol) in THF (150 mL) at −70 °C. The reaction mixture was warmed to 0 °C and stirred for 90 min at the same temperature. The mixture was cooled to −70 °C and a solution of ethyl chloroformate (14.3 mL, 150.0 mmol) in THF (15 mL) was added dropwise to the mixture. After being stirred for 30 min at −70 °C, the mixture was stirred at room temperature for 2 h. The mixture was poured into an ice-saturated ammonium chloride aqueous solution. The mixture was extracted with Et$_2$O. The organic layer was washed with water and brine and dried over anhydrous MgSO$_4$. The solvent was evaporated in vacuo and the residue was chromatographed on silica gel with CHCl$_3$-Et$_2$O (9:1) to produce **3a,b**.

Ethyl 3-methoxy-2,4-di(methoxymethoxy)benzoate (**3a**): (7.75 g, 25.8 mmol, 86% yield); ^{1}H-NMR (CDCl$_3$) δ 1.38 (t, *J* = 7.1 Hz, 3H, CH$_3$), 3.52 (s, 3H, OCH$_3$), 3.62 (s, 3H, OCH$_3$), 3.89 (s, 3H, OCH$_3$), 4.37 (q, *J* = 7.1 Hz, 1H, OCH$_2$CH$_3$), 5.18 (s, 2H, OCH$_2$), 5.28 (s, 2H, OCH$_2$), 6.97 (d, *J* = 9.0 Hz, 1H, H-5), 7.60 (d, *J* = 8.8 Hz, 1H, H-6); ^{13}C-NMR (CDCl$_3$) δ 14.3, 56.4, 57.4, 60.8, 61.0, 94.6, 100.1, 110.6, 119.3, 126.7, 143.2, 151.3, 154.4, 165.1.

Ethyl 3,4-dimethoxy-2-(methoxymethoxy)benzoate (**3b**): (5.92 g, 21.9 mmol, 73% yield); ^{1}H-NMR (CDCl$_3$) δ 1.38 (t, *J* = 7.1 Hz, 3H, CH$_3$), 3.61 (s, 3H, OCH$_3$), 3.87 (s, 3H, OCH$_3$), 3.91 (s, 3H, OCH$_3$), 4.35 (q, *J* = 7.1 Hz, 1H, OCH$_2$CH$_3$), 5.17 (s, 2H, OCH$_2$), 6.72 (d, *J* = 9.0 Hz, 1H, H-5), 7.65 (d, *J* = 8.8 Hz, 1H, H-6); ^{13}C-NMR (CDCl$_3$) δ 14.3, 56.0, 57.4, 60.7, 60.9, 100.0, 106.9, 118.2, 127.0, 142.5, 151.2, 156.8, 165.2.

3.4. The General Procedure for the Synthesis of α-(Dimethylphosphono)acetylbenzenes **4a,b**

n-BuLi (1.55 M hexane solution, 42.6 mL, 66 mmol) was added to a solution of diisopropylamine (8.4 mL, 60.0 mmol) in THF (100 mL) at −70 °C. After being stirred for 30 min at the same temperature, a solution of dimethyl methylphosphonate (4.47 g, 36.0 mmol) in THF (15 mL) was added dropwise to the mixture. The reaction mixture was stirred for 15 min at −70 °C and a solution of **3a,b** (30.0 mmol) in THF (15 mL) was added to the mixture. The mixture was stirred for 1 h at −70 °C and for 12 h at room temperature. The mixture was poured into ice and a 2 M hydrochloric acid aqueous solution. The mixture was extracted with EtOAc. The organic layer was washed with water and brine and dried over anhydrous MgSO$_4$. The solvent was evaporated in vacuo and the residue was chromatographed on silica gel with CHCl$_3$-Et$_2$O-MeOH (8:2:0.05) to produce **4a,b**.

α-(Dimethylphosphono)-3-methoxy-2,4-di(methoxymethoxy)acetophenone (**4a**): (9.87 g, 26.1 mmol, 87% yield); reddish brown viscous oil; ^{1}H-NMR (CDCl$_3$) δ 3.52 (s, 6H, OCH$_3$), 3.77 (d, *J* = 11.2 Hz, 6H, P(O)OCH$_3$), 3.86 (d, *J* = 21.5 Hz, 2H, P(O)CH$_2$), 3.88 (s, 3H, OCH$_3$), 5.23 (s, 2H, OCH$_2$), 5.28 (s, 2H, OCH$_2$), 6.98 (d, *J* = 8.8 Hz, 1H, H-5), 7.48 (d, *J* = 9.0 Hz, 1H, H-6); ^{13}C-NMR (CDCl$_3$) δ 40.3 (d, *J* = 131.0 Hz, P(O)CH$_2$), 52.9 (d, *J* = 5.8 Hz, P(O)OCH$_3$), 56.5, 58.0, 61.0, 94.7, 100.2, 110.9, 126.0, 126.9 (d, *J* = 3.3 Hz, Ar), 142.0, 150.6, 155.1, 191.9 (d, *J* = 6.6 Hz, CO).

α-(Dimethylphosphono)-3,4-dimethoxy-2-(methoxymethoxy)acetophenone (**4b**): (7.94 g, 22.8 mmol, 76% yield); reddish brown viscous oil; ^{1}H-NMR (CDCl$_3$) δ 3.51 (s, 3H, OCH$_3$), 3.77 (d, *J* = 11.0 Hz, 6H, OCH$_3$), 3.86 (s, 3H, OCH$_3$), 3.87 (d, *J* = 21.7 Hz, 2H, P(O)CH$_2$), 3.92 (s, 3H, OCH$_3$), 5.23 (s, 2H, OCH$_2$), 6.76 (d, *J* = 8.8 Hz, 1H, H-5), 7.54 (d, *J* = 8.8 Hz, 1H, H-6); ^{13}C-NMR (CDCl$_3$) δ 40.9 (d, *J* = 131.0 Hz, P(O)CH$_2$), 52.8 (d, *J* = 6.6 Hz, P(O)OCH$_3$), 56.1, 58.0, 60.8, 100.2, 107.3, 125.9 (d, *J* = 3.3 Hz, Ar), 126.2, 141.4, 150.6, 157.5, 191.7 (d, *J* = 6.6 Hz, CO).

3.5. The General Procedure for the Synthesis of Chalcones **6a–l**

A solution of benzaldehydes **5a–f** (1.2 mmol) in THF (1 mL) was added to a solution of **4a,b** (1.0 mmol) and DBU (0.30 g, 2.0 mmol) in THF (4 mL) at room temperature. The reaction mixture was poured into an ice-saturated ammonium chloride aqueous solution and extracted with Et$_2$O. The organic layer was washed with water and brine and dried over anhydrous MgSO$_4$. The solvent was evaporated in vacuo and the residue was chromatographed on a preparative thin layer chromatography (hexane:EtOAc = 3:2) to produce chalcones **6a–l**.

3′-Methoxy-4,2′,4′-tri(methoxymethoxy)chalcone (**6a**): (0.35 g, 0.78 mmol, 78% yield); yellow viscous oil; ^{1}H-NMR (CDCl$_3$) δ 3.45 (s, 3H, OCH$_3$), 3.49 (s, 3H, OCH$_3$), 3.53 (s, 3H, OCH$_3$), 3.93 (s, 3H, OCH$_3$), 5.15 (s, 2H, OCH$_2$), 5.21 (s, 2H, OCH$_2$), 5.28 (s, 2H, OCH$_2$), 7.00 (d, *J* = 8.8 Hz, 1H, H-5′), 7.06 (d, *J* = 8.5 Hz, 2H, H-3 and H-5), 7.34 (d, *J* = 15.9 Hz, 1H, H-α), 7.37 (d, *J* = 8.8 Hz, 1H, H-6′), 7.57 (d, *J* = 8.8 Hz, 2H, H-2 and H-6), 7.64 (d, *J* = 15.6 Hz, 1H, H-β); ^{13}C-NMR (CDCl$_3$) δ 56.0, 56.3, 57.5, 60.9, 94.0, 94.7, 99.9, 111.1, 116.2, 124.7, 125.0, 128.5, 128.8, 129.8, 142.4, 142.9, 149.8, 153.7, 158.7, 190.9.

3′-Methoxy-3,4,2′,4′-tetra(methoxymethoxy)chalcone (**6b**): (0.44 g, 0.91 mmol, 91% yield); yellow viscous oil; ^{1}H-NMR (CDCl$_3$) δ 3.46 (s, 3H, OCH$_3$), 3.52 (s, 3H, OCH$_3$), 3.54 (s, 6H, OCH$_3$), 3.93 (s, 3H, OCH$_3$), 5.16 (s, 2H, OCH$_2$), 5.27 (s, 2H, OCH$_2$), 5.28 (s, 2H, OCH$_2$), 5.28 (s, 2H, OCH$_2$), 7.00 (d, *J* = 8.8 Hz, 1H, H-5′), 7.17 (d, *J* = 8.5 Hz, 1H, H-5), 7.26 (dd, *J* = 2.0 and 8.3 Hz, 1H, H-6), 7.31 (d, *J* = 15.9 Hz, 1H, H-α), 7.36 (d, *J* = 8.8 Hz, 1H, H-6′), 7.43 (d, *J* = 2.0 Hz, H-2), 7.58 (d, *J* = 15.9 Hz, 1H, H-β); ^{13}C-NMR (CDCl$_3$) δ 56.1, 56.2, 56.3, 57.5, 60.9, 94.7, 94.9, 95.3, 99.8, 111.1, 116.0, 116.0, 123.5, 124.9, 125.2, 128.6, 129.2, 142.4, 143.1, 147.0, 149.0, 149.7, 153.7, 190.9.

3′-Methoxy-2,4,2′,4′-tetra(methoxymethoxy)chalcone (**6c**): (0.43 g, 0.89 mmol, 89% yield); yellow viscous oil; ^{1}H-NMR (CDCl$_3$) δ 3.47 (s, 3H, OCH$_3$), 3.49 (s, 3H, OCH$_3$), 3.50 (s, 3H, OCH$_3$), 3.53 (s, 3H, OCH$_3$), 3.93 (s, 3H, OCH$_3$), 5.14 (s, 2H, OCH$_2$), 5.20 (s, 2H, OCH$_2$), 5.25 (s, 2H, OCH$_2$), 5.29 (s, 2H, OCH$_2$), 6.73 (dd, *J* = 2.2 Hz and 8.5 Hz, 1H, H-5), 6.84 (d, *J* = 2.2 Hz, 1H, H-3), 7.00 (d, *J* = 8.8 Hz, 1H, H-5′), 7.38 (d, *J* = 8.3 Hz, 1H, H-6′), 7.41 (d, *J* = 14.6 Hz, 1H, H-α), 7.60 (d, *J* = 8.5 Hz, 1H, H-6), 8.02 (d, *J* = 15.9 Hz, 1H, H-β); ^{13}C-NMR (CDCl$_3$) δ 56.3, 56.4, 56.5, 57.7, 61.1, 94.1, 94.5, 94.8, 100.0, 103.1, 109.2, 111.1, 118.4, 124.9, 125.2, 129.2, 129.3, 138.3, 142.5, 149.9, 153.7, 157.4, 160.0, 191.3.

3,3′-Dimethoxy-4,2′,4′-tri(methoxymethoxy)chalcone (**6d**): (0.37 g, 0.82 mmol, 82% yield); ^{1}H-NMR (CDCl$_3$) δ 3.46 (s, 3H, OCH$_3$), 3.52 (s, 3H, OCH$_3$), 3.54 (s, 3H, OCH$_3$), 3.93 (s, 6H, OCH$_3$), 5.16 (s, 2H, OCH$_2$), 5.28 (s, 2H, OCH$_2$), 5.29 (s, 2H, OCH$_2$), 7.00 (d, *J* = 8.8 Hz, 1H, H-5′), 7.16–7.17 (m, 3H, H-2, H-5 and H-6), 7.36 (d, *J* = 15.9 Hz, 1H, H-α), 7.37 (d, *J* = 8.5 Hz, 1H, H-6′), 7.61 (d, *J* = 15.9 Hz, 1H, H-β); ^{13}C-NMR (CDCl$_3$) δ 55.8, 56.2, 56.3, 57.5, 60.9, 94.7, 95.0, 99.8, 110.6, 111.1, 115.6, 122.3, 124.9, 125.0, 128.6, 129.1, 142.4, 143.2, 148.3, 149.5, 149.7, 153.7, 190.9.

4,3′-Dimethoxy-3,2′,4′-tri(methoxymethoxy)chalcone (**6e**): (0.36 g, 0.80 mmol, 80% yield); ^{1}H-NMR (CDCl$_3$) δ 3.46 (s, 3H, OCH$_3$), 3.53 (s, 6H, OCH$_3$), 3.92 (s, 3H, OCH$_3$), 3.93 (s, 3H, OCH$_3$), 5.16 (s, 2H, OCH$_2$), 5.26 (s, 2H, OCH$_2$), 5.28 (s, 2H, OCH$_2$), 6.91 (d, *J* = 8.3 Hz, 1H, H-5), 7.00 (d, *J* = 8.8 Hz, 1H, H-5′), 7.26 (dd, *J* = 1.7 Hz and 8.3 Hz, 1H, H-6), 7.29 (d, *J* = 15.6 Hz, 1H, H-α), 7.35 (d, *J* = 8.8 Hz, 1H, H-6′), 7.43 (d, *J* = 1.7 Hz, 1H, H-2), 7.59 (d, *J* = 15.6 Hz, 1H, H-β); ^{13}C-NMR (CDCl$_3$) δ 55.9, 56.3, 56.4, 57.6, 61.0, 94.9, 95.5, 99.9, 111.2, 111.5, 115.6, 124.1, 124.9, 125.1, 128.0, 128.9, 142.6, 143.5, 146.6, 149.9, 151.7, 153.8, 191.3.

3,4,3′-Trimethoxy-2′,4′-di(methoxymethoxy)chalcone (**6f**): (0.35 g, 0.83 mmol, 83% yield); ^{1}H-NMR (CDCl$_3$) δ 3.47 (s, 3H, OCH$_3$), 3.54 (s, 3H, OCH$_3$), 3.93 (s, 3H, OCH$_3$), 3.93 (s, 6H, OCH$_3$), 5.17 (s, 2H, OCH$_2$), 5.29 (s, 2H, OCH$_2$), 6.88 (d, *J* = 8.3 Hz, 1H, H-5), 7.00 (d, *J* = 8.8 Hz, H-5′), 7.15 (d, *J* = 2.0 Hz, 1H, H-2), 7.20 (dd, *J* = 2.0 Hz and 8.3 Hz, 1H, H-6), 7.32 (d, *J* = 15.9 Hz, 1H, H-α), 7.37 (d, *J* = 8.5 Hz, 1H, H-6′), 7.62 (d, *J* = 15.9 Hz, 1H, H-β); ^{13}C-NMR (CDCl$_3$) δ 55.9, 56.0, 56.5, 57.7, 61.1, 94.9, 100.0, 110.0, 111.0, 111.3, 123.1, 124.7, 125.2, 127.9, 128.9, 143.7, 149.1, 150.0, 151.2, 153.9, 191.2.

3′,4′-Dimethoxy-4,2′-di(methoxymethoxy)chalcone (**6g**): (0.35 g, 0.89 mmol, 89% yield); yellow viscous oil; ^{1}H-NMR (CDCl$_3$) δ 3.45 (s, 3H, OCH$_3$), 3.49 (s, 3H, OCH$_3$), 3.91 (s, 3H, OCH$_3$), 3.93 (s, 3H, OCH$_3$), 5.15 (s, 2H, OCH$_2$), 5.22 (s, 2H, OCH$_2$), 6.78 (d, *J* = 8.8 Hz, 1H, H-5′), 7.06 (d, *J* = 8.5 Hz, 2H, H-3 and H-5), 7.39 (d, *J* = 15.9 Hz, 1H, H-α), 7.45 (d, *J* = 8.5 Hz, 1H, H-6′), 7.58 (d, *J* = 8.8 Hz, 2H, H-2 and H-6), 7.66 (d, *J* = 15.9 Hz, 1H, H-β); ^{13}C-NMR (CDCl$_3$) δ 56.1, 56.2, 57.7, 61.0, 94.1, 100.1, 107.4, 116.3, 124.8, 125.5, 127.8, 128.7, 129.9, 141.7, 142.8, 150.0, 156.4, 158.8, 190.8.

3′,4′-Dimethoxy-3,4,2′-tri(methoxymethoxy)chalcone (**6h**): (0.35 g, 0.79 mmol, 79% yield); ^{1}H-NMR (CDCl$_3$) δ 3.46 (s, 3H, OCH$_3$), 3.52 (s, 3H, OCH$_3$), 3.54 (s, 3H, OCH$_3$), 3.91 (s, 3H, OCH$_3$), 3.93 (s, 3H, OCH$_3$), 5.16 (s, 2H, OCH$_2$), 5.28 (s, 2H, OCH$_2$), 5.29 (s, 2H, OCH$_2$), 6.78 (d, *J* = 8.8 Hz, 1H, H-5′), 7.18 (d, *J* = 8.5 Hz, 1H, H-5), 7.26 (dd, *J* = 2.0 Hz and 8.5 Hz, 1H, H-6), 7.36 (d, *J* = 15.9 Hz, 1H, H-α), 7.44 (d, *J* = 8.5 Hz, 1H, H-6′), 7.44 (d, *J* = 2.0 Hz, 1H, H-2), 7.60 (d, *J* = 15.6 Hz, 1H, H-β); ^{13}C-NMR (CDCl$_3$) δ 56.0, 56.2, 56.3, 57.6, 60.9, 94.9, 95.3, 99.9, 107.3, 116.0, 116.0, 123.6, 125.3, 125.4, 127.6, 129.3, 141.7, 143.0, 147.1, 149.0, 150.0, 156.4, 191.0.

3′,4′-Dimethoxy-2,4,2′-tri(methoxymethoxy)chalcone (**6i**): (0.37 g, 0.83 mmol, 83% yield); yellow viscous oil; ^{1}H-NMR (CDCl$_3$) δ 3.46 (s, 3H, OCH$_3$), 3.49 (s, 3H, OCH$_3$), 3.50 (s, 3H, OCH$_3$), 3.91 (s, 3H, OCH$_3$), 3.93 (s, 3H, OCH$_3$), 5.14 (s, 2H, OCH$_2$), 5.20 (s, 2H, OCH$_2$), 5.25 (s, 2H, OCH$_2$), 6.73 (dd, *J* = 2.2 and 8.5 Hz, 1H, H-5), 6.77 (d, *J* = 8.8 Hz, 1H, H-5′), 6.84 (d, *J* = 2.2 Hz, 1H, H-3), 7.45 (d, *J* = 15.9 Hz, 1H, H-α), 7.45 (d, *J* = 8.8 Hz, 1H, H-6′), 7.61 (d, *J* = 8.5 Hz, 1H, H-6), 8.03 (d, *J* = 15.9 Hz, 1H, H-β); ^{13}C-NMR (CDCl$_3$) δ 55.9, 56.1, 56.2, 57.5, 60.8, 94.0, 94.4, 99.8, 103.0, 107.2, 109.1, 118.4, 124.8, 125.3, 127.9, 129.1, 137.9, 141.6, 149.7, 156.1, 157.3, 159.8, 191.0.

3,3′,4′-Trimethoxy-4,2′-di(methoxymethoxy)chalcone (**6j**): (0.33 g, 0.78 mmol, 78% yield); yellow viscous oil; ^{1}H-NMR (CDCl$_3$) δ 3.46 (s, 3H, OCH$_3$), 3.52 (s, 3H, OCH$_3$), 3.91 (s, 3H, OCH$_3$), 3.93 (s, 6H, OCH$_3$), 5.17 (s, 2H, OCH$_2$), 5.28 (s, 2H, OCH$_2$), 6.78 (d, *J* = 8.8 Hz, 1H, H-5′), 7.17 (br s, 3H, H-2, H-5, and H-6), 7.39 (d, *J* = 15.6 Hz, 1H, H-α), 7.45 (d, *J* = 8.8 Hz, 1H, H-6′), 7.63 (d, *J* = 15.9 Hz, 1H, H-β); ^{13}C-NMR (CDCl$_3$) δ 55.9, 56.0, 56.3, 57.6, 60.9, 95.1, 100.0, 107.4, 110.7, 115.6, 122.5, 125.1, 125.5, 127.6, 129.3, 141.7, 143.1, 148.4, 149.6, 150.0, 156.5, 190.8.

4,3′,4′-Trimethoxy-3,2′-di(methoxymethoxy)chalcone (**6k**): (0.37 g, 0.89 mmol, 89% yield); yellow viscous oil; ^{1}H-NMR (CDCl$_3$) δ 3.46 (s, 3H, OCH$_3$), 3.53 (s, 3H, OCH$_3$), 3.91 (s, 3H, OCH$_3$), 3.92 (s, 3H, OCH$_3$), 3.93 (s, 3H, OCH$_3$), 5.16 (s, 2H, OCH$_2$), 5.26 (s, 2H, OCH$_2$), 6.77 (d, *J* = 8.8 Hz, 1H, H-5′), 6.91 (d, *J* = 8.5 Hz, 1H, H-5), 7.27 (dd, *J* = 2.0 Hz and 8.3 Hz, 1H, H-6), 7.34 (d, *J* = 15.9 Hz, 1H, H-α), 7.43 (d, *J* = 8.5 Hz, 1H, H-6′), 7.44 (d, *J* = 1.7 Hz, 1H, H-2), 7.60 (d, *J* = 15.6 Hz, 1H, H-β); ^{13}C-NMR (CDCl$_3$) δ 55.9, 56.0, 56.2, 57.5, 60.8, 95.3, 99.8, 107.2, 111.4, 115.5, 123.9, 124.7, 125.2, 127.6, 127.9, 141.6, 143.0, 146.3, 149.7, 151.5, 156.2, 190.7.

3,4,3′,4′-Tetramethoxy-2′-(methoxymethoxy)chalcone (**6l**): (0.36 g, 0.92 mmol, 92% yield); ^{1}H-NMR (CDCl$_3$) δ 3.46 (s, 3H, OCH$_3$), 3.91 (s, 3H, OCH$_3$), 3.93 (s, 3H, OCH$_3$), 3.93 (s, 3H, OCH$_3$), 3.93 (s, 3H, OCH$_3$), 5.17 (s, 2H, OCH$_2$), 6.78 (d, *J* = 8.8 Hz, 1H, H-5′), 6.89 (d, *J* = 8.3 Hz, 1H, H-5), 7.16 (d, *J* = 2.0 Hz, 1H, H-2), 7.20 (dd, *J* = 2.0 Hz and 8.3 Hz, 1H, H-6), 7.37 (d, *J* = 15.9 Hz, 1H, H-α), 7.44 (d, *J* = 8.5 Hz, 1H, H-6′), 7.63 (d, *J* = 15.9 Hz, 1H, H-β); ^{13}C-NMR (CDCl$_3$) δ 55.8, 55.9, 56.0, 57.6, 60.9, 100.0, 107.4, 109.9, 110.9, 123.0, 124.6, 125.4, 127.7, 127.9, 141.7, 143.3, 149.0, 149.9, 151.0, 156.4, 190.9.

3.6. The General Procedure for the Deprotection of **6a–l**

A solution of **6a–l** (1.0 mmol) in methanol (5 mL) and 3 M hydrochloric acid (5 mL) was refluxed for 1 h. The mixture was extracted with EtOAc. The organic layer was washed with water and brine and dried over anhydrous MgSO$_4$. The solvent was evaporated in vacuo and the residue was chromatographed on preparative thin layer chromatography (hexane:EtOAc = 2:3) to produce aurones **7a–l**.

4,2′,4′-Trihydroxy-3′-methoxychalcone (**7a**): (0.22 g, 0.76 mmol, 76% yield); yellowish brown solid, 204–209 °C; ^{1}H-NMR (CDCl$_3$:DMSO-d_6 = 9:1) δ 3.93 (s, 3H, OCH$_3$), 6.53 (d, J = 8.8 Hz, 1H, H-5′), 6.90 (d, J = 7.8 Hz, 2H, H-3 and H-5), 7.43 (d, J = 15.9 Hz, 1H, H-α), 7.54 (d, J = 8.1 Hz, 2H, H-2 and H-6), 7.61 (d, J = 8.8 Hz, 1H, H-6′), 7.83 (d, J = 15.4 Hz, 1H, H-β), 9.25 (s, 1H, OH), 9.57 (s, 1H, OH), 13.76 (s, 1H, OH); ^{13}C-NMR (CDCl$_3$:DMSO-d_6 = 9:1) δ 60.3, 107.4, 114.0, 115.9, 116.4, 125.7, 125.7, 130.2, 134.6, 144.3, 156.2, 158.3, 159.9, 191.7; UV/Vis (3.0 × 10^{-5} M, DMSO); λ = 380.0 nm (ε, 3.0 × 10^4).

3,4,2′,4′-Tetrahydroxy-3′-methoxychalcone (**7b**): (0.25 g, 0.84 mmol, 84% yield); yellow solid, 191–195 °C; ^{1}H-NMR (DMSO-d_6) δ 3.74 (s, 3H, OCH$_3$), 6.48 (d, J = 9.3 Hz, 1H, H-5′), 6.82 (d, J = 8.3 Hz, 1H, H-5), 7.22 (dd, J = 2.0 Hz and 8.3 Hz, 1H, H-6), 7.29 (d, J = 2.0 Hz, 1H, H-2), 7.65 (d, J = 15.1 Hz, 1H, H-α), 7.69 (d, J = 15.1 Hz, 1H, H-β), 7.93 (d, J = 9.3 Hz, 1H, H-6′), 9.12 (s, 1H, OH), 9.71 (s, 1H, OH), 10.40 (s, 1H, OH), 13.74 (s, 1H, OH); ^{13}C-NMR (DMSO-d_6) δ 59.7, 107.9, 113.7, 115.7, 115.9, 117.2, 122.4, 126.2, 126.8, 134.7, 144.9, 145.6, 149.0, 157.1, 158.5, 192.0; UV/Vis (2.6 × 10^{-5} M, DMSO); λ = 400.5 nm (ε, 2.1 × 10^4).

2,4,2′,4′-Tetrahydroxy-3′-methoxychalcone (**7c**): (0.14 g, 0.47 mmol, 47% yield); reddish orange solid, 189–193 °C; ^{1}H-NMR (CD$_3$OD) δ 3.85 (s, 3H, OCH$_3$), 6.34 (d, J = 2.2 Hz, 1H, H-3), 6.36 (dd, J = 2.2 Hz and 9.5 Hz, 1H, H-5), 6.46 (d, J = 8.8 Hz, 1H, H-5′), 7.51 (d, J = 8.3 Hz, 1H, H-6), 7.68 (d, J = 9.5 Hz, 1H, H-6′), 7.69 (d, J = 15.1 Hz, 1H, H-α), 8.10 (d, J = 15.4 Hz, 1H, H-β); ^{13}C-NMR (CD3OD) δ 60.8, 103.4, 108.6, 109.0, 115.4, 115.5, 117.4, 127.2, 132.3, 136.0, 142.2, 157.6, 159.3, 160.6, 162.6, 194.3; UV/Vis (2.8 × 10^{-5} M, DMSO); λ = 399.0 nm (ε, 3.0 × 10^4).

4,2′,4′-Trihydroxy-3,3′-dimethoxychalcone (**7d**): (0.30 g, 0.95 mmol, 95% yield); orange solid, 158–163 °C; ^{1}H-NMR (DMSO-d_6) δ 3.76 (s, 3H, OCH$_3$), 3.89 (s, 3H, OCH$_3$), 6.51 (d, J = 9.0 Hz, 1H, H-5′), 6.86 (d, J = 8.1 Hz, 1H, H-5), 7.30 (d, J = 8.3 Hz, 1H, H-6), 7.56 (br s, 1H, H-2), 7.76 (d, J = 15.1 Hz, 1H, H-α), 7.81 (d, J = 15.4 Hz, 1H, H-β), 8.01 (d, J = 8.8 Hz, 1H, H-6′), 9.77 (s, 1H, OH), 10.46 (s, 1H, OH), 13.83 (s, 1H, OH); ^{13}C-NMR (DMSO-d_6) δ 55.8, 59.7, 107.7, 111.5, 113.5, 115.4, 117.2, 124.4, 125.9, 126.7, 134.5, 144.6, 147.7, 149.7, 156.9, 158.2, 191.7; UV/Vis (2.5 × 10^{-5} M, DMSO); λ = 397.5 nm (ε, 2.8 × 10^4).

3,2′,4′-Trihydroxy-4,3′-dimethoxychalcone (**7e**): (0.29 g, 0.90 mmol, 90% yield); yellowish brown solid, 180–185 °C; ^{1}H-NMR (DMSO-d_6) δ 3.77 (s, 3H, OCH$_3$), 3.87 (s, 3H, OCH$_3$), 6.52 (d, J = 8.8 Hz, 1H, H-5′), 7.02 (d, J = 8.5 Hz, 1H, H-5), 7.34 (dd, J = 1.7 Hz and 8.3 Hz, 1H, H-6), 7.39 (d, J = 1.5 Hz, 1H, H-2), 7.73 (d, J = 15.4 Hz, 1H, H-α), 7.78 (d, J = 15.4 Hz, 1H, H-β), 8.00 (d, J = 9.0 Hz, 1H, H-6), 9.24 (s, 1H, OH), 10.54 (s, 1H, OH), 13.76 (s, 1H, OH); ^{13}C-NMR (DMSO-d_6) δ 55.7, 59.8, 107.9, 111.7, 113.6, 114.9, 118.1, 122.2, 126.8, 127.3, 134.5, 144.3, 146.4, 150.2, 157.0, 158.3, 191.7; UV/Vis (2.7 × 10^{-5} M, DMSO); λ = 400.0 nm (ε, 2.2 × 10^4).

2′,4′-Dihydroxy-3,4,3′-trimethoxychalcone (**7f**): (0.32 g, 0.98 mmol, 98% yield); orange-yellow solid, 140–144 °C; ^{1}H-NMR (DMSO-d_6) δ 3.75 (s, 3H, OCH$_3$), 3.83 (s, 3H, OCH$_3$), 3.88 (s, 3H, OCH$_3$), 6.51 (d, J = 9.0 Hz, 1H, H-5′), 7.04 (d, J = 8.3 Hz, 1H, H-5), 7.57 (d, J = 2.0 Hz, 1H, H-2), 7.41 (dd, J = 2.0 Hz and 8.3 Hz, 1H, H-6), 7.78 (d, J = 15.4 Hz, 1H, H-α), 7.86 (d, J = 15.4 Hz, 1H, H-β), 8.02 (d, J = 9.0 Hz, 1H, H-6′), 10.48 (s, 1H, OH), 13.76 (s, 1H, OH); ^{13}C-NMR (DMSO-d_6) δ 55.6, 55.7, 59.7, 107.7, 110.6, 111.3, 113.5, 118.2, 124.2, 126.8, 127.1, 134.5, 144.2, 148.7, 151.2, 157.0, 158.2, 191.7; UV/Vis (3.3 × 10^{-5} M, DMSO); λ = 394.0 nm (ε, 2.3 × 10^4).

4,2′-Dihydroxy-3′,4′-dimethoxychalcone (**7g**): (0.25 g, 0.84 mmol, 84% yield); yellow solid, 152–156 °C; ^{1}H-NMR (CDCl$_3$) δ 3.93 (s, 3H, OCH$_3$), 3.96 (s, 3H, OCH$_3$), 5.75 (s, 1H, OH), 6.54 (d, J = 9.0 Hz, 1H, H-5′), 6.90 (d, J = 8.5 Hz, 2H, H-3 and H-5), 7.45 (d, J = 15.4 Hz, 1H, H-α), 7.57 (d, J = 8.5 Hz, 2H, H-2 and H-6), 7.69 (d, J = 9.0 Hz, 1H, H-6′), 7.86 (d, J = 15.4 Hz, 1H, H-β), 13.35 (s, 1H, OH); ^{13}C-NMR (CDCl$_3$) δ 56.0, 60.6, 102.6, 115.4, 115.8, 117.4, 125.6, 127.2, 130.3, 136.3, 144.3, 157.8, 157.9, 158.0, 192.1.

3,4,2′-Trihydroxy-3′,4′-dimethoxychalcone (**7h**): (0.16 g, 0.51 mmol, 51% yield); green-yellow solid, 147–151 °C; ^{1}H-NMR (CDCl$_3$) δ 3.93 (s, 3H, OCH$_3$), 3.95 (s, 3H, OCH$_3$), 5.91 (s, 1H, OH), 6.01 (s, 1H, OH), 6.54 (d, J = 9.0 Hz, 1H, H-5′), 6.92 (d, J = 8.1 Hz, 1H, H-5), 7.14 (d, J = 8.3 Hz, 1H, H-6), 7.18 (s, 1H,

H-2), 7.39 (d, *J* = 15.1 Hz, 1H, H-α), 7.67 (d, *J* = 9.0 Hz, 1H, H-6′), 7.77 (d, *J* = 15.4 Hz, 1H, H-β), 13.39 (s, 1H, OH); ^{13}C-NMR (CD3OD) δ 56.5, 60.8, 104.2, 115.8, 116.5, 116.7, 117.9, 123.7, 127.6, 128.1, 137.3, 146.6, 146.7, 150.0, 158.5, 159.6, 193.9.

2,4,2′-Trihydroxy-3′,4′-methoxychalcone (**7i**): (0.13 g, 0.41 mmol, 41% yield); reddish orange solid, 120–125 °C; ^{1}H-NMR (DMSO-d_6) δ 3.69 (s, 3H, OCH$_3$), 3.87 (s, 3H, OCH$_3$), 6.33 (dd, *J* = 1.7 Hz and 8.8 Hz, 1H, H-5), 6.38 (d, *J* = 1.7 Hz, 1H, H-3), 6.68 (d, *J* = 8.8 Hz, 1H, H-5′), 7.70 (d, *J* = 14.9 Hz, 1H, H-α), 7.73 (d, *J* = 7.6 Hz, 1H, H-6′), 7.95 (d, *J* = 9.0 Hz, 1H, H-6), 8.09 (d, *J* = 15.4 Hz, 1H, H-β), 10.33 (br s, 2H, OH), 13.57 (s, 1H, OH); ^{13}C-NMR (DMSO-d_6) δ 56.2, 59.9, 102.4, 103.5, 108.2, 113.2, 115.2, 115.4, 126.5, 130.6, 135.7, 140.5, 157.1, 157.9, 159.3, 161.8, 192.4.

4,2′-Dihydroxy-3,3′,4′-trimethoxychalcone (**7j**): (0.25 g, 0.77 mmol, 77% yield); yellowish brown solid, 117–124 °C; ^{1}H-NMR (CDCl$_3$) δ 3.93 (s, 3H, OCH$_3$), 3.96 (s, 3H, OCH$_3$), 3.98 (s, 3H, OCH$_3$), 5.96 (s, 1H, OH), 6.54 (d, *J* = 9.0 Hz, 1H, H-5′), 6.97 (d, *J* = 8.3 Hz, 1H, H-5), 7.13 (d, *J* = 1.7 Hz, 1H, H-2), 7.25 (dd, *J* = 1.7 Hz and 8.5 Hz, 1H, H-6), 7.43 (d, *J* = 15.4 Hz, 1H, H-α), 7.70 (d, *J* = 9.0 Hz, 1H, H-6′), 7.85 (d, *J* = 15.4 Hz, 1H, H-β), 13.32 (s, 1H, OH); ^{13}C-NMR (CDCl$_3$) δ 56.0, 56.1, 60.6, 102.6, 110.3, 114.8, 115.6, 117.6, 123.2, 125.7, 127.2, 136.6, 144.9, 146.6, 148.3, 158.1, 158.2, 192.2.

3,2′-Dihydroxy-4,3′,4′-trimethoxychalcone (**7k**): (0.24 g, 0.73 mmol, 73% yield); yellowish brown solid, 107–110 °C; ^{1}H-NMR (CDCl$_3$) δ 3.92 (s, 3H, OCH$_3$), 3.95 (s, 3H, OCH$_3$), 3.96 (s, 3H, OCH$_3$), 5.73 (s, 1H, OH), 6.54 (d, *J* = 9.0 Hz, 1H, H-5′), 6.89 (d, *J* = 8.3 Hz, 1H, H-5), 7.14 (dd, *J* = 2.2 Hz and 8.3 Hz 1H, H-6), 7.30 (d, *J* = 2.2 Hz, 1H, H-2), 7.44 (d, *J* = 15.4 Hz, 1H, H-α), 7.68 (d, *J* = 9.0 Hz, 1H, H-6′), 7.82 (d, *J* = 15.4 Hz, 1H, H-β), 13.32 (s, 1H, OH); ^{13}C-NMR (CDCl$_3$) δ 55.9, 56.0, 60.5, 102.6, 110.3, 112.6, 115.4, 118.0, 122.9, 125.6, 128.1, 136.4, 144.3, 145.6, 148.7, 157.9, 158.0, 192.0.

2′-Hydroxy-3,4,3′,4′-tetramethoxychalcone (**7l**): (0.28 g, 0.80 mmol, 80% yield); orange-yellow solid, 117–120 °C; ^{1}H-NMR (CDCl$_3$) δ 3.93 (s, 3H, OCH$_3$), 3.95 (s, 3H, OCH$_3$), 3.96 (s, 3H, OCH$_3$), 3.98 (s, 3H, OCH$_3$), 6.55 (d, *J* = 9.3 Hz, 1H, H-5′), 6.92 (d, *J* = 8.3 Hz, 1H, H-5), 7.17 (d, *J* = 2.0 Hz, 1H, H-2), 7.27 (dd, *J* = 2.0 Hz and 8.3 Hz 1H, H-6), 7.45 (d, *J* = 15.4 Hz, 1H, H-α), 7.72 (d, *J* = 9.3 Hz, 1H, H-6′), 7.87 (d, *J* = 15.4 Hz, 1H, H-β), 13.34 (s, 1H, OH); ^{13}C-NMR (CDCl$_3$) δ 55.9, 55.9, 56.0, 60.5, 102.4, 109.9, 110.8, 115.3, 117.6, 123.1, 125.6, 127.3, 136.4, 144.5, 148.9, 151.2, 157.9, 158.0, 191.9.

3.7. The General Procedure for the Synthesis of Flavanones **8a–l**

A solution of **7a–l** (1.0 mmol) and potassium fluoride (0.29 g, 5.0 mmol) in methanol (5 mL) was refluxed for 24 h. The water was added to a mixture solution and the mixture was extracted with EtOAc. The organic layer was washed with water and brine and dried over anhydrous MgSO$_4$. The solvent was evaporated in vacuo and the residue was chromatographed on a preparative thin layer chromatography (hexane:toluene:EtOAc = 1:1:1) to produce flavanones **8a–l**.

7,4′-Dihydroxy-8-methoxyflavanone (**8a**): (0.28 g, 0.98 mmol, 98% yield); pale yellow solid, 195–200 °C; ^{1}H-NMR (CD$_3$OD) δ 2.72 (dd, *J* = 2.9 Hz and 17.1 Hz, 1H, H-3ax), 3.07 (dd, *J* = 12.9 Hz and 17.1 Hz, 1H, H-3eq), 3.79 (s, 3H, OCH$_3$), 5.42 (dd, *J* = 2.9 Hz and 12.9 Hz, 1H, H-2), 6.55 (d, *J* = 8.8 Hz, 1H, H-6), 6.82 (td, *J* = 2.0 Hz and 8.5 Hz, 2H, H-3′ and H-5′), 7.35 (td, *J* = 1.7 Hz and 8.3 Hz, 2H, H-2′ and H-6′), 7.51 (d, *J* = 8.8 Hz, 1H, H-5); ^{13}C-NMR (CD$_3$OD) δ 44.8, 61.2, 81.3, 111.4, 115.9, 116.2, 123.7, 128.8, 131.0, 136.4, 157.4, 158.5, 158.7, 193.2; UV/Vis (1.5 × 10^{-3} M, DMSO); λ = 376.4 nm (ε, 1.2 × 10^2).

7,3′,4′-Trihydroxy-8-methoxyflavanone (**8b**): (0.20 g, 0.65 mmol, 65% yield); yellowish brown solid, 188–193 °C; ^{1}H-NMR (CD$_3$OD) δ 2.72 (dd, *J* = 2.9 Hz and 17.1 Hz, 1H, H-3ax), 3.01 (dd, *J* = 12.9 Hz and 17.1 Hz, 1H, H-3eq), 3.81 (s, 3H, OCH$_3$), 5.35 (dd, *J* = 2.9 Hz and 12.9 Hz, 1H, H-2), 6.54 (d, *J* = 8.8 Hz, 1H, H-6), 6.78 (d, *J* = 8.1 Hz, 1H, H-5′), 6.82 (dd, *J* = 1.7 Hz and 8.3 Hz, 1H, H-6′), 6.97 (d, *J* = 1.7 Hz, 1H, H-2′), 7.50 (d, *J* = 8.8 Hz, 1H, H-5); ^{13}C-NMR (CD$_3$OD) δ 44.9, 61.3, 81.3, 111.3, 114.5, 115.9, 116.1, 119.0, 123.6, 131.7, 136.4, 146.2, 146.6, 157.3, 158.4, 193.2; UV/Vis (2.6 × 10^{-5} M, CH$_3$OH); λ = 392.0 nm (ε, 2.7 × 10^3).

7,4′-Dihydroxy-8,3′-dimethoxyflavanone (8d): (0.28 g, 0.90 mmol, 90% yield); yellow solid, 193–195 °C;
^{1}H-NMR (CD$_3$OD) δ 2.67 (dd, *J* = 2.7 Hz and 16.8 Hz, 1H, H-3ax), 3.16 (dd, *J* = 12.7 Hz and 16.6 Hz,
1H, H-3eq), 3.69 (s, 3H, OCH$_3$), 3.77 (s, 3H, OCH$_3$), 5.46 (dd, *J* = 2.4 Hz and 12.9 Hz, 1H, H-2), 6.57
(d, *J* = 8.8 Hz, 1H, H-6), 6.79 (d, *J* = 8.8 Hz, 1H, H-6′), 6.93 (d, *J* = 8.8 Hz, 1H, H-5′), 7.11 (s, 1H, H-2′), 7.40
(d, *J* = 8.8 Hz, 1H, H-5); ^{13}C-NMR (CD$_3$OD) δ 43.2, 55.7, 60.2, 79.4, 110.4, 111.0, 114.4, 115.1, 119.3, 122.0,
129.9, 135.1, 146.7, 147.4, 155.7, 156.9, 190.2; UV/Vis (2.7 × 10^{-5} M, CH$_3$OH); λ = 383.8 nm (ε, 1.7 × 10^4).

7,3′-Dihydroxy-8,4′-dimethoxyflavanone (8e): (0.27 g, 0.85 mmol, 85% yield); yellowish brown solid,
180–185 °C; ^{1}H-NMR (DMSO-*d*$_6$) δ 2.69 (dd, *J* = 2.9 Hz and 16.8 Hz, 1H, H-3ax), 3.06 (dd, *J* = 12.5 Hz and
16.8 Hz, 1H, H-3eq), 3.71 (s, 3H, OCH$_3$), 3.78 (s, 3H, OCH$_3$), 5.48 (dd, *J* = 2.9 Hz Hz and 12.5 Hz, 1H,
H-2), 6.58 (d, *J* = 8.8 Hz, 1H, H-6), 6.91 (dd, *J* = 1.7 Hz and 8.3 Hz, 1H, H-6′), 6.95 (d, *J* = 8.5 Hz, 1H, H-5′),
6.97 (d, *J* = 2.4 Hz, 1H, H-2′), 7.41 (d, *J* = 8.8 Hz, 1H, H-5); ^{13}C-NMR (DMSO-*d*$_6$) δ 43.1, 55.6, 60.1, 78.9,
110.2, 111.8, 113.8, 114.3, 117.3, 121.8, 131.4, 134.9, 146.2, 147.5, 155.4, 156.6, 189.8; UV/Vis (2.9 × 10^{-5} M,
DMSO); λ = 363.6 nm (ε, 2.2 × 10^3).

7-Hydroxy-8,3′,4′-trimethoxyflavanone (8f): (0.30 g, 0.90 mmol, 90% yield); yellow solid, 143–145 °C;
^{1}H-NMR (CDCl$_3$) δ 2.87 (dd, *J* = 2.9 Hz and 16.8 Hz, 1H, H-3ax), 3.06 (dd, *J* = 12.9 Hz and 16.8 Hz, 1H,
H-3eq), 3.91 (s, 6H, OCH$_3$), 3.95 (s, 3H, OCH$_3$), 5.46 (dd, *J* = 2.7 Hz and 12.9 Hz, 1H, H-2), 6.59 (s, 1H,
OH), 6.68 (d, *J* = 8.8 Hz, 1H, H-6), 6.91 (d, *J* = 8.8 Hz, 1H, H-5′), 7.02–7.03 (m, 2H, H-2′ and H-6′), 7.65
(d, *J* = 8.5 Hz, 1H, H-5); ^{13}C-NMR (CDCl$_3$) δ 44.2, 55.8, 61.1, 80.0, 109.1, 109.3, 110.9, 115.4, 118.4, 122.9,
130.9, 134.1, 148.8, 149.0, 154.2, 155.0, 190.2; UV/Vis (2.3 × 10^{-5} M, CHCl$_3$); λ = 392.6 nm (ε, 1.4 × 10^3).

4′-Hydroxy-7,8-dimethoxyflavanone (8g): (0.26 g, 0.87 mmol, 87% yield); yellow solid, 165–170 °C;
^{1}H-NMR (CDCl$_3$) δ 2.88 (dd, *J* = 2.9 Hz and 16.8 Hz, 1H, H-3ax), 3.07 (dd, *J* = 12.2 Hz and 16.8 Hz, 1H,
H-eq), 3.88 (s, 3H, OCH$_3$), 3.94 (s, 3H, OCH$_3$), 5.45 (dd, *J* = 2.9 Hz and 12.2 Hz, 1H, H-2), 6.39 (s, 1H, OH),
6.67 (d, *J* = 9.0 Hz, 1H, H-6), 6.87 (d, *J* = 8.5 Hz, 2H, H-3′ and H-5′), 7.31 (d, *J* = 8.8 Hz, 2H, H-2′ and H-6′),
7.73 (d, *J* = 9.0 Hz, 1H, H-5); ^{13}C-NMR (CDCl$_3$) δ 44.0, 56.3, 61.1, 79.7, 105.7, 115.5, 116.0, 123.1, 127.8,
130.3, 136.7, 155.4, 156.2, 158.8, 191.6; UV/Vis (3.1 × 10^{-5} M, CHCl$_3$); λ = 391.2 nm (ε, 1.2 × 10^3).

3′,4′-Dihydroxy-7,8-dimethoxyflavanone (8h) (0.20 g, 0.63 mmol, 63% yield); yellowish brown solid,
175–177 °C; ^{1}H-NMR (DMSO-*d*$_6$) δ 2.71 (dd, *J* = 2.9 Hz and 16.8 Hz, 1H, H-3ax), 3.11 (dd, *J* = 12.5 Hz
and 16.8 Hz, 1H, H-3eq), 3.69 (s, 3H, OCH$_3$), 3.87 (s, 3H, OCH$_3$), 5.45 (dd, *J* = 2.9 Hz and 12.5 Hz, 1H,
H-2), 6.76–6.77 (m, 2H, H-6 and H-6′), 6.84 (d, *J* = 8.8 Hz, 1H, H-5′), 6.92 (d, *J* = 1.7 Hz, 1H, H-2′), 7.55
(d, *J* = 8.8 Hz, 1H, H-5); ^{13}C-NMR (DMSO-*d*$_6$) δ 43.2, 56.1, 60.2, 79.1, 105.8, 114.1, 115.1, 115.6, 117.6,
121.9, 129.6, 136.2, 144.9, 145.4, 154.7, 158.0, 190.3.

4′-Hydroxy-7,8,3′-trimethoxyflavanone (8j): (0.30 g, 0.91 mmol, 91% yield); yellow solid, 145–146 °C;
^{1}H-NMR (CDCl$_3$) δ 2.88 (dd, *J* = 2.9 Hz and 16.8 Hz, 1H, H-3ax), 3.06 (dd, *J* = 12.5 Hz and 16.8 Hz, 1H,
H-3eq), 3.87 (s, 3H, OCH$_3$), 3.91 (s, 3H, OCH$_3$), 3.93 (s, 3H, OCH$_3$), 5.44 (dd, *J* = 2.9 Hz and 12.5 Hz, 1H,
H-2), 5.78 (s, 1H, OH), 6.67 (d, *J* = 8.8 Hz, 1H, H-6), 6.92–6.99 (m, 2H, H-5′ and H-6′), 7.02 (d, *J* = 1.5 Hz,
1H, H-2′), 7.71 (d, *J* = 9.0 Hz, 1H, H-5); ^{13}C-NMR (CDCl$_3$) δ 44.1, 55.8, 56.1, 60.9, 79.7, 105.4, 108.6,
114.2, 115.9, 119.1, 122.6, 130.4, 136.7, 145.6, 146.3, 155.0, 158.4, 190.6; UV/Vis (6.1 × 10^{-4} M, CHCl$_3$);
λ = 370.0 nm (ε, 1.9 × 10^3).

3′-Hydroxy-7,8,4′-trimethoxyflavanone (8k): (0.30 g, 0.90 mmol, 90% yield); ^{1}H-NMR (CDCl$_3$) δ 2.85
(dd, *J* = 2.9 Hz and 16.8 Hz, 1H, H-3ax), 3.02 (dd, *J* = 12.5 Hz and 16.8 Hz, 1H, H-3eq), 3.87 (s, 3H,
OCH$_3$), 3.89 (s, 3H, OCH$_3$), 3.93 (s, 3H, OCH$_3$), 5.41 (dd, *J* = 2.9 Hz and 12.5 Hz, 1H, H-2), 5.94 (s, 1H,
OH), 6.66 (d, *J* = 9.0 Hz, 1H, H-6), 6.87 (d, *J* = 8.3 Hz, 1H, H-5′), 6.95 (dd, *J* = 2.0 Hz and 8.3 Hz, 1H,
H-6′), 7.08 (d, *J* = 2.0 Hz, 1H, H-2′), 7.70 (d, *J* = 9.0 Hz, 1H, H-5); ^{13}C-NMR (CDCl$_3$) δ 44.1, 55.9, 56.1,
60.9, 79.4, 105.4, 110.4, 112.4, 115.9, 117.7, 122.6, 131.6, 136.7, 145.5, 146.5, 155.0, 158.4, 190.7.

3′,4′,7,8-Tetramethoxyflavanone (8l): (0.16 g, 0.46 mmol, 46% yield); yellow solid, 141–143 °C; ^{1}H-NMR
(CDCl$_3$) δ 2.90 (dd, *J* = 3.2 Hz and 16.8 Hz, 1H, H-3ax), 3.07 (dd, *J* = 12.2 Hz and 16.8 Hz, 1H, H-eq), 3.88
(s, 3H, OCH$_3$), 3.90 (s, 3H, OCH$_3$), 3.91 (s, 3H, OCH$_3$), 3.94 (s, 3H, OCH$_3$), 5.48 (dd, *J* = 2.9 Hz and 12.2

Hz, 1H, H-2), 6.67 (d, *J* = 9.0 Hz, 1H, H-6), 6.90 (d, *J* = 8.1 Hz, 1H, H-5′), 7.01–7.04 (m, 2H, H-2′ and H-6′), 7.71 (d, *J* = 8.8 Hz, 1H, H-5); ¹³C-NMR (CDCl₃) δ 44.1, 55.8, 55.8, 56.1, 60.9, 79.5, 105.4, 109.2, 110.8, 116.0, 118.4, 122.6, 131.0, 136.7, 148.8, 148.9, 154.9, 158.4, 190.5; GC-MS 344 (M+, 44), 180 (35), 164 (100).

*3.8. The General Procedure for the Synthesis of Chalcones **9a–k** by the Selective Deprotection of the 2′-Methoxymethyl Group*

A solution of **6a–k** (1.0 mmol) and 1.5 M hydrochloric acid aqueous solution (5 mL) in THF (5 mL) was stirred at room temperature for 45 min. The mixture was extracted with Et₂O. The organic layer was washed with water and brine and dried over anhydrous MgSO₄. The solvent was evaporated in vacuo and the residue was chromatographed on a preparative thin layer chromatography (hexane:EtOAc = 3:2) to produce chalcones **9a–k**.

2′-Hydroxy-3′-methoxy-4,4′-di(methoxymethoxy)chalcone (**9a**): (0.29 g, 0.77 mmol, 77% yield); ¹H-NMR (CDCl₃) δ 3.50 (s, 3H, OCH₃), 3.53 (s, 3H, OCH₃), 3.94 (s, 3H, OCH₃), 5.23 (s, 2H, OCH₂), 5.32 (s, 2H, OCH₂), 6.75 (d, *J* = 9.0 Hz, 1H, H-5′), 7.09 (d, *J* = 8.8 Hz, 2H, H-3 and H-5), 7.47 (d, *J* = 15.4 Hz, 1H, H-α), 7.61 (d, *J* = 8.8 Hz, 2H, H-2 and H-6), 7.64 (d, *J* = 9.0 Hz, 1H, H-6′), 7.88 (d, *J* = 15.4 Hz, 1H, H-β), 13.33 (s, 1H, OH); ¹³C-NMR (CDCl₃) δ 56.1, 56.4, 60.6, 94.0, 94.5, 106.0, 116.0, 116.3, 117.9, 125.2, 128.1, 130.0, 144.3, 155.6, 158.2, 159.1, 192.1.

2′-Hydroxy-3′-methoxy-3,4,4′-tri(methoxymethoxy)chalcone (**9b**): (0.38 g, 0.87 mmol, 87% yield); orange solid, 84–88 °C; ¹H-NMR (CDCl₃) δ 3.53 (s, 3H, OCH₃), 3.53 (s, 3H, OCH₃), 3.56 (s, 3H, OCH₃), 3.95 (s, 3H, OCH₃), 5.30 (s, 2H, OCH₂), 5.30 (s, 2H, OCH₂), 5.32 (s, 2H, OCH₂), 6.76 (d, *J* = 9.0 Hz, 1H, H-5′), 7.21 (d, *J* = 8.5 Hz, 1H, H-5), 7.29 (dd, *J* = 2.0 Hz and 8.5 Hz, 1H, H-6), 7.44 (d, *J* = 15.4 Hz, 1H, H-α), 7.48 (d, *J* = 2.0 Hz, 1H, H-2), 7.66 (d, *J* = 9.0 Hz, H-6′), 7.84 (d, *J* = 15.4 Hz, 1H, H-β), 13.31 (s, 1H, OH); ¹³C-NMR (CDCl₃) δ 56.3, 56.3, 56.4, 60.7, 94.6, 95.0, 95.5, 106.2, 116.1, 116.1, 118.6, 124.1, 125.5, 129.0, 137.4, 144.3, 144.5, 147.3, 149.6, 155.8, 158.4, 192.3.

2′-Hydroxy-3′-methoxy-2,4,4′-tri(methoxymethoxy)chalcone (**9c**): (0.32 g, 0.73 mmol, 73% yield); ¹H-NMR (CDCl₃) δ 3.50 (s, 3H, OCH₃), 3.53 (s, 3H, OCH₃), 3.53 (s, 3H, OCH₃), 3.94 (s, 3H, OCH₃), 5.21 (s, 2H, OCH₂), 5.29 (s, 2H, OCH₂), 5.32 (s, 2H, OCH₂), 6.75 (d, *J* = 9.0 Hz, 1H, H-5′), 6.76 (dd, *J* = 2.2 Hz and 8.5 Hz, 1H, H-5), 6.87 (d, *J* = 2.2 Hz, 1H, H-3), 7.59 (d, *J* = 15.6 Hz, 1H, H-α), 7.61 (d, *J* = 8.5 Hz, 1H, H-6), 7.64 (d, *J* = 9.3 Hz, 1H, H-6′), 8.21 (d, *J* = 15.4 Hz, 1H, H-β), 13.46 (s, 1H, OH); ¹³C-NMR (CDCl₃) δ 56.2, 56.3, 56.4, 60.6, 94.1, 94.4, 94.5, 103.1, 105.9, 109.2, 116.1, 118.1, 118.3, 125.2, 129.8, 137.2, 139.8, 155.4, 157.6, 158.2, 160.3, 192.6.

2′-Hydroxy-3,3′-dimethoxy-4,4′-di(methoxymethoxy)chalcone (**9d**): (0.35 g, 0.87 mmol, 87% yield); ¹H-NMR (CDCl₃) δ 3.53 (s, 6H, OCH₃), 3.95 (s, 3H, OCH₃), 3.97 (s, 3H, OCH₃), 5.30 (s, 2H, OCH₂), 5.33 (s, 2H, OCH₂), 6.77 (d, *J* = 9.3 Hz, 1H, H-5′), 7.17 (d, *J* = 1.7 Hz, 1H, H-2), 7.20 (d, *J* = 8.3 Hz, 1H, H-5), 7.25 (dd, *J* = 1.7 Hz and 8.3 Hz, 1H, H-6), 7.46 (d, *J* = 15.4 Hz, 1H, H-α), 7.67 (d, *J* = 9.3 Hz, 1H, H-6′), 7.86 (d, *J* = 15.4 Hz, 1H, H-β), 13.34 (s, 1H, OH); ¹³C-NMR (CDCl₃) δ 55.9, 56.3, 56.4, 60.6, 94.4, 94.9, 105.9, 110.8, 115.5, 115.9, 118.1, 122.5, 125.2, 128.6, 137.2, 144.5, 148.7, 149.4, 155.6, 158.2, 192.0.

2′-Hydroxy-4,3′-dimethoxy-3,4′-di(methoxymethoxy)chalcone (**9e**): (0.26 g, 0.65 mmol, 65% yield); ¹H-NMR (CDCl₃) δ 3.53 (s, 3H, OCH₃), 3.56 (s, 3H, OCH₃), 3.95 (s, 6H, OCH₃), 5.30 (s, 2H, OCH₂), 5.33 (s, 2H, OCH₂), 6.76 (d, *J* = 9.0 Hz, 1H, H-5′), 6.94 (d, *J* = 8.3 Hz, 1H, H-5), 7.31 (dd, *J* = 2.0 Hz and 8.3 Hz, 1H, H-6), 7.43 (d, *J* = 15.4 Hz, 1H, H-α), 7.49 (d, *J* = 2.2 Hz, 1H, H-2), 7.67 (d, *J* = 9.3 Hz, 1H, H-6′), 7.85 (d, *J* = 15.4 Hz, 1H, H-β), 13.36 (s, 1H, OH); ¹³C-NMR (CDCl₃) δ 55.9, 56.2, 56.4, 60.6, 94.4, 95.3, 105.9, 111.3, 115.0, 115.9, 117.8, 124.5, 125.3, 127.4, 137.1, 144.5, 146.5, 151.9, 155.5, 158.2, 192.0.

2′-Hydroxy-3,4,3′-trimethoxy-4′-(methoxymethoxy)chalcone (**9f**): (0.36 g, 0.95 mmol, 95% yield); ¹H-NMR (CDCl₃) δ 3.53 (s, 3H, OCH₃), 3.95 (s, 6H, OCH₃), 3.97 (s, 3H, OCH₃), 5.33 (s, 2H, OCH₂), 6.76 (d, *J* = 9.0 Hz, 1H, H-5′), 6.92 (d, *J* = 8.5 Hz, H-5), 7.16 (d, *J* = 1.7 Hz, 1H, H-2), 7.26 (dd, *J* = 1.7 Hz and 8.3 Hz, 1H, H-6), 7.44 (d, *J* = 15.4 Hz, 1H, H-α), 7.67 (d, *J* = 9.0 Hz, 1H, H-6′), 7.87 (d, *J* = 15.4 Hz, 1H,

H-β), 13.37 (s, 1H, OH); ^{13}C-NMR (CDCl$_3$) δ 55.8, 55.9, 56.4, 60.6, 94.4, 105.9, 109.9, 110.8, 115.9, 117.5, 123.1, 125.2, 127.3, 137.2, 144.7, 148.9, 151.3, 155.5, 158.2, 192.0.

2′-Hydroxy-3′,4′-dimethoxy-4-(methoxymethoxy)chalcone (**9g**): (0.32 g, 0.93 mmol, 93% yield); yellow solid, 92–95 °C; ^{1}H-NMR (CDCl$_3$) δ 3.50 (s, 3H, OCH$_3$), 3.93 (s, 3H, OCH$_3$), 3.96 (s, 3H, OCH$_3$), 5.23 (s, 2H, OCH$_2$), 6.54 (d, *J* = 9.0 Hz, 1H, H-5′), 7.09 (d, *J* = 8.8 Hz, 2H, H-3 and H-5), 7.48 (d, *J* = 15.4 Hz, 1H, H-α), 7.61 (d, *J* = 8.8 Hz, 2H, H-2 and H-6), 7.69 (d, *J* = 9.0 Hz, 1H, H-6′), 7.87 (d, *J* = 15.4 Hz, 1H, H-β), 13.31 (s, 1H, OH); ^{13}C-NMR (CDCl$_3$) δ 56.0, 56.1, 60.5, 94.0, 102.5, 115.4, 116.3, 117.9, 125.6, 128.1, 130.0, 136.4, 144.1, 157.9, 158.0, 159.0, 192.0.

2′-Hydroxy-3′,4′-dimethoxy-3,4-di(methoxymethoxy)chalcone (**9h**): (0.38 g, 0.93 mmol, 93% yield); ^{1}H-NMR (CDCl$_3$) δ 3.53 (s, 3H, OCH$_3$), 3.56 (s, 3H, OCH$_3$), 3.93 (s, 3H, OCH$_3$), 3.96 (s, 3H, OCH$_3$), 5.30 (s, 2H, OCH$_2$), 5.31 (s, 2H, OCH$_2$), 6.55 (d, *J* = 9.0 Hz, 1H, H-5′), 7.21 (d, *J* = 8.3 Hz, 1H, H-5), 7.29 (dd, *J* = 2.0 Hz and 8.5 Hz, 1H, H-6), 7.45 (d, *J* = 15.4 Hz, 1H, H-α), 7.48 (d, *J* = 2.0 Hz, 1H, H-2), 7.70 (d, *J* = 9.0 Hz, 1H, H-6′), 7.84 (d, *J* = 15.4 Hz, 1H, H-β), 13.28 (s, 1H, OH); ^{13}C-NMR (CDCl$_3$) δ 56.0, 56.2, 60.5, 94.9, 95.3, 102.5, 115.4, 115.8, 115.9, 118.4, 123.9, 125.7, 128.8, 136.4, 144.1, 147.1, 149.3, 157.9, 158.1, 191.9.

2′-Hydroxy-3′,4′-dimethoxy-2,4-di(methoxymethoxy)chalcone (**9i**): (0.38 g, 0.93 mmol, 93% yield); light yellow solid, 93–95 °C; ^{1}H-NMR (CDCl$_3$) δ 3.50 (s, 3H, OCH$_3$), 3.53 (s, 3H, OCH$_3$), 3.93 (s, 3H, OCH$_3$), 3.96 (s, 3H, OCH$_3$), 5.22 (s, 2H, OCH$_2$), 5.29 (s, 2H, OCH$_2$), 6.54 (d, *J* = 9.0 Hz, 1H, H-5′), 6.76 (dd, *J* = 2.4 Hz and 8.8 Hz, 1H, H-5), 6.87 (d, *J* = 2.2 Hz, 1H, H-3), 7.59 (d, *J* = 15.6 Hz, 1H, H-α), 7.62 (d, *J* = 8.8 Hz, 1H, H-6), 7.69 (d, *J* = 9.0 Hz, 1H, H-6′), 8.22 (d, *J* = 15.4 Hz, 1H, H-β), 13.43 (s, 1H, OH); ^{13}C-NMR (CDCl$_3$) δ 56.0, 56.2, 56.3, 60.5, 94.0, 94.4, 102.4, 103.0, 109.1, 115.5, 118.1, 118.3, 125.5, 129.6, 136.4, 139.5, 157.6, 157.9, 157.9, 160.2, 192.4.

2′-Hydroxy-3,3′,4′-trimethoxy-4-(methoxymethoxy)chalcone (**9j**): (0.34 g, 0.90 mmol, 90% yield); ^{1}H-NMR (CDCl$_3$) δ 3.53 (s, 3H, OCH$_3$), 3.93 (s, 3H, OCH$_3$), 3.96 (s, 3H, OCH$_3$), 3.97 (s, 3H, OCH$_3$), 5.30 (s, 2H, OCH$_2$), 6.54 (d, *J* = 9.0 Hz, 1H, H-5′), 7.17 (d, *J* = 2.0 Hz, 1H, H-2), 7.20 (d, *J* = 8.5 Hz, 1H, H-5), 7.24 (dd, *J* = 1.7 Hz and 8.3 Hz, 1H, H-6), 7.46 (d, *J* = 15.4 Hz, 1H, H-α), 7.70 (d, *J* = 9.0 Hz, 1H, H-6′), 7.85 (d, *J* = 15.4 Hz, 1H, H-β), 13.30 (s, 1H, OH); ^{13}C-NMR (CDCl$_3$) δ 55.9, 56.0, 56.3, 60.5, 94.9, 102.5, 111.0, 115.4, 115.6, 118.2, 122.4, 125.6, 128.7, 136.4, 144.3, 148.7, 149.5, 157.9, 158.1, 191.9.

2′-Hydroxy-4,3′,4′-trimethoxy-3-(methoxymethoxy)chalcone (**9k**): (0.36 g, 0.95 mmol, 95% yield); ^{1}H-NMR (CDCl$_3$) δ 3.57 (s, 3H, OCH$_3$), 3.93 (s, 3H, OCH$_3$), 3.95 (s, 3H, OCH$_3$), 3.96 (s, 3H, OCH$_3$), 5.30 (s, 2H, OCH$_2$), 6.55 (d, *J* = 9.3 Hz, 1H, H-5′), 6.94 (d, *J* = 8.3 Hz, 1H, H-5), 7.31 (dd, *J* = 2.2 Hz and 8.3 Hz, 1H, H-6), 7.44 (d, *J* = 15.4 Hz, 1H, H-α), 7.49(d, *J* = 2.2 Hz, 1H, H-2), 7.71 (d, *J* = 9.0 Hz, 1H, H-6′), 7.85 (d, *J* = 15.4 Hz, 1H, H-β), 13.32 (s, 1H, OH); ^{13}C-NMR (CDCl$_3$) δ 55.9, 56.0, 56.2, 60.5, 95.4, 102.5, 111.4, 115.0, 115.4, 117.8, 124.5, 125.7, 127.5, 136.4, 144.3, 146.5, 151.9, 157.9, 158.0, 191.9.

3.9. The General Procedure for the Synthesis of Flavonols **10a–l**

To a solution of **7l** and **9a–k** (1.0 mmol) in methanol (25 mL), a 4 M sodium hydroxide aqueous solution (0.3 mL, 1.2 mmol) and a 30% hydrogen peroxide solution (0.5 mL, 5.0 mmol) were added at room temperature. After being stirred at room temperature for 12 h, the mixture was poured into ice and a 2 M hydrochloric acid aqueous solution. The precipitate was filtered, washed with water, and dried in vacuo to produce flavonols **10a–l**.

8-Methoxy-7,4′-di(methoxymethoxy)flavonol (**10a**): (0.20 g, 0.51 mmol, 51% yield); ^{1}H-NMR (CDCl$_3$) δ 3.51 (s, 3H, OCH$_3$), 3.56 (s, 3H, OCH$_3$), 4.07 (s, 3H, OCH$_3$), 5.26 (s, 2H, OCH$_2$), 5.36 (s, 2H, OCH$_2$), 7.20 (d, *J* = 9.0 Hz, 2H, H-3′ and H-5′), 7.26 (d, *J* = 9.0 Hz, 1H, H-6), 7.93 (d, *J* = 9.0 Hz, 1H, H-5), 8.26 (d, *J* = 9.0 Hz, 2H, H-2′ and H-6′); ^{13}C-NMR (CDCl$_3$) δ 56.1, 56.5, 61.6, 94.1, 95.1, 113.6, 116.0, 116.1, 116.5, 120.5, 124.7, 129.2, 129.2, 137.2, 137.7, 144.8, 149.7, 153.9, 158.4, 172.7.

8-Methoxy-7,3′,4′-tri(methoxymethoxy)flavonol (**10b**): (0.16 g, 0.36 mmol, 36% yield); ^{1}H-NMR (CDCl$_3$) δ 3.55 (s, 3H, OCH$_3$), 3.56 (s, 3H, OCH$_3$), 3.58 (s, 3H, OCH$_3$), 4.08 (s, 3H, OCH$_3$), 5.33 (s, 2H, OCH$_2$), 5.34 (s, 2H, OCH$_2$), 5.36 (s, 2H, OCH$_2$), 7.09 (s, 1H, OH), 7.26 (d, *J* = 9.0 Hz, 1H, H-6), 7.32 (d, *J* = 8.8 Hz, 1H, H-5′), 7.92 (d, *J* = 9.3 Hz, 1H, H-5), 7.99 (dd, *J* = 2.0 Hz and 8.8 Hz, 1H, H-6′), 8.18 (d, *J* = 2.0 Hz, 1H, H-2′); ^{13}C-NMR (CDCl$_3$) δ 56.2, 56.2, 56.4, 61.5, 94.9, 95.0, 95.5, 109.7, 113.5, 115.8, 116.2, 120.3, 122.5, 125.1, 137.1, 137.5, 143.9, 146.7, 148.5, 149.6, 153.7, 172.4.

8-Methoxy-7,2′,4′-tri(methoxymethoxy)flavonol (**10c**): (0.15 g, 0.33 mmol, 33% yield); ^{1}H-NMR (CDCl$_3$) δ 3.48 (s, 3H, OCH$_3$), 3.51 (s, 3H, OCH$_3$), 3.55 (s, 3H, OCH$_3$), 3.98 (s, 3H, OCH$_3$), 5.20 (s, 2H, OCH$_2$), 5.23 (s, 2H, OCH$_2$), 5.34 (s, 2H, OCH$_2$), 6.43 (s, 1H, OH), 6.85 (dd, *J* = 2.2 Hz and 8.5 Hz, 1H, H-6′), 7.00 (d, *J* = 2.2 Hz, 1H, H-2′), 7.27 (d, *J* = 9.0 Hz, 1H, H-6), 7.54 (d, *J* = 8.5 Hz, 1H, H-5′), 7.96 (d, *J* = 9.0 Hz, 1H, H-5); ^{13}C-NMR (CDCl$_3$) δ 56.1, 56.4, 61.4, 94.1, 94.9, 95.0, 104.0, 108.8, 113.4, 114.0, 117.0, 120.3, 131.4, 137.5, 137.8, 145.1, 150.2, 153.4, 156.2, 159.8, 172.4.

8,3′-Dimethoxy-7,4′-di(methoxymethoxy)flavonol (**10d**): (0.11 g, 0.26 mmol, 26% yield); ^{1}H-NMR (CDCl$_3$) δ 3.55 (s, 3H, OCH$_3$), 3.56 (s, 3H, OCH$_3$), 4.00 (s, 3H, OCH$_3$), 4.07 (s, 3H, OCH$_3$), 5.33 (s, 2H, OCH$_2$), 5.36 (s, 2H, OCH$_2$), 7.00 (s, 1H, OH), 7.27 (d, *J* = 9.0 Hz, 1H, H-6), 7.32 (d, *J* = 8.5 Hz, 1H, H-5′), 7.90 (dd, *J* = 2.0 Hz and 8.8 Hz, 1H, H-6′), 7.93 (d, *J* = 9.0 Hz, 1H, H-5), 7.95 (d, *J* = 2.0 Hz, 1H, H-2′); ^{13}C-NMR (CDCl$_3$) δ 55.8, 56.2, 56.5, 61.5, 95.0, 110.8, 113.5, 115.5, 116.2, 120.4, 120.8, 125.1, 137.1, 137.4, 144.1, 147.7, 149.1, 149.5, 153.7, 172.4.

8,4′-Dimethoxy-7,3′-di(methoxymethoxy)flavonol (**10e**): (0.27 g, 0.65 mmol, 65% yield); ^{1}H-NMR (CDCl$_3$) δ 3.56 (s, 3H, OCH$_3$), 3.58 (s, 3H, OCH$_3$), 3.98 (s, 3H, OCH$_3$), 4.08 (s, 3H, OCH$_3$), 5.34 (s, 2H, OCH$_2$), 5.36 (s, 2H, OCH$_2$), 6.98 (s, 1H, OH), 7.06 (d, *J* = 8.8 Hz, 1H, H-5′), 7.26 (d, *J* = 9.0 Hz, 1H, H-6), 7.92 (d, *J* = 9.0 Hz, 1H, H-5), 8.04 (dd, *J* = 2.2 Hz and 8.5 Hz, 1H, H-6′), 8.17 (d, *J* = 2.2 Hz, 1H, H-2′); ^{13}C-NMR (CDCl$_3$) δ 55.9, 56.2, 56.4, 61.5, 95.0, 95.5, 111.3, 113.4, 115.3, 116.3, 120.3, 122.7, 123.8, 137.0, 137.5, 144.0, 146.1, 149.5, 151.0, 153.7, 172.4.

8,3′,4′-Trimethoxy-7-(methoxymethoxy)flavonol (**10f**): (0.15 g, 0.38 mmol, 38% yield); light yellow solid, 163–166 °C; ^{1}H-NMR (CDCl$_3$) δ 3.56 (s, 3H, OCH$_3$), 3.98 (s, 3H, OCH$_3$), 4.01 (s, 3H, OCH$_3$), 4.08 (s, 3H, OCH$_3$), 5.37 (s, 2H, OCH$_2$), 7.00 (s, 1H, OH), 7.05 (d, *J* = 8.5 Hz, 1H, H-6), 7.28 (d, *J* = 7.6 Hz, 1H, H-5′), 7.93 (s, 1H, H-2′), 7.94 (d, *J* = 8.8 Hz, 1H, H-5), 7.96 (dd, *J* = 2.0 Hz and 8.1Hz, 1H, H-6′); ^{13}C-NMR (CDCl$_3$) δ 55.7, 55.8, 56.5, 61.5, 94.9, 110.1, 110.7, 113.3, 116.2, 120.4, 121.0, 123.6, 136.9, 137.3, 144.2, 148.4, 149.5, 150.2, 153.6, 172.3.

7,8-Dimethoxy-4′-(methoxymethoxy)flavonol (**10g**): (0.16 g, 0.45 mmol, 45% yield); ^{1}H-NMR (CDCl$_3$) δ 3.51 (s, 3H, OCH$_3$), 4.02 (s, 3H, OCH$_3$), 4.04 (s, 3H, OCH$_3$), 5.27 (s, 2H, OCH$_2$), 6.94 (s, 1H, OH), 7.07 (d, *J* = 9.0 Hz, 1H, H-6), 7.20 (d, *J* = 9.0 Hz, 2H, H-3′ and H-5′), 7.97 (d, *J* = 9.0 Hz, 1H, H-5), 8.26 (d, *J* = 9.0 Hz, 2H, H-2′ and H-6′); ^{13}C-NMR (CDCl$_3$) δ 56.0, 56.4, 61.4, 94.0, 109.8, 115.4, 115.9, 120.5, 124.6, 129.0, 136.7, 144.3, 149.4, 156.0, 158.1, 172.5.

7,8-Dimethoxy-3′,4′-di(methoxymethoxy)flavonol (**10h**): (0.12 g, 0.28 mmol, 28% yield); ^{1}H-NMR (CDCl$_3$) δ 3.55 (s, 3H, OCH$_3$), 3.58 (s, 3H, OCH$_3$), 4.02 (s, 3H, OCH$_3$), 4.05 (s, 3H, OCH$_3$), 5.33 (s, 2H, OCH$_2$), 5.34 (s, 2H, OCH$_2$), 6.97 (s, 1H, OH), 7.07 (d, *J* = 9.3 Hz, 1H, H-6), 7.33 (d, *J* = 8.8 Hz, 1H, H-5′), 7.96 (d, *J* = 9.0 Hz, 1H, H-5), 7.98 (dd, *J* = 2.2 Hz and 8.8 Hz, 1H, H-6′), 8.18 (d, *J* = 2.2 Hz, 1H, H-2′); ^{13}C-NMR (CDCl$_3$) δ 56.2, 56.2, 56.4, 61.4, 94.9, 95.5, 109.8, 115.3, 115.7, 115.8, 120.5, 122.5, 125.2, 136.5, 136.9, 143.8, 146.7, 148.4, 149.4, 156.1, 172.5.

7,8-Dimethoxy-2′,4′-di(methoxymethoxy)flavonol (**10i**): (0.07 g, 0.17 mmol, 17% yield); ^{1}H-NMR (CDCl$_3$) δ 3.48 (s, 3H, OCH$_3$), 3.51 (s, 3H, OCH$_3$), 3.96 (s, 3H, OCH$_3$), 4.01 (s, 3H, OCH$_3$), 5.20 (s, 2H, OCH$_2$), 5.23 (s, 2H, OCH$_2$), 6.42 (s, 1H, OH), 6.85 (dd, *J* = 2.2 Hz and 8.8 Hz, 1H, H-6′), 7.00 (d, *J* = 2.2 Hz, 1H, H-2′), 7.08 (d, *J* = 9.0 Hz, 1H, H-6), 7.54 (d, *J* = 8.8 Hz, 1H, H-5′), 8.00 (d, *J* = 9.0 Hz, 1H, H-5); ^{13}C-NMR (CDCl$_3$) δ 56.1, 56.4, 61.3, 94.1, 94.8, 104.0, 108.8, 109.6, 114.0, 116.1, 120.5, 131.4, 136.5, 137.6, 145.0, 150.0, 155.7, 156.2, 159.8, 172.5.

7,8,3′-Trimethoxy-4′-(methoxymethyl)flavonol (**10j**): (0.22 g, 0.56 mmol, 56% yield); ^{1}H-NMR (CDCl$_3$) δ 3.55 (s, 3H, OCH$_3$), 4.00 (s, 3H, OCH$_3$), 4.02 (s, 3H, OCH$_3$), 4.05 (s, 3H, OCH$_3$), 5.33 (s, 2H, OCH$_2$), 7.00 (s, 1H, OH), 7.08 (d, *J* = 9.0 Hz, 1H, H-6), 7.32 (d, *J* = 8.8 Hz, 1H, H-5′), 7.90 (dd, *J* = 2.0 Hz and 8.8 Hz, 1H, H-6′), 7.95 (d, *J* = 2.0 Hz, 1H, H-2′), 7.97 (d, *J* = 9.0 Hz, 1H, H-5); ^{13}C-NMR (CDCl$_3$) δ 55.8, 56.2, 56.4, 61.3, 94.9, 109.8, 110.8, 115.3, 115.4, 120.6, 120.8, 125.1, 136.4, 136.9, 144.0, 147.7, 149.0, 149.4, 156.1, 172.5.

7,8,4′-Trimethoxy-3′-(methoxymethyl)flavonol (**10k**): (0.24 g, 0.61 mmol, 61% yield); ^{1}H-NMR (CDCl$_3$) δ 3.58 (s, 3H, OCH$_3$), 3.98 (s, 3H, OCH$_3$), 4.02 (s, 3H, OCH$_3$), 4.06 (s, 3H, OCH$_3$), 5.34 (s, 2H, OCH$_2$), 7.00 (s, 1H, OH), 7.06 (d, *J* = 8.5 Hz, 1H, H-5′), 7.07 (d, *J* = 9.0 Hz, 1H, H-6), 7.96 (d, *J* = 9.0 Hz, 1H, H-5), 8.04 (dd, *J* = 2.2 Hz and 8.8 Hz, 1H, H-6′), 8.18 (d, *J* = 2.0 Hz, 1H, H-2′); ^{13}C-NMR (CDCl$_3$) δ 56.0, 56.4, 56.6, 61.6, 95.7, 109.9, 111.4, 115.5, 116.0, 120.7, 122.9, 124.0, 136.6, 137.0, 144.2, 146.2, 149.5, 151.1, 156.2, 172.6.

7,8,3′,4′-Tetramethoxyflavonol (**10l**): (0.12 g, 0.33 mmol, 33% yield); pale yellow solid, 215–217 °C; ^{1}H-NMR (CDCl$_3$) δ 3.98 (s, 3H, OCH$_3$), 4.00 (s, 3H, OCH$_3$), 4.02 (s, 3H, OCH$_3$), 4.05 (s, 3H, OCH$_3$), 7.01 (s, 1H, OH), 7.04 (d, *J* = 8.5 Hz, 1H, H-5′), 7.08 (d, *J* = 9.0 Hz, 1H, H-6), 7.92 (d, *J* = 2.0 Hz, 1H, H-2′), 7.95 (dd, *J* = 2.0 Hz and 8.1 Hz, 1H, H-6′), 7.97 (d, *J* = 8.8 Hz, 1H, H-5); ^{13}C-NMR (CDCl$_3$) δ 55.7, 55.8, 56.4, 61.3, 109.7, 110.2, 110.7, 115.3, 120.5, 121.0, 123.7, 136.4, 136.7, 144.2, 148.5, 149.3, 150.2, 156.0, 172.4; UV/Vis (2.1 × 10^{-5} M, CHCl$_3$); λ = 363.6 nm (*ε*, 2.8 × 10^4).

3.10. The General Procedure for the Deprotection of Flavonols **10a–k**

A solution of **10a–k** (1.0 mmol) in methanol (5 mL) and 3 M hydrochloric acid (5 mL) was refluxed for 1 h. The mixture was extracted with EtOAc. The organic layer was washed with water and brine and dried over anhydrous MgSO$_4$. The solvent was evaporated in vacuo and the residue was chromatographed on a preparative thin layer chromatography (hexane:EtOAc = 2:3) to produce flavonols **11a–k**.

7,4′-Dihydroxy-8-methoxyflavonol (**11a**): (0.18 g, 0.45 mmol, 80% yield); pale yellowish brown solid, 263–267 °C; ^{1}H-NMR (DMSO-*d$_6$*) δ 3.93 (s, 3H, OCH$_3$), 6.96 (d, *J* = 9.0 Hz, 2H, H-3′ and H-5′), 6.98 (d, *J* = 8.8 Hz, 1H, H-6), 7.68 (d, *J* = 8.8 Hz, 1H, H-5), 8.06 (d, *J* = 8.8 Hz, 2H, H-2′ and H-6′), 9.14 (s, 1H, OH), 10.07 (s, 1H, OH); ^{13}C-NMR (DMSO-*d$_6$*) δ 60.8, 114.6, 114.9, 115.3, 119.8, 122.1, 128.8, 134.4, 136.8, 144.7, 149.1, 154.1, 158.5, 171.8; UV/Vis (2.8 × 10^{-5} M, CH$_3$OH); λ = 358.5 nm (*ε*, 1.8 × 10^4).

7,3′,4′-Trihydroxy-8-methoxyflavonol (**11b**): (0.16 g, 0.49 mmol, 98% yield); yellow solid, 257–258 °C; ^{1}H-NMR (DMSO-*d$_6$*) δ 3.94 (s, 3H, OCH$_3$), 6.91 (d, *J* = 8.5 Hz, 1H, H-5′), 6.98 (d, *J* = 9.0 Hz, 1H, H-6), 7.59 (dd, *J* = 2.2 and 8.5 Hz, 1H, H-6′), 7.67 (d, *J* = 8.8 Hz, 1H, H-5), 7.72 (d, *J* = 2.2 Hz, 1H, H-2′), 9.10 (s, 1H, OH), 9.35 (s, 1H, OH), 9.52 (s, 1H, OH), 10.51 (s, 1H, OH); ^{13}C-NMR (DMSO-*d$_6$*) δ 60.9, 114.5, 114.6, 114.9, 115.4, 119.4, 119.8, 122.4, 134.4, 136.8, 144.7, 144.8, 147.0, 149.1, 154.0, 171.7; UV/Vis (2.5 × 10^{-5} M, CH$_3$OH); λ = 366.0 nm (*ε*, 2.1 × 10^4).

7,2′,4′-Trihydroxy-8-methoxyflavonol (**11c**): (0.06 g, 0.18 mmol, 36% yield); pale green-yellow solid, 265 °C (decomp.); ^{1}H-NMR (DMSO-*d$_6$*) δ 3.90 (s, 3H, OCH$_3$), 6.17 (d, *J* = 1.7 Hz, 1H, H-3′), 6.31 (dd, *J* = 2.0 Hz and 8.8 Hz, 1H, H-5′), 6.95 (d, *J* = 8.8 Hz, 1H, H-6), 7.52 (d, *J* = 8.3 Hz, 1H, H-6′), 7.68 (d, *J* = 8.8 Hz, 1H, H-5), 9.46 (s, 1H, OH), 10.32 (s, 1H, OH); ^{13}C-NMR (DMSO-*d$_6$*) δ 60.8, 104.8, 106.1, 113.2, 114.1, 115.0, 119.7, 127.9, 134.4, 142.9, 146.8, 149.4, 153.1, 159.8, 160.6, 175.9; UV/Vis (2.7 × 10^{-5} M, CH$_3$OH); λ = 395.0 nm (*ε*, 1.5 × 10^4).

7,4′-Dihydroxy-8,3′-dimethoxyflavonol (**11d**): (0.14 g, 0.43 mmol, 85% yield); pale yellow solid, 281–282 °C; ^{1}H-NMR (DMSO-*d$_6$*) δ 3.85 (s, 3H, OCH$_3$), 3.95 (s, 3H, OCH$_3$), 6.97 (d, *J* = 8.5 Hz, 1H, H-5′), 6.99 (d, *J* = 8.8 Hz, 1H, H-6), 7.68 (d, *J* = 8.8 Hz, 1H, H-5), 7.74 (dd, *J* = 2.0 Hz and 8.5 Hz, 1H, H-6′), 7.78 (d, *J* = 2.0 Hz, 1H, H-2′), 9.25 (s, 1H, OH), 9.75 (s, 1H, OH), 10.56 (s, 1H, OH); ^{13}C-NMR (DMSO-*d$_6$*)

δ 55.6, 60.9, 111.0, 114.7, 114.9, 115.5, 119.9, 121.2, 122.5, 134.4, 137.0, 144.6, 147.2, 148.2, 149.2, 154.2, 171.9; UV/Vis (2.7×10^{-5} M, acetone); λ = 353.0 nm (ε, 1.8×10^4).

7,3′-Dihydroxy-8,4′-dimethoxyflavonol (11e): (0.14 g, 0.43 mmol, 86% yield); yellow solid, 241–244 °C; ^{1}H-NMR (DMSO-d_6) δ 3.86 (s, 3H, OCH$_3$), 3.95 (s, 3H, OCH$_3$), 7.00 (d, *J* = 8.8 Hz, 1H, H-6), 7.13 (d, *J* = 8.5 Hz, 1H, H-5′), 7.69 (d, *J* = 8.8 Hz, 1H, H-5), 7.71 (dd, *J* = 2.2 Hz and 8.5 Hz, 1H, H-6′), 7.74 (d, *J* = 2.2 Hz, 1H, H-2′), 9.21 (s, 1H, OH), 9.39 (s, 1H, OH), 10.54 (s, 1H, OH); ^{13}C-NMR (DMSO-d_6) δ 55.5, 60.9, 111.7, 114.2, 114.7, 114.9, 119.1, 119.8, 123.9, 134.4, 137.2, 144.2, 146.0, 148.7, 149.1, 154.1, 171.8; UV/Vis (2.8×10^{-5} M, CH$_3$OH); λ = 361.5 nm (ε, 2.2×10^4).

7-Hydroxy-8,3′,4′-trimethoxyflavonol (11f): (0.07 g, 0.19 mmol, 38% yield); ocher solid, 202–206 °C; ^{1}H-NMR (DMSO-d_6) δ 3.85 (s, 3H, OCH$_3$), 3.86 (s, 3H, OCH$_3$), 3.96 (s, 3H, OCH$_3$), 7.00 (d, *J* = 8.8 Hz, 1H, H-6), 7.18 (d, *J* = 8.5 Hz, 1H, H-5′), 7.69 (d, *J* = 8.8 Hz, 1H, H-5), 7.80 (d, *J* = 2.0 Hz, 1H, H-2′), 7.85 (dd, *J* = 2.0 Hz and 8.5 Hz, 1H, H-6′), 9.29 (s, 1H, OH), 10.56 (s, 1H, OH); ^{13}C-NMR (DMSO-d_6) δ 55.4, 55.6, 60.8, 110.3, 111.5, 114.8, 114.9, 119.9, 120.8, 123.8, 134.4, 137.4, 144.1, 148.2, 149.2, 149.8, 154.3, 171.9; UV/Vis (2.4×10^{-5} M, CHCl$_3$); λ = 359.0 nm (ε, 1.9×10^4).

4′-Hydroxy-7,8,dimethoxyflavonol (11g): (0.09 g, 0.29 mmol, 57% yield); pale yellow solid, 235–236 °C; ^{1}H-NMR (DMSO-d_6) δ 3.93 (s, 3H, OCH$_3$), 3.96 (s, 3H, OCH$_3$), 6.97 (d, *J* = 8.8 Hz, 2H, H-3′ and H-5′), 7.27 (d, *J* = 9.0 Hz, 1H, H-6), 7.83 (d, *J* = 9.0 Hz, 1H, H-5), 8.08 (d, *J* = 8.8 Hz, 2H, H-2′ and H-6′), 9.26 (s, 1H, OH), 10.12 (s, 1H, OH); ^{13}C-NMR (DMSO-d_6) δ 56.5, 61.0, 110.4, 115.3, 116.1, 119.9, 122.0, 129.0, 135.9, 136.9 145.3, 148.4, 155.5, 158.7, 171.9; UV/Vis (2.7×10^{-5} M, CH$_3$OH); λ = 361.5 nm (ε, 2.5×10^4).

3′,4′-Dihydroxy-7,8-dimethoxyflavonol (11h): (0.13 g, 0.40 mmol, 79% yield); yellow ocher solid, 261–263 °C; ^{1}H-NMR (DMSO-d_6) δ 3.84 (s, 3H, OCH$_3$), 3.94 (s, 3H, OCH$_3$), 6.37 (dd, *J* = 2.0 Hz and 8.3 Hz, 1H, H-5′), 6.42 (d, *J* = 2.0 Hz, 1H, H-3′), 7.25 (d, *J* = 9.0 Hz, 1H, H-6), 7.26 (d, *J* = 8.3 Hz, 1H, H-6′), 7.83 (d, *J* = 9.0 Hz, 1H, H-5), 9.68 (s, 1H, OH), 9.78 (s, 1H, OH); ^{13}C-NMR (DMSO-d_6) δ 56.4, 60.9, 102.9, 106.6, 109.5, 110.3, 116.8, 119.9, 131.6, 136.0, 137.4, 147.5, 149.2, 155.3, 156.7, 160.1, 172.1; UV/Vis (2.5×10^{-5} M, CH$_3$OH); λ = 369.0 nm (ε, 2.4×10^4).

2′,4′-Dihydroxy-7,8,3′-trimethoxyflavonol (11i): (0.07 g, 0.22 mmol, 43% yield); red-clay solid, 192–196 °C; ^{1}H-NMR (DMSO-d_6) δ 3.95 (s, 3H, OCH$_3$), 3.96 (s, 3H, OCH$_3$), 6.92 (d, *J* = 8.5 Hz, 1H, H-5′), 7.26 (d, *J* = 9.0 Hz, 1H, H-6), 7.62 (dd, *J* = 2.0 Hz and 8.5 Hz, 1H, H-6′), 7.75 (d, *J* = 2.0 Hz, 1H, H-2′), 7.82 (d, *J* = 9.0 Hz, 1H, H-5), 9.22 (s, 1H, OH), 9.40 (s, 1H, OH), 9.56 (s, 1H, OH); ^{13}C-NMR (DMSO-d_6) δ 56.4, 61.1, 110.3, 114.6, 115.4, 116.0, 119.6, 119.9, 122.3, 135.8, 136.9, 144.8, 145.2, 147.2, 148.3, 155.4, 171.8.

4′-Hydroxy-7,8,3′-trimethoxyflavonol (11j): (0.08 g, 0.24 mmol, 48% yield); ocher solid, 177–181 °C; ^{1}H-NMR (CDCl$_3$) δ 4.01 (s, 3H, OCH$_3$), 4.02 (s, 3H, OCH$_3$), 4.05 (s, 3H, OCH$_3$), 6.01 (s, 1H, OH), 7.00 (s, 1H, OH), 7.07 (d, *J* = 9.0 Hz, 1H, H-6), 7.09 (d, *J* = 8.3 Hz, 1H, H-5′), 7.88 (dd, *J* = 2.0 Hz and 8.5 Hz, 1H, H-6′), 7.93 (d, *J* = 2.0 Hz, 1H, H-2′), 7.97 (d, *J* = 9.0 Hz, 1H, H-5); ^{13}C-NMR (CDCl$_3$) δ 55.8, 56.4, 61.3, 109.7, 109.9, 114.4, 115.3, 120.5, 121.4, 123.2, 136.4, 136.6, 144.3, 146.1, 147.1, 149.3, 156.0, 172.4; UV/Vis (2.8×10^{-5} M, CHCl$_3$); λ = 362.5 nm (ε, 2.3×10^4).

3′-Hydroxy-7,8,4′-trimethoxyflavonol (11k): (0.09 g, 0.27 mmol, 53% yield); pale yellow solid, 231–234 °C; ^{1}H-NMR (DMSO-d_6) δ 3.86 (s, 3H, OCH$_3$), 3.95 (s, 3H, OCH$_3$), 3.97 (s, 3H, OCH$_3$), 7.13 (d, *J* = 8.5 Hz, 1H, H-5′), 7.27 (d, *J* = 9.0 Hz, 1H, H-6), 7.72 (dd, *J* = 2.2 Hz and 8.5 Hz, 1H, H-6′), 7.75 (d, *J* = 2.2 Hz, 1H, H-2′), 7.83 (d, *J* = 9.0 Hz, 1H, H-5), 9.33 (s, 1H, OH), 9.42 (s, 1H, OH); ^{13}C-NMR (DMSO-d_6) δ 55.5, 56.4, 61.0, 110.3, 111.7, 114.2, 116.0, 119.3, 119.9, 123.8, 135.8, 137.3, 144.7, 146.0, 148.4, 148.8, 155.5, 171.9; UV/Vis (2.3×10^{-5} M, CHCl$_3$); λ = 360.5 nm (ε, 2.6×10^4).

3.11. The General Procedure for the Preparation of 4-Chloroacetylpyrogallols *12a,b*

Chloroacetyl chloride (4.3 mL, 54.0 mmol) was added to a suspension of anhydrous aluminum chloride (8.00 g, 60.0 mmol) and 1,2-dichloroethane (100 mL) was added under an argon atmosphere

at room temperature. A solution of **1a**,**b** (30.0 mmol) in 1,2-dichloroethane (30 mL) was added to the mixture and the reaction mixture was stirred at room temperature for 12 h. The mixture was poured into ice and a 2 M HCl solution and extracted with CHCl3. The organic layer was washed with water and dried over anhydrous $MgSO_4$. The solvent was evaporated in vacuo and the residue was chromatographed on silica gel with CHCl3-Et$_2$O (9:1) to produce **12a**,**b**.

1-Chloroacetyl-2,4-dihydroxy-3-methoxybenzene (**12a**): (3.77 g, 17.4 mmol, 58% yield); ^{1}H-NMR (CDCl$_3$) δ 4.00 (s, 3H, OCH$_3$), 4.64 (s, 2H, CH2), 6.56 (d, *J* = 9.0 Hz, 1H, H-5), 6.57 (s, 1H, OH), 7.41 (d, *J* = 9.0 Hz, 1H, H-6), 12.24 (s, 1H, OH); ^{13}C-NMR (CDCl$_3$) δ 44.8, 60.9, 107.2, 112.2, 126.3, 134.3, 155.9, 156.8, 195.2.

1-Chloroacetyl-2-hydroxy-3,4-dimethoxybenzene (**12b**): (3.74 g, 16.2 mmol, 54% yield); colorless solid, 155–158 °C; ^{1}H-NMR (CDCl$_3$) δ 3.89 (s, 3H, OCH$_3$), 3.95 (s, 3H, OCH$_3$), 4.65 (s, 2H, CH2), 6.54 (d, *J* = 9.0 Hz, 1H, H-5), 7.49 (d, *J* = 9.0 Hz, 1H, H-6), 11.85 (s, 1H, OH); ^{13}C-NMR (CDCl$_3$) δ 45.0, 56.2, 60.7, 103.5, 112.7, 126.1, 136.6, 157.2, 159.1, 195.0.

3.12. The General Procedure for the Preparation of Benzofuranones **13a**,**b**

A solution of **12a**,**b** (20.0 mmol) and sodium acetate (6.56 g, 80.0 mmol or 3.28 g, 40.0 mmol) in methanol (100 mL) was refluxed for 2 h. Water was added to the mixture and extracted with Et$_2$O. The organic layer was washed with brine and dried over anhydrous $MgSO_4$. The solvent was evaporated in vacuo and the residue was chromatographed on silica gel with CHCl$_3$-Et$_2$O (9:1) to produce **13a**,**b**.

6-Hydroxy-7-methoxy-3(2*H*)-benzofuranone (**13a**): (2.77 g, 15.4 mmol, 77% yield); ^{1}H-NMR (DMSO-d_6) δ 3.89 (s, 3H, OCH$_3$), 4.76 (s, 2H, CH$_2$), 6.85 (d, *J* = 8.5 Hz, 1H, H-5), 7.12 (d, *J* = 8.5 Hz, 1H, H-4), 9.37 (s, 1H, OH); ^{13}C-NMR (DMSO-d_6) δ 56.5, 75.2, 107.4, 113.7, 115.5, 131.7, 154.6, 162.1, 198.0.

6,7-Dimethoxy-3(2*H*)-benzofuranone (**13b**): (3.22 g, 16.6 mmol, 83% yield); reddish yellow solid, 119–123 °C; ^{1}H-NMR (CDCl$_3$) δ 3.97 (s, 3H, OCH$_3$), 4.01 (s, 3H, OCH$_3$), 4.67 (s, 2H, CH$_2$), 6.72 (d, *J* = 8.5 Hz, 1H, H-5), 7.41 (d, *J* = 8.5 Hz, 1H, H-4); ^{13}C-NMR (CDCl$_3$) δ 56.7, 61.0, 75.5, 107.3, 116.3, 119.1, 134.2, 159.4, 166.0, 197.8.

3.13. The General Procedure for the Protection of **13a** with a Chloromethyl Methyl Ether

A solution of **13a** (0.90 g, 5.0 mmol) in DMF (5 mL) was added to a suspension of sodium hydride (60% in mineral oil, 0.24 g, 6.0 mmol) in DMF (15 mL) at 0 °C. After being stirred at room temperature for 30 min, a chloromethyl methyl ether (0.57 mL, 7.5 mmol) was added to the mixture at 0 °C. After being stirred at room temperature for 6 h, Et$_2$O (20 mL) was added to the mixture. The reaction mixture was poured into ice water (200 mL). The mixture was extracted with Et$_2$O. The organic layer was washed with water and brine and dried over anhydrous $MgSO_4$. The solvent was evaporated in vacuo and the residue was chromatographed on silica gel with CHCl$_3$-Et$_2$O (9:1) to produce **13c**.

7-Methoxy-6-(methoxymethoxy)-3(2*H*)-benzofuranone (**13c**): (0.81 g, 3.6 mmol, 72% yield); dark brown solid, 203–210 °C; ^{1}H-NMR (CDCl$_3$) δ 3.53 (s, 3H, OCH$_3$), 4.03 (s, 3H, OCH$_3$), 4.68 (s, 2H, OCH$_2$), 5.32 (s, 2H, OCH$_2$), 6.94 (d, *J* = 8.5 Hz, 1H, H-5), 7.37 (d, *J* = 8.5 Hz, 1H, H-4); ^{13}C-NMR (CDCl$_3$) δ 56.6, 61.0, 75.4, 95.0, 110.8, 117.0, 118.8, 156.9, 166.3, 197.9.

3.14. The General Procedure for the Synthesis of Aurones **14a–l**

Aluminum oxide (basic, 2.00 g, 19.6 mmol) was added to a solution of benzofuranones **13b**,**c** (1.0 mmol) and benzaldehydes **5a–f** (1.2 mmol) in dichloromethane (5 mL). The mixture was thoroughly stirred for 2 days at room temperature. The suspension was filtered off and the residue was washed with CHCl$_3$. The filtrate was concentrated in vacuo and the residue was chromatographed on a preparative thin layer chromatography (CHCl$_3$:Et$_2$O = 9:1) to produce (*Z*)-aurones **14a–l**.

(Z)-7-Methoxy-6,4′-di(methoxymethoxy)aurone (**14a**): (0.32 g, 0.86 mmol, 86% yield); reddish yellow solid, 92–94 °C; ^{1}H-NMR (CDCl$_3$) δ 3.50 (s, 3H, OCH$_3$), 3.55 (s, 3H, OCH$_3$), 4.19 (s, 3H, OCH$_3$), 5.24 (s, 2H, OCH$_2$), 5.33 (s, 2H, OCH$_2$), 6.84 (s, 1H, H-10), 7.03 (d, J = 8.5 Hz, 1H, H-5), 7.12 (d, J = 9.0 Hz, 2H, H-3′ and H-5′), 7.48 (d, J = 8.3 Hz, 1H, H-4), 7.87 (d, J = 8.8 Hz, 2H, H-2′ and H-6′); ^{13}C-NMR δ (CDCl$_3$) 56.1, 56.5, 61.0, 93.9, 95.1, 111.7, 112.2, 116.3, 117.6, 119.0, 125.7, 132.7, 134.6, 146.1, 155.9, 157.4, 158.1, 182.7.

(Z)-7-Methoxy-6,3′,4′-tri(methoxymethoxy)aurone (**14b**): (0.23 g, 0.54 mmol, 54% yield); light yellow solid, 85–86 °C; ^{1}H-NMR (CDCl$_3$) δ 3.54 (s, 3H, OCH$_3$), 3.55 (s, 3H, OCH$_3$), 3.56 (s, 3H, OCH$_3$), 4.21 (s, 3H, OCH$_3$), 5.32 (s, 4H, OCH$_2$), 5.34 (s, 2H, OCH$_2$), 6.82 (s, 1H, H-10), 7.04 (d, J = 8.5 Hz, 1H, H-5), 7.24 (d, J = 8.5 Hz, 1H, H-5′), 7.47 (dd, J = 2.0 Hz and 8.3 Hz, 1H, H-6′), 7.48 (d, J = 8.5 Hz, 1H, H-4), 7.88 (d, J = 2.0 Hz, 1H, H-2′); ^{13}C-NMR (CDCl$_3$) δ 56.1, 56.2, 56.5, 61.0, 94.7, 95.0, 95.1, 111.5, 112.2, 115.7, 117.5, 118.4, 118.9, 126.2, 126.5, 134.5, 146.1, 146.8, 148.3, 155.8, 157.3, 182.8.

(Z)-7-Methoxy-6,2′,4′-tri(methoxymethoxy)aurone (**14c**): (0.29 g, 0.67 mmol, 67% yield); yellow solid, 105–110 °C; ^{1}H-NMR (CDCl$_3$) δ 3.50 (s, 3H, OCH$_3$), 3.52 (s, 3H, OCH$_3$), 3.67 (s, 3H, OCH$_3$), 3.99 (s, 3H, OCH$_3$), 5.22 (s, 2H, OCH$_2$), 5.27 (s, 2H, OCH$_2$), 5.33 (s, 2H, OCH$_2$), 6.78 (dd, J = 2.2 Hz and 9.0 Hz, 1H, H-5′) 6.81, (d, J = 8.8 Hz, 1H, H-5), 6.87 (d, J = 2.2 Hz, 1H, H-3′), 7.38 (s, 1H, H-10), 7.58 (d, J = 8.5 Hz, 1H, H-4), 8.27 (d, J = 8.8 Hz, 1H, H-6′); ^{13}C-NMR (CDCl$_3$) δ 56.2, 56.3, 56.5, 61.0, 93.9, 94.4, 95.1, 102.7, 106.5, 109.1, 111.4, 115.5, 117.8, 118.9, 132.4, 133.6, 146.2, 155.6, 157.2, 157.6, 159.5, 182.8.

(Z)-7,3′-Dimethoxy-6,4′-di(methoxymethoxy)aurone (**14d**): (0.28 g, 0.69 mmol, 69% yield); reddish yellow solid, 95–100 °C; ^{1}H-NMR (CDCl$_3$) δ 3.54 (s, 3H, OCH$_3$), 3.55 (s, 3H, OCH$_3$), 3.98 (s, 3H, OCH$_3$), 4.18 (s, 3H, OCH$_3$), 5.32 (s, 2H, OCH$_2$), 5.34 (s, 2H, OCH$_2$), 6.84 (s, 1H, H-10), 7.04 (d, J = 8.5 Hz, 1H, H-5), 7.24 (d, J = 8.5 Hz, 1H, H-5′), 7.44 (dd, J = 2.0 Hz and 8.5 Hz, 1H, H-6′), 7.50 (d, J = 8.5 Hz, 1H, H-4), 7.60 (d, J = 2.0 Hz, 1H, H-2′); ^{13}C-NMR (CDCl$_3$) δ 55.6, 56.2, 56.5, 60.8, 94.8, 95.1, 111.6, 112.4, 113.5, 115.4, 117.5, 119.2, 125.2, 126.2, 134.4, 146.2, 147.7, 149.2, 155.9, 157.5, 182.7.

(Z)-7,4′-Dimethoxy-6,3′-di(methoxymethoxy)aurone (**14e**): (0.34 g, 0.85 mmol, 85% yield); light yellow solid, 130–133 °C; ^{1}H-NMR (CDCl$_3$) δ 3.55 (s, 3H, OCH$_3$), 3.56 (s, 3H, OCH$_3$), 3.95 (s, 3H, OCH$_3$), 4.20 (s, 3H, OCH$_3$), 5.30 (s, 2H, OCH$_2$), 5.33 (s, 2H, OCH$_2$), 6.82 (s, 1H, H-10), 6.97 (d, J = 8.5 Hz, 1H, H-5′), 7.03 (d, J = 8.5 Hz, 1H, H-5), 7.48 (dd, J = 2.0 Hz and 8.5 Hz, 1H, H-6′), 7.48 (d, J = 8.5 Hz, 1H, H-4), 7.89 (d, J = 2.0 Hz, 1H, H-2′); ^{13}C-NMR (CDCl$_3$) δ 55.8, 56.1, 56.5, 61.0, 95.2, 95.3, 111.4, 111.7, 112.5, 117.7, 118.1, 118.9, 125.0, 126.9, 134.6, 146.0, 146.4, 151.0, 155.8, 157.3, 182.7.

(Z)-7,3′,4′-Trimethoxy-6-(methoxymethoxy)aurone (**14f**): (0.12 g, 0.31 mmol, 31% yield); light yellow solid, 157–161 °C; ^{1}H-NMR (CDCl$_3$) δ 3.55 (s, 3H, OCH$_3$), 3.95 (s, 3H, OCH$_3$), 3.98 (s, 3H, OCH$_3$), 4.18 (s, 3H, OCH$_3$), 5.34 (s, 2H, OCH$_2$), 6.84 (s, 1H, H-10), 6.95 (d, J = 8.3 Hz, 1H, H-5′), 7.04 (d, J = 8.5 Hz, 1H, H-5), 7.44 (dd, J = 1.7 Hz and 8.5 Hz, 1H, H-6′), 7.49 (d, J = 8.3 Hz, 1H, H-4), 7.60 (d, J = 1.7 Hz, 1H, H-2′); ^{13}C-NMR (CDCl$_3$) δ 55.7, 55.9, 56.6, 60.9, 95.2, 111.0, 111.7, 112.9, 113.1, 117.7, 119.3, 125.1, 125.7, 134.6, 146.1, 148.8, 150.5, 156.1, 157.6, 182.9.

(Z)-6,7-Dimethoxy-4′-(methoxymethoxy)aurone (**14g**): (0.31 g, 0.89 mmol, 89% yield); ^{1}H-NMR (CDCl$_3$) δ 3.50 (s, 3H, OCH$_3$), 3.99 (s, 3H, OCH$_3$), 4.18 (s, 3H, OCH$_3$), 5.24 (s, 2H, OCH$_2$), 6.80 (d, J = 8.5 Hz, 1H, H-5), 6.83 (s, 1H, H-10), 7.12 (d, J = 8.5 Hz, 2H, H-3′ and H-5′), 7.52 (d, J = 8.5 Hz, 1H, H-4), 7.87 (d, J = 8.8 Hz, 2H, H-2′ and H-6′); ^{13}C-NMR (CDCl$_3$) δ 56.2, 56.8, 61.1, 94.2, 108.0, 112.1, 116.6, 117.1, 119.5, 126.0, 132.9, 133.9, 146.6, 157.4, 158.4, 158.6, 183.0.

(Z)-6,7-Dimethoxy-3′,4′-di(methoxymethoxy)aurone (**14h**): (0.31 g, 0.78 mmol, 78% yield); yellow solid, 133–135 °C; ^{1}H-NMR (CDCl$_3$) δ 3.53 (s, 3H, OCH$_3$), 3.56 (s, 3H, OCH$_3$), 3.99 (s, 3H, OCH$_3$), 4.19 (s, 3H, OCH$_3$), 5.31 (s, 4H, OCH$_2$), 6.80 (s, 1H, H-10), 6.80 (d, J = 8.5 Hz, 1H, H-5), 7.24 (d, J = 8.3 Hz, 1H, H-5′), 7.47 (dd, J = 2.0 Hz and 8.3 Hz, 1H, H-6′), 7.52 (d, J = 8.5 Hz, 1H, H-4), 7.87 (d, J = 2.0 Hz, 1H, H-2′); ^{13}C-NMR (CDCl$_3$) δ 56.1, 56.2, 56.7, 61.0, 94.8, 95.2, 107.7, 111.9, 115.8, 116.7, 118.6, 119.2, 126.4, 126.5, 133.6, 146.3, 146.9, 148.4, 157.0, 158.3, 182.7.

(*Z*)-6,7-Dimethoxy-2′,4′-di(methoxymethoxy)aurone (**14i**): (0.36 g, 0.89 mmol, 89% yield); light yellow solid, 115–120 °C; ^{1}H-NMR (CDCl$_3$) δ 3.50 (s, 3H, OCH$_3$), 3.52 (s, 3H, OCH$_3$), 3.99 (s, 3H, OCH$_3$), 4.16 (s, 3H, OCH$_3$), 5.22 (s, 2H, OCH$_2$), 5.27 (s, 2H, OCH$_2$), 6.80 (d, *J* = 8.5 Hz, 1H, H-5), 6.83 (dd, *J* = 2.2 Hz and 8.8 Hz, 1H, H-5′), 6.88 (d, *J* = 2.2 Hz, 1H, H-3′), 7.38 (s, 1H, H-10), 7.52 (d, *J* = 8.3 Hz, 1H, H-4), 8.26 (d, *J* = 8.5 Hz, 1H, H-6′); ^{13}C-NMR (CDCl$_3$) δ 56.1, 56.3, 56.6, 60.9, 94.0, 94.5, 102.8, 106.2, 107.6, 109.2, 115.7, 117.0, 119.2, 132.4, 133.6, 146.4, 156.9, 157.6, 158.1, 159.5, 182.7.

(*Z*)-6,7,3′-Trimethoxy-4′-(methoxymethoxy)aurone (**14j**): (0.30 g, 0.81 mmol, 81% yield); yellow solid, 158–162 °C; ^{1}H-NMR (CDCl$_3$) δ 3.53 (s, 3H, OCH$_3$), 3.98 (s, 3H, OCH$_3$), 4.00 (s, 3H, OCH$_3$), 4.16 (s, 3H, OCH$_3$), 5.31 (s, 2H, OCH$_2$), 6.81 (d, *J* = 8.1 Hz, 1H, H-5), 6.82 (s, 1H, H-10), 7.23 (d, *J* = 8.5 Hz, 1H, H-5′), 7.43 (dd, *J* = 2.0 Hz and 8.5 Hz, 1H, H-6′), 7.53 (d, *J* = 8.5 Hz, 1H, H-4), 7.59 (d, *J* = 1.7 Hz, 1H, H-2′); ^{13}C-NMR (CDCl$_3$) δ 55.7, 56.2, 56.7, 60.8, 94.9, 107.8 112.2, 113.6, 115.5, 116.7, 119.4, 125.2, 126.3, 133.5, 146.4, 147.7, 149.2, 157.2, 158.4, 182.6.

(*Z*)-6,7,4′-Trimethoxy-3′-(methoxymethoxy)aurone (**14k**): (0.29 g, 0.78 mmol, 78% yield); yellow solid, 162–167 °C; ^{1}H-NMR (CDCl$_3$) δ 3.55 (s, 3H, OCH$_3$), 3.94 (s, 3H, OCH$_3$), 4.00 (s, 3H, OCH$_3$), 4.19 (s, 3H, OCH$_3$), 5.30 (s, 2H, OCH$_2$), 6.80 (d, *J* = 8.3 Hz, 1H, H-5), 6.80 (s, 1H, H-10), 6.97 (d, *J* = 8.3 Hz, 1H, H-5′), 7.48 (dd, *J* = 2.0 Hz and 8.5 Hz, 1H, H-6′), 7.51 (d, *J* = 8.5 Hz, 1H, H-4), 7.88 (d, *J* = 2.2 Hz, 1H, H-2′); ^{13}C-NMR (CDCl$_3$) δ 56.0, 56.3, 56.8, 61.1, 95.4, 107.9 111.6, 112.3, 117.0, 118.3, 119.3, 125.2, 126.9, 133.8, 146.3, 146.5, 151.1, 157.1, 158.4, 182.8.

(*Z*)-6,7,3′4′-Tetramethoxyaurone (**14l**): (0.27 g, 0.80 mmol, 80% yield); yellow solid, 156–157 °C; ^{1}H-NMR (CDCl$_3$) δ 3.95 (s, 3H, OCH$_3$), 3.98 (s, 3H, OCH$_3$), 3.99 (s, 3H, OCH$_3$), 4.16 (s, 3H, OCH$_3$), 6.80 (d, *J* = 8.5 Hz, 1H, H-5), 6.82 (s, 1H, H-10), 6.95 (d, *J* = 8.3 Hz, 1H, H-5′), 7.44 (dd, *J* = 2.0 Hz and 8.5 Hz, 1H, H-6′), 7.53 (d, *J* = 8.3 Hz, 1H, H-4), 7.60 (d, *J* = 2.0 Hz, 1H, H-2′); ^{13}C-NMR (CDCl$_3$) δ 55.6, 55.8, 56.6, 60.8, 107.8, 110.9, 112.4, 113.0, 116.8, 119.4, 125.0, 125.5, 133.5, 146.2, 148.7, 150.3, 157.1, 158.4, 182.6; UV/Vis (2.2 × 10^{-5} M, CHCl$_3$); λ = 406.8 nm (ε, 2.3 × 10^4).

3.15. The General Procedure for the Deprotection of **14a–k**

A solution of **14a–k** (1.0 mmol) in methanol (5 mL) and 3 M hydrochloric acid (5 mL) was refluxed for 1 h. The mixture was extracted with EtOAc. The organic layer was washed with water and brine and dried over anhydrous MgSO$_4$. The solvent was evaporated in vacuo and the residue was chromatographed on a preparative thin layer chromatography (hexane:EtOAc = 2:3) to produce aurones **15a–k**.

(*Z*)-6,4′-Dihydroxy-7-methoxyaurone (**15a**): (0.18 g, 0.63 mmol, 63% yield); yellow brown solid, 240–241 °C; ^{1}H-NMR (CDCl$_3$:CD$_3$OD = 1:1) δ 4.15 (s, 3H, OCH$_3$), 6.75 (d, *J* = 8.5 Hz, 1H, H-5), 6.80 (s, 1H, H-10), 6.90 (d, *J* = 8.5 Hz, 2H, H-3′ and H-5′), 7.37 (d, *J* = 8.3 Hz, 1H, H-4), 7.81 (d, *J* = 8.8 Hz, 2H, H-2′ and H-6); ^{13}C-NMR (CDCl$_3$:CD$_3$OD = 1:1) δ 61.1, 113.8, 114.2, 116.0, 116.5, 120.1, 124.2, 132.8, 133.9, 146.7, 158.5, 158.8, 160.0, 183.8; UV/Vis (3.0 × 10^{-5} M, CH$_3$OH); λ = 394.6 nm (ε, 2.6 × 10^4).

(*Z*)-6,3′,4′-Trihydroxy-7-methoxyaurone (**15b**): (0.27 g, 0.91 mmol, 91% yield); reddish ocher solid, 235–238 °C; ^{1}H-NMR (DMSO-*d*$_6$) δ 4.04 (s, 3H, OCH$_3$), 6.70 (s, 1H, H-10), 6.79 (d, *J* = 8.3 Hz, 1H, H-5), 6.87 (d, *J* = 8.3 Hz, 1H, H-5′), 7.27 (dd, *J* = 2.0 Hz and 8.3 Hz, 1H, H-6′), 7.35 (d, *J* = 8.3 Hz, 1H, H-4), 7.46 (d, *J* = 1.7 Hz, 1H, H-2′), 9.45 (s, 1H, OH), 9.84 (s, 1H, OH), 10.96 (s, 1H, OH); ^{13}C-NMR (DMSO-*d*$_6$) δ 60.8, 112.3, 113.3, 114.7, 115.9, 117.8, 119.3, 123.2, 124.6, 132.1, 145.3, 145.4, 148.0, 157.6, 157.8, 181.1; UV/Vis (2.9 × 10^{-5} M, DMSO); λ = 411.2 nm (ε, 2.1 × 10^4).

(*Z*)-6,2′,4′-Trihydroxy-7-methoxyaurone (**15c**): (0.25 g, 0.84 mmol, 84% yield); ocher solid, 288–290 °C; ^{1}H-NMR (DMSO-*d*$_6$) δ 3.94 (s, 3H, OCH$_3$), 6.43 (d, *J* = 2.0 Hz, 1H, H-3′), 6.45 (dd, *J* = 2.2 Hz and 9.3 Hz, 1H, H-5′), 6.96 (d, *J* = 8.5 Hz, 1H, H-5), 7.12 (s, 1H, H-10), 7.26 (d, *J* = 8.5 Hz, 1H, H-4), 8.16 (d, *J* = 8.3 Hz, 1H, H-6′), 9.82 (s, 1H, OH), 10.16 (s, 1H, OH), 10.42 (s, 1H, OH); ^{13}C-NMR (DMSO-*d*$_6$)

δ 56.6, 102.1, 106.3, 108.3, 108.3, 110.6, 114.6, 116.1, 131.3, 132.8, 145.0, 153.3, 154.5, 159.0, 160.8, 181.9; UV/Vis (2.8 × 10^{-5} M, DMSO); λ = 428.2 nm (ε, 3.3 × 10^4).

(*Z*)-6,4′-Dihydroxy-7,3′-dimethoxyaurone (**15d**): (0.24 g, 0.75 mmol, 75% yield); yellow solid, 218–220 °C; ^{1}H-NMR (DMSO-d_6) δ 3.87 (s, 3H, OCH$_3$), 4.04 (s, 3H, OCH$_3$), 6.79 (d, *J* = 8.5 Hz, 1H, H-5), 6.79 (s, 1H, H-10), 6.92 (d, *J* = 8.3 Hz, 1H, H-5′), 7.36 (d, *J* = 8.5 Hz, 1H, H-4), 7.42 (dd, *J* = 1.7 Hz and 8.3 Hz, 1H, H-6′), 7.63 (d, *J* = 1.7 Hz, 1H, H-2′); ^{13}C-NMR (DMSO-d_6) δ 55.6, 60.7, 112.3, 113.5, 114.3, 114.7, 116.0, 119.5, 123.4, 125.9, 132.1, 145.6, 147.7, 148.9, 157.8, 157.9, 181.2; UV/Vis (2.4 × 10^{-5} M, DMSO); λ = 407.2 nm (ε, 2.9 × 10^4).

(*Z*)-6,3′-Dihydroxy-7,4′-dimethoxyaurone (**15e**): (0.31 g, 0.97 mmol, 97% yield); yellow brown solid, 241–243 °C; ^{1}H-NMR (DMSO-d_6) δ 3.82 (s, 3H, OCH$_3$), 4.01 (s, 3H, OCH$_3$), 6.70 (s, 1H, H-10), 6.77 (d, *J* = 8.5 Hz, 1H, H-5), 7.05 (d, *J* = 8.5 Hz, 1H, H-5′), 7.33 (d, *J* = 8.3 Hz, 1H, H-4), 7.37 (dd, *J* = 1.5 Hz and 8.5 Hz, 1H, H-6′), 7.45 (d, *J* = 1.5 Hz, 1H, H-2′), 9.44 (s, 1H, OH), 10.97 (s, 1H, OH); ^{13}C-NMR (DMSO-d_6) δ 55.7, 60.8, 111.7, 112.1, 113.4, 114.5, 117.3, 119.4, 124.2, 124.5, 132.1, 145.7, 146.4, 149.5, 157.8, 157.9, 181.2; UV/Vis (2.7 × 10^{-5} M, DMSO); λ = 405.4 nm (ε, 2.1 × 10^4).

(*Z*)-6-Hydroxy-7,3′,4′-trimethoxyaurone (**15f**): (0.21 g, 0.65 mmol, 65% yield); yellow solid, 204–205 °C; ^{1}H-NMR (CDCl$_3$) δ 3.95 (s, 3H, OCH$_3$), 3.96 (s, 3H, OCH$_3$), 4.27 (s, 3H, OCH$_3$), 6.65 (s, 1H, OH), 6.82 (d, *J* = 8.5 Hz, 1H, H-5), 6.83 (s, 1H, H-10), 6.94 (d, *J* = 8.5 Hz, 1H, H-5′), 7.42 (dd, *J* = 2.0 Hz and 8.3 Hz, 1H, H-6′), 7.46 (d, *J* = 8.3 Hz, 1H, H-4), 7.51 (d, *J* = 2.0 Hz, H-2′); ^{13}C-NMR (CDCl$_3$) δ 55.7, 55.8, 60.6, 111.0, 111.7, 112.6, 113.0, 116.3, 119.7, 124.9, 125.4, 130.9, 146.0, 148.7, 150.4, 154.9, 115.9, 182.1; UV/Vis (2.4 × 10^{-5} M, CHCl$_3$); λ = 400.0 nm (ε, 2.6 × 10^4).

(*Z*)-4′-Hydroxy-6,7-dimethoxyaurone (**15g**): (0.27 g, 0.89 mmol, 89% yield); dark yellow solid, 230–231 °C; ^{1}H-NMR (DMSO-d_6) δ 4.00 (s, 3H, OCH$_3$), 4.17 (s, 3H, OCH$_3$), 5.76 (s, 1H, OH), 6.81 (d, *J* = 8.3 Hz, 1H, H-5), 6.84 (s, 1H, H-10), 6.95 (d, *J* = 8.3 Hz, 2H, H-3′ and H-5′), 7.54 (d, *J* = 8.5 Hz, 1H, H-4), 7.83 (d, *J* = 8.3 Hz, 2H, H-2′ and H-6′); ^{13}C-NMR (DMSO-d_6) δ 56.6, 60.6, 108.7, 112.0, 114.9, 116.0, 119.0, 119.1, 122.7, 133.1, 154.1, 156.5, 158.3, 159.2, 181.3; UV/Vis (3.0 × 10^{-5} M, DMSO); λ = 404.2 nm (ε, 2.5 × 10^4).

(*Z*)-3′,4′-Dihydroxy-6,7-dimethoxyaurone (**15h**): (0.16 g, 0.51 mmol, 51% yield); dark yellow solid, 219–220 °C; ^{1}H-NMR (CD$_3$OD) δ 3.97 (s, 3H, OCH$_3$), 4.08 (s, 3H, OCH$_3$), 6.71 (s, 1H, H-10), 6.84 (d, *J* = 8.3 Hz, 1H, H-5), 6.94 (d, *J* = 8.5 Hz, 1H, H-5′), 7.26 (dd, *J* = 2.2 Hz and 8.3 Hz, 1H, H-6′), 7.46 (d, *J* = 8.5 Hz, 1H, H-4), 7.46 (d, *J* = 2.2 Hz, 1H, H-2′); ^{13}C-NMR (CD$_3$OD) δ 57.2, 61.5, 109.7, 115.0, 116.4, 117.6, 118.8, 120.3, 125.1, 126.3, 135.0, 146.4, 147.0, 149.3, 158.7, 160.5, 184.3; UV/Vis (2.5 × 10^{-5} M, CH$_3$OH); λ = 408.2 nm (ε, 2.6 × 10^4).

(*Z*)-2′,4′-Dihydroxy-6,7-dimethoxyaurone (**15i**): (0.25 g, 0.78 mmol, 78% yield); reddish clay solid, 245 °C (decomp.); ^{1}H-NMR (DMSO-d_6) δ 3.94 (s, 3H, OCH$_3$), 4.02 (s, 3H, OCH$_3$), 6.43 (s, 1H, H-10), 6.44 (d, *J* = 7.1 Hz, 1H, H-5), 7.01 (d, *J* = 8.3 Hz, 1H, H-5′), 7.14 (s, 1H, H-3′), 7.48 (d, *J* = 8.3 Hz, 1H, H-4), 7.98 (d, *J* = 8.5 Hz, 1H, H-6′), 10.17 (s, 1H, OH), 10.36 (s, 1H, OH); ^{13}C-NMR (DMSO-d_6) δ 56.8, 60.7, 102.3, 106.8, 108.5, 108.9, 110.4, 116.4, 119.0, 132.2, 133.3, 144.7, 156.5, 158.2, 159.2, 161.0, 181.2; UV/Vis (2.4 × 10^{-5} M, DMSO); λ = 424.6 nm (ε, 2.9 × 10^4).

(*Z*)-4′-Hydroxy-6,7,3′-trimethoxyaurone (**15j**): (0.27 g, 0.81 mmol, 81% yield); dark yellow solid, 171–176 °C; ^{1}H-NMR (CDCl$_3$) δ 3.97 (s, 3H, OCH$_3$), 3.99 (s, 3H, OCH$_3$), 4.16 (s, 3H, OCH$_3$), 6.13 (s, 1H, OH), 6.80 (d, *J* = 8.3 Hz, 1H, H-5), 6.81 (s, 1H, H-10), 6.99 (d, *J* = 8.3 Hz, 1H, H-5′), 7.39 (dd, *J* = 1.7 Hz and 8.3 Hz, 1H, H-6′), 7.52 (d, *J* = 8.5 Hz, 1H, H-4), 7.56 (d, *J* = 1.7 Hz, 1H, H-2′); ^{13}C-NMR (CDCl$_3$) δ 55.7, 56.6, 60.7, 107.8, 112.7, 112.7, 114.7, 116.8, 119.3, 124.5, 126.1, 133.5, 146.0, 146.3, 147.3, 157.0, 158.3, 182.5; UV/Vis (2.8 × 10^{-5} M, CHCl$_3$); λ = 405.4 nm (ε, 1.7 × 10^4).

(*Z*)-3′-Hydroxy-6,7,4′-trimethoxyaurone (**15k**): (0.30 g, 0.91 mmol, 91% yield); dark yellow solid, 196–200 °C; ^{1}H-NMR (CDCl$_3$) δ 3.94 (s, 3H, OCH$_3$), 3.98 (s, 3H, OCH$_3$), 4.20 (s, 3H, OCH$_3$), 5.86 (s, 1H, OH), 6.78 (s, 1H, H-10), 6.79 (d, *J* = 9.3 Hz, 1H, H-5), 6.92 (d, *J* = 8.3 Hz, 1H, H-5′), 7.39 (dd, *J* = 2.0 Hz and 8.3 Hz, 1H, H-6′), 7.51 (d, *J* = 8.5 Hz, 1H, H-4), 7.57 (d, *J* = 2.2 Hz, 1H, H-2′); ^{13}C-NMR (CDCl$_3$)

δδ 56.0, 56.8, 61.1, 107.9, 110.6, 112.4, 116.7, 116.9, 119.3, 124.7, 125.6, 133.8, 145.6, 146.4, 148.0, 157.1, 158.4, 182.9; UV/Vis (2.6 × 10^{-5} M, CHCl$_3$); λ = 405.0 nm (ε, 1.8 × 10^4).

3.16. The DPPH Radical Scavenging Assay

The measurement of the 2,2-Diphenyl-1-picrylhydrazyl (DPPH) radical scavenging effect was performed according to the established procedure [8]. Sample compounds were dissolved in ethanol to obtain a 0.1 mM concentration. The DPPH free radical was dissolved in ethanol to obtain a concentration of 0.2 mM. The ethanol (100 μL) and DPPH solutions (50 μL) were added to a sample solution (100 μL) on a 96-well transparent microplate. The mix solution was mixed on a plate-mixer for 1 min. The mix solution was allowed to stand at 25 °C for 30 min in the dark, followed by measuring the absorbance with a microplate reader at 517 nm. The sample blank test (B) was performed with ethanol instead of the sample solution using a similar procedure. The blank test of the sample (C) was performed similarly, with ethanol instead of the DPPH solution. The blank test of the sample blank (D) was performed similarly, but with ethanol instead of the sample and DPPH solution. The DPPH radical scavenging rate was calculated as follows:

$$\text{DPPH Radical Scavenging Rate (\%)} = \{(B - D) - (A - C)\}/(B - D) \times 100 \tag{1}$$

where A is the absorbance of the sample, B is the absorbance of the sample blank, C is the absorbance of the blank of the sample, and D is the absorbance of the blank of the sample blank.

3.17. Tyrosinase Activity Inhibition Assay

The Tyrosinase activity was determined using the dopachrome method with L-3-(3,4-dihydroxyphenyl) alanine (L-DOPA) as the substrate [9]. Sample compounds were dissolved in DMSO to obtain a concentration of 3.0 mM. L-DOPA was dissolved in a 0.2 M phosphate buffer solution (PBS, pH 6.8) to obtain a concentration of 1.66 mM. The enzyme tyrosinase from mushrooms was dissolved in PBS to obtain a concentration of 600 units/mL. The sample solution (10 μL) was added to a L-DOPA solution (280 μL) on a 96-well transparent microplate. The mix solution was mixed on a plate-mixer for 1 min. The mix solution was left to stand at 25 °C for 5 min. The tyrosinase solution (10 μL) was added to the mixture and the mixture was incubated at 25 °C for 10 min, followed by measuring the absorbance with a microplate reader at 475 nm. The sample blank test (B) was performed with DMSO instead of the sample solution with similar procedure. The blank test of sample (C) was similarly performed with PBS instead of the enzyme solution. The blank test of the sample blank (D) was similarly performed with the DMSO and PBS instead of the sample and enzyme solutions, respectively. The percentage inhibition of tyrosinase activity was calculated as follows.

$$\text{Tyrosinase Activity Inhibition Rate (\%)} = \{(B - D) - (A - C)\}/(B - D) \times 100 \tag{2}$$

where A is the absorbance of the sample, B is the absorbance of the sample blank, C is the absorbance of the blank of the sample, and D is the absorbance of the blank of the sample blank.

4. Conclusions

In this study, chalcones, flavanones, and flavonols were easily synthesized, including 8-methoxybutin, which is a naturally occurring product from *Coreopsis lanceolata* L., using the HWE reaction as the key reaction in five to seven steps with overall yields of 18–59%, 13–53%, and 2–21% from *O*-methylpyrogallol **4a,b**, respectively. The synthesis of aurones including leptosidin was achieved in four to five steps with overall yields of 5–36% from **4a,b** using the aldol condensation reaction as a key reaction.

We found a correlation between the physiological activity and structures of the A- and B-rings of chalcone, flavanone, flavonol, and aurone. Each of chalcones **7b,h**; flavanones **8b,h**; flavonols

11b,**h**; and aurones **15b**,**h** with the 3,4-dihydroxy groups on the B-ring had high antioxidant activity. The antioxidant activity in decreasing order was flavonol, chalcone, aurone, and flavanone.

The chalcones **7c**,**i** and aurones **15c**,**i** bearing the 2,4-dihydroxy groups on the B-ring had a high inhibitory activity potential. The whitening effect in decreasing order was chalcone, aurone, flavonol, and flavanone.

References

1. Tanimoto, S.; Miyazawa, M.; Inoue, T.; Okada, Y.; Nomura, M. Chemical constituents of *Coreopsis lanceolata* L. and their physiological activities. *J. Oleo Sci.* **2009**, *58*, 141–146. [CrossRef] [PubMed]
2. Okada, Y.; Okita, M.; Murai, Y.; Okano, Y.; Nomura, M. Isolation and identification of flavonoids from *Coreopsis lanceolata* L. petals. *Nat. Prod. Res.* **2014**, *28*, 201–204. [CrossRef] [PubMed]
3. Pardede, A.; Mashita, K.; Ninomiya, M.; Tanaka, K. Kouketsu, Flavonoid profile and antileukemic activity of *Coreopsis lanceolata* flowers. *Bioorg. Med. Chem. Lett.* **2016**, *26*, 2784–2787. [CrossRef] [PubMed]
4. Rao, Y.K.; Rao, V.C.; Kishore, P.H.; Gunasekar, D. Total synthesis of heliannone A and (*R*,*S*)-heliannone B, two bioactive flavonoids from *Helianthus annuus* Cultivars. *J. Nat. Prod.* **2001**, *64*, 368–369. [CrossRef] [PubMed]
5. Oyamada, T. A new general method for the synthesis of the derivatives of flavonol. *Bull. Chem. Soc. Jpn.* **1935**, *10*, 182–186. [CrossRef]
6. Bolek, D.; Gütschow, M. Preparation of 4,6,3′,4′-tetrasubstituted aurones via aluminium oxide-catalyzed condensation. *J. Heterocycl. Chem.* **2005**, *42*, 1399–1403. [CrossRef]
7. Pelter, A.; Ward, R.S.; Heller, H.G. Carbon-13 nuclear magnetic resonance spectra of (*Z*)- and (*E*)-aurones. *J. Chem. Soc. Perkin Trans. 1* **1979**, *0*, 328–329. [CrossRef]
8. Tominaga, H.; Kobayashi, Y.; Goto, T.; Kasemura, K.; Nomura, M. DPPH radical-scavenging effect of several phenylpropanoid compounds and their glycoside derivatives. *Yakugaku Zasshi* **2005**, *125*, 371–375. [CrossRef] [PubMed]
9. Tada, T.; Nomura, M.; Shimomura, K.; Fujihara, Y. Synthesis of karahanaenone derivatives and their inhibition properties toward tyrosinase and superoxide scavenging activity. *Biosci. Biotechnol. Biochem.* **1996**, *60*, 1421–1424. [CrossRef]
10. Stratford, M.R.L.; Ramsden, C.A.; Riley, P.A. Mechanistic studies of the inactivation of tyrosinase by resorcinol. *Bioorg. Med. Chem.* **2013**, *21*, 1166–1173. [CrossRef] [PubMed]

Preliminary Quality Evaluation and Characterization of Phenolic Constituents in Cynanchi Wilfordii Radix

Takashi Uchikura [1], Hiroaki Tanaka [1], Hidemi Sugiwaki [1], Morio Yoshimura [1], Naoko Sato-Masumoto [2], Takashi Tsujimoto [2], Nahoko Uchiyama [2], Takashi Hakamatsuka [2] and Yoshiaki Amakura [1,*]

[1] Department of Pharmacognosy, College of Pharmaceutical Sciences, Matsuyama University, 4-2 Bunkyo-cho, Matsuyama, Ehime 790-8578, Japan; 46150019@g.matsuyama-u.ac.jp (T.U.); 16130815@g.matsuyama-u.ac.jp (H.T.); h_sugiwa@g.matsuyama-u.ac.jp (H.S.); myoshimu@g.matsuyama-u.ac.jp (M.Y.)

[2] Division of Pharmacognosy, Phytochemistry and Narcotics, National Institute of Health Sciences, 3-25-26 Tonomachi, Kawasaki-ku, Kawasaki, Kanagawa 210-9501, Japan; nasato@nihs.go.jp (N.S.-M.); tsujimoto@nihs.go.jp (T.T.); nuchiyama@nihs.go.jp (N.U.); thakama@nihs.go.jp (T.H.)

* Correspondence: amakura@g.matsuyama-u.ac.jp; Tel.: +81-89-925-7111

Abstract: A new phenolic compound, 2-*O*-β-laminaribiosyl-4-hydroxyacetophenone (**1**), was isolated from Cynanchi Wilfordii Radix (CWR, the root of *Cynanchum wilfordii* Hemsley), along with 10 known aromatic compounds, including cynandione A (**2**), bungeisides-C (**7**) and –D (**8**), *p*-hydroxyacetophenone (**9**), 2′,5′-dihydroxyacetophenone (**10**), and 2′,4′-dihydroxyacetophenone (**11**). The structure of the new compound (**1**) was elucidated using spectroscopic methods and chemical methods. The structure of cynandione A (**2**), including a linkage mode of the biphenyl parts that remained uncertain, was unambiguously confirmed using the 2D ^{13}C–^{13}C incredible natural abundance double quantum transfer experiment (INADEQUATE) spectrum. Additionally, health issues related to the use of Cynanchi Auriculati Radix (CAR, the root of *Cynanchum auriculatum* Royle ex Wight) instead of CWR have emerged. Therefore, constituents present in methanolic extracts of commercially available CWRs and CARs were examined using UV-sensitive high-performance liquid chromatography (HPLC), resulting in common detection of three major peaks ascribed to cynandione A (**2**), *p*-hydroxyacetophenone (**9**), and 2′,4′-dihydroxyacetophenone (**11**). Thus, to distinguish between these ingredients, a thin-layer chromatography (TLC) method, combined with only UV irradiation detection, focusing on wilfosides C1N (**12**) and K1N (**13**) as marker compounds characteristic of CAR, was performed. Furthermore, we propose this method as a simple and convenient strategy for the preliminary distinction of CWR and CAR to ensure the quality and safety of their crude drugs.

Keywords: *Cynanchum wilfordii*; phenolic glycoside; 2-*O*-β-laminaribiosyl-4-hydroxyacetophenone; cynandione A; thin layer chromatography; *Cynanchum auriculatum*

1. Introduction

Cynanchi Wilfordii Radix (CWR), the dried root of *Cynanchum wilfordii* Hemsley (family Asclepiadaceae), is a crude drug listed in the Korean Herbal Pharmacopoeia [1]. CWR has been used in Korea as a substitute for Polygoni Multiflori Radix, the dried root of *Polygonum multiflorum* Thunberg (Polygonaceae), which is used for its restorative effects and is one of the important crude drugs listed in the Japanese, Korean, and Chinese Pharmacopoeias. Recently, the use of Cynanchi Auriculati Radix (CAR), the dried root of *Cynanchum auriculatum* Royke ex Wight, instead of CWR has led to health problems in Korea [2,3]. Although CAR resembles CWR closely in appearance,

CAR, a crude drug that differs from CWR in China, is currently treated as a toxic plant by the U.S. Food and Drug Administration (FDA) [4]. Therefore, standards and methods to distinguish CWR from CAR should be established to ensure the quality and safety of the crude drugs. We recently reported a survey on the original plant species of crude drugs widely distributed as CWR in the Korean and Chinese markets. This study revealed that CAR was incorrectly used in eight of the 13 products distributed as CWR, including possible confusion of CWR and CAR [5]. Previous phytochemical investigations of CWR identified the presence of pregnane glycosides, acetophenones, and humulanolides [6–11]. Although there are several reports on ingredient research using materials of CWA and CAR available on the market, they may not be of the precise species. Therefore, detailed phytochemical information on the raw material with defined origins is necessary to ensure the quality and safety of crude drugs.

Several studies have assessed the quality of CWR and CAR and have aimed to distinguish between them using high-performance liquid chromatography (HPLC) [12,13], and many methods used to identify crude drugs ensure reliability. However, in this study, the characterization of phenolic constituents in authentic original CWR plant species is identified using DNA sequences [5], and a simple and convenient thin-layer chromatography (TLC) method for the distinction of CWR and CAR to ensure the quality and safety of their crude drugs.

2. Results and Discussion

2.1. Isolation and Characterization

A homogenate of CWR in 80% methanol (MeOH) was concentrated and further extracted with *n*-hexane, ethyl acetate (EtOAc), and *n*-butanol (BuOH) to obtain the respective extracts and water (H_2O) extract. HPLC analysis was used to monitor the ultraviolet (UV)-sensitive compounds (phenols) in the EtOAc and *n*-BuOH extracts, which were separately chromatographed using a Diaion HP-20, YMC GEL ODS-AQ, and Chromatorex ODS with MeOH-H_2O in a stepwise gradient mode. The fractions showing similar HPLC or TLC patterns were combined and further purified using column chromatography to obtain compound **1**, cynandione A (**2**) [14], uridine (**3**), guanosine (**4**), adenosine (**5**), tryptophan (**6**) [15], bungeiside-C (**7**), bungeiside-D (**8**), *p*-hydroxyacetophenone (**9**) [16], 2′,5′-dihydroxyacetophenone (**10**) [13], and 2′,4′-dihydroxyacetophenone (**11**) [16]. The known compounds **2–11** were identified by direct comparison with authentic specimens and by comparing their spectral data with those reported in the literature (Figure 1).
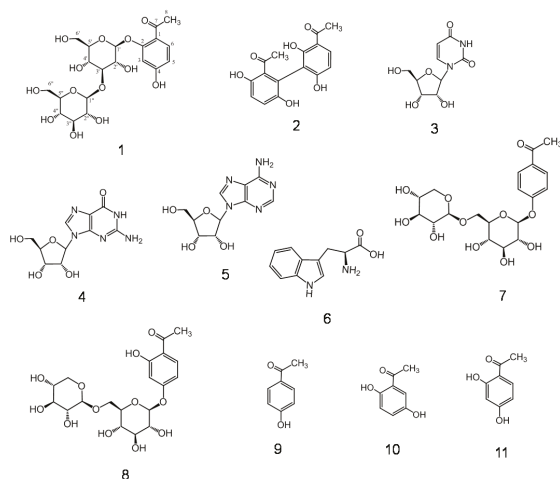

Figure 1. Structures of compounds **1–11**.

Compound **1** was isolated as a light brown amorphous powder. Its molecular formula was assigned as $C_{20}H_{28}O_{13}$ based on its high resolution-electrospray ionization (HR-ESI)-mass spectrometry (MS, *m/z* 475.1473 [M–H]⁻; calcd. for $C_{20}H_{28}O_{13}$-H: 475.1457) and ^{13}C-NMR (20 ^{13}C signals) spectra. The UV spectrum showed absorption maxima at 228, 269, and 301 nm. The proton (^{1}H)- and ^{13}C-NMR spectra of compound **1** exhibited the following signal characteristics of the 2′,4′-hydroxyacetophenone moiety. The ^{1}H-NMR spectrum (Figure S1) assigned based on the ^{1}H-^{1}H correlation spectroscopy (COSY) (Figure S2) exhibited signals due to an acetyl group (δ_H 2.62, 3H) and ABX-type proton signals due to a trisubstituted benzene proton, δ_H 6.69 (d, *J* = 2.0 Hz), 6.50 (dd, *J* = 2.0, 8.5 Hz), and 7.68 (d, *J* = 8.5 Hz), and two sets of sugar protons.

This acetophenone unit was also supported by eight carbon signals, δ_C 121.3, 160.9, 103.7, 164.9, 110.8, 133.3, 200.3, and 32.1 (C-1–8), in the ^{13}C-NMR spectrum (Figure S3) assigned based on heteronuclear single quantum coherence (HSQC) and heteronuclear multiple bond connectivity (HMBC) spectra (Figure 2, Figures S4 and S5). Additionally, an aglycone of compound **1** was chemically substantiated by acid hydrolysis followed by HPLC analysis, which showed the production of 2′,4′-dihydroxyacetophenone. The presence of two sugar units in **1** was indicated by two anomeric proton signals at δ_H 5.05 (d, *J* = 7.5 Hz) and 4.58 (d, *J* = 7.5 Hz) and others assigned based on COSY, as shown in Table 1. Thus, the sugar residues were presumed to be hexoses, as revealed by 12 aliphatic carbon signals (δ_C 102.1, 110.8, 74.1, 75.5, 88.2, 77.9, 69.7, 71.6, 78.0, 78.2, 62.4, and 62.6) in the ^{13}C-NMR spectrum.

The sugar unit obtained following acid hydrolysis of compound **1** was identified as D-glucose by the HPLC analysis of derivatives prepared by the reaction with L-cysteine methyl ester and *o*-tolyl isothiocyanate according to the previously reported method [17]. The linking position of each unit was determined by correlations among the glucose H-1′ (δ 5.05)/C-2 (δ 160.9) of the acetophenone moiety and glucose H-1″ (δ 4.95)/glucose C-3 (δ 88.2) in the HMBC spectrum. Moreover, the nuclear Overhause effect spectroscopy (NOESY) results showed a correlation between the glucose H-1′ (δ_H 5.05) and H-3 (δ_H 6.69) (Figure 2). β-Glycosidic linkages at each glucose core were assigned by a large coupling constant (*J* = 7.5 Hz). Therefore, compound **1** was established as 2-*O*-β-laminaribiosyl-4- hydroxyacetophenone.

Table 1. ^{1}H- (500 MHz) and ^{13}C-NMR (126 MHz) data of compound **1** measured in MeOH-d_4.

Positions	δ_C	δ_H (*J* in Hz)
1	121.3	
2	160.9	
3	103.7	6.69 (d, *J* = 2.0)
4	164.9	
5	110.8	6.50 (dd, *J* = 2.0, 8.5)
6	133.3	7.68 (d, *J* = 8.5)
7	200.3	
8	32.1	2.62 (3H, s)
Glucose-1′	102.1	5.05 (d, *J* = 7.5)
2′	74.1	3.74 (m) [d]
3′	88.2	3.67 (t, *J* = 9.0)
4′	69.7	3.54 (t, *J* = 9.0)
5′	78.0 [a]	3.52 (m) [d]
6′	62.4 [b]	3.94 (dd, *J* = 1.5, 12.0) [c], 3.75 (m) [c,d]
Glucose-1″	105.3	4.58 (d, *J* = 7.5)
2″	75.5	3.30 (m) [d]
3″	77.9 [a]	3.39 (t, *J* = 9.5)
4″	71.6	3.30 (m) [d]
5″	78.2 [a]	3.35 (m) [d]
6″	62.6 [b]	3.89 (dd, *J* = 2.0, 11.5) [c], 3.63 (m) [c,d]

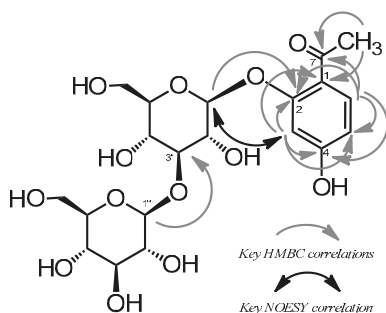[a,b,c] Assignments may be interchanged. [d] Overlapped signals.

Figure 2. Key heteronuclear multiple bond connectivity (HMBC) correlations and nuclear Overhause effect spectroscopy (NOESY) correlation of compound **1**.

Cynandionene A (**2**) is a characteristic biacetophenone derivative with a biphenyl structure, which was revised from 4,3′-diacetyl-2,3,2′,6′-tetrahydrohydroxybiphenyl by 6,3′-diacetyl-2,5,2′,6′-tetrahydrohydroxybiphenyl after the structural elucidation [14]. It was difficult to confirm the present structure based only on the HMBC spectrum because a connection between C-1 and C-1′ could not be confirmed. Therefore, in this study, we attempted to prove the connection of the biphenyl carbon–carbon bond using two-dimensional (2D) incredible natural abundance double quantum transfer experiment (INADEQUATE) for the first time. All C–C correlations were observed as shown in Figure 3. Compound **2** was shown to have C–C correlations between C-1 and C-1′. Therefore, the present biphenyl structure of compound **2** was supported by the 2D-INADEQUATE data. The positions of two acetyl groups were also confirmed using HMBC.
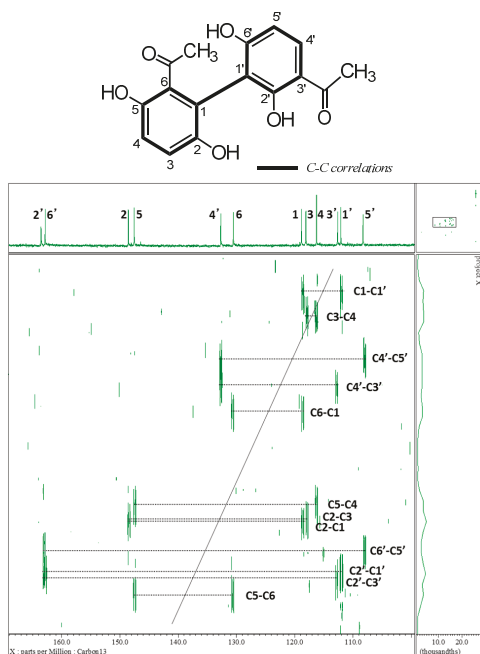
Figure 3. Two-dimensional incredible natural abundance double quantum transfer experiment (2D-INADEQUATE) spectrum of compound **2**.

2.2. Preliminary Quality Evaluation of CWR and CAR Using TLC

CAR resembles CWR closely in appearance as shown in Figure 4. In this study, CWR and CAR (four and nine samples, respectively) identified using DNA sequences [5] were used as the test samples (Table 2 and Figure 4). HPLC chromatograms of MeOH extracts (CWR-Ex and CAR-Ex) obtained from these samples are shown in Figure 5.
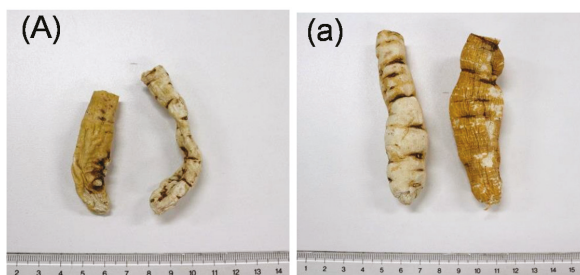

Figure 4. Crude drugs identified: (**A**) Cynanchi Wilfordii Radix (CWR, the root of *Cynanchum wilfordii* Hemsley) (Product C), and (**a**) Cynanchi Auriculati Radix (CAR, the root of *Cynanchum auriculatum* Royke ex Wight) (Product h).

Table 2. The Korean and Chinese market samples used in this study.

Products	Crude Drug	Locality	Market
A	Cynanchi Wilfordii Radix (CWR)	Korea	Korea
B	Cynanchi Wilfordii Radix (CWR)	Korea	Korea
C	Cynanchi Wilfordii Radix (CWR)	Yeongcheon	Korea
D	Cynanchi Wilfordii Radix (CWR)	Yeongcheon	Korea
a	Cynanchi Auriculati Radix (CAR)	Jiangsu	China
b	Cynanchi Auriculati Radix (CAR)	Jiangsu	China
c	Cynanchi Auriculati Radix (CAR)	Jiangsu	China
d	Cynanchi Auriculati Radix (CAR)	Jiangsu	China
e	Cynanchi Auriculati Radix (CAR)	Jiangsu	China
f	Cynanchi Auriculati Radix (CAR)	Jiangsu	China
g	Cynanchi Auriculati Radix (CAR)	Jiangsu	China
h	Cynanchi Auriculati Radix (CAR)	Korea	Korea
i	Cynanchi Auriculati Radix (CAR)	Korea	Korea

In all the HPLC analyses of CWR-Ex samples, three main peaks corresponding to cynandione A (**2**), *p*-hydroxyacetophenone (**9**), and 2′,4′-dihydroxyacetophenone (**11**) were detected. In CAR-Ex, products **b**–**e** and **g**–**i**, but not **a** and **f**, were also mainly detected, suggesting that it would be difficult to distinguish these crude drugs by detecting these three compounds as reference compounds. On the other hand, CAR exhibited a peak corresponding to wilfosides K1N (**13**), which was not clearly detected in those of CWR. Because it was difficult to distinguish the species using HPLC analyses, a TLC method was developed. The TLC chromatogram of CAR-Ex with an EtOAc/water/MeOH/acetic acid (200:10:10:3, *v/v/v/v*) solvent mixture (A) as the mobile phase provided well-separated spots under UV light (254 nm) including a clear spot with approximately *R*f 0.5 (Figure 6). This spot was revealed to be due to two compounds with almost the same *R*fs. These two compounds were isolated by preparative TLC with the other solvent system, *n*-hexane-acetone (1:1), leading to clearly separated spots and were identified as wilfosides C1N (**12**) and K1N (**13**) [18].

Several previous studies have reported strategies for distinguishing CWR and CAR. For example, one method evaluated seven compounds in each sample, whereas another study used conduritol F as a marker compound, which is a characteristic constituent in CWR [12,13]. However, one method was complicated because it required the analysis of numerous constituents in samples using HPLC, and the other involved detection using a spray reagent using TLC. Additionally, the identification

of the type of samples is vague, although the appearances are similar. The method proposed in the present study is extremely simple because the sample was extracted with MeOH, followed only by a TLC method with UV irradiation detection. Thus, this method could be useful as a distinguishing tool among the preliminary TLC methods for comparison of CWR and CAR.
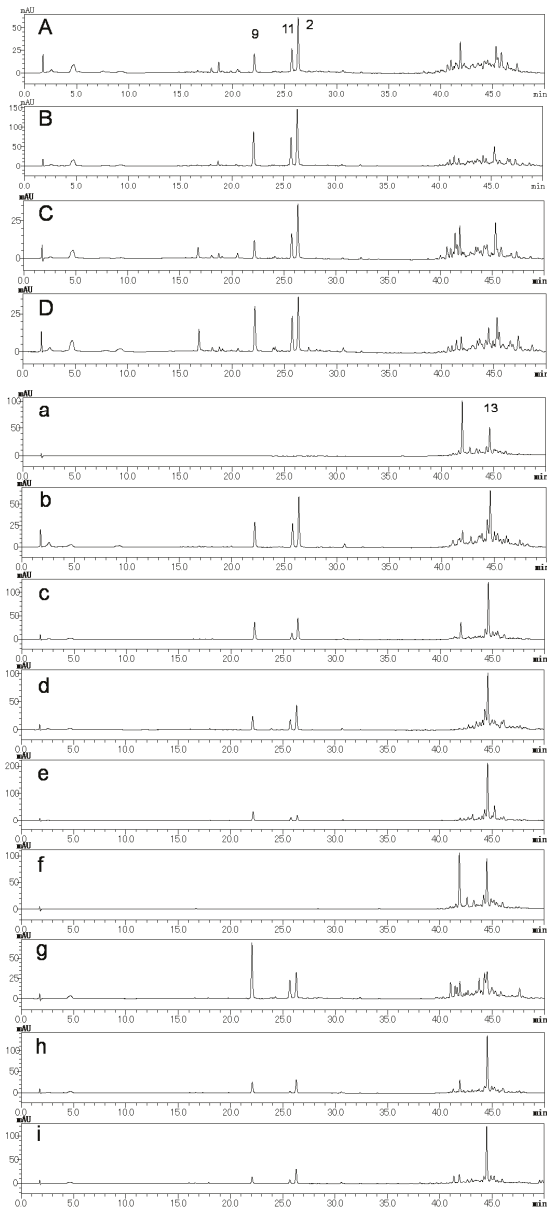

Figure 5. HPLC chromatograms of the crude drug extracts identified as Cynanchi Wilfordii Radix (CWR) (**A–D**) and Cynanchi Auriculati Radix (CAR) (**a–i**). The number on the chromatogram corresponds to the compound number. HPLC conditions are described in condition 1 of Section 3.
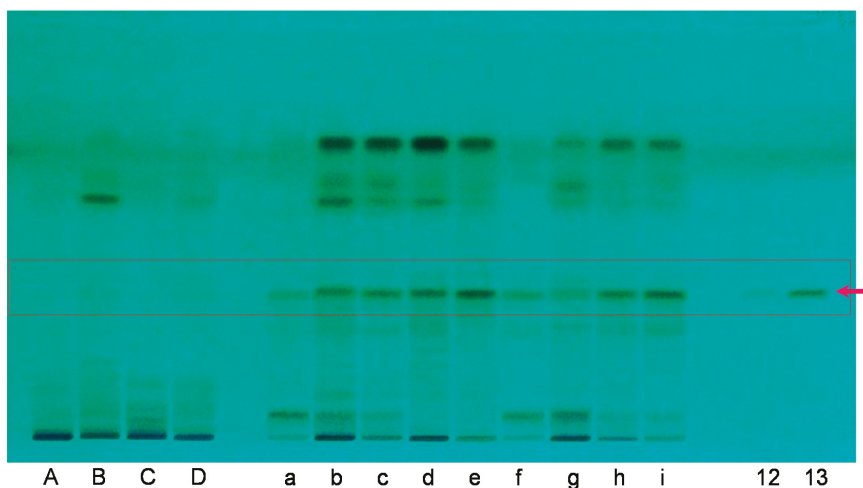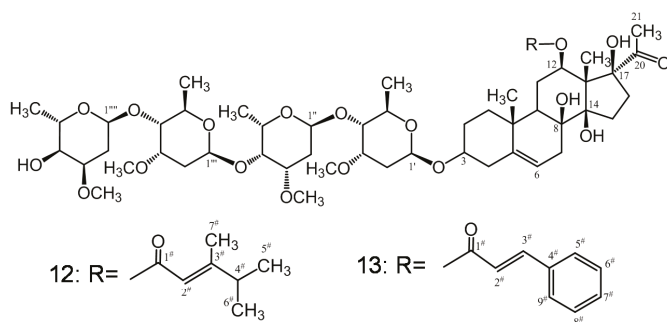
Figure 6. TLC chromatograms of the crude drugs Cynanchi Wilfordii Radix (CWR) (**A**–**D**) and Cynanchi Auriculati Radix (CAR) (**a**–**i**). TLC plate illuminated with UV 254 nm. 12: wilfoside C1N, 13: wilfoside K1N. Conditions are described in Section 3.

3. Experimental Section

3.1. General

Optical rotations were measured using a JASCO P-1020 digital polarimeter (JASCO Corporation, Tokyo, Japan). The UV spectra were recorded using a Shimadzu UVmini-1240 (Shimadzu Corporation, Kyoto, Japan). The HR-ESI-MS spectra were obtained using a micrOTOF-Q (Bruker Daltonics, Billerica, MA, USA) mass spectrometer with acetonitrile as the solvent. The NMR spectra were recorded using a Bruker AVANCE500 instrument (Bruker BioSpin, Billerica, MA, USA; 500 and 126 MHz for ^{1}H and ^{13}C, respectively) and chemical shifts were expressed as parts per million (ppm) relative to those of the solvents [MeOH-d_4 (δ_H 3.30; δ_C 49.0), and dimethyl sulfoxide (DMSO)-d_6 (δ_H 2.50; δ_C 39.5)] on a tetramethylsilane scale. The standard pulse sequences programmed for the instrument (AVANCE 500) were used for each 2D measurement (COSY, HSQC, and HMBC). The 2D-INADEQUATE spectrum was recorded using a JEOL ECA800 instrument (JEOL, Tokyo, Japan). Column chromatography was carried out using the Diaion HP-20, MCI-gel CHP-20P (Mitsubishi Chemical Co., Tokyo, Japan), Chromatorex ODS (Fuji Silysia Chemical Ltd., Aichi, Japan) and YMC GEL ODS (YMC Co. Ltd., Kyoto, Japan), respectively. Preparative TLC was carried out using TLC Silica gel 60 F$_{254}$ glass plates (Merck, Darmstadt, Germany). TLC was performed with CAMAG HPTLC equipment (CAMAG,

Muttenz, Switzerland) including a Linomat V applicator (CAMAG) and visualizer documentation system (CAMAG). The samples were spotted on HPTLC Silica gel 60 F$_{254}$ glass plates (20 × 10 cm, Merck), and the spots were detected using UV irradiation at 254 nm. The reversed-phase (RP) HPLC conditions were as follows. Condition 1: column, L-column ODS (5 μm, 150 × 2.1 mm i.d., Chemicals Evaluation and Research Institute, Tokyo, Japan); mobile phase, solvent A was 0.1% formic acid in water, and solvent B was 0.1% formic acid in acetonitrile (0–30 min, 0–50% B in A; 30–35 min, 50–85% B in A; 35–40 min, 85–85% B in A); injection volume, 2 μL; column temperature, 40 °C; flow-rate, 0.3 mL/min; and detection wavelength, 200–400 nm. Condition 2: column, YMC-pack ODS-AQ-3C2 (5 μm, 150 × 2.0 mm i.d., YMC Co. Ltd., Kyoto, Japan); mobile phase, 10 mmol/L phosphoric acid (H$_3$PO$_4$)-10 mmol/L monopotassium phosphate (KH$_2$PO$_4$)-acetonitrile (8:2); column temperature, 30 °C; flow-rate, 0.25 mL/min; and detection wavelength, 280 nm. Condition 3: column, YMC-pack ODS-AQ-3C2 (5 μm, 150 × 2.0 mm i.d., YMC Co. Ltd., Kyoto, Japan); mobile phase, 50 mmol/L phosphate buffer-acetonitrile (75:25); column temperature, 35 °C; flow-rate, 0.3 mL/min; and detection wavelength, 250 nm.

3.2. Materials

The CWR products used in the phytochemical investigation were purchased at a crude drug store at the Gyeongdong Market (Seoul, Korea). CWR and CAR for HPLC and TLC analyses were obtained from the Gyeongdong or Chinese markets and were provided by Japanese crude drug wholesalers. The identities of all the crude drugs were confirmed using DNA sequences [5]. All other reagents used were of analytical grade.

3.3. Extraction and Isolation

The CWR product (300 g) was homogenized in 3 L 80% MeOH [MeOH-H$_2$O (8:2)], the homogenate was filtered, concentrated to approximately 300 mL, and then extracted with 3 L each of *n*-hexane, EtOAc, and *n*-BuOH to obtain extracts at yields of *n*-hexane (492.9 mg), EtOAc (7.0 g), *n*-BuOH (13.2 g), and water (43.2 g), respectively. The EtOAc extract (500 mg) was chromatographed using the YMC GEL ODS with MeOH-H$_2$O (10:90→20:80→30:70→40:60→50:50→100:0) in stepwise gradient mode. The fractions showing similar HPLC patterns were combined and further purified using column chromatography with the Chromatorex ODS or preparative TLC with *n*-hexane-acetone (2:1 or 1:1), or both to obtain *p*-hydroxyacetophenone (**9**, 13.8 mg), 2′,5′- dihydroxyacetophenone (**10**, 1.0 mg), 2′,4′-dihydroxyacetophenone (**12**, 3.8 mg), and cynandionene A (**2**, 9.6 mg). The *n*-BuOH extract (12.5 g) was similarly separated using column chromatography over Diaion HP-20 with MeOH-H$_2$O (0:100→10:90→20:80→30:70→40:60→50:50→ 100:0) in stepwise gradient mode. The H$_2$O eluate (3.0 g) was separated using column chromatography using the Chromatorex ODS with aqueous MeOH to obtain uridine (**3**, 6.3 mg), and adenosine (**5**, 2.3 mg). The 10, 20, 30, and 40% MeOH eluates (120, 130, 89, and 52 mg, respectively) were purified using column chromatography with YMC GEL ODS using aqueous MeOH to obtain guanosine (**4**, 21.8 mg), tryptophan (**6**, 20.6 mg), bungeiside-C (**7**, 13.7 mg) plus compound **1** (2.4 mg), and bungeiside-D (**8**, 7.0 mg), respectively. These compounds were identified by direct comparison with authentic specimens or by comparing their spectral data with those reported in the literature. The physical spectral data of the new compound **1** are as follows.

2-O-β-Laminaribiosyl-4-hydroxyacetophenone (**1**): A light brown amorphous powder. UV λ$_{max}$ (MeOH) nm (log ε): 228 (3.01), 269 (3.14), 301 (2.94). [α]$_D^{24}$ -14° (*c* 1.0, MeOH). ^{1}H-NMR (500 MHz, MeOH-*d$_4$*) and ^{13}C-NMR (126 MHz, MeOH-*d$_4$*) data are shown in Table 1. HR-ESI-MS *m/z*: 475.1473 ([M–H]$^-$, Calcd. for C$_{20}$H$_{28}$O$_{13}$-H: 475.1457).

Cynandione A (**2**): ^{1}H-NMR (DMSO-*d$_6$*, 800 MHz) δ 12.86 (1H, s, 2′-OH), 10.31 (1H, s, 6′-OH), 9.31 (1H, s, 2-OH), 8.49 (1H, s, 5-OH), 7.68 (1H, d, *J* = 2 Hz, H-4′), 6.72 (1H, d, *J* = 8 Hz, H-3), 6.67 (1H, d, *J* = 8 Hz, H-4), 6.43 (1H, d, *J* = 8 Hz, H-5′), 2.50 (3H, s, 8-CH$_3$), 2.19 (3H, s, 8′-CH$_3$). ^{13}C-NMR (DMSO-*d$_6$*, 200 MHz) δ 203.7 (C-7′), 203.6 (C-7), 163.0 (C-2′), 162.8 (C-6′), 148.5 (C-2), 147.5 (C-5), 132.7 (C-4′),

130.7 (C-6), 118.7 (C-1), 117.9 (C-3), 116.3 (C-4), 112.8 (C-3′), 112.0 (C-1′), 108.0 (C-5′), 31.2 (C-8), 26.7 (C-8′).

The CAR product (103 g) was homogenized in 80% MeOH (1 L), and the homogenate was filtered, concentrated to approximately 100 mL, and then extracted with *n*-hexane (300 mL), EtOAc (300 mL), *n*-BuOH (3 L), and water to obtain the solvent extracts at yields of 492.9 mg, 7.0 g, 13.2 g, and 43.2 g, respectively. The EtOAc extract (100 mg) was dissolved in MeOH and subjected to preparative TLC [*n*-hexane-acetone (1:1)] to yield wilfoside C1N (**12**, 8.0 mg) and wilfoside K1N (**13**, 10.5 mg). These compounds were identified by comparing their ^{1}H- and ^{13}C-NMR data with those reported in literatures and were used as standard samples.

3.4. Partial Acid Hydrolysis of Compound **1**

A solution of compound **1** (0.2 mg) in H_2O (0.2 mL) and 1 mol/L hydrochloric acid (HCl, 0.1 mL) was heated in a boiling water bath for 8 h. After removing the solvent, the residue was analyzed using HPLC (under Condition 2), and 2′,4′-dihyroxyaetophenone was detected.

3.5. Determination of Sugar Configuration of Compound **1**

The sugar configuration was determined using a previously described method [17]. Compound **1** (1.0 mg) was hydrolyzed by heating in 1 mol/L HCl (0.2 mL) and neutralized with Amberlite IRA400. After evaporation, the residue was dissolved in pyridine (0.2 mL) containing L-cysteine methyl ester hydrochloride (1.0 mg) and heated at 60 °C for 1 h. *o*-Tolyl isothiocyanate (1.0 mg) in pyridine (0.2 mL) was then added to the mixture and heated at 60 °C for 1 h. The reaction mixture was directly analyzed using RP-HPLC (under Condition 3). The peak coincided with that of the derivative of the authentic D-glucose sample.

3.6. Preparation of Test Solution of the Crude Drugs for HPLC and TLC

A sample of each product obtained from the open market was pulverized (0.2 and 1 g for the HPLC and TLC analyses, respectively), extracted with MeOH (1.0 mL) by sonication for 5 min, centrifuged, and the supernatant obtained was used as the test solution. The HPLC was performed under Condition 1 described in Section 3.1. For the TLC, aliquots (5 μL) of each test solution were applied to the HPTLC plates, which were developed in a TLC chamber saturated with EtOAc/water/MeOH/acetic acid (200:10:10:3, *v/v/v/v*) mixture as the mobile phase. The spots were detected under a UV lamp at 254 nm.

4. Conclusions

In the present study, a new phenolic compound, 2-*O*-β-laminaribiosyl-4-hydroxyacetophenone (**1**), was successfully isolated from CWR, in addition to 11 known compounds. Cynandione A (**2**), which is one of the main constituents of CWR with a biphenyl moiety, was identified using its 2D ^{13}C–^{13}C INADEQUATE spectrum; the carbon–carbon connection of the biphenyl moiety was clearly confirmed for the first time. The component distributions of MeOH extracts of CWR using a UV-sensitive HPLC analysis revealed three peaks of cynandione A (**2**), *p*-hydroxyacetophenone (**9**), and 2′,4′-dihydroxyacetophenone (**11**), which were the main detected constituents. The emerging use of CAR in place of CWR has led to the need for a differentiating method, and therefore, we proposed and developed the present TLC method for the preliminary distinction between CWR and CAR.

References

1. Korea Food and Drug Administration. *The Korean Herbal Pharmacopoeia*; Korea Food and Drug Administration: Seoul, Korea, 2002; p. 98.

2. Ministry of Food and Drug Safety, Korea. Available online: http://www.mfds.go.kr/index.do?mid=676& seq=27270 (accessed on 25 January 2018).

3. Division of Safety Information on Drug and Food, National Institute of Health Sciences. Food Safety Information. Available online: http://www.nihs.go.jp/hse/food-info/foodinfonews/2015/ foodinfo201509c.pdf (accessed on 25 January 2018).

4. U.S. Food and Drug Administration (FDA). FDA Poisonous Plant Database. Available online: https://www.accessdata.fda.gov/scripts/Plantox/Detail.CFM?ID=11513 (accessed on 25 January 2018).

5. Sato-Masumoto, N.; Uchikura, T.; Sugiwaki, H.; Yoshimura, M.; Masada, S.; Atsumi, T.; Watanabe, M.; Tanaka, N.; Uchiyama, N.; Amakura, Y.; et al. Survey on the original plant species of crude drugs distributed as *Cynanchi Wilfordii* radix and its related crude drugs in the korean and chinese markets. *Biol. Pharm. Bull.* **2017**, *40*, 1693–1699. [CrossRef] [PubMed]

6. Tsukamoto, S.; Hayashi, K.; Mistuhashi, H. Studies on the constitunets of Asclepiadanceae plants. LX. Further studies on glycosides with a novel sugar chain containing a pair of optically isomeric sugars, D- and L-cymarose, from *Cynanchum wilfordi*. *Chem. Pharm. Bull.* **1985**, *33*, 2294–2304. [CrossRef]

7. Hwang, B.Y.; Kim, S.E.; Kim, Y.H.; Kim, H.S.; Hong, Y.-S.; Ro, J.S.; Lee, K.S.; Lee, J.J. Pregnane glycosides multidrug-resistance modulators from *Cynanchum wilfordii*. *J. Nat. Prod.* **1999**, *62*, 640–643. [CrossRef] [PubMed]

8. Yoon, M.-Y.; Choi, N.H.; Min, B.S.; Choi, G.J.; Choi, Y.H.; Jang, K.S.; Han, S.-S.; Cha, B.; Kim, J.-C. Potent in vivo antifugal activity against powdery mildews of pregnane glycosides from the roots of *Cynanchum wilfordii*. *J. Agric. Food Chem.* **2011**, *59*, 12210–12216. [CrossRef] [PubMed]

9. Li, J.-L.; Gao, Z.-B.; Zhao, W.-M. Identification and evaluation of antiepilepic activity of C$_{21}$ steroidal glycosides from the roots of *Cynanchum wilfordii*. *J. Nat. Prod.* **2016**, *79*, 89–97. [CrossRef] [PubMed]

10. Hwang, B.Y.; Kim, Y.H.; Ro, J.S.; Lee, K.S.; Lee, J.J. Acetophenones from roots of *Cynanchum wilfordii* HEMSLEY. *Arch. Pharm. Res.* **1999**, *22*, 72–74. [CrossRef] [PubMed]

11. Li, J.-L.; Fu, Y.F.; Zhang, H.-Y.; Zhao, W.-M. Two new humulanolides from the root of *Cynanchum wilfordii*. *Tetrahedron Lett.* **2015**, *56*, 6503–6505. [CrossRef]

12. Jiang, Y.F.; Choi, H.G.; Li, Y.; Park, Y.M.; Lee, J.H.; Kim, D.H.; Lee, J.-H.; Son, J.K.; Na, M.; Lee, S.H. Chemical constitunets of *Cynanchum wilfodii* and the chemotaxonomy of two species of the family Aslepiadacease, *C. wilfordii* and *C. auriculatum*. *Arch. Pharm. Res.* **2011**, *34*, 2021–2027. [CrossRef] [PubMed]

13. Li, Y.; Piao, D.; Zang, H.; Woo, M.-H.; Lee, J.-H.; Moon, D.-C.; Lee, S.-H.; Chang, H.W.; Son, J.K. Quality assessment and discrimination of the roots of *Cynanchum auriculatum* and *Cynanchum wilfordii* by HPLC-UV analysis. *Arch. Pharm. Res.* **2013**, *36*, 335–344. [CrossRef] [PubMed]

14. Lin, C.-N.; Huang, P.-L.; Lu, C.-M.; Yen, M.-H.; Wu, R.-R. Revised structure for five acetophenoes from *Cynanchum taiwanianum*. *Phytochemistry* **1997**, *44*, 1359–1363.

15. SDBSWeb. National Institute of Advanced Industrial Science and Technology. Available online: http://sdbs.db.aist.go.jp (accessed on 25 January 2018).

16. Li, J.; Kadota, S.; Kawata, Y.; Hattori, M.; Xu, G.-J.; Namba, T. Constutuents of the roots of *Cynanchum bungei* DECNE. Isoation and structures of four new glucosides, bungeiside-A, -B, -C, and -D. *Chem. Pharm. Bull.* **1992**, *40*, 3133–3137. [CrossRef] [PubMed]

17. Tanaka, T.; Nakashima, T.; Ueda, T.; Tomii, K.; Kouno, I. Facile discrimination of aldose enantiomers by reversed-phase HPLC. *Chem. Pharm. Bull.* **2007**, *55*, 899–901. [CrossRef] [PubMed]

18. Liu, S.; Chen, Z.; Wu, J.; Wang, L.; Wang, H.; Zhao, W. Appetite suppressing pregnane glycosides from the roots of *Cynanchum auriculatum*. *Phytochemistry* **2013**, *93*, 144–153. [CrossRef] [PubMed]

Sample Availability: Samples of the compounds **1**–**13** are available from the authors.